ISSN 1738-1142

Volume 18(2) **2020**

KOREAN RADIOACTIVE WASTE SOCIETY

2020 추계학술논문요약집

| 일시 |

2020. 12. 9(수) ~ 11(금)

| 온 라 인 | www.krs.or.kr

한국방사성폐기물학회

Zoom

| 오프라인 | 대전 예람인재교육센터

Abstracts of Proceedings of the
Korean Radioactive Waste Society
AUTUMN 2020

사단법인 한국방사성폐기물학회
Korean Radioactive Waste Society

2020 추계학술발표회

이 발표논문집은 2020년도 정부재원(과학기술진흥기금 및 복권기금)으로
한국과학기술단체총연합회의 지원을 받아 발간되었음

ISSN 1738-1142

Volume 18(2) **2020**

KOREAN RADIOACTIVE WASTE SOCIETY

2020
추계학술논문요약집

| 일시 |
2020. 12. 9(수) ~ 11(금)

| 온 라 인 | www.krs.or.kr
한국방사성폐기물학회
Zoom
| 오프라인 | 대전 예람인재교육센터

Abstracts of Proceedings of the
Korean Radioactive Waste Society
AUTUMN 2020

사단법인 한국방사성폐기물학회
Korean Radioactive Waste Society

Contents

KOREAN
RADIOACTIVE WASTE
SOCIETY

1분과 핵주기정책·규제 및 비확산 [ORAL]

1-O-01 The Use of Satellite Imagery for Countering Nuclear Proliferation: A Historical Review ····· 21
Jae-Jun Han, Nam Kyung Kim [KINAC]

1-O-02 A Survey of Deep Learning Based Satellite Image Analysis Technologies to Support Remote Sensing for Nuclear Nonproliferation ····· 23
Nam Kyung Kim [KINAC]

1-O-03 Proactive Adaptive Cooperative Threat Reduction Under the Three Pillar Approach ····· 25
Yongsoo Hwang [KAERI]

1-O-04 A Statistical Approach for Safeguards of a Nuclear Facility Handling Bulk Material ····· 27
Seung Min Woo, Jukyong Kim [Jeju Natl. Univ.], Jinwoo Lee [KAIST]

1-O-05 Blast Load Assessment on a Reinforced Concrete Wall ····· 29
Wooseub Kim, Seungsik Yu, Ji-Hwan Cha [KINAC]

1-O-06 A Study on Accidental Acquisition of Nuclear Material in Terms of Safeguards ····· 31
Ju-Ang Jung, Hyun-Jo Kim, In-Chul Kim, Byung-Doo Lee, Sung-Ho Lee, Hyun-Sook Kim, Jin-Ha Choi, Mun-Young Ryu [KAERI]

1-O-07 Safeguards Measures for Model Pyroprocessing Plant Developed in Collaboration With IAEA ····· 33
Seong Kyu Ahn, Ho-Dong Kim, Se-Hwan Park, Dae-Yong Song [KAERI]

1분과 핵주기정책·규제 및 비확산 [POSTER]

1-P-01 A Study on the Application of a Radiation Portal Monitoring System ····· 37
Chansuh Lee, Beomseok Shin [KINAC]

1-P-02 Progress in the Analysis of Uranium Enrichment Using LIBS+LIF ····· 39
Se-Hwan Park, Euo-Chang Jung, Seong-Kyu Ahn [KAERI]

1-P-03 Study on Emergency Operating Procedures for Fuel Cycle Facilities ····· 41
Seok-Jun Seo [KAERI]

1-P-04 Development of Emergency Operating Procedures for a Gas Leakage ····42
Seok-Jun Seo [KAERI]

1-P-05 Analysis of Vital Area Identification During Maintenance of Equipment ····43
Ji-Hwan Cha, Wooseub Kim [KINAC]

1-P-06 The Status of Nuclear Material Accountancy of R&D Facility at KAERI ····45
Hyun-Jo Kim, In-Chul Kim, Byung-Doo Lee, Sung-Ho Lee, Hyun-Sook Kim, Juang Jung, Jin-Ha Choi, Mun-Young Ryu [KAERI]

1-P-07 The Status of Practical Education for Accounting Nuclear Material at KAERI ····47
Jinha Choi, In-Chul Kim, Byung-Doo Lee, Sung-Ho Lee, Hyun-Jo Kim, Hyun-Sook Kim, Juang Jung, Mun-Young Ryu [KAERI]

1-P-08 A Study on the Need of New Safeguards International Training Course for States With Small Quantities Protocols at INSA ····49
Byung-Woo Shin [KINAC]

1-P-09 Safeguards Activities for Nuclear Power Plant in Post-operational Phases ····51
Wonjong Song [KINAC]

1-P-10 An Exploratory Study on Acquisition Path Analysis for Denuclearization Verification ····53
Jung-Hyun Lee, Minsoo Kim, Yonhong Jeong, Seung Ho Jeong, Young Wook Lee [KINAC]

1-P-11 Education of Nuclear Nonproliferation and Security Facing the COVID-19 Challenges ····55
Sung Yoon Park, Byung-Woo Shin [KINAC]

2분과 사용후핵연료 처분전관리 [ORAL]

2-O-01 Preliminary Data Analysis of Empty Weight Transportation Test and Surrogate Spent Nuclear Fuel Loaded Transportation Test Under Normal Conditions of Transport ····59
JaeHoon Lim, Woo-seok Choi, Sang Soon Cho, Gil-Eon Jeong, Jongmin Lim [KAERI]

2-O-02 Current Status of the R&D Program for Evaluating Spent Nuclear Fuel Integrity Under Normal Conditions of Road and Sea Transport in Korea ····61
Hyeong Koo Kim, Joong Jin Kim, Jang Whan Lim, Seong Ki Lee, Jong Sung Yoo [KEPCO NF]

2-O-03 Fuel Handling Process and Interlock Design of Fuel Handling Equipment ····63
Sang-Gyoon Chang, Jung-Gyu Kim, Jong-Min Kim [KEPCO E&C], Jong-Pil Jung [KHNP]

2-O-04 Creep Assessment of Domestic Spent Nuclear Fuel During Long-term Dry Storage Condition ····65
You-Jin Kang, Dongjun Lee, Wontak Lee, Eunho Choi, Sangtae Kim, Yong-Soo Kim [Hanyang Univ.]

2-O-05 A Study on the Peening Effects of 316LN Stainless Steel Using the Contour Method to Enhance the SCC (Stress Corrosion Cracking) Resistance for SNF Dry Storage Canisters ····· 67
Hwasoo Kang, Yongsoo Kim [Hanyang Univ.], Yongdeog Kim, Donghee Lee [KHNP-CRI], Ho Kyeom Kim [The Open Univ.]

2-O-06 Study of Exchange Current Densities of Zn and La on Liquid Bi Electrode in Molten LiCl-KCl Salt ····· 69
Jun Woo Park, Jong-Il Yun [KAIST]

2-O-07 Decontamination Targets for Spent Nuclear Fuel Reprocessing in the Aspect of the Radiological Risk of Human Intrusion ····· 71
Hyewon Shin, Younghwan Jeong, Jungho Hur, Jaeyeong Park, Il Soon Hwang [UNIST]

2-O-08 Prediction of Radioactive Fission Gas Release During Loss-of-Coolant-Accident in a Spent Fuel Pool ····· 73
Sun Ki Kim [KAERI]

2분과 사용후핵연료 처분전관리 [POSTER]

2-P-01 Evaluation of Commercial Alloys for Application in Carbon-anode-based Oxide Reduction System ····· 77
Min Ku Jeon, Sung-Wook Kim, Sang-Kwon Lee, Eun-Young Choi [KAERI]

2-P-02 Preliminary Analysis of the Anodic Gas Generated in the Oxide Reduction Process With Carbon Anode ····· 79
Sang-Kwon Lee, Sung-Wook Kim, Min Ku Jeon, Eun-Young Choi [KAERI]

2-P-03 Review of Spent Fuel Pool Island of SONGS Units 2/3 in USA ····· 81
Kwang Nam Kim, Sang Hoon Park, Kyong Won Han, Kwan Sik Chun [KETA]

2-P-04 Final Design Review of Sealed Container for Storage and Transportation of Spent Nuclear Fuels ····· 83
Sukwoo Hong, Myungchul Park, Hyoungmun Kwon, Sunggeun Kim, Jeongnam Jang [KAERI]

2-P-05 Criticality Analysis of GBC-32 Cask With PLUS7 Fuels in Burnup Credit ····· 85
Hyungju Yun, Seunghyun Kim, Hyeonwoo Oh [KORAD]

2-P-06 Investigation on the Performance of the Porous Multi-layer Hemisphere Crucible Cover for Cd Distillation ····· 87
Sang Woon Kwon, Junhyuk Jang, Sung Jai Lee [KAERI]

2-P-07 Studies on the Dissolution of SrO From Simulated Fuel in LiCl-KCl Molten Salt ····· 88
Chang Hwa Lee, Seungwoo Paek, Seok-Min Hong, Sung-Jai Lee [KAERI]

2-P-08 A Study on the Road Transport Test With Full-Scale Cask for the Evaluation of Transportability After Storage ····· 90
Woo-seok Choi, JaeHoon Lim, Jongmin Lim, Gileon Jeong, Sang Soon Cho [KAERI]

2-P-09 Comparison of Dimensional Conformity of Surrogate Metallic Fuels in Different Additive Manufacturing Processes ····· 92
Young-Ho Lee, Sang-Kyu Park, Kiho Kim, Jeong-Yong Park [KAERI]

2-P-10 The Effects of Hydrogen Content and Hydride Morphology on the Ductile to Brittle Transition Temperature (DBTT) for Zircaloy-4 Cladding ····· 94
Ho-a Kim, Jae-soo Noh [ACT]

2-P-11 Topology Optimization of Test Model of Tie-down Structure for the KORAD-21 Transportation Cask ····· 96
Gil-Eon Jeong, Woo-Seok Choi, Sang Soon Cho [KAERI]

2-P-12 Preparation for the Repair of Top-Nozzle Dismantled Fuel Assembly ····· 98
Myungchul Park, Sukwoo Hong, Inchan Kwon, Hyoungmun Kwon [KAERI]

2-P-13 Proposal for Interim Storage Facility of Spent Nuclear Fuel in Korea ····· 100
Jin-Seob Kwon, Chang-Lak Kim [KINGS]

2-P-14 Preliminary Logistic Simulation for Spent Fuels From Kori Site to an Assumed Interim Storage Facility ····· 102
Young-min Kim, David Kessel, Chang-Lak Kim [KINGS]

2-P-15 The Means to Apply the Definition for the License of the Design Approval of the Spent Nuclear Fuel Storage Cask ····· 104
Daesik Yook, Suji Yoon, Eunjin Seo [KINS]

2-P-16 Vibration and Shock Analysis for Ship Transportation of Spent Nuclear Fuel ····· 106
Sang Soon Cho, Kiseog Seo [KAERI], Daesik Yook [KINS

2-P-17 Reaction of RE and Mg Metals With UCl_3 in the LiCl-KCl Molten Salt ··· 108
Seungwoo Paek, Gha-Young Kim, Junhyuk Jang, Chang-Hwa Lee, Sung-Jai Lee [KAERI]

2-P-18 Design Features of the Transfer Cask (OASIS-HC) and Storage Cask (OASIS-STO) ····· 110
Soung Kyu Lee, Jin Seok Park, Min Kyu Kim, Jong Min Kim [KEPCO E&C]

2-P-19 Pyro-SFR Cycle Transition Scenario in Korean Energy Transition Policy ·· 112
Hong Jang, Hyo On Nam, Won Il Ko [KAERI]

2-P-20 SFR SF Pyroprocessing Flowsheet Model for Economic Evaluations ····· 114
Hun Suk Im, Kwang Rag Kim, Hong Jang, Hyo On Nam [KAERI]

2-P-21 Gas Circulation Drying System Control for Dry Storage of Spent Nuclear Fuel ····· 116
Kyung-Wook Shin, Gyung-Sun Chae, Geon-Hui Lee, Jae-Seok Park [SAE-AN Eng. Corp.]

2-P-22 A Framework for Integrated Oxide Reduction Process Automation in Pyroprocess Automation Mockup ····· 118
Jonghui Han, Jongkwang Lee, Dongseok Ryu, Seungnam Yu [KAERI]

2-P-23 Operation Set Based Handling Automation in Pyroprocess Automation Mockup ····· 120
Jonghui Han, Jongkwang Lee, Dongseok Ryu, Seungnam Yu [KAERI]

2-P-24 Experimental Study of Centrifugal Contactor Using Immiscible Fluids of Water and Mercury ····· 122
Youn Su Kim, Byung Gi Park [Soonchunhyang Univ.]

2-P-25 Estimation of Disposal Footprint for Wastes From the Advanced Nuclear Fuel Cycle ····· 124
Hyo On Nam, Hun Suk Im, Hong Jang [KAERI]

2-P-26 Effect of Cooling Time on the Characteristics of the Electrochemically Processed Wastes ····· 126
Hyo On Nam [KAERI]

3분과 고준위폐기물처분 [ORAL]

3-O-01 Study on the Hydro-Geological Change of Natural Barriers by Borehole Expansion Test ····· 131
Kyung-Woo Park, Byeong-Hak Park, Chang-Yong Lee, Nak-Youl Ko, Sung-Hoon Ji [KAERI]

3-O-02 Time-Resolved Laser Luminescence Properties of U(VI) Species Adsorbed on Na-Montmorillonite, Alumina, and Silica ····· 133
Euo Chang Jung, Tae-Hyeong Kim, Wansik Cha, Min Hoon Baik [KAERI]

3-O-03 Estimating Hydraulic Conductivity of Fractured Crystalline Rock Aquifer Using Pulse Test ····· 135
Byeong-Hak Park, Kyung-Woo Park, Changyong Lee, Nak-Yeol Ko, Sung-Hoon Ji [KAERI]

3-O-04 Modeling the Sequential Canister Failures and Solute Transport in the Geological Disposal System ····· 137
Minjeong Kim, Jung-Woo Kim, Jaewon Lee, Dong-Keun Cho [KAERI]

3-O-05 Technology Innovation for Future Safety and Security Enhancement of a Deep Geologic Repository ····· 139
Yongsoo Hwang, Hyo-On Nam [KAERI]

3-O-06 Numerical Estimation of Changes in Hydrogeological Characteristics Around a Disposal Hole at an Underground Research Tunnel ····· 141
Chae-Soon Choi, Kyung-Woo Park, Nak-Youl Ko, Byeong-Hak Park, Sung-Hoon Ji [KAERI]

3분과 고준위폐기물처분 [POSTER]

3-P-01 Evaluation of Water Retention Curve for Korean Bentonite Buffer Considering Dry Density and Temperature Variation ····· 145
Seok Yoon, Geon-Young Kim, Dong-Keun Cho [KAERI]

3-P-02 Comparison of Q-Equivalent Models for the Mass Transfer Around the Deposition Hole ····· 147
Heui-Joo Choi, In-Young Kim, Jong Youl Lee, Dong-Keun Cho [KAERI

3-P-03 Retrievability of Deposited Canisters in the KRS+ Repository ····· 149
Heui-Joo Choi, Jong Youl Lee, Dong-Keun Cho [KAERI]

3-P-04 Conceptual Design of Sandglass-like Separator for Immobilized Anionic Radionuclides Using Particle Tracking Based on Computational Fluid Dynamics ····· 151
Tae-Jin Park, Young-Chul Choi [KAERI], Jiwoong Ham [Chungnam Natl. Univ.]

3-P-05 Interactions Between Korean Buffer and Groundwater Under Temperature Conditions of Disposal Interest ····· 153
Tae-Jin Park, Ji-Hun Ryu, Min-Hoon Baik, Jae-Kwang Lee [KAERI]

3-P-06 Field Tracer Tests for Identifying Local Heterogeneity of Borehole Wall ···· 155
Nak-Youl Ko, Kyung-Woo Park, B.H. Park, Chang Yong Lee, Sung-Hoon Ji [KAERI]

3-P-07 Concepts of Retrieval Processes for Deposited Disposal Canisters and Bentonite Blocks ····· 157
Jong-youl Lee, In-young Kim, Heui-joo Choi, Dong-keun Cho [KAERI]

3-P-08 The Evolution History of Fractures and Fracture Fillings of Deep Granitic Rock at KURT Site ····· 159
Soolim Jung, Ji-Min Choi, Sung-Hoon Ji, Kyung-Su Kim [KAERI]

3-P-09 History of Development and Activity Patterns of the Keumwang Fault at Inje-gun, Gangwon-do ····· 161
Ji-Min Choi [KAERI], Hee-Kwon Lee [Kangwon Natl. Univ.]

3-P-10 Mechanistic Understanding of Bentonite Swelling as a Buffer Material ···· 163
Jae Owan Lee, Seok Yoon, Jin-Seop Kim, Geon Young Kim [KAERI]

3-P-11 Near-field Evolution During Thermal Period of a HLW Repository ····· 165
Min-Hoon Baik, Jae-Kwang Lee [KAERI]

3-P-12 Preliminary Performance Analysis Modeling for an Annular Metal Fuel …167
Byoung Oon Lee, Chan Bock Lee, June Hyung Kim, Jeong Yong Park, Jin Sik Cheon [KAERI]

3-P-13 Copper Corrosion Modeling in Anaerobic Environment of YS03 Borehole ··169
Minsoo Lee, Kyung-Woo Park, Sung-Hoon Ji [KAERI]

4분과 중저준위폐기물관리 [ORAL]

4-O-01 Spent Resin Management Strategy Based on Experience and Current Status ·····173
Suk Nam Lim, Kyu Sup Choi, Jae Woo Park, Hyo Sub Kim [KONES]

4-O-02 Design of Prototype (Part 2) That Treats Radioactive Waste Containing C-14 ·····174
Bong-Ki Ko, Hyeon-Oh Park, Ki-Hyun Kwon, Seung-Geon An [Sunkwang T&S]

4-O-03 Solidification of Borate Waste Using Metakaolin-Based Geopolymer Waste Form ·····176
Byoungkwan Kim, Juhyeok Lee, Jaehyuk Kang, Younglim Shin, Won-Seok Kim, Wooyong Um [POSTECH]

4-O-04 The Self-clearance Strategy of the New Fuel Container for Heavy Water Reactor (CANDU) Based on DQO ·····178
Kwangyoung Sohn, Changhwan Cho, Sungjong Kim [MIRAE-EN]

4-O-05 Seismic Analysis of the Disposal Containers Stacked in the LILW Repository Silos ·····180
Hyeongjin Byeon, Kiwon Kang, Yulim Lee, Jaeyeong Park [UNIST]

4-O-06 Development of Conceptual Design for Cover in Nearsurface Disposal Facility ·····182
Ki-jung Kwon, Mi-jin Kwon, Yu-hwa Son [KORAD]

4-O-07 A Study on the Optimized Segmentation of 560 MWe Westinghouse Pressurized Water Reactor Reactor Vessel Internals ·····184
Hyo-Jeon Kim, Jae-yong Lee, Kyung-min Kim, Young-wook Kim, Yong-soo Kim [Hanyang Univ.]

4분과 중저준위폐기물관리 [POSTER]

4-P-01 Decontamination and Treatment Technologies of Radioactive Waste for the Decommissioning of CANDU-6 (Canadian Case) ····· 189
Mugap Shin, Kwangsoon Choi, Jaihoon Jung [KEPCO E&C]

4-P-02 Adsorption of Iodide Using Silver Functionalized Magnetite Silica Composites ····· 191
Sangeun Jo, Dohyun Kim, Youngwoong Park, Sangjun Choi [Kyungpook Natl. Univ.], Jungwon Choi [KRICT]

4-P-03 Applicability of Domestic Natural Zeolite as an Additive for Solidification of Decommissioning Liquid Waste With Polymer Cement ····· 193
Seong Ho Yoo, Hyun Ki Jung, Ho Yeon Yang, Kwan Sik Chun [KETA]

4-P-04 Homogeneity Test of Cesium and Cobalt Loaded Ion Exchange Resins in Polymer Waste Form ····· 195
Jueun Kim, Byoungkwan Kim, Bhupendra Kumar Singh, Wooyong Um [POSTECH]

4-P-05 Mercury (II) Removal From Aqueous Solution Using Sulfur-functionalized Biochar ····· 197
Samiratu Atibun Isa, Sae Yun Kwon, Bhupendra Kumar Singh, Hyojoo Kim, Wooyong Um [POSTECH]

4-P-06 The Process-level Modeling and Simulation for the Underground Silo of LILW Disposal Facility ····· 199
Myunggoo Kang, Jaechul Ha, Tae-man Kim, Chun-hyung Cho [KORAD]

4-P-07 Review on the Plasma Arc Melting Technology Using Graphite Electrodes for the Treatment of Radioactive Mixed Wastes ····· 201
Jae-Hyuk Choi, Na-Young Kim, In-Sun Jang, Kung-Hwa Yang [DAWONSYS]

4-P-08 Reduction of Radioactive Concrete Waste Using Dense Medium Separation Technology ····· 203
Seokju Hong, Sangsoo Han, Seongsik Nam, Won-Seok Kim, Wooyong Um [POSTECH]

4-P-09 Solubility of Tc-99 With Various Conditions in the Wolsung Repository Site, South Korea ····· 205
Sohae Park, Sangsoo Han, Wooyong Um [POSTECH]

4-P-10 Design Concept of the Automatic Fastening Device for the Lid of the High Integrity Container Applicable to Korea ····· 207
Mi-Hyun Lee, Young Hwan Hwang, Ji-Hoon Lee [KHNP-CRI]

4-P-11 A Study on Long-term Stability of High Integrity Container ····· 209
Young Hwan Hwang, Mi-Hyun Lee, Ji-Hoon Lee [KHNP-CRI]

4-P-12 Status of Radioactive Mixed Waste Treatment Technology ····· 211
In Sun Jang, Na Young Kim, Jae Hyuk Choi, Kyung Hwa Yang [DAWONSYS]

4-P-13 Comparison of Laws and Regulations on Mixed Waste Between the USA and Korea ····· 213
Eun-Jin Sim, Sun-Kee Lee, Chang-Lak Kim [KINGS]

4-P-14 A Case Study on the Radionuclide Fraction in Activated Concrete for Abroad Decommissioning NPPs ····· 215
Yu-hwa Son, Tae-man Kim, Chun-hyung Cho [KORAD]

4-P-15 A Study on the Indirect Evaluation Method of Difficult-to-Measure Nuclides in Nuclear Decommissioning Radioactive Waste ····· 217
Hang-Rae Cho, Ji-Soo Yoon, Ji-Hoon Lee [KHNP-CRI]

4-P-16 Study on Introduction of Margin at Solid Waste Form Test for Acceptance Criteria of Final Repository ····· 219
Dae Seok Hong, Dong Ju Lee, Ji Young Song, Yoon Do Oh, Ki Baek Shin, Hyun Kyu Lee, Dong Han Yoo, Won Hyuk Jang [KAERI]

4-P-17 The Development of URSF Management System ····· 221
YuJeong Choi, Jeongguk Kim, Jongjin Kim, Jinwoo Lee [KAERI]

4-P-18 Development of Equipment of Contamination Inspection for Steel Pipe Scaffold in Nuclear Power Plants ····· 223
Hyung kwon Jeong, Dong kyu Jang, Jeong won Park [ACTRMT]

4-P-19 RESRAD Code Sensitivity Analysis and Safety Assessment for Clearance of Radioactive Waste ····· 225
Yeo Chong Cho, Jong Soon Song [Chosun Univ.]

4-P-20 Preliminary Studies on Neutron Activation of Concrete From Cyclotron Facilities and Applicability of Decay-in-storage for Decommissioning Waste Management ····· 227
Se Geun Lee, Jae Hak Cheong [Kyung Hee Univ.]

4-P-21 A Study of the Nuclear Inventory Evaluation for Decommissioning Radioactive Waste Scaling Factor Analysis ····· 229
Hwayoon Kang, Yongsoo Kim [Hanyang Univ.]

4-P-22 Pressurized Heavy Water Reactor Spent Resin Mixture Transfer System Processor Development ····· 231
Kyu-Ho Lee, Ha-Young Oh, Bong-Ki Ko, Hyeon-Oh Park, Seung-Geon An [Sunkwang T&S]

5분과 제염해체 [ORAL]

5-O-01 Synthesis of Prussian Blue Functionalized CoCr Layered Double Hydroxides to Treat Cesium and Iodate Together ····· 235
Jueun Kim, Jaehyuk Kang, Wooyong Um [POSTECH]

5-O-02 A Chemical Decontamination Process for Corrosion Oxide Layers on Carbon Steel Heat Transport System in PHWR ····· 237
Naon Chang, Yongsoo Kim [Hanyang Univ.], Heechul Eun, Huijun Won, Wangkyu Choi, Seonbyeong Kim [KAERI]

5-O-03 Evaluation of the Nuclide Inventory for the SG Crossover Leg in Kori Unit 1 ····· 239
Jonghoa Kim, Homin Jeon, Jihyun Yu, Seunggi Jeong, Sunghoon Kim, Kyeongho Han, Jangsoo Seo [Sae-An Enertech Corp.]

5-O-04 Integration of Soil Washing and Water Treatment Techniques for Separation of Radioactive Elements From Soils Impacted by Nuclear Power Plants ····· 241
Yongju Choi, Jihyeon Jung, Hojae Song, Seonyoung An, Seoyoung Choi, Jong Kwon Choe, Kyoungphile Nam [Seoul Natl. Univ.]

5-O-05 Radioactivity Concentration Derivation for Conditional Recycling of Decommissioning Wastes ····· 243
Kiwon Kang, Hyeongjin Byeon, Eunyeong Choi, Jaeyeong Park [UNIST]

5-O-06 Numerical Calculations for Performance Prediction of Ventilation Unit of Thermal Cutting System Developed for Kori Unit 1 Reactor Vessel Dismantling ····· 245
Kyuho Chang, Haewoong Kim, Kwangsoo Park, Heedong Sohn [Doosan HI&C]

5-O-07 Analysis of Plasma Cutting Process Using High Speed Camera and Cutting Signals ····· 247
Dae-Won Cho, Dong-Hyun Kim, Jeong Suh [KIMM]

5-O-08 Planning and Design of Decommissioning Site Remediation Focusing on Radionuclide and Site Media Characteristic ····· 249
In-Ho Yoon, Sung-Man Kim, Ilgook Kim, Chan-Woo Park, Hee-Man Yang, Youngho Sihn, Changyun Roh, Sang-Bum Hong [KAERI]

5분과 제염해체 [POSTER]

5-P-01 Pre-Decommissioning Activities for the Decommissioning of CANDU-6 (Canadian Case) ····· 253
Kwangsoon Choi, Mugap Shin, Jaihoon Jung [KEPCO E&C]

5-P-02 A Study for Maximizing Detection Efficiency and Image Resolution in Nuclear Power Plant ····· 255
Changyeon Yoon [KHNP-CRI], Taewoong Lee [KEPCO KPS]

5-P-03 A Study on the Dose Assessment of Workers in the Transition Period ·· 257
Jong Soon Song, Hak Yun Lee [Chosun Univ.]

5-P-04 Evaluation of the Preliminary Dose Rate of the New-type Disposal Container According to the Predicted Value of the Radionuclides Inventory of the Decommissioning Concrete Waste ····· 259
Ho-seog Dho, Tae-man Kim, Rin-ah Kim, Chun-hyung Cho [KORAD]

5-P-05 Review on Site Remediation and Release of Nuclear Power Plant During Decommissioning ····· 261
Cheon-Woo Kim, Kwang-ho Jo, Hyejin Jung [KHNP-CRI]

5-P-06 Constructability Review Considering Installation and Dismantling of NSSS Equipment in the Early Phase of the Project ····· 263
Jun Hee Lee, Sung Hyun Jeon [KEPCO E&C]

5-P-07 A Study on Assessment of Lead-free Dual-layered Shielding for Radiation Shielding Rates During Decommissioning of Steam Generator in Kori Unit 1 ··· 265
Taewoong Lee, Heechul Youn, Nakjeom Kim [KEPCO KPS]

5-P-08 Optimization of Lead-free Dual-layered Shielding for Radiation Exposure During Decommissioning of Steam Generator in Kori Unit 1 ····· 267
Taewoong Lee, Seongmin Jo, Nakjeom Kim [KEPCO KPS]

5-P-09 DOI Coded Aperture Imager Monitoring the Distribution of Gamma Nuclides in Decommissioning of Nuclear Power Plant ····· 269
Taewoong Lee, Nakjeom Kim [KEPCO KPS], Hyounggun Lee, Wonho Lee [Korea Univ.]

5-P-10 Dual-Anti Mask Methods for Monitoring the Distribution of Gamma Nuclides in Decommissioning of Nuclear Power Plant ····· 271
Taewoong Lee, Nakjeom Kim [KEPCO KPS], Wonho Lee [Korea Univ.]

5-P-11 Construction of the Advanced Remote Dismantling System Testbed ····· 273
Jonghwan Lee, Dongjun Hyun, Jae Sung Shin, Ikjune Kim, Sungmoon Joo, Jaehyun Ha [KAERI]

5-P-12 Preliminary Review of Applicability of Site Configuration Management to Nuclear Power Plants Under Decommissioning ····· 275
Ga Hyun Chun, Jae Hak Cheong [Kyung Hee Univ.]

5-P-13 Applying AOPs to Illite for Efficient Cesium Removal in Liquid Waste ····· 277
Jaeeun Kang, Juhyeok Lee, Jimo Lee, Ingyu Song, Won-Seok Kim [POSTECH]

5-P-14 Studies on Characteristics of $HMnO_4$, a Strong Oxidizing Reagent for NPP Chromium Oxide Decontamination, Prepared by Cation Ion Exchange of $KMnO_4$ ····· 279
Junho Shin, Seungyeop Han, Hyojung Kim, Jongho Jeon, Wonzin Oh, Sang-June Choi [Kyungpook Natl. Univ.], Jae Kwan Park, Byung-Chul Lee [Hannam Univ.], Ki-Chul Kim [KEPCO KPS]

5-P-15 Identification Algorithm Based on Neural Network for Gamma Spectra in Low Level Activity Measurement ····· 281
Inhye Hahm, Eunjoong Lee, Byungchae Lee, Young-Su Kim, Junha Kim, Sang Bum Hong [KAERI]

5-P-16 Tritium Removal Behaviors of Protonated Lithium Metal Compounds in Water ····· 283
Chan Woo Park, Sung-Wook Kim, Youngho Sihn, In-Ho Yoon [KAERI]

5-P-17 Logistical Simulation for Concrete Treatment Process in Decommissioning ··· 284
Bong-su Yoon, David Kessel, Chang-Lak Kim [KINGS]

5-P-18 Choosing a Knowledge Management Strategy for Decommissioning of NPP ·· 286
So-Yoon Kim, David Kessel, Chang-Lak Kim [KINGS]

5-P-19 Establishment of Restricted Recycling Scenarios of Very Low Level Waste From Decommissioning and Preliminary Radiological Assessment of Potential Risk ····· 288
In Gyu Chang, Jae Hak Cheong [Kyung Hee Univ.]

5-P-20 The Effect of ICRP's New Internal Dosimetry Models on Occupational Internal Exposure During Dismantling of Radioactive Concrete ····· 290
Siwan Noh, Seungnam Yu [KAERI]

5-P-21 A Study on Radiological Inventory Evaluation for RV/RVI and Bio-Shield Concrete of a 1,000MW PWR NPP With Three-Loop ····· 292
Jae-Hun Ko, Dong-Gyu Lee, Nak-Hoon Sung [KONES], Jae-Yong Oh, Cheon-Woo Kim [KHNP-CRI]

5-P-22 Technical Review on Release of Radioactive Building in European Commission ····· 294
Jihwan Yu, Hangrae Cho [KHNP-CRI]

5-P-23 Efficient Decomplexation of Co-EDTA Mixed Radioactive Waste by Advanced Oxidation Process ····· 296
Juhyeok Lee, Wooyong Um [POSTECH]

5-P-24 Tritium Extraction From Cement Mortar According to Heating Temperature ·· 298
Ki Joon Kang, Jun Woo Bae, Hee Reyoung Kim [UNIST]

5-P-25 Development of WBS for CANDU Nuclear Power Plant ····· 300
Minhee Kim, Chang-Lak Kim, Sanghwa Shin [KINGS]

5-P-26 Sulfate Radical Advance Oxidation Process for Degradation of Spent Resin ····· 302
Muhammad Aamir Hafeez, Junsung Jeon, Junkyu Park, Wooyong Um [POSTECH]

5-P-27 Analysis on Radioactive Waste Level of the Reactor Internals According to the Content of Impurities ····· 304
Gilyong Cha, Soonyoung Kim, Minhye Lee [RADCORE], Minchul Kim, Hyunmin Kim [KHNP-CRI]

5-P-28 Performance Evaluation of Non-radioactive Contaminated Soil Separation, Coagulation and Dewatering Using Pilot Scale Soil Decontamination System ··· 306
Seongjoo Kang, Minhyuk Yoon, Kukjin Seo, Woohyeon Rhee, Seungil Kim, Dukwon Kang [Elim-Global]

5-P-29 Fabrication of Nanocomposite-based Plastic Scintillator ····· 308
Hara Kang, Jae Hak Cheong [Kyung Hee Univ.], Sang Bum Hong, Changhyun Roh [KAERI]

5-P-30 Cutting Simulation Method Based on the 3D Scanned Environmental Information for Nuclear Facility Dismantlement ····· 310
Ikjune Kim, Dongjun Hyun, Jonghwan Lee, Sungmoon Joo, Jaehyun Ha [KAERI]

5-P-31 Integrated Control Framework of Remote Dismantling System in Radiation and Underwater Environment ····· 312
Dongjun Hyun, Ikjune Kim, Sungmoon Joo, Jaehyun Ha, Jonghwan Lee [KAERI]

5-P-32 Disposal and Treatment for Decommissioning Solid Waste of Advanced Fuel Science Building at KAERI ····· 314
Byungyoun Min, Hyojin Aan, Undong Choi, Jinho Park, Seungkook Park [NUDECOM]

6분과 방사선환경 및 안전 [ORAL]

6-O-01 Exercises of Aerial Radiation Measurements Using a Manned Helicopter ····· 319
Young-Yong Ji [KAERI], Hyon-Sock Chang [SI Detection], Hee-Jin Kim [Busan Metropolitan City]

6-O-02 Calculation of Minimum Detectable Concentrations for Mobile In-Situ Gamma Detector Using Outdoor-Field Data ····· 321
Se-Won Park, Chanki Lee, Hee Reyoung Kim [UNIST]

6-O-03 Development of Radiation Localization Algorithm Using Recursive Bayesian Inference ····· 323
Hwa Jeong Han, Beom Kyu Kim, Byung Gi Park [Soonchunhyang Univ.], Sang Hun Shin [FNC Technology]

6-O-04 Comparison of Gross and Photopeak Counts for Underwater Measurements Based on $YAlO_3$:Ce Spectrometer ····· 325
Chanki Lee, Hee Reyoung Kim [UNIST]

6-O-05 Introduction of Modular Design Based Mobile Air Cleaning System ····· 327
Jong Seong Kim, Kaphyun Yoo, Jungsu Oh [Century Corp.], Hyun Chul Lee, Doo Yong Lee [FNC Technology], Dukhee Lee [SOLTI], Junghyuk Shin [NAC], Byunggi Park [Soonchunhyang Univ.]

6-O-06 Comparison of Annual Atmospheric Dispersion Factors of Continuous and Purge Releases of Gaseous Radioactive Effluents ····· 329
Na-Hyun Kim, Chang-Lak Kim [KINGS], Won-Tae Hwang [KAERI]

6-O-07 Comprehensive Wireless Radiation Monitoring System for Decommissioning Nuclear Power Plants ····· 331
Yun-Sam Kim, Younggil Kim, Donggu Kim, Jungsik Kim, Misuk Jang, Seoung Rae Kim [NESS]

6분과 방사선환경 및 안전 [POSTER]

6-P-01 Introduction of Auto G-factor Calculation Program ····· 335
Sungyeop Joung, Young-Yong Ji [KAERI]

6-P-02 Analysis on Activation Source Term for Soil Sample at KIJANG Research Reactor ····· 337
Ji Sung Park, Gyuhong Roh, Byungchul Lee [KAERI]

6-P-03 Development of Regulatory Guidance on Conditional Clearance for the Disposal, Recycling and Reuse of Activated Medical LINAC Components ···· 339
Byeonghyeon Park, Minchul Song, Jonghoon Park, Jaeho Lee [KINS]

6-P-04 Review on Effectiveness of Current Discharge Limit Based on Radiation Dose for Gaseous Radioactive Effluent From Korean Nuclear Power Plants · 341
Soyun Kim, Ji Su Kang, Jae Hak Cheong [Kyung Hee Univ.]

6-P-05 Preliminary Safety Assessment of Incineration of Decommissioning Waste for Clearance ····· 343
Ji Hoon Han, Jae Hak Cheong [Kyung Hee Univ.]

6-P-06 Comparative Analysis of HH-XRF Spectra for UO_2 Using Monte Carlo Simulation ····· 345
Jaeyeong Jang, Woojin Kim [KINAC]

6-P-07 Evaluation of Radiological Hazard Parameter of Domestic Building Raw Materials ····· 347
Myeong-Hoon Joo, Dae-Hyeon Kim, Eun-Ji Park, Seok-Hwan Han, Sung-Gyu Leem [Hanil Nuclear]

6-P-08 Analysis of DCGL Derivation Cases at License Termination ····· 349
Gang Woo Ryu, Se Jong Lee, Min Seong Kim, Hyeok Jae Kim, Kwang Pyo Kim [Kyung Hee Univ.]

6-P-09 Review of Radiation Dose Assessment for the Processed Products ····· 351
Byung Min Lee, Jae Kwon, Jong Hyeok Park, Kwang Pyo Kim [Kyung Hee Univ.], Jung Hwan Jang [KINS]

6-P-10 Review of Studies Assessing Radiation Dose to Residents Due to the Radioactive Effluent From Nuclear Facilities ····· 353
Hyun Jun Na, Min Young Lee, Hyeung Woo Nam, Jae Bin Heo, Kwang Pyo Kim [Kyung Hee Univ.], Jin Ho Park [KINS]

6-P-11 Outdoor Air Control Unit With Heat Pipes System for Reducing Radioactive Liquid Waste ····· 355
Youngwoo Kwon, Seonho Noh, Heeseok Kang, Youngkuk Jang, Ilje Cho [KAERI]

6-P-12 Comparison of Indoor Thermal Environment by Exhaustion in Spring and Summer ····· 357
Heeseok Kang, Youngwoo Kwon, Seonho Noh, Youngkuk Jang, Ilje Cho [KAERI]

6-P-13 A New Approach to Determine Critical Distance Radius of Self Powered Neutron Detector by Using Least Square Fitted Charge Density ····· 359
Hyuk Han, ChangJe Park [Sejong Univ.]

6-P-14 Preliminary Study on Neutron Shielding of Moderating Materials Using an SiPM-based ^{4}He Detector System ····· 361
Kyung Taek Lim, Sungmin Kim, Wonjong Song, Heejun Chung [KINAC]

7분과 방사화학 [ORAL]

7-O-01 Evaluation of ^{55}Fe in Radioactive Waste With Liquid Scintillation Counting ··· 365
Kyunghun Jung, Garam Park, Jungbo Yoo, Tae-Hong Park, Jaiil Park [KAERI]

7-O-02 Manufacture of Leaching Resistance Cement Waste Form Including KJRR Simulated Liquid Waste ····· 367
Gi Yong Kim, Tae-Hong Park, Junhyuck Im, Dae Seok Hong, Jong Sik Shon [KAERI]

7-O-03 Strontium Isotope Detection by Combination of Laser-induced Breakdown Spectroscopy (LIBS) and Molecular Laser-induced Fluorescence (MLIF) ··· 369
Sung-Uk Choi, Jong-Il Yun [KAIST]

7-O-04 Coordination Mode-dependent Stability and Optical Property Changes of Am(III)-aliphatic Dicarboxylate Complexes ····· 371
H.-K. Kim, H.-R. Cho, E. C. Jung, W. Cha [KAERI], K. Jeong [KMA], K. Kwak [Korea Univ.]

7-O-05 Anodic Dissolution Behaviors of Inconel-600 Depending on Ni and Fe Additives in LiCl-KCl ····· 373
Younghwan Jeon, Jungho Hur, Seungmin Ohk, Jaeyeong Park [UNIST]

7-O-06 Two-step Zr Metal Preparation Combining Electrorefining and Thermal Decomposition ····· 375
Jungho Hur, Younghwan Jeon, Seungmin Ohk, Jaeyeong Park [UNIST]

7-O-07 Thermal Behaviors of Nuclear Fuel Samples and Cladding Materials by Using In-Situ High-Temperature XRD ····· 377
Sang Ho Lim, Jeongmook Lee, Dong Woo Lee, Jong-Yun Kim, Tae-Hyung Kim, Junghwan Park [KAERI], Young-Sang Youn [Yeungnam Univ.]

7분과 방사화학 [POSTER]

7-P-01 Determination of ^{90}Sr and ^{63}Ni in Low-and Intermediate-level Radioactive Waste ····· 381
Kyeonghui Bae, Sora Choi, Kyunghun Jung, Jung Bo Yoo, Tae-Hong Park [KAERI]

7-P-02 Effect of H_2O Adsorption on Cladding Material ····· 383
Dong Woo Lee, Jeongmook Lee, Jong-Yun Kim, Sang Ho Lim [KAERI], Sangjune Park, Young-SangYoun [Yeungnam Univ.], Ki-jeong Kim [POSTECH]

7-P-03 Measurement of Recovery for the Validation of Pretreatment Method in Decontamination Paper Samples ····· 385
Kwang-Soon Choi, Simon Oh, Jae-seok Lee, Hye-Ryun Cho, Tae-Hong Park [KAERI]

7-P-04 Determination of Reduction Yield of Metallic-Metal Oxide Products From Pyroprocessing of Spent Nuclear Fuels: Development of In-Hotcell Procedure ····· 387
Young Hwan Cho, Tae Hong Park, Sang Eun Bae [KAERI]

7-P-05 In-Situ Qualitative Monitoring of Metal Ions in LiCl-KCl Melt ····· 389
Chan-Yong Jung, Hwa-Kyeung Jeong, Sang-Eun Bae [KAERI]

7-P-06 Determination of EDTA in Radioactive Wastes in the Presence of Iron Using UV-Vis Spectrophotometer ····· 391
Hyejin Cho, Jail Park [KAERI]

7-P-07 Synthesis of Actinide Chloride Complexes From Actinide Oxide in High Temperature Molten Salt ····· 393
Hwakyeung Jeong, Sang-Eun Bae [KAERI]

7-P-08 Studies on the Chemical Synthesis and Characterization of Lead (II) Oxide Nanoparticles Prepared With Cationic, Anionic and Non-ionic Surfactants ····· 395
Viktoriya Kim, Jung Hwan Park [UST], Dong Woo Lee, Jeongmook Lee, Tae-Hyeong Kim, Jong-Yun Kim, Sang Ho Lim [KAERI]

7-P-09 Characterization of Material for Immobilization of Radioactive Waste : Structure, Leaching Test and γ-irradiation ····· 397
Hye Ran Noh [UST], Dong-Woo Lee, Tae-Hyeong Kim, Jeongmook Lee, Jong-Yun Kim, Sang Ho Lim [KAERI

7-P-10 Determination of Lanthanides in a High Salt Matrix Using Liquid-Liquid Extraction ····· 399
Jihye Kim, Sang-Eun Bae [KAERI]

7-P-11 Sample Preparation and Characterization of ε-particles in CeO_2 ····· 401
Hyun Myung Choe [Sogang Univ.], Hye Ran Noh, Dong Woo Lee, Jeongmook Lee, Junghwan Park, Tae-Hyeong Kim, Jong-Yun Kim, Sang Ho Lim [KAERI]

7-P-12 Investigation on Crystallographic Properties of Zr and its Alloy Through the Use of In-situ High Temperature X-ray Diffraction ····· 403
Tae-Hyeong Kim, Dong Woo Lee, Jeongmook Lee, Junghwan Park, Jong-Yun Kim, Sang Ho Lim [KAERI], Young-Sang Youn [Yeoungnam Univ.]

7-P-13 Study on Improving the Sensitivity of Nuclear Material Analysis With LA-ICP-MS Using Desolvator ····· 405
Jeongmook Lee, Dong Woo Lee, Tae-Hyeong Kim, Junghwan Park, Jong-Yun Kim, Sang Ho Lim [KAERI]

1분과

핵주기정책·규제 및 비확산(Oral)

The Use of Satellite Imagery for Countering Nuclear Proliferation : A Historical Review

Jae-Jun HAN* and Nam Kyung KIM
Korea Institute of Nuclear Nonproliferation and Control,
1418 Yuseong-daero, Yuseong-gu, Daejeon, Republic of Korea
*jjhan@kinac.re.kr

1. Introduction

Satellite imagery is being used as useful information in that it has high accessibility to the target objects. This paper aims at sharing implications on the availabilities and limitations of satellite imagery for countering nuclear proliferation. The main objective is not to deliver scientific aspects in satellite technology, but to take cognisance of its use, providing historical events to members of the Technical Division of Nuclear Fuel Cycle Policy, Regulation and Non-proliferation in the Korean Radioactive Waste Society.

2. The Use of Satellite Imagery in Nuclear Nonproliferation

Among the Treaties that have already entered into force, the International Atomic Energy Agency (IAEA) has had the ground to use satellite imagery to fulfil the agency missions, in accordance to the paragraph 6 of the INF/ CIRC153 [1], "the Agency shall take full account of technological developments in the field of safeguards." In 1997, the IAEA adopted the Additional Protocol [2] for strengthening the Safeguards Agreements by expanding the scope of declarations and the access to information to verify the state declarations.

As for countering nuclear proliferation, satellite imagery is also being used to identify nuclear activities in rogue states which do not comply with the global nuclear nonproliferation regime. From small-scale objects (such as building expansion, vehicle movement, steam venting, etc.) to large-scale changes (such as subsidence in a mountain area), the satellite information supports to interpret the relevance of nuclear proliferation.

Similarly, it also can be exploited in denuclearisation. From the DPRK De-nuclearization Roadmap [3], the process will take over a decade, including to halt, roll back, and eliminate the nuclear program. Given the duration of denuclearisation, satellite imagery can play an essential role in verifying the long-term process, and in monitoring even after its completion.

3. Aspects of Interpreting Satellite Imagery for Countering Nuclear Proliferation

As aforementioned, the use of satellite imagery in nuclear nonproliferation can be conceptually understandable. In practical, however, use in countering nuclear proliferation namely monitoring rogue states requires much more attention than the implementation of IAEA safeguards in that not verifying the declared information but inferring the relevance of observed characteristics to nuclear activities. To identify nuclear proliferation activities with satellite imagery, such as the production of weapons-grade fissile material, the expertise in not only the nuclear fuel cycle but also remote sensing is essentially required for interpreting satellite imagery. Further, the understanding of states' nuclear proliferation history helps imagery analysts to derive rational inference.

Regarding quality and quantity of satellite information, the spatial, temporal and spectral resolutions of satellite imagery are gradually increasing, which refer to the degree of visibility, a chance to imagery acquisition, and information beyond the visible, respectively. These resolutions delineate technical capabilities (limitations) of using satellite imagery for countering nuclear proliferation.

4. Historical Events Captured by Satellite Imagery for Countering Nuclear Proliferation

Since the access to rogue states is generally prohibited, satellite imagery is the only means to provide direct and physical information on target facilities. Accordingly, the imagery analysts from the non-profit organisations, such as 38 North, ISIS, CSIS, etc., have interpreted them for countering nuclear proliferation since the mid-2000s.

This paper focuses on nuclear fuel cycle facilities in North Korea to investigate historical events captured by satellite imagery. The facilities for fuel fabrication, uranium enrichment, reactor operation and reprocessing are known to be located in the Yongbyon Nuclear Complex.

Therefore, suspicious activities therein, such as retrofits, steam plumes, dredging, vehicle movement, etc. [4-6], have been monitored by the imagery analysts. Although the significance of activities relevant to nuclear proliferation varies depending on the types of signs on the imagery, it showed that the credibility of the imagery interpretation could be improved by other information besides the satellite imagery. For lack of space, the more details are discussed in the presentation.

A few historical events proved that the capabilities in capturing the signs are determined by the quality and quantity of satellite imagery. As to the spatial resolution, the degree of currently available visibility is about a half meter, meaning that one pixel contains a 50 cm × 50 cm area on the ground. For example, an average person is represented in one pixel; thus, it is difficult to distinguish whether the pixel represents a person or not. On the other hand, an object larger than that, such as vehicles, can be distinguished with 50 cm of spatial resolution.

The clouds have a significant influence on the acquisition frequency of electric-optical satellite imagery, implying that the imagery suitable for interpretation may take several days, even if satellites re-visit the target spots every day.

5. Conclusions

This work intended to deliver how satellite imagery supports to counter nuclear proliferation, providing historical events of interpretation. The facilities for fuel fabrication, uranium enrichment, reactor operation and reprocessing in the Yongbyon Nuclear Complex have been reviewed with suspicious activities, such as retrofits, steam plumes, dredging, vehicle movement, etc. Further, the limitations of currently available technology (resources) in remote sensing were discussed in the quality and quantity perspectives.

ACKNOWLEDGEMENT

This work was supported by the Nuclear Safety Research Program through the Korea Foundation Of Nuclear Safety (KoFONS), granted financial resource from the Nuclear Safety and Security Commission (NSSC), Republic of Korea (No. 1905009).

REFERENCES

[1] IAEA, INFCIRC/153(corrected), The Structure and Content of Agreements Between the Agency and States Required in Connection with the treaty on the Non-Proliferation of Nuclear Weapons, (1972).

[2] IAEA, INFCIRC/540, Model Protocol Additional to the Agreement(S) Between State(S) and the International Atomic Energy Agency for the Application of Safeguards, (1997).

[3] Siegfried S. Hecker et al., A technically-informed roadmap for North Korea's denuclearization, Available at https://cisac.fsi.stanford.edu/research/dprk-denuclearization-roadmap/ (Accessed: 20 Oct 2020).

[4] Articles – Topic: Satellite Imagery, Available at https://www.38north.org/topics/satellite-analysis/ (Accessed: 20 Oct 2020).

[5] Articles – Imagery, Available at https://beyondparallel.csis.org/imagery/ (Accessed: 20 Oct 2020).

[6] Articles – Satellite Imagery Analysis, Available at https://customer.janes.com/janes/home (Accessed: 20 Oct 2020).

A Survey of Deep Learning Based Satellite Image Analysis Technologies to Support Remote Sensing for Nuclear Nonproliferation

Nam Kyung KIM
Korea Institute of Nuclear Nonproliferation and Control, 1418, Yuseong-daero, Yuseong-gu, Daejeon, 34101, Republic of Korea
*namkkim@kinac.re.kr

1. Introduction

As the spatial resolution of commercial satellite imagery has been enhanced less than 1 m, satellite image analysis has been utilized as an indispensable technology to support remote sensing for nuclear nonproliferation.

However, to efficiently utilize the rapid increasing number of satellite information, it is necessary to perform the computer-based image analysis rather than the human interpretation. In recent years, the Convolutional Neural Networks (CNN) based deep learning models that do not lose spatial information of images were developed and applied to various image analyses: classification, object detection, and semantic (or instance) segmentation (Fig. 1) [6].

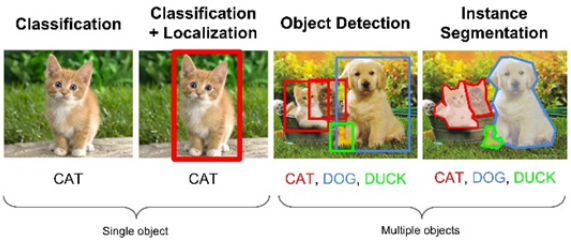


Fig. 1. Classification, object detection, and semantic (or instance) segmentation [6].

Furthermore, deep learning based technologies can overcome the limitations of the traditional image analysis methods: (1) the difficulty of feature extraction and (2) the ambiguity of threshold selection [1]. CNN of deep learning methods can extract features of images without considerable expertise and determine an appropriate thresholds (parameters) through the loss reduction calculation between the ground truth data and the predicted data.

Therefore, this paper investigated deep learning based technologies for remote sensing of satellite imagery from the nuclear nonproliferation perspective. The latest trends of R&D on deep learning methods, introduced in the proceedings of the Korean Society for Remote Sensing (KSRS) autumn conference held in Nov. 2020, were mainly examined.

2. R&D trends of deep learning methods for remote sensing of satellite imagery

2.1 Change detection by semantic segmentation with Fully Convolutional Networks (FCN)

In the field of remote sensing for nuclear nonproliferation, satellite image analysis has mostly focused on the pixel- or object-based change detection. Further, the change detection can be regarded as a binary semantic segmentation into two objects, i.e., changes and no-changes (or the unclassified), with the Fully Convolutional Networks (FCN) (Fig. 2) [2].

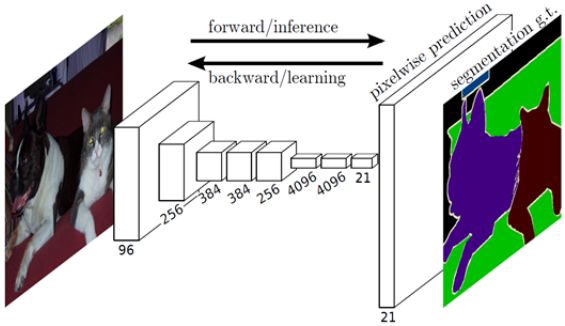


Fig. 2. FCN for sematic segmentation, which consists of only convolutional layers [2].

Two studies about the change detection using deep learning methods, i.e., the semantic segmentation, were summarized as follows.

M. Jeong and J. Choi evaluated the change detection performance of FC-DenseNet, which is one of FCN based deep learning architectures [3]. Notably, they tried to overcome false positives due to seasonal effects by utilizing the no-change training dataset shown in Fig. 3 [3].



Fig. 3. No-change datasets to remove seasonal effects [3].

A. Song et al. proposed the change detection method in hyperspectral images using the

Recurrent 3D FCN (Re3FCN) combining FCN and the Recurrent Neural Networks (RNN), which is mainly used to process natural languages (Fig. 4) [1]. Re3FCN can eventually extract spectral-spatial-temporal features for change detection [1].

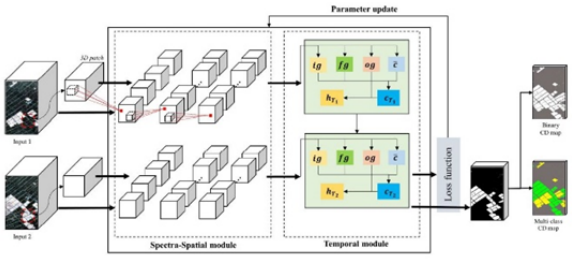


Fig. 4. Re3FCN for change detection, which is composed of spectral-spatial module and temporal module [1].

2.2 Construction of training datasets with KOMPSAT satellite imagery

From the perspective of developing deep learning based technologies, the verification with the qualified training dataset is an essential prerequisite. For example, AlexNet, VGG, GoogLeNet, and ResNet, which are the contemporary CNN models for image classification [2], were developed by evaluating their performance with the ImageNet dataset including 1.2 million object images and 1,000 object categories.

To promote the domestic R&D of deep learning based technologies, Korea Aerospace Research Institute (KARI) and National Information Society Agency (NIA) have established the AI (including machine and deep learning) training datasets for detecting (1) objects of interest, (2) buildings, (3) roads, (4) clouds, and (5) water bodies with KOMPSAT satellite imagery [4]. The established dataset would be distributed as public data on the website and utilized as the training dataset for the AI challenge of object detection [4]. Table 1 represents characteristics of the KARI-NIA dataset for object detection compared with the widely used datasets, i.e., xView and DOTA [5].

Table 1. Characteristics of deep learning training datasets [5]

Dataset	# of images	# of categories	Satellite sensor
xView	1,000,000	60	WorldView-3
DOTA	188,282	15	(N/A)
KARI-NIA	500,000	15	KOMSAT-3(A)

3. Conclusion

In this paper, South Korea's the latest R&D trends of deep learning methods for remote sensing can be divided as follows.

① Change detection (semantic segmentation) with FCN-based models
② Construction of large-scale training datasets with KOMPSAT images

As a future work, researches regarding deep learning in this paper need to be applied to detect changes which can imply suspicious nuclear activities.

ACKNOWLEDGMENTS

This work was supported by the Nuclear Safety Research Program through the Korea Foundation Of Nuclear Safety (KoFONS), granted financial resource from the Nuclear Safety and Security Commission (NSSC), Republic of Korea. (No. 1905009).

REFERENCES

[1] A. Song, J. Choi, Y. Han, and Y. Kim, "Change Detection in Hyperspectral Images Using Recurrent 3D Fully Convolutional Networks", Remote Sensing, 10(11), 2018.
[2] J. Long, E. Shelhamer, and T. Darrell, "Fully convolutional networks for semantic segmentation", Proc. of the IEEE conference on computer vision and pattern recognition, 2015.
[3] M. Jeong and J. Choi, "Performance Evaluation of Convolutional Neural Network for the Change Detection according to the Characteristics of Training Data", Proc. of the KSRS 2020 Autumn Conference, November 4-6, 2020, Online.
[4] H. Oh, T. Jeon, M. Kim, J. K. Lee, and T.-B. Chae, "AI Training Datasets for KOMPSAT Images and Application Techniques", Proc. of the KSRS 2020 Autumn Conference, November 4-6, 2020, Online.
[5] J. Koo, H. Oh, M. Kim, J. K. Kim, and T. Jeon, "Introduction and Analysis of Satellite Imagery Dataset for Object Detection", Proc. of the KSRS 2020 Autumn Conference, November 4-6, 2020, Online.
[6] A. Ouaknine, "Review of Deep Learning Algorithms for Object Detection", https://medium.com/zylapp/review-of-deep-learning-algorithms-for-object-detection-c1f3d437b852.

Proactive Adaptive Cooperative Threat Reduction Under the Three Pillar Approach

Yongsoo Hwang*
Korea Atomic Energy Research Institute
*yshwang@kaeri.re.kr

1. Introduction

The impact of the Military Parade at Kim Il Sung Square to celebrate the 75th Anniversary of the Worker's Part of Korea(WPK) has been significantly. How to work on the dialogues and other defense measures have created a lot of concerns and new ideas even though there are still big uncertainties throughout the outcomes of the US November election and the advent of new Administration and a task force to manage the nuclear DPRK impasse later-on. Many prominent political leaders have emphasized the importance of the declaration of the Korean War. However, to solve the everlasting DPRK issues, the political measure only might not work. The author proposes the Three Pillar Approach to solve the issues, the combination of the step by step political measures to assure the regime stability of the DPRK and eventual peace implementation in the North East Asia region, along with two other pillars, the major step by step denuclearization starting from the Yongbyon Plus option and the Adaptive Cooperative Threat Reduction(ACTR) approach covering key areas, the energy solution, medical measures, agricultural package and limited infra-structure development. In this short paper, the author shall focus on the outline of the three-pillar approach and the role of the nuclear sector for the ACTR and etc.

2. The Impact of the Parade

Throughout the three hour long military parade to celebrate the birth of the WPK, the DPRK through the compact tape delay video display through her state run KCNA and the all international deliveries clearly demonstrates her full capacity of her weaponry and firm and persistent will for the self-deterrence. The full fleet of missiles covers the entire spectrum of the ranges, from short & medium, intermediate, and inter-continental ones. The KN23 missiles, clones of the Russian Iskander systems., extensively test fired recently, are targeting the entire range of the PRK, The KN17, Hwasong12 in the other name, actively tested in 2017, is apparently targeting entire Japan and Guam is there also. Also, two black and while colored new missiles such as a Pukguksong 4A or Polaris 4A, and a KN27 or Hwasong16, is demonstrated possibly targeting the US. The detailed function analysis over these is not the main subject of this paper. The real purpose of this paper is to develop the proper approach to accelerate the dialogue after the US election, to achieve the ultimate goal, the denuclearization of Korean Peninsula.

3. Three Pillar Approach

Many political agendas are proposed to meet the request from the DPRK over the regime stability. The options such as the Proclamation of the End of the Korean War and the Peace Treaty are the good examples. Still they are at the stage of available options. How to integrate these viable options in association with the actual denuclearization is the core part to achieve the ultimate agreement among critical stakeholders such as two Koreas and the United States. In addition, the DPRK needs the pragmatic solution to revitalize her economy, two fundamental goals of Kim Jong Un under the flagship of the Byongjin Policy.

These ambitious goals cannot meet the expectations among stakeholders which have different views at this moment. For example, the major concern of the US is to eliminate the ICBM's, SLBL's targeting at her along with nuclear war heads. The major concern from Japan might be more, worrying about the additional measures such as SCUB-ER, KN17 and more. It is quite natural to introduce the step by step approaches for constructing the three pillars, political, actual denuclearization, and the ACTR. It shall require the innovative approaches to develop the reference scenarios with time line action plan and financial arrangement to back-up long-term implementation.

4. The ACTR

The ACTR should act as critical incentive package to assist the reform of the DPRK society in a timely manner. It should include the medical cooperation package to deal with the pandemic such as Covid-19, the aviation flue, and other syndromes. The DPRK's ambitious

project to complete Pyongyang General Hospital was not successful probably due to the Pandemic as well as the sanctions. The global society can assist the medical cooperation without significant difficulty. The same effort is recommended to be applied for the agricultural cooperation to relieve the shortage of crop supply in the DPRK. The critical component of the ACTR package is on the energy supply because it is a viable option to stimulate the heavy industries such as the chemical industries and more in the DPRK. The author proposes the detailed step by step approach for the energy cooperation. When there is any significant political and verification measure implementation, there should be the corresponding immediate action to deliver the appropriate amount of the heavy oil and other resources as attempted in the old Agreed Framework(AF) cooperation. In parallel, the ROK should act as a prime consultant to introduce the pragmatic energy solution for the DPRK covering three different subjects;

(1) Introduction of the step by step approach for power generation plants,
(2) Development of local and nation-wide grid network, and
(3) Creating descent job opportunities for many DPRK staff members currently working at the WMD sectors.

Of course, throughout the all lessons from the previous AF implementation, the DPRK shall prefer the immediate as well as the long-term actions. To meet the demands, the author proposes the followings;

(1) Immediate implementation of small-scale wind mill systems for valuable mines in the remote areas in the DPRK to assist the revival of the cash cow business, the export of the valuable resources to the global market with systematic after care services for continuous operation at the beginning,
(2) Replacement and upgrade of old critical components of the conventional fossil fuel fired power stations such as Pukchang, Unghi, Pyongyand and Dong-Pyongyang by supplying the new turbines and more to enhance the energy efficiency, and
(3) Construction of large scale PWR's as promised by the AF or the fleet of the distributed SMR's to meet the specific local key demands.

The author trusts that the implementation of the nuclear energy supply is critical for the following reasons;

(1) Firstly, it was the stipulated promise throughout the AF negotiation and implementation,
(2) Secondly, it can certainly suit the demand from the DPRK to establish the domestic energy supply system,
(3) Thirdly, the only multi-lateral agreement to solve the DPRK issues, the 2005 Bejing Six Party Talks explicitly claims to support the realization of the peaceful nuclear power generation option in the DPRK, and
(4) Finally, it shall create a lot of stable and good job opportunities and also fully support the operation of the uranium mining business, the big job market in the DPRK.

The practical implementation of the nuclear installation shall require the precise design of the so called the Fuel Leasing and Take Back Option to eliminate any possibility of future EnR (Enrichment and Reprocessing) in the DPRK.

As stated the different types of reactors can be implemented in association with the pragmatic plan to build the local and the nation-wide grid network, which can also create the many jog opportunity.

5. Conclusions

In this paper, the very schematic view of the ACTR is reviewed. When implemented, the energy solution described in this paper long with the active decontamination of relevant nuclear installations and the corresponding waste management along with cooperative monitoring shall also contribute significantly to manage the DPRK staff members.

A Statistical Approach for Safeguards of a Nuclear Facility Handling Bulk Material

Seung Min Woo[1,*], Jinwoo Lee[2], and Jukyong Kim[3]
[1] Department of Nuclear and Energy Engineering, Jeju National University, Jeju 64243, Republic of Korea
[2] The Cho Chun Shik Graduate School of Green Transportation, Korea Advanced Institute of Science and Technology, Daejeon 34141, Republic of Korea
[3] Department of Public Administration, Jeju National University, Jeju 64243, Republic of Korea
*woosm@jejunu.ac.kr, lee.jinwoo@kaist.ac.kr, agelead@jejunu.ac.kr

1. Introduction

There are two forms of material in nuclear facilities, such as items and bulk materials. The item material, for example nuclear fuel assemblies and spent nuclear fuel assemblies, can be safeguarded by counting items and checking a serial number of them. However, safeguarding bulk materials should be more carefully conducted because bulk materials in a loose form such as gas, liquid, powder are not always explicitly identified [1]. Nuclear material accountancy is one of the crucial methods for safeguarding bulk materials.

Nuclear material accounting of bulk material generally relies on the detection system, including radiation detection. That detection system contains two types of errors: (i) the random error; and (ii) the systematic error. Those errors can be propagated through processes in a nuclear facility, and the propagated error could negatively affect nuclear material accountancy and safeguards of the nuclear facility. Therefore, in this study, a statistical approach is applied to evaluate a nuclear facility's material accountability, handling bulk materials.

2. Methodology

The statistical concepts and terminologies are mainly referred from Avenhaus' book [2].

2.1 Closed box model

Nuclear facilities consist of multiple areas for individual purposes. Either the entire facility or each processing area can be defined as a closed box that is called the Material Balance Area (MBA) as depicted in Fig. 1. The throughput (D) of MBA is the sum of materials entering (R, receipt) and leaving (S, shipment) the MBA during a certain period. The physical inventories, I_0 and I_1, are defined as the material contained in the MBA at the beginning (t_0) and end (t_1) of that period, respectively. Given those parameters, the material balance model can be defined as follows:

$$MUF = I_0 + D - I_1 = I_0 + R - S - I_1 \quad (1)$$

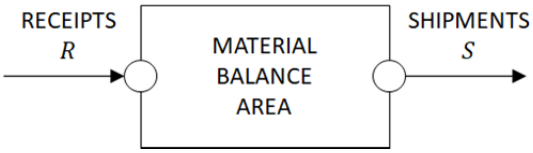


Fig. 1. Material Balance Area.

where the variable, MUF, represents to the Material Unaccounted For. The case that MUF is equal to zero can be the best case in nuclear material accountancy; however, it would not always be zero due to various uncertainty sources. Each variable is associated with uncertainties, and the combined uncertainty is represented as e. The expectation and variance of e are assumed to be zero and σ^2, respectively. Therefore, the expectation and of MUF, $E(MUF)$=0, can be zero. Based on the error propagation theory, the variance of MUF, σ^2_{MUF}, in Eq. 1 can be evaluated by the sum of variances of all the variables based on the assumption of independence among them. Last, the random variable, MUF, is assumed to follow the Gaussian distribution.

2.2 Hypothesis testing

Two hypotheses, null and alternative, should be established to apply the hypothesis testing method. First, the null hypothesis (H_0) is the expectation of MUF is equal to zero:

$$H_0: E(MUF) = 0. \quad (2)$$

Second, the alternative hypothesis (H_1) is the expectation of MUF is equal to M, which is greater than zero as follows:

$$H_1: E(MUF) = M. \quad (3)$$

Rejecting the null hypothesis means that the alternative hypothesis is correct. In contrast, accepting the null hypothesis means that the alternative hypothesis is rejected. The probability of detection, β, of the alternative hypothesis test can be evaluated by:

$$\beta \equiv prob\left\{\frac{MUF-M}{\sigma} \leq \frac{s-M}{\sigma}\right\} = \Phi\left\{\frac{s}{\sigma} - \frac{M}{\sigma}\right\}. \quad (4)$$

The term s stands for the significant threshold value of the null hypothesis test, set by the value that leads to a specific Type-I error (false positive) for given reliability for the one-tailed test. In the alternative hypothesis test, if the red colored area (1- β) is higher than the error level (i.e., 5% if the targeted reliability α is 95%), H_1 is accepted. The above procedure is graphically described in Fig. 2.

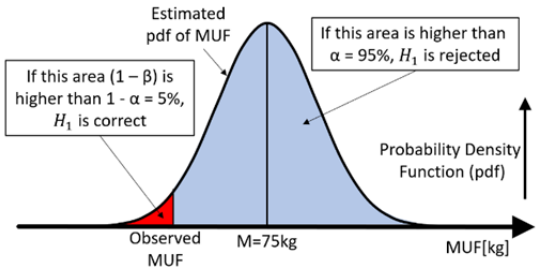


Fig. 2. Hypothesis testing.

3. Case study

For the case study, the observed MUF for Low-Enriched Uranium (LEU) of the nuclear fuel manufacturing facility in 2011 is -250kg. The standard deviation of the MUF is 502kg. The value of M is pre-given as 75kg, which is the significant quantity of LEU [1]. Using those values, we estimate the probability of detection as 99.5%. Therefore, we could conclude that the *MUF* in 2011 is not statistically significant. In other words, it could be claimed that the nuclear material diversion in this facility did not occur in 2011.

4. Conclusion

In this study, the statistical methodology to evaluate the nuclear material accountancy for a nuclear facility treating bulk material is reviewed. Particularly, the hypothesis testing for the MUF is conducted to analyze the possibility of occurrence for nuclear material diversion in a nuclear facility using bulk material. In this study, there is a lack of detailed data to evaluate; therefore, performing further analysis is impossible. However, we will try various statistical analyses after obtaining useful data in the future.

REFERENCES

[1] International Atomic Energy Agency, "IAEA Safeguards Glossary-2001 Edition.", International Atomic Energy Agency International Nuclear Verification Series No.2 (2002).

[2] R. Avenhaus, "Material accountability: Theory, verification, and applications", John Wiley & Sons, (1977).

Blast Load Assessment on a Reinforced Concrete Wall

Wooseub Kim*, Seungsik Yu, and Ji-Hwan Cha
Korea Institute of Nuclear Nonproliferation and Control (KINAC)
1418, Yuseong-daero, Yuseong-gu, Daejeon, 34101 Republic of Korea
*wskim@kinac.re.kr

1. Introduction

Since Korea decided to introduce nuclear technologies in 1956, radioactive wastes have been steadily produced, and the places for managing and storing the wastes have inevitably increased. Because such places can be the attractive target of bombing, sabotage, and theft for malicious purposes, the importance of a physical protection system (PPS), which opposes and limits the capabilities of the potential adversaries, has been emphasized.

In particular, the excellent explosion resistance performance of the reinforced concrete (RC) wall containing radioactive wastes allows to prevent an illegal intrusion with the use of high explosives, and contributes to the enhancement of the PPS.

In this research, the blast loads on a RC wall generated by the detonation of trinitrotoluene (TNT) were assessed depending on charge weight and standoff distance. For the blast load assessments, experimental data provided by "Structures to Resist the Effects of Accidental Explosions" (UFC 3-340-02) were used, and the explosive charge was assumed to be detonated almost at ground surface. The results showed that the peak reflected pressure and impulse on a RC wall increase with increasing charge weight but drastically decrease as standoff distance increases. Thus, blocking explosive detonation in close proximity of a RC wall can play an important role for intrusion prevention.

2. Materials and methods

2.1 Description of blast-loading environment

As shown in Fig. 1, it was assumed that the blast-loading environment is categorized as hemispherical surface burst explosion that the initial shock is amplified by ground reflections and the blast wave is perpendicularly propagated to the 3×3 m RC wall. To identify variations in the blast loads with the TNT charge weights of 3—30 kg and standoff distances of 0.5—10 m, the experimental data presented in UFC 3-340-02 were used.

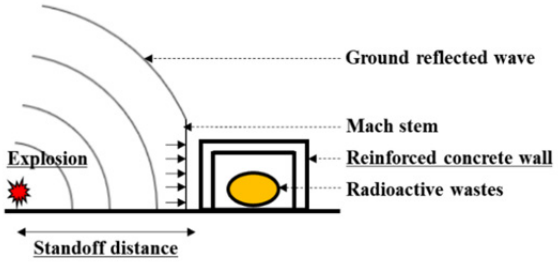


Fig. 1. Description of surface burst blast environment.

2.2 Determination of blast-loading parameters

The process of determining blast-loading parameters is illustrated in Fig. 2. For a conservative assessment, UFC 3-340-02 recommends that the effective TNT charge weight (W_e) multiplied by 1.2 be used to compensate unknown factors such as unexpected shock wave reflections [1]. Therefore, in the same principle, the effective TNT charge weight was defined depending on each explosion scenario.

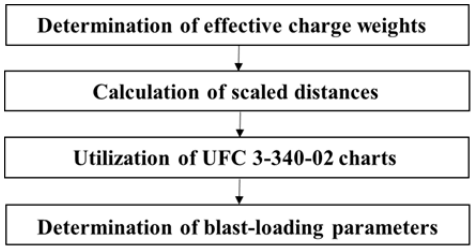


Fig. 2. Flow diagram of blast-loading parameters determination process.

Then, to utilize UFC 3-340-02 charts, the scaled distance (Z) was calculated according to equation (1) [1].

$$Z = \frac{D}{W_e^{\frac{1}{3}}} \quad (1)$$

Where D is the standoff distance between a RC wall and a TNT.

As summarized in Table 1, the values of the blast-loading parameters were determined by using the calculated scaled distances and the experimental data given in UFC 3-340-02 charts.

Table 1. The list of reference charts in the UFC 3-340-02

Blast-loading parameters	Reference chart
Peak positive incident pressure (P_{so})	Figure 2-15
Unit positive incident impulse (I_s)	Figure 2-15
Peak positive reflected pressure (P_r)	Figure 2-193
Unit positive reflected impulse (I_r)	Figure 2-194
Sound velocity in reflected region (C_r)	Figure 2-192
Peak drag pressure ($C_D q_0$)	Figure 2-3

Based on the abovementioned blast-loading parameters, the fictitious durations for the positive phase of the blast wave (t_{of}) and for the normal reflected wave (t_{rf}) were calculated using equation (2, 3) [1].

$$t_{of} = \frac{2\,I_s}{P_{so}} \quad (2)$$

$$t_{rf} = \frac{2\,I_r}{P_r} \quad (3)$$

The clearing time for reflected pressures (t_c) was also computed using equation (4) [1].

$$t_c = \frac{4\,S}{\left(1+\frac{S}{G}\right) C_r} \quad (4)$$

Where S is the smaller value, and G is the larger value between the height of a RC wall or one-half its width. In this study, S is 1.5 m and G is 3 m because the 3×3 m RC wall was assumed.

2.3 Assessment of blast loads

According to UFC 3-340-02, the front wall loads for a rectangular above-ground structure can be described as Fig. 3. The curve with the smallest value of the impulse should be selected to calculate the wall loading [1]. Therefore, the areas under a linear curve and a bilinear curve for each scenario were compared to figure out the smallest value. Then, the peak reflected pressure and impulse were defined.

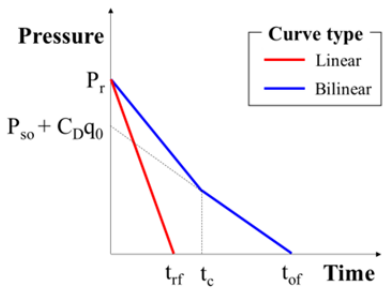


Fig. 3. Pressure-time load curves for front wall loading.

3. Results and discussion

Figs. 4 and 5 show that the peak reflected pressure and impulse tend to increase as either the standoff distance decreases or the TNT charge weight increases. Especially, the peak reflected pressure and impulse are more heavily influenced by the standoff distance than the TNT charge weight. In addition, when the standoff distance is increased from 0.5 m to 2 m, the pressure and impulse are dropped to almost a tenth in the same condition of charge weight.

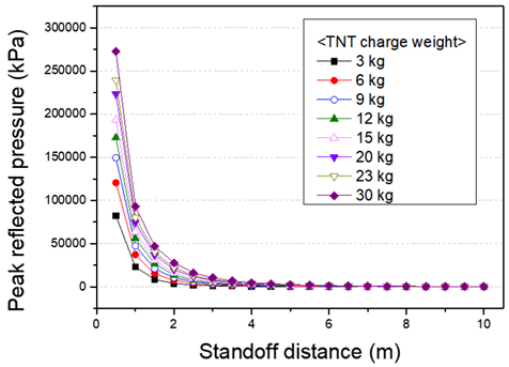


Fig. 4. Peak reflected pressures with the TNT charge weights of 3—30 kg as a function of standoff distance.

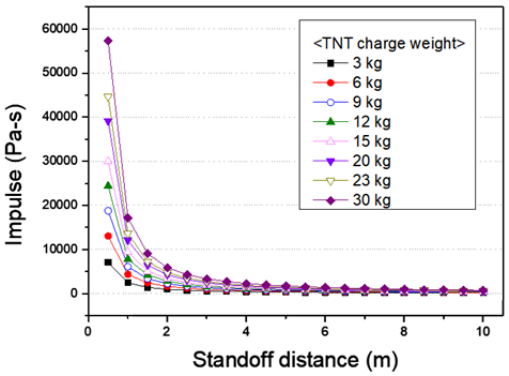


Fig. 5. Impulses with the TNT charge weights of 3—30 kg as a function of standoff distance.

4. Conclusion

In this study, it was verified that blast loads are highly affected by standoff distance. Blocking the explosive detonation close to a RC wall can be the most effective way of restraining an illegal intrusion with the use of explosives.

REFERENCES

[1] U.S. Department of Defense, “Structures to Resist the Effects of Accidental Explosions”, UFC 3-340-02 (2008).

A Study on Accidental Acquisition of Nuclear Material in Terms of Safeguards

Ju-Ang JUNG*, Hyun-Jo Kim, In-Chul Kim, Byung-Doo Lee,
Sung-Ho Lee, Hyun-Sook Kim, Jin-Ha Choi, and Mun-Young Ryu
KAERI, 989-111 Daedeok-daero, Yuseong-gu, Daejeon, Republic of Korea
*jajung@kaeri.re.kr

1. Introduction

The Nuclear Non Proliferation Treaty (NPT) is the cornerstone of the global nonproliferation regime. The NPT parties shall promise and fulfill their obligations in the areas of non-proliferation, disarmament and peaceful use of nuclear materials and related technologies. To fulfill its commitments under NPT, South Korea has signed a binding protection contract with the International Atomic Energy Agency (IAEA) to apply IAEA protection measures in Korea. Under the safeguards agreement, South Korea is obliged to report to the IAEA on all nuclear materials and specific types of nuclear energy research and manufacturing, and accept IAEA inspections in the region. And South Korea is obliged by the IAEA to ensure that the Safeguards are applied to all nuclear materials in South Korea to ensure that all nuclear materials in the country are not diverted for non-peaceful purposes.

In terms of safeguards, this is what nuclear material accidental gains. Old laboratories and sites dealing with nuclear materials have late detection of nuclear materials used long ago when the concept of safeguards measures was not secured. This has become an issue recently. So we discussed the reasons for the discovery of the accidental gain nuclear material and how to respond to it.

2. The Issue of Accidental Acquisition of Nuclear Material

2.1 Definition

In terms of safeguards, the nuclear material of accidental gains is unforeseen nuclear material that is present in a material balance area, except when detected in the course of a physical inventory taking by the facility operator.

2.2 Cause

In facilities that use nuclear material for a long period of time, accidental acquisition of nuclear material may occur occasionally. When the nuclear material is brought in and used, safeguards measures in Korea have not been established 40 to 50 years ago, and there have been cases where poor management is later found.

2.3 Trace amounts of nuclear material

There are many cases where such accidental gain nuclear material is usually in trace amounts. Usually, in case of large quantities, the manager consistently manages well. In most cases, trace amounts of nuclear material are omitted due to the carelessness of the manager or an error in handover and are mixed with general materials.

2.4 Establish a standard minimum amount

Natural Uranium or Depleted Uranium are materials that do not have a significant radiation safety problem unless they are radiation-emitting materials. The facility's position is to establish a standard for the amount of substances in question as a concept of safety measures, so that trace amounts (the amount of the sample to be tested) of substances below that amount can be used without notification.

3. Improvement plan for contingent acquisition nuclear material

3.1 Self test

In order to detect the nuclear material of accidental gain, it is advisable to periodically self-inspect the office at a facility that uses nuclear material or a laboratory that previously used nuclear material.

3.2 Exchange inspection

Lab managers often visit their labs and often don't see strange things because of the illusion of knowledge. I think I know everything in my lab. To prevent this, it's also a good idea to switch to other lab managers and test each other.

3.3 Regulatory body inspection

Periodic visits and inspections of laboratories with a history of nuclear material by the regulatory body are of utmost importance, but in reality, it is almost impossible for the regulatory body to visit all laboratories nationwide.

3.4 Training

The nuclear Safety Culture is the core values and behaviors resulting from a collective commitment by leaders and individuals to emphasize safety over competing goals to ensure protection of people and the environment [4]. One of the biggest accidents caused by the lack of this can be seen as the Fukushima accident.

Establishing and maintaining a positive Safeguards culture directly contributes to the safe and secure use of nuclear materials. The use of regulated materials and other users are responsible for ensuring that they are used safely. NRC encourages licensees to maintain a positive safety culture because the weakness or deteriorating safety culture in safety culture seems to increase the likelihood and consequences of performance problems.

It is desirable to alert the aforementioned safety culture, as well as the important contents of Safeguards, through periodic education and to find the nuclear material by itself.

4. Conclusion

Forty-five years have passed since South Korea joined the Nuclear Nonproliferation Treaty in 1975 and signed the Korea-IAEA Safeguards Agreement. Since then, the concept of Safeguards has gradually been created and systematized in the country. In the case of laboratories that have been around since the 1960s, trace amounts of nuclear material that used to be no problem are sometimes found. Under current laws and regulations, the report is required to be made unconditionally. In the case of NU, DU, which is not an issue in terms of radiation safety, it is hoped that minimal requirements will be established in terms of Safeguards to exempt substances below them, which will help research or experimentation.

REFERENCES

[1] Treaty on the Non-Proliferation of Nuclear Weapons (NPT), United Nations, (1970).

[2] IAEA SAFEGUARDS GLOSSARY 2001 Edition.

[3] John L, Jaech et al, Statistical Methods in NUCLEAR MATERIAL CONTROL, UNITED STATES ATOMIC ENERGY COMMISSION, (1973).

[4] James Harold Warren Jr et al, Safety Culture Monitoring: A Management Approach for Assessing Nuclear Safety Culture Health Performance Utilizing Multiple-Criteria Decision Analysis, (2015).

Safeguards Measures for Model Pyroprocessing Plant Developed in Collaboration With IAEA

Seong Kyu Ahn*, Ho-Dong Kim, Se-Hwan Park, and Dae-Yong Song
Korea Atomic Energy Research Institute, 111, Daedeok-daero 989beon-gil, Yuseong-gu, Daejeon, Republic of Korea
*skahn76@kaeri.re.kr

1. Introduction

The nuclear society recommends "Safeguards-by-Design" for the implementation of effective and efficient safeguards to a future nuclear system. One of the effort to address this, the IAEA and the ROK started an member state support program (MSSP) titled "Development of Safeguards Measures and Equipment for a Pyroprocessing Plant using Related Facilities" in 2017. The task is to contribute to key objective 6 entitled, "Develop generic safeguards approach for electrochemical recycling plants and small modular and/or GEN IV reactors" from the project SGCP-003 in the D&IS Program for nuclear verification, 2016 – 2017. The task is also to support the long-term strategic plan of the IAEA. The MSSP task covers development and/or field testing of safeguards approaches, measures, and equipment.

2. Main

2.1 Pyro Safeguards Measures

Through the new MSSP from 2017, a conceptual electrochemical recycling facility named REPF+ is designed. In the REPF+, PWR spent fuel assemblies are received, and SFR fuel assemblies and U ingots are produced. The throughput is about 30 MTHM/yr., and the total operation days are about 250/yr. The mass balance of U and Pu, a process diagram, process equipment, and a flow sheet for nuclear materials are included in the design of the REPF+. Four MBAs and flow and inventory KMPs are assigned to the REPF+. The operator's accounting methods for nuclear material in all of its forms are identified based on an instrument performance analysis and research result. The facility description, the facility layout and containment features, and procedures for nuclear material accountancy and control are included in the model DIQ the REPF+. Sixteen scenarios are selected as major diversion scenarios in the REPF+. Verification approaches in the REPF+ have been identified: verification methods of PIV, verification methods of IIV, verification methods of inventory changes, and verification methods within MBA for each MBA. For each diversion scenario, the details of the diversion strategy and the corresponding safeguards measures are summarized. Also, the safeguards measures and safeguards considerations are evaluated.

2.2 Consideration for Pyro Safeguards

The safeguards considerations, which are drawn from the evaluations, are as follows.

- NRTA and accompanying verification play an essential role.
- The access route to the transfer path between the hot cells (including penetrations) is to be minimized.
- Less-frequent but short-notice, random and unannounced inspections that can provide added assurance for the operations as declared.
- It is important to confirm that no undeclared material has been introduced into the hot cell.
- The importation of unnecessary containers into the hot cell is to be avoided.
- Optical surveillance of areas with high-Pu concentrations, such as the ER salt, U/TRU ingot storage, and slug-casting furnace, is important, so camera either inside the hot cell or outside near the penetration window would plays a key roles.
- Process monitoring of, for example, operation current, voltage, operation time, and released gas amount plays an important role.
- If the waste is managed by type, the applied safeguards measures are more effective.
- Since the recovered U/TRU product has a very high Pu content, special attention has to be paid.

2.3 Report for a Model Safeguards Measures

The safeguards measures explored and exercise using model plant is summarized as a final report. The new model plant, REPF+, is an upgraded model of the previous study[1] that reflects the progress of electrochemical recycling technology. The throughput of the REPF+ is three time larger than that of the REPF, and the SFR fuel fabrication process is included in the REPF+. The operator's nuclear material accounting methods and verification approach in the REPF+ are outlined. The technical objectives applicable

to the REPF+ as well as diversion and misuse scenarios are proposed, as is the MBA/KMP structure in the REPF+. The detailed verification approach for the REPF+ is also proposed. Finally safeguards considerations and recommendations are summarized in the report.

The safeguards measures and instruments in the operator's nuclear material accounting system and the verification approach of the REPF+ are designated based on the published data and the results of technology assessment. Although international collaboration on the exploration of the safeguards technologies applicable to electrochemical recycling is in progress, further research for more effective and efficient safeguards in the electrochemical recycling facility is necessary.

3. Conclusion

SSBD is an approach to the design and construction of a nuclear facility whereby nuclear safeguards provisions and features are designed into the facility from the very beginning of the design process. In the previous MSSP on electrochemical recycling, the roles of process developers, developers for facility safeguards, national authorities, and IAEA are summarized. Although a detailed safeguards approach for the new electrochemical recycling facility is usually developed at the end of the design stage, it should be developed and updated in the pre-conceptual and conceptual design stages.

These efforts will be helpful to the implementation of safeguards and the more effective and efficient attainment of the technical objectives of a electrochemical recycling facility.

Acknowledgement

This work was supported by a National Research Foundation of Korea (NRF) grant funded by the Korean government's Ministry of Science and ICT (MSIT) (No. NRF-2017M2A8A5015084).

REFERENCES

[1] Hee-Sung Shin, et. Al., "Development of a safeguards approach for a pyroprocessing plant by IAEA Member State Support Program", KAERI/RR-3342 (2011).

1분과

핵주기정책·규제 및 비확산(Poster)

A Study on the Application of a Radiation Portal Monitoring System

Chansuh Lee* and Beomseok Shin
The Korea Institute of Nuclear Nonproliferation and Control, 1418, Yuseong-daero, Yuseong-gu, Daejeon, Republic of Korea
*chans@kinac.re.kr

1. Introduction

Government agencies in South Korea are conducting radiation inspections on imported cargo: including the Korea Customs Service (KCS), the Nuclear Safety and Security Commission (NSSC), the Ministry of the Food and Drug Safety (MFDS), the Ministry of Agriculture, Food and Rural Affairs (MAFRA), the Ministry of Environment (ME) and the Korea Forest Service (KFS). A 2020 parliamentary audit emphasized the need for information sharing and overall management of information among government agencies. Currently, the NSSC conducts monitoring of household radiation and recycled scraps at customs through the Radiation Portal Monitor (RPM) system. The NSSC deals with nuclear nonproliferation and nuclear security as well as nuclear and radiation safety. This study reviews Korea's overall RPM system along with its current status to determine whether the RPM system can be used for other areas of the NSSC work.

2. RPM Overview

2.1 Purpose of RPM

The Radiation Portal Monitor (RPM) is a radiation detection device used to inspect individuals, vehicles, cargo, or other vectors to detect illegal sources at borders or security facilities [01]. Many countries, for example, the United States, Canada, and many in Europe, operate RPMs for national security. RPMs are installed and operated at border ports and airports to block nuclear materials and radioisotopes that are not authorized by the government that can be used for nuclear weapons or dirty bombs. Korea enacted and operated related laws in 2011.

2.2 Legal Basis for the RPM in South Korea

In South Korea, RPMs are installed and operated at airports and ports under Article 19 of the Act on Protective Action Guidelines against Radiation in the Natural Environment (referred to here as the "PAGR Act"). Since the Radon Bed incident in May 2018, the safety management of radiation has been strengthened [02]. The operator of airports and port facilities must cooperate with the installation of RPMs and may entrust their operation to the operator. Currently, the Nuclear Safety and Security Commission (NSSC) has entrusted the management supervision of RPMs to the Korea Institute of Nuclear Safety (KINS), which conducts the response, investigation, processing and reporting in the event of major alarms. The PAGR Act limits RPMs to only two targets, Article 2.1 (a) and (d). The first is radiation emitted from natural radionuclides contained in raw materials, residues, and processed products, and the second is radiation emitted from a radioactive substance contained in scrap metal collected within the Republic of Korea or in a foreign country and sold or recycled.

2.3 RPM Status in South Korea

What we commonly see in harbors is the primary surveillance equipment for the RPM. A large-area plastic scintillator is used to provide fast detection speed and is relatively inexpensive and easy to produce. However, it is impossible to analyze nuclei with it because there is no photoelectric effect peak. Therefore, further examination is required to identify specific nuclei.

A secondary monitoring system uses a dosimeter and a portable nuclide analyzer, which is used to analyze a nuclear species after primary surveillance. It provides remote support through the KINS expert remote support system to allow field operators to conduct secondary searches.

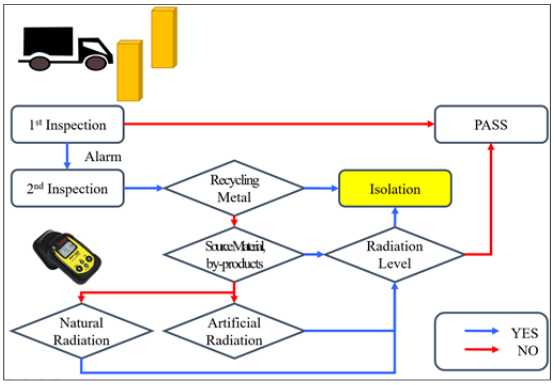


Fig. 1. RPM System Procedure.

In order to fundamentally block the inflow and distribution of illegal radioactive materials into the country and to identify and manage the

distribution status of natural radionuclide-containing materials in Korea, a total of 130 RPMs have been installed and are operated at 17 locations (15 ports and 2 airports). As of June 30, 2020, a total of 180 monitors in 17 locations have been installed and are operated, and about six additional monitors are expected to be installed each year [03]. The operation procedure for RPMs is shown in Figure 1.

3. Application of RPMs for Nuclear Nonproliferation and Security

3.1 Trade Control and Antiterrorism Utilization

In accordance with the Safeguards Agreement with the IAEA, the Foreign Trade Act, and the Nuclear Safety Act, exports and imports of nuclear materials and nuclear items are reported to the IAEA and inventory management is performed. Licensing and clearance information on the export and import of nuclear materials and items is shared between the NSSC and Korean Customs. If the material or items consist of a single item it is very easy to identify. On the other hand, if the exporter is not familiar with or intentionally avoids the mixture or some partial items containing a small quantity of nuclear material, the means to identify them are very limited.

Adding neutron detectors to the RPMs currently in operation or linking information to other systems operating in customs may improve the identification. With these improvements, it will be easier to identify such nuclear materials or reusable equipment because difficult identification of Naturally Occurring Radioactive Material (NORM) is also possible.

If the means are in place, control and safeguards against nuclear imports and exports and anti-terrorism tasks can be strengthened.

In addition, as shown in the Table 1, the current departmental radiological inspection of imported cargo may be integrated and managed. Of course, consultation with the relevant ministries and legal issues need to be resolved in the future.

Table 1. Radiation Inspection Items and Jurisdiction for imported cargo

NSSC	KCS	MFDS	MAFRA	ME	KFS
NORM Metal Scrap	Industri-al product	Agricultural livestock product	Feed	Coal Ash	Wood

3.2 Additional Reviews

The combination of RPMs, HS-Code and X-ray images, as well as the current link between RPMs and UNI-PASS, could further enhance regulatory completeness. Currently, there is no data for this link, but if data accumulates after connection, it will provide a basis for easy detection and response of abnormalities through big-data and machine learning.

4. Conclusion

This study reviewed the overview of RPMs, the target items of RPMs, the current status of operation, and the application of RPMs. If the first inspection information related to radiation is shared with the relevant agencies, integrated monitoring and management of the items under the jurisdiction of each agency will be possible.

In addition, strengthening nuclear non-proliferation work can be expected if the RPM includes a nuclide classification module for monitoring nuclear materials and used nuclear items. Furthermore, it could also be used as a basic material for anti-terrorism.

ACKNOWLEDGEMENT

This work was supported by the Nuclear Safety Research Program through the Korean Foundation Of Nuclear Safety (koFONS) using the financial resource granted by the Nuclear Safety and Security Commission (NSSC) of Korea. (No. 1075000985).

REFERENCES

[1] Fehlau, P. E.; Brunson, G. S. (1983). "Coping with Plastic Scintillators in Nuclear Safeguards". IEEE Transactions on Nuclear Science. 30 (1): 158–161.

[2] Act on Protective Action Guidelines against Radiation in the Natural Environment, June, 9, 2020, NSSC.

[3] https://cisran.kins.re.kr/intro/norm/recycled/PortDockintro.do, 2020.10.11.

Progress in the Analysis of Uranium Enrichment Using LIBS+LIF

Se-Hwan Park*, Euo-Chang Jung, and Seong-Kyu Ahn
Korea Atomic Energy Research Institute, Yuseong-gu, Daejeon, 34057, Korea
*ex-spark@kaeri.re.kr

1. Introduction

The isotopic ratio analysis is used in a large number of fields such as nuclear forensics and non-proliferation monitoring, archaeology, geology, biology, medical, and environmental applications. The isotopic ratio of uranium (U enrichment) is especially important in the non-proliferation monitoring, since the U enrichment can indicate that the uranium is intended to be used for the nuclear weapon or explosive.

The U enrichment can be measured with couple of methods such as mass spectrometry, gamma-ray spectroscopy, neutron counting, and optical spectroscopy. The optical spectroscopy, which can be used for the U-enrichment measurement, are Laser-Induced Breakdown Spectroscopy (LIBS), Laser Absorption Spectroscopy (LAS), and Laser Induced Fluorescence (LIF). KAER is developing an analysis method of U enrichment using LIF and LIF. In LIBS, the plasma is generated using the laser pulse and the isotopic ratio can be obtained by measuring the plasma emission using a high-resolving spectrometer. Second laser with precise frequency is incident on the plasma and the isotopic ratio can be obtained by measuring the fluorescence from the resonance induced by the second laser. In this presentation, we present our progress in the analysis of U enrichment using LIBS+LIF.

2. Methods and Results

The selected U lines for the measurement of U enrichment were U II 424.437 nm and U I 682.691 nm for LIBS, and U I 394.38 nm and U I 682.691 nm for LIF. Gd was selected as surrogate of U, and the Gd I 405.822 nm line was selected for the isotopic ratio measurement.

An optical spectroscopy chamber for the measurement of U enrichment was fabricated. A laser beam was introduced into the chamber vertically and irradiated on the sample to generate plasma, and a laser beam was introduced horizontally into the chamber to induce the fluorescence. The pressure and gas type in the chamber could be controlled.

The LIBS spectrum of Gd was measured in the optical spectroscopy chamber changing the gas condition in the chamber. The gas conditions in the chamber was 1) air atmospheric pressure, 2) Ar 700 Torr, 3) Ar 300 Torr, 4) Ar 100 Torr, 5) Ar 10 Torr, and 6) Ar 5 Torr. The peak intensity was highest at Ar 300 Torr, and the background was flattened at Ar 10 Torr and Ar 5 Torr.

The LIBS spectrum of U was measured using a spectrometer (EMU-120/65, IXU1) with resolution of 0.0135 nm at 430 nm to assess if the U enrichment can be measured with the spectrometer with resolution of ~ 0.01 nm. The U enrichment of the U samples were 1, 4, and 19.9 %. The U-235 peak could be identified when the U enrichment of the sample was 19.9 %. Though the highly enriched U can be determined with the moderate resolving spectrometer, a spectrometer with higher resolving power is necessary to measure the U enrichment of low enriched U.

The fluorescence of U near the U I 682.691 nm was measured using a hollow cathode lamp of depleted U. As the frequency of the incident laser from External Cavity Diode Laser (ECDL) was changed, the spectrum of the emission from the hollow cathode was measured. The U-238 resonance was identified in the measurement.

3. Summary

The measurement of U enrichment is important in the non-proliferation monitoring, and the optical spectroscopy is one of the measurement method of U enrichment, especially it is developed as the field measurement method of U enrichment. The measurement of U enrichment using LIBS+ LIF is developed at KAERI. The measurement setup was built up, the measurement condition was optimized, and the U enrichment will be measured soon.

Acknowledgement

This work was supported by a National Research Foundation of Korea (NRF) grant funded by the Korean government's Ministry of Science and ICT (MSIT) (No. NRF-2017M2A8A5015084). This work also was partly supported by the Nuclear Safety Research Program through the

Korea Foundation Of Nuclear Safety (KoFONS) using the financial resource granted by the Nuclear Safety and Security Commission (NSSC) of the Republic of Korea (No. 1903014).

Study on Emergency Operating Procedures for Fuel Cycle Facilities

Seok-Jun Seo*
Nuclear Fuel Cycle Enabling Technology Division, Korea Atomic Energy Research Institute,
989-111 Daedeok-daero, Yuseong-gu, Daejeon, South Korea
*sjseo@kaeri.re.kr

1. Introduction

There are several domestic and international guidelines [1, 2] for developing emergency operating procedures (EOPs). In this study, one of international guidelines is selected and its characteristics are examined. The meaning of 'emergency' is defined in the reference as "a nonroutine situation or event that necessitates prompt action primarily to mitigate a hazard or adverse consequences for human health and safety, quality of life, property or the environment" [1].

In order to establish the EOP, it is also necessary to distinguish among normal operation, abnormal operation, design basis accidents (DBAs), beyond design basis accidents (BDBAs), and severe accidents. Thus, definitions of those terms are considered in this study and scope of EOP preparation is confirmed. EOPs are divided into scenario dependent procedure and scenario independent procedure according to an existence of specific target events. In addition, event based procedures were widely used before the Three Mile Island (TMI) accident. On the other hand, symptom/state based procedures are introduced to a need for a reliable and continuous plant diagnosis. Finally, basic principles and general approach for EOP development are summarized and discussed.

2. Results and Discussion

An operation region consists of the normal operation and some of abnormal operation as shown in Fig.1. Because some of abnormal events could shift to normal operation quickly as long as no harmful effects are occurred on a process, process equipment, systems, and facility. Operation limit includes most of the operation such as normal operation and abnormal operation. Thus, the operating document for both normal operation and abnormal is termed normal and abnormal operating procedures (AOPs), respectively. Accident condition is more severe than the abnormal condition such as DBAs, BDBAs, and severe accident. Therefore, the purpose of EOP is to provide a guidance for operators to deal with accident conditions in the range of between abnormal operations and DBAs.

REFERENCES

[1] Safety Report Series No. 48, Development and Review of Plant Specific Emergency Operating Procedure, IAEA (2006).
[2] NUREG-0899, Guidelines for the Preparation of Emergency Operating Procedures, NRC (1982).

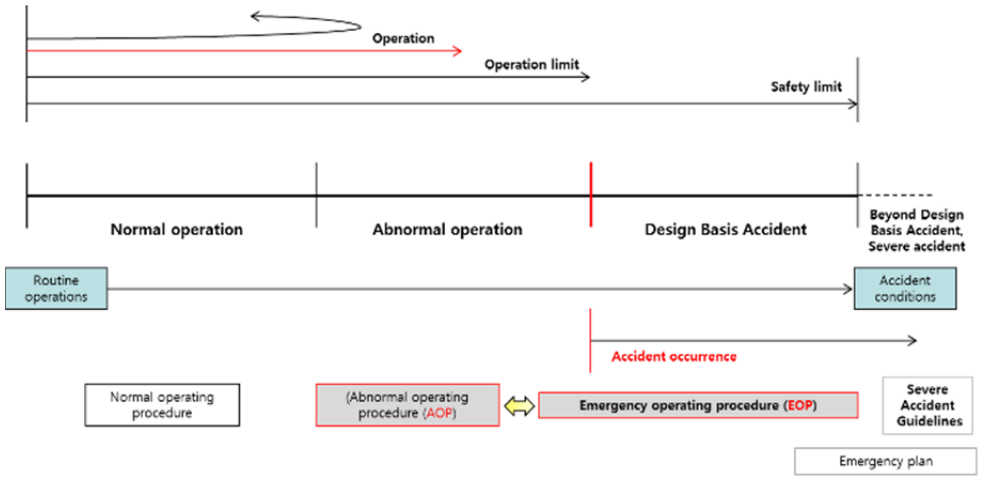


Fig. 1. Scope of development of emergency operation procedure.

Development of Emergency Operating Procedures for a Gas Leakage

Seok-Jun Seo*
Nuclear Fuel Cycle Enabling Technology Division, Korea Atomic Energy Research Institute,
989-111 Daedeok-daero, Yuseong-gu, Daejeon, South Korea
*sjseo@kaeri.re.kr

1. Introduction

There have been abundant interests on safety of nuclear-related facilities since Fukushima Daiichi accident in 2011. In order to secure a safety of a fuel cycle facility, an integrated safety analysis (ISA) is required by U.S. NRC [1]. Thus, it is necessary to precisely conduct a hazard analysis to examine and find hazardous and abnormal operational circumstances. Then, an accident analysis is conducted by calculating their hazardous effects quantitatively on workers, public, and environments in terms of radiological and chemical hazards. After the quantitative analysis, it is categorized into abnormal operation, design basis accidents (DBAs), beyond-DBAs, and severe accidents. In the ISA, the hazardous consequences are prevented and mitigated by selecting items relied on for safety (IROFS). The IROFS include not only engineered IROFS, but also administrative IROFS such as abnormal operating procedure (AOP) and emergency operating procedure (EOP). Here, the meaning of 'emergency' is defined as "a nonroutine situation or event that necessitates prompt action primarily to mitigate a hazard or adverse consequences for human health and safety, quality of life, property or the environment" [2]. In this study, examples of EOP are prepared for process specific EOPs in fuel cycle facilities, which include general description of purpose, scope, definitions, references, responsibilities, procedure, and attachments. These attachments also contain automatic actions, immediate actions, and subsequent actions, etc [2-4].

2. Results and Discussion

An example of EOP is shown below with a content of the attachment for a leakage of asphyxiant gas which would have possibilities to happen during a period of operation in a facility. This attachment example shows the event sequence and automatic, immediate, and subsequent actions.

< EOP attachment A: Leakage of asphyxiant gas >

A.1. Event Sequence
- A.1.1. Occurrence of leakage of an asphyxiant gas
- A.1.2. Failure of a facility ventilation system
- A.1.3. Detection and alarm of an oxygen concentration detector
- A.1.4. Harm or suffocation of a worker when it is below the standard oxygen concentration

A.2. Automatic Actions
- A.2.1. Oxygen concentration alarm sounds when ventilation equipment is stopped → immediate evacuation

A.3. Immediate Actions
- A.3.1. Alert nearby workers
- A.3.2. Alert operation manager
- A.3.3. Alert process area manager

A.4. Subsequent Actions
- A.4.1. Alert nearby workers
- A.4.2. Check operability of the ventilation system (if not operate, evacuate and use a portable oxygen tank)
- A.4.3. Check the oxygen detector
- A.4.4. Find a breakage part and leakage
- A.4.5. Emergency stop of processes

REFERENCES

[1] NUREG-1520, Standard Review Plan for Fuel Cycle Facilities License Applications, U.S. Nuclear Regulatory Commission (2015).
[2] Safety Report Series No. 48, Development and Review of Plant Specific Emergency Operating Procedure, IAEA (2006).
[3] NUREG-0899, Guidelines for the Preparation of Emergency Operating Procedures, NRC (1982).
[4] Emergency Operating Procedure, NRC website.

Analysis of Vital Area Identification During Maintenance of Equipment

Ji-Hwan Cha* and Wooseub Kim
Korea Institute of Nuclear Nonproliferation and Control, 1418 Yuseong-Gu, Daejeon, Korea
*jh_cha@kinac.re.kr

1. Introduction

Identification of vital areas is an important step in the process of protecting against sabotage. Vital area identification (VAI) is the process of identifying the area in a nuclear facility around which protection will be provided in order to prevent or reduce the likelihood of sabotage. INFCIRC/225/Rev. 5 (IAEA Nuclear Security Series No. 13) indicates that nuclear material in an amount which if dispersed could lead to high radiological consequences (HRCs) and a minimum set of equipment, systems, or devices needed to prevent HRCs, should be located within one or more vital areas, and be located inside a protected area. All measures that have been designed into the facility for safety purposes should be taken into account when identifying vital areas [1]. 10 CFR 73.55 specifies requirements for protection of nuclear power plants against radiological sabotage, including the location of vital equipment in vital areas and protection measures to be applied to vital areas [2]. However, in building logic models for the VAI analysis, it is not necessary to assume that a vital equipment maintenance outage occurs concurrently with an attack. Vital equipment maintenance outages that occur during operations should be addressed as specified in VAI assumptions. It should require the implementation of compensatory measures such as designating and protecting alternate vital areas containing redundant equipment [3].

Although VAI focuses on the consequences of malicious acts, equipment unavailability could conceivably occur by chance, or as a result of maintenance outages, concurrent with a malicious act. The results of the VAI need to be deterministic; that is, an area is either vital or it is not. Therefore, the assumptions that establish the requirements for the VAI should specify whether the analysis should include concurrent equipment unavailability due to random failure or maintenance. It is therefore necessary for each nuclear power reactor licensee and new reactor applicant to identify the vital areas during maintenance to which the required protection measures will be applied.

2. VAI during Maintenance of Equipment

The schematic of VAI flow chart showed in Fig. 1. The requirements should be clearly established prior to attempting to set up VAI. Through VAI process, it was notice that there are some more assumptions and policy considerations to make in order to analysis more realistic, and gain mutual understanding form engineers, plant operators, and regulators at the same time. Therefore, approached to protection during maintenance of equipment strongly involve to policy considerations step.

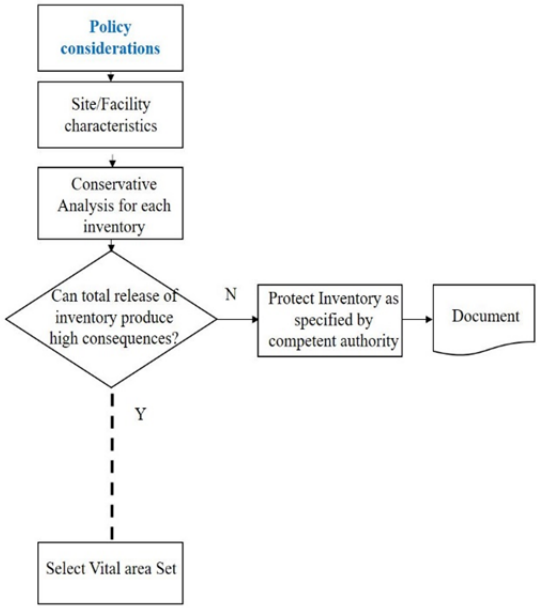


Fig. 1. Schematic of vital area identification(VAI) flow chart.

All distinct operating states (normal operation, hot standby, cold standby, and refueling) should addressed in the VAI. The different operational states may rely on different equipment to perform safety functions and require protection of different areas to ensure protection and to prevent release against sabotage.

In order to ensure that a facility is adequately protected when maintenance is being performed in a vital area, the competent authority may require the operator to designate and protect temporary vital areas or take other compensatory measures. VAI process identifies a minimum set

of equipment needed to prevent sabotage. There are two concepts of approaches to accommodate maintenance outages. First, select vital areas to contain more than the minimum set of equipment needed to prevent sabotage. Second, designate temporary vital areas to maintain a minimum set of protected equipment. Considering competent authority, second concept is more effective method to VAI.

3. Conclusion

In this study, analysis vital area identification during maintenance of equipment performed from VAI process flow sequence. VAI during maintenance process was overlooked at the beginning stage of policy considerations. However, these alternate vital areas should be set for preventing sabotage. The suggestions for VAI during maintenance of equipment could be drawn.

(1) Select vital areas to contain more than the minimum set of equipment needed to prevent sabotage.
(2) Designate temporary vital areas to maintain a minimum set of protected equipment.

REFERENCES

[1] International Atomic Energy Agency, Nuclear Security Recommendations on Physical Protection of Nuclear Material and Nuclear Facilities (INFCIRC/225/Revision 5), IAEA Nuclear Security Series No. 13, IAEA, Vienna (2011).
[2] 10 Code of Federal Regulations, Part 73.55.
[3] Sandia National Laboratories, Vital Area Identification for U.S. Nuclear Regulatory Commission Nuclear Power Reactor Licensees and New Reactor Applicants, SAND2008-5644, (2008).

The Status of Nuclear Material Accountancy of R&D Facility at KAERI

Hyun-Jo Kim*, In-Chul Kim, Byung-Doo Lee, Sung-Ho Lee, Hyun-Sook Kim, Juang Jung, Jin-Ha Choi, and Mun-Young Ryu
KAERI, 989-111 Daedeok-daero, Yuseong-gu, Daejeon, Republic of Korea
*keiki@kaeri.re.kr

1. Introduction

The KAERI-Daejeon site consists of 11 nuclear facilities subject to IAEA safeguards. The overall safeguards system at KAERI is shown in figure 1. The Nuclear Material Control Team (NMCT) responsibility for the overall implementation of the safeguards matter arising at each facility. A facility manager is designated at each nuclear facility for the implementation of safeguards work at the facility level.

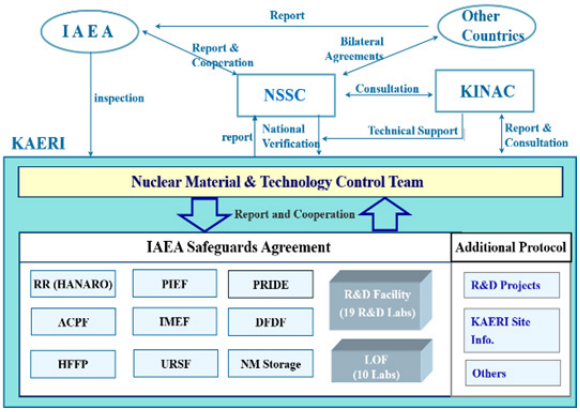


Fig. 1. Overall Safeguards System at KAERI.

The small amount of nuclear material handling facilities at KAERI are the R&D facility and the LOF at KAERI. The R&D facility consists of the nuclear fuel cycle related R&D laboratories and LOF at KAERI consists of the basic R&D laboratories which are not related with nuclear fuel cycle.

The R&D facility has small amount of nuclear material, but the experiments are performed most actively. The R&D facility consisting of 19 inventory KMPs is operated on a project basis and the laboratories for each project are designated as an inventory KMP. Many researchers conduct experiments using small amount of nuclear material in the laboratories.

Therefore, the R&D facility is the most difficult facility to prepare the nuclear material accounting documents for IAEA inspections.

This paper describes the status of nuclear material accountancy of the R&D facility at KAERI.

2. Status of Nuclear Material accountancy of the R&D facility at KAERI

2.1 Nuclear Material Accounting System at KAERI

The most basic of the safeguards obligation that the nuclear facility must comply with is to manage the nuclear material accounting data.

KAERI had been developing its computerized nuclear material accounting system since the end of 1980s. It was developed as a stand-alone system and thus there were some limitations in collecting the inventory change data from the nuclear facilities at KAERI. That is, when the inventory changes occurred in a facility, the operator provided the inventory change information in hard copy to the NMCT, and the NMCT entered the data into the system.

As Integrated Safeguards (IS) has been applied to ROK since 2008, it is difficult to prepare the inspection documents within 2 hours if the nuclear material accounting data is not periodically managed at each facility.

Therefore, KAERI has developed a web-based accounting system, called KASIS (KAERI Safeguards Information treatment System), with the function of a near real-time account system to cope with short notice inspection under IS.

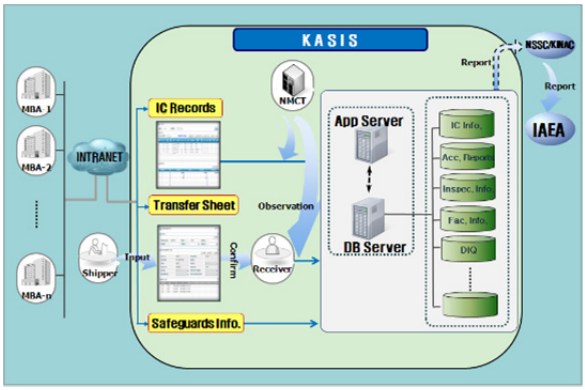


Fig. 2. Schematic Diagram of KASIS.

The facility operators and NMCT can access and work together on the intranet. The facility operators should input the inventory changes such as re-batching and nuclear material transfer into KASIS.

2.2 Nuclear Material Accountancy R&D facility at KAERI

Since KASIS was developed based on the item counting facility, it does not have a function to manage the nuclear material in process of bulk handling facility.

The HANARO fuel fabrication facility which is the large bulk handling facility at KAERI has established its own inventory management system. The system is connected to KASIS and the inventory of nuclear material in process is managed with its own system and the re-batching is applied if necessary.

On the other hand, in the case of the R&D facility, it is practically difficult to develop the own inventory management system due to budget etc. Also, there are a lot of researchers who conduct experiments using small amount of nuclear material within one KMP. Therefore, it is difficult to prepare the nuclear material inventory list within 2 hours during RII (Random Interim Inspection).

So, the facility operators have often reported the internal inventory changes for process nuclear materials that do not have to report to the IAEA to manage the inventory list in preparation for RII. Some KMPs were even managed the losses using arbitrary batches to manage the amount of losses occurred during experiments.

The NMCT has discussed with the facility managers several times and decided to apply the re-batching when the nuclear material is taken out of the storage for the experiments and when the experiments are completed and brought into the storage. However, the inconvenience remains that the amount of nuclear materials in the process should be managed separately.

3. Conclusion

This paper reviewed the status of nuclear material accountancy of the R&D facility at KAERI. The nuclear facilities at KAERI have managed the nuclear material accounting data using KASIS. However, KASIS does not have the function to treat the loss occurred during the experiments and manage the inventory of nuclear materials in the process for the bulk handling facility. For efficient inventory management of nuclear materials in process, it is necessary to develop the own inventory management system for the R&D facility and connect to KASIS in the future.

REFERENCES

[1] IAEA, “Nuclear Material Accounting Handbook”, (2008).

[2] IAEA, “Safeguards Implementation Practices Guide on Provision of Information to the IAEA”, (2016).

[3] B.D.Lee, “The Status of Development on a Web-Based Nuclear Material Accounting System at KAERI”, KNS 2014 Spring Conference, May 29-30, (2014), Jeju.

The Status of Practical Education for Accounting Nuclear Material at KAERI

Jinha Choi*, In-Chul Kim, Byung-Doo Lee, Sung-Ho Lee, Hyun-Jo Kim,
Hyun-Sook Kim, Juang Jung, and Mun-Young Ryu
KAERI, 989-111 Daedeok-daero, Yuseong-gu, Daejeon, Republic of Korea
*choijh@kaeri.re.kr

1. Introduction

Since agreement between Korea and IAEA for the application of safeguards in connection with the NPT (INFCIRC/236), it reached a comprehensive conclusion that means all nuclear materials and nuclear activities in Korea are performed for the peaceful purposes.

In 2007, nuclear control education was enacted and workers who handle nuclear material or project managers who research related nuclear fuel cycle take annual education.

To enhance recognition of safeguards at KAERI, moreover, Nuclear Material and Technology Control (NMTC) team has provided additional training course focused on practical education for worker of nuclear material accounting and safeguards.

In 2019, NMTC conducted two practical education and three occasional training for worker in charge of nuclear material accounting [1].

2. Practical and Occasional Education for Safeguards at KAERI

In 2007, nuclear control education was enacted in the domestic law system by reflecting IAEA Safeguards Agreements and Additional Protocol, Therefore persons in chare of nuclear material accounting are have to take nuclear control education according to the defined education hours, methods, and training contents on every year based on Article 141 of the Enforcement Rules.

This part about nuclear control education is also specified in internal regulation for accounting and control of nuclear materials in KAERI. The internal regulation include also additional training course like practical education.

2.1 Practical Education

To strengthen the implementation of on-site safeguards, NMTC has provided practical education for those in charge of nuclear material accounting and control since 2009[2]. However, there were frequent cases of overlapping schedules and contents with legal education, resulting in decrease participation rates and educational effects.

Occasionally, there is a difference between person in charge of nuclear material accounting and actual user for nuclear material. It could not rule out the possibility of problems for the accounting. Personnel for nuclear material accounting was newly defined to prevent these problems in advance.

They are not obliged to complete the nuclear control education, legal education. Internal regulation is revised so that the personnel must complete the practical education for safeguards every year, thereby reflecting facility's characteristics and improving the recognition.

2.2 Occasional Education

It is not easy to adjust the schedule of the personnel in facilities and laboratories. Therefore, frequency of education was changed to twice a year instead of once a year. Occasional education was also added for newly appointed representative or personnel of facility and laboratory if it is difficult to wait for regular education or when work is urgent.

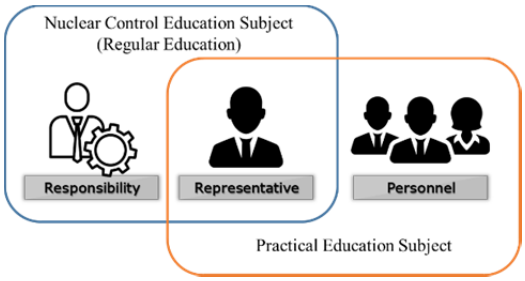


Fig. 1. Scheme of Education for Safeguards.

2.3 Characteristics of Education for Safeguards

Practical education for safeguards at KAERI includes contents used in actual practice. The contents consist of inventory management of nuclear material, how to use the system for change or transfer, how to write reports etc.

Features of education are as follows [3]:

1. How to use the KAERI Safeguards Information treatment System(KASIS)
2. Practical respects for method and procedure of nuclear material accounting (how to do RM/RP, Batch and MD code)
3. Preparation, procedure for IAEA/national

inspection and improvements in the results of inspection
4. The safeguards implementation system and obligations of KAERI
5. Other things necessary for accounting and control of nuclear material

3. Conclusion

Based on Article 141 of the Enforcement Rules, nuclear control education, regulation education, is conducted for workers in various nuclear facilities. It mainly contains formal content rather than practical content. Although the education is recently tried to cover the practical aspects, but it is difficult to deal with working-level contents considered the characteristics of each facility.

Practical educations and occasional educations are conducted to carry out to effective implementation of safeguards and improve the recognition at KAERI. The educations are also focused on working-level aspects. In particular, KAERI is equipped with a specific system for accounting nuclear material.

If procedures and contents of the education is supplemented by some guidelines and is replaced legal education, the burden of education recipients will be reduced and the effect of education will be increase as well as expertise. As a result, our institute will be effectively able to carry out implementation of safeguards.

REFERENCES

[1]In-Chul Kim, "Nuclear Environment, Emergency Preparedness and Control / Nuclear Control and Management", KAERI/MR-669/2019.
[2]Byung-Doo Lee, "Nuclear, Radiation Environment Protection/Nuclear Control and Management", KAERI/MR-515/2011.
[3]In-Chul Kim "Nuclear, Radiation Environment Protection/Nuclear Control and Management", KAERI/MR-636/2018.

A Study on the Need of New Safeguards International Training Course for States With Small Quantities Protocols at INSA

Byung-Woo Shin*
Korea Institute of Nuclear Nonproliferation and Control
*sbw97@kinac.re.kr

1. Introduction

After the establishment in 2014, INSA has contributed to strengthening international nuclear nonproliferation regimes by holding Safeguards (SG) International Training Courses (ITCs) for IAEA member states. INSA has also continued to make efforts to develop an effective curriculum for the states based on IAEA SG agreements because the SG environment of each state is very different depending on what kind of SG agreement the states have signed.

This paper reviews the characteristics of main SG agreements and the status of IAEA member states. It also explores the current module status of INSA SG ITC and suggests why the INSA should develop a new SG ITC for Small Quantities Protocol (SQP) for strengthening the international nuclear nonproliferation regime.

2. Background and Current Status of IAEA Main SG Agreements

All non-nuclear-weapon States party (NNWSs) to the NPT, as well as state parties to the regional nuclear-weapon-free zone treaties, are required to conclude the Comprehensive Safeguards Agreement (CSA) with the IAEA. So, the CSA is considered as the representative agreement. In concluding the CSA with the IAEA, the states must declare the type and quantity of material. The CSA gives the IAEA the authority to independently verify that all nuclear material in the state or jurisdictional control of a state is not diverted for non-peaceful purposes.

The Additional Protocol (AP) is designed for States that have any type of safeguards agreement with the IAEA. The main objective of the AP is expanding the IAEA's ability to check for nuclear facilities.

Contrary to the AP, the SQP suspends the application of many provisions of the CSA (in Part II). This simplifies the implementation of safeguards, but States with a modified SQP are required to submit more information like an initial report to the IAEA.

Table 1 shows that the number of the states of the CSA, the AP, and the SQP as of December 31, 2019. In this paper, an SQP State is a State that has an operational SQP. A full CSA state is a state that has the CSA in force and that does not have an operational the SQP. The number of states that concluded the CSA is 175, while 94 states (54%) out of 175 states are SQP states and even 34 states (19%) have concluded SQP without AP. It shows not only the CSA and the AP are the main agreement but also the SQP.

Table 1. Number of the states of Full CSA, AP and SQP, as of December 31 2019

Agreement	With AP	Without AP	Total(%)
Full CSA	71(41%)	10(6%)	81(46%)
SQP	60(34%)	34(19%)	94(54%)
Total	131(75%)	44(25%)	175(100%)

3. Status of INSA SG ITCs

There are three SG courses in INSA ITC. It consists of one introductory and two specialized courses. The most content in each SG ITC is focused on the CSA and the AP. Table 2 shows the objective of each INSA SG ITC.

Table 2. The Contents of Safeguards ITCs at INSA

Couese Theme	Description
Fundamentals of Nuclear SG (Introductory, 5days)	The course aims to raise awareness to participants at the beginner level about the concept on the State system of accounting for and control of nuclear material in accordance with SG agreements and AP.
Provision of information to the IAEA (Specialized A, 5day)	The course aims to provide participants with practical knowledge and skills required to prepare the SG to be provided to the IAEA under SG and AP.
Strengthening State Safeguards Regulatory Authority (Specialized B, 5days)	The course aims to assist participants' countries to establish and maintain their SG infrastructure. The structure and contents are primarily based on IAEA Services Series 31.

Three INSA SG courses are consist of 57 modules. Table 3 shows the number of modules related to each SG agreement in the point of module objective.

Table 3. The Number of Modules related to SG Agreement in INSA SG ITCs

Course	SQP	AP	CSA	Others
Itroductory	0 (0%)	4 (20%)	14 (70%)	2 (10%)
Specialized A	0 (0%)	2 (13%)	10 (50)	3 (20%)
Specialized B	0 (0%)	3 (13%)	17 (77%)	2 (10%)
total	0 (0%)	9 (16%)	41 (72%)	7 (12%)

*Others includes modules like overview, facility tour, etc.

72% of modules in INSA SG ITCs are consist of CSA related contents. The AP modules can be helpful to the SQP states with the AP but are just 16% and there are no modules for only SQP states. It means that INSA SG ITCs are not effective for the states with the SQP.

4. Conclusions

Six years have passed since INSA was established. INSA has strengthened its educational capabilities by providing ITCs. INSA ITCs have focused on providing SG ITCs related to the CSA and the AP to newcomer countries most of which concluded the CSA and the AP. But, over 50% of member states with the CSA have concluded the SQP to their CSA which holds in abeyance many procedures in Part II of the CSA. So, developing a new ITC for SQPs could be a good opportunity to broaden INSA's roles.

Additionally, INSA can contribute to strengthening not only the nuclear nonproliferation regime but also the nuclear security regime by providing the new course. The human resource improvement by providing the new course is also related to the improvement of domestic nuclear material accounting and control (NMAC) in the state.

By providing various ITCs related to safeguards, INSA will contribute steadily to strengthen international nuclear nonproliferation and security regime as one of the major COE (Center of Excellence).

References

[1] Annual Report 2014~2019, KINAC/INSA.
[2] Safeguards Implementation Guide for States with Small Quantities Protocols, IAEA.
[3] Is training provided to SQP States enough, N. Miyaji, JAEA.
[4] 2019 Safeguards Implementation Report (SIR) , IAEA.

Safeguards Activities for Nuclear Power Plant in Post-Operational Phases

Wonjong Song
Korea Institute of Nuclear Nonproliferation and Control (KINAC)
1418, Yuseong-daero, Yuseong-gu, Daejeon, Republic of Korea
*wjsong47@kinac.re.kr

1. Introduction

A state in force undertakes to declare the type and quantity of all nuclear material in the state and accept IAEA safeguards inspection under the Comprehensive Safeguards Agreement (CSA). The implementation of IAEA safeguards for a nuclear facility begins when a Design Information Questionnaire (DIQ) is submitted to the IAEA. The safeguards activities are then enforced until the nuclear facility is decommissioned.

Currently, there are 46 Material Balance Areas (MBAs) under safeguards in ROK including the Kori unit 1 and Wolsong unit 1 in the permanent shutdown phase. In the IAEA's reference data, the number of nuclear reactors in the operation phase changed from 437 to 443 in 2020 compared to 2010. However, the number of reactors in the permanent shutdown phase changed from 123 to 186. Furthermore, the number of reactors in the decommissioned or decommissioning phase was changed from 108 to 150 [1,2]. It is expected that more nuclear reactors will be decommissioned based on the reported statistics. The ROK's authority declared that the Kori unit 1 would be decommissioned without issuing an operation-license extension. Therefore, the safeguards activities in the post-operational phase are investigated in this study.

2. Considerations in Post-operational Phases

The number of nuclear facilities in post-operational phases is increasing globally, and the IAEA has been developing the guidelines for these facilities. In this study, several important considerations in the post-operational phases for the IAEA's safeguards are reviewed.

2.1 Post-operational phases

The post-operational phases consist of three steps: the permanent shutdown phase, the closed-down phase, and the decommissioned phase. The permanent shutdown refers to a nuclear facility that has been stopped permanently, but the nuclear material has not been removed. The closed-down phase is subdivided into preservation and decommissioning phase. If the nuclear material has been removed completely, a facility's state will change from the permanent shutdown phase to the closed-down in preservation phase. A facility can be restarted at any moment in the closed-down in preservation phase because all essential equipment for operation remains at a facility. If removing or rendering the essential equipment inoperable gets underway, a facility's state has to change from the preservation phase to the decommissioning phase. The IAEA then carries out final Design Information Verification (DIV) in order to confirm that all essential equipment is removed adequately or rendered inoperable. If the IAEA's confirmation is obtained, a facility's state changes to the decommissioned phase.

According to the IAEA, the decommissioned phase means that a facility is decommissioned for safeguards purpose, which can no longer be used to store, handle, and utilize the nuclear material. Therefore, the efforts and resources to reactivate a facility may equal or even exceed the requirements for constructing a new facility [3].

2.2 Nuclear material

A facility's state changes from the permanent shutdown to the closed-down in preservation phase if all nuclear material is removed or transferred to other MBAs. In this phase transition, retained waste, exempted nuclear material, and terminated nuclear material should be considered rather carefully.

The retained waste generated during facility operation does not satisfy conditions for termination of safeguards. All retained waste recorded as 'transfer to retained waste' (TW) should be returned to 're-transfer from retained waste' (FW) in the nuclear material accounting reports. After reporting changes in inventory quantity, all retained waste should be removed or transferred to other MBAs.

Safeguards for the nuclear material that satisfies the paragraph 36 or 37 of the CSA can be exempted and de-exempted in any MBAs. Therefore, the existence of the exempted nuclear material does not affect the phase transition between the permanent shutdown and closed-

down in preservation. If a state concluded Additional Protocol (AP) with the IAEA, the location of the exempted nuclear material should be tracked because it is subject to the 2.a.(vii) of the AP. Nevertheless, most nuclear power plants in ROK do not need to consider such this issue as there are no exempted nuclear material.

Safeguards for the nuclear material can be terminated by the paragraph 11 or 13 of the CSA. The existence of the terminated nuclear material also does not affect the phase transition between the permanent shutdown and closed-down in preservation. If a state concluded the AP with the IAEA, the information of the terminated nuclear material, including Highly Enriched Uranium (HEU), U-233, and Pu, should be reported according to the 2.a.(viii) of the AP [3].

2.3 Essential equipment

The IAEA determines the essential equipment by reviewing a DIQ submitted by a state authority. In particular, the essential equipment list is provided to a facility in the closed-down in decommissioning phase. Based on this information, the essential equipment is removed or rendered inoperable by an operator. The essential equipment may be considered inoperable by many ways such as cutting, crushing, melting, filling with cement, and drilling. If the essential equipment is removed without rendering inoperable and instead utilized again in another facility, such information must be reported to the IAEA [3].

3. Safeguards in Post-operational Phases

ROK had concluded the CSA and AP with the IAEA. Therefore, the authority of ROK provides a variety of information and supports regarding the IAEA inspections. If a facility is in the post-operational phases, some changes are required in providing information and the IAEA inspections.

3.1 Provision of Information

All nuclear material should be removed or transferred for the phase transition between the permanent shutdown and closed-down in preservation. Therefore, null nuclear material accounting reports are submitted from the closed-down in preservation phase. The submission of the null nuclear material accounting reports can be stopped by an agreement with the IAEA. The present DIQ form of reactor does not include the decommissioning information. Therefore, an operator should submit the updated DIQ including question 58 and 59 [3,4].

3.2 IAEA Inspection

Even if a facility enters the permanent shutdown phase, the type and frequency of the IAEA inspections are not altered compared to those of the normal operation phase. The IAEA inspections, such as interim, Physical Inventory Verification (PIV), and DIV, are performed. If a facility becomes the closed-down in preservation phase, the interim and PIV are not performed because it does not contain any nuclear material. In the closed-down in decommissioning phase, the final DIV is carried out to confirm that the essential equipment is removed adequately or rendered inoperable. If a state concluded the AP with the IAEA, Complimentary Access (CA) could always be carried out from the normal operation to the decommissioned phase [3].

4. Conclusion

Since the Kori unit 1 will be decommissioned, the authority of ROK is obligated to support the IAEA safeguards activities related to its decommissioning. Unfortunately, ROK has not yet experienced the decommissioning of a commercial reactor. Thus, several safeguards issues possibly caused in the post-operational phases are reviewed in this paper. This work will help to develop the national safeguards guidance on decommissioning strategy.

Acknowledgment

This work was supported by the Nuclear Safety Research Program through the Korea Foundation of Nuclear Safety (KoFONS) using financial resources granted by the Nuclear Safety and Security Commission (NSSC) of the Republic of Korea (No. 1804025).

REFERENCES

[1] IAEA, Nuclear Power Reactors in the World, Reference Data Series No.2, (2010).
[2] IAEA, Nuclear Power Reactors in the World, Reference Data Series No.2, (2020).
[3] IAEA, Guidelines for the Post-Operational Phase of Nuclear Facilities or Locations Outside Facilities, TBD.
[4] IAEA, A DIQ Completion Guidelines (Reactors), TBD.

An Exploratory Study on Acquisition Path Analysis for Denuclearization Verification

Jung-Hyun LEE*, Minsoo KIM, Yonhong JEONG, Seung Ho JEONG , and Young Wook LEE
Korea Institute of Nuclear Non-proliferation and Control, 1418, Yu Sung Dae Ro, Yu Sung Gu, Daejon, Korea
*leejh@kinac.re.kr

1. Introduction

The acquisition path analysis (APA) is a useful tool to establish safeguards strategies of the IAEA as it allows identifying the plausible technical routes for acquiring weapons-usable material of a State [1].

The purpose of this paper is to describe how structured acquisition path analysis can be used to define denuclearization verification priorities and to prevent rearmament. Through the examination of the relevant literatures, the authors suggest considerations for verification of North Korean nuclear program.

2. Background

2.1 Literature Review

The APA model of IAEA can deal with the civil nuclear fuel cycle only and it is not fully standardized [2].

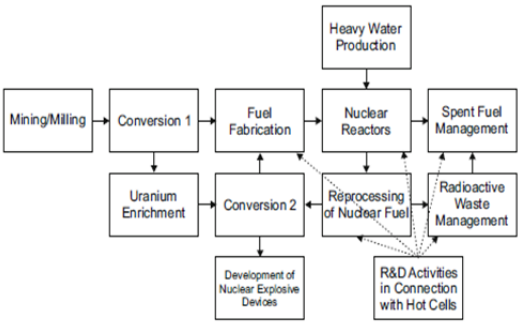


Fig. 1. Overview of the APA model of IAEA.

To solve this problem, Researchers at the Forschungszentrum Jülich GmbH (FZJ) in Germany have been actively conducted modification in the following two directions.

The first is to expand the model to deal with the case of acquiring nuclear material from a military nuclear fuel cycle or nuclear weapons complex [3].

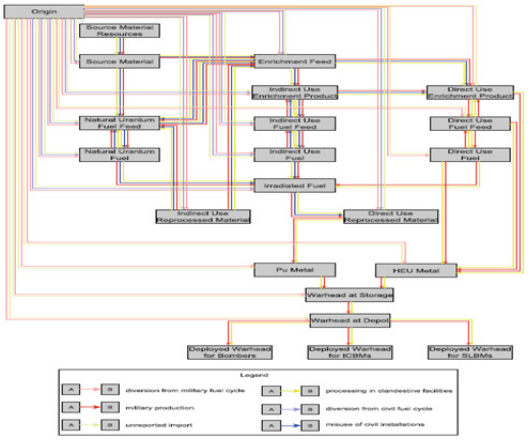


Fig. 2. Overview of the APA model of FZJ in Germany.

The second is to apply mathematical models and statistical concept such as directed graph theory and two-person non-cooperative inspection game theory to the APA for quantifying effectiveness of a verification regime [4].

Table 1. Graph theory and the element of the APA

No.	Graph theory	APA model
1	Node	IAEA model : Facilities,FZJ model : Materials
2	Edge	IAEA model : Materials FZJ : Process
3	Path	Weapons-usable material Acquisition path
4	Edge weight	Attractiveness and/or Evaluation Methodology

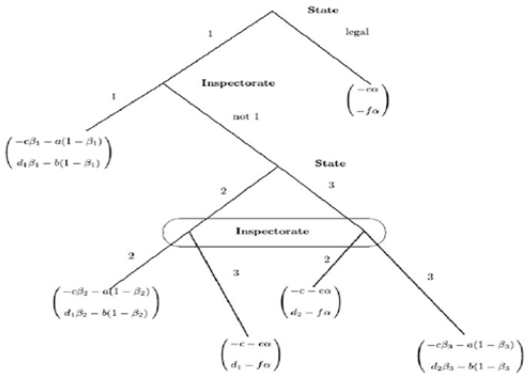


Fig. 3. Non-cooperative two-person inspection game model for disarmament verification.

Table 2. Summary of literature review

	IAEA physical model	FZJ APA model
Purpose	Safeguards (State-level approach)	Nuclear disarmament Verification
Scope (Material, Facilities/ Process)	15 nuclear material forms(Edge)	22 nuclear material forms(Node)
	11 civil nuclear fuel cycle processes(Node)	6 processes(Edge) -include military nuclear fuel cycle process
Evaluation Methodology	Classified	3 measures proposed by Gen IV international Forum - Proliferation Technical Difficulty(TD) - Proliferation Cost(PC) - Proliferation Time(PT)
Findings/ Limitations	- Not applicable to military nuclear program - Proven but classified model	- Nat applicable to H-bomb program - Not applicable to the disassembly and disposition of nuclear weapons - Not applicable to a State that has completed indigenous development of its nuclear program

3. Considerations for North Korean Denuclearization Verification

Due to lack of available information, this study was limited to suggest considerations for verification of North Korean denuclearization.

3.1 North Korean nuclear program

North Korea claims to have developed nuclear weapons with its own technology. Since its 4th nuclear test in 2016, North Korea has claimed to have used hydrogen bombs. In order to verify North Korean H-bomb program, this paper suggested a model including 12 facilities(H-facilities) and 5 types of fusional fuel material (H-materials) as shown in fig 3. H-materials are not defined as nuclear materials under the NPT regime, and among H-facilities, nuclear reactors can be categorized as nuclear facilities [5].

3.2 Nuclear Weapons lifecycle

As shown in Figure 3, nuclear weapons are conceptually designed, developed, produced, deployed and maintained in the stockpile then retired and dismantled. This sequence is known as the 'nuclear weapons lifecycle' [6]. The forms of the weapon-usable materials in each lifecycle vary - metal part, scrap, waste, hold up on process equipment and surrounding enclosures. All of these should be eliminated. For sustainable denuclearization, it is very important to ensure that weapon-usable materials from disassembly of nuclear weapons should be introduced into the verification and monitoring systems, and finally should be dispositioned to prevent rearming the nuclear weapons. Disposition of HEU is possible by blending down its concentration of U-235. Compared to HEU, plutonium deposition is a far less straightforward and require higher technology [7].

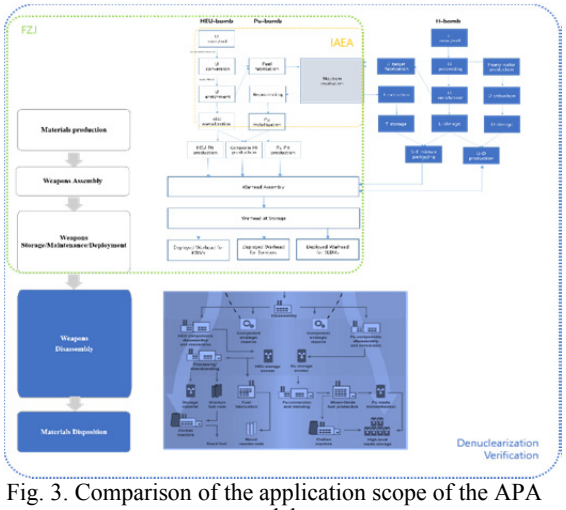


Fig. 3. Comparison of the application scope of the APA models.

3.3 Evaluation Methodology

Evaluation criteria of the FZJ model shown in Table I are not suitable to a State that has already completed development of nuclear weapons with its own technology and materials. This paper suggested detection probability, proliferation time (shortest path) and detection resource efficiency.

REFERENCES

[1] IAEA, GOV/2014/41, Supplementary Document to the Report on The Conceptualization and Developments of Safeguards Implementation at the State Level, (2014).
[2] Jill N.Cooley, The Evolution of Safeguards, (2020).
[3] Irmgard Niemeyer, Joshua Rukowski, Gotthard Stein, Physical Model and Acquisition Path Analysis: Applicability to Nuclear Disarmament Verification, (2020).
[4] Morton Canty, Clemens Listner, Formalizing Acquisition Path Analysis, (2020).
[5] Jung-Hyun LEE*, Minsoo KIM, Young Wook LEE, 2019 Korean Nuclear Society Autumn meeting, Consideration on Technical Support to Denuclearization: Focused on H-program, (2019).
[6] DOD, Nuclear Matters Handbook, (2020).
[7] Thomas Shea, Verifying Nuclear Disarmament, (2019).

Education of Nuclear Nonproliferation and Security Facing the COVID-19 Challenges

Sung Yoon Park* and Byung-Woo Shin
1418 Yuseong-daero, Yuseong-gu, Daejeon, Republic of Korea
*sypark12@kinac.re.kr, sbw97@kinac.re.kr

1. Introduction

Since the Covid-19 outbreak in 2020, there have been many changes in international cooperation. In particular, in the field of training and education, the concept of online education and so-called 'on-tact' education have got more attention than ever.

Since its establishment in 2014, KINAC/ INSA has been offering international training for nuclear newcomer countries and partner countries to help them establish or enhance their nonproliferation and security regime. KINAC/ INSA also provides mandatory national training courses for nuclear facility operators, researchers, and inspectors to improve their nuclear nonproliferation and security competence.

There emerges a need to change the form of education to prepare for the advent of 'on-tact' education. This paper aims to present a new direction of KINAC/INSA's program by reviewing the new trends in education with the COVID-19 outbreak, the government's 2021 R&D policy, and IAEA's guidelines for training centers.

2. Analysis of Internal and External Environment of KINAC/INSA

2.1 Present State of KINAC/INSA

KINAC/INSA is an educational institution specialized in the field of nuclear nonproliferation and security. In 2019, it offered five mandatory national nuclear nonproliferation training courses and 43 mandatory national nuclear security training courses. Ten additional but non-mandatory courses for the general public were also hosted. For the international community, nine international training courses were hosted. Five of them were KINAC/INSA's indigenous courses, and the others were the IAEA's regional, international, or joint training courses. About 2,000 people completed the mandatory national courses, and 120 attended the international courses. The course hours varied from two hours to two weeks, depending on the type of education. Main form of education was collective offline education, and the online program was partially tried to alter the offline courses. Most of the courses that KINAC/INSA provides were theoretical education despite its possession of practical training infrastructure. While it has an advantage that is well equipped with practical training facilities, its programs were more devoted to theoretical education [1].

2.2 KINAC/INSA's Response to the Pandemi

In 2020, the education industry faced a situation that has not been experienced. Most of the offline education courses have been canceled or suspended due to the epidemic. Some of the mandatory offline education had to increase the number of providing programs with fewer participants to comply with the government's quarantine guidelines.

KINAC/INSA was no exception, and all of the international educations planned this year, except for one session held in January, have been postponed for the next year. For mandatory education, most of the courses initially planned in the first half of the year were postponed to the second half. While the epidemic got more severe in the second half of the year, KINAC/ INSA proposed to amend the Nuclear Safety Act and relevant regulations to allow training courses using the online platform to alter the offline education. Moreover, KINAC/INSA is now upgrading existing textbooks to online course materials to prepare for the prolonged pandemic situation.

2.3 Government's R&D Plans in 2021

The government set its 2021 R&D plan to weigh on localization in the materials sector by funding the development of chip materials, components, and equipment, improving contact-free service and digital content, and growing artificial intelligence technology [2]. It results from significant changes in 2020, such as Japan's export restriction, COVID-19 outbreak, and the grown notification on the fourth industrial revolution.

2.4 IAEA's Guideline for the National Nuclear Security Support Centres

With the growing awareness of nuclear security after the Nuclear Security Summits, numerous states established institutions that may provide training and education in this field. IAEA recently published a technical document for those institutions, a guideline on establishing and operating a National Nuclear Security Support Centre (NSSC) [3]. The essential role and functions of the NSSC in the guideline are human resource development, technical support, and scientific support. The guideline also advises that practical exercises can enhance the effectiveness of the NSSC's programs.

3. SWOT Analysis of KINAC/INSA

The above-mentioned current status and environmental changes of KINAC/INSA is organized as following SWOT table:

Table 1. SWOT Analysis of KINAC/INSA

Strength	Weakness
- Seven years of experience - Well equipped facilities for practical training and exercise - Conformed professor - Experience in the implementation, not only education	- Obsolescence of education materials - Lack of capacity to develop its own content - Devoting to theoretical education - Pandemic - Lack of experience in R&D fields
Opportunity	**Threat**
- Awareness of contact-free service - Government's R&D plan - Gradual shifts in generation - Secure short-term budget	- Devaluation on KINAC/INSA operation - Devaluation on the effectiveness of online education - Insecure long-term budget

4. Conclusion

Since its establishment in 2014, KINAC/INSA has made great efforts to develop educational programs, equip practical exercising facilities, and increase professors' number.

As a result, KINAC/INSA's scale and quality of education are evaluated to be better than those of Japan or China. After the recent pandemic outbreak, KINAC/INSA is taking the current situation as an opportunity to check its operational capabilities once again. In conclusion, KINAC/INSA should establish a technical and legal foundation for non-face-to-face education. It also needs to develop digital contents that can be used in both contact-free education and in-person education. To differentiate offline educations from digital content, more practical exercises rather than theoretical education should be developed to raise the course's effectiveness.

REFERENCES

[1] Annual Report of KINAC-INSA, KINAC.

[2] The 4th Basic Plan for National Science and Technology (2018-2022), Ministry of Science and ICT.

[3] Establishing and Operating a National Nuclear Security Support Centre(TECDOC-1734), IAEA.

2분과

사용후핵연료 처분전관리 (Oral)

Preliminary Data Analysis of Empty Weight Transportation Test and Surrogate Spent Nuclear Fuel Loaded Transportation Test Under Normal Conditions of Transport

JaeHoon Lim*, Woo-seok Choi, Sang Soon Cho, Gil-Eon Jeong, and Jongmin Lim
Korea Atomic Energy Research Institute
*jhlim85@kaeri.re.kr

1. Introduction

Currently, the development of evaluation technology for vibration and shock loads transmitted to spent nuclear fuel and structural integrity of spent nuclear fuel under normal conditions of transport is progressing in Korea by the present authors [1]. To identify the dynamic characteristics results from the different test conditions, empty weight road transportation tests were prepared and performed in June 2020 [2]. Road transportation tests under normal conditions of transport using surrogate spent nuclear fuel were performed in September, 2020, and the coastal ship transportation test is planned for June, 2021.

The test model KORAD-21, transportation cask-cradle system, was manufactured in Doosan Heavy Industries and Construction for the transportation tests.

Preliminary data analysis of empty weight transportation test and surrogate spent nuclear fuel loaded transportation test will be conducted along with detailed review in the aspect of durability.

2. Test Conditions

The transportation test composes of the empty weight transportation test, and loaded transportation test including the handling test. In order to investigate amplification or attenuation characteristics, according to the load transfer path, thirty-five accelerometers were attached on the trailer platform, cradle, cask, canister, disk assembly, basket, and surrogate fuel assemblies. To investigate the durability of spent nuclear fuel rods, thirty-two strain gages were attached on surrogate fuel assemblies. All tests were conducted in Doosan Heavy Industries and Construction.

2.1 Handling Test

Acceleration and strain data were measured while the cask was moved by the overhead crane. The data was measured when the cask was handled vertically, seated on the cradle, and loaded and unloaded on the trailer.



Fig. 1. Handling Test.

2.2 Empty Weight and Loaded Transportation

As shown in Table 1, five test conditions were established based on the events that might occur when a tractor-trailer transports heavy weight [2]. Each condition will be performed three times for consistency. For the speed bump test, the test velocity of loaded tests was lowered compared to the empty weight tests for the safety of the trailer.

Table 1. Empty Weight and Loaded Transportation Test Conditions

Test	Item	Velocity (km/h)
Speed bump	General speed bumps, L-shape and U-shape interferences	Empty: 5, 10, 15 Loaded: 5
Lane change	Lane width 2.5 m and 3.5 m	30
Deceleration	Braking distance 10, 13, 16 m	30
Obstacle avoidance	Steering away from the obstacle at 10, 13, and 16 m	30
Pilot test	Uncontrolled test	Arbitrary

The test conditions were experimented in a more severe operating condition than actual transportation conditions. The actual spent nuclear fuel will be transported by road with a few guide vehicles arranged in front of the trailer and behind the trailer to avoid sudden stop or maneuver.

3. Preliminary Data Analysis

The preliminary data analysis on the empty weight, and loaded transportation tests, tested in June to September, is being analyzed. As a result of initial data analysis of the empty

weight test, the maximum acceleration was observed when the vehicle passes U-shape interference.

Further, acceleration and strain data, determined through the handling and transportation tests, will be analyzed. It will investigate whether the load generated for each transport mode was amplified or attenuated according to the load transfer path. The load transfer characteristics is expected to be different according to the transportation mode and loading path. The effects of strain on the structural integrity of the spent nuclear fuel will also be investigated.

4. Conclusion

Road transportation tests under normal conditions of transport using surrogate spent nuclear fuel were performed in September, 2020. Preliminary data analysis of empty weight transportation test and surrogate spent nuclear fuel loaded transportation test is being conducted along with detailed review in the aspect of durability.

Acknowledgements

This work was supported by the Korea Institute of Energy Technology Evaluation and Planning (KETEP) and the Ministry of Trade, Industry & Energy(MOTIE) of the Republic of Korea (No. 2018170201770).

REFERENCES

[1] Lim, J. H., Cho, S. S., Yang, Y. Y., Seo, K. S., and Choi, W. S., “Establishment of Data Acquisition System for Road and Sea Transportation Test of Surrogate Spent Nuclear Fuel under Normal Conditions of Transport,” Korea Radioactive Waste Society Fall Conference, (2019).

[2] Lim, J. H., Yang, Y. Y., Jeong, G. E., Lim, J. M., Cho, S. S., and Choi, W. S., “Scenarios and Instruments Locations for Heavy Trailer Empty Weight Test to Calibrate Multi-body Dynamics Modeling,” Korea Radioactive Waste Society Spring Conference, (2020).

Current Status of the R&D Program for Evaluating Spent Nuclear Fuel Integrity Under Normal Conditions of Road and Sea Transport in Korea

Hyeong Koo Kim*, Joong Jin Kim, Jang Whan Lim, Seong Ki Lee, and Jong Sung Yoo
KEPCO Nuclear Fuel, 242, Daedeok-daero 989beon-gil, Yuseong-gu, Daejeon, Republic of Korea
*hkkim@knfc.co.kr

1. Introduction

Along with the long history of nuclear power generation, various types of SNF are stored in spent fuel pool of each power plant, and the storage pools are expected to be saturated in the near future. Therefore, in order to prevent the saturation of the spent fuel pool and continue to operate the power plants, normal transport of SNF through land and sea must be accompanied. As the first step of SNF management, the Korean multi-modal transportation test (MMTT) project has been launched in order to clarify the vibration and shock loads under normal conditions of transport (NCT) and to evaluate the integrity of SNF under the transportation loads.

In this project, four institutes are carrying out researches as follows:

Korea Nuclear Fuel (KNF), a leading organization, develops technology to evaluate the integrity of SNF against vibration and shock loads under NCT.

Korea Atomic Energy Research Institute (KAERI) carries out normal transport test and analyzes the vibration and shock load characteristics under NCT.

Korea Radioactive Waste Agency (KORAD) analyzes the carrying system and test route.

And Acts Ltd. develops a standard for failure of SNF cladding under NCT.

2. Status of the Research

2.1 Participating Organizations and Scopes

Four organizations are participating in this project. Fig. 1 shows the overall work scope of this project and the interface between the organizations. KNF, the leading organization of the project, is responsible for developing the SNF integrity evaluation methodology under NCT, developing both fuel assembly level and fuel rod level analysis models, and performing fuel assembly and fuel rod tests such as fatigue and wear. KORAD develops the representative transportation scenarios and analyzes the transport system, and is responsible for the transport system necessary for the land and sea transport test in Korea. KAERI conducts actual land and sea transportation tests according to the transport scenarios developed by KORAD and identifies the vibration and shock loads under NCT. Then, the vibration and shock load characteristics are analyzed to produce the reference loads required for fuel assembly and fuel rod level tests which will be performed by KNF. And ACT studies the degradation mechanisms and material characteristics of irradiated Zirconium alloy cladding to establish the failure criteria of the cladding under vibration and shock loads [1].

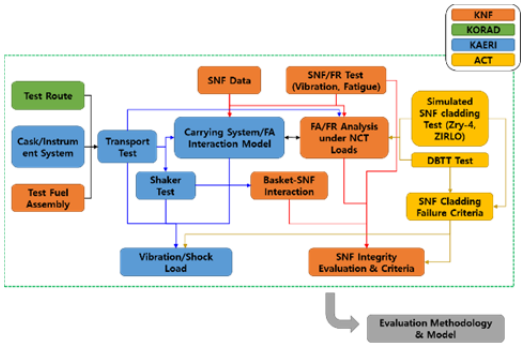
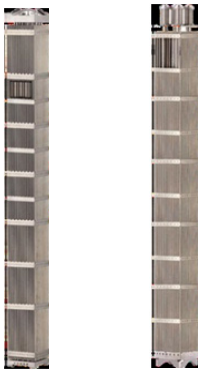


Fig. 1. Work scopes and interface of the organizations.

2.2 Status of the Research

2.2.1 Preparation of Transportation Test

For the normal transport test, two test assemblies and a full-size KORAD21 transportation cask were manufactured as shown in Fig.2 and Fig.3, respectively.



(a) WH 17x17 type (b) KSNP 16x16 type

Fig. 2. Configuration of surrogate fuel assemblies.



Fig. 3. Configuration of full-size KORAD21 Transportation Cask.

2.2.2 Truck Transportation Test

Fig.4 shows the scene of a road transportation test using a 10 axle truck trailer. The transportation cask is a weigh of about 150 tons, so the transport test was not able to perform on the public road because of overweight. Therefore, the captive track test was performed by selecting an appropriate section within Doosan Heavy Industries campus.

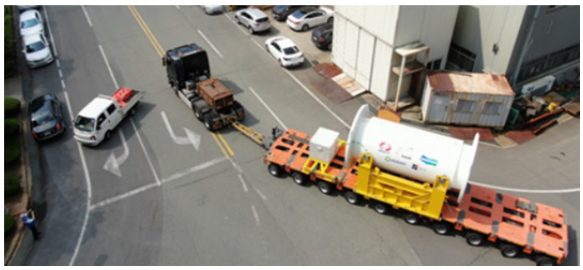


Fig. 4. Configuration of Truck Transportation Test.

2.3 Further Study

The next test is scheduled for a sea transportation according to the sea transportation scenario developed by KORAD next year.

Fig.5 shows the fuel rod fatigue and wear test equipment established through this project. The fatigue and wear tests will be performed using the vibration and shock loads obtained from these transportation tests to evaluate the integrity of SNF.



Fig. 5. Configuration of fuel rod fatigue and wear test setup.

3. Conclusion

In this paper, we introduced the current status of Korean MMTT project. Through this project, we will construct SNF normal transport and measurement systems and identify the vibration and shock loads acting on the transportation cask and the SNFs. With this test result, we will develop the analysis models, methodology and database to evaluate the integrity of SNF under normal land and sea transport conditions in Korea.

ACKNOWLEDGEMENT

This work was supported by the Korea Institute of Energy Technology Evaluation and Planning (KETEP) grant funded by the Korea government (MOTIE) (20181710201770, Development of Evaluation Technology for Vibration and Shock Load Characteristics and PWR Spent Nuclear Fuel Integrity under Normal Conditions of Road and Sea Transport).

REFERENCES

[1] H.K. Kim, et al. “Overview of R&D Program for Evaluating SNF Integrity under Normal Conditions of Road and Sea Transportation in Korea,” Proceedings of the 2019 TopFuel Conference, Seattle, Washington, USA, Sep. 22-26, (2019).

Fuel Handling Process and Interlock Design of Fuel Handling Equipment

Sang-Gyoon Chang[a,*], Jung-Gyu Kim [a], Jong-Min Kim [a], and Jong-Pil Jung [b]
[a] NSSS Division, KEPCO Engineering & Construction Company, Inc., Daejeon-si, Korea
[b] Korea Hydro & Nuclear Power Co., Ltd, Korea
*sgchang@kepco-enc.com

1. Introduction

This study provides technical information for the fuel handling process from new fuel receipt to spent fuel shipment at nuclear power plant and interlock design of the fuel handling equipment. The fuel handling equipment should be designed in the viewpoints of safety functions for fuel handling, efficiency for operation and maintenance of fuel handling equipment and decommission for nuclear power plant. Technical information provided in this paper would be beneficial suggestion to enhance the safety and the efficiency of the fuel handling equipment.

2. New and Spent Fuel Handling Process

The fuel handling equipment (FHE) consists of various equipment performing safety functions for fuel handling. Fig. 1 shows the new and spent fuel transfer path between the Containment Building and the Fuel Handling Area of Aux. Building.

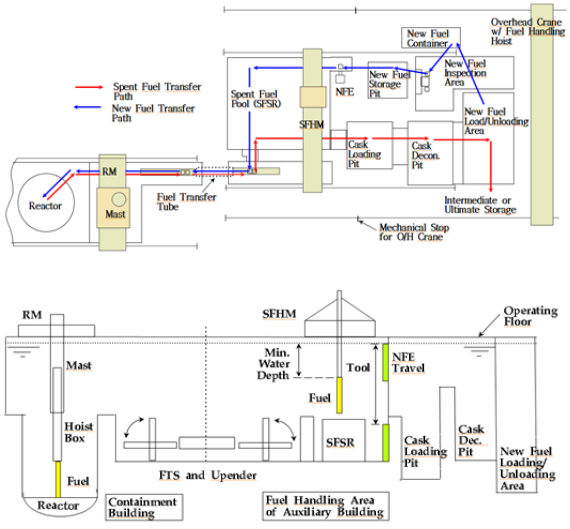


Fig. 1. Typical New and Spent Fuel Transfer Path of Fuel Handling Equipment.

After arrival of the new fuel shipping containers, the containers are transferred and secured to the operating floor. New fuel is inspected in the new fuel inspection device before placement into the new fuel racks and this operation is repeated until all fuel assemblies are placed in the racks. The New Fuel Elevator (NFE) lowers a fuel assembly into the spent fuel storage pool to allow the Spent Fuel Handling Machine (SFHM) to transfer new fuel to the spent fuel rack of the spent fuel storage pool or to the transfer upender. During refueling operations, new fuel is transferred to a reactor in the containment building through the transfer tube. For unloading from a reactor, spent fuels are moved underwater to the transfer upender in the containment building by the Refueling Machine (RM). The SFHM removes the spent fuel from the upended transfer carriage and places it to the spent fuel storage rack. The SFHM transfers spent fuels from the storage racks to the spent fuel cask for the intermediate storage. This operation will be implemented when the fuel cask loading pit is filled with spent fuel storage pool water. After the spent fuels are loaded into the cask, it will be sealed and transferred to the cask decontamination pit by the cask handling hoist. Then it is transferred to the truck loading & unloading area with the cask handling hoist for intermediate and /or ultimate storage.

3. Interlock Design for Fuel Handling Equipment

The fuel handling equipment should be designed to prevent damage to a fuel assembly and to ensure personal safety in accordance with interlock design requirements [1]. The domestic acts regulate the technical criteria for the structure, performance, operation and quality assurance of nuclear fuel periodic facilities. The interlock design of the FHE is based on regulatory guidelines [2] and engineering codes and standards. In order to meet acceptance criteria for the FHE design, the provisions for a protection from a physical fuel damage and a radiological protection, adequate cooling and a prevention of a criticality, and the operability and maintainability should be considered.

3.1 Protection from a fuel damage and a radiological material release

The mechanical and electrical safety devices for the FHE should be designed to prevent any damage to the fuel assemblies that pose a radiation hazard or an unintentional radiation exposure risk to personnel. Grapples and mechanical latches which carry a fuel assembly should be designed for the fuel assemblies not to drop and to be damaged. The interlock of the FHE(see Table 1) should be designed as follows: 1) Underload and Overload interlock, 2) Up-Limit for a physical limitation to a hoisting, 3) Non-simultaneous Motion interlock against simultaneous hoisting and translation motions, 4) Grapple Release interlock, 5) Bridge and Trolley Travel interlock, 6) Translation Inhibit interlock, 7) Interfaced interlock between the RM (or SFHM) and the Fuel Transfer System (FTS) to ensure a proper equipment positioning during fuel transfer operations.

Table 1. Typical Interlock Design Requirement of Fuel Handling Equipment

	Overload/ Undeload	Up-Limit	Non-Simultaneous Motion	Grapple Release	Bridge /Trolley Travel	Trans-lation Inhibit
SFHM	X	X	X[a]	X	X[a]	X[a,b]
NFE		X				
FTS Carrier	X					
RM	X	X	X[a]	X	X[a]	X[a,b]

[a] Except when hand or manually actuated.
[b] Except with jogging circuit with approximately 1.5-mm (1/16-in.) increments.

3.2 Cooling, shielding and prevention of criticality

All the fuel handling equipment should be designed to prevent an accidental criticality during a fuel handling. In the event of an unexpected failure, the fuel assembly should remain in a safe condition and location with an adequate cooling and shielding. The component of the FHE should be designed so that the operator will not be exposed to $\geq$ 2.5 mrem/h from an irradiated fuel assembly elevated to the up position interlock in the pool at a normal operating water level.

3.3 Operability and maintainability

The FHE should be designed to operate in an efficient manner with a high degree of reliability. A high degree of efficiency can be achieved in the FHE by using simple and direct operations. Design life, radiation damage resistance, maintainability, and the ease of a decontamination should be evaluated during the design of the components of the FHE and they should be located in the accessible areas for an operation, testing, inspection, and maintenance. All the components which are normally submerged refueling water should be removable and replaceable with ease without lowering the refueling pool water levels.

4. Conclusions

The fuel handling process and interlock design requirements for the FHE based on the regulatory documents and the industrial codes and standards are reviewed. The design requirements for a protection from physical fuel damage and a radiological protection, adequate cooling and a prevention of a criticality, and the operability and maintainability for the FHE were established.

REFERENCES

[1] KEPIC NDD 57.1-2010 (ANSI/ANS-57.1, Design Requirements for Light Water Reactor Fuel Handling Systems), 1992 (Re-affirmed 2005).
[2] SRP 9.1.4, Light Load Handling System and Refueling Cavity Design, (2014).

Creep Assessment of Domestic Spent Nuclear Fuel During Long-Term Dry Storage Condition

You-Jin Kang, Dongjun Lee, Wontak Lee, Eunho Choi, Sangtae Kim, and Yong-Soo Kim*
Department of Nuclear Engineering, Hanyang University, 222 Wangsimni-ro, Seongdong-gu, Seoul 04763, Republic of Korea
*yongskim@hanyang.ac.kr

1. Introduction

In Korea, spent nuclear fuel has been stored in wet storage at the reactor site with safe method and regulation. After 2022, wet storage capacity approaches tolerance. Therefore, government have considered dry storage system. Dry storage is expected to have long term storage period of 40 years or more. In dry storage system, spent fuel suffer degradation. To avoid degradation, foreign government regulate peak cladding temperature and cladding hoop stress. But, there is no regulatory guideline in Korea [1]. In this study, we numerically evaluate creep behavior using computational method to consider effect of hydrogen effect on creep behavior.

2. Experimental

2.1 Selection of representative spent fuel

We employed 7 power history scenario proposed by Kim [2] to characterize the initial characteristic of spent nuclear fuel for dry storage condition. Figure 1 shows postulated power history by Kim [2]. For each cases, we assumed (1) spent fuel type is V5H-17 X 17 and (2) spent fuel has only 27, 42 and 55 GWD/MtU burnup.

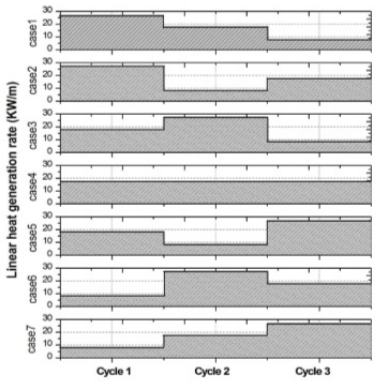


Fig. 1. Postulated power history [1].

2.2 Creep evaluation model

In this study, we used Chin model [3] to evaluate creep strain of spent fuel cladding. Table 1 shows Chin creep model. To treat the effect of absorbed hydrogen on Zircaloy cladding creep, we chose the Yamananka model [4]. This model stated that the hydrogen content changes the cladding property (Eq. 1). E_H and E_O is elastic modulus respectively. And C_H is hydrogen concentration.

$$E_H = (1 - 2.518 \times 10^{-4} \times c_H) \times E_O \quad (1)$$

Since the creep is critically affected by temperature history, we adopted temperature model by Dunham [5]. Dunham studied the temperature history during dry storage for high burnup fuel (>60GWd/MtU) using FALCON code. And we assumed that spent nuclear fuel has been stored in wet storage for 7 years and initial temperature after vacuum drying is exactly 400℃. Storage period is 60 years.

2.3 Computational Method

We used Fortran language to numerically evaluate creep behavior. Figure 2 shows the computational flow chart for creep assessment. Input 4 types of data, and computer go through 6 steps. After 6 steps, we obtained creep strain after 60 years.

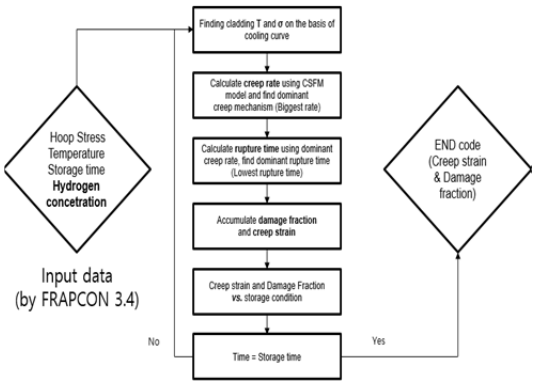


Fig. 2. Computational flow chart for creep evaluation.

3. Result & Discussion

3.1 Temperature decay

Figure 3 shows the temperature decay in dry storage condition for 60 years. This model does

not decay below 240℃. Thus, we can evaluate more conservatively.

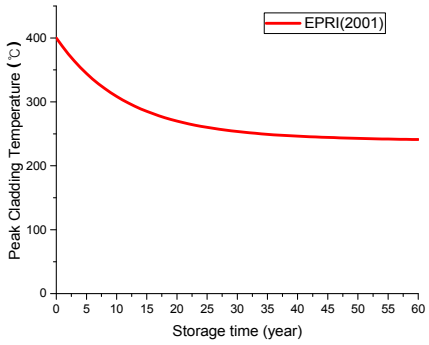


Fig. 3. Expected temperature decay in dry storage system.

3.2 Creep strain in dry storage condition

Figure 4 – 6 shows creep strain under dry storage for 60 years. We observed that strain dramatically increase during the first 5 years, and nearly saturates after 6 years. Maximum creep strain rate reaches 0.259% for case 7 of 27,000MWD/MtU fuel. For 42,000MWd/MtU fuel, creep strain rate reaches 0.402% for case 5. And strain rate for 55,000MWD/MtU fuel reaches 1.31% for case 5. Only high burnup fuel case (55GWD/MtU) exceeds regulatory guideline (strain rate = 1.0%). Furthermore, to understand trend and range of cladding damage with respect to the fuel burnup, we compared our results and Kim's data [1] with fuel burnup. At the low burnup (< 45,000 MWD/MtU), creep strain barely increases. However, creep strain increases dramatically at the high burnup fuel (> 45,000 MWd/MtU) (Fig. 7).

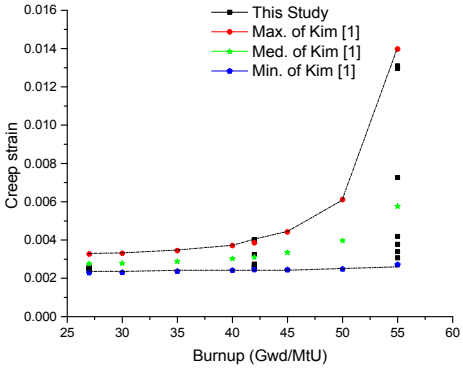


Fig. 4. The range of creep strain from this study and Kim.

4. Conclusion

In this study, we evaluated the creep strain rate of spent nuclear fuel during dry storage according to their power history and hydrogen effects. We adopted Chin creep model [3] and Yamananka hydrogen model [4]. Low burnup fuel (< 45,000 MWD/MtU) has low creep strain rate (<0.4%). But for some high burnup fuel (>45,000 MWD/MtU), strain rate exceeds regulatory guideline (strain rate=1.0%). Thus, this work can provide helpful guideline for establishment of dry storage regulation for high burnup fuel.

ACKNOWLEDGEMENT

This work was supported by the Human Resources Program in Energy Technology of the Korea Institute of Energy Technology Evaluation and Planning (KETEP) granted financial resource from the Ministry of Trade, Industry & Energy (No. 20204030200100) and the National Research Foundation of Korea(NRF) grant funded by the Korean government (MSIP: Ministry of Science, ICT and Future Planning) (No. 2017M2B2B10 72 888).

REFERENCES

[1] J.S. Kim, D.H. Kook, J.H. Sim, Y.S. Kim, "Review on Spent Nuclear Fuel Performance and Degradation Mechanisms under Long-term Dry Storage", JNFCWT 11(4): 333-340, (2013).

[2] J.S. Kim, H.K. Yoon, D.H. Kook, Y.S. Kim, "A Study on the Initial Characteristic of Domestic Spent Nuclear Fuels for Long-term Dry Storage", Nuclear Engineering and Technology, 45(3), (2013).

[3] B.A. Chin, M.A. Khan, J, Tarn, E.R. Gilbert, "Deformation and Facture Map methodology for Predicting Cladding Behavior during Dry Storage," Pacific Northwest Laboratory, PNL-5998, (1986).

[4] S. Yamanaka, M. Kuroda, D. Setoyama, "Mechanical Properties of Zirconium Hydride and Hydrogen Solid Solution." Transactions of the Atomic Energy Society of Japan, 1(4), (2002).

[5] R.S. Dunham, Y.R. Rashid, "Creep Modeling and Analysis Methodology for Spent Fuel in Dry Storage", Electric Power Research Institute, EPRI-1003135, (2001).

A Study on the Peening Effects of 316LN Stainless Steel Using the Contour Method to Enhance the SCC (Stress Corrosion Cracking) Resistance for SNF Dry Storage Canisters

Hwasoo Kang[a], Yongsoo Kim[a,*], Yongdeog Kim[b], Donghee Lee[b], and Ho Kyeom Kim[c]
[a] Department of Nuclear Engineering, Hanyang University,222 Wangsimni-ro, Seongdong-gu, Seoul 133-791, Korea
[b] KHNP-CRI, 70 Yuseong Daero 1312, Yuseong-gu, Daejeon, Republic of Korea, 305-343
[c] Materials Engineering, The Open University, Walton hall, Milton Keynes, MK7 6AA, UK
*yongskim@hanyang.ac.kr

1. Introduction

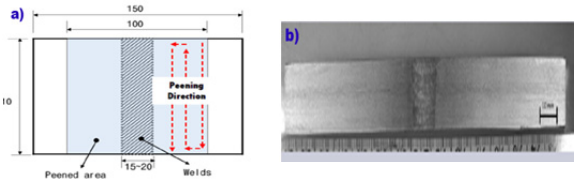
Chloride Induced Stress Corrosion Cracking (CISCC), a recently developed standing crack at the welded part of the spent fuel canister, is divided into three main causes: residual stress, corrosion environment, and type of metal materials. Residual stresses among these may occur in material processing such as welding and metal bonding and residual stresses have a significant impact on integrity depending on external load conditions.

In this paper, we would like to examine the peening effect on welds using the test piece of the Stainless steel 316LN machined as dry storage container material. Because the actual welded HAZ (Heat Affected Zone) area has a high residual stress, it is assumed that the result of residual stress before and after the test can be mitigated. And the same conditions shall be applied to the peened welded test specimen and the welded basic specimen respectively.

The distribution measurement of residual stress was carried out using the CM (Contour Method)[1]. Residual stress distribution of transverse surface in vertical direction, cutting surface of specimen is analyzed.

2. Methods

The test material used in laser peening was used in the SS 316LN. In this experiment, as a technology for improving metal surface with excellent application effect and low adverse effect, ALP (Air Laser Peening) which generates strong shock waves on the surface using high energy laser pulses is applied.



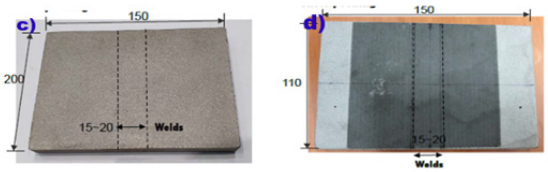


Fig. 1. Specimen arrangement; a)Peened layout, b)Welding, c)Before peening, and d)After peening [2].

The measurements of the residual stress in the test-pieces were conducted using CM at The Open University. The experiment was divided into two types of specimens before and after peening to confirm the change in residual stress. The CM used here is a technique that can provide a 2D residual stress map that acts on a plane or surface of interest using Bueckner's elastic superposition principle. The basic analysis stage consists of sample cutting, surface measurement, and data analysis (FE modeling) through finite element analysis methods.

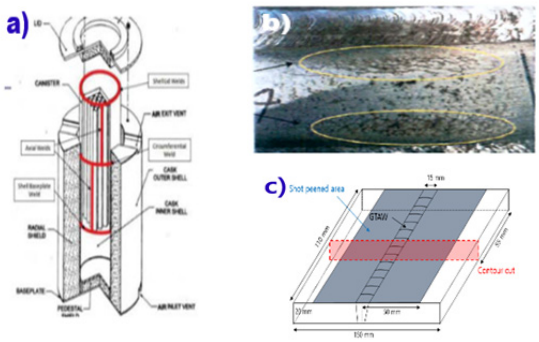


Fig. 2. a) Susceptible area, b) CISCC(HAZ), and c) Cutting arrangement.

Carefully cut the central part of the metal welding machine within the yield strength using WEDM(Wire Electric Discharge Machine), and use the elastic coefficient of metal considering the material characteristics of SS316LN. The precisely measured height difference of the cutting surface using laser is interpreted inversely by finite element method to analyze the actual residual stress.

The WEDM metal cutting technique is a non-

contact technique using electrically charged thin mobile wires. By ionizing and cutting materials with electrical energy, all cutting processes can be carried out in water where the temperature remains constant, minimizing plastic deformation by temperature.

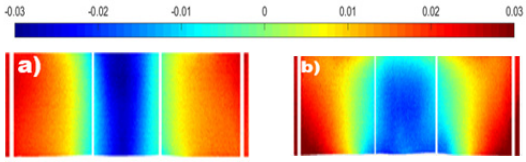


Fig. 3. Averaged surface raw data; a) Non peening and b) Peened.

Centering around the peening area, the height difference of the cutting surface perpendicular to the direction of the peening was measured by Contour, and Figure 3 shows the distribution of raw data of the mean values of both cut surfaces after Contour measurement.

The finite element analysis used the commercial program ABAQUS program, and the material value of the test specimen was applied equally with the Young's Modulus (Elastic coefficient, E=193 GPa) and the poisson's ratio (υ=0.30). After 3D FE Model Meshing, an analysis of elastic micro-modulation with 8 points of node isometric material properties is used.

3. Results

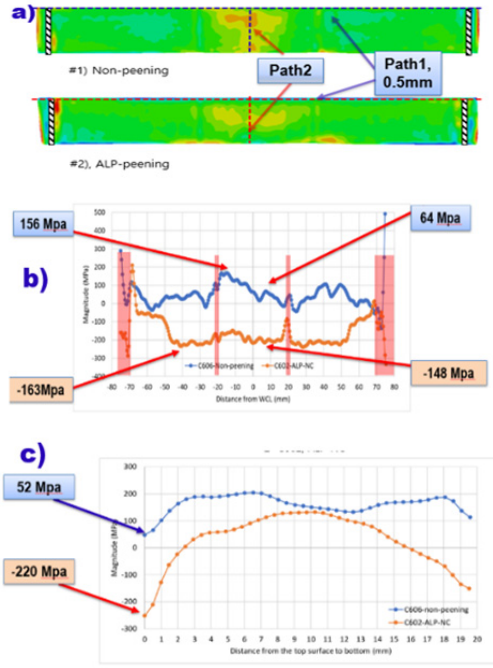


Fig. 4. a) Contour map, b) Line profiles for path 1, and c) path 2.

Figure 4. a) shows a comparison of residual stress distributions of specimens before and after peening, for Path 1& 2. b) shows the residual stress in the lateral direction at a location of 0.5 mm below the cutting plane for Path 1. The blue line is the BKG specimen that shows the residual stress of the weld area before peening. Residual stresses of up to 156 MPa are distributed around the welded parts. The red line shows the change in residual stress from -50 mm to 50 mm with peening technique. Up to − 148 MPa of compressive force has been applied to the weld area since the peening process. This comparative analysis indicates that the compression stress caused by the peening effect is being applied, and that effect shows a change of up to 300 MPa. c) Path 2 can identify the distribution of residual stress on the peening effect according to the depth direction at the weld centerline. It is observed that the compression stress on the surface is applied up to 220 MPa on the surface, and the effect on the peening gradually decreases with the depth direction.

Based on the above results, it was confirmed that the actual peening effect was acting within 2mm of the metal surface.

4. Conclusion

In this study, CM analysis, which is a residual stress measurement method, was performed using welding specimen applied with air laser peening technique. The above experiments used welded specimen made by Doosan used in dry storage containers.

As in the results of the experiment, because HAZ areas have high residual stresses, the CM analysis results predict that the application of the peening can mitigate tensile stress.

To supplement the reliability problem of the residual stress measurement results of CM analysis in the future, accurate residual stress evaluation shall be accompanied by comparison with the Hole Drilling measurement results, which is the result of different methods of measurement in the same specimen.

REFERENCES

[1] Prime M.B, 'Cross-sectional mapping of residual stresses by measuring the surface contour after a cut', (2001).

[2] Doosan, Residual Stress Measurement Report, Aug, (2020).

Study of Exchange Current Densities of Zn and La on Liquid Bi Electrode in Molten LiCl-KCl Salt

Jun Woo Park and Jong-Il Yun*
Department of Nuclear and Quantum Engineering, KAIST, Daehak-ro 291, Yuseong-gu, Daejeon 34141, Republic of Korea
*jiyun@kaist.ac.kr

1. Introduction

Pyroprocessing is one of the technological options to reduce the volume of spent nuclear fuel. In general, liquid metal electrodes used in the electrowinning process of pyroprocessing should avoid recovering Pu alone through the co-deposition of other transuranic elements (TRU). However, lanthanides can also be deposited on liquid metal electrodes together with TRU. Such a co-deposition of lanthanides with a high neutron absorption cross-section makes it inappropriate to recycle TRU nuclear fuel [1].

To utilize liquid metal electrodes effectively, the understanding and prediction of the electrochemical behaviors of elements should be clarified. One of the key electrochemical properties is the exchange current density. However, so far only a few studies have examined the exchange current density of elements on liquid metal electrodes.

In this study, Zn and La are selected as target materials due to their distinctive electrochemical behavior on the liquid Bi electrode. The exchange current density is analyzed by the linear polarization (LP) method. The electrochemical behavior of Zn and La on the liquid Bi electrode is investigated by comparing both results of Zn and La, which have to be taken into account when determining their exchange current densities.

2. Experimental

The electrochemical experiments were carried out in a glove box with concentrations of O_2 and H_2O less than 5 ppm. An electrical furnace was set to maintain the operation temperature of system at 773K. The current and voltage were applied with a potentiostat (SP-240, Biologics).

The three-electrode system was employed to measure electrochemical properties. Granular type Bi (99.999%, Sigma-Aldrich) was liquefied by melting in a cylindrical quartz cell and utilized as a working electrode. The tungsten (W) rod (99.95%, Nilaco) surrounded by a quartz tube was used as a lead electrode to connect the liquid Bi and the potentiostat. A 2 mm thick cylindrical W electrode (99.95%, Nilaco) was used as a counter electrode. An Ag rod (99.99%, Nilaco) was dipped into the LiCl-KCl melt with 10wt% AgCl (99.99%, Sigma-Aldrich), dissolved in a thin-end pyrex tube, in order to construct a 10wt% Ag|AgCl reference electrode.

Anhydrous LiCl-KCl (99.99%, Sigma-Aldrich) were utilized as background electrolyte. $ZnCl_2$ (99.999%, Sigma-Aldrich) and $LaCl_3$ (99.99%, Sigma-Aldrich) were prepared as target elements.

3. Result and Discussion

3.1 LiCl-KCl-$ZnCl_2$ on liquid Bi electrode

The cyclic voltammetry (CV) is performed before and after adding 1wt% $ZnCl_2$ in molten LiCl-KCl on the liquid Bi electrode. As shown in Fig. 1, the A/A' redox couple, which is unambiguously assigned to the Li redox reaction on the liquid Bi electrode, is observed. The B/B' redox couple is observed after the addition of $ZnCl_2$, indicating the Zn redox reaction.

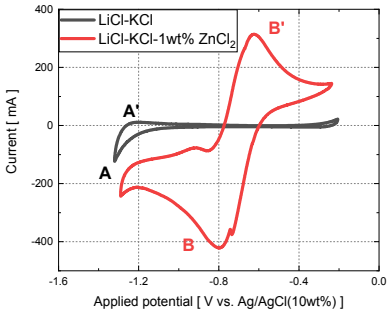


Fig. 1. CV of LiCl-KCl and $ZnCl_2$ at 1wt% in LiCl-KCl on the liquid Bi electrode.

It can be clearly seen that the B/B' peak is far away from the A/A' peak and the current of the blank electrolyte is comparatively small. Therefore, the Zn redox reaction is rarely affected by the Li redox reaction.

The LP method is applied to calculate the exchange current density. The LP method consists of a pre-deposition step and a linear sweep voltammetry (LSV) step. Chrono-amperometry (CA) is employed for the pre-deposition step and a scan rate of 3 mV/s is applied to the LSV

step. The exchange current density is calculated based on equation (1).

$$j_0 = \frac{RT}{nFA} \times \frac{i}{\eta} \quad (1)$$

Where j_0 is the exchange current density, R is the gas constant, T is the temperature, n is the number of transferred electrons, F is the faraday constant, A is the electrode surface area, i is the current, and η is the overpotential. The term of i/η is the slope of i-η near the equilibrium potential during the LSV step.

Fig. 2 shows the LP results of Zn. As the CA potential of the pre-deposition step is negative enough, the slope of the LSV and the equilibrium potential are reached similar values. The exchange current density of Zn on the liquid Bi electrode is calculated to be 6.62 ± 0.17 mA/cm^2 by using the LSV with pre-deposition for 3 seconds at -0.90 V, -0.95 V, and -1.00 V.

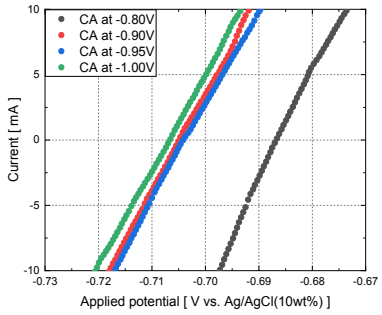


Fig. 2. LSV of LiCl-KCl-1wt% $ZnCl_2$ near the zero current region with various pre-deposition potentials.

3.2 LiCl-KCl-$LaCl_3$ on liquid Bi electrode

Contrary to the LiCl-KCl-$ZnCl_2$ system, the LiCl-KCl-$LaCl_3$ system shows a different electrochemical behavior in the CV of LiCl-KCl-$LaCl_3$, as shown in Fig. 3.

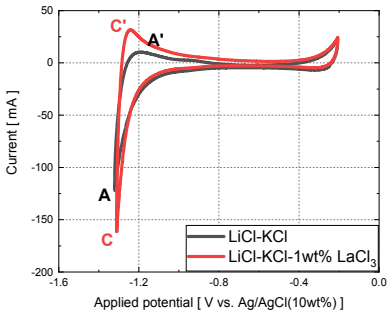


Fig. 3. CV of LiCl-KCl and LiCl-KCl-1wt% $LaCl_3$ on the liquid Bi electrode.

The C/C' redox peak overlaps very closely with the A/A' peak of the blank electrolyte. This infers that it is hard to distinguish the La redox reaction from the Li redox reaction on the liquid Bi electrode.

LP is also performed to calculate the exchange current density of La on the liquid Bi electrode. Fig. 4 shows the LP result of La. The slope and the equilibrium potential are changed drastically with varying CA potentials. In this system, as shown in Fig. 3, the Li reduction occurs almost simultaneously with the non-negligible current signal magnitude in the electrochemical window range of the La reduction. Therefore, it is difficult to achieve the electrochemical properties of only La on the liquid Bi electrode.

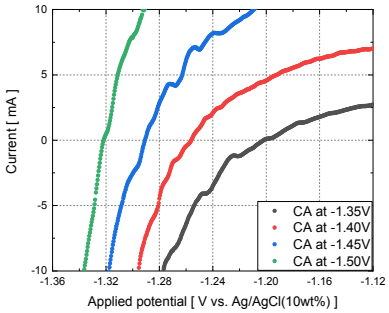


Fig. 4. LSV of LiCl-KCl-1wt% $LaCl_3$ near the zero current region with various pre-deposition potentials.

4. Conclusion

In this study, the electrochemical behavior of Zn and La on the liquid Bi electrode was examined. The CV was first performed to find out the redox behavior of Zn and La, and then the LP method was used to calculate the exchange current density. The exchange current density of Zn on the liquid Bi electrode is the value of 6.62 ± 0.17 mA/cm^2. However, the determination of the exchange current density of La was not possible due to the Li reduction overlapping with the reduction of La. This study shows that the exchange current density on the liquid metal electrode is only determined if the redox reaction of the elements is not affected by Li reduction.

REFERENCES

[1] J. Jang, T. Kim, G. Kim, D. Yoon, S. Lee, "Uranium recovery via electrochemical deposition with a liquid zinc cathode followed by electrochemical oxidation of rare earth metals", J. Nucl. Mater. 520, 245-251, (2019).

Decontamination Targets for Spent Nuclear Fuel Reprocessing in the Aspect of the Radiological Risk of Human Intrusion

Hyewon Shin, Younghwan Jeong, Jungho Hur, Jaeyeong Park*, and Il Soon Hwang
Department of Nuclear Engineering, Ulsan National Institute of Science and Technology, 50 UNIST-gill, Eonyang-eup, Ulju-gun, Ulsan, 44919, Republic of Korea
*jypark@unist.ac.kr

1. Introduction

The decontamination targets of spent nuclear fuel (SNF) reprocessing should be determined based on the radiological risks of a potential repository for the final wastes. Inadvertent human intrusion after the institutional control periods (ICP) would be the most critical factor leading to the radiological consequence and limiting the radioactivity concentration of the repository, because of the absence of the active control measure. In this paper, the DF of actinides is derived so that the radiological consequences of the inadvertent human intrusion into the repository are below 1 mSv or 20 mSv per a single intrusion.

2. Dose for the Inadvertent Human Intrusion

2.1 Dose Calculation Method

The radiological effect of the inadvertent human intrusion for the final reprocessing waste repository was estimated based on the Posiva's report [1]. The total dose rate the drilling worker or geologist is received was evaluated by considering external irradiation, inadvertent ingestion, and inhalation of dust. The shielding effect was not considered. The equations used are as follows:

$$D_{ext} = 1.4 \cdot 10^{-13} \cdot f_1 \cdot f_2 \cdot \frac{1}{x^2} \cdot \rho \cdot V \cdot t_{exp} \cdot \sum_i (E_i \cdot S_i) \quad (1)$$

$$D_{ing} = t_{exp} \cdot m \cdot \sum_i (I_{ing,i} \cdot S_i), \text{ and} \quad (2)$$

$$D_{inh} = t_{exp} \cdot R \cdot d \cdot \sum_i (I_{inh,i} \cdot S_i). \quad (3)$$

where D_{ext}, D_{ing}, D_{inh} are effective dose equivalent from external irradiation, ingestion, inhalation, f_1 is conversion factor from exposure to effective dose equivalent, f_2 is self-shielding factor, x is distance from source, E_i is, S_i is average activity concentration of radionuclide i in the sample, ρ is density of sample, V is volume of sample, t_{exp} is exposure time, m is intake by ingestion, $I_{ing,i}$, $I_{inh,i}$ are dose per unit intake by ingestion and inhalation of each radionuclide i, R is respiration rate, and d is air dust concentration.

The exposure time and distance from the excavated sample are assumed to be 1 hour and 1 meter. The volume of the excavated sample is 0.02 m^3. The variables in dose equations were obtained from the Posiva's report referring the conventional drilling technique and the diamond core drilling.

The SNF inventory of pressurized water reactor (PWR) with 3.1% enrichment and 45 GWd/t burnup, which is calculated by Monte Carlo simulation, is utilized.

2.2 Required DF for the Inadvertent Human Intrusion

Based on the dose calculation in the Posiva's report, DF was calculated to satisfy the dose criteria. The dose criteria 1 mSv and 10 mSv were set in the following reason. The IAEA's specific safety requirements of No. SSR-5 (Disposal of Radioactive Waste) states that when the annual dose is less than 1 mSv, the efforts to reduce the radiological consequences are not required [2]. The 10mSv of the Notice of the Nuclear Safety and Security Commission (NSSC) is considered as an alternative option for waste disposal. The final waste form is assumed as waste glass form whose conventional acceptable waste loading is about 10 - 20 wt.% [3].

3. Results & Discussion

3.1 Dose Calculation Method

The external, ingestion and inhalation doses from the excavated sample from PWR SNF are represented in Figure 1. The total dose from the excavated sample lies almost 1E+04 mSv even after 100,000 years, and the ingestion dose is the most dominant than others. For the ingestion and inhalation, TRUs contributes the largest portion for overall periods, and the doses of Sr and Cs are considerable for up to 300 years.

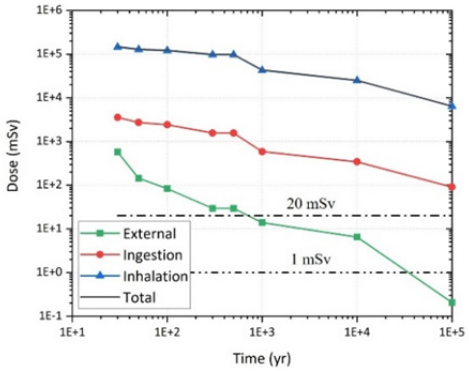


Fig. 1. Dose for the inadvertent human intrusion into the PWR SNF repository.

3.2 Required DF for the Inadvertent Human Intrusion

Since the ICP in Korea is less than 300 years, the dose of SNF for human intrusion must be lowered through reprocessing. LiCl-KCl salt waste, which contains the most TRU, was selected as a target among the waste in pyroprocessing of Korea Atomic Energy Research Institute (KAERI). After 300 years of institutional management in Korea, the human intrusion dose of LiCl-KCl salt waste is 103mSv, 100 times of 1mSv, and 10 times more than 10mSv. Almost all doses are occupied by the TRU. Therefore, partitioning of the PWR SNF should focus on actinide elements for the human intrusion and reduce the ICP for the final waste repository.

The DFs of Sr and Cs are fixed as 100 and 10,000 by the final stream of KAERI pyroprocessing [4]. The required DFs of U/TRU to meet 1 and 20 mSv are calculated according to the ICP and waste loading ratio of the final waste as shown in Table 1. To satisfy 1 mSv when used with pyroprocessing of KAERI, additional 8 and 110 U/TRU DFs are required for 10% and 20%, respectively.

Table 1. Required DF of U/TRU according to the dose criteria for the inadvertent human intrusion into the SNF reprocessing final waste repository when DFs of Sr and Cs are 100 and 10,000

Dose criteria (mSv)		1		10	
Waste loading (wt.%)		10	20	10	20
Required DF by ICP 300 years	U/TRU	8,000	110,000	700	3,000
Required DF by ICP 500 years	U/TRU	8,000	110,000	700	3,000
Required DF by ICP 1,000 years	U/TRU	3,000	12,000	300	1,100

When the TRU DF is 50,000 or more, the Sr dose occupies the second largest portion. Therefore, if Sr DF becomes 200, the required DF of TRU decreases to 55,000 and if 500, it goes to only 40,000.

4. Conclusion

KAERI Pyroprocessing also satisfies 10 mSv/event for human intrusion scenarios when 10 w.t.% of waste is charged, so that it can meet the standards of the Nuclear Safety and Security Commission notice. However, a DF of 1E+05 is required to increase the waste loading ratio to 20 w.t.% to reduce the volume of waste and to reduce the human intrusion radioactive hazard to 1 mSv/event.

ACKNOWLEGEMENTS

This work was supported by the National Nuclear R&D program funded by Ministry of Science and ICT and by the National Nuclear R&D program (NRF-2019M2D1A1067205) organized by the National Research Foundation (NRF) of South Korea in support of the Ministry of Science and ICT.

REFERENCES

[1] S.M. Smith, et al., Human Intruder Dose Assessment for Deep Geological Disposal, Posiva, Finland (2013).
[2] IAEA, Disposal of Radioactive Waste, IAEA, Vienna (2011).
[3] National Research Council, Waste Forms Technology and Performance: Final Report, The National Academies Press, Washington (2011).
[4] KAERI, An analysis and assessment of pyroprocess flow sheets for effective disposition of spent fuel, KAERI, Korea (2014).

Prediction of Radioactive Fission Gas Release During Loss-of-Coolant-Accident in a Spent Fuel Pool

Sun Ki Kim*
Korea Atomic Energy Research Institute,
Daedeok-daero 989-111, Yuseong-gu, Daejeon, Republic of Korea
*kimsk@kaeri.re.kr

1. Introduction

The accident scenario in a spent fuel pool (SFP) is classified into two types of accident scenario. The first scenario is a loss of cooling accident which causes a boil-off in the SFP. The second scenario is a loss of coolant accident which causes a partial or a full drainage in the SFP [1-4]. During the accident, Zircaloy-4 spent fuel cladding begin to react with high temperature air, and the heat generates by exothermic reaction between Zr and air. If the zirconium fire occurs during the accident in a SFP, the spent fuel cladding and pellets would be severely fragmented and powdered and it may lead to a massive radioactive fission gas release. Therefore, it is crucial to predict the quantity of radioactive fission gas release. In this paper, the prediction of fission gas release, CsI, in the spent fuel in Zircaloy-4 cladding ignition condition in a SFP.

2. Fission Gas Release during an Accident

2.1 Mechanism of Fission Gas Release

The assessment of the source term of spent nuclear fuel may be used for quantitative assessment of the proliferation of nuclear materials due to loss of coolant accident in the SFP. In the event of loss of coolant in the spent fuel pool, failure of the spent fuel rods is carried out by the immediate release of fission products. The fission gas in the free space of the fuel rod is immediately released, and the fragmentation and powdering of the UO_2 pellet are carried out under oxidation conditions between 400°C~500°C. Fission gases exhibit strong diffusion as the temperature rises, and most gases are released outside. During air oxidation at high temperatures of UO_2 pellet, the cracks and the grain boundary are separated into grain units. In addition, oxidation proceeds to the grain surface and is crushed in the form of popcorn, accelerating the powder conversion of U_3O_8. In this process, most fission gases contained in nuclear fuel materials are released externally.

2.2 Burn-up Effect of Fission Gas Release

Un-irradiated UO_2 pellet and spent UO_2 pellet differ in the release behavior of fission products by degree of burn-up. In the case of high burn-up UO_2 pellet, the amount of fission product is high, and various oxides result in small oxidation characteristics depending on temperature. In particular, the rim in the outer region is not nearly oxidized and the release of fission gases inside rarely occurs. Generally, in the case of intermediate burn-up UO_2 fuel, the separation and oxidized grain boundary shows typical oxidation characteristics, but the composition of the uranium compound, etc. hinders the release of fission gases by delaying some oxidation. In the case of low burn-up UO_2 fuel, the distinction between the grain boundary and grains, the UO_2 fuel appears to have been oxidized unambiguously fast, the conversion of U_3O_8 appears to be rapid, and most fission gases are released externally. The effects of c burn-up by the main influencing factors are as follows.

- Effect of temperature: Low BU < Middle BU < High BU
- Effects of burn-up: Low BU > Middle BU > High BU
- Oxygen potential: Low BU = Middle BU = High BU

3. Prediction of CsI during an Accident

Fig. 1 shows the calculation of the release of CsI. As shown in Fig. 1, CsI can be seen to be released rapidly at any point after a temporary incubation period. This point is immediately after the Zircaloy-4 cladding ignition in the event of an accident, which means that the integrity of the cladding is severely damaged and CsI is released in large quantities. Fig. 2 shows the Zircaloy-4 cladding ignition point and CsI release point compared to each other. As shown in Fig. 2, the CsI are shown to be released in large quantities immediately after the ignition point of Zircaloy-4 cladding in a spent fuel assembly with an initial decay heat of 5 kW. Early decay heat (4kW to 20kW) of the spent fuel accident scenario using MELCOR_SFP

code indicates that the initial decay heat is high, accelerating boiling, completely evaporating the coolant in the pool and rapidly increasing the temperature of the fuel cladding. If the initial decay heat is greater than 5 kW, Zircaloy-4 cladding ignites regardless of the initial level of the pool, which can be predicted to result in a large release of fission products (CsI).

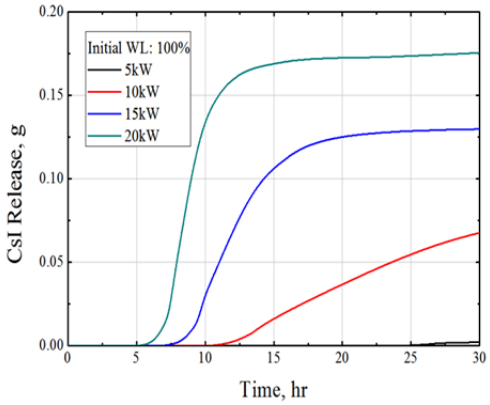


Fig. 1. CsI release during loss of coolant accident in a SFP with variation of decay heat.

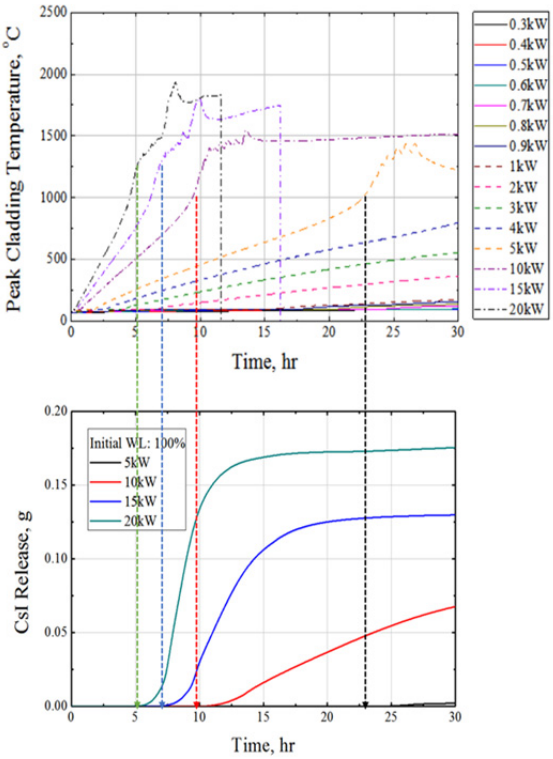


Fig. 2. Comparison of Zr-ignition time and CsI release time.

4. Conclusion

Since the ignition of the fuel cladding leads to the mass release of fission product such as CsI, it is necessary to evaluate the characteristics of the cladding ignition or fire which bring about massive release of fission products. This paper presents preliminary findings on the quantitative release of CsI, one of the fission products. It is expected that these findings would enhance the knowledge of fission gas release prediction.

REFERENCES

[1] S. Park, Effect of nitriding during air oxidation of zircaloy-4, Proc. of TopFuel 2015, September 13-17, 2015, Zurich, Switzerland.
[2] M. Steinbrück, A. Miassoedov, G. Schanz, L. Sepold, U. Stegmaier, J. Stuckert, Nuclear Engineering and Design 236, 14-16 (2006).
[3] C. Duriez, T. Dupont, B. Schmet, F. Enoch, Journal of Nuclear Materials, 380, 1-3 (2008).
[4] S. K. Kim, Zr-based Cladding Fire During Loss-of-Coolant-Accident in a Spent Fuel Pool, Proceeding of Korea radioactive Waste Society Autumn Meeting, October 2019.

2분과

사용후핵연료 처분전관리 (Poster)

Evaluation of Commercial Alloys for Application in Carbon-Anode-Based Oxide Reduction System

Min Ku Jeon[1,2,*], Sung-Wook Kim[1], Sang-Kwon Lee[1], and Eun-Young Choi[1,2]
[1]Korea Atomic Energy Research Institute, 989-111 Daedeok-daero, Yuseong-gu, Daejeon, Republic of Korea
[2]Department of Quantum Energy Chemical Engineering, University of Science and Technology, 217 Gajeong-ro, Yuseong-gu, Daejeon, Republic of Korea
*minku@kaeri.re.kr

1. Introduction

Recently, a new approach was introduced to oxide reduction (OR) process, in which oxide type used nuclear fuels are converted into metallic forms as a part of pyroprocessing. This new approach is a carbon-anode-based OR system which operates at higher voltage than the decomposition potential of LiCl (3.46 V at 650℃)[1]. Operating at a higher voltage indicates that the new system can achieve higher current than the traditional Pt anode system. However, the carbon-anode-based OR system produces Cl_2 and O_2 gases simultaneously at the anode. Due to the highly corrosive behavior of Cl_2 especially at high temperatures, the integrity of structural materials previously designed for O_2 environment needs revision.

Three commercial alloys of Stainless steel 316 (SS-316), Inconel X-750, Hastelloy C-276 were employed in this work to quantitatively evaluate corrosion characteristics of these alloys for application in the carbon-anode-based OR system. The nickel alloys were selected owing to their excellent corrosion resistance under a chlorine atmosphere[2].

2. Experimental

Specimens of the alloys were prepared by shearing 1.0 mm thick plates into 1 cm × 3 cm size. Four specimens were employed for each experiment (average 9.371 g for SS-316, 10.172 g for Inconel X-750, and 10.474 g for Hastelloy C-276). A quartz tube with a diameter of 4 cm was used as a reactor for corrosion experiments. The specimens were weighed and then loaded in the middle of the reactor, which was positioned horizontally. A heater was employed in the middle of the reactor in order to control the reaction temperature.

The corrosion experiments were conducted at various reaction temperatures (300–700℃) and gas compositions (30 mL·min^{-1} Cl_2, 20 mL·min^{-1} Cl_2 + 10 mL·min^{-1} O_2, and 10 mL·min^{-1} Cl_2 + 20 mL·min^{-1} O_2) with an Ar flow to maintain total flow rate at 200 mL·min^{-1}. The effect of reaction time was also investigated along with the above experiments.

The HSC chemistry software (version 9.5.1) was employed for thermodynamic calculations.

A scanning electron microscopy (SEM) with an energy dispersive X-ray spectroscope (EDS) was used for analysis of changes in the surface morphology and the composition, respectively.

3. Results and discussion

3.1 Stainless steel 316

The effects of reaction temperature and Cl_2–O_2 composition on the corrosion rate were investigated, and the results are shown in Fig. 1. It was found that the presence of oxygen significantly suppress the corrosion reaction and that the corrosion rate exponentially increased with an increase in the reaction temperature in a range of 300–600℃.

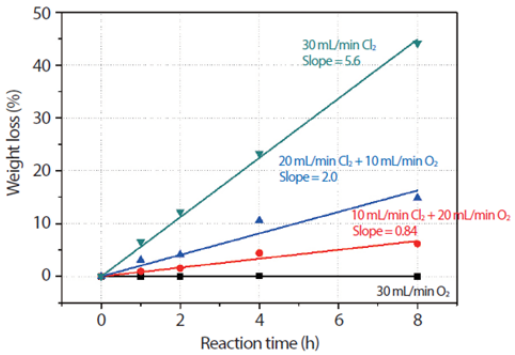


Fig. 1. Effect of Cl_2–O_2 composition on the reaction time–weight loss relationship at 600℃.

3.2 Inconel X-750

Superior corrosion resistance was observed in Inconel X-750 compared to that of SS-316. As shown in figure below, the corrosion rate of Inconel X-750 was only 1/22–1/41 of SS-316 under various Cl_2–O_2 compositions. It was identified that the presence of oxygen is a key factor which can profoundly reduce the corrosion rate as shown in Fig. 2.

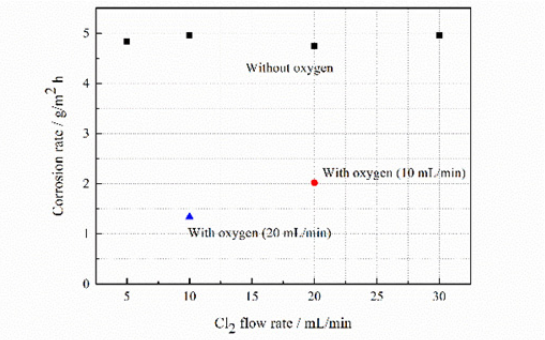


Fig. 2. Effect of Cl_2–O_2 composition on the corrosion rate of Inconel X-750.

3.3 Hastelloy C-276

Hastelloy C-276 exhibited similar corrosion rate values to those of Inconel X-750 under a 30 $mL \cdot min^{-1}$ Cl_2 + 170 $mL \cdot min^{-1}$ Ar flow in the temperature range of 300–700℃. However, the significant reduction in the corrosion rate under a Cl_2–O_2 mixed flow, which was found in SS-316 and Inconel X-750, was not observed in Hastelloy C-276 as shown in Fig. 3.

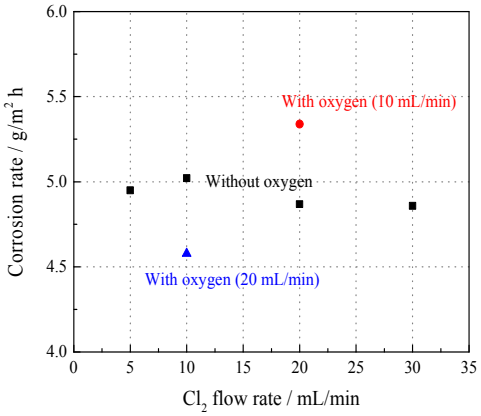


Fig. 3. Corrosion rate of Hastelloy C-276 as a function of Cl_2–O_2 composition at 600℃.

4. Conclusion

Among the three commercial alloys evaluated in this work, Inconel X-750 was identified as the best option for caron-anode-based OR application due to its slow corrosion rate especially under a Cl_2–O_2 mixed atmosphere. Hastelloy C-276 exhibited similar corrosion resistance to that of Inconel X-750 under a Cl_2–Ar condition, while the suppressing role of oxygen was not found in Hastelloy C-276. Although SS-316 exhibits severe corrosion in the presence of chlorine, it can be used at low temperatures (around 300℃), and the presence of oxygen is beneficial for lowering the corrosion rate.

REFERENCES

[1] S.-W. Kim, D.H. Heo, S.K. Lee, M.K. Jeon, W. Park, J.-M. Hur, S.-S. Hong, S.-C. Oh, and E.-Y. Choi, “A preliminary study of pilot-scale electrolytic reduction of UO2 using a graphite anode”, Nucl. Eng. Technol., 49(7), 1451-1456 (2017).

[2] M.H. Brown, W.B. DeLong, and J.R. Auld, “Corrosion by chlorine and by hydrogen chloride at high temperatures”, Ind. Eng. Chem., 39(7), 839-844 (1947).

[3] M.K. Jeon, S.-W. Kim, and E.-Y. Choi, “Corrosion behavior of stainless steel 316 for carbon anode oxide reduction application”, J. Nucl. Fuel Cycle Waste Technol., 18(2), 169-177 (2020).

[4] M.K. Jeon, S.-W. Kim, S.-K. Lee, and E.-Y. Choi, “Corrosion behavior of Inconel X-750 for carbon anode oxide reduction application”, J. Nucl. Fuel Cycle Waste Technol., 18(3), 355-362 (2020).

[5] M.K. Jeon, S.-W. Kim, S.-K. Lee, and E.-Y. Choi, “Corrosion behavior of Hastelloy C-276 for carbon-anode-based oxide reduction applications”, J. Nucl. Fuel Cycle Waste Technol., 18(3), 383-393 (2020).

Preliminary Analysis of the Anodic Gas Generated in the Oxide Reduction Process With Carbon Anode

Sang-Kwon Lee*, Sung-Wook Kim, Min Ku Jeon, and Eun-Young Choi
Korea Atomic Energy Research Institute
Daedeok-daero 989-111, Yuseong-gu, Daejeon, 34057, South Korea
*sklee79@kaeri.re.kr

1. Introduction

As we confirmed the possibility of the oxide reduction (OR) process with carbon anode we are struggling to replace the cost platinum anode with a carbon anode. The key issues in the carbon-based oxide reduction process are lowering the carbonate concentration in the molten salt below a certain level and applying higher cell potential than the platinum-based oxide reduction process [1]. Due to higher cell potential, it is inevitable to generate a mixture of anodic gases containing toxic and corrosive chlorine gas (Cl_2), oxygen (O_2), carbon monoxide (CO), and carbon dioxide (CO_2) gases. Considering the stability of the component of electrolytic reducer and control of operation conditions, it is essential to know the composition of the mixed gases generated on the carbon anode with respect to the electrolyte composition and operating cell potential, and so on.

2. Experimental

Figure 1 shows the schematic experimental apparatus utilized for this study. This study was performed in an electrochemical cell as shown in Fig.1. LiCl molten salt containing 1.28 wt.% Li_2O and 0.75 wt.% Li_2CO_3 as an electrolyte is prepared at 650 ^oC. Stainless steel rod (3mm dia.) and graphite (Alfa aser 3mm dia.) was used as a cathode and anode, respectively, and its immersion depth in the electrolyte was about 2.5 cm. Ni/NiO reference electrode was used to measure and control potential. Autolab 302N potentiostat was used for cyclic voltammetry to identify the standard potential for Li/Li^+ reaction. A Keysight E3633A power supply and Keysight 34461A digital multimeter were employed to control anode potential and current and to measure a cell potential, respectively. For analysis of mixed gases MAX300 -LG Mass spectrometer (Extrel) was used and calibrated with Cl_2 (1%, Ar base), CO/CO_2 (100/100 ppm, Ar base), O_2/CO_2 (500/ 100 ppm, Ar base) standard gases before the experiment.

The salt sample taken during the experiment was analyzed with Titrator Compact G20S (Mettler Toledo).

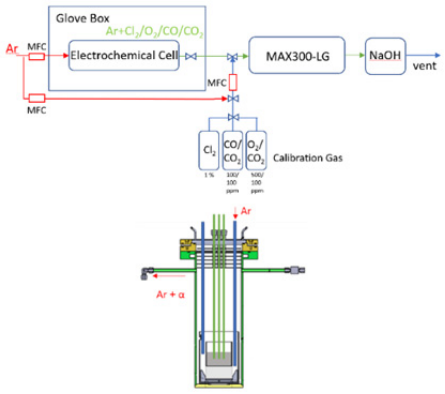


Fig. 1. Schematic experimental apparatus.

3. Results and Discussion

Figure 2 (a) shows the measured current and cell potential at various applied anode potential in the range of 2.5 to 5.5 V vs Ni/NiO. It was determined from the CV (not shown) that Li/Li^+ standard potential is -2.23 V vs Ni/NiO. Anode potential was controlled for 2 min at 2.5, 3.5, 4.5, and 5.5 V and then for 10 min at 4.5 V two times, which was repeated. Figure 2(b) shows the concentration of the O_2, CO, CO_2, Cl_2 generated in the cell during the experiment.

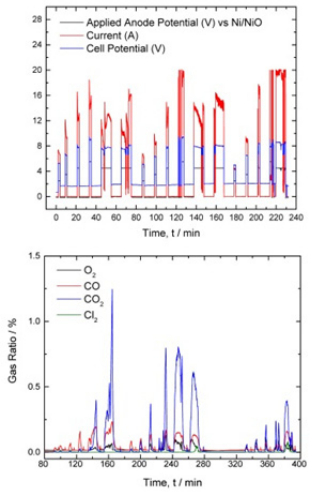
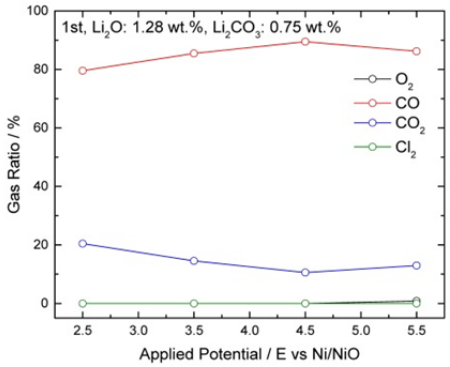
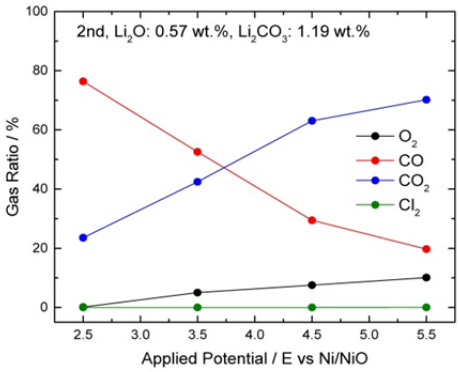


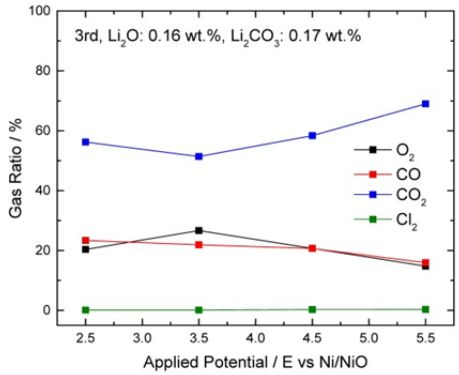
Fig. 2. Measured (a) electrochemical data and (b) gas concentration during the experiment.

Figure 3 shows the gas ratio at each potential (for 2 min at 2.5V ~ 5.5V) and cycle (for 10min at 4.5V). In the beginning, the salt contains Li_2O

1.28 wt.% and Li_2CO_3 0.75 wt.% and CO gas was the main component (80~90%) of mixed gas generated for 2 min at 2.5 V to 5.5 V. CO and CO_2 gases had a similar portion in the mixed gas generated for 10 min at 4.5 V and CO_2 gas became the main gas at second cycle. After these steps, the concentrations of Li_2O and Li_2CO_3 in the salt were changed to 0.57 wt.% and 1.19 wt.%, respectively. Oxygen ion was consumed from the anodic reaction with carbon and carbonate ion was increased from a reaction with the generated CO/CO_2 gas on the anode. In the second experiment for 2 min at several potentials, CO gas portion was reduced (76% ->20%) when the anode potential was increased to 5.5 V, whereas CO_2 gas portion was increased and O_2 gas was also increased gradually. CO_2 gas was the main gas during the 2 cycles for 10 min at 4.5 V.







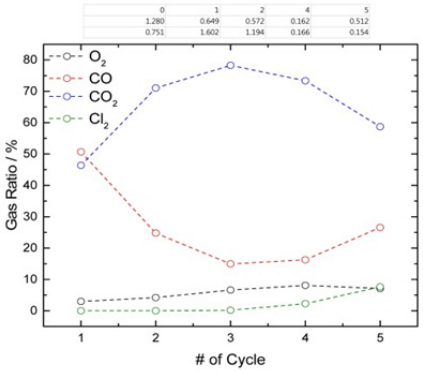


Fig. 3. Gas ratio at each potential (for 2 min at 2.5V ~ 5.5V) and cycle (for 10min at 4.5V).

After these steps, the concentrations of Li_2O and Li_2CO_3 in the salt were changed to 0.16 wt.% and 0.17 wt.%, respectively. Oxygen ion was continuously consumed from the anodic reaction with carbon and carbonate ion was also decreased. In the third experiment for 2 min at several potentials, CO_2 gas portion was about 60% and CO and O_2 had a similar portion (~20%) in the mixed gas regardless of the applied potential. CO_2 gas was the main gas during the cycle for 10 min at 4.5 V but decreased a little (~59%) and CO gas portion was increased (~27%) and Cl_2 gas was identified in this cycle.

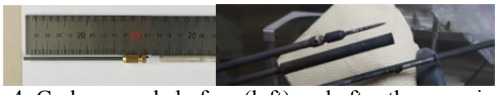


Fig. 4. Carbon anode before (left) and after the experiment (right).

Figure 4 shows the carbon anode before and after the experiment. It was confirmed that a large amount of carbon was consumed.

4. Conclusions

The ratio of $CO/O_2/CO_2/Cl_2$ in the mixed gas generated on the carbon anode during the experiments is significantly influenced by the applied potential and compositions of the salt, and the possibility of the toxic and corrosive Cl_2 gas generation increases with removing the oxygen ion sources in the salt.

REFERENCES

[1] S.-W. Kim, M.K. Jeon. H.W. Kang, S.-K. Lee, E.Y. Choi, W. Park, S.-S. Hong, S.-C. Oh, J. M. Hur, J. Radioanal. Nucl. Chem., 310, 463-467 (2016).

[2] J.-M. Hur, J.-S. Cha, E.-Y. Choi, ECS Electrochem. Lett., 3, E5-E7 (2014).

Review of Spent Fuel Pool Island of SONGS Units 2/3 in USA

Kwang Nam Kim, Sang Hoon Park, Kyong Won Han, and Kwan Sik Chun*
Korea Environment Testing and Analysis Laboratory, 63-1, Wondoo-ro, Gwangsan-gu, Gwangju, Republic of Korea
*kschun44@hotmail.com

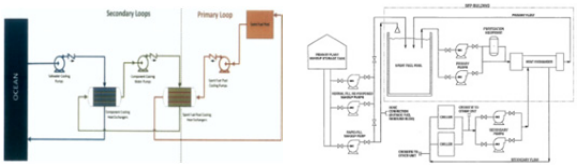
1. Introduction

Since the completion of construction in June 1977, Kori Unit 1 has ended 40 years of operation and has been permanently suspended on June 18, 2017, and is being pursued with the aim of completing the decommissioning by 2032, and subsequent nuclear decommissioning will continue. During decommissioning, spent nuclear fuel, which is the main source of radiation, should be stored in the storage pool for at least 5 years after permanent shutdown, and also appropriate management options should be established. Due to the permanent shutdown, the original cooling system of the SFP exceeds the required capacity, and so there can be a need to find a more efficient plan for the SFP management. And so, the project for SFP Islanding of SONGS Unit 2/3, which were shutdown in January of 2012 in USA, were reviewed to provide information which can be helpful to find more efficient plan for the management of SFP after permanently shutdown.

2. Difference between the original SFP and the SFPI cooling systems[1~3]

SFP water is circulated by the SFP pump through the cooled SFP heat exchanger. Heat is transferred to the equipment cooling water system, which is transferred to the seawater cooling system and eventually discharged to the Pacific Ocean, shown in Fig. 1[1]. The seismic category of the original SFP cooling system is classified as Category I, the quality is reclassified as Group D, and the quality grade is classified as Class III-AQ[3].

The cooling system of SFPI consists of a primary loop and a secondary loop, and the primary loop consists of 2 pumps with 100% capacity and 1 heat exchanger with 100% capacity, shown in Fig. 1[2]. The water of SFP is circulated through the heat exchanger by the primary pump, and the differential pressure in the heat exchanger is monitored to ensure that the secondary system is operating at a higher pressure than the primary system to suppress contamination to the secondary side. And the purification loop of this cooling system consists of two ion exchangers, which flow through the outlet in front of the primary heat exchanger. The Independent Cooling System is classified as the quality grade Class III-AQ and seismic Category III.



(a) Original system[1] (b) Islanding system[2]

Fig. 1. Schematic flow diagram of the SFP cooling systems.

3. Project cost for SFP Islanding

By the evidence on the decommissioning of in December 2014[4], the construction cost of SFPI for SONGS units 2 and 3 was estimated at $18,270,000 (based on US$ in 2014). Initially, it was planned for 15 months to select the best company for the decommissioning of SONGS units 2 and 3, but it took 2 years and 9 months. Practically the SFPI cost was reduces by $10,000,000 from the expected cost, and so $8,400,000 was recorded for the project of SFPI[5].

The reasons why the significant cost savings were done are due to the “Development of Request for Proposal” and the “Bid review process” and also to the operation of the “Cross-functional team”[5]. In addition, through the process of installation and competition, the most suitable supplier was selected and the optimal value was created on behalf of the customer. Some components were designed to meet the seismic requirements of the Uniform Building Code rather than seismic design requirements for nuclear power plant. And it was possible to reduce this cost because the implementation of some scopes such as the security mode for storage pools was not required[5].

4. Safety analysis of SFPI [6,7]

4.1 Design basis accidents

Although the probability of a fuel handling accident is very low, the impact stress applied to

the fuel clad by the fall of the spent fuel assembly during fuel handling does not exceed the allowable stress (49,000 psi.) of the unirradiated Zircaloy-4 fuel clad. On the other hand, the category in which the fuel assembly can fall into the storage pool and impact the stored spent fuel assembly can not exceed one assembly. However, if it were assumed that the fuel rods of 472 would be damaged by falling accident, the total effective dose equivalent in Exclusion Area Boundary(EAB) and Low Population Zone(LPZ) would be much lower values than the limit of 6.3rem[7].

Transport casks are handled in the cask loading pool area, and the liner of this pool is designed to withstand the impact of the transport cask falling[8]. Even if the transport cask falls to the bottom of the loading pool from the top and impacts the floor, the incident will not occur through the liner. However, assuming that all the fuels of 32 assemblies loaded in the cask were damaged due to the fall of the transport cask, the total effective exposure dose in the control room, EAB, and LPZ areas would be less than the limit values[6,7].

Assuming that the loss of all SFP cooling function would caused leakage of some of the stocks of spent fuel assemblies and release of radionuclides by boiling the SFP water, the estimated effective equivalent doses according to each location in the vicinity of such a boiling accident would be much lower than the limit values[6].

4.2 Beyond design basis accidents

Under the adiabatic heating of the hottest assembly in the SFP, of which the heat generation rate as of June 12, 2014 is 2,653 Watts, the time which takes to reach 900°C in an enclosed space can be estimated to meet the limit(10 hours).

As of June 12, 2013, the maximum dose rate in EAB based on direct and scattered radiation from spent fuel assemblies due to loss of water inventory in SFP was much lower than the limit[7].

5. Conclusion

It is possible to reduce the capacity of SFPI cooling system facilities and to adjust the grade down, and by introducing an air-cooled type, it is possible to simplify the overall cooling system by cutting off the use of seawater, thereby improving operational efficiency and economics. In addition, safety can be improved by reducing radiation exposure to the public as well as workers.

Even if there is a loss of pool water due to an accident/event in the storage pool, it is judged that there is no safety problem as the related systems are configured so that there is sufficient time to replenish the cooling water to the pool before boiling of the pool water.

It is quite encouraging that the facilities for SFP islanding of SONGS units 2 and 3 were able to be installed at a much lower cost than the originally estimated cost. So, the SONGS process applied for cost savings will be of great help in reviewing the introduction of SFPI at decommissioning of Korean nuclear power plants.

REFERENCES

[1] California Coastal Commission, “Notice of Coastal Development Permit : de Minimis Waiver”, Permit No.9-15-0162-W, 2015.04.03.

[2] SCE, Spent Fuel Pool ‘Island’ Description, Attachment A of ML15236A018, 2015.

[3] SCE, Response to NRC Request for Additional Information (RAI-016) Regarding Emergency Planning Exemption Request, Enclosure of ML14309A195, 2014.11.03.

[4] SCE, “Testimony on the Nuclear Decommissioning of SONGS 2 & 3”, 2014.12.10.

[5] SEC, “Testimony on the Reasonableness of the SONGS 2&3 Nuclear Decommissioning Activities and Costs Incurred during 2016-2017”, 2018.03.15.

[6] SCE, Updated Final Safety Analysis Report – Accident Analysis, Chapter 15, 2016.12.15.

[7] SCE, “Evaluation of Proposed License Amendment Request – Permanent Defueled Emergency Plan”, Enclosure of ML14092A314, 2014.03.31.

[8] SCE, “SONGS Spent Fuel Pool Island LAR-Draft RAI Responses”, Enclosure of ML15327 A410, 2015.11.19.

Final Design Review of Sealed Container for Storage and Transportation of Spent Nuclear Fuels

Sukwoo Hong*, Myungchul Park, Hyoungmun Kwon, Sunggeun Kim, and Jeongnam Jang
Korea Atomic Energy Research Institute, 111, Daedeok-daero 989beon-gil, Yuseong-gu, Daejeon, Republic of Korea
*hongsw@kaeri.re.kr

1. Introduction

KAERI-PIEF stores various types of spent nuclear fuels(SNF), such as assemblies, rods, specimens and fragments left after performing post-irradiation tests. In this regard, the National Assembly and citizen expressed concern about the storage of SNF in large city. Accordingly, KAERI announced the 'Comprehensive Measures for Safety of Nuclear Research' and decided to establish a technology base to transport the SNF in storage to the generation site, nuclear power plant(NPP). However, in order to safely store and transport such intact and damaged nuclear fuels, it must be sealed in a separate container. Overseas, sealed containers capable of storing or transporting SNF in the form of fragment and specimens, including intact and damaged rods, have already been developed and commercialized. However, there has been no case of developing or using such the sealed container until now in Korea. In this situation, uncertainty and risk must be minimized in order to fulfill the promises to the public. Therefore, KAERI tried to introduce the sealed container commercially available abroad. After careful evaluation internally and externally, the Westinghouse Electric Sweden AB(WSE)'s sealed container, Quiver, was introduced. And so far, the final design has been made to suit the situation of Korea such as KAERI and NPP. In this paper, KAERI briefly introduce the Quiver design and safety analysis results.

2. Final Design of Quiver

The Quiver that KAERI will use is designed to be handled safely throughout the nuclear cycle based on the type of nuclear fuel being stored. As shown in Fig. 1, Quiver was designed by dividing into two types according to the type of nuclear fuel. First, there is Type 1, which can seal intact and damaged nuclear fuel rods, and Type 2, which can seal nuclear fuel in the form of fragments and specimens. When nuclear fuel maintains the shape of a rod, it can be loaded directly in Quiver Type 1 like a general fuel rod basket. However, since the fuel rods subjected to the post-irradiation tests were cut into fragments and mounted specimens, they are first placed in a specimen container(SC), and SC was designed to be loaded in Quiver Type 2. In addition, these SCs were designed into two types. SC Type A was designed to contain fragments and SC Type B was designed to contain the mounted specimen. Each SC has a built-in filter, so the SC itself has a particle tight function. All sections and specimens will be loaded onto the SC in the PIEF hotcell, and the prepared SCs will be loaded onto the Quiver Type 2 in the pool. Quiver Type 1 can load up to 60 rods and Quiver Type 2 can load up to 28 rods of nuclear fuel. Both Quivers were designed to be lighter in weight compared to the assembly even when they are full of nuclear fuels or SCs. And it was designed so that there is no problem in handling or storage in PIEF and NPP by making the outer dimensions of Quiver the same as that of the existing assembly.

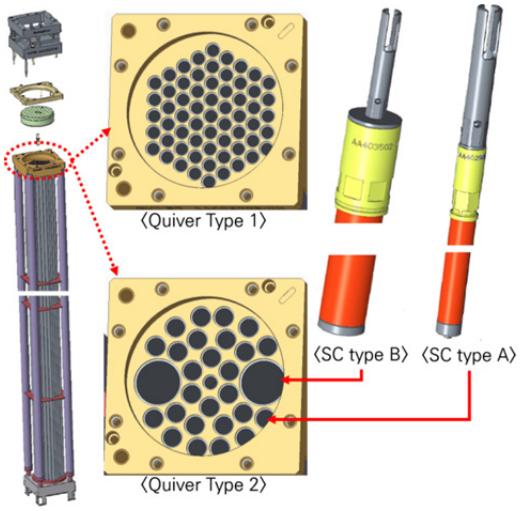


Fig. 1. Schematic of designed Quiver type 1 and type 2.

3. Safety Analyses of Quiver

The safety was confirmed by performing thermal, structural and criticality analysis for the two types of Quiver, respectively. However, the sealed containers such as Quiver, there are no clear laws or technical standards at home and abroad, so it was reasonably reflected by referring to the existing technical standards.

3.1 Thermal Analysis

In the case of thermal analysis, it was performed by applying very conservative values for the cooling time, heat transfer coefficient, thermal conductivity coefficient, ambient temperature and etc. As a result of the analysis, the function and safety of the Quiver were not affected in the storage conditions of the pool and the transportation conditions of the transport cask.

3.2 Structural Analysis

In the case of structural analysis, the structural safety of Quiver in various conditions was analyzed, such as the seismic load during storage, the stress when handling the Quiver, the drop test criteria (normal and accident conditions) of the transport cask according to IAEA SSR-6 and etc. As a result, the safety of Quiver was not affected under all conditions.

3.3 Nuclear Criticality Analysis

In the case of criticality analysis, the analysis was performed under very conservative conditions such as enrichment, density, 100% fission material in the Quiver tube and etc. As a result, it showed a very low effective multiplication factor, and it was very stable as it showed a much lower effective multiplication factor compared to that of a general nuclear fuel assembly.

4. Conclusion

In this paper, the shape of the final designed Quiver and the contents of safety analysis in the design process are described. All designs were made to be handled in various conditions such as KAERI-PIEF, transport cask, NPP and etc. Also, through safety analysis, it was possible to confirm the safety of the Quiver in various conditions.

Criticality Analysis of GBC-32 Cask With PLUS7 Fuels in Burnup Credit

Hyungju Yun*, Seunghyun Kim, and Hyeonwoo Oh
Korea Radioactive Waste Agency, 174 Gajeong-ro, Yuseong-gu, Daejeon 34129, Republic of Korea
*yhjnet1@korad.or.kr

1. Introduction

The capacity of on-site interim storage pools for used nuclear fuels (UNFs) generated by pressurized water reactors in South Korea is expected to saturate from 2024. This estimation accounts for the re-racking and on-site transportation of UNFs. One solution to this situation is to take UNFs out of on-site interim storage pools and store them in dry storage casks (DSCs). It is necessary to perform the accurate criticality safety evaluations of a cask system. The application of burnup credit which takes credit for the reduction of reactivity resulted from fuel depletion can increase the capacity in storage casks. However, the burnup credit application introduces lots of complexity into a criticality safety analysis such as the accurate estimation of the isotopic inventories and the burnup of UNFs. In this work, the criticality evaluations considering burnup credit were performed for Generic 32 PWR-assembly Burnup Credit (GBC-32) cask [1] with the UNFs discharged after Hanbit Nuclear Power Plant Unit 3 (HBN #3) using the SCALE 6.1/STARBUCS code and the MCNP 6 code.

2. Methods and results

2.1 Regulatory requirement

The criticality evaluation ensures that UNFs contained into a DSC remains subcritical under normal, off-normal, and accident conditions during dry storage. The effective neutron multiplication factor (k_{eff}) should not exceed 0.95 under all conditions [1].

2.2 Axial burnup distribution

The determination of the axial burnup profiles for the UNFs discharged from HBN #3 requires the design data of the nuclear fuels and reactor operation conditions. The initial uranium enrichment range of the nuclear fuels is between 4.10 and 4.52 wt. %. Fig. 1 shows the normalized axial burnup distributions for the reference and 20 NFAs discharged from HBN #3. The reference profile is a representative normalized PWR axial burnup distribution with an assembly-averaged burnup greater than 30,000 MWD/MTU [2].

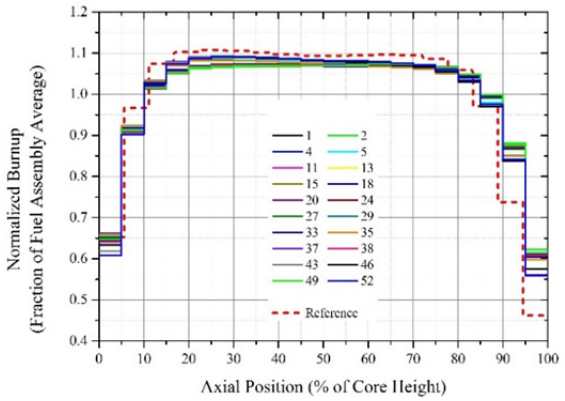


Fig. 1. Axial burnup distributions.

2.3 Depletion and criticality analyses

The evaluations consist of a two-step process: (1) the determination of isotopic compositions within UNFs loaded into a DSC by a depletion calculation and (2) the determination of the k_{eff} value for the cask by a criticality calculation [1]. The first step is to perform the depletion analysis by the SCALE 6.1/ORIGEN-S code with the new one-group cross-section libraries. The libraries were generated using the SCALE 6.1/TRITON code. The second step is to perform Monte Carlo neutron transport calculations using the SCALE 6.1/STARBUCS code and the MCNP 6 code to estimate the criticality for the GBC-32 cask. Fig. 2 shows the radial cross section of the GBC-32 DSC loaded with the PLUS7 UNFs.

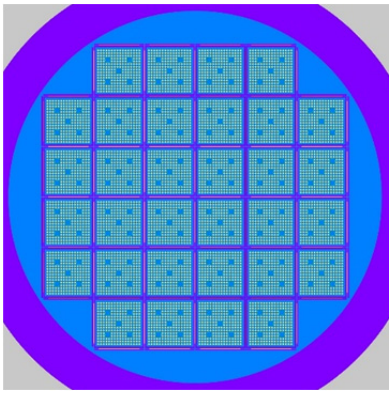


Fig. 2. GBC-32 DSC with PLUS7 UNFs.

2.4 Results and analyses

k_{eff} values of the GBC-32 cask system were calculated for the cooling times of 0, 20, and 30 years and plotted in Figs. 3, 4, and 5.

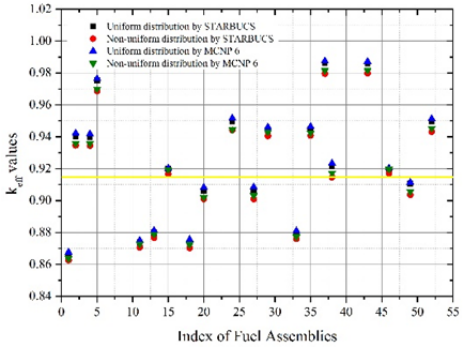


Fig. 3. k_{eff} values for the cooling time of 0 year.

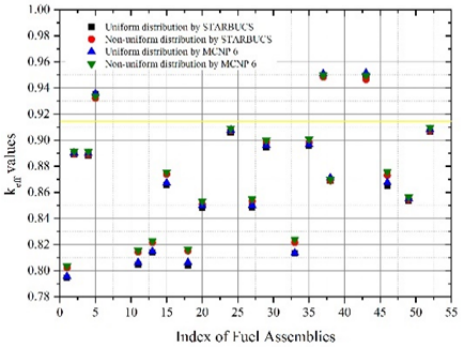


Fig. 4. k_{eff} values for the cooling time of 20 year.

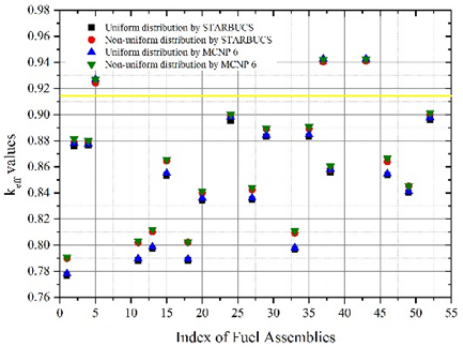


Fig. 5. k_{eff} values for the cooling time of 30 year.

The upper criticality safety limit, the yellow line, was set to be 0.9146 due to the uncertainties in Ref. 1. In Fig. 3, 12 UNFs for the cooling time of 0 year were not allowed to be stored in the cask because the k_{eff} values exceeds the safety limit. In Figs. 4 and 5, the UNFs except for 3 UNFs were allowed to be stored for the cooling times of 20 and 30 years. The UNFs that were not allowed to be stored had high initial enrichments and low discharge burnups.

However, the more UNFs were allowed to be stored in the cask as the cooling time of UNFs was longer. Because it occurred the disintegration of Pu-241 and the buildup of Am-241 due to β^--decay of Pu-241. In other words, Pu-241 of the fissile nuclides decreased with time and k_{eff} values of the cask system decreased. Fig. 6 shows the axial distributions for the atomic densities of Pu-241 at 3 cooling times.

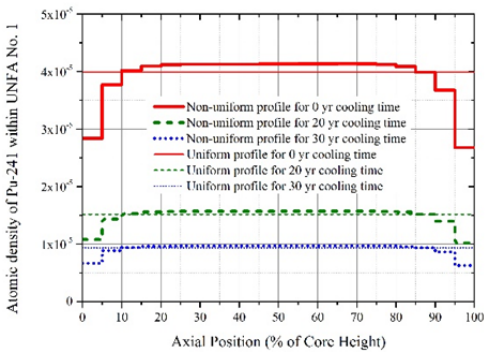


Fig. 6. Atomic density profile of Pu-241 with cooling time.

3. Conclusion

The criticality evaluation for burnup credit was performed for the GBC-32 cask with the PLUS7 UNFs using the STARBUCS and MCNP6 codes. k_{eff} values were calculated for the cooling times of 0, 20, and 30 years. From the results, the following conclusions are drawn.

(1) 12 discharged fuel assemblies for the cooling time of 0 year were not allowed to be stored in the cask. Most of the discharged fuel assemblies except for 3 discharged fuel assemblies were allowed to be stored for the cooling times of 20 and 30 years.

(2) The more UNFs were allowed to be stored in the cask as the cooling time of UNFs was longer. Because it occurred the disintegration of Pu-241 and the buildup of Am-241 due to β^--decay of Pu-241.

(3) In other words, Pu-241 of the fissile nuclides decreased with time and k_{eff} values of the cask system decreased.

REFERENCES

[1] J.C. Wagner, "Computational Benchmark for Estimation of Reactivity Margin from Fission Products and Minor Actinides in PWR Burnup Credit", NUREG/CR-6747, U.S. NRC (2001).

[2] J.C. Wagner, M.D. DeHart, and C.V. Parks, "Recommendations for Addressing Axial Burnup in PWR Burnup Credit Analyses", NUREG/CR-6801, U.S. NRC (2003).

Investigation on the Performance of the Porous Multi-Layer Hemisphere Crucible Cover for Cd Distillation

Sang Woon Kwon*, Junhyuk Jang, and Sung Jai Lee
Korea Atomic Energy Research Institute, 989-111 Daedukdaero, Yuseong, Daejeon, 34057, Korea
*swkwon@kaeri.re.kr

Abstract

The distillation of liquid cathode is necessary to separate cadmium from the actinide elements in the pyroprocessing since the actinide deposits are dissolved or precipitated in a liquid cathode. It is needed to separate the cadmium from the liquid cathode deposit to recover actinide elements in pyroprocessing. Vacuum distillation has been used for the separation of the cadmium from the liquid cadmium cathode deposit (LCC). It is important to avoid the escape of the liquid cadmium drops from the crucible of the LCC during the distillation. In this study, the performance of the Porous Multi-layer Hemisphere Crucible Cover was examined to develop a cadmium distiller for the pyroprocessing. Cadmium distillation experiments were carried out with the Porous Multi-layer Hemisphere Crucible Cover at various temperatures. A liquid or solid metal such as bismuth (Bi) or tungsten (W) was used as a surrogate for the actinide elements. The weights of the surrogate were compared before and after the cadmium distillation to examine the liquid Cd drop escape from the crucible. The surrogate loss was not found at 570 ℃ in the crucible equipped with the cover, whereas small loss was found in the crucible without the cover. The amount of the surrogate loss increased with increasing temperature in the crucible without the cover. There is a salt layer on the LCC crucible when the salt separation step is omitted prior to the distillation step. The cover salt should be distilled along with a cadmium. The covered salt raises the amount of the liquid cadmium escape from the crucible. The distillation experiments for the electrolyte salt and cadmium were carried out to examine the operation conditions of the distiller at various temperatures. The effect of the salt layer on the Cd loss was very high and the crucible cover was essential for the distillation of Cd with salt. From the results of this work, it can be concluded that the Porous Multi-layer Hemisphere Crucible Cover can be used to minimize the deposit loss by prevention of escape of liquid cadmium drop.

ACKNOWLEDGEMENT

This work was supported by a National Research Foundation of Korea (NRF) grant funded by the Korean Government (MSIP) (No. 2017M2A8A5015079).

Studies on the Dissolution of SrO From Simulated Fuel in LiCl-KCl Molten Salt

Chang Hwa Lee*, Seungwoo Paek, Seok-Min Hong, and Sung-Jai Lee
Korea Atomic Energy Research Institute (KAERI)
*chwalee@kaeri.re.kr

1. Introduction

Pyroprocessing is a technology that uses molten molten salt electrochemistry to recover U and fission products (FPs) from spent nuclear fuel to reduce the amount of high-level wastes and to recover U/TRUs and recycle them as metal fuel to enhance the resource utilization [1]. The pyroprocess consists of a head-end process that separates the spent PWR nuclear fuel from the cladding waste, an oxide reduction process that converts the oxide fuel to metal, and an electrorecovery process that recovers metallic U and U/TRU products from the converted fuel [2]. Various FPs can be captured separately in the head-end process or recovered by salt treatment to manage them separately, thereby significantly reducing the disposal area.

Cesium (Cs) and strontium (Sr) are representative high decay heat fission products, and are radioactive nuclides that must be specially managed to reduce the disposal area. Cs is volatilized together with Kr-85, C-14, Tc-99, I-129, etc. during the heat treatment step of the head-end process, On the other hand, the oxide form of Sr is dissolved as a chloride form through a chemical reaction with LiCl in 650°C LiCl-Li_2O salt during the oxide reduction process. However, only about 70% Sr is removed from the simulated fuel and the rest in the oxide form is remained in the converted metal fuel and transferred to the subsequent electrorefining (ER) process [3], which could affect the ER salt (eutectic temperature, UCl_3 concentration, etc.) as well as the following salt treatment process.

In this study, we examine the dissolution effect of Sr and Ba, a daughter nuclide of Sr in oxide forms, using LiCl-KCl salt for their efficient separations from the simulated fuel pretreated in the head-end process.

2. Experimental

An anhydrous LiCl-KCl eutectic salt was used with various concentrations of SrO and BaO for this study. Table 1 shows the components of simulated nuclear fuel based on standard PWR reactors (4.5% enrichment, 55,000 Mwd/tU burn-up, and 10-year cooling). First, assuming that the simulated fuel was dissolved in LiCl-KCl salt of 4 times amount of the fuel mass, 1/3, 1/2, 1, 2, and 3 times of SrO and BaO corresponding to the concentrations in the simulated fuel were added in the form of powder into 10 g LiCl-KCl salt to perform the dissolution tests. Second, the simulated fuel pellet was pulverized by heat treatment for 1 hour in an air atmosphere at 500°C, and then the microstructure of particles was observed using SEM. The difference in the solubility of SrO and BaO between the pellet- and powder-type simulated fuel in LiCl-KCl salt.

Table 1. Sessions for KRS conference

Element	wt %	Element	wt %
UO_2	95.3253	SrO	0.7589
Y_2O_3	0.0815	ZrO_2	4.2815
La_2O_3	0.2077	BaO	1.8178
CeO_2	0.4275	MoO_3	4.4321
Pr_6O_{11}	0.1956	RuO_2	3.5458
Nd_2O_3	0.6901	Rh_2O_3	0.4589
Sm_2O_3	0.1386	PdO	1.5496
Eu_2O_3	0.0232	TeO_2	0.5230
Gd_2O_3	0.0275	Total	100.00

3. Results and discussion

3.1 Dissolution of SrO and BaO in LiCl-KCl molten salt

Figure 1 shows the concentrations of Ba and Sr equivalent to 1/3, 1/2, 1, 2, and 3 times of SrO and BaO (as indicated in the inset) corresponding to the concentration of simulated fuel added in 10 g LiCl-KCl, which were analyzed by sampling the salt after a certain period of time. SrO and BaO are spontaneously chlorinated by the reaction with LiCl in 500°C LiCl-KCl salt as the following reactions.

$$2LiCl + SrO = Li_2O + SrCl_2 \quad (\Delta G = -7.213 \text{ kJ at } 500^oC) \qquad (1)$$

$$2LiCl + BaO = BaCl_2 + Li_2O \quad (\Delta G = -63.2 \text{ kJ at } 500^oC) \qquad (2)$$

The Sr and Ba concentrations at 0 hour present the added initial concentrations and the

concentrations at 1 and 3 hours indicate the quantitatively measured concentrations of Sr and Ba in the salt samples taken from the salt top using ICP-OES. Even considering the error of the initially measured values, it was confirmed that the most of SrO and BaO was dissolved within the initial 1 hour and there was no significant difference even in the 3-hour dissolution. This shows that the reaction of SrO and BaO with LiCl is kinetically fast and that most of them can be dissolved when SrO and BaO are solely exposed to the salt.

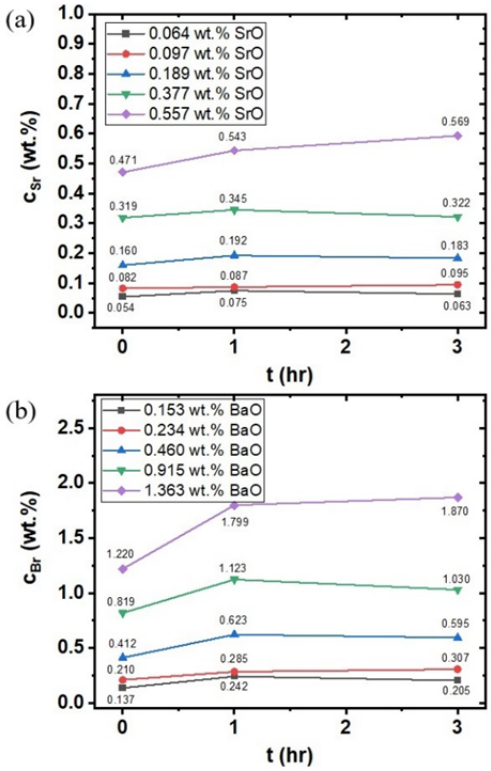


Fig. 1. Concentrations of Sr and Ba in 500°C LiCl-KCl salt with dissolution time.

3.2 Dissolution of Simulated fuel in LiCl-KCl molten salt

Figure 2 shows the simulated fuel containing SrO and BaO in pellet and powder forms by the oxidative heat treatment. The UO_2 pellets are pulverized by a volume expansion as the oxidation proceeds. The weight difference between the heat treatment reveals that the most of UO_2 was converted to U_3O_8. In the result of observing the microstructure of the pulverized simulated fuel particles using SEM (Fig. 3), the size of particles was ranged from 5 to 20 μm and fine cracks were also found on the particles.

In order to compare the dissolution characteristics of the simulated fuel in LiCl-KCl salt between pellet- and powder-type samples, dissolution experiments were performed by adding the pellets of 4.4 g and powder of 3.3 g in 500°C LiCl-KCl salt of 10 g for 3 hours, respectively. The color of the salt sample taken from the salt with powder-type fuel was revealed to be light brown compared to that of the salt with pellets, which might be associated with a partial dissolution of surrogate nuclides from the simulated fuel. The quantitative measurement for the samples will be conducted afterward.



Fig. 2. Simulated spent fuel pellets (a) before and (b) after heat treatment at 500°C for 1 hr.

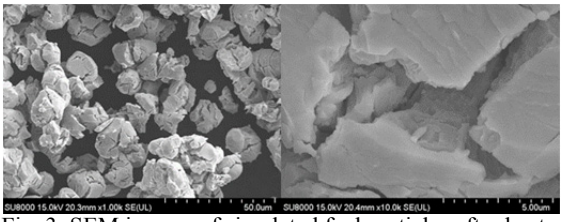


Fig. 3. SEM images of simulated fuel particles after heat treatment at 500°C for 1 hr.

4. Conclusions

The chlorination reactions of powdered SrO and BaO with LiCl were kinetically fast in 500°C LiCl-KCl salts for the concentration up to 3 times of the concentrations included in the simulated fuel. The dissolution experiments of simulated fuel revealed that the pulverization is more effective to remove the fission products by dissolving in LiCl-KCl salts.

REFERENCES

[1] J. J. Laidler et al., "Development of Pyroprocessing Technology", Prog. Nucl. Energ., 31, 131-140 (1997).

[2] G.-I. Park et al., "Recent Progress in Waste Treatment Technology for Pyroprocessing at KAERI", J. of Nucl. Fuel Cycle Waste Technol., 17(3), 279-298 (2019).

[3] E.-Y. Choi and S. M. Jeong, "Electrochemical Processing of Spent Nuclear Fuels: An Overview of Oxide Reduction in Pyroprocessing Technology", Prog. Nat. Sci.: Mat. Int., 25, 572-582 (2015).

A Study on the Road Transport Test With Full-Scale Cask for the Evaluation of Transportability After Storage

Woo-seok Choi*, JaeHoon Lim, Jongmin Lim, Gileon Jeong, and Sang Soon Cho
Korea Atomic Energy Research Institute, 111 Daedeok-daero989beon-gil, Korea
*wschoi@kaeri.re.kr

1. Introduction

The spent nuclear fuel discharged from nuclear power plants shall be safely managed for a long time. Currently, most of spent nuclear fuels in Korea are stored in wet storage facility in nuclear power plants, and will be transferred to an interim storage facility in the future, stored for a certain period of time, and transferred to the final disposal site. The spent nuclear fuel is degraded during the long-term storage period, which reduces structural integrity. Thus, the transport safety of degraded spent nuclear fuel is a major concern in many countries.

For the first time in Korea on September 15 and 16, a full-scale transport cask loaded with surrogate spent nuclear fuel was loaded onto a large trailer and the transport test was carried out. Load and strain data from the main locations of the fuel assemblies, transport cask and trailer were obtained.

Supported by the Ministry of Industry and Energy, the KAERI, KEPCO NF, KORAD, ACT, and DOOSAN participated in the test. The full-scale transport cask used for the test was manufactured by DOOSAN as a KORAD-21 transport cask developed with domestic technology. The fuel loaded into the transport cask was manufactured and provided by KEPCO NF as a simulated fuel assembly in the form of ACE7 and PLUS7. The KORAD conducted an analysis of transport routes.

2. Test Model

(Transport Cask) Transport tests using full-scale transport casks were planned to assess the 'transportability after storage' of spent nuclear fuel. The full-scale cask test model was selected as KORAD-21 [1]. Therefore, this test had an incidental effect of verifying the manufacturability of the KORAD-21 cask.

(Surrogate fuel assembly) The surrogate spent fuel assemblies used in this test were new fuel assemblies with no history of combustion. This is because it is impossible to use the spent nuclear fuel assembly as it is, and it is also impossible to attach sensors to the spent fuel assembly. In addition, the pellets inside the fuel rods were replaced with the same shape of lead because the nuclear material could not be used, so the weights were equally matched. Therefore, the fuel assembly used in the test does not emit heat and radioactivity. Two bundles of ACE7 and PLUS7 were used in the test. For the remaining 19 bundles, a pile of concrete equal to the weight of the fuel assembly was produced to keep the overall weight similar.

(Decision of Sensor locations) As trailers carrying transport cask of spent nuclear fuel drive on the road, the spent nuclear fuel receives vibrations and shocks. The load passed from the ground to the trailer platform via the trailer's wheels is passed through the cradle to the transport cask. The load is then transferred into the fuel assembly via the disk assembly and basket inside the transport cask [2]. In some sections of this load path, the load is amplified and in others the load is attenuated. The characteristics of load transfer within the load path must be identified to ultimately reduce the load reaching the spent nuclear fuel and to ensure safety during transport.

For this test, a total of 100 channels of sensors were attached to the major positions of trailers, cradle, casks, canisters, disk assemblies, baskets and fuel assemblies located on the load transfer path. The accelerometers and strain gauges were also attached in the direction of the length of the fuel rod located in the center of the fuel assembly as shown in Fig. 1 and Fig. 2 to assess the behavior of the fuel rods under the transferred load. Through the transport test, the integrity and durability of the nuclear fuel rods will be evaluated based on the data measured from the fuel rods.

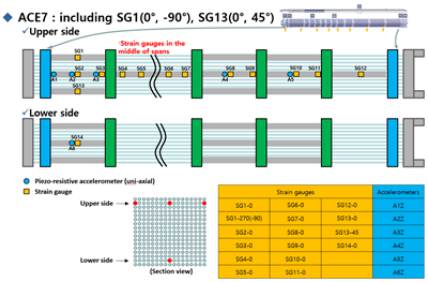


Fig. 1. Sensor type and location of fuel assembly ACE7.

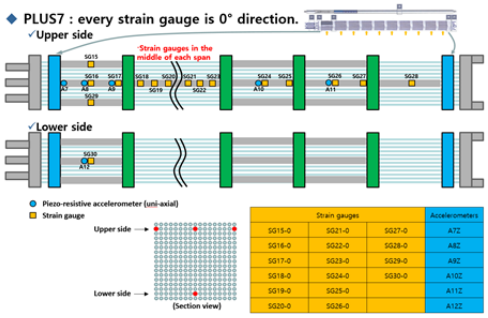


Fig. 2. Sensor type and location of fuel assembly PLUS7.

3. Performance of Transportation Test

The road transport test was carried out on a road inside DOOSAN. Handling test, circulation test, and straight lane test were performed for normal transport conditions. In the circular test, a trailer loaded with cask circled the 4.5 km road in DOOSAN eight times to measure the data as shown in Fig. 3. There were sections such as uphills, downhills, rails, curved lanes, and 90 degrees of turn. The test data was successfully obtained for each test condition. Quantitative assessments of what loads have been delivered from key locations of the transport system, including the fuel assembly, using the acquired data will be carried forward in the future.


Fig. 3. Road transport test.

4. Summary

Test data from various road conditions obtained through this test will be used as a safety demonstration data for spent nuclear fuel transportability and is expected to contribute greatly to enhancing public acceptance of spent fuel transport.

Acknowledgements

This work was supported by the Korea Institute of Energy Technology Evaluation and Planning (KETEP) and the Ministry of Trade, Industry & Energy(MOTIE) of the Republic of Korea (No. 2018170201770).

REFERENCES

[1] Choi, W. S., Lim, J. H., Lim, J. M., Yang, Y. Y., Jeong, G. E., Cho, S., "Current Status of Korean Multi-modal Transportation Test(MMTT)," Korea Nuclear Society Virtual Spring Meeting, (2020).

[2] Lim, J. H., Cho, S. S., Yang, Y. Y., Seo, K. S., and Choi, W. S., "Establishment of Data Acquisition System for Road and Sea Transportation Test of Surrogate Spent Nuclear Fuel under Normal Conditions of Transport," Korea Radioactive Waste Society Fall Meeting, (2019).

Comparison of Dimensional Conformity of Surrogate Metallic Fuels in Different Additive Manufacturing Processes

Young-Ho Lee*,[1], Sang-Kyu Park[2], Kiho Kim[2], and Jeong-Yong Park[2]
[1]Advanced 3D Printing Technology Development Division, Korea Atomic Energy Research Institute
[2]Innovative Fuel Technology Development Division, Korea Atomic Energy Research Institute
*leeyh@kaeri.re.kr

1. Introduction

Recently, additive manufacturing (AM) technology is significantly attractive in all fields of manufacturing industries. In particular, the development of innovative systems for the next-generation nuclear power plant is underway by introducing AM technology. Although the AM technologies are necessary to advance the manufacturing process specific to the material systems in nuclear energy, they do not deal with the uranium fuel itself, which is the most important material of the reactor. The advantages of AM for manufacturing intermetallic uranium compounds such as U_3Si_2, they have a narrow compositional range, which requires specialized techniques that are distinct from the conventional fabrication methods. Until now, it is difficult to show meaningful results of AM studies for achieving acceptable density and microstructures for fuel materials. Unlike air processing of UO_2 manufacturing, however, metallic fuels such as U-Zr alloys should be processed in inert atmospheres because applicable AM methods require their powers that are vulnerable in air. Although there are many practical problems in handling uranium powder in AM methods, it was proposed that the most promising areas where AM can have significant impact on conventional nuclear fuel fabrication are known to the area of advanced matrices for particle and dispersion fuels free from the constraints of conventional processing [1]. This study presents a preliminary trial, focusing on the dimensional stability of manufactured surrogate metallic fuels by applying various additive manufacturing (AM) methods, which significantly impacts the metallic fuel fabrication process.

2. Fuel fabrication

There are many AM processes that used in a wide variety of industry including powder bed fusion (PBF), selective laser melting (SLM), Directed energy deposition (DED), material extrusion, stereolithography, etc. Among those, PBF and DED methods can be suitable for metal printing to heap up conventional fuel shapes. Table 1 summarized typical advantages and disadvantages of these two methods for fabrication of nuclear fuel.

Table 1. Summary of Advantage and Disadvantages of AM method that used in this study

Method		Remarks
PBF	A	Large investment in development in the industry Possible to apply complex geometry
	D	Limited size of printed component Poor surface finish (post processing)
DED	A	Less metal powder and heat input Better microstructures due to low heat input and high solidification rate Very large or small parts are feasible Variety of composition
	D	Difficult to overhung features Process complexity and slow build rate Expensive infrastructure Safety issues such as the use of inert gas, metal powders and a high power laser

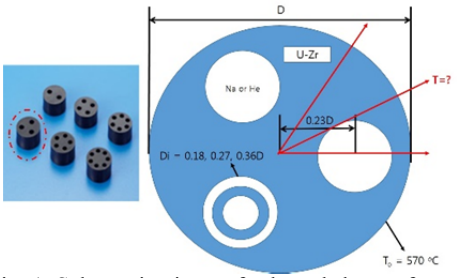


Fig. 1. Schematic views of selected shape of metallic fuel for application to AM process [3].

Previous study focused on the shape of innovative fuel shapes, which has various holes for improve thermal conductivity and fuel performance [2-3]. In this study, a cylinder fuel with 3 holes dispersed at 120° intervals is selected for manufacturing surrogate metallic fuel with Fe-based alloys powder in PBF and DED methods. Also, different hole sizes were also selected to have 0.18, 0.27 and 0.36 with ratio of hole to fuel pin diameter (i.e., diameter ratio, Fig. 1) and this area is assumed to fill with

sodium or helium gas for comparing heat conductivity effects.

3. Dimension conformity

Fig. 2 shows the schematic views and measured surface roughness of as-fabricated surrogate metallic fuels by using PBF and DED methods. The designed dimension of metallic fuel is 5.54 mm in outer diameter and 10 mm of height. Internal hole size is designed to 1.0, 1.5 and 2.0 mm. In cased of the DED method, however, internal hole buckling occurred during the stacking process, which made it difficult to maintain its complete shape. So, the cylinder shape without internal holes was fabricated to compare the dimension conformity according to the AM methods. Unlike the DED method, it was confirmed that metallic fuel can be manufactured with stable dimensions regardless of the internal hole in the PBF method. Consequently, the PBF method is considered as a suitable method for fabricating metallic fuel in a view point of dimension conformity and mass production. However, there are many problems related to U handling, powder consumption, and contamination by heating and melting, etc., it is necessary to carefully consider the productivity and suitability of AM methods, development of improved manufacturing process, etc.

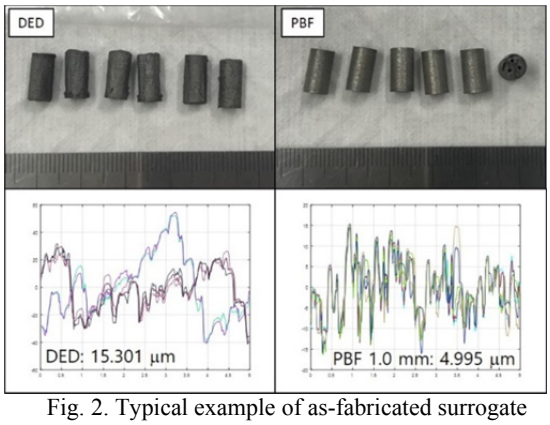


Fig. 2. Typical example of as-fabricated surrogate metallic fuel with three internal holes and measured surface roughness.

ACKNOWLEDGEMENT

This work was supported by a National Research Foundation of Korea (NRF) grant funded by the Korean government (MSIP) (2017M2A8A5014888).

REFERENCES

[1] A.T. Nelson, “Features that further Performance Limits of Nuclear Fuel Fabrication: Opportunities for Additive Manufacturing of Nuclear Fuels”, ORNL/SPR-2019/1183.

[2] Y.H. Lee, S.U. Lee, S.G. Park, B.O. Lee, K.H. Kim, J.Y. Park, “Temperature Distribution of Innovative Metallic Fuel with Multi-hole Shapes”, Proc. Of the KRS 2019 Autumn Conference, 17(2), October 30~November 1, 2019, Jeju.

[3] Y.H. Lee, S.G. Park, B.O. Lee, K.H. Kim, J.Y. Park, “A Study on Innovative Metallic Fuel Shapes and Their Manufacturing Requirements”, Proc. of the KRS 2018 Fall Conference, 16(2), October 31-November 2, 2018, Jeju.

The Effects of Hydrogen Content and Hydride Morphology on the Ductile to Brittle Transition Temperature (DBTT) for Zircaloy-4 Cladding

Ho-a Kim* and Jae-soo Noh
Atomic Creative Technology Co., Ltd., 1434, Yuseong-daero, Yuseong-gu, Daejeon, Republic of Korea
*pissan@hanyang.ac.kr

1. Introduction

As the fuel burnup increases, the concerning of brittle failure for the spent fuel cladding becomes greater. The brittle failure of the claddings may occur in handling, storage and transportation of SNF.

Ductility of SNF claddings can be reduced due to zirconium hydrides which are generated during reactor operation and transformed afterwards, i.e. during dry storage.

Shock and vibration are expected to occur during the transportation. It is understood that the hydrogen content and hydride morphology could affect the ductility of the claddings against these external loads. Therefore, it is important to know ductile to brittle transition temperature (DBTT) of metal cladding which can suffer cooling process in dry storage.

The most probable failure mode during transportation of SNF shall be longitudinal crack due to pinch loads and it may occur depending on the temperature of the cladding.

The object of this study is to understand how the content of hydrogen and hydride morphology in the cladding affects the functioning of the cladding, especially when confronting pinch load by estimating the DBTTs of the various conditions of the claddings by Ring Compression Test (RCT) which is believed to simulate the pinch load.

RCT were conducted to measure offset strain of Zircaloy-4 cladding against pinch-load and then DBTT was evaluated through the transition of offset strain to certain level.

2. Experimental

2.1 Specimen preparation

Stress-relieved (SR) Zircaloy-4 cladding tube was used in this study. Three types of specimen were used: CH, RH-90, and RH-150. CH is circumferential hydride specimen and RH is radial hydride specimen. Hydrogen was charged in CH and RH specimens using a Sievert type apparatus aimed at 200-700 wppm, and RH specimens were pressurized with Ar gas under 90 and 150 MPa hoop stresses. CH and RH specimens were classified in Table 1.

Table 1. Classification of the CH and RH specimens

Specimen	Hoop stress (MPa)	Hydrogen concentration (wppm)		
		1	2	3
CH	0	200	400	700
RH-90	90	200	400	700
RH-150	150	200	400	700

2.2 Ring compression test (RCT)

Ring compression test is a test method that can simulate pinch-load during the normal transportation of RCT. RCT was used to evaluate the relative effect of the circumferential and radial hydride. Compression tests were conducted with 10 mm rings of the CH and RH specimen using a universal testing machine. Load-displacement curves were obtained from the RCT test results and offset strain [1] was calculated from the load-displacement curves. Before and after the tests, images on hydride morphology of the specimens were observed by optical microscope and crack path and length will be evaluated by analyzing the hydride morphology images.

3. Results and discussions

3.1 Specimen hydride morphologies

Fig. 1 and Fig. 2 show hydride morphologies of the CH and RH specimens before/after the RCTs. As hydrogen concentration increases, the content of precipitated hydride also increases in both the CH and RH specimens. In the RH specimens, the fraction of radial hydride decreases as hydrogen content increases. In Fig. 2, cracks of the CH specimen occurred at 3 o'clock and 9 o'clock, but cracks of the RH-150 specimen occurred at 6 o'clock and 12 o'clock. At the beginning of deformation, the stress at 12 o'clock and 6 o'clock is the highest and the stress at 3 o'clock and 9 o'clock is higher as the deformation progresses. Therefore, 12 o'clock and 6 o'clock are brittle fracture and 3 o'clock and 9 o'clock are ductile fracture.

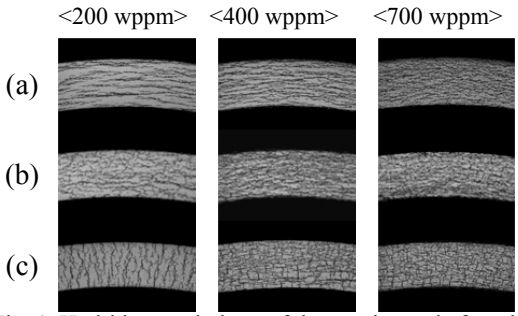


Fig. 1. Hydride morphology of the specimens before the RCTs: (a) CH, (b) RH-90, and (c) RH-150 specimens.

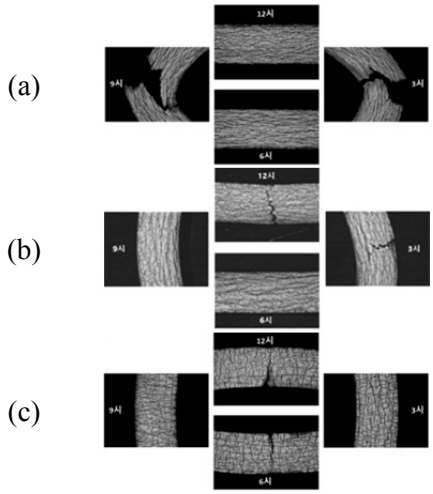


Fig. 2. Hydride morphology of the specimens (RT, 400 wppm) after the RCTs: (a) CH, (b) RH-90, and (c) RH-150.

3.2 Ductile to brittle transition temperature (DBTT) by offset strain

To classify ductile and brittle failure, Billone [1] suggests "offset strain" concept. Offset strain is determined from the permanent change in ring diameter after unloading and/or by the offset displacement [2]. Offset strain vs. temperature of the specimens is shown in Fig. 3. From the transition of offset strain, DBTTs were evaluated. In the CH specimens, DBTTs are located around 50 ℃ regardless of hydrogen content. The CH specimens are sufficiently ductile even at room temperature and very ductile even at a temperature of 50 ℃. In the RH-90 specimens, DBTTs of 200 and 400 wppm are located around 75 ℃ and DBTT of 700 wppm is located around 125 ℃. Overall, as the hydrogen content increases, the ductility tends to decrease, and therefore resulting in higher DBTT. However, in RH-150 specimens, DBTTs of specimen with 200 and 400 wppm H are located around 225 ℃ which is higher than DBTT of the specimen with 700 wppm H (175 ℃). It seems that as the hydrogen content gets lower, the proportion of radial hydrides that can act as crack paths gets higher, accordingly resulting in more brittle.

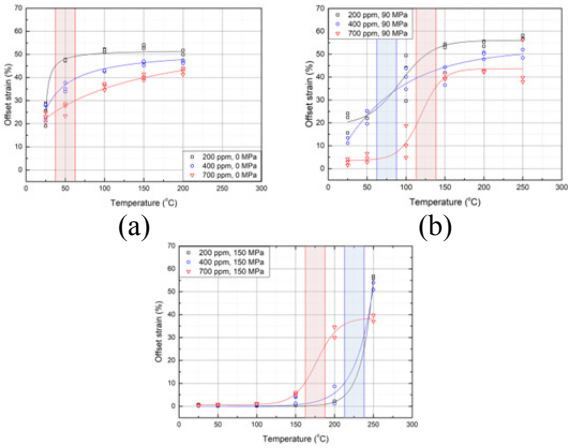


Fig. 3. Offset strain vs. temperature of the specimens: (a) CH, (b) RH-90, and (c) RH-150 specimens.

4. Conclusions

Ring compression tests were conducted to measure offset strain of Zircaloy-4 cladding against pinch-load which can occur during spent nuclear fuel (SNF) handling and transportation depending on the morphology of zirconium hydride. Then DBTT was evaluated through the transition of offset strain. The test results are as follows:

1. The specimens fractured at 12 o'clock and 6 o'clock are brittle than the specimens fractured at 3 o'clock and 9 o'clock.
2. In CH and RH-90 specimens, as the hydrogen content increases, the ductility tends to decrease, therefore, resulting in higher DBTT.
3. In RH-150 specimens, the lower hydrogen content, the higher the proportion of radial hydrides that can act as crack paths, and thus became more brittle.

Acknowledgement

This work was supported by the Korea Institute of Energy Technology Evaluation and Planning (KETEP) and the Ministry of Trade, Industry & Energy(MOTIE) of the Republic of Korea (No. 20181710201770).

REFERENCES

[1] M. C. Billone et al., FCRD-USED-2012-000039, ANL-13/05 (2011).
[2] M. C. Billone, NUREG/CR-7139, ANL-11/52 (2012).

Topology Optimization of Test Model of Tie-Down Structure for the KORAD-21 Transportation Cask

Gil-Eon Jeong*, Woo-Seok Choi, and Sang Soon Cho
Korea Atomic Energy Research Institute (KAERI)
*ong@kaeri.re.kr

1. Introduction

Most countries with nuclear power plants are paying critical attention to the issue of safe transportation of spent nuclear fuel [1], which could either be degraded during long-term storage or become high burnup spent fuel in the near future. In general, the spent nuclear fuel is transported by its own transportation cask. The cask and its associated parts must have sufficient structural integrity to meet the domestic and international regulations. Therefore, this paper presents the way to design an optimized tie-down structure to satisfy the regulations and to be used for the normal transportation test of the KORAD-21 transportation cask.

2. KORAD-21

2.1 KORAD-21 transportation cask

The KORAD-21 dual purpose transportation cask was developed for the purpose of safe transportation of the spent nuclear fuel. The schematic description of the KORAD-21 transportation cask is shown in Fig.1.

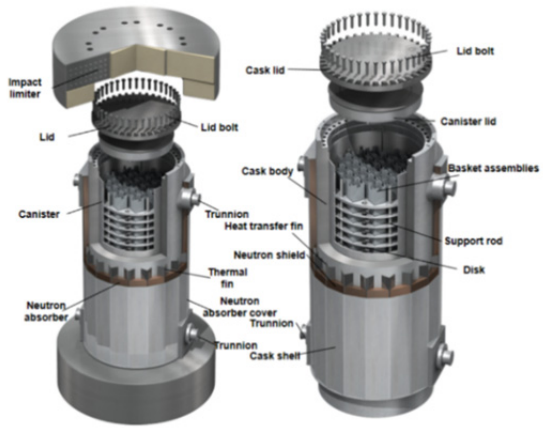


Fig. 1. Schematic description of KORAD-21 transportation cask.

2.2 Test model of tie-down structure

In order to safely transport and support the KORAD-21 transportation cask, the tie-down structure is essential. The Assembly of the KORAD-21 transportation cask and its test model of tie-down structure is shown in Fig.2.

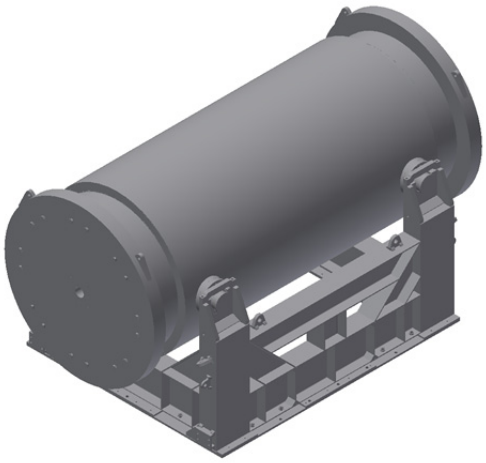


Fig. 2. Assembly of KORAD-21 transportation cask and test model of tie-down structure.

The tie-down structure must have a stress lower than the yield stress under the load conditions required by the regulation [2]. For the simplest test model of the tie-down structure, the von Mises stress contour is shown in Fig.3. In the corner of each main pillar, the von Mises stress (484 MPa) exceeds yield stress (350 MPa). Therefore, more supports are needed to meet the regulation. In this paper, the topology optimization is used to find an optimized conceptual design of the test model of tie-down structure based on the simplest test model by adding a number of supports.

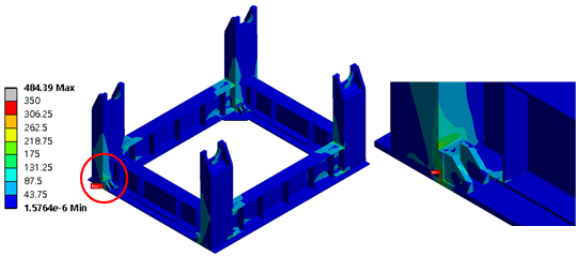


Fig. 3. von Mises stress of the simplest tie-down structure of the KORAD-21 transportation cask.

3. Topology optimization of test model of tie-down structure for the KORAD-21

In this paper, to find an optimum topological layout of the supports based on the simplest test model of tie-down structure, the commercial

software ANSYS Workbench is applied. The design domain is the regions between the main pillars. The optimized topological layout of the supports is shown in Fig. 4.

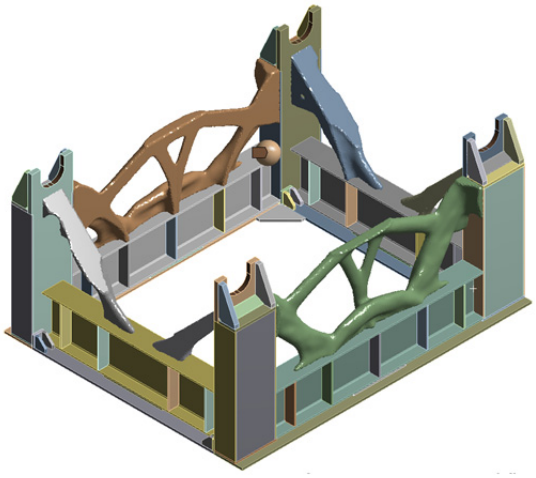


Fig. 4. Optimum topological layout of test model of tie-down structure.

In order to verify whether the optimum topological layout meets the regulation or not, the structural analysis is performed. The von Mises stress contour is shown in Fig. 5. Unlike the simplest test model, the von Mises stress (261 MPa) within the yield stress is derived.

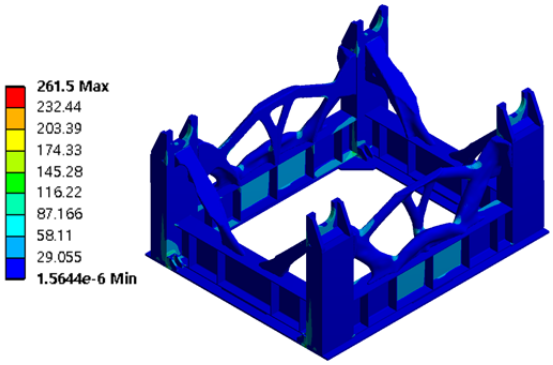


Fig. 5. Von-mises stress contour for optimized KORAD-21 tie-down structure.

By applying the results of the topology optimization and considering producibility, the test model of the tie-down structure is redesigned as shown in Fig. 6 and manufactured as shown in Fig. 7.

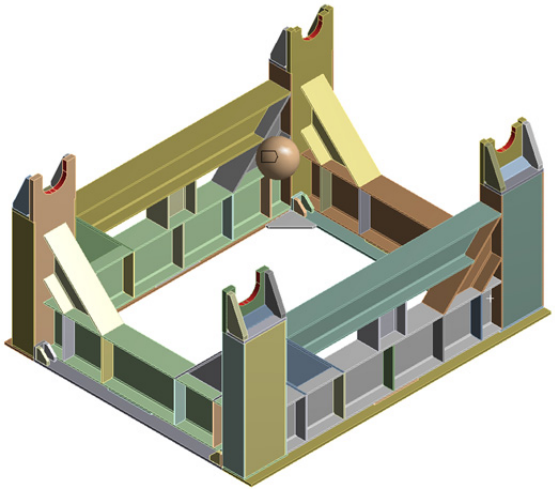


Fig. 6. Redesigned test model of tie-down structure.



Fig. 7. Manufactured KORAD-21 tie-down structure.

4. Conclusion

This study presents a way to find an optimum design of the test model of tie-down structure for the KORAD-21 transportation cask using topology optimization by applying a commercial software ANSYS. Because of its simplicity and effectiveness, the presented approach will be universally applied to the design of tie-down structures to be developed in the future.

Acknowledgement

This work was supported by the Korea Institute of Energy Technology Evaluation and Planning (KETEP) and the Ministry of Trade, Industry and Energy (MOTIE) of the Republic of Korea. (No. 2018170201770).

REFERENCES

[1] T. Saegusa et al., 2010, “Review and future issues on spent nuclear fuel storage,” Nucl. Eng. Technol., vol. 42, no. 3, pp. 237~248.
[2] IAEA Safety Standard Series No. SSR-6, 2019, “Regulations on Packaging and Transportation of Radioactive Material”.

Preparation for the Rair of Top-Nozzle Dismantled Fuel Assembly

Myungchul Park*, Sukwoo Hong, Inchan Kwon, and Hyoungmun Kwon
Korea Atomic Energy Research Institute, 111, Daedeok-daero 989, Yuseong-gu, Daejeon, Korea
*mcpark@kaeri.re.kr

1. Introduction

Top-nozzle of fuel assembly is in charge of handling function for the fuel assembly and has a structure to be compatible with the handling tools used in nuclear facilities. If the top-nozzle is separated from the main body to take out the fuel rod in it, the handling capability of the fuel assembly is in a lost state. In that case, a repair work to restore the handling function is required.

Top-nozzle has a structure to be connected to the guide tubes of fuel assembly using screws or some other parts. However, if the reassembly is impossible due to the damage of joint part, special components shall be developed to re-connect between the top-nozzle and the guide tubes.

General way to connect between them is to insert expandable component into the guide tube and fix it[1]. However, the guide tube of spent fuel is mechanically weaker than fresh status due to the oxidation and hydrogen peak-up during the burnup. Considering these degradation, it is needed to investigate the material properties of the guide tube of spent fuel. In addition, if the height or the shape at upper site of the guide tube is changed, these changes should be considered when the repair components are developed.

Therefore, in the present study, the preparation required to develop the repair components for top-nozzle dismantled fuel assembly was carried out. Actual survey of spent fuel assembly, evaluation of the irradiated guide tubes and the design of the repair component were performed.

2. Methods and Results

2.1 Actual survey of spent fuel assembly

The height and the shape of the guide tube in dismantled fuel assembly was measured using the extended tools and radiation resistant camera. The height of each guide tubes had difference and some deformation at upper site was observed. Therefore, the discrepancy between the design information and the actual fuel status shall be considered while the repair components are designed.

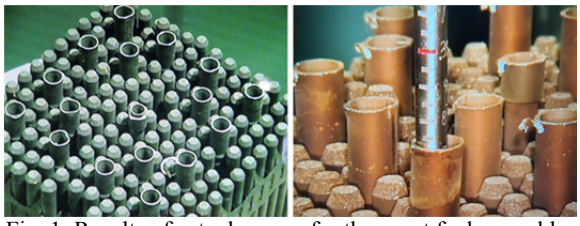


Fig. 1. Results of actual survey for the spent fuel assembly.

2.2 Evaluation of the irradiated guide tubes

The cut of guide tube from the spent fuel was investigated to evaluate its properties. As a factor to evaluate the degradation of irradiated guide tubes, hydrogen concentration and oxide layer thickness was measured. To choose optimized position for installing expandable component, the samples were taken from various height in the range of span 5-6, as shown in Fig. 2.

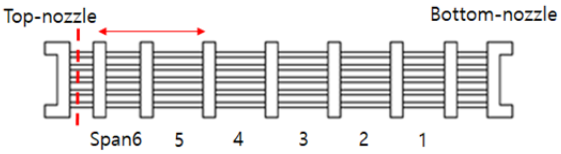


Fig. 2. Height range of evaluated guide tubes.

In hydrogen analysis results, hydrogen concentration of guide tube was less than cladding tube and average value was about 150 ppm. To evaluate the ductility of irradiated guide tubes, ring compression tests[2] were also carried out using 10 mm ring sample, as shown in Fig 3. In the test results, the certain range of elastic deformation was observed. Accordingly, proper torque value for installing the repair component will be determined in the elastic deformation range based on these data.



Fig. 3. Ring compression test.

2.3 Design of the repair components

For the repair of top-nozzle dismantled fuel assembly, expandable component installed into the guide tube and new top-nozzle was designed. The basic structure of the expandable component referred to that of commercial anchor bolt. The specific dimensions were determined based on the status of spent fuel and the test results of guide tube. From the results of strain vs torque tests, load tests using manufactured components and dummy/irradiated guide tubes, final design of the repair components will be determined.

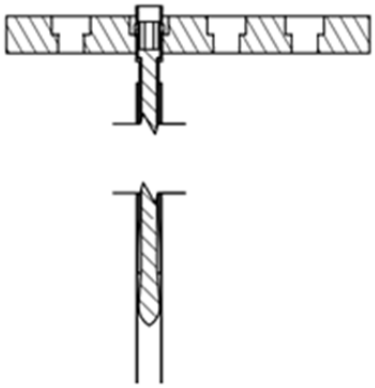


Fig. 4. Concept design of expandable component.

3. Conclusions

To prepare the repair components for top-nozzle dismantled fuel assembly, actual survey of spent fuel assembly, evaluation of the irradiated guide tubes and the design of the repair component were performed. It is expected that final design of the repair components will be determined based on various test results.

REFERENCES

[1] Korean patent, 10-0216503.
[2] M.C. Billone, FCRD-UFD-2013-000401 (2013).

Proposal for Interim Storage Facility of Spent Nuclear Fuel in Korea

Jin-Seob Kwon* and Chang-Lak Kim
KEPCO International Nuclear Graduate School, 658-91 Haemaji-ro, Seosaeng-myeon, Ulju-gun, Ulsan, Republic of Korea
*kwonjs1977@gmail.com

1. Introduction

This study was conducted to recommend the optimal interim storage option for Spent Nuclear Fuel (SNF) generated from Nuclear Power Plants (NPPs) in Korea. There are 2 technical options to be compared: Wet and dry storage types, which were divided into on-site and off-site facilities depending on the location, and off-site facilities were only considered for centralized types.

Finally, one of the decision-making processes, the Analytic Hierarchy Process (AHP), analyzed the preferred interim storage options from the perspective of various stakeholders (government, public and owner).

2. Technical Options for Interim Storage

2.1 Wet Storage Technologies

For a long period of time, wet storage of SNF using pools has been a major storage option. From the beginning of nuclear power generation, the pool type was the only method for initial cooling and radiation shielding of SNF emitted from the reactor. It was also mainly used for temporary storage of SNF in reprocessing plants. It can be broadly classified into 3 categories: single, serial and parallel pool [1].

However, In general, safety issues such as loss of cooling, radiation exposure, operational accidents, and criticality have been continuously raised for wet storage facilities.

2.2 Dry Storage Technologies

In general, SNF assemblies are suitable for dry, natural cooling storage after initial cooling in water pools. Reviews of SNF storage facilities implemented over the past few decades show that natural cooling dry storage technologies are becoming more common and attractive option than wet storage, especially for long-term storage, in terms of economics and safety [1].

Dry storage technology can be broadly classified into cask systems and other systems. Cask systems include canister-based casks and bare fuel casks, while other systems include vault, silo, hardened storage and cavern or tunnel storage.

3. Global Status of Interim Storage

The SNF is once stored in the spent fuel pools. Since then, the management method varies from country to country. Table 1 shows the recent global status of interim storage facilities. Unfortunately, there are no interim storage facilities in Korea. In this table, we can check the global preferred option are on-site dry storage facilities. The operation period of the facilities is generally in operation for about 40 to 60 years.

Table 1. Global status of SNF interim storage facilities [2]

Options	On-site	Off-site	On & Off-site
Wet	Finland, Slovakia	France, Sweden	
Dry	U.S., Canada, Spain, Czech Re., Hungary, South Africa, Romania, Armenia	Nether-lands	
Wet & Dry	Ukraine, India, Belgium, Bulgaria, Argentina		China, Japan, Russia, U.K, Germany, Swiss

4. Comparisons of Interim Storage Technologies

Table 2 below provides a comparison of general advantages and disadvantages between dry and wet storage.

Table 2. General pros and cons of interim storage options [3]

	Dry storage	Wet storage
Pros	- No SNF corrosion - Passive cooling - Mobility of SNF - No purification system - No liquid waste - Only SNF impact of the accident casks	- Inspection - Changing SNF location
Cons	- Indirect inspection	- SNF Corrosion - Forced cooling - No Mobility of SNF - Purification sys. Liquid waste - All SNF impacted in case of a accident

In addition, the two options were compared in details in terms of safety, security, economy, flexibility and public acceptance. After the Fukushima nuclear accident and the 911 terrorist attack, dry storage was considered to be advantageous in terms of public acceptance because of its relatively excellent safety and security in case of power loss or aircraft impact. Dry storage was also considered advantageous in terms of economics and flexibility for long-term maintenance and response to future changes. Table 3 shows estimated storage cost analysis between 2 options over 54 years from construction to decommissioning and disposal.

Table 3. Estimated storage cost analysis of 5,000tHM facility in japan [4]

Cost (100s of million 1998 yen)	Wet storage	Dry storage
Capital cost	1,561	1,310
- Construction cost	1,328	105
- Cask cost	100	1,195
- Decommissioning and disposal cost	133	10
Operation cost	1,395	238
Transportation cost	41	60
Total cost (2020 US$)	2,977 (3.60 billion)	1,608 (1.94 billion)

5. Decision Making Process

AHP is the widely used synthesis methodology for combining judgment and data to effectively rank options and predict outcomes. Fig. 1 shows AHP hierarchical arrangement.

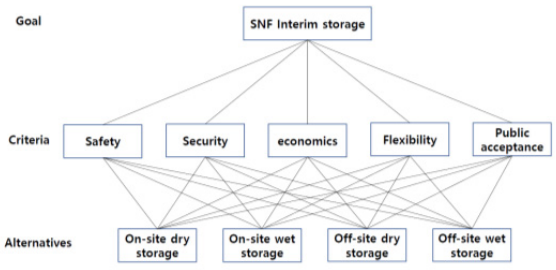


Fig. 1. AHP hierarchical arrangement.

The analysis results in Table 4 shows that regardless of the stakeholders, on-site dry storage was selected the optimal SNF interim storage option in Korea.

Table 4. Analysis result of AHP by each stakeholder

Ranking	Government perspective	Public perspective	Owner perspective
1	On-site dry / 1.000000*	On-site dry / 1.000000	On-site dry / 1.000000
2	Off-site dry / 0.342927	Off-site dry / 0.327019	Off-site dry / 0.423257
3	On-site wet / 0.312971	On-site wet / 0.314631	On-site wet / 0.259598
4	Off-site wet / 0.140484	Off-site wet / 0.140370	Off-site wet / 0.179229

* Priority value: the best choice has a priority of 1.0

6. Conclusion and Future Works

As can be seen form the results of AHP analysis, in Korea, dry storage type is the most preferred option for major stakeholders, and it will also be the optimal technology option by reflecting the recent global nuclear industry trend.

Siting is a socially and politically important. Since it is not easy to secure new sites other than the currently operating NPP sites, on-site facilities are judged to be an option to minimize social conflicts and accelerate the installation time.

It would be also possible to consider a tunnel or cavern storage at NPP sites in Korea. SNF interim storage facilities should be installed promptly to safely store SNF and prepare for final disposal or recycling in the future.

ACKNOWLEDGEMENT

This work was supported by the Korea Institute of Energy Technology Evaluation and Planning (KETEP Project No. 20204010600130) and the Ministry of Trade, Industry & Energy (MOTIE) of the Republic of Korea.

REFERENCES

[1] International Atomic Energy Agency, “Selection of Away-From-Reactor Facilities for SNF Storage, A Guidebook”, IAEA-TECDOC-1558, September 2007.
[2] Korea Energy Economics Institute, “World Nuclear Power Market Insight”, November 31 2018.
[3] Romanato. Luiz Sergio, Rzyski. Barbra Maria, “Advantages on Dry Storage for SNF”, First American IRPA Congress 2006, Mexico, September 2006.
[4] A Joint Report From the Harvard University Project on Management the Atom and the University of Tokyo Project on sociotechnics of Nuclear Energy, “Interim Storage of SNF-A Safe, flexible, and Cost-Effective Near-Term Approach to SNF Management”, June 2001.

Preliminary Logistic Simulation for Spent Fuels From Kori Site to an Assumed Interim Storage Facility

Young-min Kim*, David Kessel, and Chang-Lak Kim
KEPCO International Nuclear Graduate School
658-91 Haemaji-ro, Seosaeng-myeon, Ulju-gun, Ulsan, Republic of Korea
*minmin0903@naver.com

1. Introduction

Korean government had declared to the cancellation of the construction of new nuclear power plants and early closure of old nuclear power plants. As a result, Kori NPP unit 1 and Wolsong NPP unit 1 were permanently shut-down and these nuclear power plants are now preparing to decommission. According to these energy paradigm change in the nuclear environment, off-site transportation of spent fuels, which must precede decommission of nuclear power plants, has now become top priority issue. For these reason, this report was intended to propose the optimized spent fuels transport method from Kori NPP unit 1, 2, 3 and 4 to an assumed interim storage facility by evaluating the scenarios using the Flexsim simulation software which is widely used for simulation of logistic and manufacturing industrials.

2. Basic Assumption

2.1 Quantity of SNFs

The amount of transporting spent fuels from Kori NPP units 1, 2, 3 and 4 were assumed to 6,573 spent fuel assemblies (2,675 Ut) in total, referring to the data of the Public Debate Committee in 2015[1]. The spent fuels which were already transferred to other plants, high-burn spent fuels and damaged fuels were excluded from the total quantity.

2.2 Location of the facility

The location of an interim storage facility was assumed within the site or out of the site. It is clear that there is no specific meaning to the location assumption and it's just an assumption for calculating the transport schedule.

2.3 Sailing time

To assume the sailing time, the distance from the power plant to an interim storage facility was divided by the average speed. The average speed of ship operation was assumed to be 10 knots (18.52km/h). For accurate distance measurement, an ocean distance measurement system provided by the Korea Hydrographic and Oceanographic Agency was used [2]. As a result, the sailing time assumed for 2 days.

2.4 Transport Method

It was assumed that the transport method used multi-transport method. Transporting using trailer was conducted within NPP site and an assumed interim facility, and marine transport was used off-site and assumed interim facility.

2.5 Operation time

The operation time is assumed for the evaluating the data of each scenarios as shown in Table 1.

Table 1. Operation time assumption

Categories	Operation	Assumed day (day/cask)
Site operation	Loading SNF to canister	3.5
	Loading canisters with SNF to transport casks & cask closure	0.5
Inland Transport	Loading/unloading casks onto a vessel	0.5
	Inland transportation within site (or interim facility)	0.5
Maritime Transport	Loading/unloading casks onto a vessel	0.5
	Maritime transportation	2
Interim facility operation	Storing the canister with SNF	3
	Decontamination and inspection of transport cask	2

3. Simulation

Based on the location of interim storage, each main simulation model was created and the optimized plan was proposed by adjusting the variables such as number of trailers, casks and vessels.

3.1 On-site simulation model

The 24 assemblies of spent fuel were loaded in a canister and then the canister was inserts into a transport cask. After ready to departure at site, the cask was transported to an assumed

interim facility using the trailer. After arrival, the canister was unloaded from cask and then storing operation was conducted during interim operation. And then, the spent fuels stored in interim storage and empty decontamination operation for cask was conducted and finally empty cask was returned. Figure 1 shows the main simulation model.

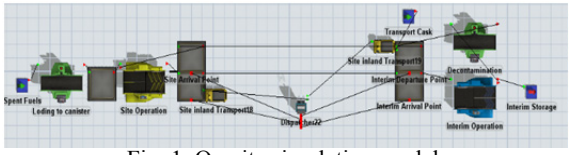


Fig. 1. On-site simulation model.

3.2 Off-site Simulation model

The simulation model was constructed as shown in Figure 2. The major difference from the previous model was the application of maritime transport.

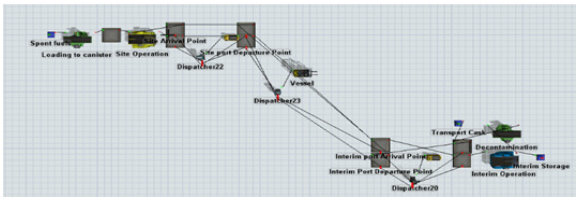


Fig. 2. Off-site simulation model.

4. Results

4.1 Result for on-site simulation model

As a result of the simulations, most optimized scenario was scenario 1 which was to use 10 casks and a trailer as shown in Table 2. If the number of trailers and casks increased, the waiting time for subsequent processes was increased as well, but the total duration was not reduced. This means that the critical path was in the site (or facility)'s process, not in the transportation. Increasing the capacity of the facility to shorten the schedule is not a realistic alternative.

Table 2. Result for on-site simulation model

Scenario	# 1	# 2	# 3	# 4
Variable	10 casks, 1 trailer	10 casks, 2 trailers	20 casks, 1 trailer	20 casks, 2 trailers
Total duration	990d	990d	990d	990d
Avg. waiting time				
At site	12.70d	13.48d	24.31d	29.86d
At facility	2.94d	1.18d	12.51d	1.85d

4.2 Result for off-site simulation model

As a result of the simulations, scenario 4 and 8 were most likely to shorten the schedule based on total duration. According to the utilization rate of ships and trailers in each scenario, scenario 4 could be determined to be optimized and it was also more economical to use one vessel in case of scenario 4.

Table 3. Result for off-site simulation model

	#3	#4	#7	#8
Variable	1 vessel, 20 casks, 2 trailers	1 vessel, 20 casks, 4 trailers	2 vessels, 20 casks, 2 trailers	2 vessels, 20 casks, 4 trailers
Total duration	1,534	1,130	1,477	1,073
Utilization (%)				
Trailer at Site	69	46	72	49
Vessel	48	62	33	40
Trailer at facility	75	50	78	53

* Hided other scenarios because of space

5. Conclusion

This might be the first study to simulate the SNFs transport using Flexsim software. The study was evaluated on a schedule basis. Once the future schedule becomes more clearly, the final scenario needs to be evaluated by adding an economic assessment.

ACKNOWLEDGEMENT

This work was supported by the Korea Institute of Energy Technology Evaluation and Planning (KETEP Project No. 20204010600130) and the Ministry of Trade, Industry & Energy (MOTIE) of the Republic of Korea.

REFERENCES

[1] "Recommendations on the management of spent nuclear fuel", Spent Fuel Public Debate Committee, (2015).

[2] Korea Hydrographic and Oceanographic Agency, "Ocean distance measurement system".

The Means to Apply the Definition for the License of the Design Approval of the Spent Nuclear Fuel Storage Cask

Daesik Yook*, Suji Yoon, and Eunjin Seo
Korea Institute of Nuclear Safety
*dsyook@kins.re.kr

1. Introduction

The Nuclear Safety and Security Commission (NSSC) is now trying to introduce of the design approval of spent nuclear fuel to the nuclear safety act. According to the draft of the amendment of the nuclear safety act, spent fuel storage cask which is approved and manufactured can be installed in the nuclear power plant site or centralized interim spent nuclear fuel storage facility. In order to that, normal, off-normal, accident condition scenario have to be well defined in the safety analysis report of storage cask.

The aim of this study is to arrange the meaning of the definition which is used in the safety analysis report of storage cask in order to avoid the confusion of the terminology which are used in the nuclear safety act and the subordinate.

2. Development of the Definition for the Design Approval of the Storage Cask

2.1 Introduction of design approval of spent nuclear fuel storage cask in the nuclear safety act

The amendment of the nuclear safety act was passed the Cabinet meeting, which includes the provision of design approval of spent nuclear fuel storage cask on 1st, September in 2020.

According to amendment of the nuclear safety act[1], any nuclear enterpriser (defined in article 71, nuclear safety act) can apply to get the licensing of theirs own unique storage cask. Naturally, the approved storage cask can be installed both in the nuclear power plant site or centralized interim spent nuclear fuel storage facility as shown in Fig 1.

2.2 Development of the notice on the guide for the safety analysis report of storage cask

As introducing the design approval of storage cask in the nuclear safety act and subordinate, the draft of the notice on the guide for the safety analysis report of storage cask are under development by the NSSC and KINS. The article 2 of the notice draft is the definition and there are the definition of normal operation, off-normal event, and accident condition. The term "normal operation" means an operation in a storage cask performed within the limiting conditions for operation, which refers to the acceptance, handling, storage, and retrieval of spent fuel, as well as the monitoring, maintenance, and testing of the related equipment.

The term "off-normal condition" means any operation conditions that deviates from normal operation and which is expected to occur several times during the operational lifetime of an storage cask, but which does not cause any significant damage to important safety installations or lead to accident conditions.

The term "accident condition" means both design-basis accidents and design- basis natural phenomenon.

The definitions of the terms used in the draft notice shall be the same as those provided in the Nuclear Safety Act, the Enforcement Decree thereof, the Enforcement Rule thereof, the Regulations on Technical Standards for Nuclear Reactor Facilities, etc., the Regulations on Technical Standards for Radiation Safety Control, etc., and the related notices of the Nuclear Safety and Security Commission, excluding those definitions provided under the article 2 (definition) of the notice draft.

2.3 The relationship of the definition between the notice draft and the existing regulations

As mentioned before, the approved storage cask can be installed both in the nuclear power plant site or centralized interim spent nuclear fuel storage facility. In order to that, it is necessary that the compatibility of storage cask with the existing facilities (nuclear power plant or interim storage facility) shall be reviewed during the licensing procedure. For this, the relationship of the definition between the notice draft and the existing regulations shall be arranged. For example, the terms of design basis (design criteria), design-basis accident, anticipated operational occurrence and limiting conditions for operation [2]. Table 1 describes the terminology which can be used in the safety analysis report of storage cask. It must be careful to use the same or similar

terminology which are used in the existing safety analysis report of commercial nuclear power plant or interim storage facility while the licensing procedure for design approval of storage cask.

3. Conclusion

The approved storage cask can be installed both in the nuclear power plant site or centralized interim spent nuclear fuel storage facility. It means that the appropriate term shall be used to setup scenarios for the normal, off-normal, and accident conditions when the safety analysis report is prepared for the design approval of the storage cask.

ACKNOWLEDGEMENT

This work was supported by the Nuclear Safety Research Program though the Korean Foundation of Nuclear Safety (KOFONS) using the financial resource granted by the Nuclear Safety and Security Commission (NSSC) of Korea. (No. 1803015).

REFERENCES

[1] KINS, “Development of Technical Requirements & Regulatory Guide for the Spent Nuclear Fuel Demonstration Program”, NSTAR-20RS23-72, (2020).

[2] NSSC, Nuclear Safety Act and the Subordinate, (2020).

Table 1. The same or similar terminologies which are used in the SAR among design approval of storage cask, the existing commercial NPP, and the interim storage facility

Terminology	facility	Definition
Design basis	NPP	in order to prevent the conditions of reactor facilities from exceeding prescribed limits in respect of operational states or accidents of reactor facilities expected to occur during the lifetime of a nuclear power plant, which apply as the standards to ensure the minimum functions or performance of installations of reactor facilities, that must be considered in design of such installations.
(Design criteria)	Interim storage	The criteria set to ensure that the conditions of an interim storage facility do not exceed the specified limits of its operational status or of events expected during its lifetime, i.e. the criteria for the minimum functions and performances to be considered when designing the installations to be installed in the interim storage facility.
Anticipated operational occurrence	NPP	The operational condition that deviates from normal operation but does not cause any significant damage to the facilities important to safety, or leads to accident conditions, which are expected to occur several times during the lifetime of reactor facilities.
	Interim storage	Any operation conditions that deviates from normal operation and which is expected to occur several times during the operational lifetime of an interim storage facility, but which does not cause any significant damage to important safety installations or lead to accident conditions.
Design basis accident	NPP Interim storage	an accident that must be considered in design of facilities to ensure that such facilities meet the design basis
Limiting conditions for operation	NPP	The minimum level of functions or performance required to ensure the safety of reactor facilities. When a limiting condition for operation is not met, the reactor shall be shutdown or any remedial action shall be followed.
	Interim storage	The minimum functions and performance levels required to maintain an interim storage facility in a safe state.

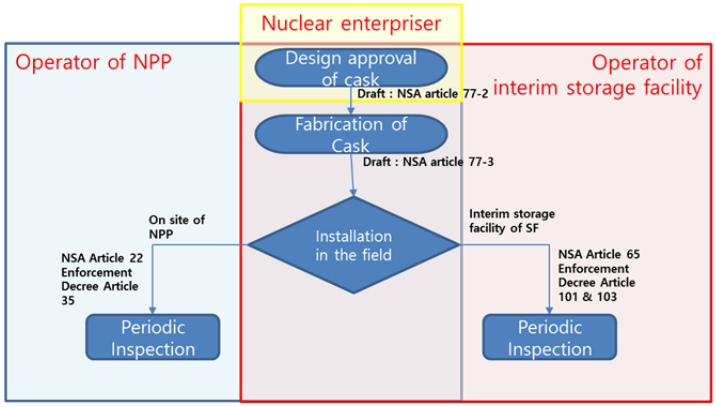


Fig. 1. Framework of storage cask licensing procedure in the Nuclear Safety Act.

Vibration and Shock Analysis for Ship Transportation of Spent Nuclear Fuel

Sang Soon Cho[1,*], Kiseog Seo[1], and Daesik Yook[2]
[1]Korea Atomic Energy Research Institute(KAERI)
[2]Korea Institute of Nuclear Safety(KINS)
*sscho96@kaeri.re.kr

1. Introduction

Spent nuclear fuel must be transported from the storage facility in the nuclear power plant to the storage facility, and its structural integrity must be maintained in normal condition of transport. In general, the transportation of spent nuclear fuel is carried out in three kinds of modes: road, rail and sea, and the repeated vibration and shock loads are applied by the truck, train and ship during transportation [1]. It has to be checked whether the structural integrity of the spent fuel is maintained under these load conditions.

All domestic nuclear power plants are located on coastal sites, and the storage facility for spent nuclear fuel is likely to be decided as a coastal site as well. Therefore, it is expected that the candidate mode of transporting spent nuclear fuel in Korea is the marine transport mode by ship. In the marine transportation mode, the wave load of the sea creates a vibration phenomenon which the ship mainly shakes in the rolling motion, and the spent nuclear fuel inside the transportation cask fixed to the ship is affected. In other words, in marine transportation, the path of load is transmitted in the order of waves, ship, transportation cask, internal structures and spent nuclear fuel.

The purpose of this study is to examine the response of a ship by waves in order to evaluate the vibration and shock loads generated in the transportation cask when the spent fuel metal cask is transported during the marine transportation.

.

2. Vibration and Shock Analysis

2.1 Analysis Model

The ship model used in this study is HANJIN 3006, and because an accurate size of ship model was not known, the CAD model of Stena Teknic was scaled to satisfy the geometric information of the HANJIN 3006 model. The draft of the ship is assumed to be 5.35m. An analysis model is prepared in which a total of 20 casks for Fig. 2. Finite Element model with sea, ship and casks.

Transporting spent nuclear fuel were loaded in the ship's analysis model. The commercial software is SeaFEM for vibration and shock analyses in the marine transportation.

2.2 Analyses Conditions

The boundary condition used in the response amplitude operator (RAO) analysis is set to infinite depth in the case of bathymetry, and the white noise spectrum is used as the wave spectrum type used in the analysis. The amplitude is set to 1 m, the shortest period of the wave was set to 3 seconds, and the longest period was set to 25 seconds. Here, the white noise spectrum generates a number of waves having the same amplitude and direction as the frequency uniformly distributed over the periods.

In the transient analysis, the wave direction is set to the rolling direction of ship, which is the greatest responsive direction in the results performed in many kinds of RAO analyses. The significant wave height is 0.5m, the significant wave period is set to 9.3 seconds. The center of gravity and radius of rotation of the ship are the same as those of the RAO analysis, and the JONSWAP spectrum is applied to this analysis.

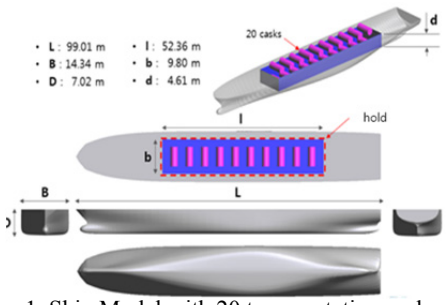


Fig. 1. Ship Model with 20 transportation casks.

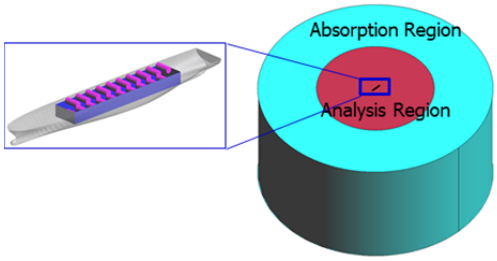


Fig. 2. Finite Element model with sea, ship and casks.

3. Conclusion

The purpose of this study is to evaluate the vibration and shock responses of a ship generated by the sea waves when the spent fuel cask is transported in the mode of marine transportation. The response amplitude operator (RAO) analysis using white noise spectrum was performed for the vibration analysis of the ship, and the transient analysis using JONSWAP spectrum was performed for the wave direction with the most outstanding response to confirm the RAO of the transport cask. As a result of the RAO analysis, it was confirmed that the response of the rolling direction of the ship was remarkably high. The transient analysis was also performed with the wave direction of the rolling motion of the ship wave, and a response similar to the result of RAO analysis was obtained. This transient analysis results will be used as input conditions for vibration and fatigue analysis acting on the transport cask and spent nuclear fuel.

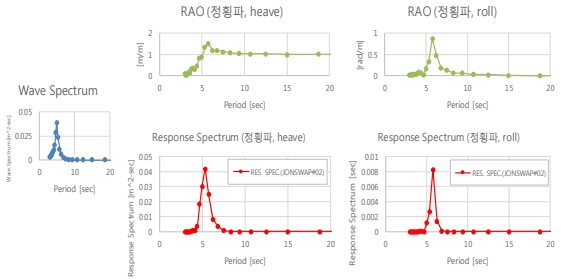


Fig. 3. RAO Analyses Results.

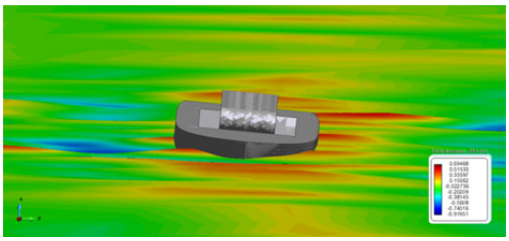


Fig. 4. Transient Analysis Result with the rolling motion of ship.

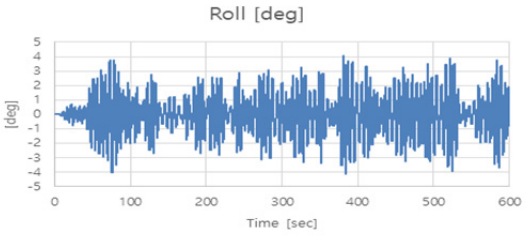


Fig. 5. Time History of Rolling Angle.

Acknowledgements

This study was partially supported by the Nuclear Safety Research Program through the Korea Foundation of Nuclear Safety(KOFONS), granted financial resource from the Nuclear Safety and Security Commission(NSSC), Republic of Korea (No.1803015).

REFERENCES

[1] Lim, J. H., Cho, S. S., Yang, Y. Y., Seo, K. S., and Choi, W. S., “Establishment of Data Acquisition System for Road and Sea Transportation Test of Surrogate Spent Nuclear Fuel under Normal Conditions of Transport,” Korea Radioactive Waste Society Fall Conference, (2019).

Reaction of RE and Mg Metals With UCl_3 in the LiCl-KCl Molten Salt

Seungwoo Paek*, Gha-Young Kim, Junhyuk Jang, Chang-Hwa Lee, and Sung-Jai Lee
Korea Atomic Energy Research Institute, 111, Daedeok-daero 989beon-gil, Yuseong-gu, Daejeon, Republic of Korea
*swpaek@kaeri.re.kr

1. Introduction

The RE content in TRU product recovered from pyroprocessing should be as low as possible when used as metal fuel for an SFR. Because the RE content in the TRU product may affect the integrity of the fuel claddings [1]. Recent study has shown that UCl_3 can effectively remove RE elements from U/RE ingot, but experiments using TRU elements could not be carried out [2]. However, experiments with TRU materials are generally very difficult and usually use surrogate materials. Recently, a study in electrochemical experiment with molten salt revealed that Mg could be used as a surrogate material for Pu [3].

In this study, the reaction characteristics of Mg and RE by the reaction of U-Mg-RE metals and UCl_3 in the LiCl-KCl molten salt were observed.

2. Experimental

The metals Mg, Nd, and Ce with 99.9% purity used in the experiment were Alfa Aesar products, and depleted uranium (DU) ingot was cut to a desired size and used. The reactor used in the experiment used a 5 cm diameter alumina crucible. Anhydrous LiCl-KCl eutectic salt (99.99% purity, Sigma Aldrich) was used as an electrolyte and the reaction temperature maintained at 773K. Metal concentrations of molten salt according to reaction time was analyzed using ICP-AES.

3. Results and Discussion

3.1 The experiment using UCl_3 and Gd

RE removal process from TRU product using UCl_3 is based on the difference in Gibbs free energy of chloride formation between TRU and RE elements. TRU element also has a – ΔG value that is smaller than RE element but can react. In other words, TRU element can also react in part to form TRU chloride by reacting with UCl_3. To recover the RE as chloride and TRU as a metal, a two-step reaction experiment was performed. That is, in the first step, UCl_3 was used as an oxidant to dissolve RE in the form of chloride, and in the second step, some dissolved TRU chloride was converted to TRU metal using Gd.

$$TRUCl_3 + Gd = GdCl_3 + TRU \qquad (1)$$

The TRU/RE ratio of the TRU product of pyroprocessing under study in KAERI is in the range of 0.25 ~ 1. This study seeks to obtain a final product with a large TRU/RE value by removing RE elements from recovered TRU product. Thus, the experiments were conducted with a different TRU(Mg)/RE ratio of 3 sets.

3.2 Concentration change of metals in the molten salt by 2-step reaction

Figure 1 shows the concentration changes of the U, Ce, Nd, Gd, and Mg in the salt by the reaction with UCl_3 of 1st step and the reaction with Gd of 2nd step in the set 1 experiment (Mg/RE=1.3). Figure 2 and 3 also show the experimental results in a set of experiments with different Mg/RE values.

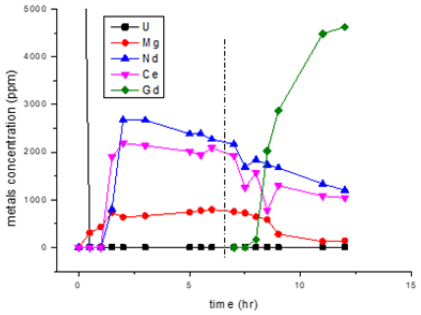


Fig. 1. Concentrations changes in the set 1(Mg/RE=1.3).

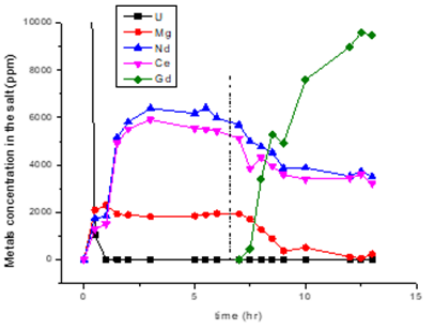


Fig. 2. Concentrations changes in the set 2(Mg/RE=0.57).

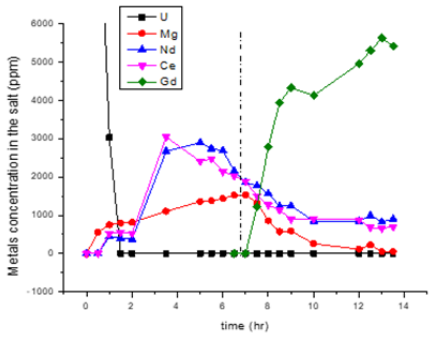


Fig. 3. Concentrations changes in the set 2(Mg/RE=0.24).

In the experiment of 3 sets, the concentration change of metal elements in the salt showed almost similar changes. In the 1st step reaction with UCl_3, uranium concentration decreased to a near zero in 1 hour after reaction. The concentration of Ce and Nd increased rapidly and reached almost constant values from about two hours after the reaction. The concentration of Mg was also shown in reaction with UCl_3. In the 2nd step of reaction with Gd metal, the concentration of Mg continued to decrease, resulting in a concentration of below 100 ppm and the RE concentration also decreased. It is estimated that the decrease in the concentration of RE chlorides is due to the properties of RE forming alloy with Mg. From this study, it was shown that the RE elements was effectively removed via two-step reaction using UCl_3 and Gd metal.

ACKNOWLEDGEMENT

This work was supported by a National Research Foundation (NRF) grant funded by the Korean government (MSIP) (No.2017M2A8A5015079).

REFERENCES

[1] A. B. Cohen et al., "Fuel/cladding Compatibility in U-19Pu-10Zr/HT9-clad Fuel at Elevated Temperature", J. Nuclear Materials, 204, 244-252 (1993).
[2] S. Paek et al, "Removal of Rare Earth Elements from a U/RE ingot via a Reaction with UCl_3", Journal of Radioanalytical and Nuclear Chemistry, 322, 495-502 (2019).
[3] M. Simpson et al, "Galvanic Reduction of Uranium (III) Chloride from LiCl-KCl Eutectic Salt using Gadolinium Metal", Journal of Nuclear Materials, 493, 120-123 (2017).

Design Features of the Transfer Cask (OASIS-HC) and Storage Cask (OASIS-STO)

Soung Kyu Lee*, Jin Seok Park, Min Kyu Kim, and Jong Min Kim
Mechanical System Engineering Dept., KEPCO E&C, 989-111, Daedeokdaero Yuseong-gu, Daejeon, 34057, Korea
*hikyu@kepco-enc.com

1. Introduction

As storage pools for the spent nuclear fuel (SNF) in the domestic operating nuclear power plants are getting saturated, the construction of SNF dry storage facility has long been discussed to dispose of the high-level radioactive waste of on-site.

Expecting the demand for the SNF casks to increase in near future, KEPCO E&C has been working on the development of our new SNF cask models and associated engineering capability buildup. We firstly proposed a dual purpose metal cask OASIS-32D [1] that can be utilized for both transport and storage of SNFs. Based on the technology and experience of the OASIS-32D, we are now developing two more cask models: OASIS-HC metal cask dedicated for on-site transfer and handling of SNFs, and OASIS-STO concrete cask for storage.

This paper introduces the key design features of OASIS-HC and OASIS-STO.

2. Design Features

2.1 Design considerations

The transfer cask and storage cask were designed for the same SNF with one for the OASIS-32D. The SNF design parameters are given in Table I.

Table 1. SNF Design Parameters

Parameter	Design Features
Fuel types	ACE 7 & PLUS 7 PWR SNF (32 bundles)
Initial enrichment	Maximum 5.0 w/o (U-235)
Discharge burnup	45,000 MWD/MTU
Cooling periods	10 years

2.2 Components of OASIS-HC and OASIS-STO

2.2.1 Canister

The canister is a cylindrical shell that stores up to 32 bundles of PWR SNFs. Its top lid is welded for complete seal which provides the containment boundary after the SNFs are loaded. The inside of the canister is composed of a basket and reinforcement supports. The basket contains the neutron absorbers capturing the neutron source generated from the SNFs and reinforcement supports hold the basket as being welded to the outer surface of basket.

The canister that have been developed for OASIS-32D is applied to the OASIS-HC and OASIS-STO design to be compatible with various cask models.

2.2.2 OAISIS-HC

OASIS-HC as shown in Fig. 1 consists of a cask body and 2 bottom lids called pool lid and transfer lid, each used separately. The cask body materials surrounding the canister are composed of carbon steel, neutron shielding material and heat transfer pin. The materials of 2 bottom lids installed under the cask are stainless steel.

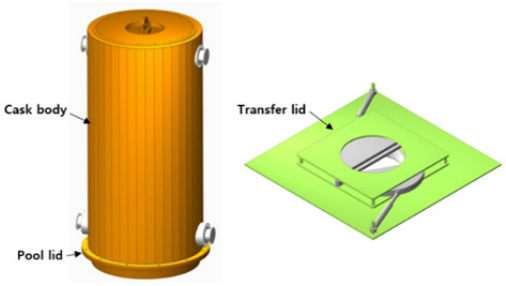


Fig. 1. Configuration of OASIS-HC.

2.2.3 OASIS-STO

OASIS-STO as shown in Fig. 2 consists of a cask body, top lid and bottom lid. The cask body materials surrounding the canister are composed of carbon steel and high density concrete. In a same manner, the top lid and bottom lid materials bolted to the top and bottom of a cask body are composed of carbon steel and high density concrete. The top lid has 4 outlet vent ports and the bottom lid has 4 inlet vent ports, unaligned.

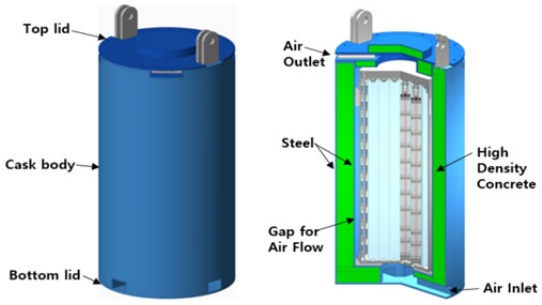


Fig. 2. Configuration of OASIS-STO.

2.3 Design Features of OASIS-HC

The cask body is a cylindrical vessel with thick walls which are composed of cask shell and outer shell.

The cask shell located between the canister and outer shell performs the role of structural materials as a main body. The materials of cask shell are carbon steel effective for shielding gamma rays.

The outer shell surrounding the outside of the cask shell contains neutron shielding materials and heat transfer pins. The neutron shielding is designed to optimize circumferential neutron shielding by optimal combination of various composition materials. Heat transfer pins embedded in the neutron shielding materials are designed for heat transfer efficiency and weldability to the inside and outside wall of the outer shell.

The pool lid bolted to the cask body is used in cask loading pit, cask decontamination pit and on-site storage building for fuel loading and canister moving sequence. The contact surface between the cask body and bottom lid is sealed with the double O-rings. So that, As sealing with double O-rings, the annular space is charged with water or helium for cask cooling.

The transfer lid, after the cask with pool lid is drained and dried, is installed instead of pool lid at the bottom of the cask in on-site storage building. It is composed of lid housing, 2 bottom doors, base plate. 2 bottom doors are operated separately by the power of actuator and allow the canister to be lowered into the storage cask through the opening space of cask bottom (refer to Fig. 3).

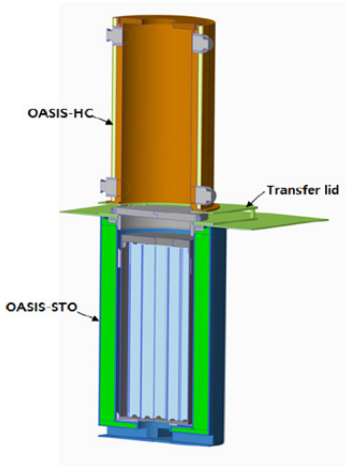


Fig. 3. Transferring the canister to OASIS-STO.

2.4 Design Features of OASIS-STO

The cask body is a cylindrical vessel with thick walls of hybrid shield which are composed of high density concrete and carbon steel(steel-concrete-steel). The role of the high density concrete is to perform the shielding against gamma and neutron radiation. The thickness of high density concrete and carbon steel is sufficiently considered to satisfy the allowable radiation dose rate.

The channels are installed around the inner cavity of the cask body to position the canister at the center of the cask body.

The top lid and bottom lid provide path natural convection cooling through the 4 inlet vent ports and 4 outlet vent ports. The air flows vertically from the 4 inlets in the bottom lid to 4 outlets in the top lid through the gap between the cask body and canister.

The shielding plates are installed within the inlet vent ports and outlet vent ports to minimize the dose rates. The shielding plates are designed in lattice shape to scatter the radiation and to allow the air flow unblocked for cooling.

3. Conclusion

Based on the technology and experience of the SNF cask OASIS-32D that developed for dual purposes of transport and storage of spent fuels, KEPCO E&C is now developing two new casks OASIS-HC and OASIS-STO. OASIS-HC is metal cask dedicated for on-site transfer and handling of SNFs, and OASIS-STO is a concrete cask for the storage. Both casks can handle 32 bundles of PWR fuels and will be technically and economically optimized to comply for the market demands.

REFERENCES

[1] K. J. Ko, et al., Design Features of an OASIS-32D Metal Cask for both Transport and Storage of SNF, The Korea Nuclear Society Spring Meeting, (2017).

Pyro-SFR Cycle Transition Scenario in Korean Energy Transition Policy

Hong Jang*, Hyo On Nam, and Won Il Ko
Korea Atomic Energy Research Institute, Daejeon, Republic of Korea
*janghong@kaeri.re.kr

1. Introduction

In the past, system analysis studies of fuel cycle transition scenario assumed continuous future nuclear power generation based on the past national basic plan for electricity supply and demand. However, the recent basic plan contained a gradual nuclear phase-out stance, which is completely different from the assumptions of past studies. Apart from the plan, KAERI has been developing a pyro-SFR cycle technology, a fuel cycle technology that could be an alternative to the once-through (OT) cycle, with government support. If the nuclear phase-out persists, the transition scenario to the pyro-SFR cycle assumed in previous system analysis studies is no longer valid. Therefore, in this study, a new transition scenario to the pyro-SFR cycle in the nuclear phase-out situation is proposed and the validity of the scenario is verified based on mass flow for the scenario.

2. Transition Scenario Setting

In our previous study [1], transition scenarios to the OT cycle were proposed in consideration of the nuclear phase-out situation, and the mass flows of those scenarios were analyzed. The OT cycle transition scenarios were based on the government's HLW management plan [2], but assumed that implementation of the plan would be delayed by 5 or 10 years, taking into account that the plan is currently being reviewed. Proposed OT cycle transition scenario includes operation plans for the interim storage and the final disposal facility as shown in Table 1.

The pyro-SFR cycle transition scenario additionally requires operation plans for the pyro facilities and SFRs. If commercial pyro facility can be secured in a timely manner, it can be assumed that PWR spent fuels (SFs) are not stored in the interim storage and processed directly in the pyro facility. Based on this assumption, as the default scenarios (S1-1 and S2-1), the start of the pyro facility operation is set to either 2041 or 2046, the same as the start of the interim storage operation in scenario S1 and S2.

In addition, as alternative scenarios (S1-2 and S2-2) assuming the delay in securing commercial pyro facility, the start of the pyro facility operation is set to be 10 years later than the default scenarios. In this alternative scenarios, the PWR SFs are stored in the interim storage from 2041 or 2046 until the pyro facility is secured.

In all scenarios, the SFR operation is set to start three years after the start of the pyro facility operation so that the pyro facility could produce enough SFR fuels for the initial core. And a pyro facility is assumed to be capable of handling 450 tHM PWR SFs annually for 60 years to process the full amount of PWR SFs generated. And 5 fleets of 1,500 MWe SFR are assumed to be constructed every 4 years and operated for 60 years each to burn the TRUs in the PWR SFs. It is also assumed that radioactive wastes generated from the pyro facility are stored in the facility and disposed of from the same year as at the beginning of disposal of the PWR SFs in scenarios S1 and S2, to the additional 40 years of cooling required to dispose of spent fuels discharged from the last SFR shutdown.

The proposed four pyro-SFR cycle transition scenarios are summarized in Table 2. Other details are excluded due to lack of space.

Table 1. OT cycle transition scenario set

Scenario	S1	S2
Interim storage start	2041	2046
Interim storage end	2092	2092
PHWR SF disposal start	2058	2063
PHWR SF disposal end	2069	2074
PWR SF disposal start	2070	2075
PWR SF disposal end	2122	2122

Table 2. Pyro-SFR cycle transition scenario set

Scenario	S1-1	S1-2	S2-1	S2-2
Interim storage start	-	2041	-	2046
Interim storage end	-	2092	-	2092
Pyro facility start	2041	2051	2046	2056
Pyro facility end	2101	2111	2106	2116
SFR start	2044	2054	2049	2059
SFR end	2120	2130	2125	2135
PHWR SF disposal start	2058	2058	2063	2063
PHWR SF disposal end	2069	2069	2074	2074
Pyro waste disposal start	2070	2070	2075	2075
Pyro waste disposal end	2160	2170	2165	2175

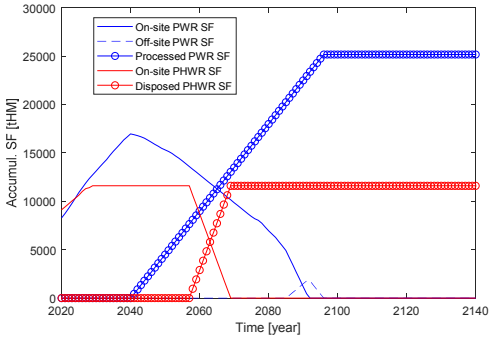


Fig. 1. Accumulated SF amounts stored in the reactor, interim storage, and processed in the pyro for scenario S1-1.

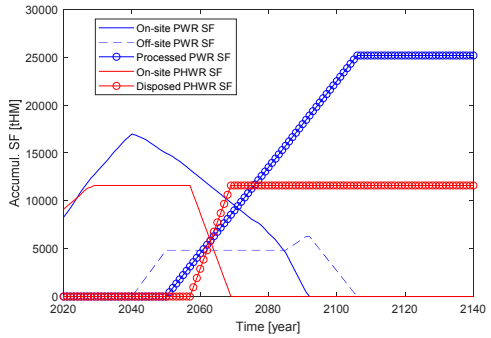


Fig. 2. Accumulated SF amounts stored in the reactor, interim storage, and processed in the pyro for scenario S1-2.

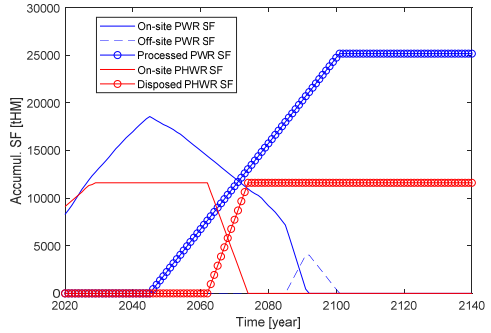


Fig. 3. Accumulated SF amounts stored in the reactor, interim storage, and processed in the pyro for scenario S2-1.

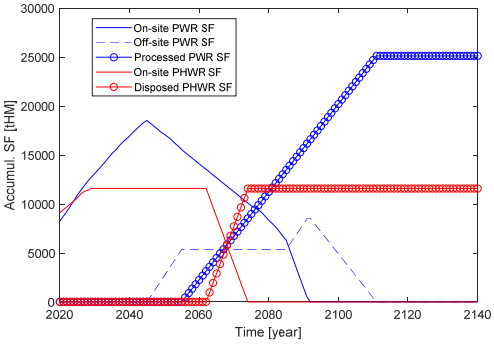


Fig. 4. Accumulated SF amounts stored in the reactor, interim storage, and processed in the pyro for scenario S2-2.

3. Mass Flow Analysis

The scenario sets in Table 2 were implemented in the dynamic mass flow model, and the mass flows were derived. Fig. 1~4 show the cumulative storage of spent fuels in on-site and off-site storages and the cumulative throughput in the pyro facility for scenario S1-1~S2-2.

Comparing the peak amount of the PWR SFs stored in the on-site storage can be seen that S1-1 and S1-2 (17,000 tHM) are lower than S2-1 and S2-2 (18,600 tHM). This is because in S1-1 and S1-2, the PWR SFs escape earlier from the on-site storage to the off-site storage or the pyro facility. In S1-2 and S2-2, 4,800 tHM and 5,400 tHM of the PWR SFs generated before the pyro facility is secured are stored in the interim storage and then sent to the pyro facility. Although S1-1 and S2-1 set the pyro facility to replace the interim storage, it can be seen that a storage is needed to temporarily store the PWR SFs that is no longer acceptable on site after the last PWR shutdown (1,800 tHM for S1-1 and 4,000 tHM for S2-1). S1-2 and S2-2 also show additional off-site storage masses for the PWR SFs taken out after the last PWR shutdown (1,400 tHM for S1-2 and 3,200 tHM for S2-2). This result indicates that the pyro facility should have a co-located interim storage that can store the PWR SFs for the site closure.

4. Conclusion

In this study, transition scenarios to the pyro-SFR cycle were proposed and their dynamic mass flows were analyzed. As a result, it was possible to derive the quantity information that can suggest capacity of the on-site and off-site storages for the transition to the pyro-SFR cycle. The proposed transition scenarios in Table 1 and 2 will be used to analyze the mass or volume of radioactive wastes generated from the fuel cycle as well as to assess economic viability of the pyro-SFR cycle transition compared to the OT cycle transition in the nuclear phase-out situation.

REFERENCES

[1] H. Jang et al., Once-through Cycle Transition Scenario in Korean Energy Transition Policy, KRS spring meeting, Online, Jul. 29~31, (2020).

[2] MOTIE, Basic Plan on High-level Radioactive Waste Management (Draft), MOTIE, (2016).

SFR SF Pyroprocessing Flowsheet Model for Economic Evaluations

Hun Suk Im*, Kwang Rag Kim, Hong Jang, and Hyo On Nam
Korea Atomic Energy Research Institute, 111, Daedeok-daero 989beon-gil, Yuseong-gu, Daejeon, Republic of Korea
*Ihs95@kaeri.re.kr

1. Introduction

In Korea, since the commercial operation of Kori 1 in 1979, 24 nuclear reactors have been in operation until now, and management of all nuclear power plants is scheduled according to the Basic Plan for long-term Electricity Supply and Demand. However, the cumulative amount of spent nuclear fuel(SF) is increasing due to the operation of nuclear power plants. As part of management for accumulated spent nuclear fuel KAERI has joined "Pyro-Sodium cooling Fast Reactor(SFR) fuel cycle system" according to the long term R&D plan for future nuclear system decided by the 255th Atomic Energy Commission in December, 2008. Along with the steady development of PWR SF mass SFR SF mass balance began to be developed in line with SFR core system design. And the geologic disposal and the economic evaluation for Pyro-SFR fuel cycle system are also studied based on the mass balance. This waste information from mass balance of SFR SF Pyro are used for economic evaluations. Since domestic SFR SF has never been produced so far, we have established the mass balance for SFR SF pyroprocessing based on the data related to EBR-Ⅱ in the past.

2. SFR SF

As shown in Fig. 1[1], 1) SFR SF has a containment structure in which a fuel rod is surrounded by bond-sodium in the cladding. Since SFR has no neutron moderation bond-sodium is used as a coolant. Thus bond-sodium removal process is added to deal with SFR SF by pyroprocessing. And some compounds of nuclides and bond-sodium are predicted to be produced thermodynamically. Since several nuclides like volatile Xe, Kr, and Cs released from fuel matrix are contained despite of high temperature and high pressure. Thus purification of bond-sodium is required to separate some nuclides as well. 2) Since SFR SF is metal type, the kind of volatile nuclides is different from that of PWR SF and the volatility behavior is also different [2]. So the behavior study of metal fuel in head-end process should be conducted forward. And this metal fuels are fed directly into ER process without Oxide Reduction process in pyroprocessing.

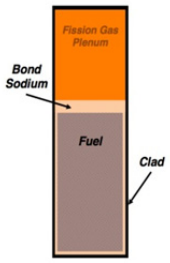


Fig. 1. Structure of Metal SFR SF.

3. Process Flow of SFR SF pyro and Material Stream

The process flow of SFR SF is summarized in Fign.2. The differences from PWR SF are found at head end process and oxide reduction process, respectively. In the head end process, new unit processes related to bond-sodium treatment are introduced while some processes such as low-temperature oxidation, reduction, and high-temperature treatment have been reduced. In order to remove bond-sodium some part of Melt Drain Evaporate Carbonate (MEDEC) process [3] was applied into SFR SF pyro. During the removal and the separation processes of bond-sodium, the radioactive nuclides are expected to be recovered in the various wastes according to the treatment method.

In the Electro-refining process, metal fuel is fed into eutectic salt with cladding hull since cladding hull is not removed in the head end process. All radioactive nuclides except noble metal are dissolved into eutectic salt. U ingot and U/TRU ingot are produced through electro-refining and winning processes, respectively. However U ingot process can be omitted according to the fuel composition of SFR SF. Since the composition of fuel can be changed in line with the improvement of SFR core system design. In the salt purification process, salt-soluble nuclides in the eutectic salt are recovered vis reactive distillation process and the unreacted nuclides such as Cs and I are separated with crystallization method.

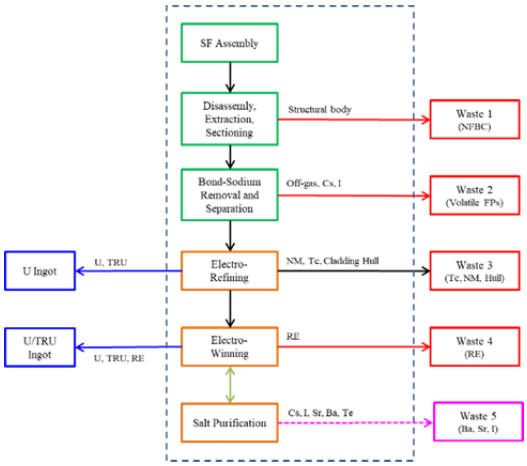


Fig. 2. Schematic flowchart of SFR SF pyro.

4. Mass Balances and Constraints

There are several constraints to calculate mass balances. First, the last concentration ratio of TRU to U in the electro-refining process is limited to 3.52~3.54[4] to keep high purity electrodeposit U. The second, the ratio of TRU to RE in the U/TRU ingot is assumed to be 6 or higher in the electro-winning step. The quantity of U/TRU ingot($x_{TRU(Cd)}$) is mathematically derived from mass balance equations with the initial of nuclides in the salt, the residual in the salt after process and separation factors(SF) with (1) and (2). The last, the residual TRU in the salt is set up less than 0.1wt% as irreversible loss in the salt.

$$\frac{x_{TRU(Cd)}}{x_{RE(Cd)}} = 6 \quad (1)$$

$$\begin{aligned} x_{RE(s)} &= x_{RE(ini,s)} - x_{RE(Cd)} \\ &= x_{RE(ini,s)} - {}^{x_{TRU(Cd)}}/_{6} \end{aligned} \quad (2)$$

5. Conclusions

The process flow and mass balance were established based on the pyroprocessing process technology. Compared to the PWR SF Pyro, improvements were conducted in head end process to suit the fuel characteristics of SFR SF and were based on the data from EBR-Ⅱ data when no actual data were available. Further for the detailed undeveloped process technology, processes were considered with logical approach and the wastes that could be generated during SFR SF pyro were considered. Although many part of this study were not perfect to explain the whole process for SFR SF pyro, it will be used as basic data to guide further research.

ACKNOWLEDGEMENT

This work was supported by a National Research Foundation (NRF) grant funded by the Ministry of Science and ICT(2017M2A8A501507214).

REFERENCES

[1] D. Grabaskas et al, “Regulatory Technology Development Plant Sodium Fast Reactor Mechanistic source term development”, ANL-ART-3, (2015).
[2] D. Grabaskas et al, “Regulatory Technology Development Plant Sodium Fast Reactor Mechanistic source term Development-Metal Fuel Radionuclide Release”, ANL-ART-38, (2016).
[3] K. L. Toews, et al, “Application of the MEDEC process to treat FERMI-1 Sodium-Bonded Spent Nuclear Fuel”, ANS Topical meeting on spent nuclear fuel and fissile materials, (2002).
[4] K. Uozumi, et al, “Electrochemical behavios of uranium and plutonium at simultaneous recoveries into liquid cadmium cathode”, J. of Nuclear Materials, 325, (2004).

Gas Circulation Drying System Control for Dry Storage of Spent Nuclear Fuel

Kyung-Wook Shin*, Gyung-Sun Chae, Geon-Hui Lee, and Jae-Seok Park
SAE-AN ENGINEETING CORPORATION. #910, 184, Gasan digital 2-ro, Geumcheon-gu, Seoul, Republic of Korea
*And9211@sae-an.co.kr

1. Introduction

In domestic nuclear power plants, spent nuclear fuel is stored in wet storage facilities. However, due to the lack of storage space in wet storage facilities, the operation of temporary intermediate storage facilities that can be stored is planned. As a method of temporary intermediate storage, dry storage, in which containers are filled with an inert gas, is suggested as a realistic alternative. Dry storage is advantageous in terms of stability and economy compared to wet storage. After the spent nuclear fuel is withdraw from the wet storage facility, it is necessary to remove the moisture in the container to transport it to the dry storage facility. This is to secure the integrity of spent nuclear fuel by safely storing spent nuclear fuel that is stored for a long time. Commercially available moisture removal methods include vacuum drying and gas circulation drying.

This paper is concerned with the control of the gas circulation drying system during the dry process for dry storage of spent nuclear fuel.

2. Gas Circulation Drying System

2.1 General Information

The basic concept of the forced gas dehydration process is a method of removing moisture by flowing heated inert gas to the canister, and the main component is as follows.

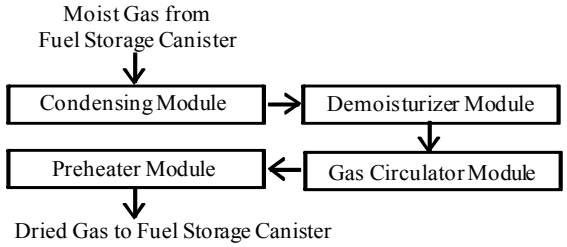


Fig.1. Block flow diagram of the forced gas dehydration.

2.2 System Configuration

The gas circulation system is a method of drying by circulating a heated inert gas through the inside of a storage container loaded with spent nuclear fuel. The basic configuration of the system consists of a cooling device that removes moisture, a heater that increase the temperature of the gas, a circulator that circulates the gas, a valve, a temperature sensor that measures the state of the gas and a pressure sensor.

This system is programmed by programmable logic controller(PLC), so it is possible to record the operation and measurement values of each component. In addition, when the system is configured with PLC, installation cost is low and maintenance or expansion is easy. The control and monitoring of the system is connected to human machine interface(HMI) to check the operation and measurement status of each component on a screen designed by the user, and remote control and monitoring are also possible.

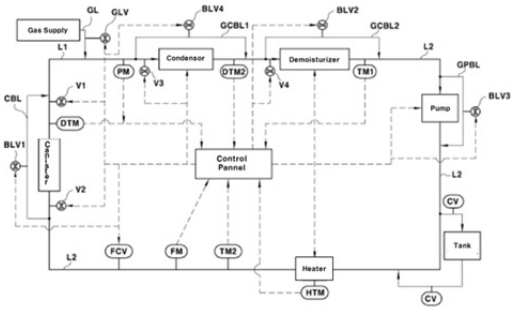


Fig. 2. System schematic diagram.

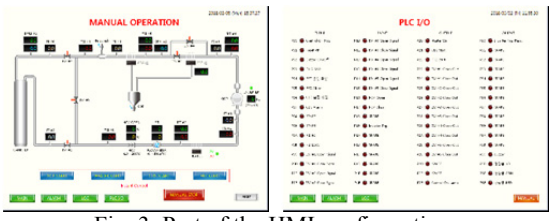


Fig. 3. Part of the HMI configuration.

2.3 System Control Flow

The control of the drying system is divided into a preparatory process stage, a drying process stage, and a drying confirmation stage. The components of the drying system are programmed to operate at each stage.

The preparation process stage is the stage of operating with the default settings of each component for the drying process. At this stage, a gas circulation line is formed and consist of supplying inert gas, checking gas pressure in the gas circulation line, stopping inert gas, starting a gas circulation pump, starting a cooling device, and starting a heater.

The drying process stage is a stage of drying

the container loaded with spent nuclear fuel when the preparation process stage is completed. This stage include adjusting the temperature of the gas entering the container, the temperature at which the gas exiting the container is cooled, and the flow rate of the gas. In the drying process, it is the stage of confirming the set values as the drying standard and isolating the container and the drying system.

The drying confirmation stage is a stage to check the dry state inside the container after thedrying process stage is finished. This stage confirms that the set value, which is the drying standard, is satisfied for a constant time while the container and the drying system are isolated. The drying process is terminated if it is maintained below the set value that is the drying standard for a constant time and is confirmed in an appropriate state. If a nonconformity condition is identified, the container and the drying system are separated and the drying process returns.

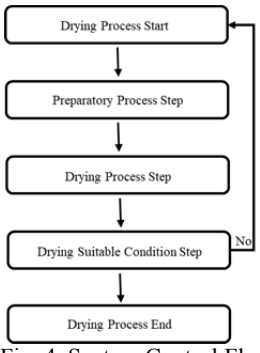


Fig. 4. System Control Flow.

3. Conclusion

The system control method in this paper is applied to the control method by PLC. The reason for applying PLC is high reliability and good compatibility with industrial devices in the industrial field. In addition, when the system is configured with PLC, installation cost is low and maintenance or expansion is easy. It is also an advantage that the control method of the system can be modified according to the procedures or needs of the drying process.

Acknowledgement

This work was supported by Korea Institute of Energy Technology Evaluation and Planning (KETEP) and the Ministry of Trade, Industry & Energy (MOTIE) of the Republic of Korea (No. 20181720201020).

REFERENCES

[1] ASTM C1553-6, “Standard Guide for Drying Behavior of Spent Nuclear Fuel”, ASTM, (2016).

A Framework for Integrated Oxide Reduction Process Automation in Pyroprocess Automation Mockup

Jonghui Han*, Jongkwang Lee, Dongseok Ryu, and Seungnam Yu
Korea Atomic Energy Research Institute
*jhan@kaeri.re.kr

1. Introduction

Pyroprocess automation mockup is a facility for evaluating durability and operability of automated pyroprocess equipment in a high temperature salt environment [1]. For this purpose, a gantry system for handling and transfer automation, and three simulated units for oxide reduction (OR) process were installed in the mockup.

To operate integrated OR process automatically, a framework is required, which can manage whole process sequences and can arrange material handling equipment based on the signals or events of all equipment in the floor. This paper addresses the development of a framework for operation automation of the integrated OR process handled by the gantry system in the mockup.

2. Automation Framework for Integrated OR Process

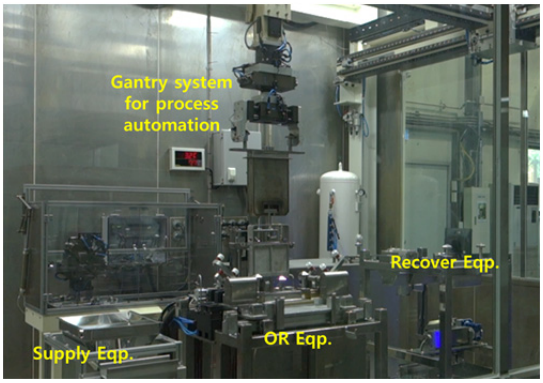


Fig. 1. Gantry system and process equipment.

Figure 1 shows the gantry system and process equipment for process automation study in the pyroprocess automation mockup. For operation automation, a process controller is required, which can command each device's controller and the gantry controller according to process sequences. Hence, in this paper, a framework has been developed based on the pyroprocess execution system (PES) for pyroprocess [2].

2.1 Design of automation control framework

In the mockup, the process sequence is relatively simple since the number of units is much smaller than the integrated pyroprocess. So, PES is simplified to design the control framework. Figure 2 shows the designed control framework. The designed framework has three modules: dispatcher for process sequence control, pEC for process equipment control, and mhEC for gantry control.

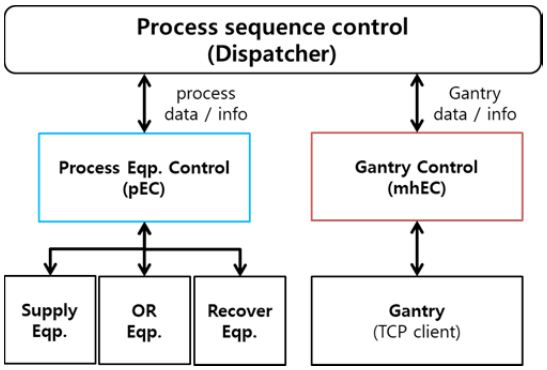


Fig. 2. Control framework.

Dispatcher manages the sequence of process steps and commands to pEC and mhEC according to the sequence and it waits reports or messages from them before sends the commands to proceed to the next step.

pEC and mhEC perform actions based on the commands from the dispatcher, and report the states or events such as start or end of action, or alarm/error.

2.2 Implementation of framework

Figure 3 shows the hardware diagram to implement the designed framework into the integrated OR process automation in the mockup.

The roles of pEC were assigned to a programmable logic controller (PLC) that could control three process devices, and pEC can communicate with dispatcher via OPC (open platform communication). Gantry controller as mhEC was modified so that it could receive the commands from dispatcher and report its states via TCP/IP communication.

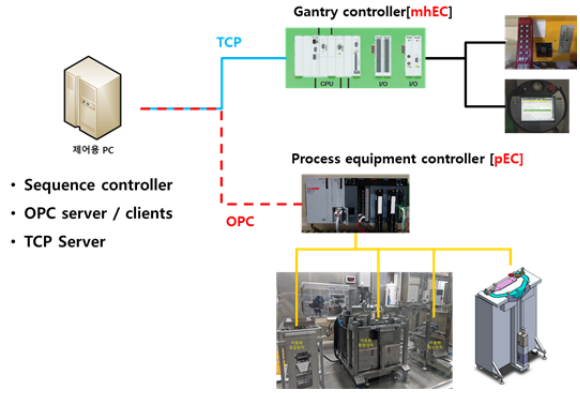


Fig. 3. Hardware diagram for implementation.

Dispatcher is implemented into a computer, and it manages and control the states of process equipment and the gantry system using a unified control program which can handle equipment data from OPC and TCP. Figure 4 shows the captured user interface of the program.

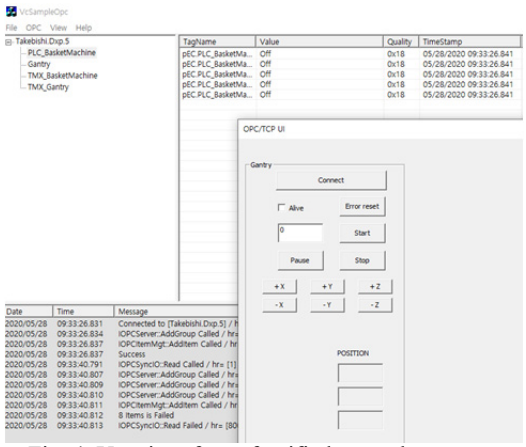


Fig. 4. User interface of unified control program.

3. Conclusion

In this paper, a framework for unit process operation automation was designed and implemented. This framework can provide the base for the pyroprocessing automation studies.

REFERENCES

[1] J. Han, et al., “Construction of Dry Room for Pyroprocessing Automation Verification Mock-up”, Proc. of the KRS 2018 Spring Conference, May 30-June 27, 2018, Busan.
[2] M.S. Shin, et al., “Preliminary design of a production automation framework for a pyroprocessing facility,” NET, 50, 2018.

Operation Set Based Handling Automation in Pyroprocess Automation Mockup

Jonghui Han*, Jongkwang Lee, Dongseok Ryu, and Seungnam Yu
Korea Atomic Energy Research Institute
*jhan@kaeri.re.kr

1. Introduction

Pyroprocess is a batch process that proceeds with the series of transfer of baskets filled with nuclear materials from the equipment to another. And since the process equipment is fixed at a certain location, the locations for handling baskets in the equipment are not changed during processes. Hence, in this paper, the operation set based gantry automation is developed and its performance was verified by automation operation of the integrated oxide reduction (OR) process handled by the gantry system in the pyroprocess automation mockup.

2. Integrated Oxide Reduction Process Automation

The automated OR process in the pyroprocess automation mockup is composed of three process units that are the supply equipment, the oxide reduction, and the recovery equipment. Cathode basket (CB) and cover are mainly handled objects by the gantry system in this process.

Figure 1 shows the process sequence of the integrated oxide reduction process in the pyroprocess automation mockup.

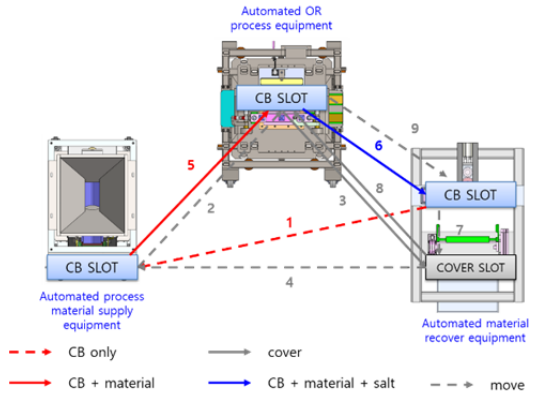


Fig. 1. Scenario of integrated oxide reduction process.

2.1 Sequence of OR process

The OR process starts from the recovery equipment. The gantry picks the empty CB from the recover equipment, and transfers it to the supply equipment (red dotted line). Then, the CB is filled with simulated process materials at the supply, and it is transported to the OR equipment (red line) and loaded into the molten salt. A few hours later, the CB is unloaded from the OR equipment, and it is transferred to the recover equipment for retrieving materials (blue line).

To implement this sequence, the sequence diagram for signals between equipment controls is shown as in figure 2. The details of the signals were defined in [2], and they are simplified for this study.

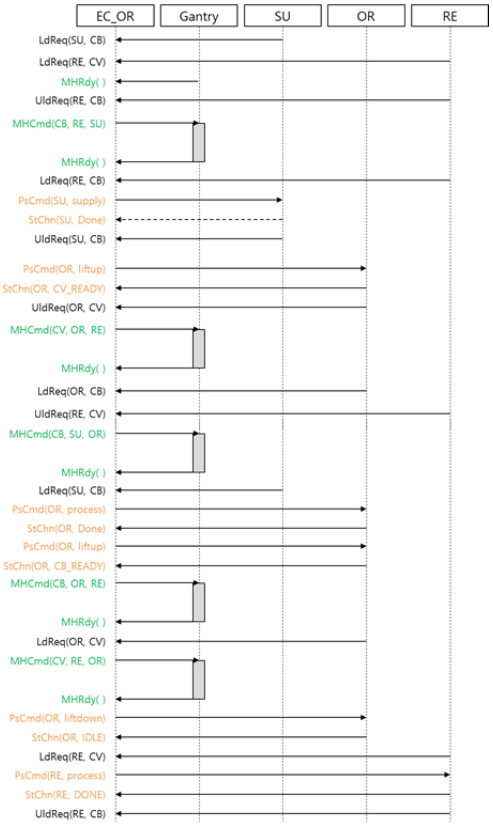


Fig. 2. Sequence diagram for integrated oxide reduction process automation.

2.2 Process operation set design

For process automation, the handling locations according to the sequence are required for gantry control. The main handling locations of the OR process are 4 points, which are 1 point on the supply equipment, 1 point on the OR equipment, and 2 points on the recover equipment. In these locations, the gantry picks or releases the handling targets (CB or cover) and transfers them to the next locations.

In addition to the main location, another 17 locations are considered for avoiding the collision

with equipment or for improving handling safety.

Since those locations are not changed during the process, gantry operations can be defined based on the locations. In other words, the gantry operations can be defined the final location, waypoints to the final location, and handling events (pick or release of basket) on the location. The 12 operation sets are implemented for the OR process as shown in figure 3.

1. Planar_gripper_attach
   - GRPS1_WORK_Z1
2. RE_pick_CB
   - RE_CB_WORK
   - planar_gripper_clamp
3. SU_release_CB
   - RE_CB_SHIFT → SU_CB_SHIFT → SU_CB_WORK
   - planar_gripper_unclamp
4. OR_pick_Cover
   - OR_CB_WORK
   - planar_gripper_clamp
5. RE_release_Cover
   - RE_COVER_WORK
   - planar_gripper_unclamp
6. SU_pick_CB
   - SU_CB_WORK
   - planar_gripper_clamp
7. OR_release_CB
   - OR_CB_SHIFT → OR_CB_WORK
   - planar_gripper_unclamp
8. OR_pick_CB
   - OR_CB_WORK
   - planar_gripper_clamp
9. RE_release_CB
   - OR_CB_OFFSET → RE_CB_SHIFT → RE_CB_WORK
   - planar_gripper_unclamp
10. RE_pick_Cover
    - RE_COVER_WORK
    - planar_gripper_clamp
11. OR_release_Cover
    - OR_CB_WORK
    - planar_gripper_unclamp
12. Planar_gripper_detach
    - GRPS1_WORK_Z1

Fig. 3. Gantry operation set.

2.3 OR process automation using gantry operation sets

As shown in figure 4, the OR process can be operated automatically using the gantry operation sets. Before the operation, the main handling locations are taught by operator using hand-held human machine interface outside the mockup.

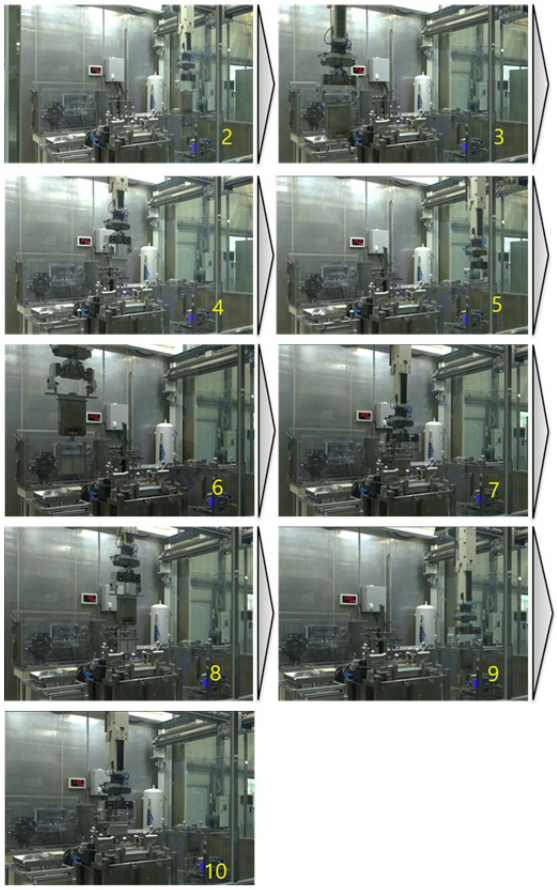


Fig. 4. OR process automation using gantry operation set.

3. Conclusion

In this paper, the gantry operation sets for the OR process automation has been defined based on handling locations and gripping event on the point. This operation set base automation was demonstrated in automation mockup.

REFERENCES

[1] M.S. Shin, et al., “Preliminary design of a production automation framework for a pyroprocessing facility,” NET, 50 (2018).

Experimental Study of Centrifugal Contactor Using Immiscible Fluids of Water and Mercury

Youn Su Kim and Byung Gi Park*
Energy Environment Departure of Soon Chun Hyang University
*rladbstn2018@sch.ac.kr

1. Introduction

The purpose of this study is to evaluating the parameters affecting efficiency of a centrifugal contactor to mix and separate immiscible fluids. Mixing and separation occur continuously in the centrifugal contactor, so parameters that affect mixing and separation may be different. Efficiency of mixing and separation is evaluated by changing parameters using water and mercury as immiscible fluids at room temperature.

2. Experimental

2.1 Centrifugal Contactor

Centrifugal Contactor is composed of housing and rotor. Immiscible fluids enter the device through the inlets of housing, pass through the gap between housing and rotating rotor (Annular Mixing Zone), and enter into rotor through rotor inlet and exhaust through weirs (Upper Weir and Lower Weir) to outlets [1].

Mixing and separating occur in different regions in the centrifugal contactor. Mixing of fluids occurs in the gap between housing inner wall and rotor outer wall by rotating rotor. Inside the rotor, centrifugal force and different density make two fluids separated and exhausted to the other weirs and outlets [1].

2.2 Immiscible Fluids

Water and mercury were used as the two immiscible liquids. At room temperature(20℃), the density of water and mercury is 0.998(g/mL) and 13.543 (g/mL).

2.3 Parameters

Parameters affecting mixing and separating are classified to physical parameters and operation parameters. Physical parameters are numerical size of the device, for example housing inner diameter, rotor outer and inner diameters and diameters of weirs. Operation parameters, which are experimentally adjustable, have flow rate ratio (M/W: mercury flow rate/water flow rate), flow rate and rotation speed (rpm) [2][3][4].

Physical parameters of mixing are housing inner diameter and rotor outer diameter affecting size of annular mixing zone. Operation parameters have flow rate of fluids and rpm. Separating parameters are rotor inner diameter, diameter of weirs, have flow rates, M/W that is wide ranges, due to start-up and shutdown, and rpm as operation parameters.

2.4 Evaluation

The evaluations of efficiency are shown in various papers. Mixing is evaluated through ALH (Annular Liquids Height) and overflow that is flowing over Annular Mixing zone to Light Phase Outlet. ALH and overflow are observed and measured through video recording and snapshot.

Evaluations of Separating are carryover and nominal total flow of two fluids. Carryover is phenomenon, other phase liquid is exhausted to outlet of the other phase liquid and described as follows [2][3][4]:

$$carrover(\%) = \frac{V_{out,other\ outlet}}{V_{in}} \times 100 \quad (1)$$

where $V_{out,other\ outlet}$ is the volume of the other liquid exhausted through the other outlet, V_{in} is the volume of injected liquid. Nominal total flow of two fluids is defined by carryover below 1%.

3. Method

The methods of mixing and separating are different. Device is made with 3D printing. To recording video, the housing is made of clear acrylic. The Flow rates were adjusted by changing the height from outlet inlet of housing to the outlet of feed tank.

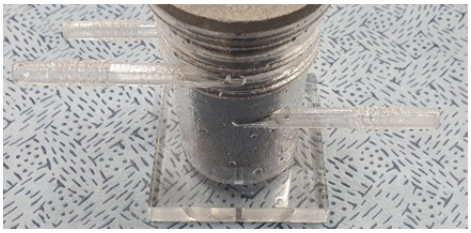


Fig. 1. 3D printing.

3.1 Mixing Evaluation

In all cases, M/W was fixed to 1. Water was continuously injected at the specified flow rate and mercury was injected when the flow of water was stable. Video was started at same time as the mercury injection. This experiment was performed by changing parameters.

3.2 Separating Evaluation

Same volumes of water and mercury were injected simultaneously at each parameter. Beakers were placed at the outlet to receive exhausted liquids. The volume of liquids were measured with a graduated cylinder.

4. Conclusion

In the study, the efficiency of centrifugal contactor was evaluated according to the parameters. ALH increased as flow rates increasing or as gap narrows. But when ALH was higher than the height of Annular Mixing Zone, overflow occurred. Separating was varied as each parameter influenced each other.

REFERENCES

[1] Leonard, Ralph. (2010). Design Principles and Applications of Centrifugal Contactors for Solvent Extraction. 10.1201/9781420059700-c10.

[2] Zhao, Mingming & Cao, Shuo & Duan, Wuhua. (2014). Effects of some parameters on mass-transfer efficiency of a 20 mm annular centrifugal contactor for nuclear solvent extraction processes. Progress in Nuclear Energy. 74. 154–159. 10.1016/j.pnucene.2014.02.024.

[3] Duan, Wuhua & Song, Chongli & Wu, Qiulin & Zhou, Xiuzhu & Zhou, Jiazhen. (2005). Development and Performance of a New Annular Centrifugal Contactor for Semi□Industrial Scale. Separation Science and Technology - SEPAR SCI TECHNOL. 40. 1871-1883. 10.1081/SS-200064531.

[4] Cao, Shuo & Duan, Wuhua & Wang, Chengqian. (2013). Effects of Structure Parameters on the Hydraulic Performance of the ϕ20 Annular Centrifugal Contactor. Energy Procedia. 39. 461-466. 10.1016/j.egypro.2013.07.237.

Estimation of Disposal Footprint for Wastes From the Advanced Nuclear Fuel Cycle

Hyo On Nam*, Hun Suk Im, and Hong Jang
Korea Atomic Energy Research Institution, Daejeon, Republic of Korea
*hnam@kaeri.re.kr

1. Introduction

Footprint of the disposal facility is one of the most important factors for the development of back-end nuclear fuel cycle strategy due to the high population and small territory in Korea. And disposal footprint for high-level radioactive waste is one of the criteria which needs to be assessed when the national policy for the management of spent nuclear fuels is discussed. In this study, at first, we have developed a baseline flowsheet of the pyroprocessing (pyro) assuming that all the PWR spent fuels (SF) is being processed and transuranic (TRU) nuclides in the PWR spent fuels will be recycled back as a fresh fuel for sodium-cooled fast reactors. Secondly, from the mass balance analysis of the advanced nuclear fuel cycle system, which is recycling spent fuels in combination with the pyroprocessing and SFR technologies, the amount of waste and their radiological characteristics were predicted. Lastly, disposal footprint for each type of waste forms were estimated assuming their disposal concepts.

2. Analysis on the Waste Streams

2.1 Total amount of PWR spent fuels

As of June 2020, 19,632 PWR assemblies and 469,044 CANDU bundles have been generated from 22 PWR and 4 CANDU reactors, which includes Kori unit 1 and Wolsong unit 1.

Based on the 8th Basic Plan on the Power Demand and Supply (BPPDS), which was established in 2017, four more PWRs will be constructed and start their operation. Therefore, total 30 nuclear power plants will be deployed in Korea. And it is estimated that total amount of spent fuels generated from the 30 NPPs will be about 61,949 assemblies (about 26,700 tons) and 632,764 bundles from the PWRs and CANDU reactors, respectively.

2.2 Flowsheet analysis

In order to assess mass balances for nuclides in PWR spent fuels through pyroprocess, various assumption such as separation ratio at each unit processes were decided.

A schematics of flowsheet of pyroprocess for PWR spent fuels is shown in Fig. 1. At first, spent fuel assemblies are disassembled and sectioned. And then fuel rod is decladded. Fuel pellets then go through several steps of heat treatment at various temperatures and gas environments. During the heat treatment process, volatile nuclides such as Cs, I, and Tc are separated and captured in the filtration system. In the next oxide reduction (OR) process, oxide form of fuel is reduced to a metallic form, and then a metallic form of fuel is delivered to the next electro-refining (ER) process. During the OR process, high heat emitting element such as Sr is eluted from the fuel to molten salt and then be separated during salt purification process. The ER process recovers uranium from the fuel anode to the solid cathode, and noble metal (NM) in the anode basket is sent to the waste treatment. After the ER process, dissolved TRUs are recovered in the electro-winning process and rare earth (RE) elements are separated.

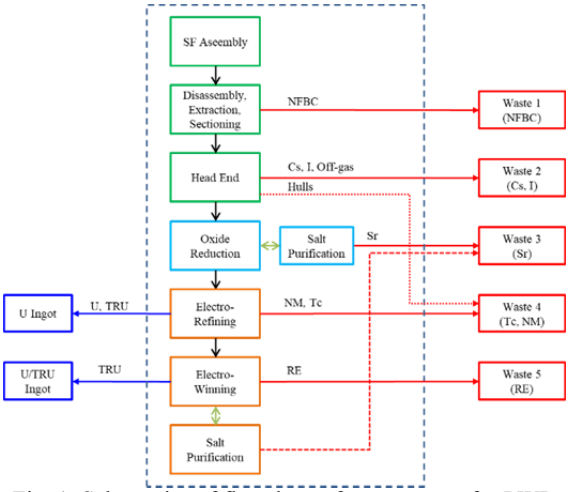


Fig. 1. Schematics of flowsheet of pyroprocess for PWR spent fuels.

3. Estimation of Disposal Footprint

3.1 Disposal concept for each waste stream

In the mass balances based on the baseline flowsheet, eight waste streams were identified. And those waste streams are classified according to the concept of disposal as assumed in previous study [1]. In case of the waste form which contains rare earth (RE) element, it is assumed

to be disposed in a deep geological repository referring to the Swedish disposal concept for the deep geological disposal [2], because it contains small amount of alpha emitting TRU nuclides. And we consider RE element waste forms as a HLW although RE element waste form is not classified as a high-level waste (HLW) according to current Nuclear Safety Act in Korea. In case of waste forms for filter wastes for capturing I and Tc is also assumed to be disposed in deep geological repository although it is not a HLW considering their high mobility in the geologic media.

In case of metallic waste from structural materials such as NFBC of fuel assemblies and cladding, and noble metal in the fuel basket from ER process are supposed to be disposed in the depth of 200~300 meters referring to the French concept for the reprocessed waste deployed in ANDRA. The waste form which contains high-emitting elements such as Cs and Sr are assumed to be stored in the decay storage for about 300 years. And the footprint for the decay storage is also estimated.

Same disposal concept is also assumed to be deployed for the waste streams from the process of SFR spent fuels except that one more waste stream is generated. Because the SFR SF is a metallic fuel which do not need OR process unlike the PWR SF, more Sr is being saturated in the molten salt and, therefore, salt wastes contains relatively high concentrations of Sr is generated. And it is assumed to be disposed in the deep geology with the RE element waste forms which is considered as a HLW.

3.2 Estimation of disposal footprint

Based on the assumed disposal concept with the estimated amount of waste forms from the mass balance analysis, disposal footprint is estimated.

In case of the direct disposal of PWR spent fuels, 15,488 canisters are needed for the disposal of 61,949 fuel assemblies. And considering a thermal limit on the bentonite buffer, spacing between the disposal tunnels (40 m) and the distance between the deposition holes (9 m) was decided. And then footprint is calculated to be about 6.02 km^2 based on the above assumptions.

In case of the disposal footprint for each disposal concept for the processed wastes is shown in Table 1. And it is estimated that the disposal footprint of HLW is about 0.089 km^2. If we are focusing on the disposal footprint for HLW, it is found that total footprint for HLW from the advanced nuclear fuel cycle system can be significantly reduced compared to the direct disposal of PWR spent fuels.

Table 1. Estimated disposal footprint for each disposal concept for the processed wastes (unit: km^2)

Disposal Concept		Wastes from PWR SF Pyro	Wastes from SFR SF Pyro	Sum
Deep Geological Disposal	HLW	0.032	0.057	0.089
	LILW	0.082	0.007	0.089
Medium Depth Disposal	LILW	0.018	0.044	0.062
Decay Storage	LILW	0.044	0.014	0.058

4. Conclusion

In this study, disposal footprint for wastes from the advanced nuclear fuel cycle was estimated from the mass balances based on the baseline flowsheet of pyroprocess in combination with the sodium-cooled fast reactors. Total about 26,700 tons of PWR spent fuels are assumed to be processed and 1,730 tons of SFR spent fuels are going through multiple recycling from the system dynamic analysis. Considering characteristics of waste forms, disposal concepts are assumed referring to the Swedish disposal concept for the deep geological disposal and the French concept for the reprocessed waste deployed in ANDRA for the medium depth disposal as described in previous study. It is found that total footprint for HLW from the advanced nuclear fuel cycle system is estimated about 0.089 km^2. And it shows a possibility of substantial reduction in the footprint compared to the direct disposal of PWR spent fuels.

REFERENCES

[1] KAERI/TR-6872, Preliminary Feasibility Study on Pyroprocessing, (2017).

[2] Final Storage of Spent Nuclear Fuel, KBS-3, Summary. SKBF/KBS, (1983).

[3] M.I. Ojovan, Handbook of Advanced Radioactive Waste Conditioning Technologies, (2011).

Effect of Cooling Time on the Characteristics of the Electrochemically Processed Wastes

Hyo On Nam*
Korea Atomic Energy Research Institution, Daejeon, Republic of Korea
*hnam@kaeri.re.kr

1. Introduction

Radioactive nuclides in spent nuclear fuel decay in the course of time. Hence it is worth assessing the effect of cooling time before electrochemical recycling process, which is so called pyroprocess, on the waste characteristics. In this study, PWR spent fuel of 4.5 wt% U-235 initial enrichment with a burnup of 55,000 MWD/MTiHM is assumed to be processed. And waste characteristics such as activity, decay heat, radiotoxicity, are analyzed as the cooling time at the time of separation process varies at 10, 40, 100, 300 years, respectively.

2. Spent Fuel Characteristics

2.1 Activity and Radiotoxicity

Radiotoxicity of total spent nuclear fuel, total actinides, and total fission products are shown in Fig.1 with the toxicity of major nuclides such as Am-241, Pu-239, and Pu-240, and so on. It is shown that the toxicity of SNF depends on the toxicity of actinides after about 250 years, because the half-life of nuclides is usually larger than fission products.

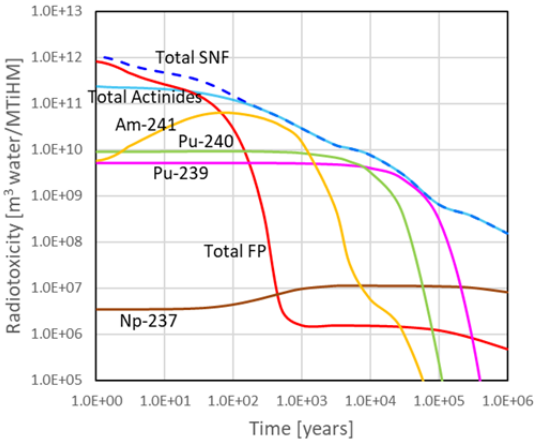


Fig. 1. Radiotoxicity of PWR spent fuel as a function of time.

2.2 Decay Heat

Decay heat of total spent nuclear fuel, total actinides, and total fission products are shown in Fig.2 with the decay heat of major nuclides. At shorter time range, decay heat of fission products, mainly Sr-90, Cs-137, and their daughter nuclides prevails than others.

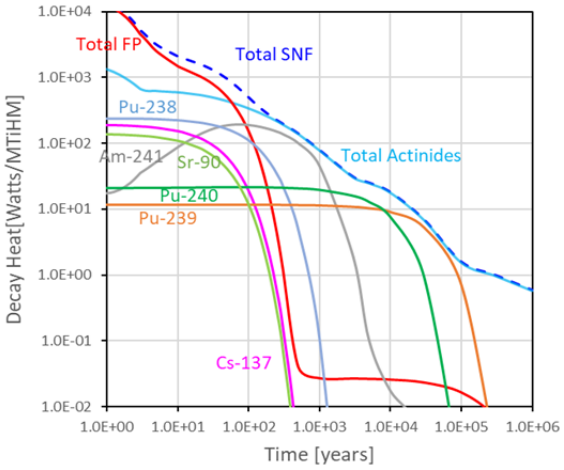


Fig. 2. Decay heat of PWR spent fuel as a function of time.

2.3 Inventory Change

Because relative short time frame about 10 to 300 years for the separation time are considered in this study, we identified nuclides with large mass variations as shown Fig. 3. At shorter time frame, nuclide mass of Cs-137, Sr-90 and Pu-241 changes dramatically, because those nuclides have a shorter half-life of about 30.18 years, 28.79 years, and 14.4 years, respectively.

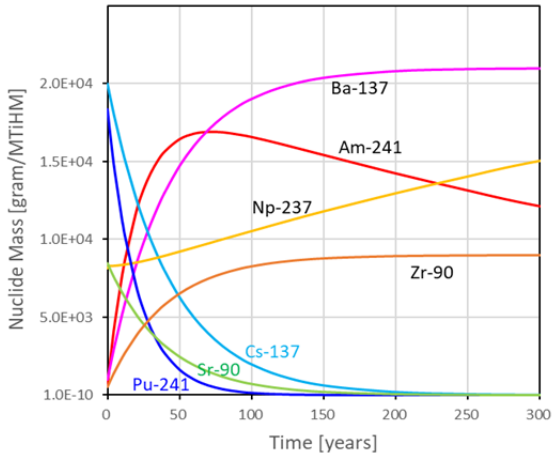


Fig. 3. Nuclide mass change as a function of time.

As the Cs-137, Sr-90 and Pu-241 decays, the amount of daughter nuclides Ba-137, Zr-90, Am-241 and Np-237 increases rapidly.

3. Electrochemically Processed Waste Characteristics

3.1 Assumed composition of waste

In this study, two different waste streams from the electrochemical process was analyzed. One is a RE waste, which is assumed to contain about 99% of rare earth elements with about 0.1% of transuranic elements(TRUs) as an impurity (See Table 1). And the other is a Sr waste from the oxide reduction process, which is assumed to contain about 97% of Sr with several elements as shown in Table 2.

Table 1. Separation efficiency of electrochemical processing for RE wastte

	RE	TRU
RE waste	99%	0.1%

Table 2. Separation efficiency of electrochemical processing for Sr waste

	Sr	Sb	Te	Ba	Eu
Sr waste	97%	50%	50%	97%	84%

3.2 Waste Characteristics

The effect of cooling time on the waste characteristics, such as activity, decay heat, and toxicity, was analyzed for the RE waste and Sr waste. The cooling time at the time of separation process(T_s) is varied at 10, 40, 100, 300 years as shown in Fig. 4 and Fig. 5. Although only decay heat of the wastes is provided in the manuscript, it is found that the cooling time for the separation does not have a significant impact on all of the waste characteristics (activity, decay heat, toxicity) considered in this study.

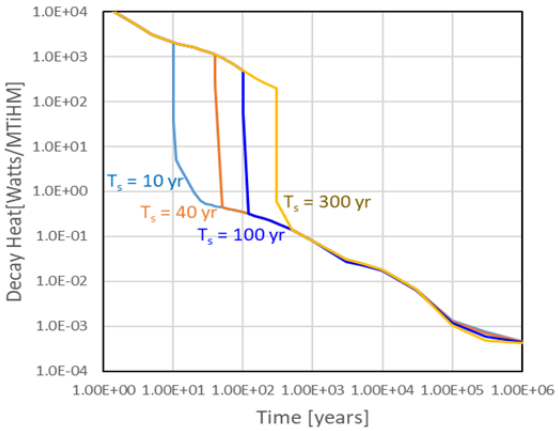


Fig. 4. Decay heat of the electrochemically processed RE waste.

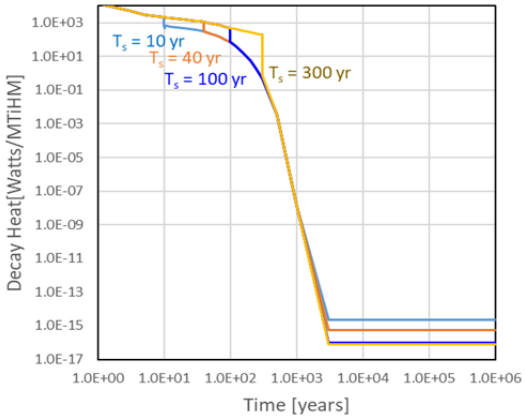


Fig. 5. Decay heat of the electrochemically processed Sr waste.

4. Conclusion

Several major nuclides such as Cs-137, Sr-90, Pu-241 which has relatively shorter half-life decays in a short time frame. And, mass of their daughter nuclides, such as Ba-137, Zr-90, and Am-241 increases. Therefore, it was assumed that the separation time of the SNF is one of the important parameters which decides the waste characteristics. And, in this study, the effect of cooling time of the spent nuclear fuel for the separation process on the waste characteristics was analyzed.

From the analysis on the waste characteristics for the RE waste, which contains higher amount of TRU elements, and the Sr waste, which contains higher amount of heat heat-emitting Sr-90, it is found that the cooling time for the separation does not have a significant impact on all of the waste characteristics.

Although it is not directly discussed in this study, the separation time is still an important factor in the electrochemical process point of view. First, as the amount of Pu-239, Am-241, and Np-237 changes as time varies, the composition will affect fuel performance if those fissile elements are recovered and recycled as a fuel. Second, sufficient cooling time is needed because the amount of decay heat generated from the waste should be limited to a certain temperature or below considering the integrity of the mechanical and chemical waste form.

REFERENCES

[1] KAERI/TR-7996, Analysis on Characteristics of Reference SNF for KRS+ Design – I. PLUS7 SNF, (2019).

3분과

고준위폐기물처분 (Oral)

Study on the Hydro-Geological Change of Natural Barriers by Borehole Expansion Test

Kyung-Woo Park*, Byeong-Hak Park, Chang-Yong Lee, Nak-Youl Ko, and Sung-Hoon Ji
Korea Atomic Energy Research Institute, 111 Daedeok-daero 989 beongil, Yuseong-gu, Daejeon, Republic of Korea
*woosbest@kaeri.re.kr

1. Introduction

The hydraulic tests described in this paper were conducted to evaluate the short-term evolution of hydrogeological properties around the borehole surface due to the expansion of borehole. For this purpose, BDZ-1 borehole with a 3-inch diameter was drilled in KURT in 2018, and it was expanded to a 4-inch diameter in 2019, which the expanded borehole was called as BDZ-E-1. Compared with the results of BDZ-1 borehole, we would like to evaluate the changes in the hydrogeological properties according to the borehole expansion. The results of this paper will be used to understand the short-term evolution of hydrogeological characteristics according to the excavation of a disposal hole.

2. Test method

Pulse test, slug test and constant head test were carried out to obtain the hydrogeological properties at BDZ-1 borehole (3-inch diameter) and BDZ-E-1 borehole (4-inch diameter) in KURT. Pulse and slug test are hydraulic test methods that observe the instant pressure change over time when the water level changes in an aquifer and then returns to the stable hydraulic head in the test section. The slug test and pulse test differ in the recovery method of the hydraulic head according to pressure displacement. The constant head withdrawal test can be carried out in the artesian aquifer. When the pressure is removed from the aquifer that has an artesian condition because the hydraulic head is higher than the elevation of the surface, groundwater in the test section is discharged to the surface. It is possible to derive the hydrogeological properties of the medium by observing the discharged flow rate.

3. Hydrogeological evolution of Natural barriers

As a result of observing the hydraulic head for each test section before and after the BDZ-1 borehole was expanded, the hydraulic head decreased in the entire test section compared to the hydraulic head before expansion (Fig. 1). The decrease in the hydraulic head results from the change in the hydraulic connectivity due to the borehole expansion. In addition to the change in the hydraulic network, a damage zone may cause a decrease of hydraulic head in the borehole, which is occurred during the process of expanding the borehole.

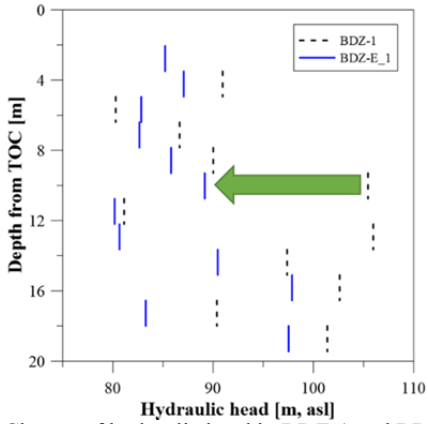


Fig. 1. Change of hydraulic head in BDZ-1 and BDZ-E-1.

When comparing the permeability before and after the borehole expansion, it can be seen that the permeability of the overall test section is increased in the pulse test, slug test, and constant head test performed after the borehole is expanded (Fig. 2). This increase in permeability may explain the increase in permeability in the excavated damage zone caused by the excavation of borehole.

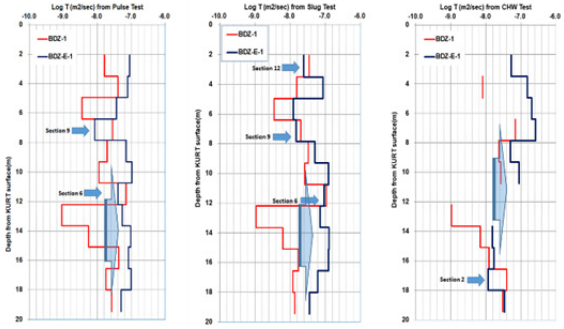


Fig. 2. Change of transmissivity before and after borehole expansion in BDZ-1 borehole.

When calculating the ratio of increase in transmissivity after expansion for each test method for the entire test section, the ratio in transmissivity decreases as the test section in the

lower region goes to the pulse test, slug test, and constant head test, while the upper section showed the opposite results (Fig. 3). The ratio in the transmissivity before and after the expansion of the borehole at each test shows that the hydraulically affected area around the excavated damage zone is getting expanded in the section adjacent to the KURT wall.

	Pulse Test	Slug Test	CHW Test
Section 1	1.88	2.62	1.14
Section 2	5.59	5.18	0.29
Section 3	1.91	7.33	1.41
Section 4	Excl. from calc.	Excl. from calc.	2.23
Section 5	Excl. from calc.	Excl. from calc.	-
Section 6	0.57	0.86	-
Section 7	9.37	4.77	3.2
Section 8	3.64	1.56	2.1
Section 9	0.30	0.75	3.81
Section 10	10.17	3.51	-
Section 11	1.95	5.54	Excl. from calc
Section 12	5.50	0.70	3.52
Average	4.09	3.28	2.24

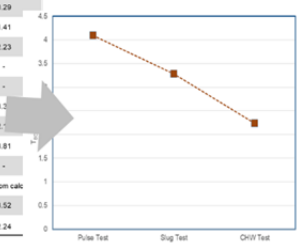


Fig. 3. Ratio of increase in transmissivity after expansion for each test method.

4. Concluding Remarks

The hydraulic test described in this paper was conducted to evaluate the short-term evolution of hydrogeological properties around the borehole surface due to the excavation of expanded borehole. Compared with the results of the previously studied hydrogeological properties in this BDZ-1 borehole, we evaluated the changes in the hydrogeological properties according to the borehole expansion. After the BDZ-1 borehole was expanded, the hydraulic head for each test section decreased compared to the hydraulic head before borehole expansion. This can predict the change of hydraulic connectivity in the excavated damage zone due to the expansion of the borehole and the impact of the damage to the KURT wall that may occur during the expansion of the borehole. Before and after the expansion, the transmissivity of the test section calculated using the hydraulic test was increased. The value of transmissivity was increased from several times to up to several tens of times, and this increase in transmissivity could be explained in the same way as the increase in transmissivity in the excavated damage zone when excavating a disposal hole.

Acknowledgments

This work was supported by the National Research Foundation of Korea (NRF) funded by the Korean government, Ministry of Science and ICT (Grant No. 2017M2A8A5014858).

Time-Resolved Laser Luminescence Properties of U(VI) Species Adsorbed on Na-Montmorillonite, Alumina, and Silica

Euo Chang Jung*, Tae-Hyeong Kim, Wansik Cha, and Min Hoon Baik
Korea Atomic Energy Research Institute, 111 Daedeok-daero 989 beon-gil, Yuseong-gu, Daejeon, Republic of Korea
*ecjung@kaeri.re.kr

1. Introduction

The release of uranium (U) from repository, entering the biosphere must be prevented for the long-term safety of radioactive waste disposal. The sorption processes of U onto several metal oxides and minerals have a significant effect on migration properties of U. The microscopic sorption characteristics at a molecular scale can be investigated using spectroscopic techniques, such as an extended X-ray absorption fine structure spectroscopy and time-resolved laser luminescence spectroscopy (TRLLS).

Although the TRLLS study of the sorption behaviors of U(VI) surface species has been studied extensively, the chemical speciation of U(VI) surface species has not been fully identified yet. A wide range of luminescence spectral shapes and lifetime values have been reported for these U(VI) surface species prepared under comparable experimental conditions. Until now, the reason of these inconsistent experimental data remained ambiguous.

In this study, TRLLS were performed for the adsorbed U(VI) on montmorillonite, alumina, and silica samples. The luminescence properties (the excitation, luminescence peak position, and lifetime) were compared between these samples.

2. Materials and Methods

Na-montmorillonite, 2:1 structured alumino-silicate clay mineral saturated with sodium, was prepared from KJ-II Gyeongju bentonite by using separation, refinement, washing, and saturation processes. The solid concentration of the prepared Na-montmorillonite suspension in 0.1 M NaCl medium was approximately 5.2 g/L. The properties of KJ-II bentonite were investigated in the previous study [1]. Commercially available alumina and silica powders were prepared with the solid concentration of 1 g/L. The experimental setup of TRLLS is described in the previous study [2].

3. Results and Discussion

Normalized luminescence spectra measured with λ_{ex} = 266 nm at the laser pulse energy of 0.1 mJ are shown in Fig. 1. The gate delay time (t_d) and width (t_w) of ICCD (intensified charge-coupled device) were set at 1 μs and 1000 μs, respectively.

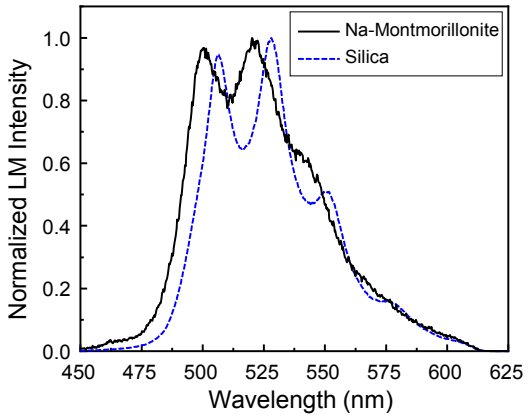


Fig. 1. Comparison of normalized luminescence (LM) spectra of U(VI) surface species measured from the silica and Na-montmorillonite at pH of 7.5. The spectra were measured at t_d = 1.0 μs and t_w = 1000 μs.

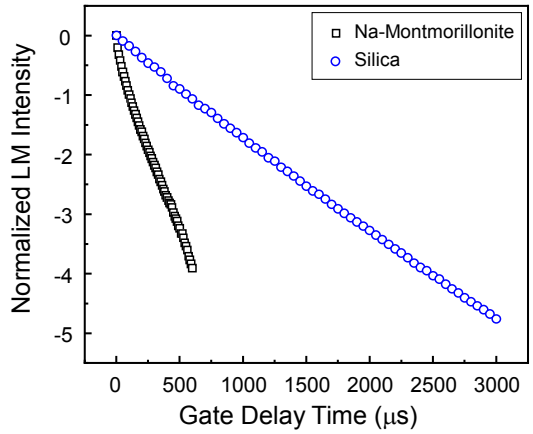


Fig. 2. Luminescence lifetimes measured from the samples used in Fig. 1. Symbols represent the normalized luminescence intensity in the natural logarithmic scale.

The luminescence measured from the silica sample showed the peak positions of 507, 528, 549, and 577 nm. On the other hand, the peak

positions at 501, 521, 538, and 563 nm were obserevd for the Na-montmorillonite.

The luminescence lifetimes of U(VI) surface species measured from the samples used in Fig. 1 are shown in Fig. 2. The luminescence intensities were measured using the kinetic mode of the ICCD for the lifetime determination. The t_d varied from 1−601 μs and 1−3001 μs with a gate delay step of 10 μs and 50 μs for the Na-montmorillonite and silica, respectively. Consequently, the luminescence intensities of 61 spectra were used to determine the lifetimes. Much longer lifetimes of approximately τ_1 = 340 μs and τ_2 = 667 μs were determined for silica than τ_1 = 40 μs and τ_2 = 187 μs for Na-montmorillonite.

Differences in luminescence peak positions and lifetimes observed in Figs. 1 and 2 imply that the U(VI) surface species adsorbed onto silanol sites of Na-montmorillonite are not predominant as compared to the those adsorbed onto aluminol sites. The luminescence characteristics of U(VI) surface species adsorbed onto Na-montmollironite, silica, and alumina will be discussed in detail.

Acknowledgement

This study is supported by the Nuclear Research and Development program of the National Research Foundation of Korea (Grant code: 2017M2A8A-5014719).

REFERENCES

[1] M. Yoo, H. Choi, M. Lee, S. Lee, “Measurement of Properties of Domestic Bentonite for a Buffer of an HLW Repository”, Journal of Nuclear Fuel Cycle and Waste Technology, 14(2), 135−147 (2016).

[2] Euo Chang Jung, Min Hoon Baik, Hye-Ryun Cho, Hee-Kyung Kim, Wansik Cha, Journal of Nuclear Fuel Cycle and Waste Technology, 15(2), 101−116 (2017).

Estimating Hydraulic Conductivity of Fractured Crystalline Rock Aquifer Using Pulse Test

Byeong-Hak Park, Kyung-Woo Park, Changyong Lee, Nak-Yeol Ko, and Sung-Hoon Ji*
Radioactive Waste Disposal Research Division, Korea Atomic Energy Research Institute, Republic of Korea
*shji@kaeri.re.kr

1. Introduction

This paper presents the hydrogeological characteristics estimated from four-inch diameter boreholes (BDZ-E_1 and BDZ-E_2) in a crystalline rock aquifer which is preferred as a host rock for high-level radioactive waste disposal repositories. For this objective, hydraulic tests (pulse, slug, and constant head withdrawal tests) were performed at BDZ-E boreholes in 2019 and 2020. By comparing three different methods, the applicability and limitation of pulse tests is discussed.

2. Hydraulic Tests

2.1 BDZ-E_1

The depth of BDZ-E_1 borehole ranges from 2.05 to 19.45 m from top of casing (TOC). Since hydraulic tests were conducted at intervals of 1.45 m using a double packer system, the borehole can be divided into 12 sections. Pulse and slug tests were performed for all sections, while constant head withdrawal tests could not be carried out at sections 5 and 6 where stable hydraulic head was relatively low.

2.2 BDZ-E_2

BDZ-E_2 borehole has 11 sections, ranging between 2.35 and 19.75 m from TOC. As in BDZ-E_1, pulse and slug tests could be performed over the entire section. Because stable head in almost sections was around TOC (80 m, ASL), constant head withdrawal test was conducted only at section 9.

3. Results and Discussions

The hydraulic conductivity values estimated from three different methods were comparable for BDZ-E_1 borehole. This indicates that pulse tests are applicable to estimate the hydraulic parameters of a fractured crystalline rock aquifer. However, there were some deviations among the estimated values when hydraulic conductivity is relatively high. This is partly due to the influence of the hydraulic radius. The greater the influence of the hydraulic radius, the higher the estimated hydraulic conductivity. Thus, the hydraulic conductivity has the highest value in constant head withdrawal tests and the lowest value in pulse tests.

Such difference in the estimated hydraulic conductivity can be partly due to the effect of nonlinear flow. When flow velocity is fast, hydraulic conductivity estimated can be distorted by nonlinear flow [1, 2]. As a result, the hydraulic conductivity is relatively low in the results of slug tests which has larger initial displacement than pulse and constant head withdrawal tests.

For BDZ-E_2 borehole which has relatively high hydraulic conductivity ($> 6.9 \times 10^{-8}$ m/s in most sections), the estimated values from pulse tests responses were 1 order of magnitude higher than those from slug and constant head withdrawal tests. This suggests the upper limit of pulse tests, which is in agreement with the previous study [3].

4. Conclusion

To evaluate hydraulic parameters of BDZ-E boreholes, pulse, slug, and constant heat withdrawal tests were performed. The results of the present work indicate that pulse tests can be applicable to estimate the hydraulic conductivity of a fractured crystalline rock aquifer. However, pulse tests have also a limitation that it can overestimate the hydraulic conductivity in a relatively permeable aquifer.

Acknowledgments

This study was supported by the Nuclear Research and Development Program of the National Research Foundation of Korea (NRF) funded by the Ministry of Science and ICT (No. 2017M2A 8A5014858).

REFERENCES

[1] S.-H. Ji and Y.-K Koh, “Nonlinear groundwater flow during a slug test in fractured rock”, Journal of Hydrology, 520, 30–36 (2015).
[2] S.-H. Ji, B.-H. Park, and K.-W. Park, “Distortion of the estimated hydraulic conductivity from a hydraulic test in fractured rock due to

excessive injection or extraction", Water, 12, 2712 (2020).
[3] S. Walter, T. Arno, F. Hansruedi, and G. Hans-Jurg, "Geohydraulic tests in rock", (2006).

Modeling the Sequential Canister Failures and Solute Transport in the Geological Disposal System

Minjeong Kim*, Jung-Woo Kim, Jaewon Lee, and Dong-Keun Cho
Korea Atomic Energy Research Institute, 111, Daedeok-daero 989beon-gil, Yuseong-gu, Daejeon, 34057, Korea
*mjkim1@kaeri.re.kr

1. Introduction

The APro is a process-based total system performance assessment framework which simulates the multi-physics in a geological disposal system for high-level radioactive waste [1]. The APro takes into account the failure of copper canisters by corrosion due to dissolved oxygen in groundwater. The existing model assumes that failures of all canisters in the same near-field domain would occur simultaneously. However, this assumption disregards the sequential canister failures that could potentially occur in the near-field domain. Multiple near-field domains can represent the sequential canister failures, but increase the computational load including multiple component couplings.

The objective of this study is to simulate the sequential canister failures and consequent solute transport by improving the APro to calculate the canister failures based on not the near-field domain but the repositories which are included in a near-field domain.

2. Method

2.1 Model description

The APro has been developed in MATLAB by coupling COMSOL for THMC and PHREEQC for geochemical reaction. The APro calculates the canister thickness (Th_{Cu}) in the COMSOL engine by following equation (1):

$$\frac{\partial Th_{Cu}}{\partial t} = -\frac{R_{Cu|O_2} \cdot Q_{O_2} \cdot W_{Cu}}{\rho_{Cu}} \quad (1)$$

where, $R_{Cu|O_2}$ is the mass loss rate of Cu to O_2 (4 [-]), Q_{O_2} is the normal flux of O_2 [mol/m^2·s] computed by COMSOL, W_{Cu} is the atomic weight of Cu (63.546·10^{-3} [kg/mol]), and ρ_{Cu} is the density of Cu (8,900 [kg/m^3]).

Canister failure is expected to occur in a repository if the thickness of any point of a canister in the repository is below the minimum thickness threshold. The initial thickness of a copper canister is assumed to 0.05 m, while the minimum thickness threshold is set to 0.001 m.

After the canister failure, the boundary of a canister becomes permeable, and the solute inside the canister is released.

2.2 Model set-up

To simulate the sequential canister failures in the near-field domain, this study intentionally placed nine disposal repositories with six canisters each in the fractured zone where the Darcy velocity is relatively high (Fig.1). In addition, this study pessimistically assumed that groundwater at the repository level has high dissolved oxygen (0.1 [mol/m^3]).

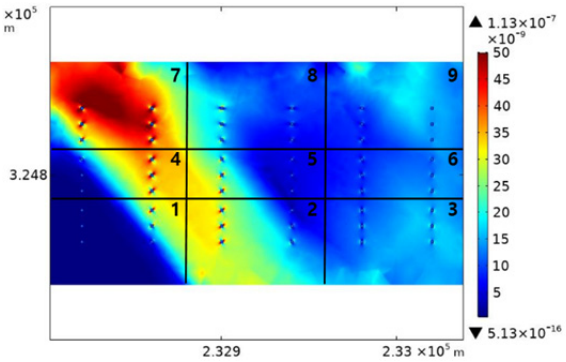


Fig. 1. Spatial distribution of Darcy velocity in the model domain.

The study simulated thermal, hydraulic, and chemical processes for 1,000,000 years. Chloride of 1 mol/m^3 was inserted in each canister as a conservative tracer.

3. Results and discussion

Canister failures occurred at five different years in the order of repositories that were located in the outside with high Darcy velocity, the outside with low Darcy velocity, and the inside, as described in Table 1. The spatial distribution of the total flux of O_2 computed when the first failure occurred is depicted in Fig. 2. As expected, the total flux of O_2 (Fig. 2) was highly correlated with the Darcy velocity (Fig. 1). From the comparison between Table 1 and Fig. 2, it could be confirmed that the sequence of canister failures was dominantly affected by the O_2 flux. However, there is still an uncertainty;

for instance, Repository 5 was lastly failed although some boreholes in the Repository 5 had the comparable O_2 flux with other repositories failed earlier. This will need to be further analyzed later.

Table 1. Times of canister failures

Failure Order	Repository #	Year
1	2,3,4,7,8	348,743
2	6	353,520
3	9	356,495
4	1	377,079
5	5	389,265

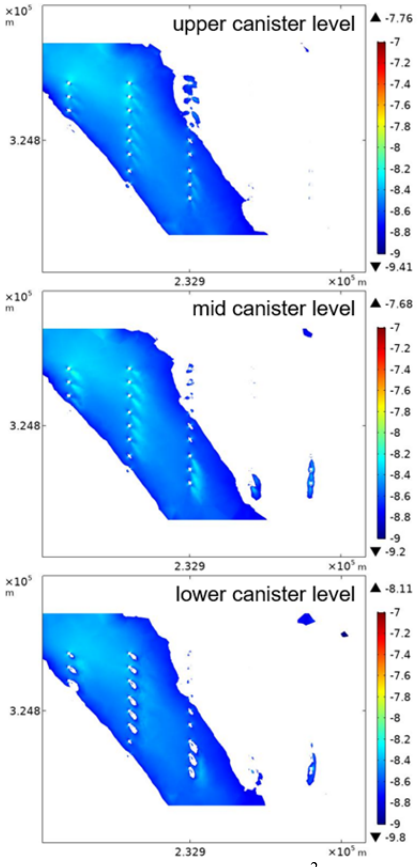


Fig. 2. 2D total flux of O_2 [log(mol/m^2·s)], which is greater than 1E-8.7 mol/m^2·s, when the first failure occurred.

The spatial distribution of chloride concentration at 1,000,000 year, when all the canisters are failed, is shown in Fig. 3. During the time span, most of the released chloride has been transported outward, while the relatively high concentration was still observed near the Repository 1 where solute transport was slow due to the low Darcy velocity.

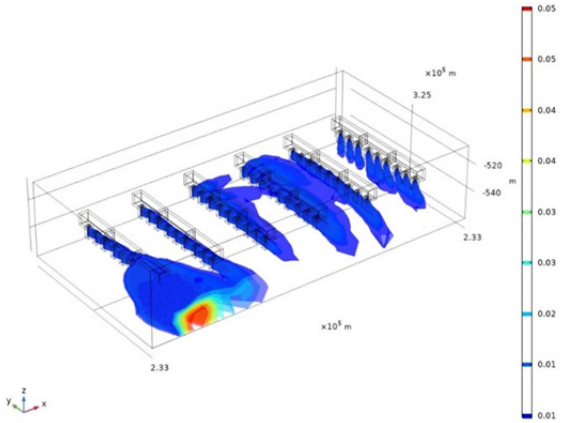


Fig. 3. Spatial distribution of chloride concentration at 1,000,000 years.

4. Conclusion

This study improved the APro to simulate the canister failures based on the repository. Canister failures preferentially occurred in the area with high Darcy velocity and correspondingly high O_2 flux. This model can be used for safety assessment for the full-scale geological disposal system.

ACKNOWLEDGEMENT

This work was supported by the National Research Foundation of Korea Nuclear Research and Development Program (2017M2A8A5014856) funded by the Ministry of Science and ICT.

REFERENCES

[1] Kim, J. W., Lee, J., & Cho, D. K. (2019). Development of User-friendly Modeling Interface for Process-based Total System Performance Assessment Framework (APro) for Geological Disposal System of High-level Radioactive Waste. JNFCWT, 17(2), 227-234.

Technology Innovation for Future Safety and Security Enhancement of a Deep Geologic Repository

Yongsoo* Hwang and Hyo-On Nam
Korea Atomic Energy Research Institute
*yshwang@kaeri.re.kr

1. Introduction

It has been almost forty years since the Swedish SKB publicized the world famous KBS-3V concept. Even though there have been series of alternative studies, still, it is the reference concept for the final disposal of spent nuclear fuels and the high- level radioactive wastes world-wide for sedimentary rock formations. The principle of defense in-depth by multiple barrier systems is the core of the KBS-3V concept. For the last decade, many innovative technologies are introduced which can be applied in the frame of the traditional KBS-3V type repository and the other innovative new repository concepts. In this paper, the technical status and the perspectives are to be discussed.

2. Technological Innovation

2.1 Canister Design and Manufacturing

The traditional waste container developed through the early phase of the KBS-3 concept development has been changed a little bit to ensure the long-term resistance against the pitting corrosion and other mechanisms and the mechanical stability against the pressures from the lithostatic and the bentonite buffer swelling. To eliminate the possibility of corrosion through the electrical wedding processes, practical measures have been implemented. Recently, in Canada, NWMO has implemented the cold spray to copper particle coating against the pitting corrosion. In addition, the 3D printing technologies are under evolution quite rapidly. These new technologies can be integrated with the traditional waste container concept development to fundamentally eliminate the possibility of initial waste container failure event and any potential defect creation to accelerate the corrosion later. The cost to manufacture the KBS-3 waste containers is high so that the application of the 3D printing shall contribute the reduce the cost significantly.

2.2 Security Measures

The spent nuclear fuels contain sensitive nuclear materials such as Pu-239 and U-235. Also, a certain amount of radioactive wastes can be used to manufacture a dirty bomb. Therefore, it is important to protect the repository against any malicious activity to excavate the access pathways to theses nuclear materials. To protect the adversary attempts, it is desirable to consider the nuclear security issues from the design concept development. In the ROK, both CANDU and PWR spent nuclear fuels are deposited into a same repository. How to develop the repository design with these two mixtures of the spent nuclear fuels shall be the one subject to enhance the nuclear security. Moreover, the extremely long batteries using special radioactive isotopes have been developed mainly throughout the space traveling. If the special detection measures are developed in combination of the new batteries ensuring quite long-time detection operation, and properly embedded when spent nuclear fuels are disposed of and when the repository is closed, it shall contribute to enhance the nuclear security significantly.

2.3 Excavation Measures

When the Swedish SKB developed the KBS-3 concept in early 1980's, they were considering both controlled blast and TBM's for tunnel excavation and a certain raising borehole machine to emplace a deposition hole under the tunnel floor. To do the technical constraint to excavate the tunnel, the tunnel size was limited to 5.5 meters so that the specific installation of a waste container was conceptualized. Nowadays, the tunnel size has been enhanced a lot throughout the evolution of the TBM's and the excavation technologies. In addition, the new generation of excavation technologies have been commercialized throughout the borehole drilling for deep geologic oil drilling and especially shale gas drilling. The deep borehole(DB) as well as the inclined borehole disposal concepts such as Deep Isolation System(DIS) become the practical solutions to permanent dispose of high level waste whose canister diameter size is around one foot at this moment. Also, there shall be great technology development in this area for a larger diameter borehole drilling. The author trusts that these technologies can be readily applicable to a potential HLW repository in soft rock formations

such as sedimentary rocks even though there might be a certain technical challenge to deal with a potential EDZ around a borehole for a repository in a hard rock such as crystalline granite. When the excavation and backfilling technologies are developed it will be important to adopt the development for a repository design concept for spent nuclear fuels as well as HLW. The deeper one can go down deeper for a repository without inadvertently creating the EDZ the potential pathway of the groundwater and radionuclide in dissolved in the groundwater, the much significantly it will contribute to enhance the long-term post closure radiological safety of a repository.

2.4 Solidifications

At this moment, the major concept for the permanent management of spent nuclear fuels in the ROK is the implementation of the direct disposal. When the proper technical innovation has been accomplish to properly isolate volatile fission products such as I, Tc, Sr, and Cs throughout the vol-oxidation process in association with the practical measure to form a stable solid form for these radionuclides, then the deep borehole disposal(DBD) or the DIS can be applied to further enhance the radiological safety as discussed above. Key advanced solidification researches have been undertaken in Japan to develop the compact solid forms while reducing the stresses by applying heat sources during the three-axial compression. When these technologies are properly combined, the compact solid wastes to isolate the troublesome volatile fission products suitable for deep disposal can be materialized. In that context, it will be important to further study the vol-oxidation processes which has been developed throughout the DUPIC and pyro-processing projects. If the additional measures are developed throughout the proper modification of the electrolytic reduction process technology development, a much more stable ceramic type waste solid form for all TRU's can be available within a foreseeable future. A ceramic waste from shall contribute significantly to limit the potential dissolution of TRU's when contacted by introducing groundwater after the breach of a waste container in a repository. This will enhance the long-term post closure radiological safety also.

3. Conclusions

The importance of safety assurance for a permanent spent nuclear fuel and HLW repository cannot be emphasized too strongly. The old Swedish KBS-3 repository concept is the backbone for this mission, The recent technology innovations in many areas can certainly enhance the long-term post closure radiological safety of a repository significantly while in many cases contributing the reduction of disposal cost. The proper combinations of technical options are recommended to be properly cultivated throughout future research.

Numerical Estimation of Changes in Hydrogeological Characteristics Around a Disposal Hole at an Underground Research Tunnel

Chae-Soon Choi*, Kyung-Woo Park, Nak-Youl Ko, Byeong-Hak Park, and Sung-Hoon Ji
Korea Atomic Energy Resea ch Institute, 111, Daedeok-daero 989 beon-gil, Yuseong-gu, Daejeon, Republic of Korea
*cschoi@kaeri.re.kr

1. Introduction

A construction of disposal tunnel and borehole through an excavation in underground rock mass can induce changes in geological structure and state of in-situ stress. Characteristics changes of discrete fracture can be intensively occured around the disturbed region which affect the stability of the geological disposal system of radioactive wastes. In this study, a numerical model had been implemented to simulate field tests conducted in the KAERI underground research tunnel(KURT) to examine the hydrogeological features around the borehole. The model was expected to analyze the hydraulic behavior of the borehole according to the stress release and extended borehole size. The simulation indicated that the field test results of the change in transmissivity of the borehole could be greatly affected by the hydraulic condition in the geological formation as well as the in-situ stress state.

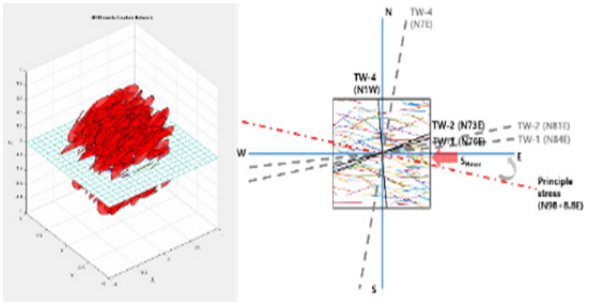
2. Procedure for numerical simulation

The purpose of the numerical model is to examine a dependence of the aperture changes to a princial stress direction and which is important factors to affect an increase in transmissivity.

2.1 Generation of DFN model with boundary conditions

The hydrogeological field tests were subjected to the borehole of BDZ-1 in research gate (RG#6) of KURT. In order to construct a representative numerical model of BDZ-1, a discrete fracture network that can be possible to exist within the research gate had been created using a DFN generator developed by Park et al. [1]. Input parameters of the fracture sets like fisher constant and dip/dip direction information were determined by a geological survey of RG#6.

The fracture density and mean trace length of the generated fracture set were indicated in Fig. 1. Considering the construction site of BDZ-1 on the free-surface from bottom to depth of 20 m in KURT (elevation 80 m), it can be seen that the vertical stress expressed as a function of depth is not significant. Therefore, numerical domain with 2D trace fracture network geometry was composed in distinct element method program, UDEC. And the boundary condition of principal stress was assigned in 6 MPa and 4 MPa according to the depth of the on-site test section (BDZ-1 section2, E.L 63.3 m) which was measured by hydraulic fracturing test [2]. A direction of maximum and minimum principal stress was also adopted in a parallel direction to the x-and y axis of the rotated domain.

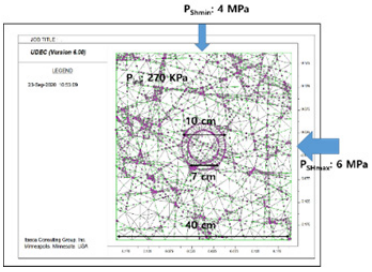


Fisher constant	Dip/Dip direction	Fracture density(m^{-2})	Mean trace length(m)
25.5	60/354	36	0.23
16.6	54/351	34	0.24
24.4	76/277	40	0.24

Fig. 1. DFN model and information of joint set.

2.2 Application of hydraulic environment

The artesian well of BDZ-1 was implemented in hydraulic-mechanical coupled simulation with a specific hydraulic head mesured by slug test [3]. A initial hyrauliuc pressure was assigned by 270 KPa and key input parameter of aperture size at high and zero normal stress was also determined by matching the transimissivity of the field test. The transimissivity of the test section 2 in BDZ-1 was 1.77 e-8 m2/s and constructed numerical model with corresponding aperture size had a transmissivity of 1.25 e-8 m2/s. Fig. 2 shows the numerical model and key input parameter for fracture properties.



Normal stiffness	$151.2e^{9}$ (N/m)	Shear stiffness	$4.9e^{9}$ (N/m)
Aperture at high stress	$1.2e^{-6}$ (m)	Aperture at zero normal stress	$1.5e^{-5}$ (m)

Fig. 2. Initial condition and input parameter.

3. Results

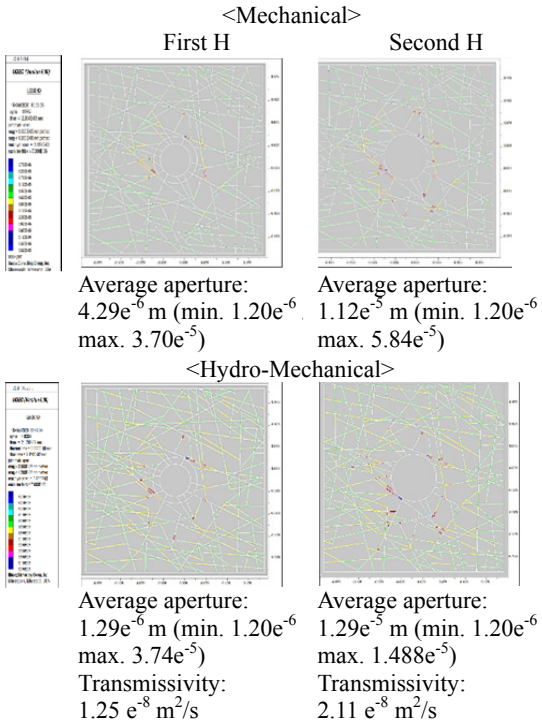


Fig. 3. Hydraulic results of the numerical model.

Mechanical model and hydraulic-mechanical coupled model were compared to investigate an effect of principal stress and complex aspect of hydraulic and stress state to changes in aperture and transmissivity. Figs. 3 and 4 show a results depending on the borehole size and numerical simulation mechanism. Much larger fracture aperture can be found in coupled model in a first borehole excavation process. And also, it is confirmed that a disturbed zone around the borehole had been propagated into a wide size through a fluid flow path. After the second expanded borehole process, the hydraulic aperture changes in coupled model was not significant compared to the mechanical model. However, the transmissivity value through the inflow rate into the borehole had been confirmed to increase about 2-order. These results were somewhat consistent with the on-site test data of the increased transmissivity after the expansion of the borehole size of BDZ-1. Based on the above results, it is assumed that hydraulic status become a major factor in evaluation model for the disposal site in KURT geological formation.

4. Conclusion

A numerical model had been implemented to estimate field test results to examine the hydrogeological features in the disturbed zone around the borehole. The simulation indicated that the change in transmissivity of the borehole could be greatly affected by the hydraulic condition in the geological formation as well as the in-situ stress state. This interpretation will require further expansion to a three-dimensional model considering the geological structure feature of KURT.

ACKNOWLEDGEMENT

This work was supported by the Nuclear Research and Development Program of the National Research Foundation of Korea (NRF) funded by the Ministry of Science and ICT (No. 2017M2A8 A5014858).

REFERENCES

[1] Park, S., Kwon, H., Yoo, L., Xie, L., Min, K.B., Kim, K.Y., Development of a hydraulic stimulation simulator toolbox for enhanced geothermal system design, Renew. Energ. 118(118), 879-895.

[2] Jo, Y., Chang, C., Park, K.W., Ji, S.H., Lee, C., In situ stress estimation in KURT site, J. Geol. Soc. Korea, 53(2017), 689-701.

[3] Park, K.W., Ko, N.Y., Ji, S.H., A study on the applicability of the hydraulic test method performed at an underground research facility in crystalline rock, Econ. Environ. Geol. 51 (2020), 121-131.

3분과

고준위폐기물처분 (Poster)

Evaluation of Water Retention Curve for Korean Bentonite Buffer Considering Dry Density and Temperature Variation

Seok Yoon*, Geon-Young Kim, and Dong-Keun Cho
Korea Atomic Energy Research Institute, 989-111, Daedeok-daero, Daejeon, Korea
*syoon@kaeri.re.kr

1. Introduction

An engineered barrier system (EBS) is suggested to dispose high level waste (HLW). It is composed of a disposal canister with packed spent fuel, a buffer material, a backfill material, and a gap-filling material [1]. A buffer material is very essential to guarantee the disposal safety of HLW, and play a very important role to protect the waste and canister against any external mechanical impact. After closure of the repository, the bentonite buffer is unsaturated. Initially, the bentonite buffer near the canister will become dry due to the decay heat from the container. Decades or hundreds of years later, the buffer becomes gradually saturated because of groundwater penetration. The saturated or unsaturated process of the bentonite buffer can be determined by water-retention curve (WRC). In this reason, dry density of bentonite buffer is changed, and it also experiences temperature variation in real repository environment. Therefore, in this study, among the thermal-hydro-mechanical properties of the bentonite buffer, WRC according to the conditions under which the saturation by temperature is constant and by dry density variation were obtained using Korean compacted bentonites.

2. Experimental Setup

2.1 Measurement of water suction

The water suction of the Korean bentonite buffer was measured. The suction can be can be calculated using the Kelvin equation like Eq. (1), which expresses the thermodynamic relationship between the total suction and relative humidity of the vapor space in bentonite [2].

$$\psi = -\frac{RT}{M}\ln\left(\frac{RH}{100}\right) \quad (1)$$

Where P is the vapor pressure of air (kPa), P_o denotes the saturation vapor pressure at the specimen temperature (kPa), R is the gas constant (8.31 J/ (mol K)), T is the Kelvin temperature of the specimen, and M is the molecular mass of water [3].

2.2 Results and Discussion

The initial water content of compacted bentonite used in the test was approximately 12% and the dry density was 1.61 g / cm³. The WRC experiment was conducted under the case where the saturation of bentonite was constant with temperature increase. Fig. 1 shows water suction values of compacted bentonite according to the temperature from room temperature to 100 ℃. The water suction was also measured under the completed confined condition according to various dry density variation between 1.40~1.73 g/ cm³. Fig. 2 shows WRC considering dry density variation. Higher water content resulted in greater increases in thermal conductivity. Bentonite is a three-phase system consisting of soil particles, water and air, and the thermal conductivity of soil is known to increase with temperature. Furthermore, there was no significant difference for suction above about 10 MPa, and higher water content with small dry density. It is though that dry density variation leads to change macro-pores of compacted bentonite [4].

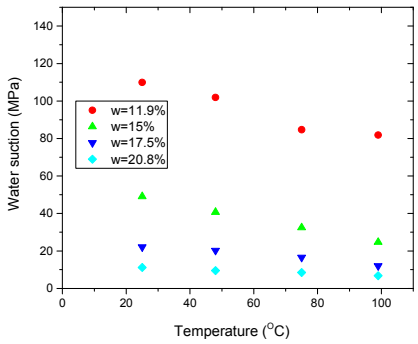


Fig. 1. Water suction vs temperature increase.

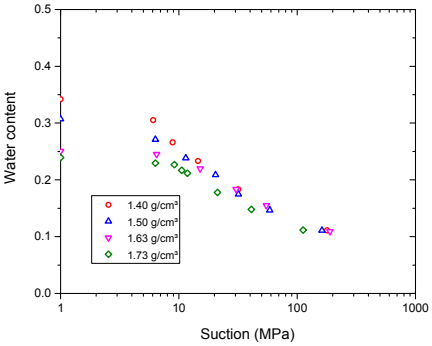


Fig. 2. Water suction considering dry density.

3. Conclusion

In this study, the water suction of Korean compacted bentonite buffer was measured according to the temperature and dry density variation. The water suction decreased as temperature increased, and there was no significant difference for suction above about 10 MPa.

ACKNOWLEDGEMENT

This research was supported by the Nuclear Research and Development Program of National Research Foundation of Korea (NRF) funded by the Minister of Science, ICT and Future Planning.

REFERENCES

[1] Lee, J.W., Choi, H., Lee, J.Y., Thermal conductivity of compacted bentonite as a buffer material for a high-level radioactive waste repository, Ann. Nucl. Energy 94 848-855, (2016).
[2] Nguyen-Tuan, L., Coupled thermos-hydro-mechanical analysis: experiment and back analysis, Ph.D Thesis, Ruhr-Universität Bochum, (2014).
[3] Yoon, S., Jeon, J.S., Chang, S., Lee, D.H., Lee, S.R., Kim, G.Y., Characteristics of water suction for a Korean compacted bentonite, Nucl. Technol. 206(2020), 514-525.

Comparison of Q-Equivalent Models for the Mass Transfer Around the Deposition Hole

Heui-Joo Choi*, In-Young Kim, Jong Youl Lee, and Dong-Keun Cho
Korea Atomic Energy Research Institute, 1045 Daeduk-daero, Yuseong, Daejeon
*HJCHOI@kaeri.re.kr

1. Introduction

One of the final solutions for the safe management of the spent nuclear fuels generated from the nuclear reactors is to use the geological disposal. KAERI is developing a geological disposal repository called KBS-3 type repository. This type repository was first proposed by Swedish several tens years ago. Two most important engineered barriers are the disposal canister and the bentonite buffer.

The safety of this concept mainly relies on a copper canister. The lifetime of the copper canister should be correctly estimated. For this purpose, mathematical modeling was introduced. In addition, radionuclide transport from the canister to the groundwater flowing in the rock was assessed using mathematical modeling techniques.

Generally, a disposal canister is located in a deposition hole surrounded by a compacted buffer which is intersected by one or more fractures with seeping groundwater. The term and concept of equivalent flowrate [Q-equivalent] was introduced to calculate the mass transport from or to the canister from the groundwater flowing in the rock by Neretnieks [1]. This model is still used to calculate the amount of corrosive agent to the canister surface. The authors developed a numerical model using Q-equivalent model [2] and found that there were lots of differences in the models used for the same situations.

In this paper, we derived the equivalent flowrate according to the definition by Neretnieks. Many authors who used the Q-equivalent model did not use the models with clear definitions. Thus we reviewed their equations and compared them with the illustrative calculations.

2. Q-Equivalent models

2.1 Definition

According to Neretnieks et al., the equivalent flowrate was introduced to assess the rate of solute transport to or from a canister (Fig. 1) [2]:

$$\mathrm{N} = Q_{eq}^{overall}(c_w - c_o) \qquad (1)$$

Q-equivalent is the transport capacity for a given concentration difference and the product of the mass transfer coefficient and the contact area.

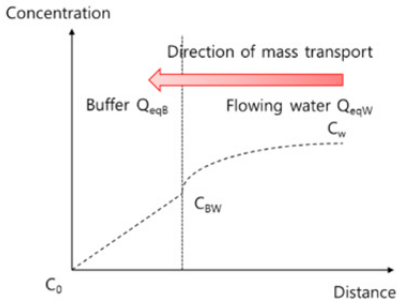


Fig. 1. Corroding agent transport from groundwater to canister surface through a buffer.

It is assumed that the mass transport within a boundary layer around the deposition hole was governed by diffusion (Fig. 2). Then the following analytical solution was easily found in many literatures:

$$\frac{c(z,t)}{c_\infty} = 1 - erf\frac{z}{\sqrt{4D_v t}} \qquad (2)$$

Then, the flux at the canister surface was obtained as follows:

$$\mathrm{N}(z=0) = -D_v \frac{dc}{dz}\Big|_{z=0} = \sqrt{\frac{D_v}{\pi t}} \qquad (3)$$

$$\eta_{mean} = \int_0^{t_0} N(t, z=0)dt = \sqrt{\frac{4D_v t_0}{\pi}} \qquad (4)$$

Thus, mass transfer coefficient was calculated:

$$k_v = \sqrt{\frac{4D_v}{\pi t_0}} \qquad (5)$$

Finally, equivalent flowrate was obtained:

$$Q_{eq} = Area \times k_v = 8b_v\sqrt{D_v r_t u_f} \qquad (6)$$

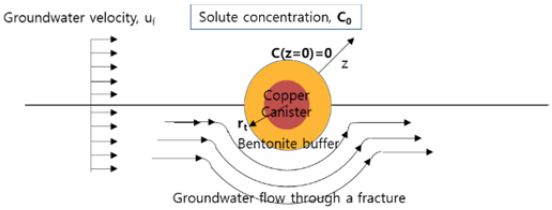


Fig. 2. Groundwater flow around the deposition hole.

2.2 Comparison of models

Moreno and Gylling used the following equivalent flowrate model in COMP23 code to calculate the transport of radionuclides from a possible defective canister into the far field [3]:

$$Q_{eq} = 2WU_0\eta_{mean} = 2WU_0\sqrt{\frac{4D_v t_w}{\pi}} = 8b_v\sqrt{D_v r_t U_0} \quad (7)$$

Lindgren and Lindström [4] used the Q_{eq} model for the calculation of the rate of transport in the near-field compartment for SR-97 project. They followed the equation proposed by Romero:

$$Q_{eq} = q_0W\eta_{mean} = q_0W\sqrt{\frac{4D_v t_w}{\pi}} = 4b_v\varepsilon_f\sqrt{D_v r_t u_f} \quad (8)$$

Smith et al. carried out the safety assessment for a KBS-3H repository [5]. They cited the Vieno and Nordman and used the equivalent flowrate as follows:

$$Q_{eq} = \frac{4\pi b_v r_t}{\pi}\sqrt{\frac{2D_v Ti_0}{r_t b_v}} = 4b_v r_t\sqrt{\frac{2D_v Ti_0}{r_t b_v}} = 8b_v\sqrt{D_v r_t u_f \epsilon_f} \quad (9)$$

Vieno and Nordman carried out TILA-99 safety assessments using REPCOM model for near-field transport of radionuclides. They used the equivalent flowrate:

$$Q_{eq} = 2\pi r_t 2b_v\sqrt{\frac{4D_v u_f}{\pi^2 r_t}} = 8b_v\sqrt{D_v r_t u_f} \quad (10)$$

2.3 Illustrative calculation

In this paper five different models used for the safety assessment were reviewed. In order to compare differences of the models, an illustrative calculation was carried out with the data in Table 1.

Table 1. Parameters used for the Q-equivalent model comparison

Parameter	Value	Unit
r_t	0.875	m
$2b_v$	1.58×10^{-5}	m
D_v	1.0×10^{-9}	m^2/s
U_0	1.0×10^{-11}	m/s
u_f	6.32×10^{-7}	m/s
porosity	1.58×10^{-5}	-

The results of the illustrative calculation were given in Table 2. Depending on the models, the results showed big differences.

Table 2. Results of illustrative calculation

Model	Equation	Value [m^3/s]
Neretnieks	$8b_v\sqrt{D_v r_t u_f}$	1.49×10^{-12}
Moreno-Gylling	$8b_v\sqrt{D_v r_t U_0}$	5.92×10^{-15}
Lindgren-Lindström	$4b_v\varepsilon_f\sqrt{D_v r_t u_f}$	1.18×10^{-17}
Smith et al.	$8b_v\sqrt{D_v r_t u_f \varepsilon_f}$	5.92×10^{-15}
Vieno-Nordman	$8b_v\sqrt{D_v r_t u_f}$	1.49×10^{-12}

3. Conclusion

Q-equivalent model has been widely used to describe the mass transport around the deposition hole. However, due to unclear definition of the model, several kinds of equations were used. In this paper, we tried to clarify the exact equation.

Acknowledgement

This work was supported by the Ministry of Science and ICT within the framework of the national long-term nuclear R&D program (NRF-2017M2A8A5014856).

REFERENCES

[1] Neretnieks I., Transport of oxidants and radionuclides through a clay buffer, SKB 79, (1978).

[2] I. Neretnieks, L. Liu, L. Moreno, Mass transfer between waste canister and water seeping in rock fractures, SKB TR-10-42. (2010).

[3] L. Moreno and B Gylling, Equivalent flow rate concept used in near field transport model COMP23, SKB R-98-53 (1998).

[4] M. Lindgren and F. Lindstrom, SR97 Radionuclide transport calculations, SKB TR-99-23 (1999).

[5] P. Smith et al., Safety assessment for a KBS-3H spent nuclear fuel repository at Olkilouto, POSIVA 2007-08 (2007).

[6] T. Vieno and H. Nordman, Updated compartment model for near-field transport in a KBS-3 type repository, POSIVA WR 2000-41 (2000).

Retrievability of Deposited Canisters in the KRS+ Repository

Heui-Joo Choi*, Jong Youl Lee, and Dong-Keun Cho
Korea Atomic Energy Research Institute, 1045 Daeduk-daero, Yuseong, Daejeon
*HJCHOI@kaeri.re.kr

1. Introduction

Although the final goal of the geological disposal is to permanently isolate the high-level waste from the human environments, it has been required to design a repository in which we can retrieve the deposited waste if necessary. The authors have developed the KBS-3 type repository with the KURT geological data. This type repository consists of important engineered barriers, a disposal canister, bentonite buffer and backfill.

According to the Nuclear Safety and Security Commission (NSSC) Notice 2017-74, the following articles are required for the design of a geological repository related to the retrieval:

- Article 2 (definition). Retrieval of radioactive waste refers to returning the deposited waste to the previous state of management before disposal.
- Article 14-4. Deep geological repository shall have a plan to safely retrieve radioactive waste if necessary during the operational period, and secure the spaces and facilities to manage the retrieved waste at appropriate locations above and below ground.

Some scenarios were assumed to provide solutions to meet the above mentioned requirements. We reviewed the previous designs and tried to find a way to manage the retrieved waste and bentonite blocks.

In addition, we reviewed the KRS+ design [1], and re-evaluate the height of buffer blocks above the disposal canister from the viewpoint of canister corrosion and retrievability.

2. Scenarios for retrieval

Assuming the future events that may happen just after the operation of a repository, we presumed three scenarios. Scenario-1 concerned a single deposition hole. That is, this scenario was related to the case that unidentified severe defects of a disposal canister were reported after the deposition of the canister. Scenario-2 was related to the case that the retrieval of the whole deposited canisters in a single disposal tunnel. In this case we assumed that a large-scale fault near the disposal tunnel was found during the operation of a repository. It was more severe case than the scenario-1. The scenario-3 was related to the political decision of the future government. A future government would decide not to dispose of the spent nuclear fuels but to reuse the fissile materials within them. In this case, we assumed that all the deposited canisters should be retrieved. However, we did not try to find the solution for the scenario-3.

3. Management of retrieved materials

As mentioned before, we tried to find solutions to manage the retrieved waste for two scenarios.

3.1 Retrieval processes

The technique to retrieve the disposal canister containing spent nuclear fuels was challenging itself. Swedish SKB reviewed several techniques and selected the best [2].

The major interest of our research was not to develop the technique itself but to apply the best technique currently available to the KRS+ repository. The procedure related to the retrieval of waste was briefly presented in Fig. 1. According to NSSC Notice, we have to prepare a spaces for the retrieval of a canister, buffer and backfill as shown in Figure.

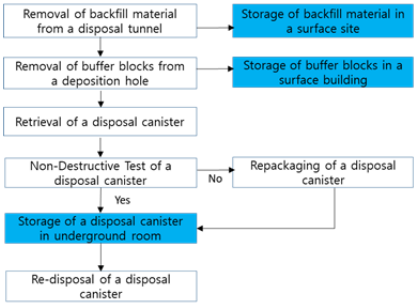


Fig. 1. Procedures for retrieval of a canister.

3.2 Storage of retrieved materials

As marked in blue in Fig. 1, the repository should prepare spaces for three materials. The underground facilities of the KRS+ repository were divided into two areas, controlled area and uncontrolled area. The disposal canisters were designed to be transported within the controlled area. Thus, we prepared a space for the retrieved disposal canister containing spent nuclear fuels.

The canister would be stored in a room (retrieved SNF storage room) close to the Operation waste hall after the inspection at the encapsulation plant (see Fig. 2). The maximum number of retrieved canisters was determined to be fifty based on the Scenario-2. Similarly, the spaces and location for the storage of retrieved buffer and backfill were proposed.

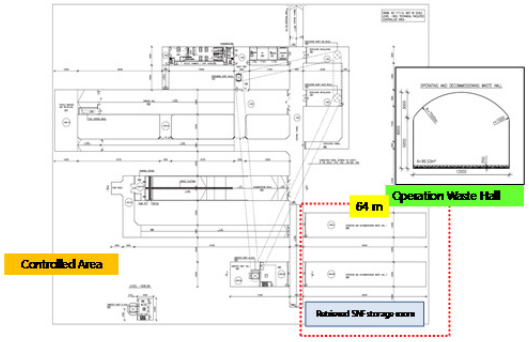


Fig. 2. Retrieved SNR storage room.

4. Retrievability and buffer dimension

One of the big challenges for retrieval of a canister was to remove the backfill and buffer material. Thus, we tried to improve the KRS+ design from the viewpoint of Retrievability.

The primary safety function of buffer was to protect a canister from corrosion by limiting groundwater flow. The current design of buffer was shown in Fig. 3. The height of buffer above the canister was set to be 2.5 m. From the viewpoint of retrieval of a canister, the height of buffer was too thick. In this study, we assessed the corrosion lifetime of a canister by changing the height of buffer.

The authors currently developed a computer program based on the Finnish Posiva approach [3]. The corroding agents for copper canister were dissolved oxygen and sulphide in groundwater under the deep geological environment. The amount of oxygen in the repository was limited, and it was assumed that all the oxygen in buffer was consumed for the corrosion of a canister. By changing the height of buffer from 2.5 m to 1.0 m, the corrosion depth by oxygen was calculated.

Similarly, the corrosion of a copper canister by sulphide in backfill was calculated by changing the height of buffer. The lifetime of a canister lid was calculated with the following equation:

$$\frac{F_{DV}}{A_{DV}} = \frac{2C_s}{\pi r_c^2}\frac{\pi r_t^2}{L} D_e \sqrt{\frac{2D_{et}q}{r_t}} \Big/ \left(2\sqrt{\frac{2D_{et}q}{r_t}} + \frac{\pi}{L} D_e\right) \quad (1)$$

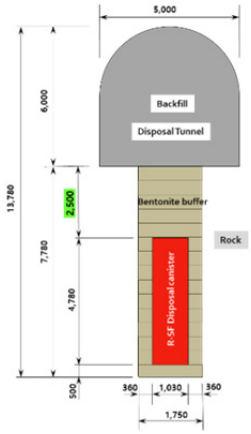


Fig. 3. Schematic of a deposition hole with buffer.

The calculation results showed that the buffer height above the canister can be reduced from 2.5 m to at least 2.0 m.

5. Conclusion

NSSC Notice 2017-74 requests to secure spaces and facilities to manage the retrieved waste. To this end, three scenarios were developed, and the technical solutions to meet the requirements for the management of retrieved materials were proposed. Finally, current design of buffer height was technically reviewed in terms of corrosion. The current height of buffer could be reduced from 2.5 m to 2.0 m.

Acknowledgement

This work was supported by the Ministry of Science and ICT within the framework of the national long-term nuclear R&D program (NRF-2017M2A8A50 14856).

REFERENCES

[1] J. Lee, I. Kim, H. Choi, and D. Cho, “An Improved Concept of Deep Geological Disposal System Considering Arising Characteristics of Spent Fuels From Domestic Nuclear Power Plants,” J. of Nucl. Fuel Cycle Waste Technol., 17(4), 405-418 (2019).

[2] P. Kalbantner and R. Sjoblom, Techniques for freeing deposited canisters, SKB TR-00-15 (2000).

[3] H. Choi, et al., Estimation of corrosion lifetime of a disposal canister based on the Finnish Posiva methodology, KAERI/TR-7612/2019 (2019).

Conceptual Design of Sandglass-Like Separator for Immobilized Anionic Radionuclides Using Particle Tracking Based on Computational Fluid Dynamics

Tae-Jin Park[1,*], Young-Chul Choi[1], and Jiwoong Ham[2]
[1]Korea Atomic Energy Research Institute, Daedeok-daero 989-111, Yuseong, Daejeon, 34057, South Korea
[2]Chungnam National University, 99, Daehak-ro, Yuseong, Daejeon, South Korea
*etjpark@kaeri.re.kr

1. Introduction

Anionic radionuclides pose one of the highest risks to the long-term safety assessments of disposal repositories [1]. Therefore, techniques to immobilize and separate such anionic radionuclides are of crucial importance from the viewpoints of safety and waste volume reduction. The main objective of this study is to design a separator with minimum pressure disturbance, based on the concept of a conventional cyclone separator. We hypothesize that the anionic radionuclides can be immobilized onto a nanomaterial-based substrate and that the particles generated in the process can flow via water (Figure 1) [2]. These particles are denser than water; hence, they can be trapped within the cyclone-type separator because of its design. We conducted particle tracking analysis using computational fluid dynamics (CFD) for the conventional cyclone separator and discussed the morphology-associated factors resulting in the high efficiency of particle separation. To validate the design, we manufactured a laboratory-scale prototype separator and tested it for iron particles. We subsequently discuss the effects of the magnetic properties introduced in the sandglass-like separator.

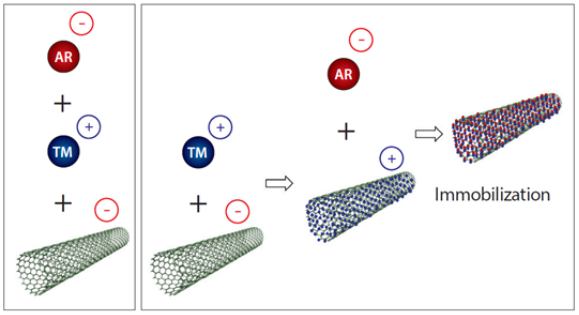


Fig. 1. Principle of the immobilization of anionic radionuclides using carbon nanotubes, a nanomaterial-based substrate.
*(a) describes the components with the charge notation (e.g., + and –) needed for immobilization and (b) shows step-wise approach. AR and TM represent anionic radionuclides and transition metals, respectively.

2. Analysis of sandglass-like separator

From the results obtained for the basic model of the conventional cyclone separator, it is obvious that we cannot achieve and effective separation. Thus, a need for a new design for the cyclone separator arises, by which the particles will be retained in the separation zone. The density difference is still the key principle for the cyclone separator; thus, the fluid must rotate within the separator. However, the particles must not escape from the separation zone through the flow.

We propose a sandglass-like morphology for the separators (Figure 2). The inlet is installed in the upper part of the separator in a direction vertical to the radius; thus, the inlet fluid rotates in the separator. The model have a vertical outlet pipe located at the center of the upper part of the separators. When the fluid enters the separator, it flows downward to the bottom and then flows out through the outlet pipe. The results of the particle tracking analysis are shown. We found that almost no particles escaped from the separation zone (i.e., only one out of 10,000 particles flowed out from the outlet).

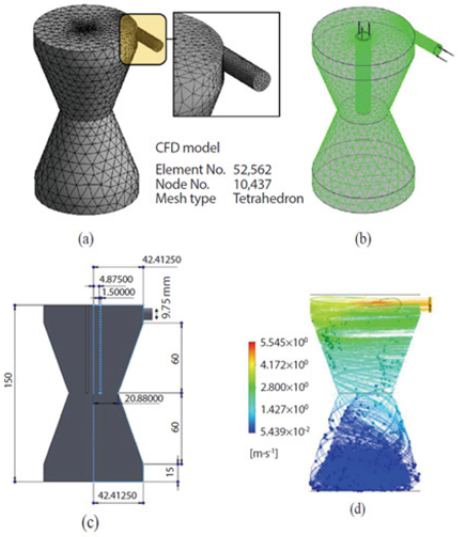


Fig. 2. (a) Meshed sandglass-like separator, (b) the boundary conditions, (c) sandglass-like separator with dimensions, and (d) simulation results for the particle tracking for (c).

To validate the separation efficiency of the sandglass-like separator, we designed and manufactured actual experimental setup. We used iron as the particles. After 5 min of operation, we collected the particles, dried, and weighed them.

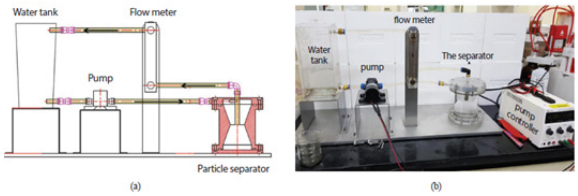


Fig. 3. (a) Design and (b) image of the experimental setup for validation of separation efficiency of the proposed sandglass-like separator.

3. Conclusions

A sandglass-like separator, based on the concept of a conventional cyclone separator, for the aqueous fluid was proposed using a particle tracking analysis based on CFD. It was seen that only one out of 10,000 particles escaped from the separation zone through the flow of the separator. In comparison, a conventional cyclone separator showed unsatisfactory results of the separation of the particles from the aqueous fluid. The manufactured sandglass-like separator in this study showed an efficiency of 99%. With an additional magnetic effect, the efficiency reached ca. 100%. The sandglass-like separator can be used for the effective separation and recovery of the particles including the immobilized anionic radionuclides. Applicability to the field of separation and filtration for the removal of foreign substances without pressure disturbances in the pipe needs to be investigated.

ACKNOWLEDGEMENT

We acknowledge the Korean government, Ministry of Science and ICT, for support (No. 2017M2A 8A5014859).

REFERENCES

[1] Y. Hwang and C.-H. Kang, "The development of a safety assessment approach and its implication on the advanced nuclear fuel cycle," Nucl. Eng. Technol., 42(1), 37-46 (2010).
[2] T.-J. Park, Y.-C. Choi, and J. Ham, "Conceptual design of sandglass-like separator for immobilized anionic radionuclides using particle tracking based on computational fluid dynamics," J. Nucl. Fuel Cycle Waste Technol., 18(3), 363-372 (2020).

Interactions Between Korean Buffer and Groundwater Under Temperature Conditions of Disposal Interest

Tae-Jin Park*, Ji-Hun Ryu, Min-Hoon Baik, and Jae-Kwang Lee
Korea Atomic Energy Research Institute, Radwaste Disposal Research Division, 989-111 Daedeok-daero, Yuseong, Daejeon, 34057, South Korea
*etjpark@kaeri.re.kr

1. Introduction

Buffer materials in a geological repository will face several geological condition changes with time. The spent nuclear fuels generate decay heats for a very long time. Thus, the thermal criteria for the hosting buffer materials must be set for the safety [1]. In addition, the underground redox condition will change from oxidizing to reducing. Then, the buffer will eventually undergo possible reactions with the radionuclides released from the spent nuclear fuels. Thus, the interactions between the buffer and groundwater under the redox conditions of disposal interest, at a specific disposal timeframe, is of importance.

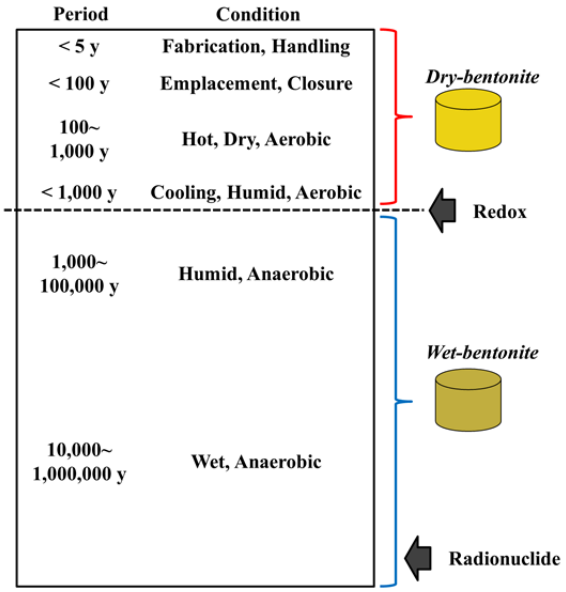


Fig. 1. Illustration of the geological conditions that the Korean buffer will face with time (modified from Peter Keech's work).

To understand the processes and obtain results related to the buffer-groundwater-radionuclides mentioned above, KAERI has been working on a stepwise approach: (i) strategy and methodology development for the Korean bentonite [2], (ii) buffer reactions with groundwater under the elevated temperatures [3], and (iii) then the interactions between the buffer and the radionuclides. Here, we report Korean buffer-groundwater interaction under the redox and temperature conditions of disposal interest.

2. Buffer-KURT GW interactions under the reducing conditions

2.1 KURT Groundwater

The groundwater obtained from the DB-3 borehole was located in the KURT (KAERI Underground Research Tunnel). To maintain the initial reducing conditions as best as possible, the containers with proper design were used during the sampling (Figure 2). Then, the containers with full of groundwater, were subsequently placed in the glovebox.



Fig. 2. KURT groundwater sampling.

2.2 Korean bentonite-KURT groundwater reactions as a function of temperatures

We first weighed the Korean bentonite (*a.k.a* KJ-II) at the ambient environment then, placed them into the glovebox (*i.e.* inert condition) with several purging steps. The bentonite to groundwater ratios were 1 to 100 for acid digestion vessels (*i.e.*, autoclaves) that were previously placed in the glovebox. Once we maintain the environment, the vessels placed in the forced convection oven with the temperatures set to 60, 90, 120, and 150 ℃. We left one in the glovebox for 25 ℃. The bentonite-groundwater reactions were continued for 45 days.



Fig. 3. Bentonite-KURT groundwater reactions.

The concentration of the ions generated from the Korean bentonite-KURT groundwater interactions, as a function of temperatures, were analyzed and compared with that from the MX80-KURT groundwater interactions (Figure 3).

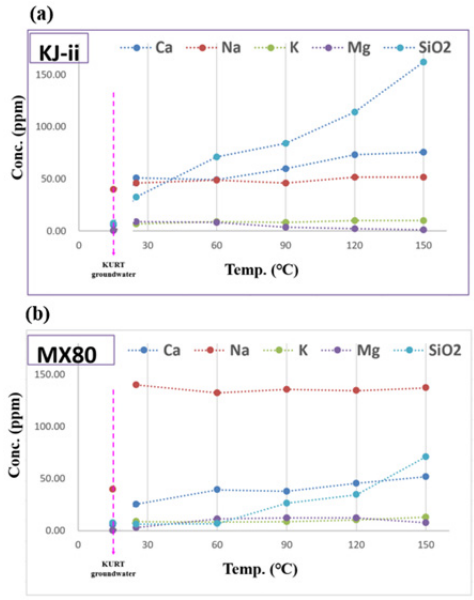


Fig. 4. Concentrations of the ions generated from the bentonite-KURT groundwater interactions as a function of temperatures.

3. Conclusions

We experimentally study the Korean bentonite and KURT groundwater interactions based on a stepwise approach. The specially designed groundwater containers were used to maintain the redox conditions of KURT groundwater as best as possible. The concentration of the ions generated from interactions between the KJ-II bentonite and KURT groundwater were analyzed and compared with that from MX-80 bentonite.

ACKNOWLEDGEMENT

We acknowledge the Korean government, Ministry of Science and ICT, for support (No. 2017M2A8 A5014859).

REFERENCES

[1] Cho, W.-J. and Kim, G. Y., “Reconsideration of thermal criteria for Korean spent fuel repository,” Annals Nucl. Ener. 88, 73-82 (2016).
[2] Park, T.-J., Ryu, J.-H., Cho, W. H., and Lee, J.-K., "Buffer retardation experiments for radionuclides under the elevated temperature conditions: Strategy and methodology development for the Korean bentonite," Proc. Kor. Rad. Waste Soc., 16(2), 203-204 (2018).
[3] Park, T.-J. and Seoung, D., "Thermal behavior of groundwater-saturated Korean buffer under the elevated temperature conditions: In-situ X-ray powder diffraction study for the montmorillonite in Korean bentonite," Nucl. Eng. Technol., in press.

Field Tracer Tests for Identifying Local Heterogeneity of Borehole Wall

Nak-Youl Ko*, Kyung-Woo Park, B.H. Park, Chang Yong Lee, and Sung-Hoon Ji
Korea Atomic Energy Research Institute, 111, Daedeok-daero 989 beon-gil, Yuseong-gu, Daejeon, Republic of Korea
*nyko@kaeri.re.kr

1. Introduction

Excavation of boreholes could form unexpected features in the wall of boreholes. The damaged zone of excavated deposition holes would be one of these features and should be checked to confirm the performance of barriers in deep geological disposal of radioactive wastes.

In this study, we performed some tracer tests to identify the damaged zone of a borehole wall, especially in terms of hydrogeological properties of the zone. The device for the trace test was installed at the test borehole, and the tracer tests, including DFTT (Dipole Flow Tracer Test), were conducted. The results of test were analyzed to find evidences for existence of the damaged zone and to expect the hydrogeological effects by the zone.

2. Study Site

The field tracer tests were conducted at the borehole (BDZ-1) in research gallery (RG) #6 of expanded zone of KURT (KAERI Underground Research Tunnel). Hydraulic properties and heads at BDZ-1 were investigated previously [1].

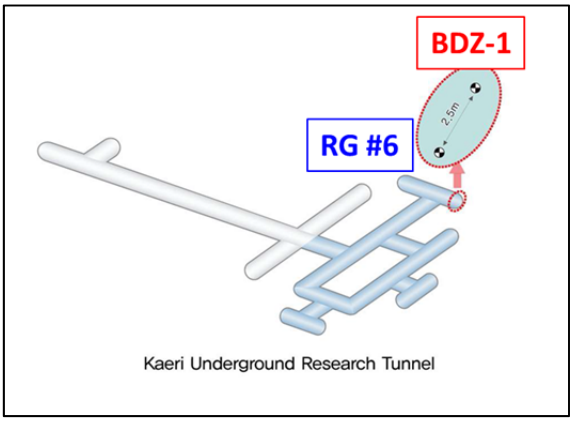


Fig. 1. Study site in KURT.

3. Field Tests

Triple packers were installed at BDZ-1 to perform tracer tests. To conduct DFTT, artificial groundwater flow was establish by injecting water with constant flow rate in the lower chamber and extracting water with constant flow from the upper chamber (Fig. 3). When the hydraulic heads at the upper and lower chambers had remained stable, the tracer was injected into the lower chamber and the concentration of the tracer in groundwater extracted from the upper chamber was observed.

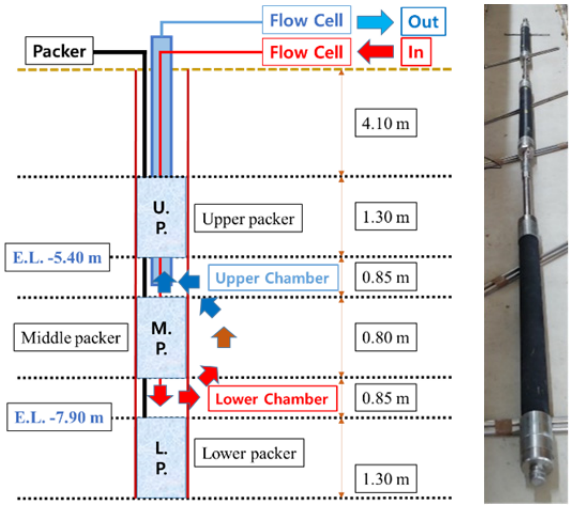


Fig. 2. Schematic diagram of the device for DFTT in the field condition, and the triple packer system.

4. Results

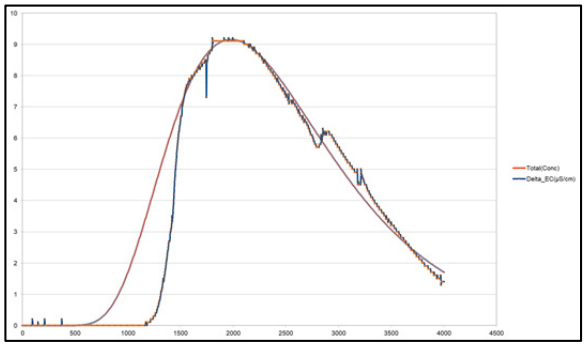


Fig. 3. Distribution of tracers under the basic condition.

The concentration of the tracer in the extracted groundwater was observed and the breakthrough curve of the tracer was evaluated. The breakthrough curve was compared with the value calculated by an analytical solution for one-dimensional transport of solute. From comparing the linear velocity obtained by the tracer test with the groundwater discharge rate derived from the previous hydraulic tests and the dipole flow test (DFT) for building stable groundwater flows, the porosity for the test interval was estimated.

The porosity had a range from 1 to 10 %, but the assumptions used in estimating the porosity were required to examine their validity in detail.

5. Conclusions

The field tracer test using DFTT was performed and the result of the test was evaluated to identify a hydraulic property of local heterogeneity of the borehole wall. From the result, the porosity of the wall, which would be damaged by excavation for reaming the borehole, was estimated. Although the evaluation of the test result and estimation of the porosity have some doubtful points to be resolved, the method in this study would be able to show hydraulic properties of the locally damaged zones in the excavated boreholes.

Acknowledgement

This work was supported by the Ministry of Science, ICT and Future Planning within the framework of the national long-term nuclear R&D program (NRF- 2017M2A8A5014858).

REFERENCES

[1] K.W. Park, N.Y. Ko, S.H. Ji, A Study on the Applicability of the Hydraulic Test Method Performed at an underground Research Facility in Crystalline Rock, Econ. Environ. Geol., 53(2), 121-131, (2020).

Concepts of Retrieval Processes for Deposited Disposal Canisters and Bentonite Blocks

Jong-youl LEE*, In-young Kim, Heui-joo CHOI, and Dong-keun CHO
Korea Atomic Energy Research Institute
*njylee@kaeri.re.kr

1. Introduction

From the 1970s, Interest of the retrievability in a geological repository for spent nuclear fuels has been increasing steadily. In 2008 the NEA RWMC, concluded that "There is general recognition that it is important to clarify the meaning and role of retrievability for each country, and that provision of reversibility and retrievability must not jeopardize long-term safety." [1].

Consideration for retrievability technology in high-level radioactive waste repository has been maintained continuously, and also in Korea, the retrievability during repository operation is specified in relevant regulation.

Therefore, analyses of retrievability technologies under consideration in international organizations and advanced foreign countries was carried out in order to derive a measure to apply retrievability to the spent nuclear fuel disposal concept under developing currently.

In this paper, the preliminary concepts of retrievability for the geological repository for spent nuclear fuel were described. To this end, reviewed the domestic related regulation. With review results and based on the procedure for retrieval of disposal container, buffer and back material in a disposal tunnel [2], the process of each retrieved material from disposal tunnel to management area are specified.

2. Requirements for Retrievability

As mentioned previously in the introduction, the retrievability during repository operation is specified in relevant regulation in Korea, that is the Nuclear Safety and Security Commission (NSSC) Notice 2017-74.

According to the regulation, the following articles are required for the design of a geological repository related to the retrieval:

- Article 2 (definition). Retrieval of radioactive waste refers to returning the deposited waste to the previous state of management before disposal.
- Article 11-3. Disposal systems shall be developed in such a way that there is no need to retrieve disposed radioactive wastes or there is no room for retrieval after the closure of the disposal facility, and the retrieval of radioactive wastes shall not be considered as part of the disposal safety.
- Article 14-4. Deep geological repository shall have a plan to safely retrieve radioactive waste if necessary during the operational period, and secure the spaces and facilities to manage the retrieved waste at appropriate locations above and below ground.

3. Processes for Retrievability of Canisters

3.1 Retrieval procedures

According to the domestic regulation on retrievability, NSSC Notice, spaces for the retrieval of a canister, buffer and backfill should be prepared in the underground facility and the surface facility. The procedure related to the retrieval of disposal canisters, bentonite block and backfill material was briefly presented in Fig. 1.

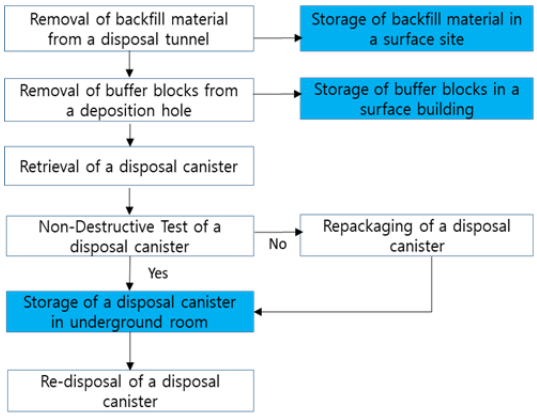


Fig. 1. Procedures for retrieval of cani. & buf [1].

3.2 Processes for canister retrieval & management

Based on procedure for retrieval of canister and bentonite block, the detailed process of canister retrieval was developed. It was divided into two process. The one was the processes in the disposal tunnel and the other was the processes in the management tunnel of underground facility shown in the figure 2.

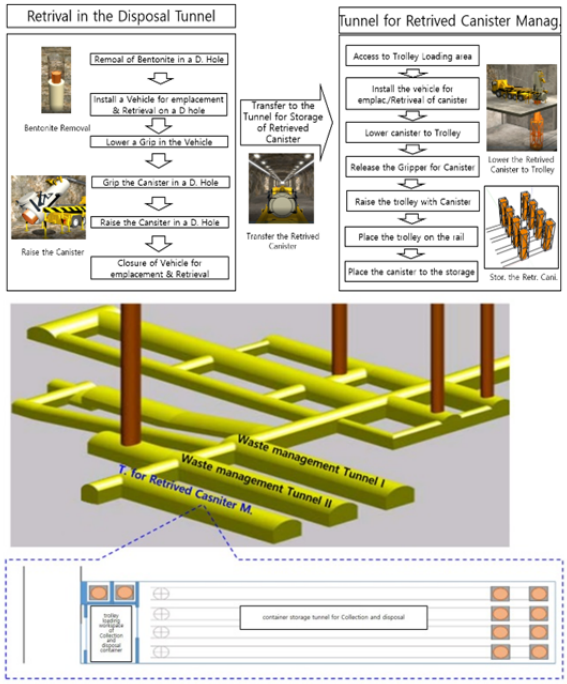


Fig. 2. Retrieval/management process of canister.

3.3 Processes for buffer retrieval & management

As shown in the fig 1, bentonite as a buffer was retrieved in the disposal tunnel and managed in a space of surface facility. Fig. 3 showed the bentonite retrieval process from disposal tunnel to surface facility.

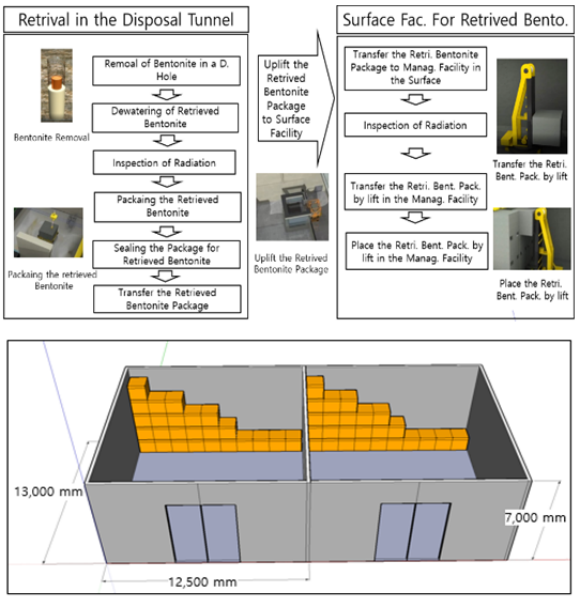


Fig. 3. Retrieval/management process of bentonite.

4. Conclusion

In this paper, based on the domestic regulation related to the retrieval of disposal canister, (NSSC) Notice 2017-74, the preliminary concepts of retrievability for the geological repository for spent nuclear fuel were described. To this end, with review of the procedure for retrieval of disposal container, buffer and back material in a disposal tunnel [2], the detailed process of each retrieved material from disposal tunnel to management area were specified.

The results of this study will be used to establish measures to apply retrievability to the disposal concept of spent nuclear fuels. Based on this, it can also be used for cost estimation of high-level waste disposal system. To do this, such as clear definitions of terms and on-site testing with basic study for the retrievability of repository should be conducted.

Acknowledgement

This work was supported by the Ministry of Science and ICT within the framework of the national long-term nuclear R&D program (NRF-2017M2A8A501 4856).

REFERENCES

[1] Reversibility and Retrievability(R&R) for the Deep Disposal of High-Level Waste and Spent Fuel, Final Report of the NEA R&R Project (2007-2011),NEA/RWM/R(2011)4, (2011).
[2] H.J Choi, Retrievability of deposited canisters in the KRS+ repository, autumn annual conference of KRS, (2020).
[3] J.Y. LEE, et al., PRE-CONCEPTUAL DESIGN OF KOREAN REFERENCE HLW VERTICAL DISPOSAL SYSTEM, KAERI/TR-3012/2005, (2005).

The Evolution History of Fractures and Fracture Fillings of Deep Granitic Rock at KURT Site

Soolim Jung*, Ji-Min Choi, Sung-Hoon Ji, and Kyung-Su Kim
Korea Atomic Energy Research Institute, 111, Daedeok-daero 989beon-gil, Yuseong-gu, Daejeon, Republic of Korea
*sljung@kaeri.re.kr

1. Introduction

Fractures in granitic rock generally act as primary pathways for groundwater flow. However, groundwater flow is the most effective pathways for the radioactive nuclides in the deep underground. Thus, for safety assessment of the disposal site, it is necessary to find out fracture network system and its long-term behavior. Understanding evolution history of the fractures and fracture fillings can attribute to understand fracture networks and to assess long-term safety of geological environments. In this study, we observed the site-specific characteristics of the fractures and fracture-filling minerals around KURT site, and tried to reconstruct the fracture evolution history of the site.

2. Methods

2.1 Study area

The research was performed around KURT (KAERI Underground Research Tunnel), Daejeon, Korea. The KURT is located on the boundary between Okcheon Belt and Kyunggi Massif. The area is composed of Mesozoic intrusive granitic body, which was formed by Daebo-Orogeny. The major rock type consisting KURT area is two-mica granite.

2.2 Sample preparations

4 types of fracture fillings were sampled from drilling rock cores in two ways. Standard samples for each type were picked every 100m interval with depth and with changing of rock types. The types of fracture fillings were distinguished by their mineral colors, textures and altered textures of surrounding rock.

2.3 Observations

Geological observation along the outcrops exposed in the KURT and fracture studies using borehole data were performed to understand the distribution and orientation of fractures and fracture fillings. The distribution of fractures was observed until 500m in depth. Also, microstructures of the fracture filling minerals were observed to understand the hydrothermal alteration history. The results from KURT and borehole were synthesized to verify the fracture evolution history of the site.

3. Results

The fracture systems observed in the borehole are somewhat correlated with the major joint sets from field survey. Most of distinctive directions were corresponded to the 6 major joint sets (Set 1 ~ 6) recognized in the outcrop of KURT, including three major sets of joints measured from the regional scale field survey.

Fractures in this site have 3 major types according to the characteristics of the fracture fillings. First is sealed fracture with filling minerals showing altered features in adjacent host rock. Second is filled fracture without altered features in adjacent host rock, which is usually calcite vein. Third is open fracture without fillings and altered zone, but sometimes having thin altered films on the fracture plane.

The directions of altered fractures in borehole are restricted from N15E to N70W with about 65W in dip, which are similar with the joint sets 1-2 from KURT. The directions of calcite vein have two major directions, N76E/63SE, N74E/62NW, which are similar with the joint sets 1 and 5. The open fractures are more randomly oriented, but have similar directions with the joint sets 3-4 as well.

The microstructures of fracture filling minerals indicate the evidences of several hydrothermal events during the cooling stage of intrusive granite body in the area. Most of the filling minerals are epidotes. Calcite veins are distributed with all depth of the borehole and KURT.

4. Discussion

According to the results, the oldest fractures (Sets 1-2) were formed by cooling and shrinking of the intrusive magma body. The cooling of magma could raise hydrothermal activity and the alteration reactions might be overlapped for a long geological period through the granite body uplifting. Some fractures might be altered and sealed with Epidote minerals. Then fractures

could be growth continuously associated with unloading and tectonic processes and new fractures could be formed as well (Sets 3-4). After local fracturing by fault activity, low temperature groundwater caused calcite precipitation along the fractures (Sets 1 and 5) and formed calcite veins. Finally, granite body was exposed by continuous uplifting and erosion, and recent underground flow of meteoric- and groundwater could react with fracture surface making thin chloritized film.

Acknowledgement

This work was supported by the Nuclear Research and Development Program of the National Research Foundation of Korea (NRF) funded by the Ministry of Science and ICT (No. 2017M2A 8A5014858).

History of Development and Activity Patterns of the Keumwang Fault at Inje-Gun, Gangwon-Do

Ji-Min Choi[1,*] and Hee-Kwon Lee[2]
[1]Korea Atomic Energy Research Institue, Yuseong-gu, Daejeon, 34057, Republic of Korea
[2]Division of Geology & Geophysics, Kangwon National University, Chuncheon, 24341, Republic of Korea
*jiminchoi@kaeri.re.kr

1. Introduction

In this study, the Keumwang fault is used to investigate the development history of fault core generated from cataclasite using the structural characteristics, and temporal-spatial activity patterns after 510 ka years ago through ESR dating.

2. Study Area

The study area, where Paleoproterozoic-Gombaeryeong granite, Jurassic-Osaek granite, Garibong granite, Biotite granite, granodiorite, Inje granite, Cretaceous-Seoraksan granite, dikes are embedded in the Paleoproterozoic-gneisses (host rock), and overlyied Quaternary-alluvium unconformably is located in Inje-gun, Gangwon-do. Keumwang fault, which has extended from the northwestern boundary of the Eumseong-basin to Searaksan area with strikes N20˚-30˚E and 170-km-long, is developed in the study area. The lineation of the fault at study area was grasped through aerial and DEM(Digital Elevation Model) imges, and 2 outcrops of fault core and 3 outcrops of subsidiary fault were discovered through geological and trench surveys.

3. Methods

3.1 Fault rocks

Identified the distribution of fault rocks along the lineation of the fault based on their characteristics. The fault zone is a complex, not a simple surface structure, and is divided into fault core where deformation is concentrated and a subsidiary fault damage zone around it. Fault rocks which comprises of fault zone are classified depending on the type of host rock, temperature, fluid pressure, depth, kinematics and lithology. Mylonite is formed in a depth of about 11 km or less with the mylonitic foliation and recrystallized matrix in a plastic condition. Catatlasite is formed in a depth of about 4-11 km by brittle deformation. Near the earth's surface, fault breccia consisting of more than 30% visible fragments, and fault gouge consisting of less than are developed in unconsolidated state.

3.2 Direction of foliations & shear surfaces

Measured the orientations of foliations and shear surfaces developed within the fault core, and classified the type of shear surfaces(R, P, R' and Y) formed by strke-slip movement. And also, the kinematic of the fault was interpreted by analyzing the shear surfaces identified the kinesthetic sensation.

3.3 ESR dating

We determined the ESR ages of last movement of each sample of fault breccia and fault gouge developed within the fault core. Temporal and spatial activity patterns were analyzed with previous studies.

4. Results

The 23 m thick fault core occurs in cataclasite derived from Jurassic biotite granite. Fault core is composed of fault breccia dominated zone(FB) and fault gouge dominated zone(FG). Clasts shaped of floating on the matrix within fault breccia and fault gouge consist of quartz and rock fragments.

The strike of foliations in the fault core appears from N30˚W to N80˚E, and most dominant direction is N-S. The strike of shear surfaces appears differently than foliations, and is dominant in the same direction of the strike of Keumwang fault.

There are 39 samples gathered, 3 of which are fault breccia and 36 are fault gouge at fault cores and subsidiary faults. 31 samples were able to determine the ESR age, but the remaining 8 samples were unable, because the ESR signals were saturated. ESR ages of 31 samples from both 2 fault cores and 3 subsidiary faults range from 510 to 210 ka and have five active periods(about 510, 440, 320, 270 and 210 ka).

5. Discussions

The 23 m thick fault core of Keumwang fault is the strike-slip fault with strike N26°E and dips 81°NW, and is composed of FZ and FG occurs in cataclasite derived from Jurassic biotite granite.

History of development of Keumwang fault, which analyzed fault kinematics using the directions of foliations and shear surfaces, and compared this study and the previous studies is as follows. 1) Mylonite derived from Jurassic biotite granite was developed in the fault damage zone by the ductile deformation. 2) Cataclasite series was loaded in mylonite series by the brittle deformation at the depth of 4-11 km. 3) Fault breccia derived from cataclasite is formed by distributed crush brecciation, frictional sliding of particles past one another increased roundness of rock fragments. 4) The shear strain is localized, and shear surfaces and fault gouge bands are developed within FB. 5) Penetrative foliations are developed by the preferred orientation of clay minerals in FG with attrition brecciation and wear mechanism.

As a result of comparing and analyzing the ESR ages from both 2 locations of the fault core and 3 locations of the subsidiary fault in this study, and both 3 locations of the fault core and 4 locations of the subsidiary fault in previous study, the Keumwang fault at the Inje-gun area has 5 times of temporal clustering into active periods(about 510, 440, 320, 270 and 210 ka). We could determine the age of last movement (210 ka) which is consistent northwestern boundaries of the 4 in 5 fault cores, except for 1 that couldn't find the boundary, especially.

ACKNOWLEDGEMENT

This study was supported by See-At Project funded by the Korea Meteorological Administration (KMI2018-02010) and subsidy for scientific research of Kangwon National University(No. D1001551-01-01).

REFERENCES

[1] Choi, J.M. and Lee, H.K., "Evolution and space-time activity patterns of the Keumwang fault at Girin-myeon, Inje-gun, Gangwon-do", Journal of the Geological Society of Korea, 56(4), 425-452 (2020).

[2] Choi, S.J., Kim, B.C., Chun, H.Y. and Kim, Y.B., "Charophytes from the Chopyeong formation (Cretaceous) of the Eumsung basin, Korea", Journal of the Geological Society of Korea, 31, 523-528 (1955).

[3] Kee, W.S., Kim, H.C., Kim, B.C., Choi, S.J., Park, S.I. and Hwang, S.K., "Geological report of the Seoraksan sheet (1:50,000)", Korea Institute of Geoscience and Mineral Resources, 6-49 (2010).

[4] Kim, M.J. and Lee, H.K., "Internal structure and movement history of the Keumwang fault", Journal of the Petrological Society of Korea, 25, 210-230 (2016).

[5] Scholz, C.H., "The brittle-plastic transition and the depth of seismic faulting", Geologische Rundschau, 77, 319-328 (1988).

Mechanistic Understanding of Bentonite Swelling as a Buffer Material

Jae Owan Lee*, Seok Yoon, Jin-Seop Kim, and Geon Young Kim
Korea Atomic Energy Research Institute (KAERI)
*jolee@kaeri.re.kr

1. Introduction

Bentonite is favored as a buffer material for an HLW repository because it has a high swelling ability (i.e., sealing capacity) and thus can effectively block groundwater from entering the repository. Bentonite after closure the repository should have a high swelling ability to fill gaps around the deposition boreholes and fractures of the surrounding rock mass when saturated with groundwater, and should also have a low swelling pressure so as not to overload the disposal container and surrounding rock mass. Therefore, understanding the swelling of bentonite as a buffer material is very important in the design of a HLW repository. The present paper reviews the bentonite swelling mechanisms, factors affecting swelling pressure, and its predictive model, and presents major considerations when measuring the swelling pressure of bentonite buffer and using a predictive model for the design of a repository.

2. Swelling mechanisms

Bentonite is a kind of clay with montmorillonite as its major constituent and quartz, feldspar, zeolite etc. as auxiliary constituents (Fig. 1(a)). The swelling of bentonite, when in contact with water, depends on the montmorillonite. The montmorillonite, a phyllosilicate group of minerals (Fig. 1(b)) has the structural chemistry of $(Al,Mg)_3(Si,Al)_4O_{10}(OH)_2$. The basic unit layer comprises two tetrahedral sheets of silica on either side of an octahedral sheet of alumina in the ratio of 2:1. The montmorillonite has high negative charge, which can be balanced by a variety of cations in the interlayers, principally Ca^{2+} and Na^{+}. It is also characterized by the ability to take up a large amount of water hydrating cations in the interlayers. The water molecules exist as a sheet in the interlayers, which are not rigidly held so that the lattice is able to expand or contract.

When the montmorillonite particles come into contacted with water, the particles become separate and remain apart each other due to the forces of interactions. This is what is called swelling. The amount of swelling is determined by the type of cation in the interlayers. Na-montmorillonite is capable of swelling up to 15 times its original volume. By contract, Ca-montmorillonite swells only to 30% of its original volume (Fig. 2).

There are six forces of interactions involved in the swelling of bentonite: hydration force of particle surfaces and cations, osmotic force with electrical double layer repulsion, breakup and formation of montmorillonite particles, demixing of exchangeable cations, co-volume swelling, and Brownian swelling. Among these forces, the major is actually the hydration force and osmotic force, and the remaining four forces are the secondary effects of the major forces. When the major forces are absent, the remaining forces do not appear.

3. Factors affecting swelling pressure and predictive models

Swelling pressure is the pressure at which bentonite acts on a system of limited volume. When bentonite is used as a buffer material for the repository, its swelling pressure should not put an excessive load on the disposal container and the surrounding rock mass. The reported swelling pressure in the literature were within a wide range of 0.027 MPa to 59 MPa depending upon the experimental conditions: dry density and initial moisture content of compacted bentonite, salinity of pore water, temperature, montmorillonite content and interlayer cations. The swelling pressure increased with an increase in the dry density, and it had lower value at higher initial moisture content. The swelling pressure decreased with an increase in the salinity of the solution. For the effect of temperature, there were conflicting results. Pusch et al. [1] reported that the swelling pressure increased with an increase in temperature, while Suzuki and Fujita [2] presented the opposite result. The higher the content of montmorillonite, the higher the swelling pressure was, and the swelling pressure of Na-bentonite was higher than that of Ca-bentonite. Predictive models of swelling pressure were proposed on the basis of the experimental results and detailed mechanisms, and three groups of models were applied to predict swelling pressure.

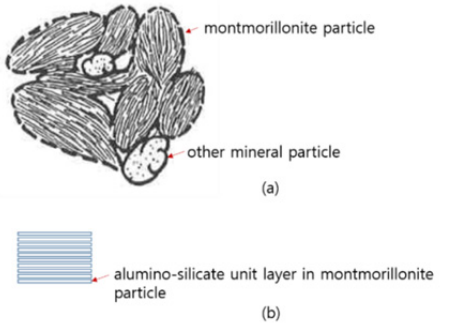


Fig. 1. Schematic (a) bentonite particle arrangement and (b) montmorillonite microstructure.

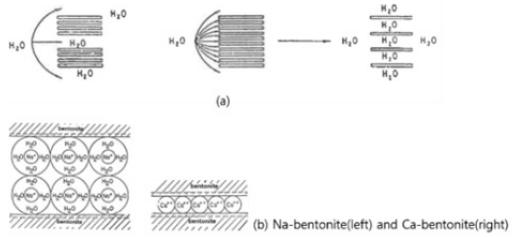


Fig. 2. (a) Swelling of montmorillonite particle in contact with water and (b) Na- & Ca-bentonite.

4. Conclusions

The swelling of bentonite involved six forces of interactions. Among them, the major forces were hydration forces of montmorillonite particle surfaces and interlayer cations and osmotic forces with electrical double layer repulsion. The swelling pressure of the bentonite buffer was dependent on factors such as dry density and initial moisture content of compacted bentonite, salinity of pore water, temperature, montmorillonite content and interlayer cations. Three models were applied to predict swelling pressure, and predictive models based on hydration force and osmotic force were widely used.

ACKNOWLEDGEMENT

This research was supported by the Nuclear Research and Development Program of the National Research Foundation of Korea (NRF-2017M2A8A5014857 and NRF-2020M2C9A1062949) funded by the Minister of Science and ICT.

REFERENCES

[1] R. Pusch, “Hydrothermal field test with French candidate clay embedding steel heater in the Stripa mine,” SKB-TR-93-02 (1993).
[2] H. Suzuki and T. Fujita, “Swelling characteristics of buffer material,” JNC TN8400, 99-038 (1998).

Near-Field Evolution During Thermal Period of a HLW Repository

Min-Hoon Baik* and Jae-Kwang Lee
Korea Atomic Energy Research Institute, 111 Daedeok-daero 989 beongil, Yuseong-gu, Daejeon, Republic of Korea
*mhbaik@kaeri.re.kr

1. Introduction

In general, the evolution of high-level radioactive waste (HLW) disposal system can be classified into the evolution during thermal period affected by the heat generated from HLW and the long-term eolution after the heat is dissipated [1]. The evolution of a HLW disposal system in the thermal period is more important in the near-field (see Fig. 1). In this study, we investigated and summarized important evolution processes in the near-field during thermal period after repository closure in terms of safety assessment.

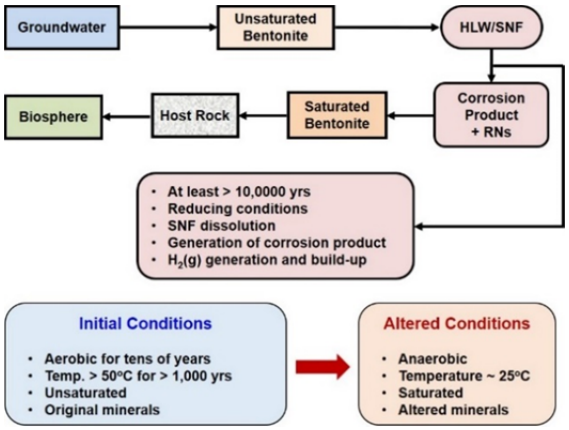


Fig. 1. Schematic illustration for the near-filed evolution of a HLW disposal system.

2. Initial Conditions of Near-field Components

HLW disposal system mainly consists of waste package (iron-cast copper canister), buffer (compacted bentonite), backfill, engineering materials such as sealing material, and surrounding rock and groundwater. It is of importance to define the initial conditions of the components of the disposal system to invstigate the evolution of the disposal system quantitatively. Thus we summarized the initial conditions of KRS+ disposal system being developed by Korea Atomic Energy Research Institute (KAERI) for the deep geological dusposal of spent nuclear fuels from PWR and PHWR [2]. The design data and analysis results from Swedish KBS-3 concept [1] which is very similar to our disposal system were also used when lacking in domestic data.

3. Near-field Evolution during Thermal Period

In this study, we investigated the evolution characteristics of following processes during thermal period, related with the performance of near-field components:

- thermal evolution of near-field,
- mechanical evolution of rock,
- hydrogeological evolution,
- chemical evolution in and around repository
- saturation of buffer and backfill,
- swelling and swelling pressure,
- chemical evolution of buffer and backfill,
- colloid release from buffer and backfill, and
- canister evolution

4. Related Safety Functions

Safety functions related with the near-filed evolution during thermal period after closure are listed and summarized in Table 1.

Table 1. Safety functions of near-field components for the iniital thermal period after closure

Component	Safety fucntion
Rock	• Provide favorable chemical conditions: • Eh (reducing), salinity(TDS < 12 g/L), ionic strength (> 4 mM equivalent), pH (< 11), [Cl^-] (< 2 M) • Provide favorable hydrologic and tranport conditions: high transport resistance (F) in fracture, low equivalent flow rate (Q_{eq}) in buffer/rock interface • Provide mechanically favorable conditions: limited GW pressure, shear movements at deposition holed (< 0.05 m), shear velocity at deposition holes (< 1 m/s) • Provide thermally favorable conditions: T at buffer (> -4°C), T near canister (> 0°C)
Buffer	• Limit adveactive transport: hydralulic conductivity (< 10^{-12} m/s), swelling pressure (> 1 MPa) • Reduce microbial activity • Damp rock shear: saturated buffer density (< 2.050 kg/m^3) • Resis transformation (T < 100°C) • Prevent canister sinking • Limit pressure on canister and rock (Swelling pressure < 15 MPa, T > -4°C)
Backfill	• Counteract buffer expansion
Canister	• Provide corrion barrier • Withstand isostatic load • Withstand shear load

5. Concluding Remarks

Based on the results obtained by investigating major processes on the near-field evolution during thermal period, it is suggested that all processes considered in the near-field during thermal periods could not inflict harm on the long-term performance of the near-field including buffer and backfill. However, there are still some remaining uncertainties to be considered in the near-filed evolution processes during thermal period which can affect on radionuclide migration and long-term evolution of the HLW disposal system.

Acknowledgments

This work was supported by the National Research Foundation of Korea (NRF) funded by the Korean government, Ministry of Science and ICT (Grant No. 2017M2A8A5014859).

REFERENCES

[1] SKB, “Long-term safety for the final repository for spent fuel at Forsmark”, Technical Report SKB TR-11-01, Stockholm, (2011).

[2] J. Lee, I. Kim, H. Choi, D. Cho, “An improved concept for deep geological disposal system considering arising characteristics of spent fuels from domestic nuclear power plants”, Journal of Nuclear Fuel Cycle and Waste Technology, 17(4), 405-418 (2019).

Preliminary Performance Analysis Modeling for an Annular Metal Fuel

Byoung Oon Lee*, Chan Bock Lee, June Hyung Kim, Jeong Yong Park, and Jin Sik Cheon
Korea Atomic Energy Research Institute, 111, Daedeok-daero 989beon-gil, Yuseong-gu, Daejeon, Republic of Korea
*bolee@kaeri.re.kr

1. Introduction

An annular metallic fuel with a helium gap has been considered for the higher burnup and safety [1]. The annular fuel also can eliminate the need for sodium waste treatment by removing the sodium as bonding material. In this paper, the preliminary performance analysis modeling for an annular metal fuel was established with the MACSIS code [2]. The preliminary performance evaluation including the fuel temperature and the fuel constituent migration was carried out.

2. Preliminary Performance Analysis Modeling

In order to evaluate the performance of an annular fuel, the preliminary performance analysis modeling has been carried out by using the MACSIS code.

The temperature distribution analysis modeling of an annular metal fuel was developed, and the modeling in connection with gap conditions was established in the MACSIS code.

The Ross and Stoute model was used for the calculation of gap conductance. For example, the gas conductance of Ross and Stoute is given by;

$$H_{gas} = \frac{k_m}{C(r_f + r_C) + (g_f + g_C) + GAP} \quad (1)$$

where k_m = the gas mixture conductivity in the fuel-cladding gap, GAP = fuel-cladding hot gap, g_f & g_c = the temperature jump distances, $C(r_f+r_c)$ = a term dealing with the fuel and cladding surface roughness, and C = a fitting parameter.

For the FGR model, the GRSIS model [3] was inserted into the MACSIS code. The preliminary swelling model of the annular metal fuel was derived, and then inserted into the GRSIS model.

Therefore, it is possible to simulate the fuel slug swelling behavior according to the burnup, and to calculate the fuel temperature distribution with the inward swelling into fuel center according to helium and sodium gap conditions.

The evaluation of fuel constituent migration is also possible considering the inward swelling.

Fig. 1 shows the calculation flow in the MACSIS code.

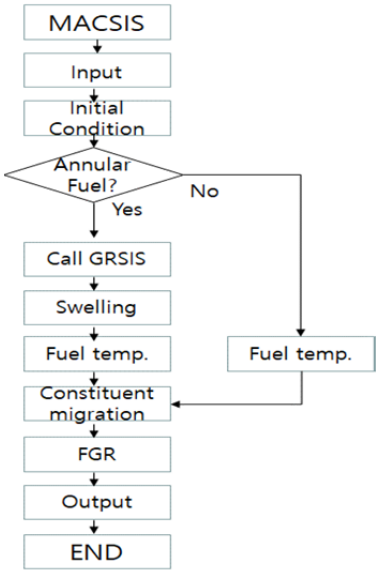


Fig. 1. Calculation flow in the MACSIS code.

3. Preliminary performance evaluation of an annular fuel

3.1 Irradiation history for performance evaluation

AFC-4C ATR irradiation test is in progress including the annular metal fuel. In order to evaluate the performance preliminarily, the irradiation history of ATR was applied [4].

In the case of the fuel constituent migration analysis, EBR-II DP81 experience was applied for the sensitivity analysis.

3.2 Evaluation of the temperature distribution and the fuel constituent migration

Fig. 2 shows the annular fuel radial temperature distribution with gap conditions.

The maximum temperature of the fuel with a helium gap can be somewhat higher due to the increase of temperature in the gap between the fuel slug and the clad. However, the maximum temperature with a sodium gap is very low.

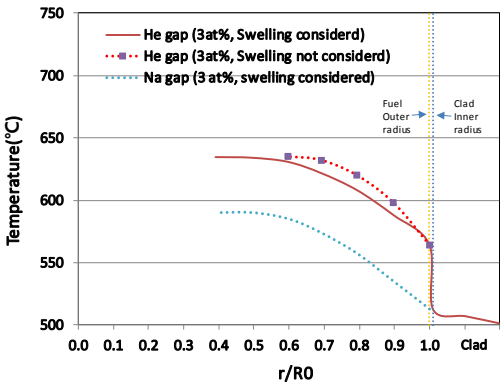


Fig. 2. Fuel radial temperature distribution with gap conditions.

The inner radius of the annular fuel decreases with burnup due to inward swelling into the fuel center.

When inward swelling occurred, it was calculated that the maximum temperature of the fuel with the helium gap was about 635℃ at r/R0 = 0.4, the fuel slug outer temperature was 564℃, and the clad inner temperature was 512℃. If the swelling was not considered, the maximum temperature of the fuel with the helium gap was 635℃ at r/R0 = 0.6.

The maximum temperature of the fuel with the sodium gap was calculated to be about 590℃.

The fuel temperature distribution is affected by the gap condition, so it is necessary to review continuously the model sensitivity including the gap model.

Fig. 3 shows the calculated radial distribution profile of Zr. The empty rectangular points mean the initial Zr concentration.

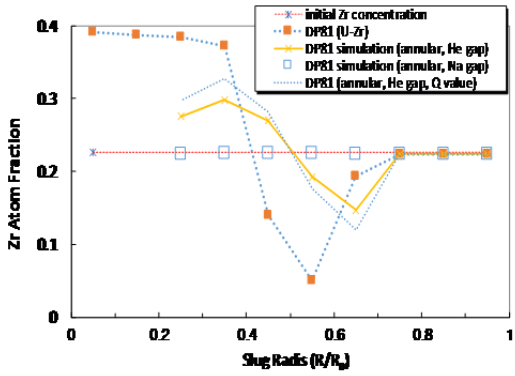


Fig. 3. Calculated profiles of Zr migration.

The calculated results for DP81 show the depletion of Zr in the middle region, and the significant migration of Zr in the center region. It was calculated that the depletion of Zr in the middle zone was simulated well for DP81, in this case the value of the heat of transport (Q*) was about -50,000kJ/mole.

Fig. 3 also shows the calculated Zr migration of the annular fuel with same irradiation history of DP81. Due to the low temperature gradient of the annular fuel, it was calculated that the Zr migration to the fuel center was not large.

If the Q* value was increased to -100,000 kJ/mole, the amount of Zr migration to the center also increased.

In the case of sodium gap, it was calculated that little migration of Zr occurred due to the low fuel temperature with low temperature gradient.

The model parameters such as Q value will be adjusted and benchmarked according to the post-irradiation examination results etc.

4. Conclusion

It is possible for an annular fuel to eliminate the need for sodium waste treatment by removing the sodium as bonding material. In order to evaluate the performance of the annular fuel, the preliminary modeling was developed and inserted into the MACSIS code.

It was calculated that the temperature distribution of the annular fuel was affected by the gap conditions. It was also expected that the Zr migration of the annular fuel was affected by temperature gradient and the fuel temperature. The results of this study will be helpful to establish the performance analysis code and to evaluate the annular fuel performance

ACKNOWLEDGEMENT

This work has been carried out under the National Nuclear R&D program supported by the Ministry of Science and ICT. The authors would like to express their appreciation to INL for the cooperation of metal fuel development.

REFERENCES

[1] Wright A. E. et al., Transactions of the ANS, Vol. 106, Chicago, Illinois, June, 2012.
[2] W. Whang et al., Nuclear Technology, vol 123, Aug, 1998.
[3] C. B. Lee et al., Journal of Nuclear Materials, Vol. 288, pp.29-42, 2001.
[4] Personal communication with INL.
[5] Hofman, G. L. et al., J. of Nuclear Materials, 227, 277, 1996.

Copper Corrosion Modeling in Anaerobic Environment of YS03 Borehole

Minsoo Lee*, Kyung-Woo Park, and Sung-Hoon Ji
Korea Atomic Energy Research Institute, 111 Daedeok-daero 989 beon-gil, Yuseong-gu, Daejeon, Republic of Korea
*minm@kaeri.re.kr

1. Introduction

High-level waste disposal containers should be kept tight in deep geologic environment for several thousand years according to the regulations. As for the corrosion resistant material of the disposal container, copper with excellent corrosion resistance is applied in many countries, such as Sweden, Finland, and Canada. Many experiments have been conducted to determine the degree of copper corrosion in the disposal environment, but it was difficult to evaluate corrosion depth only by field experiments. Therefore, in many countries, corrosion models are on developing to evaluate copper corrosion depth over a long period in disposal environment.

As for the uniform corrosion model for copper, the CCM (Copper corrosion Model) is well known [1]. The CCM model made by Fraser King assuming that copper is corroded uniformly by oxygen in a porous medium. The CCM model included electrochemical, redox, precipitation /dissolution, adsorption/desorption, and mass transfer processes.

KAERI is currently conducting a long-term corrosion experiment using YS03 borehole. There is no oxygen, but HS (Hydrogen Sulfide) was rich in YS03 borehole. We tried to predict the long-term corrosion of copper in YS03 borehole by constructing a basic corrosion model based on the diffusion of HS in bentonite buffer.

2. Simulation

2.1 Modeling Scheme

The corrosion model assumes that HS passes through the bentonite buffer, reaches on copper surface, and reacts with the copper immediately. Then, a Cu_2S layer forms on the surface. Once the Cu_2S layer was formed, the copper(I) cations formed by an anodic reaction on the copper surface diffused out of the Cu_2S layer and reacted with the HS that had diffused from the buffer material. Electrons by cathodic reaction on the copper surface generate hydrogen gas, and the hydrogen gas diffuses out through the buffer. The overall reaction system is shown in Figure 1.

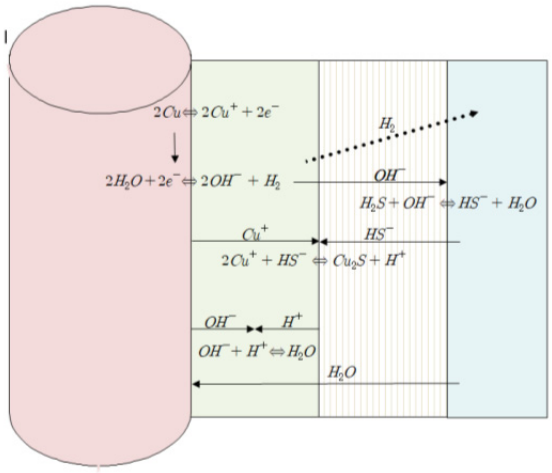


Fig. 1. Reaction Scheme for the Copper Corrosion Model by hydrogen sulfide in YS03 anaerobic environment.

2.2 Analysis tools and structures

To express the HS diffusion through a buffer layer, the cell structure of Excel(Microsoft office) was used, and the flux was calculated in conjunction with Visual Basic to give the concentration change over time. The Excel cells were divided into 22 layers. The top layer is the groundwater layer, and the bottom is the copper layer. The concentration of HS in the groundwater was fixed at about 4 ppm of HS measured in the YS03 borehole. In the Cu layer, it was assumed that all the reached HS was consumed to the concentration zero. Since the thickness of the buffer material is 2 cm, one layer divided into 20 layers corresponds to 1 mm thickness. Since there is a concentration gradient between the layers, it was considered that the movement of the HS flux according to the diffusion coefficient of the buffer material between the layers was performed according to equation (1).

$$C_i' = C_i + (J_{in} - J_{out})/dx \quad (1)$$

C_i is the HS concentration in the i layer, C_i' is the HS concentration after unit time in the i layer, J_{in} is the HS flux entering the i layer, J_{out} is the HS flux leaving the i layer, and dx is the layer thickness.

On the other hand, the interlayer flux movement was calculated using Fick's first law. And the diffusion coefficient of bentonite buffer

was from the experimental value $2x10^{-12}$ m^2/s for MX-80 at density 2000 kg/m^3 [2]. And the Stokes–Einstein equation was applied to adjust the temperature effect on the diffusion coefficient.

2.3 Simulation

It was assumed that the diffusion coefficient of the buffer layer in contact with the copper was affected by the corrosion products. When the pores of the buffer material are blocked, the diffusion coefficient decreases, but when the corrosion product degrade the swelling property of the buffer material, the diffusion coefficient increases. The transfer of HS over time was calculated considering both cases. The simulation results are shown in Figure 2.

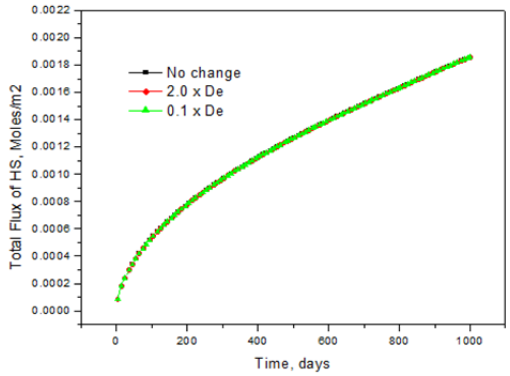


Fig. 2. Simulation results of the total flux of Hydrogen Sulfide onto copper through 20 mm thick bentonite buffer over time.

3. Conclusion

Copper corrosion by HS in YS03 borehole was modeled using an Excel program combined with Visual Basic. The HS concentration in the groundwater was set to 4ppm, and the diffusion of HS through a 2cm bentonite buffer was simulated according to YS03 long term corrosion experiment. It was assumed that all of the HS that had reached, reacted with copper immediately.

As a result of modeling, the corrosion thickness over 1000 years was about 5.63 mm. In addition, the change in the diffusion coefficient of the buffer material due to the corrosion product had no effect because the thickness of the buffer material was too large compared to the corrosion thickness.

The modeling process is currently in progress, and in the future, it is planned to additionally model the effects of oxide film and hydrogen generation.

Acknowledgement

This work was supported by the Nuclear Research and Development Program of the National Research Foundation of Korea (NRF) funded by the Ministry of Science and ICT (No. 2017M2A 8A5014858).

REFERENCES

[1] Fraser King, "Theory Manual for the Copper Corrosion Model for Uniform Corrosion in Sedimentary Rock CCM-UC.1.1", NWMO TR-2008-07 (2008).

[2] K. Pedersen, “Analysis of copper corrosion in compacted bentonite clay as a function of clay density and growth conditions for sulfate-reducing bacteria“, Journal of Applied Microbiology 108, 1094–1104 (2010).

4분과

중저준위폐기물관리 (Oral)

Spent Resin Management Strategy Based on Experience and Current Status

Suk Nam Lim*, Kyu Sup Choi, Jae Woo Park, and Hyo Sub Kim
KONES, IL-Heung Building, 65, Myeongdal-ro, Seocho-gu, Seoul, Korea
*limsn53@hanmail.net

1. Introduction

Spent resin (SR) from PWR is periodically conditioned and stored in the interim storage facility for permanent disposal while SR from CANDO reactor is stored in the large concrete vaults as ILW. SR has not been disposed yet because of issue regarding acceptance criteria.

SR treatment methods for domestic NPPs have been developed step by step to reduce the volume and enhance the waste form quality. Fee for LILW disposal has increased from 3,935 USD per 200 L drum in 2008 to 13,137 USD now.

SR management experience and current status are reviewed to find out the practical strategy for SR management.

2. SR Management Experience in Korea

2.1 Evolution History of Applied Technology

The evolution history of technology applied to SR treatment is divided into 4 generations shown in the table 1.

Table 1. The evolution history of technology for SR

Generation	Technology	Method
1st (1978)	Dewatering	Gravity
2nd (1980s)	Solidification	Cement
3rd (1990s)	Drying with HIC	Warm air
4th (2000s)	Drying/Solidification	Warm air/Polymer

2.2 Spent Resin Storage before Treatment

There are mainly 2 types of resin storage system in NPPs. One type is that spent resin is stored during short term and periodically conditioned. Another is that high activity spent resin is stored for long term while low activity spent resin is shortly stored and periodically packaged.

2.3 Inventory of the Radionuclides

NPPs had selected the scaling factor methodology for radionuclide measurement in the package. The scaling factor has been developed in 2000s. Non-destructive assay system was installed in interim storage facility in each site in 2000s.

The scaling factor for SR is not available now and expected to be applied to in the near future.

2.4 Treatment Cost Comparisons for SR

The dewatering SR retreatment cost of two available technologies is estimated based on material costs needed and disposal fee for LILW. The result is shown in table 2. The polymer solidification process is not simple and quality of waste form is more dependent on worker skill.

Table 2. Dewatering SR retreatment cost

Technology	Drying with HIC	Polymer solidification
Cost(USD)	195.5 / L	204.7 / L

2.5 Disposal Fee for LILW

Fee for LILW disposal has increased gradually as shown in table 3.

Table 3. LILW Disposal Fee (1,143 KRW/USD)

Year	2014	2016	2018	2020
USD	10,437	10,664	12,012	13,289

3. SR Management Strategy

SR management strategy, based on experience and current status reviewed, is suggested as follows.

- To reduce the volume, space in package
- To work out to comply with acceptance criteria for LIIW disposal facility especially establishing radionuclide analysis system and sampling for SR quickly
- To simplify treatment and conditioned process for SR
- To consider transport route and system before packaging design

Acknowledgement

This work was supported by the Korea Institute of Energy Technology Evaluation and Planning (KETEP) granted funds by Ministry of Trade, Industry and Energy (MOTIE), Republic of Korea. (No. 20193210100040).

REFERENCES

[1] NPPs FSAR.

Design of Prototype (Part 2) That Treats Radioactive Waste Containing C-14

Bong-Ki Ko*, Hyeon-Oh Park, Ki-Hyun Kwon, and Seung-Geon An
Sunkwang T&S Co.,Ltd, Sunkyung Officetel 20F, #3, Gongwon-ro, Guro-gu, Seoul 08298, KOREA
*bkko@sktns.co.kr

1. Introduction

Wolseong 1 and 2 nuclear power plants, the only PHWR(Pressurized Heavy Water Reactor) nuclear power plants in Korea, use ion exchange resin to purify liquid radioactive wastes generated from the moderator cleanup system, heat transport purification system, nuclear fuel exchange system and annular gas system and to reduce the concentration of radionuclides. Spent resin is stored in the spent resin storage tank with activated carbon and zeolite (mixture), and treatment technology of the spent resin generated by the PHWR nuclear power plant has not been secured so far. The spent resin generated by PHWR nuclear power plants is classified as medium-level radioactive waste due to the high concentration of C-14 radionuclides with a long and half-life of 5,730 years (KHNP Final Safety Analysis Report), and also shall be treated to silo disposal of in accordance with Nuclear Safety Commission Notice 2020-6 "Limits of Radiation Concentration of Low Level Radioactive Wastes". But, the total radioactivity (1.50E+ 15Bq) of the C-14 nuclide in spent resin is about 10 times higher than the total radioactive limit (3.04E+14Bq/g) of the radioactive waste disposal facility, and thus cannot be disposed of under the current storage conditions. In order to ensure the stability of disposal of spent resin containing high concentrations of C-14, the 'process of spent resin treatment microwave automation' was developed in this study, which removes C-14 in the spent resin and absorbs C-14 in a physically/chemical stable form.

2. Main Title

For the disposal of spent resin, which is a difficult radioactive waste, a radioactive waste disposal process containing C-14 was developed, consisting of an "automated process for separation of spent resin mixture" and an "automated process for disposal of spent resin treatment microwave" with a treatment capacity of 1 ton/8 hr. The automated spent resin treatment microwave process is part 2 process of the prototype that treats radioactive waste containing C-14, which is a process of desorption of C-14 nuclides in the wastewater using microwave, a gas condensation process and an adsorption process using adsorption towers, and a microwave generated gas circulation system.

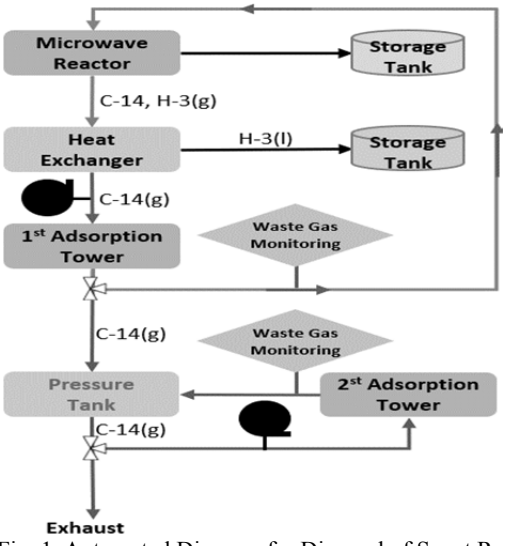


Fig. 1. Automated Diagram for Disposal of Spent Resin Treatment Microwave.

In the case of a C-14 desorption process in a spent resin using a microwave, the C-14 radionuclide is desorbed in the form of CO2 gas under the optimal desorption conditions. In addition, the representative H-3 radionuclide of PHWR nuclear power plants is vaporized in the form of $^{3}H_2O$ gas. In the gas condensation process, more than 90% of the H-3 nuclides vaporized in the wastewater treatment process are collected in the condensate storage tank, and in the case of the C-14 adsorption process, C-14 radionuclides detached from the desorption process are absorbed in a physical/chemical stable condition. In addition, desorption, condensation, and adsorption processes of the automated spent resin treatment microwave process can be using an enclosed internal circulation system and prevent radioactive gas leakage. (Block/Prevent).

2.1 Design of C-14 Desorption Process in Spent Resin

In the case of a PHWR nuclear plant spent resin storage tank, spent resin and mixture are stored in the ratio of 8 to 2, and in the case of spent resin, they contain about 50% moisture. If

the storage ratio and the processing capacity of the spent resin storage tank are considered, a maximum of 800 kg of spent resin must be treated per day. Considering the reaction time of C-14 desorption process after moisture evaporation in spent resin, the design of two microwave reactors was applied, and the throughput capacity per unit was designed at 100 kg/2 h. To evaporate 50 kg of water containing spent resin, 31,000 kcal/h of water drying energy is needed, and if this reflects the output efficiency of microwave, it is derived that more than 45 kW/h of microwave output is needed.

2.2 Design and Fabrication of Microwave Reactor

Based on the desorption process design of C-14 in spent resin, the design of a microwave reactor with 15 water-cooled 3 kW magnetron is applied. In the treatment of waste resin, a horizontal reaction machine and top-to-bottom, left-to-right impeller was designed to prevent carbonization of waste resin, taking into account the area of reaction, reaction time and treatment efficiency between microwave and spent resin.

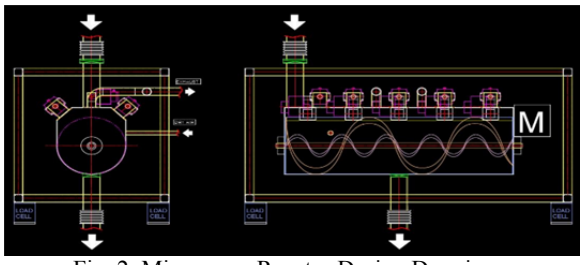


Fig. 2. Microwave Reactor Design Drawings.

In addition, simulations of temperature changes over time and electric fields were carried out, and the optimal microwave location was selected based on them.

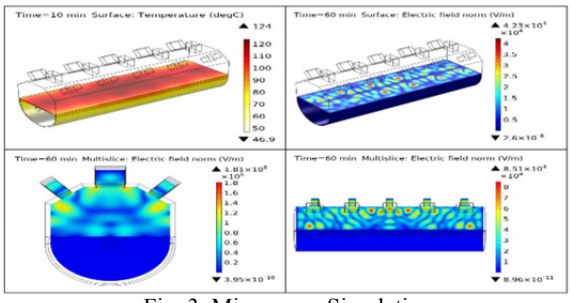


Fig. 3. Microwave Simulation.

2.3 Condensation process and internal circulation system design

Microwave cause a lot of moisture when the response. A small amount of water may improve the performance of the adsorbent, but a large amount of water decreases the performance of the adsorbent. In addition, the H-3 nuclide in moisture converts the adsorbent into a physically unstable form. To solve these problems, we designed the condensation process. In addition, an enclosed internal circulation system with real-time C-14 monitoring system was designed to ensure leakage of these radioactive gases and worker stability.

3. Conclusion

In this study, we developed an automated spent resin treatment microwave process consisting of a C-14 nuclide desorption, gas condensation, C-14 adsorption and internal circulation system in the spent resin using microwave, which is a key process for removing C-14 in the spent resin.

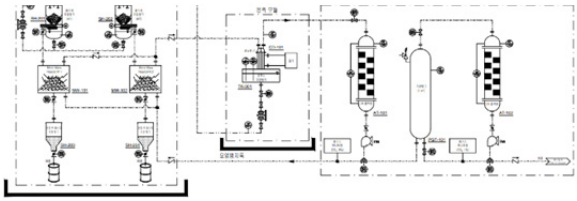


Fig. 4. Automated Process for Disposal of Spent Resin Treatment Microwave.

However, it should be accompanied by a demonstration test to optimize the process for removal of C-14 from spent resin. Through this, it is deemed that the residual C-14 removal method in condensate and the recycling feasibility assessment according to C-14 recovery should be carried out.

Acknowledgement

This Study was supported by a Korea Institute of Energy Technology Evaluation and Planning (KETEP) grant funded by the Korean government (No. 20191510301110).

REFERENCES

[1] KAREI, “Development of Adsorbent for C-14 Gas Trapping and Characteristics Evaluation, (2005).

[2] V. P. Yadav “Kinetics of Esterification of Ethylene Glycol with Acetic Acid Using Cation Exchange Resin Catalyst, (2011).

Solidification of Borate Waste Using Metakaolin-Based Geopolymer Waste Form

Byoungkwan Kim[1], Juhyeok Lee[1], Jaehyuk Kang[1], Younglim Shin[1], Won-Seok Kim[1], and Wooyong Um[1,2,*]
[1]Division of Advanced Nuclear Engineering, POSTECH, 77, Cheongam-ro, Nam-gu, Pohang, Korea
[2]Division of Environmental Science & Engineering, POSTECH, 77, Cheongam-ro, Nam-gu, Pohang, Korea
*wooyongum@postech.ac.kr

1. Introduction

The cement waste form is conventionally used for solidification of radioactive wastes. Borate waste, however, which has high boron concentration is difficult to be solidified using the cement, because boron can react with the reactive calcium compounds such as CaO and $Ca(OH)_2$ present in the cement and forms the insoluble calcium borate compounds [1]. Then, they deposit on the surface of cement particles and hinder the cement hydration reaction, resulting in the problems such as setting (or curing) retardation and low compressive strength of cement waste form [1].

Geopolymers are inorganic binders that are formed at low or room temperatures using inorganic geo-materials [2]. They are fabricated by combining amorphous aluminosilciate materials such as coal ash and metakaolin with alkaline activators [2]. The structure of a geopolymer is composed of disorderly connected Si tetrahedrons with part of their Si substituted by Al [2]. The charge imbalance arising from these cation substitutions is compensated by alkaline ions contained in activator solution (NaOH or KOH) [2].

According to the previous study, 4-coordinated boron unit can replace for the Si, similar to the role of Al [3]. Considering these characteristics of boron and geopolymer, we investigated the potential of borate waste as a raw material for metakaolin-based geopolymers. In addition, the physical and chemical characteristics of geopolymer waste form were evaluated.

2. Materials and methods

2.1 Preparation of simulated borate waste

The simulated borate waste (BW) was prepared according to the chemical composition (Table 1). Borax decahydrate ($Na_2B_4O_7{\cdot}10H_2O$), sodium nitrate ($NaNO_3$), potassium nitrate (KNO_3), calcium nitrate ($Ca(NO_3)_2{\cdot}4H_2O$), zinc nitrate ($Zn(NO_3)_2{\cdot}6H_2O$), and magnesium nitrate ($Mg(NO_3)_2{\cdot}6H_2O$) were dissolved into 1 L of deionized water (DIW) and dried at 105 ℃ for 1 day.

Table 1. The target chemical composition of BW

Element	Concentration (mg/L)
B	221,490
Na	76,000
K	2,333
Ca	1,600
Zn	583
Mg	495

2.2 Synthesis of metakaolin-based geopolymer waste form

Metakaolin, NaOH, KOH, fumed silica, and DIW were used as raw materials of geopolymer. The geopolymers were synthesized following to the mixing conditions (Table 2). Thinky mixer was used for mixing of geopolymer ingredients. Mixing was performed for 2 min at 1800 RPM, then 30 s at 2100 RPM during defoaming process. After homogeneous mixing, geopolymer mixtures were transferred into cylindrical molds with a diameter of 25 mm and a height of 50 mm, cured at 60 ℃ for 6 days, and kept at room temperature for 1 day.

Table 2. Mixing conditions of metakaolin-based geopolymers (molar ratio)

Sample name	Si/(Al+B)	Na/(Al+B)	Water content	BW content (wt%)
N1.5	1.5	1.0	H_2O/(Al+B) =9.0	10
N1.4	1.4			12
N1.3	1.3			15
Sample name	**Si/(Al+B)**	**(Na+K)/(Al+B)**	**Water content**	**BW content (wt%)**
M1.5	1.5	1.0 (Na:K=0.1:0.9)	H_2O/(Al+B) =9.0	9
M1.4	1.4			12
M1.3	1.3			14

2.3 Characterizations of borate waste and metakaolin-based geopolymer waste form

X-ray diffraction (XRD), 7-day compressive strength, and ^{11}B solid-state magic angle spinning (MAS) nuclear magnetic resonance (NMR) were conducted.

3. Results and discussions

3.1 Chemical characteristics of borate waste

XRD result showed that BW consists of crystalline phases such as tricalconite, borax decahydrate, calcium penta borate, potassium penta borate, nitratine, boric acid, and frolovite.

^{11}B MAS-NMR result of borate waste showed that 3-coordinated boron (BO_3) unit and 4-coordinated boron (BO_4) unit present in the borate waste (Fig. 1).

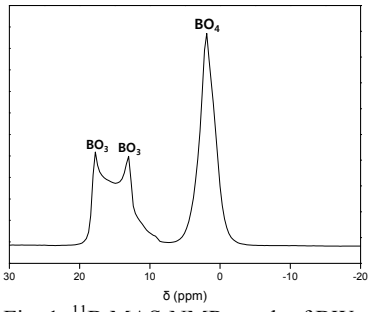


Fig. 1. ^{11}B MAS-NMR result of BW.

3.2 Physical and chemical characteristics of metakaolin-based geopolymer waste form

Geopolymers using mixed activator (NaOH and KOH) showed the highest compressive strength compared to the geopolymers using NaOH activator. Regardless of different cations, the compressive strength was proportional to the Si/(Al+B) ratio (Fig. 2).

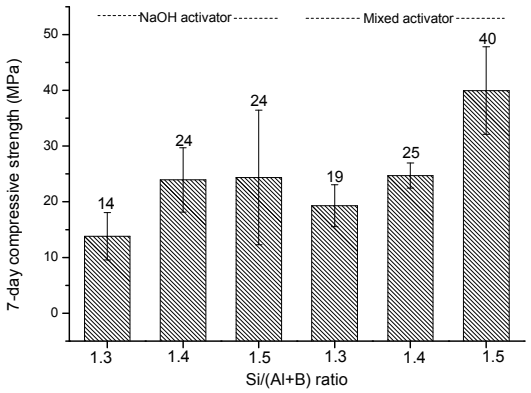


Fig. 2. 7-day compressive strength of metakaolin-based geopolymer waste form.

XRD results of geopolymers showed that BW was incorporated into geopolymer network and potassium borates were formed as new crystalline phases.

After geopolymerization, most of BO_3 units were converted to BO_4 units (Fig. 3). The highest peak was attributed to the ^{4}B(1B, 3Si) peak, showing BO_4 unit surrounded by one B atom and three Si atoms (Fig. 3).

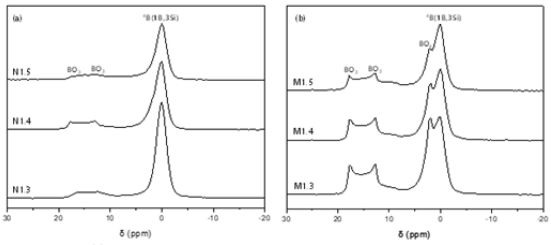


Fig. 3. ^{11}B MAS-NMR results of geopolymers using (a) NaOH and (b) mixed activator. (NaOH and KOH).

4. Conclusions

In this study, BW was solidified using metakaolin -based geopolymer waste form. The physical and chemical characteristics of geopolymers were evaluated. The highest 7-day compressive strength (40 MPa) was found in the geopolymers prepared at 1.5 Si/(Al+B) ratio using mixed activator. The BO_3 units present in BW were converted to BO_4 units which connected with the Si after geopolymerization. This study provides insight of the geopolymer solidification process for the borate waste.

ACKNOWLEDGEMENT

This work was supported by the Korea Institute of Energy Technology Evaluation and Planning (KETEP) and the Ministry of Trade, Industry & Energy (MOTIE) of the Republic of Korea (No. 20181510300870).

REFERENCES

[1] J. H. Kim, B. G. Ahn, H.Y. Kim, and H. H. Park, “A study on the solidification of borate waste using cement”, Journal of Korea Society of Waste Management, 137-142 (1989).

[2] B. Kim and S. Lee, "Review on characteristics of metakaolin-based geopolymer and fast setting”, Journal of the Korean Ceramic Society, 57, 368-377 (2020).

[3] G. Taveri, J. Tousek, E. Bernardo, N. Toniolo, A.R. Boccaccini, and I. Dlouhy, “Proving the role of boron in the structure of fly-ash/borosilicate glass based geopolymers”, Materials Letters, 200, 105-108 (2017).

The Self-Clearance Strategy of the New Fuel Container for Heavy Water Reactor (CANDU) Based on DQO

kwangyoung sohn*, changhwan cho, and sungjong kim
Nuclear Engr. Dept., MIRAE-EN Co., Ltd, D403, Techno 4-ro 17, YuSung-ku, Daejon, 34013, Korea
* kwangyoung.sohn@mirae-en.co.kr

1. Introduction

To perform the self-clearance of fresh fuel containers such as wood pallet, Styrofoam and corrugated cardboard for CANDU type of heavy water reactors (referred to as "*waste*" hereafter), it is required to define the methodology to enhance the quality of data generated during the processes of self-clearance. The level of contamination shall be tolerable for nuclides, especially tritium and C-14. Waste generator needs to establish the strategy based on Data Quality Objective (DQO) [2] [1], statistics and data science as in Table 1, and for ensuring the data quality of self-clearance for regulatory approval, and this suggests one of those approaches in consideration of the statistics and data science.

2. The primitives

To enhance the quality of data for self-clearance of fresh fuel container, the followings are analyzed;

1) The clearance reference of Canada fuel company such as BWXT and Cameco, and infra for law, standard and regulation for clearance,
2) DQO QA/QC plan and procedure[2] including the sampling design and data management (temperature and humidity, half-life etc.).

To assess the inventory status of the fresh fuel containers, the site(storage) simulation of the exposure might be helpful to understand the contamination patterns, and the stratified sampling[3] is selected for each type of wastes like wood pallet, Styrofoam and corrugated cardboard. Once the segregation and categorization are done, the application of DQO is implemented as one of the attempts for the regulatory approval.

3. The clearance strategy based on DQO

Table 1 shows a DQO template to achieve the data quality as found in [1] and [2], which is one of the approaches to prove the appropriateness of clearance, diagrammed in Figure 1[4].

Table 1. DQO 7 steps

Step	The strategy for "waste" self-clearance
1	STATE THE PROBLEM • The scope of this DQO application is for the self-clearance of the fresh fuel containers from CANDU NPPs. It normally includes wood pallet, Styrofoam, and corrugated cardboard("waste"). • The site modeling for the exposure pattern or behavior of wastes • The unambiguous objective of this project is to prove that the degree of waste contamination is in self-clearance level.
2	IDENTIFY DECISIONS • Decision statement needs to address that the waste in inventory is in the self-clearance level on radionuclides as well as tritium and C-14. • Due to the outstanding characteristics of the heavy water reactor, the tritium and C-14 shall be detected by considering the environmental changes like temperature and humidity with other nuclides.
3	IDENTIFY INPUTS • Informational inputs required to resolve the decisions identified in Step 2: (1) Environmental variables - Temperature and humidity for monitoring exposure behavior of some nuclides such as C-14 an tritium etc. (2) Sources for data - Law and act, standard and/or regulatory guideline applicable (3) Level of quality needed for the decision(s) - On-site lab and field screening for cost-effectiveness (4) Usability of existing data sets measured in the time point of waste generation or collection if; - Quality assured - Statistically valid - Commensurate with conceptual site model (5) Information needed to establish action levels (thresholds) - See (2) and (3) (6) Analytical methods and detection limits. - The activity of waste assumed as clearance level is probably very low level, and the percentage of the uncertainty of radioactivity measurement is relatively very high.

[1] Under development in ISO TC85 SC5 WG5 by UK with author.

2 Internal plan and procedure for DQO

	- Thus, the measurement method isolating the background activity is highly recommended. For this, the bag monitor or equivalent could be utilized to enhance the quality of measured data. This should be considered for the margin of detection limits as well.
4	SPECIFY BOUNDARIES • Scale of decision making: (1) Population of interest - As mentioned in Section 2, the population in inventory storage is sampled using stratified sampling to evaluate the pattern of contamination level. Based on this, the type of waste is categorized which is motivating the actual sampling design. - After categorization of wastes, the bootstrapping [3] is used to enhance the quality of sample data. (2) Geographical (spatial) boundaries of the decision statement - The source of waste in this project is clearly limited, so no geographical or spatial consideration is not required otherwise site modeling. (3) Temporal boundaries of the decision statement - Chorological history shall be recorded and traced considering the environmental condition and half-live of nuclides (4) Constraints to sampling. - *Sampling will be completed based on the data science instead of using classical sampling design [4][5].* No constraint for sampling.
5	DEFINE DECISION RULES • Decision Rules (“if…then” statements) - If the activities including other chemical properties of all the radionuclides from the bootstrapping samples in certain environment is in the clearance level (with acceptance limit for self-clearance), then perform the self-clearance. Otherwise, consider an appropriate method for different disposal.
6	SPECIFY ERROR TOLERANCES • In consideration of the relatively simple project, the expected range of data values, possible decision errors, consequences of decision errors, severity of consequences, and tolerable limits on decision errors are ignored. Simply define the null hypothesis and alternative hypotheses to prove the hypothesis. (1) Null hypothesis and alternative hypothesis
7	OPTIMIZE SAMPLE DESIGN • Select the most resource-effective data collection and analysis design from the table that satisfies the DQOs specified in the preceding six steps.

This strategy needs to be submitted for discussion and approval of the regulatory body before commencing the clearance activity. Each step in Figure 1 could be revisited for iteration and update.

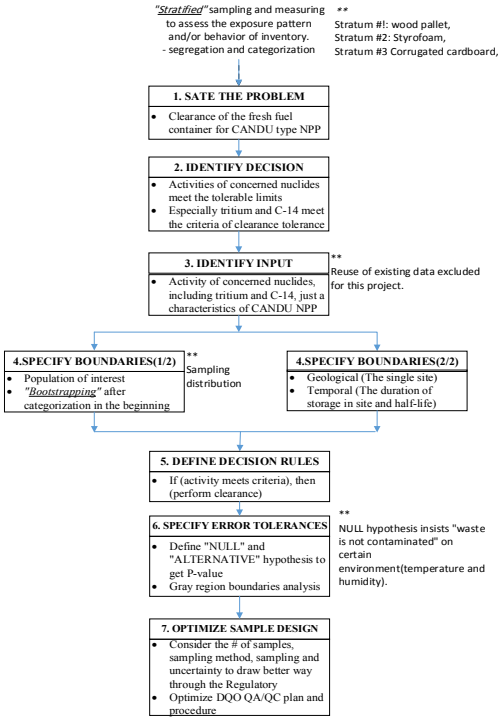


Fig. 1. The clearance strategy diagram.

4. Conclusion

This provides one of the approaches to self-clearance of the container for the fresh CANDU fuel in consideration of “data science” surpassing the classical statistics. Thus, these activities to enhance the data quality using data science for the regulatory approval will be an alternative for radioactive waste certification and approval.

REFERENCES

[1] The introduction of DQO application in radioactive waste management life cycle process, O-04-005, KRS 2020 Fall, On-line conference, 7.29 ~ 7.31.

[2] ISO NP 23580, Risk-Based Approach to Developing Data Quality Objectives in Support of the Characterization and Management of Radioactive Materials .

[3] Peter Bruce and Andrew Bruce, “Practical Statistics for Data Scientist”, O’REILLY.

[4] Mark E. Byrnes, “Sampling and surveying radiological environment”, Lewis Publishers

[5] MIL-STD-105E, Sampling procedures and table for inspection by attributes, 10-May-1989.

Seismic Analysis of the Disposal Containers Stacked in the LILW Repository Silos

Hyeongjin Byeon, Kiwon Kang, Yulim Lee, and Jaeyeong Park*
Department of Nuclear Engineering, Ulsan National Institute of Science and Technology, 50 UNIST-gil, Ulju-gun, Ulsan, Republic of Korea
*jypark@unist.ac.kr

1. Introduction

In Korea, the frequency of the earthquake was small compared to the other countries around. In September 12, 2016, the earthquake with Richter magnitude 5.8 occurred in Gyeongju, Korea which damaged several buildings. In addition, the earthquake with Richter magnitude 5.4 occurred in Pohang, Korea in November 15, 2017. However, under those severe earthquakes, the facilities related to the nuclear power plant maintained its structural stability as they are designed to endure earthquake with magnitude 6.5. Although those facilities maintained its structural stability, the risk awareness for the earthquake in Korea was enlarged to the public.

Unlike ground, the magnitude of the earthquake acceleration decreases at the underground. Therefore, structures located at the underground secures its structural stability from effect of the earthquake. Stability of silos of the Gyeongju low- and intermediate level waste (LILW) repository had been proven under the effect of the earthquake. However, the seismic analysis for the disposal containers has not been conducted which is directly related to the stability of the waste. Therefore, seismic analysis for the disposal containers need to be conducted.

2. Method

2.1 Geometry

The disposal container stacked in the silo is 16-pack disposal container which contains 16 solidified radioactive wastes in the drum. The geometry of the 16-pack disposal container is shown in Fig 1.

As shown in Fig 2, the 26 disposal containers are stacked in the silo. To describe earthquake, the square shaped ground plate is designed between disposal containers and foundation plate which is fixed.

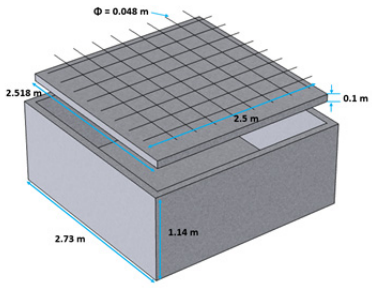


Fig. 1. Geometry of the 16-Pack disposal container.

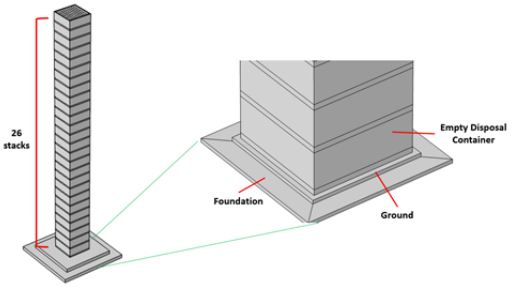


Fig. 2. Geometry of the stacked 26 disposal containers.

2.2 Boundary Conditions

The foundation plate was totally fixed and the prescribed displacement condition is applied to the ground plate which limits the displacement of the ground plate to move only in x-direction in this study. By applying this condition, the gravity into x-direction is applied in the modeling.

2.3 Input Data for Seismic Analysis

There are two big ways of doing the seismic analysis with the Finite Element Method (FEM) modeling program. One is using time-acceleration data as an input while the other is using response spectrum data. As COMSOL Multiphysics does not provide seismic analysis using response spectrum for the pressure-dependent materials like rock, the seismic analysis using time-acceleration data was conducted in this study. The input data is earthquake data with magnitude 5.9 from Jiashi, China as shown in Fig 3.

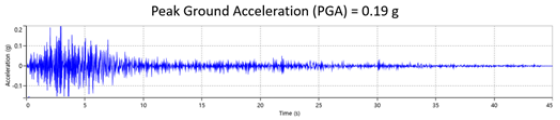


Fig. 3. Time-acceleration history obtained from Jiashi, China.

2.4 Material Property

The 16-pack disposal container is consisted of reinforced concrete and the compressive strength of the disposal container is set as 35 MPa in this study.

The Original Drucker-Prager (DP) yield criterion was applied to the concrete which is well-known yield criterion for the pressure-dependent brittle materials, for example, rock, soil and concrete, etc. The occurrence of the plastic strain of the disposal container was check by plotting DP graph as shown in Fig 4.

3. Results

The seismic analysis was done by COMSOL without any external force to check the structural stability before closure of the repository. For the shortening of the calculation time, the analysis was done for 6 seconds which is long enough to check its effect. The displacement in horizontal acceleration was checked to decide the contact between disposal container in horizontal direction due to the earthquake. The displacement is less than 2 cm which is space between disposal containers in horizontal direction in all the time as shown in Fig 4. The third principal stress representing the maximum compressive stress was compared with container's compressive strength, 35 MPa, which is less enough compared to the its compressive strength.

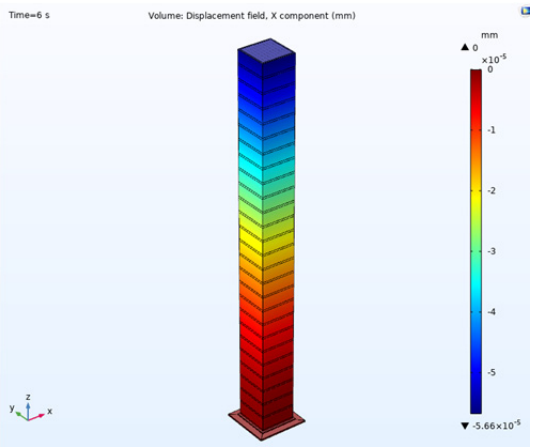


Fig. 4. Horizontal displacement done by earthquake.

4. Discussion

The empty space generated while stacking the disposal container inside the silo is 2 cm. When the earthquake occurs, there is possibility that contact between disposal container in horizontal direction and it may require additional modeling with geometry including disposal containers near the original geometry. However, the result showed that the displacement in horizontal direction is much less than the 2 cm.

5. Conclusion

The seismic analysis was conducted in this study to check structural stability of the 26 stacked disposal containers in the silo of LILW silo-type repository under about 100 m depth below sea level. Under the earthquake in horizontal acceleration, it maintains tis structural stability well and cause no contact with surrounding disposal containers. Therefore, in the further study, it is enough to apply geometry used in this study for the other seismic analysis. However, in the future work, the seismic analysis under pressure of backfilling material should be conducted.

ACKNOWLEDGEMENTS

This work was supported by the Nuclear safety Research Program through the Korea Foundation Of Nuclear Safety(KoFONS), granted financial resource from the Nuclear Safety and Security Commission(NSSC), Republic of Korea (No. 1903005).

REFERENCES

[1] Committe, A. C. I. "Building Code Requirements for Structural Concrete (ACI 318-95) and Commentary (ACI 318R-95)." American Concrete Institute, (1995).

[2] Pul, S., Ghaffari, A., Öztekin, E., Hüsem, M., Demir, S. Experimental determination of cohesion and internal friction angle on conventional concretes. ACI Mater. J., (2017), 114(3).

Development of Conceptual Design for Cover in Nearsurface Disposal Facility

Ki-jung Kwon*, Mi-jin Kwon, and Yu-hwa Son
Korea Radioactivewaste Agency (KORAD), R&D Institute of Radioactive wastes Gajeong-ro, Yuseong-gu, Daejeon 34129, South Korea
*kjkwon@korad.or.kr

1. Introduction

A Korean Low and Intermediate Level Radioactive Waste (LILW) disposal site is in Gyeongju, South Korea. The first phase construction of the disposal system was completed in 2015 as underground silos, and the second phase is a near-surface vault disposal system.

The near-surface Low and Intermediate Level radioactive Waste (LILW) vault disposal cover and concrete degradation analyses are performed to support a safety assessment for the Gyeongju Nuclear Waste Disposal Facility in South Korea.

2. Approach

The disposal concept is given in Figure 1, and two proposed (existing & alternative) designs of the disposal covers are shown in Figure 2. One of the main objectives of this project is to incorporate realistic and practical conditions to evaluate the safety margin of the proposed designs of the disposal covers and concrete structures.

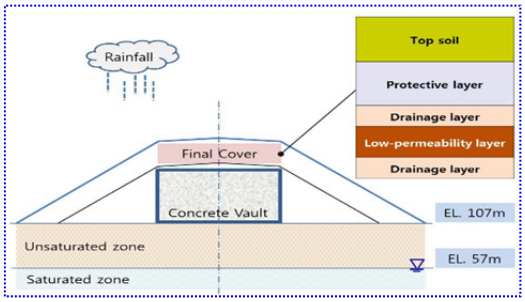


Fig. 1. Vault Facility Disposal Concept.

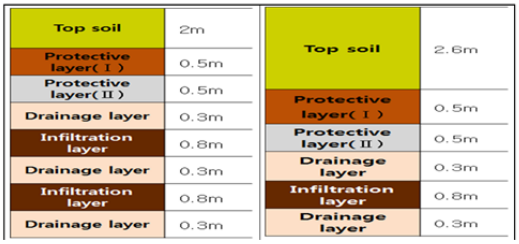


Fig. 2. (a) Existing Design (proposal) Total 5.5m and (b) Alternative Design (proposal) Total 5m.

3. Conceptual model

3.1 The water flow model

Because limiting water flow through the disposal facility is one of the main functions of the earth cover, an in-depth though qualitative description of possible water redistribution processes in the earth cover limiting downward water flow and deep percolation is provided here. In general, three water redistribution processes limiting deep percolation in systems applicable to the earth cover are evapotranspiration, the presence of capillary barriers and infiltration barriers.

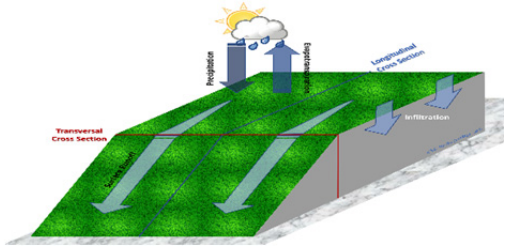


Fig. 3. Concept of Water balance model.

Water flow in variably-saturated porous media is frequently described by the Richards equation. Hydraulic properties are described with the van Genuchten-Mualem model in which the unsaturated conductivity relationship is predicted using the statistical pore-size distribution model of Mualem [132] based on the water retention characteristic parameters. The functional form of the water retention characteristic is the basic form introduced by van Genuchten.

3.2 Erosion Assessment Model

Erosion can result from both wind and rainfall, but water erosion is far more powerful, so that a cover designed to resist water erosion will generally resist wind erosion as well. Many historical approaches to estimating erosion, such as the Universal Soil Loss Equation, were developed for relatively flat agricultural land and are therefore not accurate for steeper slopes such as the proposed cover side-slopes at the LILW disposal site. Therefore, methods developed by the United States Nuclear Regulatory

Commission (USNRC, NUREG 1623 Design of Erosion Protection for Long-Term Stabilization as noted above) for closing piles of uranium mill tailings in semi-arid environments will be used. These methods are intended to eliminate the need for maintenance over time periods on the order of 1,000 years, and so they are applicable to the timespan of the LILW disposal site.

These methods consider probable maximum precipitation events, so actual climate data for the site will be most useful. If site-specific data is not available, then climate data from the literature will be used. Separate methods are available for cover slopes less than 10% and greater than 10%, so that the top surface and side-slopes of the disposal facility will be analyzed separately. The results provide the size of gravel or larger rock that must be mixed into the KJKsurface layers of the cover to resist erosion and will thereby establish design requirements for this layer.

3.3 Concrete Degradation Model

The objective of the concrete degradation analysis is to assess the adequacy of current engineered barrier system (EBS) designs of the vault cover and the concrete structures of the vaults based on the prediction of long-term evolution of its integrity.

To achieve this objective, possible degradation processes are listed and evaluated in the perspective of what their expected effect on concrete degradation is, what time frames they operate in and consequently what changes are expected to occur in chemical and mineralogical composition, fracture spacing, porosity and permeability of the vault concrete.

4. Conclusions

The time period from 0 to 300 years after closure is the Institutional Control (IC) Period. The project assumes that a kind of maintenance will be performed during this period. Especially erosion and slope stability.

Acknowledgments

This work was supported by the Radioactive Waste Management of the Korea Institute of Energy Technology Evaluation and Planning (KETEP) grant funded by the Korea government Ministry of Knowledge (20193210100130).

REFERENCES

[1] Koerner, G.R. 2020. Durability & Aging of Geosynthetics. GSI Webinar W-30. Geosynthetic Institute, Folsom, PA. May 28.

[2] A. V. Benin, A. S. Semenov, S. G. Semenov (2010): Modelling of fracture process in concrete reinforced structures under steel corrosion. Journal of Achievements in Materials and Manufacturing Engineering, Vol. 39, Issue 2, pp. 168-175.

[3] C. Q. Li, W. Lawanwisut, J. J. Zheng, W. Kijawatworawet (2005): Crack Width Due to Corroded Bar in Reinforced Concrete Structures. International Journal of Materials & Structural Reliability, Vol. 3, No. 2, pp. 87-94.

[4] Smart, N. R., & Hoch, A. R. (2010). A survey of steel and zircaloy corrosion data for use in the SMOGG gas generation model. SA/ENV, 841.

A Study on the Optimized Segmentation of 560 MWe Westinghouse Pressurized Water Reactor Vessel Internals

Hyo-Jeon Kim, Jae-yong Lee, Kyung-min Kim, Young-wook Kim, and Yong-soo Kim*
Department of Nuclear Engineering, Hanyang University, 222 Wangsimni-ro, Seongdong-gu, Seoul, Republic of Korea
*yongskim@hanyang.ac.kr

1. Introduction

The aging of nuclear power plants around the world is accelerating, Also recently permanent shutdown of Wolsong-1 was determined following to Kori-1 in Korea. This year On August 29, the public inspection procedure for the preliminary decommissioning plans for Kori- 1 was ended at Korea Hydro & Nuclear Power. As a decommissioning strategy, cold-to-hot method was proposed.

Therefore, disposal and management of waste is important for successful decommissioning. According to the previous case, the reactor vessel internals is intermediate level waste. Except for spent fuel, it has the highest radiation dose.

In This poster show cases of storage of RVI(Reactor Vessel internal) and it shows a study on the number of casks when 560 MWe Westinghouse PWR RVI are segment and put in the MOSIAK casks.

2. Case Study on Overseas Intermediate-level Waste Disposal

2.1 United States of America

In the United States, according to 10 CFR 61 Federal Regulations, wastes of higher doses than Class C are prohibited from landfilling at disposal sites. Wastes level of GTCC or higher were segmented and disposed in the spent fuel dry casks [1]. There were 22 casks generated in Zion, 3 casks in Connecticut and 4 casks in Main Yankee [2,3,4].

2.2 Germany

Germany applied MOSAIK cask(GNS) when disposing of Stade nuclear power plant internals. (PWR 640MWe) 158 casks were generated. MOSAIK cask was approved and made for transportation and storage of intermediate level waste [5]. Depending on the radiation dose, internal shielding can be added.

Table 1. MOSAIK cask scales(GNS) [6]

MOSAIK	M Ⅱ-10 T	M Ⅱ-12 T	M Ⅱ-15KKI 1	M Ⅱ-15 EI	M Ⅱ-15 U EI*
	Type IP-2	Type IP-2	Type IP-2	Type U (U)	
Outer height (mm)	1500				
Outer diameter (mm)	1060				
Internal height (mm)	1220		1140		
Internal diameter (mm)	860	820	740		
Wall thickness (mm)	100	120	160		
Lead shielding (mm)	-	-	-	0-120	
Empty weight app (kg)	4300	4700	5730	5730-9230	
Volume max (dm^3)	690	620	490	165-490	

* Under water loading

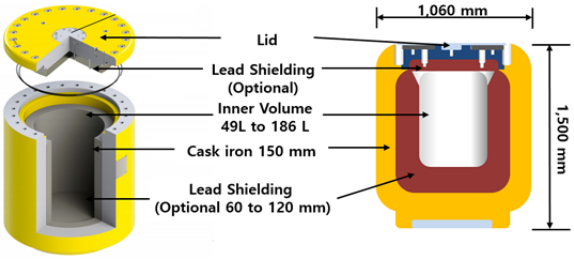


Fig. 1. MOSAIK cask shape [6].

3. Optimized Segmentation of RVI

Optimized study is conducted with the aim of minimizing volume, reducing worker exposure and minimizing cost. If the segment internals are too small, the amount of waste will decrease. But worker exposure is increased by increasing working time. Conversely, if the segment internals are too large, worker exposure decreases, but the amount of waste increases.

In this study, derive the most optimal scenario based on the ALARA(As Low As Resonably Achievable) law is conducted. The cost will be

calculated automatically when the size of the segment internals, the working time and worker exposure are determined. Figure 2 shows the segment optimization process.

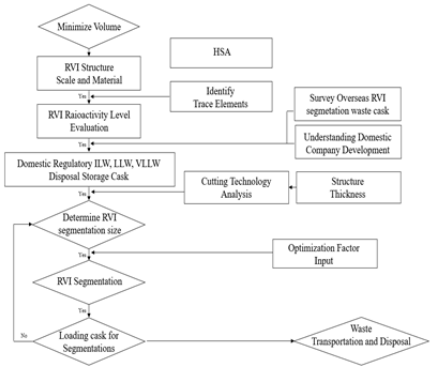


Fig. 2. RVI Segmentation process diagram.

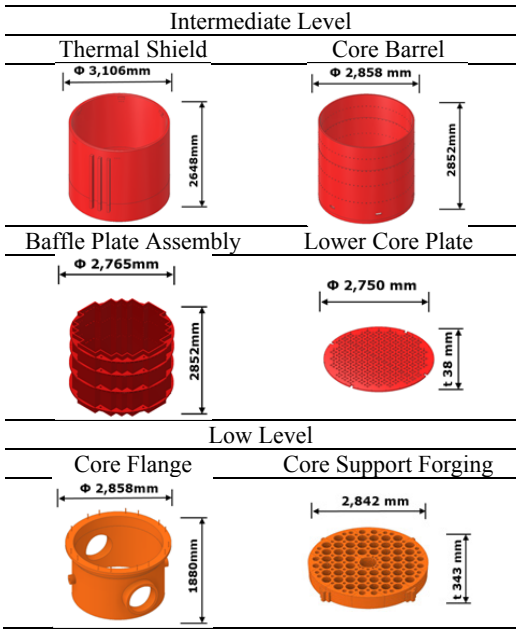


Fig. 3. RVI scales.

Region	Reactor Vessel Internals	Total Activity (Bq)	Radioactive Level
Upper Region	Core Flange	-	LLW
Belt line	Baffle Assembly	3.11E+ 16	ILW
	Core Barrel	3.54E+16	ILW
	Thermal shield	8.21E+ 15	ILW
	Lower core plate	1.21E+ 12	ILW
Lower Region	Core support forging	-	LLW
	Secondary Support Assembly (Tie plate, Cruciform column, Bottom column)	-	VLLW
			VLLW
			VLLW



Fig. 4. RVI Radioactive Level.

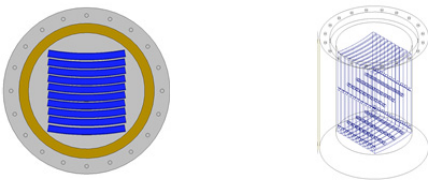


Fig. 5. Packaged Piece form the Core Barrel.



Fig. 6. Packaged Piece form the Thermal Shield.

5. Conclusion

When 560MWe Westinghouse PWR RVI segments optimally. MOSAIK casks were generated at 9 thermal shield, 5 core barrel, 4 baffle assembly and 2 low core plate. In the scenario, a total of 20 MOSAIK casks occurred.

Decommissioning of Kori-1 is expected to generate 80,000 drums of waste. But, to meet the goal of 14,500 drums. we should be reduction volume of waste of generated during decommissioning through optimized segmentation of RVI.

Acknowledgement

This work was supported by the National Research Foundation of Korea(NRF) grant funded by the Korea government 2019M2C9A1057808, 2017M2 B2B1072830.

REFERENCES

[1] WMDB-ST-3. “Decommissiong of Nuclear Facilities”, IAEA.
[2] Conrad Cook and Dr. Holger Spann. “Reactor Vessel and Reactor Vessel Internals Segmentation at Zion Nuclear Power Station”, WM2013 Conference, Feb 24-28, Phoenix, Arizona, USA.
[3] EPRI, Maine Yankee Decommissioning – Experience Report, “Detailed Experience 1997-2004”
[4] EPRI, Connecticut Yankee Decommissioning – Experience Report, “Detailed Experience 1996-2006”
[5] T.D. Baldwin and T.W. Hicks, “Robusat Shielded Container Criticality Safety Assessment : Generic Description of RSCs, 5 Sep, 2013.
[6] GNS. MOSAIK “Transport and Storage Casks for ILW.

4분과

중저준위폐기물관리 (Poster)

Decontamination and Treatment Technologies of Radioactive Waste for the Decommissioning of CANDU-6 (Canadian Case)

Mugap Shin*, Kwangsoon Choi, and Jaihoon Jung
KEPCO E&C, 269 Hyeoksin-ro, Gimcheon-si, Gyeongsangbuk-do, Republic of Korea
*mgshin@kepco-enc.com

1. Introduction

This paper summarizes the decontamination and treatment technologies of radioactive waste from pre-decommissioning activities in the CANDU (CANada Deuterium Uranium)-PHWR(Pressurized Heavy Water Reactor) decommissioning waste management review report developed through technical cooperation with CNL(Canadian Nuclear Laboratories).

2. Decontamination

2.1 Mechanical Decontamination

Mechanical decontamination relies on the use of mechanical tools that may be combined with a liquid or solid media. CANDU Clean™ and Siemens Siva-blast ™ are proven technologies that could be used for decontamination of CANDU steam generators. Both techniques involve the removal of deposits by abrasion with stainless steel grit. The blast material is conveyed through the steam generator. After passing through the tubes, the reusable blast material is separated from dust and debris and separated abrasive material is re-circulated. The reuse of the blast material is capable of minimizing generation of secondary waste.

2.2 Chemical Decontamination

There are available oxidizing processes such as alkaline permanganate (AP), nitric permanganate (NP), and permanganic acid (HP). AP is not corrosive to carbon steel whereas NP and HP are corrosive to carbon steel. In all cases, AP, NP and HP can be applied to 300 and 400 stainless steel and alloy 600 surfaces.

In addition, reduction processes are employed to assist in the dissolution of oxide layers and in many cases they are combined with complexing agents to keep the dissolved metals and associated radionuclides in solution. CAN-DECON™, CAN-DEREM™, CAN-DEREM Plus™ is to dilute regenerative process for full or sub-system decontamination. CITROX™ contains dilute oxalic and citric acids and dissolved oxygen.

HP/CORD UV™ is to dilute process consists of a HP step followed by an oxalic acid reduction step. The addition of ultraviolet light (UV light) makes it a more aggressive process to the base metal.

3. Treatment

3.1 Volume Reduction

The volume reduction technologies such as super-compaction and incineration are widely used in Canada. The main goal of the use of these technologies is to minimize the storage space. In addition, various cutting technologies, such as diamond wire cutting, are employed for large equipment to size for packaging materials in a container. Separately, metal melting is also widely used as no residual material is returned to the waste generator [1].

3.2 Thermal Processes

Incineration and pyrolysis are widely used to reduce volume of organic-contaminated waste. Residuals are then packaged and dispositioned. Metal melting can be used for reducing the volume of metal waste and if possible, recycle material. The pyrolysis process separates the organic fraction of the waste from the radionuclides by gasification of the volatile organic species; the radioactivity remains in the solid residue in the form of metal oxides. In incineration, contaminated material is heated to high temperatures in the presence of oxygen.

Plasma processing is a commercially available technology. It has the benefits of a stable final form and volume reduction. However, both capital and operating costs for a plasma processing facility are quite high.

3.3 Cutting Technologies

Plasma arc, electric and metal discharge machining, high pressure abrasive grit, milling cutters, and diamond wire saw are considered as cutting technologies. These technologies are employed to the nuclear industry in order to cut adequate size in accordance with specifications acceptable to either packaging or the receiving facility.

3.4 Immobilization

Cementation and vitrification are common technologies. The waste-cement mixture is made by combining waste, cement, water and additives either directly in the container (in-drum mixing) or prior to pouring into the container. Vitrification comprises several stages, in general, and can be applied to spent ion-exchange resin.

Immobilization is also possible through various absorbents, but may be subject to review for acceptance within the disposal facility.

Cementation for immobilization has been employed in Canada for liquid and sludge wastes with higher activities.

4. Conclusion

Wolsong Unit 1 is also CANDU 6 reactor, and we expect that the radioactive waste generated during decommissioning will be similar to decommissioning waste in Canada as confirmed through technical cooperation with CNL. Therefore, the methodology for decontamination and treatment in Canada can be used as a reference for Wolsong Unit 1 Decommissioning Project.

REFERENCES

[1] A. Taylor, “30 Years of Experience, Proceedings of Waste Management Symposia, Paper 19157, (2019).

Adsorption of Iodide Using Silver Functionalized Magnetite Silica Composites

Sangeun Jo[1,*], Dohyun Kim[1], Youngwoong Park[1], Sangjun Choi[1], and Jungwon Choi[2]
[1]Kyungpook National University, 80 Daehak-ro, Buk-gu, Daegu 41566, Republic of Korea
[2]Korea Research Institute of Chemical Technology (KRICT), 141, Gajeong-ro, Yoseong-gu, Daejeon 34114, Republic of Korea
*jse0722@knu.ac.kr

1. Introduction

Radioactive iodine released into the sea is dissolved in various forms such as iodide, iodate, and organ o-iodide in water. Each iodine can change into a different form, and this phenomenon affects the formation of iodine-treated disinfection by-products while disinfecting drinking water or wastewater. Also, because iodine exists in various chemical forms, it is not easy to remove iodine mixtures present in aqueous solution or wastewater. There are various methods for adsorbing and removing iodine ions in aqueous solutions. Some inorganic anion exchangers are used to adsorb chloride or iodide anions in solution. However, inorganic anion exchangers have the disadvantage of being toxic for use in drinking water or groundwate [1].

Therefore, in this study, the study of iodine adsorption using silver was conducted based on the results of previous studies. In previous studies, I-adsorbents using various supports such as CAM (cellulose acetate membrane), activated carbon, and zeolite have been developed. In this study, silica was used. The results of previous studies that the adsorption efficiency of silver-impregnated zeolite is better than activated carbon was the basis for carrying out this study [2].

2. Experiments

2.1 Preparation of the adsorbents

The silver functionalized magnetite silica (mag@silica-Ag), were synthesized by the following method. The magnetite-silica (1 g) were stirred in 100 mL of silver nitrate (0.1 M) using agitator until the pH is above 9.5. Subsequently, the solution was stirred at 50 ℃ for 20 h using shaking incubator (250 rpm). After reaction for 20 h, the product was separated by centrifugation and washed three times with DI water. The resulting precipitate was dried in an oven at 60 ℃ for 12 h.

2.2 Method

The iodide anion adsorption isotherm was determined by measuring the concentration of I- remaining in the solution after equilibrating with a 10 ml NaI solution having an I- concentration in the range of 1 to 200 ppm for 24 hours. It was used to prepare a calibration curve (R^2 value of the calibration curve: 0.999) and convert the UV-vis data before and after adsorption to the actual I- concentration.

3. Results

The Langmuir sorption isotherms are presented in Figure 1 and the isotherm parameters obtained by fitting the experimentally observed sorption equilibrium data to the isotherm models. The amount of iodide adsorbed onto the synthetic sorbents increased with an increase in the initial iodide concentration, which causes a driving force such as concentration gradient. The Langmuir model provides an adequate fit ($R^2 > 0.80$) to the experimental data for iodide sorption onto the synthetic sorbents. The maximum sorption capacities (q_m) of mag@silica-Ag was 0.82 mmol/g. The presence of silver on the surface of mag@silica is thought to be responsible for the higher q_m value of the mag@silica-Ag composite. Based on the good fit of the experimental data to the Langmuir isotherm model, it may be concluded that the I ion was sorbed onto the homogeneous surface of mag@ silica-Ag composite via monolayer sorption and that the silver was uniformly distributed throughout the surface.

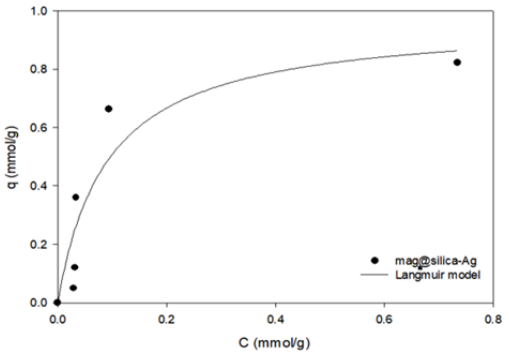


Fig. 1. Sorption isotherm of I on mag@silica-Ag composite.

4. Conclusion

In previous study, magnetite silica has higher maximum adsorption ability than silica [3]. And in this study, we figured out magnetite silver silica has higher adsorption ability than magnetite silica. Also, these results demonstrate that magnetic separation based on permanent magnets is a promising technology because of their high separation efficiency and short contact time.

REFERENCES

[1] S. Hosseini, T.S.Y.CHOONG, and L.C. ABDULLAH, “Removal of iodide ions from aqueous solution by electric arc furnace slag”, Journal of Engineering Science and Technology, 5(1), 73-81 (2015).

[2] Jay S. Hoskins, Tanju Karanfil, and Steven M. Serkiz, “Removal and sequestration of iodide using silver-impregnated activated carbon”, Environmental Science & Technology, 36(4), 784-879 (2002).

[3] Hyun-Kyu Lee et al., “Copper Ferrocyanide Functionalized Core-Shell Magnetic Silica Composites for the Selective Removal of Cesium Ions from Radioactive Liquid Waste”, Journal of Nanoscience and Nanotechnology, 16(6), 6223-6230 (2016).

Applicability of Domestic Natural Zeolite as an Additive for Solidification of Decommissioning Liquid Waste with Polymer Cement

Seong Ho Yoo, Hyun Ki Jung, Ho Yeon Yang, and Kwan Sik Chun*
Korea Environment Testing and Analysis Laboratory,
63-1, Wondoo-ro, Gwangsan-gu, Gwangju, Republic of Korea
*kschun44@hotmail.com

1. Introduction

To convert radioactive liquid waste from decommissioning of a nuclear power plant into a suitable waste form for its disposal, the project of "Development of High Performance Cement Materials and Solidification Technology for Immobilization of Liquid Radioactive Wastes" was launched in May 2020, and is being continued to the end of October 2022. Here, the addition of zeolite is considered to obtain the aggregate from the treatment of radioactive liquid waste and then polymer cement is being injected into the aggregate. Based on the previously published papers, the applicability of natural zeolite produced in Korea for the decontamination of radionuclides from the liquid waste and then for the solidification of the dried waste with polymer cement was reviewed.

2. Properties of domestic natural zeolite [1]

2.1 Mines and minerals of zeolites

Deposits under development or with potential for development in Korea are limited to the Yeongil, Gampo and Gyeongju areas in Gyeongbuk, where the tertiary volcanic sedimentary rocks are concentrated. Among the zeolites found in Korea, the usable minerals include clinoptilolite, mordenite, heulandite, and ferrierite.

Most of the zeolites in the Yeongil-Gampo area are being run on ore bodies with clinoptilolite as the main component and a little mordenite, and the content of zeolite is known to be more than 60wt%.

2.2 Characteristics of cation exchange of zeolite [1]

A corresponding negative charge is derived according to the degree of substitution of Al^{3+} for Si^{4+} in the $(Si,Al)O_4$ tetrahedral structure, which is the basic unit in the crystal structure of zeolite. In order to compensate for the loss of charge generated in this substitution process, cations such as Ca^{2+} and Na^{+} intervene in the cavity structure of the zeolite, which is weakly bound, have a tendency to be easily exchanged with other cations in aqueous solution.

The theoretical cation exchange capacity (CEC) of natural zeolite is known to be 2.2 meq/g for clinoptilolite and mordenite, 3.2 meq/g for hollandite, and 2.3 meq/g for ferrierite. However, the CEC of zeolites mined in Gyeongbuk region shows a remarkable difference not only by quality but also by mineral type, but the CEC of clinoptilolite-based ores is in the region of 60 meq/100g to 170 meq/100g, shown in Fig. 1. As shown in this figure, though the relationship between the zeolite content and the CEC value is likely proportional, it does not show a consistent correlation. This suggests that the CEC of zeolites does not simply depend on the mineral phase and the content of zeolite. That is, it is interpreted that this is because the CEC value per unit mineral varies depending on the crystallographic diversity of zeolite (Si/Al ratio representing the skeleton composition) and exchangeable cation composition (especially the content of Ca and K).

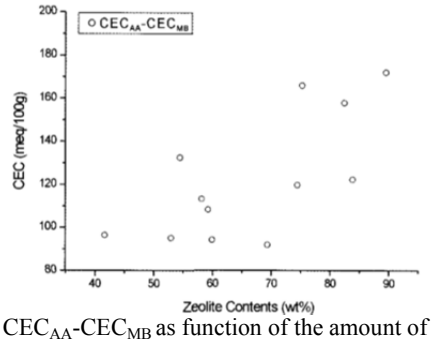


Fig. 1. CEC_{AA}-CEC_{MB} as function of the amount of natural zeolite [1].

The distribution coefficients of radionuclides at different pH values by natural zeolite (clinoptilolite) obtained from Gordes, located in the western Turkey, was comparatively high within 4 ~ 8, shown in Fig. 2.

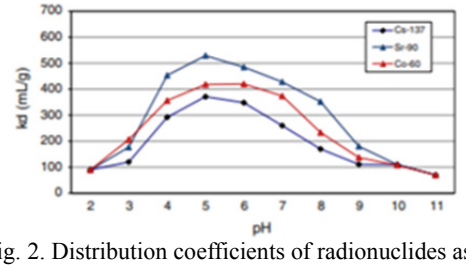


Fig. 2. Distribution coefficients of radionuclides as a function of pH of solution [2].

3. Properties of solidified cement with zeolite

3.1 Characteristics of Hydrated cement with zeolite [3,4]

As the content of zeolite (mainly clinoptilolite with a little mordenite) was increased, the initial and termination of curing cement was accelerated. This is due to acceleration of the hydration of C_3S in the cement by the addition of zeolite. On the other hand, the volume of pores increased in comparison with the plain as the content of zeolite and the curing age increased, given in Table 1. This may be due to the formation of pores with a mesopore size around the boundary between the zeolite particles and cement hydrate.

Table 1. Pore volume and mean pore diameter of cured cement pastes [3]

	Age	Plain	10%	20%
Total volume (cm^3/g)	7 days	0.048	0.051	0.078
	28 days	0.036	0.043	0.073
Average diameter (nm)	7 days	9.2	8.3	8.4
	28 days	7.9	8.6	8.4

3.2 Compressive strength of solidified cement with zeolite [3,4]

The compressive strength of the cured mortar was increased with the increase of the curing age, but sluggishly increased after 28 days, shown in Fig. 3. On the other hand, the strength was increased up to around the 15% of zeolite, then decreased. This may be due to increasing pores by the decrease of cement following the increase of zeolite content. This suggests that the content of zeolite should be around 10wt% of mortar in terms of compressive strength.

3.3 leachability to the stages of zeolite added.

The leach rate of Cs-137 from the decontaminated solidified waste was slightly lower than the direct solidified waste with the mixture of cement and zeolite, shown in Fig. 4 [2].

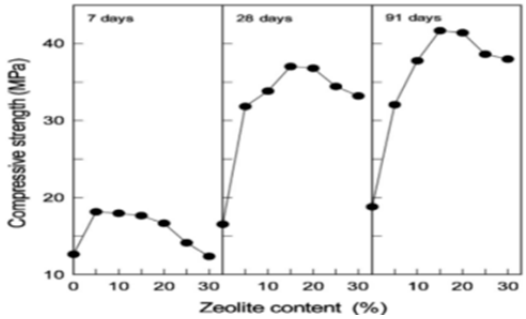


Fig. 3. Compressive strength of cured mortar as a function of the amount of zeolite [3].

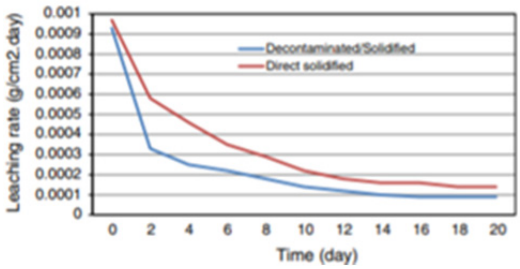


Fig. 4. Leach rates of Cs-137 from solidified cement wastes as a function of time [2].

4. Conclusion

Domestic natural zeolite would be very useful to reduce leach rate from solidified waste with polymer-cement as well as to decontaminate radionuclides from liquid waste. In terms of compressive strength, it would be better to replace around 15wt% of cement with zeolite.

REFERENCES

[1] Jin Hwan Noh, "Study of utilization of natural zeolites as functional materials for water purification (I): Cation exchange propertiy of domestic zeolite", J. Miner. Soc. Korea, 16(2), p.135-149, (2003).

[2] A.E. Osmanlioglu, "Decontamination and solidification of liquid radioactive waste using natural zeolite", J. Mater Cycles Waste Manag, 17, p.690-694, (2015).

[3] Chang-Yong Lee, Youn Cheol Kim, and Jong-Jib Lee, "Hydration characteristics of cement containing zeolite", Appl. Chem. Eng., 22(4), p.423-428, (2011).

[4] Chang-Bok, Han-Seung Lee, "Study on the effect of finess and substitution rate of natural zeolits on chemical reaction and physical properties of cement mortar", J. Korea Institute for Struc. Maintenance and Inspection, 24(3), p.96-103, (2020).

Homogeneity Test of Cesium and Cobalt Loaded Ion Exchange Resins in Polymer Waste Form

Jueun Kim[1], Byoungkwan Kim[1], Bhupendra Kumar Singh[1], and Wooyong Um[1,2,3,*]
[1]Division of Advanced Nuclear Engineering, POSTECH, 77, Cheongam-ro, Nam-gu, Pohang, Korea
[2]Division of Environmental Science & Engineering, POSTECH, 77, Cheongam-ro, Nam-gu, Pohang, Korea
[3]Nuclear Environmental Technology Institute (NETI), POSTECH, 77, Cheongam-ro, Nam-gu, Pohang, Korea
*wooyongum@postech.ac.kr

1. Introduction

Ion exchange resins (IERs) were widely used to maintain nuclear facility conditions and remove radioactive wastes. Approximately 44,500 L/yr of spent IERs were produced in Shin Wolsong 1&2 nuclear power plant (NPP), and contained 1850 MBq of ^{137}Cs and 37 MBq of ^{60}Co [1]. These spent IERs have high dispersibility and must be solidified homogeneously before permanent disposal. Cement, bitumen, and polymers were generally used to solidify the spent IERs, however, the study about evaluating the homogeneity of these waste forms were rarely done. In this study, we evaluate the homogeneity of two kinds of epoxy polymer waste forms by Laser-induced breakdown spectroscopy (LIBS) analysis, and try to identify the effect of homogeneity on waste acceptance criteria.

2. Experimental

2.1 Fabrication of Cs and Co loaded IER in epoxy polymer waste form

Mixed IER (TULSION MB-106) were added into the 30 mM CsCl and $CoCl_2$ solution at solid to solution ratio of 1 kg/10 L and reacted for 3 days. After reaction, the spent IERs were dried at 60 °C inside an oven for 3 days. The spent IERs were ground by planetary ball mill (ProPM2L, Pronextech) with 500 mL stainless steel grinding jar with SUS ball at 500 rpm for 5 hours. 120 g of simulated ion exchange resin were added to 100 g of YD-128H epoxy, 20 g of hardener (IPDA), and 1 mL of defoamer (BYK-1790), cured for 1 day at room temperature, and aged in 60 °C oven for 1 day. Polymer waste forms containing ball mill ground IERs and withour ground IERs were labelled as BG polymer and NG polymer, respectively.

2.2 Analytical methods

The compressive strength were measured at 0.3 MPa/s according to ASTM C39 methods. LIBS (J200, Applied Spectra) was used to investigate Cs and Co distribution in the epoxy polymer waste form. Polymer waste form were divided into 3 parts (Top, Middle, Bottom), and each part was analyzed in 5 sections. The leaching test were performed until 90 days according to ANSI/ANS 16.1 [2]. The concentration of Cs and Co in the leachates were measured by inductively coupled plasma mass spectrometry (NexION 300D, PerkinElmer).

3. Results and Discussion

3.1 The effect of the size of IERs on homogeneity in polymer waste form

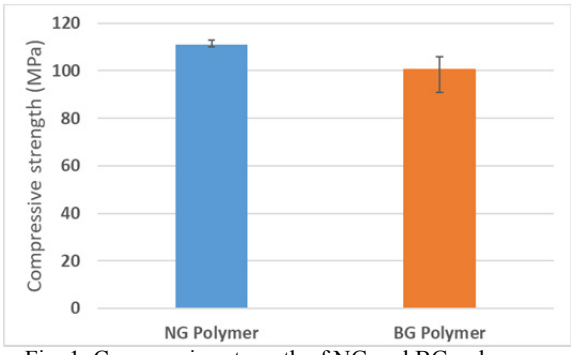


Fig. 1. Compressive strength of NG and BG polymers.

The compressive strength of NG and BG polymers were 111 MPa, and 100 MPa, respectively (Figure 1). Although the BG polymer had a slightly lower compressive strength than the NG polymer, both epoxy polymer showed that the compressive strengths satisfied 30 times higher than 3.44 MPa of waste acceptable criteria.

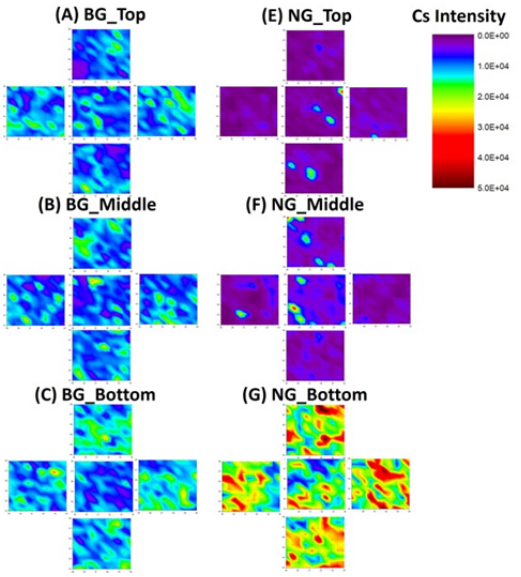


Fig. 2. Cs elemental 2D mapping of NG and BG polymer.

The Cs distribution in the epoxy polymer waste form was illustrated in in Figure 2. Both NG and BG polymers showed that Cs distributed homogeneously in radial direction even at 3 different height. However, NG polymer revealed that Cs was clustered and found more in the bottom, which means heterogeneous in vertical direction. This results suggest that granular sized IERs were easily settled down than powder sized IERs, which can lead to heterogeneity in final polymer waste form. The same results were found for Co distribution as well.

3.2 The effect of the homogeneity on leaching behavior

Table 1. Leachability index (LI) of Cs and Co

NG Polymer		BG Polymer	
Cs	Co	Cs	Co
14.44	10.49	15.18	11.13

The leaching test were performed to identify the effect of homogeneity on leaching behavior of Cs and Co from spent IERs. Both NG and BG polymer showed higher LI than the waste acceptable criteria of LI (= 6) for Cs and Co (Table 1). The total leached amount of Cs and Co from NG polymers were ~3.4 and 4.8 times higher than those of BG polymers.

4. Conclusion

In this study, we conducted the homogeneity test using polymer waste form with the Cs and Co loaded IERs and its effect on leaching behavior. BG polymer showed homogeneity in both radial and vertical directions. However, NG polymer seem to be heterogeneous in vertical direction; due to settlement of IERs. Both NG and BG polymer waste forms were satisfied the compressive strength and leachability index of waste form acceptable criteria to repository. However, the total leached amount of Cs and Co in NG polymer were ~3.4 and 4.8 times higher than those of BG polymer. The homogeneity could affect the long-term stability of the waste form.

ACKNOWLEDGEMENT

This work was supported by the Korea Institute of Energy Technology Evaluation and Planning (KETEP) granted financial resource from the Ministry of Trade, Industry & Energy, and Republic of Korea (No. 20171520000410). We appreciate to Seonggon Ryu researcher from Nuclear Engineering Services and Solutions (NESS) for supporting us to make polymer waste forms.

REFERENCES

[1] Han Jang, Nam-Hee Yang, Won-Seon Jeong, Young-Su Cho, and Geong-Jin Lee, “Design and Evaluation of Shielding for the Continuous Common Decontamination System for Radioactive Spent Resin Disposal”, Journal of Radiation Industry, 13 (2),103~108, (2019).
[2] ANS 16.1, “measurement of the leachability of solidified low-level radioactive wastes by a short-term test procedure”, (2013).

Mercury (II) Removal From Aqueous Solution Using Sulfur-Functionalized Biochar

Samiratu Atibun Isa[a], Sae Yun Kwon [a], Bhupendra Kumar Singh[b], Hyojoo Kim[b], and Wooyong Um[a,b,*]
[a]Division of Environmental Science and Engineering (DESE), POSTECH, Republic of Korea
[b]Division of Advanced Nuclear Engineering (DANE), POSTECH, Republic of Korea
*wooyongum@postech.ac.kr

1. Introduction

Mercury (Hg) has various uses in nuclear fuel reprocessing and nuclear weapon production, and so it is often present in radioactive and mixed (radioactive and hazardous) wastes. This poses threat in storage/disposal facilities and nearby resources such as underground waters due to its dispersibility and toxicity [1][2]. Palm kernel and coconut shells are major waste problems in Ghana posing threat to the environment. In this study, removal of aqueous Hg(II) was tested using sulfur-functionalized biochars produced from palm kernel and coconut shell in Ghana via slow pyrolysis.

2. Method

2.1 Biochar preparation, characterization, and sulfuration

Palm kernel and coconut shell biochar; PKSB and CSB, respectively was produced via pyrolysis at 600°C in the presence of N_2 gas at a heating rate of 10 °C/min. These materials were characterized via scanning electron microscopy with energy dispersive spectroscopy (SEM/EDS), Fourier transform infrared spectrometry (FTIR), Brunauer-Emmitt-Taylor surface area (S_{BET}), elemental, and proximate (moisture content (MC), volatile matter (VM), fixed carbon (FC), ash content (ASH)) analyses. Both PKSB and CSB were sulfurated using 2M $Na_2S.9H_2O$, and the resultant sorbents were named as SPKSB and SCSB, respectively. Biochar beads were also fabricated using polysulfone and N-methyl-2-pyrrolidin-one solvent via liquid-liquid phase separation technique. The beads were cut horizontally, and their cross-sections were analyzed by SEM. The diameter and porosity of the beads was calculated using the following equations.

$$\text{Diameter} = \frac{6\left[\frac{Wa}{\rho p}+\frac{(Wb-Wa)}{\rho w}\right]}{\pi}\Bigg\}^{\frac{1}{3}} \quad (1)$$

$$\text{Porosity} = \frac{\frac{(Wb-Wa)}{\rho p}}{\frac{Wa}{\rho p}+\frac{(wb-Wa)}{\rho w}} x100 \quad (2)$$

2.2 Sorption tests

The effect of initial Hg (II) concentration (1 - 350 mg L^{-1}), contact time (0.16 - 24 h), sorbent mass (0.01 - 1 g) and solution pH (2 - 11) on the sorption efficiency and capacity of PKSB and CSB were investigated. Pseudo first and second order, and Elovich models were used to describe the experimental kinetic data. Langmuir, Freundlich, and Temkin isotherm models were applied for Hg sorption data analysis at pH 6. Sorption of Hg(II) by sulfurated biochars (SPKSB and SCSB) is an ongoing kinetic test at 1 mg/L and pH 6. Moreover, the efficiency of the polymer beads (PSF), pristine biochar beads (PSFP and PSFC,) and sulfurated biochar beads (PSFSP and PSFSC) were also tested for Hg removal at 1 mg/L for 24 hours.

3. Results and Discussion

3.1 Characteristics of biochar and beads

Both biochars (PKSB and CSB) showed high surface area (S_{BET}), which could effectively contribute to their sorption capacity (Table 1).

Table 1. Characteristics of PKSB and CSB

Biochars	C	H	N	S
PKSB (%)	86.1	2.1	1.4	0.1
CSB (%)	90.9	2.4	1.1	0.2
	MC	VM	FC	ASH
PKSB (%)	0.1	47.8	48.54	3.59
CSB (%)	0.1	34.1	65.41	1.36
	S_{BET}	V_T	V_m	D_p
PKSB	312.2	0.14	0.03	4.79
CSB	372.1	0.17	0.02	5.11

*[S_{BET} = m^2/g; V_t, V_m = cm^3/g; D_p = nm; MC= Moisture content VM= Volatile matter FC= Fixed carbon ASH = Ash]

The pH and pH_{pzc} of PKSB was 8.45 and 6.99, respectively, while that of CSB was 9.47 and 7.15, respectively. The $pH_{biochars}$ >pH_{pzc} which indicates that the surfaces of the biochar are all negatively charged and Hg(II) removal is by electrostatic attraction, possibly with phenolic hydroxyl (-OH) and lactone groups (-C=C-, -C=O-) on the biochar surfaces [3]. The EC was

0.07 and 0.24 mS/cm for PKSB and CSB respectively. Large pores were observed on the biochar beads which is due to rapid formation of a skin layer during the liquid-liquid phase separation which results in formation of many pores in the beads [4]. Shown in figure 1.

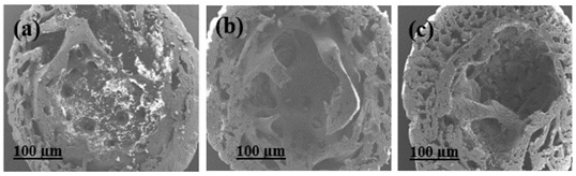


Fig. 1. Cross-sectional SEM images of PSF (a), PSFC (b), and PSFP (c).

3.2 Removal of Hg(II) from solution

Figure 2 presents the sorption data Hg(II) removal by SPKSB and SCSB. The sorption capacity improved from ~0.75 mg/g at 1 and 12 hr (when pristine biochars were used) to ~1.5 mg/g and ~1.9 mg/g at 1 and 12 hr respectively This can be attributed to the high affinity mercury has for sulfur on the biochar surface.

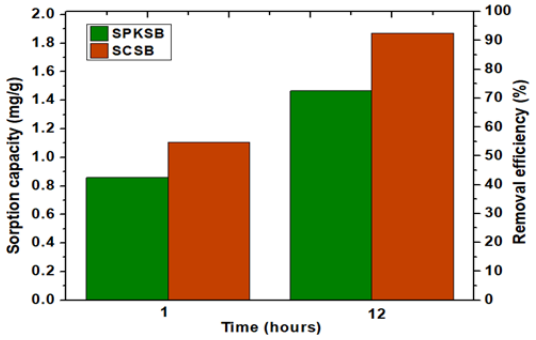


Fig. 2. Hg(II) sorption by sulfurated biochars (SPKSB and SCSB).

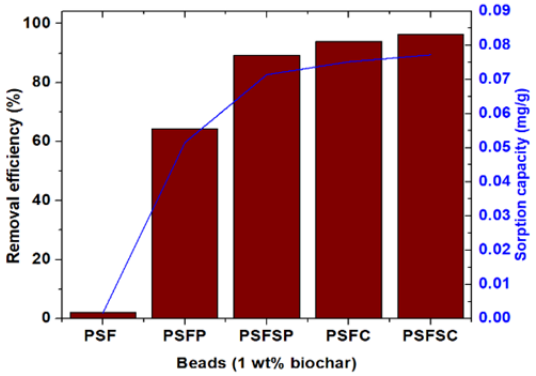


Fig. 3. Hg(II) sorption by beads of polymer, pristine, and sulfurated biochars.

The beads produced had a diameter of ~3.3mm and average porosity of ~ 80.5 %. PSF bead was not able to efficiently remove Hg(II) from solution as compared to the PSFP and PSFC. PSFSP and PSFSC had the highest Hg(II) removal efficiency evidently due to the increased sulfur content. The sorption efficiency was rather low which could be due to the wt% of biochar used in preparing the beads (1 wt %), thus an increase in wt% will give a higher sorption capacity of the polymer-biochar beads.

4. Conclusion

Biochars were produced from palm kernel and coconut shells from Ghana. Sorption of Hg (II) by sulfurated biochars was tested at different time intervals to evaluate the effect of contact time on removal efficiency of the biochars. Results show that sulfur-functionalized biochars and beads were effective in Hg(II) removal from solution. Removal mechanism of Hg(II) onto the surface functional groups of the PKSB and CSB will also be studied using X-ray absorption and photoelectron spectroscopy (XAS & XPS) on batch test samples. This result demonstrates that the biochars have a potential for treatment of aqueous streams affected by Hg(II) from medium or low level radioactive and mixed (radioactive and hazardous) wastes.

Acknowledgement

This research was supported by the BK+21 program to DANE/POSTECH through the National Research Foundation of Korea (NRF).

References

[1] Soelberg N., Enneking J., "Carbon bed mercury emissions control for mixed waste treatment." Journal of the Air & Waste Management Association, pp. 1341-1352, (2010).

[2] Wilmarth W., "Studies of mercury in high level waste systems.", Savannah River Site (United States). Funding organisation: US Department of Energy (United States); (2004).

[3] Guo X, Li M, Liu A, Jiang M, Niu X, Liu X., "Adsorption mechanisms and characteristics of Hg^{2+} removal by different fractions of biochar.", Water, pp 2105, (2020).

[4] Zhao, S., Wang, Z., Wei, X., Zhao, B., Wang, J., Yang, S. and Wang, S., "Performance improvement of polysulfone ultrafiltration membrane using PANiEB as both pore forming agent and hydrophilic modifier.", *Journal of Membrane Science*, *385*, pp.251-262, (2011).

The Process-Level Modeling and Simulation for the Underground Silo of LILW Disposal Facility

Myunggoo Kang*, Jaechul Ha, Tae-man Kim, and Chun-hyung Cho
Korea Radioactive Waste Agency, 174, Gajeong-ro, Yuseong-Gu, Daejeon, 34129, Korea
*kkang09@korad.or.kr

1. Introduction

Disposal facilities for radioactive waste are designed to provide long-term isolation from the human environment by means of a system of both natural and engineered barriers. In any optimization procedure the individual doses, as well as the corresponding risks, must be evaluated. Hence, it is essential to assess the performance of the waste disposal system quantitatively through safety assessment models. Depending on the method or depth of considering various complex phenomena affecting nuclide transfer, safety assessment model can be classified into system-level and process-level.

Traditionally, the system-level model that has been used in the safety assessment of the disposal facility is a method of simplifying and applying complex phenomena occurring in the disposal system to several constants and focusing on the final dose calculation. However, as the model is simplified, this approach has many limitations in considering the evolutionary characteristics of the disposal system over time.

In this regard, we focus on the development of the process-level model for the underground silo of Wolseong low and immediate level waste (LILW) disposal facility in Korea. The modeling and simulations were performed by using COMSOL Multiphysics based on a finite element computer code.

2. Numerical modeling and material proper

2.1 Code and model

In the present study, the nuclide transfer analysis of the waste disposal was carried out using the Subsurface Flow Module and Transport of Diluted Species Module of COMSOL Multiphysics ver. 5.5. The following Darcy's law, which is applicable for an saturated flow in porous media, is used in the Subsurface Flow Module:

$$\frac{\partial}{\partial t}(\rho\varepsilon_p) + \nabla\cdot(\rho u) = Q_m \qquad (1)$$

$$u = -\frac{\kappa}{\mu}(\nabla p + \rho g) \qquad (2)$$

where ρ is the fluid density, ε_p is the porosity, Q_m is a mass source term, u is the Darcy's velocity or specific discharge vector, κ is the permeability of the porous medium, μ is the fluid's dynamic viscosity, p is the pore pressure, g is the vector of gravitational acceleration.

In the Transport of Diluted Species Module in Porous Media, the following governing equation (3), which is applicable to calculate the species concentration and transport in porous media, is used:

$$\frac{\partial}{\partial t}(\varepsilon_p c_i) + \frac{\partial}{\partial t}(\rho c_{P,i}) + u\cdot\nabla c_i = \nabla\cdot\left[(D_{D,i} + D_{e,i})\nabla c_i\right] \qquad (3)$$

where ε_p denotes the porosity, c_i is the concentration of the species, ρ is the fluid density, $c_{P,i}$ is the amount adsorbed to solid particles, $D_{D,i}$ denotes the dispersion tensor of the species, $D_{e,i}$ denotes the effective diffusion of the species, u is the Darcy's velocity or specific discharge vector.

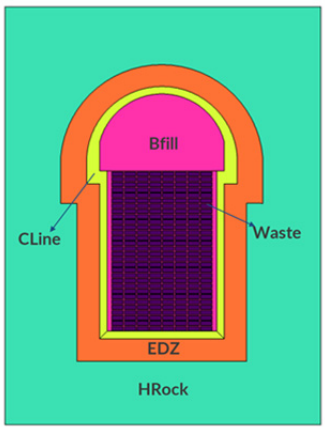


Fig. 1. The model geometry of the waste disposal facility.

The model geometry for the simulation is based on the underground silo #1 layout of Wolseong LILW disposal facility in Korea, shown at Fig. 1. The model geometry consists of the waste, the backfill (Bfill), the concrete line (CLine), the excavation damaged zone (EDZ) and the host rock (HRock).

2.2 Material properties

The material properties of each component are based on Safety Assessment Report (SAR) of 1 stage.

3. Simulation and discussion

All domains were initially saturated condition. Hydraulic boundary conditions were assumed as follows:

- No flux boundary conditions were assigned at the top and bottom.
- Constant velocity was assigned at the left side.

Firstly, flow analysis was performed under static state condition. Next, the transfers of nuclides were conducted by applying the pre-calculated Darcy velocity during 1000 years. The decay of nuclide was not considered.

3.1 Groundwater flow

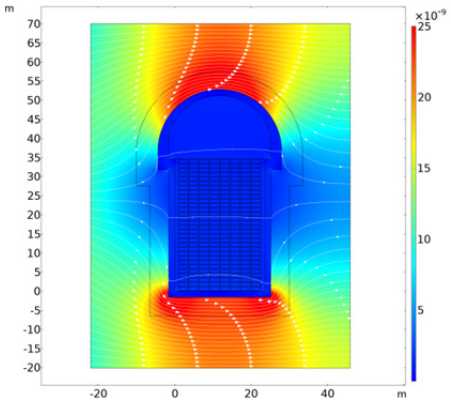


Fig. 2. Groundwater flow streamlines of the silo.

Fig. 2. shows the groundwater flow streamlines passing the underground silo of obtained from the static state case calculation. The calculated Darcy velocity was displayed by the color legend. Higher flow velocities are observed the up and down site of the silo than other region. The lower Darcy flux inside the silo results from the low permeability feature of the CLine.

3.2 Species release

After 1000 years, it was confirmed that the most of nuclides did not appear to be discharged from the silo. However, the nuclides with a low partition coefficient (such as H-3, C-14, I-129 and Tc-99) were released outside the disposal site as shown in Fig. 3.

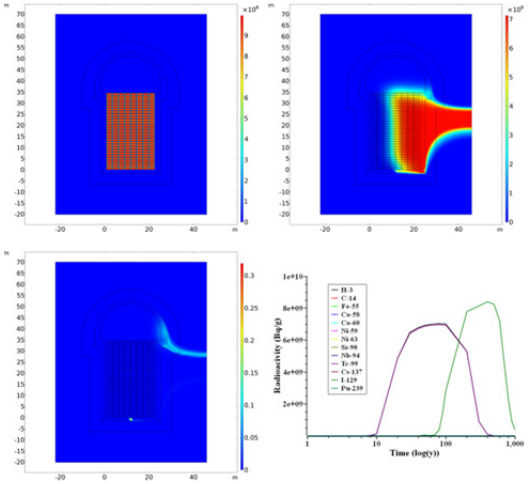


Fig. 3. The species release of the waste repository facility.

4. Conclusion

This study has developed the process-level models for near-field to describe radionuclide transport at the underground silo of Wolseong LILW disposal facility in Korea. In the case of nuclides with a low partition coefficient, leakage of nuclides dramatically appeared outside the silo. This result indicates that the adsorption is major mechanism of nuclide transfer under saturation condition. So, further study of the partition coefficient is needed to precisely characterize the migration of nuclides.

ACKNOWLEDGMENTS

This work was supported by the Korea Institute of Energy Technology Evaluation and Planning (KETEP Project No. 20193210100120) and the Ministry of Trade, Industry & Energy (MOTIE) of the Republic of Korea.

REFERENCES

[1] T. Kim, J. Jang, C. Cho, J. Kim, “Consideration of the need for the diversification on the source-term assessment model at the near-field of LILW disposal system”, Proc. of the KRS 2020 Spring Conference, 18(1), July 29-31, 2020, Online.

[2] J. Ha, T. Kim, C. Cho, “Examination and preliminary evaluation of radionuclide leakage model on waste disposal facilities”, Proc. of the KRS 2020 Spring Conference, 18(1), July 29-31, 2020, Online.

Review on the Plasma Arc Melting Technology Using Graphite Electrodes for the Treatment of Radioactive Mixed Wastes

Jae-Hyuk Choi*, Na-Young Kim, In-Sun Jang, and Kung-Hwa Yang
Dawonsys Co. Ltd, 485, Sihwahosu-ro, Danwon-gu, Ansan-si, Gyeonggi-do, Republic of Korea
*Jaehyuk1017@dawonsys.com

1. Introduction

Radioactive mixed waste is a waste that must be managed in consideration of both radioactive and non-radioactive components because it is both radioactive and hazardous. Therefore, it is necessary to develop a technology that the waste can be treated and disposed of in an environmentally and radioactively safe waste form. In the case of foreign countries, radioactive mixed wastes generated from nuclear facilities are wastes containing asbestos, organic pollutants such as PCBs(Poly Chlorinated Biphenyls), heavy metals, toxic chemicals, and so on. In Korea, it has not been investigated the amount and characteristics of radioactive mixed waste generated during NPP(Nuclear Power Plant) operation and decommissioning.

Technologies for treating radioactive waste depends on the type and characteristics of the waste and the purpose of treatment. In the case of very diverse types and characteristics, such as radioactive mixed waste, therefore, it is difficult to develop an optimum technology suitable for radioactive mixed waste.

Among various waste treatment technologies, plasma arc melting using graphite electrodes is assumed to be suitable for radioactive mixed waste. It operates at a high temperatures (about 2000℃) that can melt both metals and inorganic substances. It has high thermal efficiency than plasma torch melting and can reduce the dispersion of volatile heavy metals or harmful organic matters by melting waste in a stable condition.

This technology has been mainly studied in the United States. In particular, PNNL (Pacific Northwest National Laboratory), ALRC (Albany Research Center), and INEL (Idaho National Engineering Laboratory) under DOE (Department of Energy) developed facilities from laboratory scale to pilot scale using AC and DC arc methods. And they conducted experimental studies with various types of simulated radioactive wastes.

In this paper, we investigated plasma arc facilities developed by those organizations to refer to develop the technology for radioactive mixed waste generated in Korea.

2. Electrode Arc Melting Facility

2.1 facility type

There are two main types of electrode arc melting processes. The first is to use DC current and the second is to use AC current. Generally, AC facility with three electrodes is applied to non-conductive materials, with installed at the top. The construction cost of AC system is lower than DC system, but it has the disadvantage of high noise during operation than DC system. The DC facility has two electrodes and is applied to conductive materials. This system is difficult to repair and replace the furnace due to the electrode installed at the bottom of the furnace. Table 1 shows the characteristics of AC/DC arc facility.

Table 1. Comparison of Features by Plasma Arc Facility

No	Category	AC System	DC system
1	Main Waste	Non-conductive	Conductive
2	Number of Electrodes	3	2
3	Electrode Consumption	2~3kg/ton (Iron melting)	1~1.5kg/ton (Iron melting)
4	Facility Cost	Low	High
5	Maintenance Cost	Low	High
6	Operating Noise	High	Low (50~60% of AC)

2.2 DC Arc Engineering-Scale Facility

Fig. 1 shows a schematic diagram of a DC arc melting system with 100 kW capacity developed by PNNL. They tested with various types of wastes such as concrete, metal, soil, and combustibles. As shown in Fig.1, the DC arc melting system consists of a graphite electrode, melting hearth, two waste feeder, an off-gas outlet, and two drain lines for metal and slag. One 7.6cm diameter graphite electrode is installed on the top of the furnace, and a protective ceramic sleeve with a nitrogen purge function is installed around the electrode to reduce the corrosion of it. The lower part of the

furnace is made of a graphite material to act as an anode. In addition, an induction heating device is used to discharge the molten metal. By many pilot test, PNNL obtained a result that submerged electrode operation and cold-cap formation can reduce the evaporation of dust and volatile nuclides. In addition, they found that the graphite electrode and hearth were easily damaged by the moisture contained in the refractory.

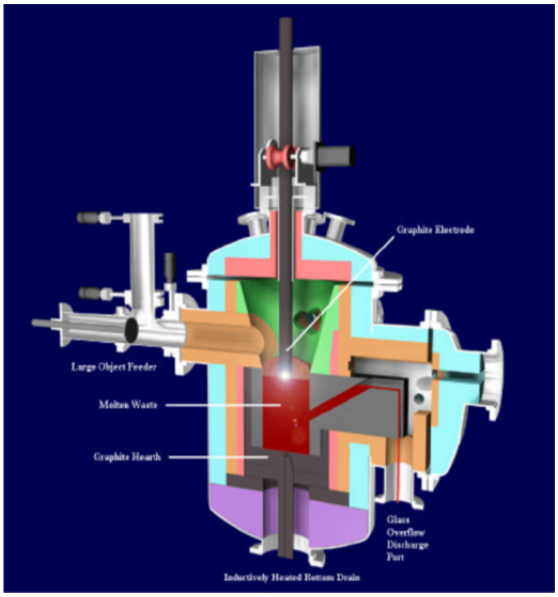


Fig. 1. A Schematic diagram of the 100kW DC Plasma Arc Melter by PNNL.

2.3 AC Arc Engineering-Scale

Fig. 2 shows a schematic diagram of the 800 kW engineering-scale AC arc melting facility manufactured by ALRC. This AC arc melting system is 140L of total capacity. It consists of three 10.2cm diameter graphite electrodes, a waste feeding system of 1ton/h, an off-gas outlet with a diameter of 20.3cm. Similar to PNNL facility, it also has two molten drain devices for metal and slag drain. The outside of the furnace is made of carbon steel and the inside is made of various refractory materials depending on the local temperature. INEL improved the facility of ALRC to conduct a test for TRU(Transuranic) contaminants. The phase 1 test was conducted to treat 5 types of TRU waste and the phase 2 test was for radioactive mixed wastes such as combustible solids, organic solvents, and metal hydroxide sludge. By years of tests, they evaluated and found the efficiency of the electrode arc melting technology.

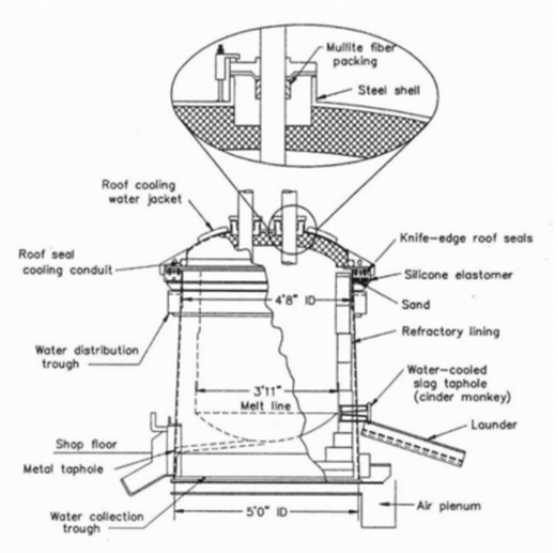


Fig. 2. A Schematic diagram of the 800kW AC Plasma Arc Melter by ALRC.

3. Conclusion

Plasma arc melting technology using a graphite electrode is considered to be useful and effective for treating radioactive mixed waste because it contains harmful heavy metals and environmentally hazardous substances.

In this paper, electrode arc melting facilities developed in the U.S were reviewed. As a large amount of radioactive mixed waste is expected to generate during NPP decontamination and dismantling, it is necessary to develop an optimum technology that can satisfy both the environmental and nuclear regulations in Korea.

ACKNOWLEDGMENTS

This works was supported by the Korea Institute of Energy Technology Evaluation and Planning (KETEP) and the Ministry of Trade, Industry & Energy(MOTIE) of the Republic of Korea (No. 20203210100050).

REFERENCES

[1] Alan D. Hartman, Laurnace L. Oden, Jack C. White, Facility for Melting Residues From Municipal Waste Combustion: Design Criteria and Description of Equipment, December, (1993).

[2] R. W. Goles, et al,. Engineering-Scale Arc Furnace Testing Summary, RL3-6-MW-51, September, (1998).

Reduction of Radioactive Concrete Waste Using Dense Medium Separation Technology

Seokju Hong, Sangsoo Han, Seongsik Nam, Won-Seok Kim, and Wooyong Um*
Division of Advanced Nuclear Engineering (DANE), Pohang University of Science and Technology (POSTECH), Pohang, South Korea, 37673
*wooyongum@postech.ac.kr

1. Introduction

In the process of Nuclear Power Plant (NPP) decommissioning, concrete waste is one of the problematic radioactive wastes because of its large volume and high quantities. Thus, radioactive concrete waste should be reduced in volume through the proper decontamination process. In general, the most representative process performed to reduce radioactive concrete waste is acid treatment. However, concrete waste has a very high pH, so it has to use more highly concentrated acid than other wastes to decontaminate. Thus, the conventional acid treatment process can cause the generation of large quantities of secondary wastes.

In this study, mining technology was applied, considering the characteristics of radioactive concrete waste generated in large quantities. Various technologies are used in the mine, such as comminution, sieving, classification, gravity separation, dense medium separation, magnetic separation, electric separation, flotation, etc. [1]. Among them, classification and dense medium separation were applied in this study, and only a small amount of acid was used to minimize the secondary waste solution.

2. Materials and Methods

2.1 Concrete preparation and thermal treatment

Concrete coupons were made with 9.25g of sand, 6g of aggregates, 5.25g of Portland cement (Type I/II), 3.25g of DI water, and 1.25g of fly ash. Cobalt nitrate hexahydrate ($Co(NO_3)_2 \cdot 6H_2O$) was used to contaminate the concrete coupons. A thermal treatment condition was optimized in our previous study like 550°C for 1hour.

2.2 Decontamination process

The decontamination process of radioactive concrete waste is shown in Figure 1. During the carbonation process, cement paste separated from concrete waste after thermal treatment was reacted with ejected CO_2 gas in DI water. This reaction produces $CaCO_3$ precipitates, which are very small in particle size. There are two ways to separate these.

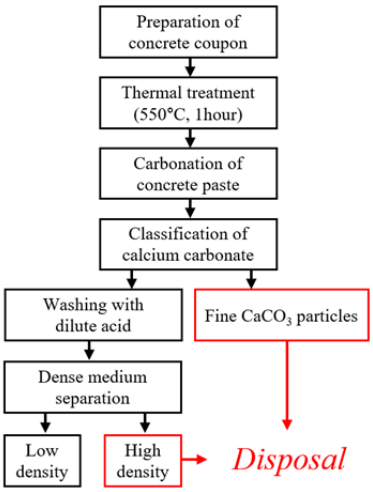


Fig.1. Flow chart of decontamination process.

$CaCO_3$ precipitates from the sand. One is sieving by size difference, and another is size classification by density difference. Both processes are well commercialized, inhere, classification was used to simplify the process. The principle of classification can be explained with Stokes law (Eq.1).

2.3 Stokes law – $CaCO_3$ classification

$$V = \frac{d^2(\rho_s - \rho_l)g}{18\eta} \quad (1)$$

Where V is the rate of settling (cm/s), η is the viscosity of the medium (g/cm·s), d is the diameter of the particle (cm), ρ_s is the density of the particle (g/mL), ρ_l is the density of the medium (g/mL), g is the gravitational constant (cm/s^2).

3. Results and Discussions

3.1 Classification

Hydrocyclone classification was conducted and carbonated paste was separated into two groups based on the settling time. According to the Stokes law (eq. 1), large size particles settle

down rapidly, and small size particles settle down slowly. Through the XRD data (Figure 2), we could identify that the fast settling particles were mainly quartz, and the slow settling particles were mainly calcite. Minor crystal phases, such as muscovite and albite were also found in both particle groups.

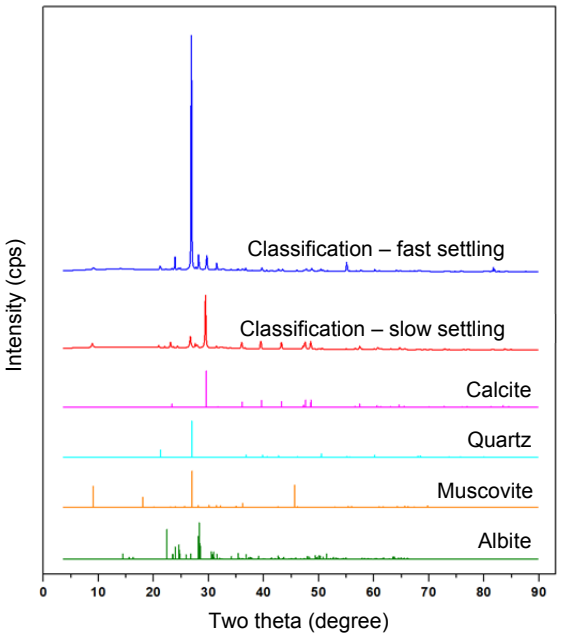


Fig. 2. XRD results of classification.

3.2 Dense medium separation

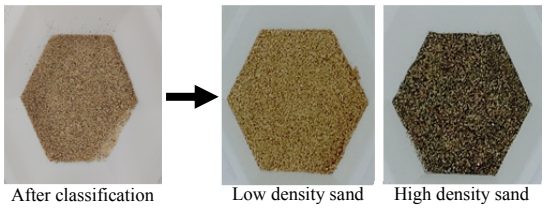


Fig. 3. Dense medium separation of sand.

After the classification, fast settling sand was separated with dense medium separation method. High density sand has a much darker color than low density sand as shown in Figure 3.

This color darkness is due to the mineral phase of edenite and hornblende that confirmed with XRD results (Figure 4). Both minerals have high density value, thus, they are clearly identified in the high density sand.

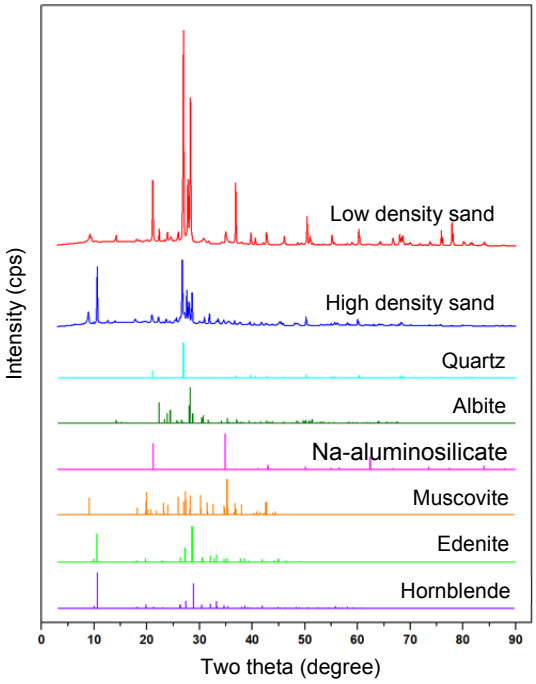


Fig. 4. XRD results of DMS separation.

4. Conclusion

To reduce the volume of radioactive concrete waste, we separated the concrete paste using mining technology. Further research and experiment about cobalt present in each separated material will be conducted.

Acknowledgement

This research was supported by Advanced Nuclear Environment Research Center (ANERC) from the National Research Foundation of Korea (NRF), NRF-2017M2B2B1072374 and NRF-2017M2B2B1072404.

References

[1] Physical Separation and Recovery of Metals from Wastes, 1993, T.J. Veasey, Wilson and D.M. Squires ed., Gordon and Breach Science Publishers.

Solubility of Tc-99 With Various Conditions in the Wolsung Repository Site, South Korea

Sohae Park, Sangsoo Han, and Wooyong Um*
Division of Advanced Nuclear Engineering (DANE), Pohang University of Science and Technology (POSTECH), Pohang, South Korea
*wooyongum@postech.ac.kr

1. Introduction

Technetium (^{99}Tc) is a β^- emitter with a long half-life ($t_{1/2} \sim 2.13 \cdot 10^5\ years$)and high yield formed fission product in nuclear reactors [1]. Due to the ^{99}Tc particular concerns such as the high mobility, long half-life, and human health, it is one of the most important radionuclides in the safety assessment of environmental radioactivity and repository of radioactive waste [2]. ^{99}Tc as a result of the disposal of radioactive wastes can be released into the environment over a long period from the repository. Generally, in environmental conditions, Tc primarily exists in two oxidation states Tc (IV) and Tc (VII). The predominant form of Tc under oxidizing conditions is the pertechnetate anion (TcO_4^-), which is highly soluble in water. On the other hand, Tc (IV) forms TcO_2 that has limited solubility under reducing conditions [2]. Thus, under various environmental conditions such as natural water composition, pH, Eh and etc., ^{99}Tc exhibits significantly different solubility behaviors that may influence the potential release and migration of ^{99}Tc from the repository. In this research, the solubility behaviors of ^{99}Tc were investigated under oxidizing and reducing conditions with seasonal waters (groundwater, seawater, and porewater) collected in the Wolsung repository site, South Korea.

2. Method

2.1 Material preparation and pretreatment

For approximation to realistic field conditions, pretreatment was conducted for each liquid and solid samples. According to the solution pH at equilibrium, four different types of pretreated solutions were prepared by reacting with natural solution samples (groundwater, seawater, rainwater) with core solid samples (rock, sea sediment, and concrete), respectively, collected from the second-stage of repository site in Wolsung, South Korea, during four seasons. The pH, electrical conductivity (EC), and dissolved oxygen (DO) were measured in the field by using electrometrically probes. After pretreatment, the total dissolved carbon was measured by total organic carbon analyzer (TOC). The major cations and anions in the collected solutions were analyzed by inductively coupled plasma optical emission spectroscopy (ICP-OES) and ion chromatography (IC), respectively.

2.2 Calculation of SLSP and modeling

Before starting the solubility experiments, Solubility Limiting Solid Phase (SLSP) and solubility modeling of ^{99}Tc under oxidizing and reducing conditions were conducted using Geochemist's workbench (GWB) with NEA-TDB and JAEA-TDB.

2.3 Solubility experiments

Technetium solubility experiments were conducted using enough amount of SLSP for ^{99}Tc; TcO_2 was prepared and reacted with 10mL ~ 30mL of pretreated solutions for two different redox environments (one is open to atmosphere for oxidizing condition, another is inside a glove box for reducing condition). The sampling was carried out for different reaction times (3h, 1d, 7d, 21d, 50d, 90d). The activities of collected samples were analyzed by using liquid scintillation counter (LSC).

3. Results & Discussion

Figure 1 shows Eh-pH diagrams for each solution collected in summer and winter seasons. In the case of groundwater, GW-1 and GW-2 under oxidizing condition, pH values were 7.97, 8.07, 7.98 and 8.09 and Eh values were 216.6, 186, 215.5, and 177 mV, respectively. Under the result of GWB calculating TcO_2 as SLSP of technetium, modeling of Tc solubility oxidizing condition was not limited for all samples regardless of seasons. Table 1 shows the solubility results under oxidizing condition.

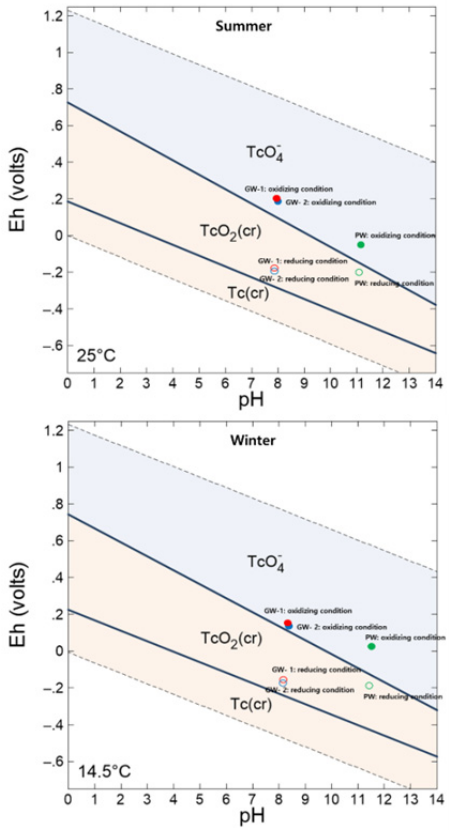


Fig.1. Eh-pH diagram for pretreated solutions under various conditions.

Table 1. Solubility values of Tc for summer and winter solutions under oxidizing condition

Samples/ season	*Summer (mol/ L)*	*Winter (mol/ L)*
GW-1	>1.64E-03	>1.44.E-03
GW-2	>1.51E-03	>1.57.E-03
SEA	>1.62E-03	>1.15E-03
PW	>1.34.E-03	>1.07E-03

In spite of different seasonal environment which is showing markedly different conditions, eg, major ion concentrations in pretreated solutions (Al varying from 10.98 to 0.65 mg/L and Li 4.96 to 7.49 mg/L), pH, Eh, and temperature throughout four seasons, the solubility of Tc showed similar values of around 1.64E-03 to 1.07E-03 M in an oxidizing environment of groundwater (GW), seawater (SEA), and pore water (PW) reacted rainwater with concrete. This result shows that the solubility behavior of Tc barely changed and most of Tc exists as TcO_4^- in solutions over a wide pH range. In other words, due to the week sorption properties of TcO_4^- in various environmental media, Tc is considered to be one of the most mobile radionuclides in the environment.

Table 2. Solubility values of Tc for summer and winter solutions under reducing condition

Sample/ season	*Summer (mol/ L)*	*Winter (mol/ L)*
GW-1	< 1.0 E-09	< 1.0 E-09
PW	< 0.5 E-10	< 0.9 E-10

Solubility experiment of Tc under reducing condition was also conducted and the results are listed in Table 2. The solubility of Tc showed similar values of around 1.0E-09 to 0.5E-10 M under reducing condition irrespective of solution types. Despite the different solution chemistries between summer and winter samples, Tc solubility data showed the same results. Comparing the data under oxidizing state, Tc barely dissolved in solutions under reducing condition, which means that Tc remains mostly solid form in reducing condition.

4. Conclusion

Despite the markedly different characteristics of seasonal solution samples, Tc solubility barely changed. On the other hand, depending on the redox potential, Tc showed significantly different solubility values. Under oxidation condition, Tc was very soluble among all the sample, while Tc showed very low solubility under reducing condition. These results can be used as a database for the safety assessment of a domestic repository site and a thermodynamic database for potential Tc transport while various conditions change.

REFERENCES

[1] T. Kobayashi, A.C. Scheinost, D. Fellhauer, X. Gaona, M. Altmaier, “Redox behavior of Tc (VII)/Tc (IV) under various reducing conditions in 0.1 M NaCl solutions”, RCA, 101, 323-332 (2013).

[2] A.H. Meena, Y. Arai, “Environmental geochemistry of technetium”, Environ Chem Lett, 15, 241-263 (2017).

Design Concept of the Automatic Fastening Device for the Lid of the High Integrity Container Applicable to Korea

Mi-Hyun Lee*, Young Hwan Hwang, and Ji-Hoon Lee
KHNP Central Research Institute, 70, Yuseong-daero 1312beon-gil, Yuseong-gu, Daejeon, Korea
*mihyun.lee@khnp.co.kr

1. Introduction

The safety and integrity suitable for regulatory requirements must be secured when handling and disposing of low and intermediate level radioactive waste generated in the nuclear industry. Among them, concentrate waste and spent resin that do not meet the disposal acceptance criteria must be solidified or disposed of using high integrity container (HIC). When handling a waste transport container with a surface dose exceeding 10 mSv, remote processing equipment that can work while maintaining a certain distance is required to protect workers. In addition, it is necessary to evaluate the adequacy of worker exposure reduction by automating container lid fastening after loading waste into HIC. Therefore, it is necessary to develop remote devices and operating procedures to reduce worker exposure when handling high dose spent resin. In this study, the design concept of a HIC remote lid fastening device applicable to Korea for the protection of workers was studied.

2. Configure and Conceptual diagram of automatic lid fastening device

2.1 Automatic lid fastener configuration

It consists of high integrity container automatic lid installation device, automatic lid installation device operation control panel, automatic lid installation device control line, essential tools for inspection, maintenance and self-calibration, etc.

2.2 Concept of automatic lid fastening device

Fig. 1 shows the conceptual diagram of the automatic lid fastener. It consists of 7 components, such as a drive motor, clutch and a lid rotating plate.

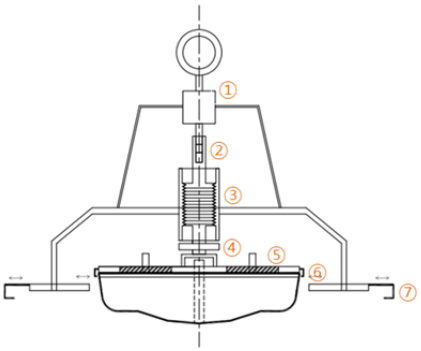


Fig. 1. Concept of automatic lid fastening device.

At the top of the automatic lid fastening device, a component that can handle the lid fastening device using an existing 10 ton crane should be installed. And if necessary, appropriate handles should be installed on the device and control panel so that the operator can transport and handle them.

① Drive motor

It provides the rotational force necessary for the installation and removal of the automatic lid fastening device, and the rotational speed is variable and has a rotational speed suitable for operation.

② Variable sleeve

③ A brunch of gears

It has the function of stably operating the rotating plate up and down by the internal screw being combined.

④ Clutch

It has a function of stably separating the lid rotating plate after locking the lid or separating the rotation of the rotating shaft for installing the rotating plate when removing the installed lid.

⑤ Lid rotating plate

It has the function of combining or separating the lid by the force of the steel plate and magnet on the top of the lid.

⑥ Lid tongs

It has the function of holding or releasing the lid according to the lid installation or removal step.

⑦ Container tongs

The tongs composed of a total 4 have the

function of stably fixing and supporting the automatic lid fastening device to the container.

3. Main Design Requirement

The automatic lid fastening device should be capable of automatic operation and manual or field operation. It also consists of a device, and operation control panel and a control line. It should be easy to move the nuclear power plant in the site and be suitable for the operation environment of the nuclear power plant, such as the movement route, installation place, crane and power supply. Operation control panels are properly spaced to reduce radiation exposure to workers. All diving of the automatic lid fastening device should use electric power, and the installation and removal of the top of the container should be performed by the operator using an existing crane. The lid installation process consists of preparing the device for installation, installing the lid, and removing the device, and it should not exceed 30 minutes to tighten the lid once.

Table 1. Lid installation process

Process	Time
Daily inspection and work preparation	5 minutes at a time
Device installation and condition check	10 minutes at a time
Lid installation and condition check	5 minutes at a time
Device removal and packaging	10 minutes at a time

4. Conclusion

In this study, the design concept and main design requirements of the HIC automatic lid fastening device were described in order to derive measures to reduce the exposure of workers, such as the development of remote treatment technology when handing high dose spent resin. It is necessary to develop a HIC remote lid fastening device applied in Korea by analyzing the technical standards for suitability of high integrity container according to the dose rate. In addition, it should be designed in consideration of the requirements of domestic and foreign regulatory agencies and the applicability of the site.

REFERENCES

[1] Jhon W. McConnell, Michael J. Tyacke, Richard C. Schmitt and Harley W. Reno, “Disposal demonstration of a high integrity container (HIC) containing an Epicor-II prefilter from three mile island”, (1985).
[2] “The drip-dry waste job”, nuclear engineering international, (2014).

A Study on Long-Term Stability of High Integrity Container

Young Hwan Hwang*, Mi-Hyun Lee, and Ji-Hoon Lee
Central Research Institute, Korea Hydro and Nuclear Power, 70, Yuseong-daero 1312 beon-gil, Yuseong-gu, Daejeon, Korea
*yhhwang7@khnp.co.kr

1. Introduction

Various types of radioactive wastes are generated during operation of nuclear power plant (NPP). The representative radioactive wastes are dry active waste (DAW), spent resin, boron concentrates, spent filters, etc. The DAWs are usually compacted in 200L drum and sent to disposal facility. Since the DAWs have been disposed in the disposal facility for many years, the data, satisfaction of waste acceptance criteria (WAC), pre-treatment, characterization, etc., are well established.

The WAC indicates that the homogeneous wastes, such as concentrates, spent resin, etc., should be solidified. It is also indicated that the solidified waste satisfies the following requirements.

- Compressive strength over 500 psig
- Radiation exposure stability
- Leaching index of Cs, Sr, Co over 6
- Compressive strength over 500 psig after flooding test
- Compressive strength over 500 psig after thermal stress

The technical standard for solidified form of cement, thermoset type resin, or glass is shown in Table 1. The periodic validation should perform every 4 years. And compressive test should perform every 10 batch or within 1 year.

Table 1. Technical standard for waste solidified form [1]

Category		Technical standard
Structural stability	Compressive strength	KS F2405
	Flooding test	NRC Technical Position on Waste Form Rev.1
	Radiation exposure test	
	Thermal stability	ASTM B553
Leaching property	Leaching index	ANS 16.1
Free standing water	Solidified form	ANS 55.1
	Sample and DAW	Pain Filter Liquid Test

Recently, high integrity container (HIC) attracts lot of attention for the disposal of spent resin and boron concentrates. The HIC is a waste package that sustains its stability over 300 year under Korean generic underground environment and disposal condition [2]. Since the waste packaged in HIC does not require solidified process or periodic validation, the treatment process become simple and economical. In Korea NPP, three types of HIC have been applied, ferralium (FE) HIC, polyethylene (PE) HIC, and polymer concrete (PC) HIC. The figure of polyethylene (PE) HIC is shown in Fig. 1. The spent resin is sent to the PE HIC and stored in many NPPs. However, the PE HIC is not acceptable in disposal facility in this moment. The KHNP has been developing PC HIC for the disposal of spent resin and concentrates.

In this paper, the long-term stability evaluation method for HIC is studied.



Fig. 1. Polymer concrete HIC [3].

2. Long Term Stability Evaluation

Since the HIC is a package that sustains over 300 years, the evaluation of long-term stability is important. Its long-term stability is categorized into mechanical, chemical, and radiation stability, when considering Korean generic underground disposal environment. The commercial PC HIC is shown in Fig. 2.



Fig. 2. Commercial PC HIC [3].

2.1 Mechanical Stability

The fundamental object of HIC is a packaging of radioactive waste. It is generally understood that the HIC would be exposed to external loading after disposal. It is important to evaluate the mechanical stability from external force. The representative test methods are KS F2405 or ASTM C39. The creep test, shown in Fig. 3., is also a good method to evaluate its property. The creep test with specific loading gives a significant information about the primary material of HIC.



Fig. 3. Creep test (example) [3].

2.2 Chemical Stability

The HIC is exposed to chemical reaction in the disposal facility. The expected chemical species are EDTA, citric acid, acid materials, and base materials. Since the WAC strictly restricts the concentration of such chemicals and water dilutes the chemicals, the expected concentration of them are relatively low. However, it is important to understand the short and long term stability from the chemical reactions to prevent the unexpected defect of the composition material.

2.3 Radiation Stability

It is expected that the HIC is exposed to alpha, beta, and gamma radiation. The HIC contains various resins from CVCS, LRS, SG blowdown, etc. The primary nuclides that affects the material stability are ^{60}Co and ^{137}Cs. The spent resins stored in high activity are classified as intermediate or low level waste. The expected radiation exposure and effect will be discussed in the paper.

3. Conclusion

In this paper, the method and related technical standards are studied. The expected important long-term stability factors are mechanical, chemical, and radiation stability. Since the HIC is defined as a package that sustains its stability over 300 years, the evaluation of the long-term stability is important. This paper describes the method of the evaluation program and its expected results.

REFERENCES

[1] FSAR Chap. 8.3, KORAD Disposal facility.

[2] “Regulation guide for high integrity container for disposal of ILW, VLW, and VLLW” KINS/RR-681(2009).

[3] “Stability analysis report of polymer concrete high integrity container” submitted.

Status of Radioactive Mixed Waste Treatment Technology

In Sun Jang*, Na Young Kim, Jae Hyuk Choi, and Kyung Hwa Yang
DAWONSYS Co., Ltd., 485, Sihwahosu-ro, Danwon-gu, Ansan-si, Gyeonggi-do, Republic of Korea
*isjang@dawonsys.com

1. Introduction

According to the radioactive waste disposal regulations, a waste with explosive, flammable, hazardous, infectious component is not allowed to the disposal facility and shall be treated to remove its hazardous characteristics. RMW (Radioactive mixed waste) refers to the wastes that both radioactive and hazardous. This waste includes many types and kinds of waste; solid or liquid, organic or inorganics, bulk or trace of amount.

Over the years, many countries have tried to find an optimum treatment technology suitable for their RMW. They investigated the waste streams, analyzed the characteristics, performed an optional study for various treatment technologies, and develop a waste treatment process and technology.

In Korea, many amounts of RMW will be expected to generate during decommissioning of NPPs (Nuclear Power Plants) in the near future. In this regard, the reviewing on the overseas status of technology will be the first step to develop the suitable treatment process in Korea.

2. Radioactive mixed waste treatment technology

2.1 U.S.

In the case of foreign countries, RMW generated from nuclear facilities includes asbestos such as building structures and insulators, PCBs (Poly Chlorinated Biphenyls)-painted or coated concretes or metals, heavy metal containing wastes such as electrical parts and sludge, and chemicals like acid, base, spent decontamination liquid.

In the U.S., RMW generated from nuclear facilities is managed separately from general radioactive waste. Also, due to its radioactive and hazardous properties, RMW is regulated by both EPA (Environmental Protection Agency) and NRC (Nuclear Regulatory Commission). Figure 1 shows the comparison of waste management regulation in Korea and U.S.

Noting that RMW could have a great effect in time and cost of a waste management project, the U.S. has carried out researches on the characteristics of RMW and evaluated various treatment technologies. As shown in Figure 2, waste handling process was developed to categorize and separate RMW from radioactive waste [1].

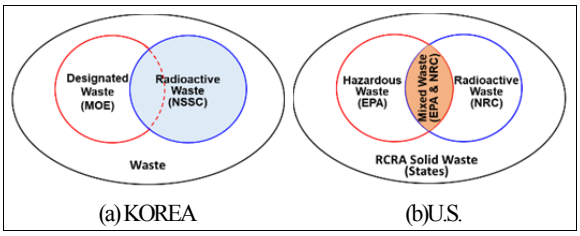


Fig. 1. Comparison of waste management regulation in Korea and U.S.

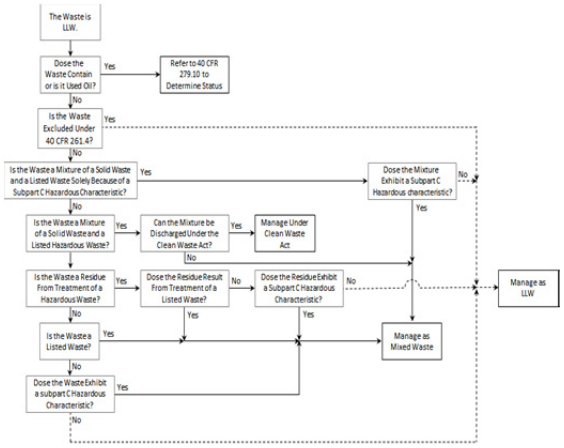


Fig. 2. US radioactive waste classification process.

DOE (Department of Energy) and EPA signed an agreement (Hanford Federal Facility Agreement and Concent Order) to improve and comply with the disposal requirements for RMW stored on the Hanford site. Through this study, a characteristic analysis and treatment technology for the RMW was selected in to dispose the waste in accordance with the disposal requirements. In other to select the optimal technology, following factors were considered: 'reducing the amount of harmful substances', 'reducing the amount of waste', 'reducing management costs', 'complying with regulatory requirements', 'reducing health risks', 'increasing treatment efficiency', 'reducing accident risk', and 'Increase resident acceptance'. As a result of this evaluation, heat treatment (vitrification, incineration) was selected for the most of the mixed waste, and the concept of the RMW treatment process was established [2].

2.2 UK

The UK estimates that decommission of NPPs will generate tens of thousands tons of asbestos waste over the next 20 years [3].

Asbestos waste was evaluated to be a difficult problem for the NPPs decommissioning project because it has a greater amount of generation than other RMWs, and has a large impact on environment and disposal costs.

Accordingly, the Low Level Waste Repository conducted an in-depth feasibility study to find an technology applicable to radioactive asbestos wastes. In this study, technical maturity, commercialization potential, investment costs, risks, health safety, and environmental impact were analyzed in detail. Finally, the melt-solidification technology by plasma arc or joule heating was evaluated as the most suitable one.

2.3 Korea

RMW cannot be disposed of due to the harmfulness according to the nuclear regulations and also it is excluded from the environmental regulations due to its radioactivity. The effective way to solve this problem is removing the harmfulness in the RMW.

Environmental regulations on the non-radioactive waste specifies the high-temperature melting as an appropriate treatment method for hazardous wastes containing asbestos and PCBs. And other hazardous organic substances are also recommended to be treated by high temperature.

There have been various studies on the heat treatment technologies, but studies for the treatment and disposal of RMW have not been conducted much.

KAERI (Korea atomic energy research institute) conducted research on treating halogen-containing plastics (PVC, PTFE), ion exchange resins, organic solvents (CCl_4, Chlorobenzen, etc.), and PCBs containing oils using a MSO (molten salt oxidation) technology [4].

Hazardous components such as halogen substances and heavy metals contact with alkali molten salts in a bubble state and immediately react with them and removed from the waste. When the waste is heat-treated in a melter or a reactor, various environmental pollutants such as dust, unburned substances, volatile radionuclides, heavy metals, acid gases, and dioxins could be generated as exhaust gases. By passing through the MSO, the exhaust gas can be purified to meet the environmental effluent limits. It was evaluated that the efficiency of hazardous gas removal was much higher than general off gas treatment equipment.

3. Conclusion

RMW treatment technology has not yet been established in Korea. In overseas, heat treatment method was evaluated as the most suitable option for the RMW. Also, the performance and efficiency of the MSO technology was demonstrated in a pilot scale facility.

Reflecting to the technology review results, we plans to develop the RMW treatment process by combining the plasma arc and MSO technology. Through this research, the RMW generated from NPP decommissioning could be safely and economically treated following to the present environmental and nuclear regulations.

ACKNOWLEDGMENTS

This works was supported by the Korea Institute of Energy Technology Evaluation and Planning (KETEP) and the Ministry of Trade, Industry & Energy(MOTIE) of the Republic of Korea (No. 20203210100050).

REFERENCES

[1] C. Hornibrook, et al,. Mixed Waste Management Guidelines, EPRI TR-103344, 1993.
[2] D. G .Black, et al,. 1996 Hanford Site Report on Land Disposal Restrictions to Mixed Waste, DOE/RL-96-08, US DOE, April 1996.
[3] ED. Ghosn, National Waste Programme: LAW Asbestos and Asbestos Containing Waste Gate B (Preferred Options) Study, LLW Repository Ltd., March 2016.
[4] H. C. Yang, et al., Destruction of chlorinated organic solvents in a two-stage molten salt oxidation reactor system, Chemical Engineering Science, Volume 62, Issues 18–20, September –October 2007.

Comparison of Laws and Regulations on Mixed Waste Between the USA and Korea

Eun-Jin Sim*, Sun-Kee Lee, and Chang-Lak Kim
KEPCO International Nuclear Graduate School, 658-91 Haemaji-ro, Seosaeng-myeon, Ulju-gun, Ulsan, Republic of Korea
*dangns83@gmail.com

1. Introduction

Kori Nuclear Power Plant Unit 1, which was permanently shut down in 2017, is preparing decommissioning the NPP. A large amount of waste is expected to be generated when the NPP is decommissioned, and in particular, low-level radioactive waste is expected to be 60% of the total waste. Among these, mixed waste is also included. Since mixed waste contains both radioactive and hazardous properties, there are many considerations for disposal. However there are no clear guidelines for mixed waste in Korea. Accordingly, this report was intended to derive methods applicable to Korea by reviewing the relevant laws and regulations of the United States, which have extensive experience in the decommissioning NPPs and is strictly managed mixed waste.

2. Status of Laws and Regulations related to Mixed Waste in the USA

2.1 General

The U.S. Nuclear Regulatory Commission (NRC) and the U.S. Department of Energy (DOE) regulates the radioactive component of mixed waste under the Atomic Energy Act (AEA). The AEA delegates the control of nuclear energy mainly to DOE, NRC, and the Environmental Protection Agency (EPA).[1]While the EPA regulates the hazardous component of mixed waste under the Resource Conservation and Recovery Act (RCRA). Therefore, mixed waste must follow both AEA and RCRA requirements.

2.2 EPA Regulations

Under the RCRA, the EPA has defined a hazardous waste. It also has developed disposal criteria that must be met before land disposal. In addition, the EPA provides standards for the construction and operation of hazardous waste treatment facilities [2].

2.3 NRC Regulations

The NRC has the authority to license and regulate the civil use of “by-products, sources and special nuclear materials” under the AEA. It also has the authorized to ensure public health and safety, common defense and security, and adequate protection for the environment when using nuclear materials in the USA [3].

2.4 DOE Regulations

The DOE has Authority under the AEA for radionuclides, but non-radioactive hazardous substances are regulated by EPA or RCRA [1]. DOE has developed Site Treatment Plans to handle its mixed wastes under the review of EPA.

3. Status of Laws and Regulations related to Mixed Waste in Korea

Generally, hazardous waste is subject to waste the regulations of the Ministry of Environment (MOE) in Korea. However, the Environmental Laws and regulations do not be applicable to radioactive waste and contaminated materials by radioactivity pursuant to the Nuclear Safety Act.

Therefore, radioactive waste is managed under the guidelines of the Nuclear Safety & Security Commission (NSSC). However, there are only comprehensive regulations related to the radioactive waste. In other words, relevant laws and regulations do not provided clear guidelines for hazardous substances. There are currently no regulations for mixed waste.

4. Comparison of Laws and Regulations

4.1 Regulatory Authority

Fig.1 compares the regulatory authority of mixed waste in the USA and Korea.



Fig. 1. Comparison of mixed waste regulation framework.

4.2 Laws and Regulations

The Table 1 and Table 2 is compared laws and regulations on mixed waste between the USA

and Korea. The USA has “strict” environmental regulations with the EPA's authority on hazardous waste. However, the MOE in Korea does not regulate radioactive materials.

Table 1. Comparison of environmental regulations

USA(40CFR Part ~)[2]	Korea
Overview and definitions(60)	Radioactive materials are supposed to follow the rules of the NSSC under Nuclear Safety Act[4]
Identification and listing of hazardous waste(261)	
Generators of hazardous waste(262)	
Transporters of hazardous waste(263)	
Standards for hazardous waste management facilities(264~266 and 267)	
Permit requirements for hazardous waste management facilities(270 and 124)	
Land Disposal Restrictions (268) All waste must be approved to EPA.	
Administered Permit Programs(270)	
Toxicity Substance Control Act (700~799); PCBs (761), Asbestos(763) Presenting the Test Method 1311	
Environmental Radiation Protection Standards; SNF,HLW,TRU Waste(191)	
National emission Standards for hazardous air pollutants(63)	

In the USA, the NRC and DOE are regulated on “hazardous waste” under the RCRA. The nuclear laws and regulations in Korea do not provide clear guidelines on hazardous waste.

Table 2. Comparison of nuclear regulations

USA(10CFR Part ~)[3]	Korea
Licensing requirements of radioactive waste (61)	Comprehensive standards for radioactive waste are provided
Radiation Protection Standard(20)	
Alternative disposal (20.2002) Disposal of VLLW under RCRA	
Byproduct Material (962) Nonradioactive hazardous component will be regulated RCRA	N/A

4.3 Proposal of Applicability in Korea

The Fig.2 provides a more stringent regulation plan of mixed waste that threatens human health and the environment by benchmarking the USA. case. Unlike existing treatment method, when hazardous components are identified among the deregulated ILW, LLW, VLLW, the generator must immediately notify the Ministry of Environment (MOE) and follow the regulatory guidelines of the MOE. The MOE needs to present specific treatment standards for the removal of hazardous substances. In addition, the generator must treat the waste after receiving approval from the MOE that the hazardous components have been removed after neutralizing according to the guidelines of the MOE. At this time, it will be necessary to secure appropriate neutralization technology.

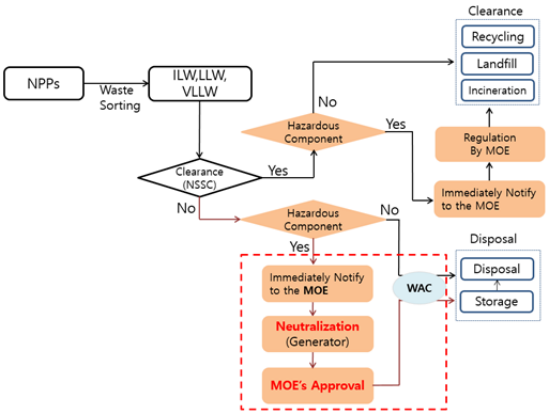


Fig. 2. Proposal of treatment option for mixed waste.

5. Conclusion

In Korea, radioactive mixed waste cannot be disposed of in radioactive waste repository due to its hazardous, and environmental regulations exclude radioactive waste from regulation. Therefore, strict management of domestic mixed waste which is expected to be generated in the near future is required by benchmarking the U.S. case. In order to treat mixed waste, a procedure approved by MOE must be established.

In order to treat mixed waste with Fig.2, it is necessary to prepare clear guidelines on the identification form of the mixed waste, treatment and disposal. In addition, it is necessary to prepare clear waste acceptance criteria for treating and disposing of mixed waste. Furthermore, securing technology capable of treating mixed waste should be given priority.

ACKNOWLEDGEMENT

This work was supported by the Korea Institute of Energy Technology Evaluation and Planning (KETEP Project No. 20193210100120) and the Ministry of Trade, Industry & Energy (MOTIE) of the Republic of Korea.

REFERENCES

[1] Atomic Energy Act, USA, (1954).
[2] The US EPA Regulations Title 40, Chapter I.
[3] The US NRC Regulations Title 10, Chapter I.
[4] Waste management Act, Korea, No.16614.

A Case Study on the Radionuclide Fraction in Activated Concrete for Abroad Decommissioning NPPs

Yu-hwa Son*, Tae-man Kim, and Chun-hyung Cho
Korea Radioactive Waste Agency, 174, Gajeong-ro, Yuseong-Gu, Daejeon, 34129, Korea
*slowstrider@korad.or.kr

1. Introduction

Kori 1, the first nuclear power plant in Korea, was permanently suspended after 39 years worktime due to comprehensive reasons such as economic feasibility, acceptance, and fostering of the decommissioning industry. Kori Unit 1 is expected to be decommissioned immediately, and the decommissioning operator KHNP is expected to prepare the decommissioning plan approving by 06.2022. The decommissioning plan should contain the site characteristic including evaluation of the nuclide inventory about the decommissioned radioactive waste [1].

Focusing only activated concrete which is difficult to process and reduce such as bio-shield, the fraction of radioactive concrete nuclides was analyzed in overseas NPPs decommissioning cases.

2. Radioactive concrete nuclide fraction and measurement method by abroad decommissioned NPPs

2.1 U.S [2]

(1) Maine Yankee [3]

Main Yankee analyzed the radionuclide fraction in two activated concrete core samples in 1/1/2004. The table-1 shows only the nuclides that were determined to be measured constituted the fraction. Nuclides that cannot be measured performed on the MDC, it was confirmed that the contribution to the annual dose rate was less than 10%. Comparing with NUREG/CR-3474, nuclides that were not measured were ignored. The main nuclides in Maine Yankee NPP are Fe-55, Eu-152, and Co-60, and they accounted for 12.4%, 11.1%, and 4.0%, respectively. Fe-55 seems to be the effect of reinforcement impurities.

(2) Connecticut Yankee (Haddam Neck)

Connecticut Yankee analyzed core samples from concrete under the Neutron Shield Tank where the Containment In-Core (CIC) Sump is located. The length of the core sample was 51 cm (20 inches), and the highest radioactivity was always measured at the top 1.5 inches. The major nuclides of Connecticut Yankee NPP are Fe-55, Eu-152, and Co-60, which are 12.0%, 16.9% and 13.0%, respectively.

(3) Yankee Rowe [4]

Yankee Rowe analyzed cores samples varying depths between 3 inches and 10.6 inches at two locations in RVC and STC, and one at the highest radiation exposure rate. Several more core samples were collected from the existing core area after the initial analysis. Core samples were analyzed by slicing them into wafers approximately 0.2 inches (0.5 cm) thick. The major nuclides of Yankee Rowe NPP are Cs-137 and Co-60, and they accounted for 87.8% and 7.4% respectively. In Yankee Rowe, Cs-137 was a principal nuclide.

(4) Rancho Seco

Rancho Seco analyzed 6 core samples at different elevations and locations within bio-shield area. The result of the reactor core level of the double vessel is the analysis result of the core sample extracted from the altitude east of the -2'5" Bio-shield. It is characterized that Eu nuclides (Eu-152, Eu-154, Eu-155) were found only in Reactor Bio-shield. The major nuclides of Rancho Seco are Eu-152 and Co-60, and they accounted for 27.6% and 10.1%, respectively.

(5) Zion 1&2 [5]

Zion 1&2 analyzed a series of concrete core samples extracted from the 568-foot concrete floor, 541-foot in-core tunnel floor, and in-core tunnel wall of two isolated buildings. And a sample of a single concrete core was taken from the centerline of the reactor in Unit 1 Bio-Shield. A total of 39 concrete core samples were analyzed, 20 from Unit 1 containment chamber and 19 from Unit 2 containment chamber. The location most likely to present the worst boundary radiation conditions was to select as many as possible. The main nuclides of Zion1&2 are Cs-137,Co-60, and Ni-63, 79.4% respectively, and they accounted for 7.1% and 5.0%. Like Yankee Rowe, Zion case had a high Cs-137 and Ni-63 value.

2.2 Sweden

(1) Forsmark [6]

The radioactivity contribution of nuclide through the bio-shield follows drill samples taken from Barsebäck 1 and 2. Nuclide inventory is calculated

for three Forsmark reactors F1, F2, F3. The major nuclides of Forsmark are Fe-55, Eu-152, and Co-60, and they accounted for 9.5%, 5.9%, and 2.4%, respectively.

(2) Oskarsham [7]

SKB analyzed the nuclide inventory of each Oskarshamn power plant (O1, O2, O3), and the arithmetic averaged results was shown in table-1. The radioactivity distribution of bio-shield are shown in the table, and the data presented are based on calculations adjusted with empirical data. The major nuclides of Oskarsham are Fe-55, Eu-152, and Co-60, and they accounted for 7.6%, 5.6%, and 2.9%, respectively. In the case of Swedish NPP, Fe-55 tended to be high.

3. Conclusion

The LILW and ILW radioactive waste disposal facility is being managed by KORAD in Gyeongju, and the radioactive waste generated from the Kori NPP Unit 1 decommissioning will also be taken and disposed to this disposal site within near future.

Information on the radioactive nuclides inventory of decommissioned NPP's radioactive waste can be used as source term prediction for ensuring the safety of the disposal facility. Radioactive nuclides analysis of NPP's decommissioning waste are being obtained through sampling and actual measurement. On average, it was confirmed that two key nuclides Eu-152 and Co-60 accounted for 9.7% and 6.7% respectively.

Through foreign decommissioned cases, it was confirmed that radioactive waste generated from decommissioning NPPs has a various nuclides distribution according to the construction and operation history. Therefore, for the safe decommissioning of Kori 1 and other NPPs facing permanent suspension, it is believed that accurate production of nuclide distribution data should be performed.

Table 1. Nuclide fraction of activated concrete for decommissioned & decommissioning NPPs abroad

		Maine Yankee	Yankee Rowe (Reactor vessel cavaty)	Conneticut Yankee	Rancho Seco	Zion 1&2	Fosmark (average)	Oskasham (average)
	Nuclide	Fraction	Fraction	Fraction	Fraction	Fraction	Fraction	Fraction
1	H-3	6.47E-01		5.51E-01	5.33E-01	8.35E-04	8.09E-01	8.31E-01
2	C-14	5.80E-02		2.80E-04	8.51E-04	8.69E-05	1.98E-04	2.79E-04
3	Fe-55	1.24E-01		1.20E-01	6.26E-02		9.46E-02	7.59E-02
6	Co-60	4.00E-02	7.04E-02	1.30E-01	1.01E-01	7.13E-02	2.92E-02	2.43E-02
7	Ni-63	7.00E-03		6.25E-04	2.01E-02	5.03E-02	1.60E-04	2.12E-04
8	Sr-90			2.33E-05		4.25E-04		
9	Nb-94			3.58E-05		3.34E-04		
10	Tc-99			6.41E-05		1.06E-04		
12	Cs-137		8.78E-01	9.00E-05		7.94E-01		
14	전알파			3.90E-04		2.20E-04		6.62E-07
22	Cs-134	8.40E-03	4.45E-02	7.94E-04		2.94E-04	3.33E-03	1.98E-03
23	Pm-145					7.87E-02		
26	Eu-152	1.11E-01	7.11E-03	1.69E-01	2.76E-01	1.61E-03	5.64E-02	5.87E-02
27	Eu-154	9.00E-03		2.42E-02	2.01E-02	8.12E-04	3.05E-03	2.54E-03
28	Eu-155			2.29E-03	2.46E-04	2.85E-04	1.33E-03	1.06E-03
	Total	100.44%	100.00%	100.00%	101.41%	100.00%	99.97%	100.00%

Acknowledgement

This work was supported by the Korea Institute of Energy Technology Evaluation and Planning (KETEP Project No. 20193210100120) and the Ministry of Trade, Industry & Energy (MOTIE) of the Republic of Korea.

REFERENCES

[1] KHNP(2020). Final Decommissioning Plan.

[2] Concrete Characterization and Dose Modeling During Plant Decommissioning. EPRI.168p.

[3] Main Yankee License Termination Plan_Rev 5(2009).US NRC.

[4] Yankee Rowe License Termination Plan. Rev1 (2004).US NRC.

[5] Zion Nuclear Power Station, Unit 1 and 2 License Termination Plan.Rev2(2018).US NRC.

[6] Decommissioning study of Forsmark NPP (2013). SKB.

[7] Decommissioning Study of Oskarshamn NPP (2013).SKB.

A Study on the Indirect Evaluation Method of Difficult-to-Measure Nuclides in Nuclear Decommissioning Radioactive Waste

Hang-Rae Cho*, Ji-Soo Yoon, and i-Hoon Lee
KHNP Central Research Institute
*hrcho6795@khnp.co.kr

1. Introduction

In order to efficiently dispose of the radioactive wastes generated during decommissioning of nuclear power plants, an indirect evaluation of difficult-to-measure (DTM) alpha/beta emitting nuclides is required, as in the waste from operating plants. A typical indirect evaluation method is a scaling factor (SF) that is a method for evaluating the radioactivity of DTM nuclides from the radioactivity of easy-to-measure (ETM) key nuclides, based on the correlations between DTM nuclides and ETM nuclides.

In general, a SF is derived from the direct analysis method for representative sampling and laboratory analysis of the radioactive wastes generated. However, since large amounts of waste are generated in a short period of time during the decommissioning of nuclear power plants, it is necessary to prepare a scaling-factor in advance for the disposal of waste as early as possible.

Therefore, we have reviewed a theoretical SF method that use the analysis results of representative samples from the source of waste considering the behavior of nuclides in the process of handling and treatment of the waste.

2. Scaling factor method

2.1 Grouping for representative sample

For the decommissioning of nuclear power plant, a detailed characteristic survey for radiological assessment of structures, systems and equipment by destructive sampling will be carried out. Based on assumptions, scenarios, and supporting data, the radiological contamination sources and patterns of structures, systems, and equipment are predicted, and the grouping for the application of scaling factors can be carried out through analysis of detailed characterization results.

If necessary, additional representative samples of each group will be collected and analyzed to identify the presence ratio of DTM nuclides and ETM key nuclides in each group's sources, and to derive SFs for each type of decommissioning radioactive waste by reflecting the behavior of nuclides that may occur during decontamination and treatment.

2.2 Applicability of scaling factor method

Scale factors are applicable when there is a reliable correlation between the key ETM nuclide and the DTM nuclide. The correlation between the two variables can be determined by the correlation coefficient of statistical method, and typically, correlation coefficient values above 0.6 have been taken to indicate evidence of significant positive correlation [1]. Thus, the radioactivity of DTM nuclides can be indirectly predicted by applying a SF to the key ETM nuclide value.

2.3 Calculation of scaling factor

There are two kinds of statistical techniques applied to derive a SF. The first is the geometric mean method that is used when the analysis values of ETM nuclides and DTM nuclides are in a linear relationship. This is the average of the multiples for the individual ratios of the ETM nuclides and DTM nuclides, which is the best estimator of a median, and most appropriate even when outliers exist [1].

In addition, the geometric mean is less than or equal to the mean of sum, the arithmetic mean, and is reasonably predictable for two variables in a linear relationship. The formula for calculation is as follows:

$$f_{SF} = \sqrt[n]{(a_{d,1}/a_{k,1} \times \cdots \times a_{d,i}/a_{k,i} \times \cdots \times a_{d,n}/a_{k,n})} \quad (1)$$

where

$a_{k,i}$: the specific radioactivity of ETM nuclide in sample i(i=1…n)
$a_{d,i}$: the specific radioactivity of DTM nuclide in sample i(i=1…n)
n : the number of samples

The second method is the logarithmic regression. This is a technique that is applied when the relationship between the two variables is nonlinear, since it is a technique that linearizes the relationship by taking logs for each variable and then applies linear regression analysis. The formula for calculation is as follows:

$$\ln(a_d) = \alpha' + \beta \times \ln(a_k) \qquad (2)$$

where

a_d : is the specific radioactivity of DTM nuclide to be determined

a_k : is the specific radioactivity of key nuclide

α, α' are constants

β: is the regression coefficient

However, the regression analysis is affected to a great degree by outliers [1].

3. Other methodology

If there is no correlation or lack of reliability of it between ETM nuclides and DTM nuclides, other indirect evaluation methodology need to be applied instead of the scaling factor method. The average values, theoretical values or upper bound values are used instead of calculated SF values in several countries such as USA.

3.1 Mean activity

If applicability of SF method cannot be confirmed, another evaluation method for determining the DTM nuclides may be used, such as mean activity method as shown in Figure 1. This is based on calculating the mean values from measurements on representative samples and applying this value to other packages.

Alternatively, the upper bound value from measurement or by theoretical calculation can be used instead of the mean value to produce a conservative estimate [2].

3.2 Theoretical value

Theoretical SF also can be developed based on physicochemical processes and models for nuclides that are difficult to sample or for radioactivity below minimum detectable activity (MDA) that are difficult to determine by radiological analysis [1].

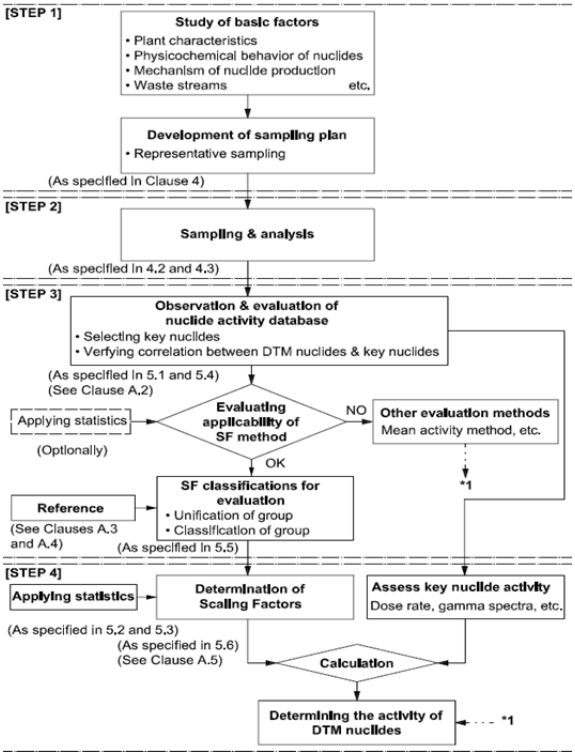


Fig. 1. Basic flow of application for SF method [2].

4. Conclusion

It will be necessary to prepare a scaling factor in advance for smooth disposal of waste as early as possible, since large amounts of waste are expected to be generated in a short period of time during the decommissioning of nuclear power plant.

Therefore, reliable indirect evaluation method such as theoretical SFs, mean activity, upper bound values will be able to be determined by considering contamination sources and patterns of radionuclides, physicochemical mechanisms and assumptions, scenarios, supporting data in the process of decontamination and treatment for decommissioning radioactive waste.

REFERENCES

[1] Determination and Use of Scaling Factors for Waste Characterization in Nuclear Power Plants, IAEA Nuclear Energy Series, No. NW-T-1.18, (2009).

[2] Nuclear Energy-Nuclear Fuel Technology-Scaling Factor Method to Determine the Radioactivity of Low-and intermediate-level Radioactive Waste Packages Generated at Nuclear Power Plants, ISO 21238, (2007).

Study on Introduction of Margin at Solid Waste Form Test for Acceptance Criteria of Final Repository

Dae Seok Hong*, Dong Ju Lee, Ji Young Song, Yoon Do Oh, Ki Baek Shin, Hyun Kyu Lee, Dong Han Yoo, and Won Hyuk Jang
Korea Atomic Energy Research Institute, 111, Daedeok-daero 989 beon-gil, Yuseong-gu, Daejeon, Republic of Korea
*dshong@kaeri.re.kr

1. Introduction

Solid waste forms are generated at nuclear facilities as a final product of some radioactive waste such as liquid waste, spent resin and so on. And these waste forms should be sent to final repository for isolation from the environment i.e., final disposal. For that, the solid waste forms should be tested for proving that those forms meet the acceptance criteria (WAC) set up by the disposal institute.

To show whether specific solidified radioactive forms are satisfied the WAC or not, each waste form generator has to test samples taken from real radioactive waste drum.

During the tests, though quality of specimen should be managed according to the WAC and related test procedure, some errors often to happen and this could be affect the test results. So, some margins should be introduced for testing waste form for its integrity.

The purpose of this study is to show why the margin is necessary during testing waste form and is to suggest degree of margin for some test items.

2. Tests for Acceptance Criteria

Solid waste forms should show their integrity for final disposal by various tests. Those tests can be categorized by their type as non-compressive strength related tests and compressive strength related tests.

The non-compressive strength related tests are free-standing water (i.e., unbounded water) content measurement and leaching test for which compressive strength measurement is not necessary before and after the tests. On the other hand, immersion test, thermal cycling test and radiation resistance test are required to measure compressive strength of specimen after the test. For the compressive strength measurement, a specimen with L(length)/D(diameter)=2 is required by WAC. So, the compressive strength related tests are affected by errors which can be occurred during specimen preparation.

3. Reasons for Margin Introduction

3.1 Errors on specimen preparation

The specimen used for tests are prepared by manufacturing cores sampled from real solidified wastes drum. One reason for errors on specimen preparation is due to tools for preparation.



Fig. 1. Tools for specimen preparation (Wheel saw blade (left) and coring drill blade (right)).

As wheel saw blade is 2.2 mm thick and coring drill blade is 5.2 mm thick, it is hard to make a specimen with L/D=2 due to vibration during manufacturing.

Additionally, competence level of tester cause error on specimen dimension.

3.2 Deviation in homogeneity

During making a solidified waste, waste may not be mixed well with solidifying agent. So there can be a hot spot in solidified waste and this means there is a non-homogeneous spot.

Also during curing concrete, crack or void can be introduced in solidified waste. This can introduce a non-homogeneous spot too.

As a result, the deviation in homogeneity is dependent on waste for treatment, procedure for solidification, curing process and so on.

Until now, there is no study on quantification of homogeneity for waste generated in Korea.

4. Result

Correction factors applicable for the specimen with L/D =1.9 is larger than 0.98 and this means that difference of compressive strength between specimen with L/D=2.0 and specimen with L/D=1.9 is less than 2%. In addition to that, as size of the specimen becomes larger, compressive strength becomes less [1]. So, it can be acceptable in a conservative view. As a result, L/D=2.0± 0.1 (i.e., L/D=1.9~2.1)may be applicable for testing solidified specimen for its integrity.

Table 1. Correction Factors for L/D Ratios Less than 2.0

L/D	1.75	1.50	1.25	1.00
Factor	0.98	0.96	0.93	0.87

In view of homogeneity, there is no enough data for discussing its margin. So, more testing using real solidified waste is required for quantifying the margin for homogeneity.

5. Conclusion

This study reviewed a margin can be introduced in testing and making solidified waste. As solidified waste should be tested for WAC, a margin is needed to be defined by regulatory body or final disposal repository.

REFERENCES

[1] Kim Ki Hong, Ryu Young Gerl, Kim Tae-Kuk, Comparison of various Standard Test Methods for Characterization of Radioactive Waste Forms, KAERI/TR-3695/2008.

The Development of URSF Management System

YuJeong Choi*, Jeongguk Kim, Jongjin Kim, and Jinwoo Lee
Integrated Radwaste Management Center, KAERI, 111, Daedeok-daero 989beon-gil, Yuseong-gu, Daejeon, Korea
*choiyj@kaeri.re.kr

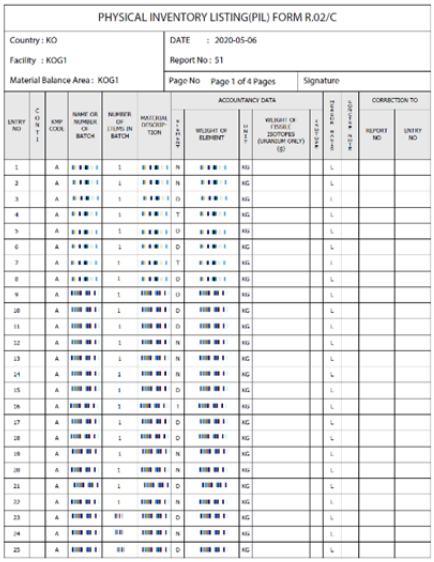
1. Introduction

The Korea Atomic Energy Research Institute (KAERI) is managing residue uranium in the centralized facility called Uranium Residue Storage Facility (URSF). This facility managed based on KAERI Advanced Nuclear Safety Information Management (ANSIM) system. This system is inconvenient for managing facility to manager. Therefore, to manage URSF Integrated Radwaste Control Team started to develop the URSF management system.

2. URSF management

2.1 Information to be managed

URSF is one of the IAEA inspected facility. Therefore, we got inspection every year. Inspectors check the items, numbers and location with each information and existence based on Physical Inventory Lists (PIL). The example of PIL is shown on Fig. 1.


PHYSICAL INVENTORY LISTING(PIL) FORM R.02/C

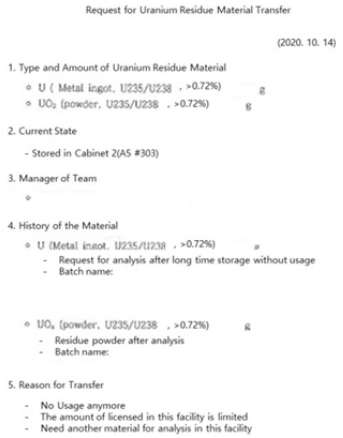
Country : KO | DATE : 2020-05-06
Facility : KOG1 | Report No : 51
Material Balance Area : KOG1 | Page No Page 1 of 4 Pages | Signature

ENTRY NO	COUNT	KMP CODE	NAME OR NUMBER OF BATCH	NUMBER OF ITEMS IN BATCH	MATERIAL DESCRIPTION	ACCOUNTANCY DATA: TYPE OF ELEMENT	WEIGHT OF ELEMENT	UNIT	WEIGHT OF FISSILE ISOTOPES (URANIUM ONLY) (g)	ESTIMATED ERROR	VERIFICATION CODE	CORRECTION TO: REPORT NO	ENTRY NO
1	A			1		N		KG			L		
2	A			1		N		KG			L		
3	A			1		D		KG			L		
4	A			1		T		KG			L		
5	A			1		D		KG			L		
6	A			1		D		KG			L		
7	A			1		T		KG			L		
8	A			1		D		KG			L		
9	A			1		D		KG			L		
10	A			1		D		KG			L		
11	A			1		D		KG			L		
12	A			1		N		KG			L		
13	A			1		N		KG			L		
14	A			1		N		KG			L		
15	A			1		D		KG			L		
16	A			1		T		KG			L		
17	A			1		D		KG			L		
18	A			1		D		KG			L		
19	A			1		N		KG			L		
20	A			1		N		KG			L		
21	A			1		D		KG			L		
22	A			1		N		KG			L		
23	A			1		D		KG			L		
24	A			1		N		KG			L		
25	A			1		D		KG			L		

Fig. 1. Example of PIL.

These lists composed of item name, number, description and weight of each item. However, the description of each item written in MD code, so it is not instinctively recognized what it is. Even we cannot check the history of materials and location of each item in URSF.

Therefore, it needs other documents for managing this information. One of the document what we collect are shown in Fig. 2. It includes chemical and physical form of each item and history of each material.


Request for Uranium Residue Material Transfer

(2020. 10. 14)

1. Type and Amount of Uranium Residue Material
   - U (Metal ingot, U235/U238 , >0.72%) g
   - UO_2 (powder, U235/U238 , >0.72%) g
2. Current State
   - Stored in Cabinet 2(A5 #303)
3. Manager of Team
4. History of the Material
   - U (Metal ingot, U235/U238 , >0.72%) g
     - Request for analysis after long time storage without usage
     - Batch name:
   - UO_4 (powder, U235/U238 , >0.72%) g
     - Residue powder after analysis
     - Batch name:
5. Reason for Transfer
   - No Usage anymore
   - The amount of licensed in this facility is limited
   - Need another material for analysis in this facility

Fig. 2. Example of Request of Consignment.

The location of each item in a facility is managed with image file manually drag and drop the item every time when it comes in. The information it includes are batch name and item location.



Fig. 3. Example of item location management format.

Those documents and formats are essential information to manage items but each document do not have all the information. Therefore, we should find and check each documents to get the information what we need.

2.2 Development of URSF management system

The purpose of URSF management system is development of visualized integrated management system as shown in Fig. 4. location of each item

are shown in the display. If user click the item then it shows the description of item and highlights the same batch. This system combined all the information of each item based on location management format. Therefore, user can easily find and get information from the system.

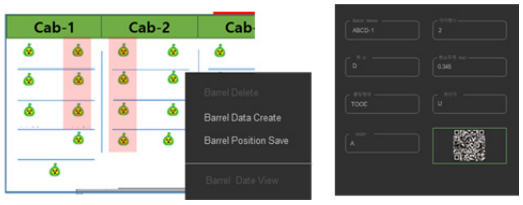


Fig. 4. Example of item location management format.

2.3 On Site Management

This system has QR code print out menu. Therefore, user can check the information of item on site which out any documents. If they scan the QR code with tablet pc then it shows the information and history of each item. This system link with tablet pc by Bluetooth.

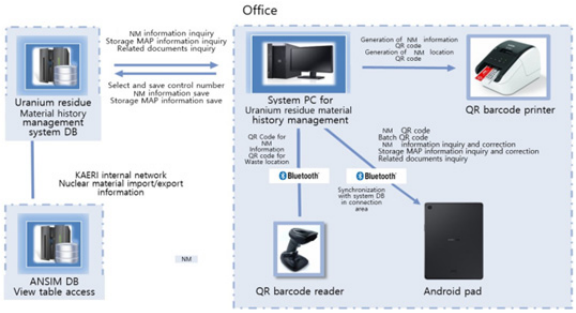


Fig. 5. Network of URSF Management System.

3. Conclusion

The URSF should be managed transparently with location, description, history and etcs. However, current system cannot covet up the information what manager need. Especially location of the item could check on the current system. It should be separately managed with image file but it was inconvenient. Integrated radwaste control team is developing the URSF management system as visualized integrated system. This system will be helpful to manage URSF system more transparently.

REFERENCES

[1] The Development of Uranium Residue Storage Management System, Remtech, (2020).

Development of Equipment of Contamination Inspection for Steel Pipe Scaffold in Nuclear Power Plants

Hyung kwon Jeong*, Dong kyu Jang, and Jeong won Park
Actrmt Co., Ltd., 219, Gasan digital 1-ro, Geumcheon-gu, Seoul, Republic of Korea
*jhk0502@actrmt.co.kr

1. Introduction

The steel pipe scaffold(SPS) generated in nuclear power plants is taken out to the general environment after measuring radioactive contamination using surface contamination monitors. It can be taken out to the general environment only when it is proved that the degree is less than the export standard value. The development of automatic survey technology is very important thing to obtain the accurate value for decision making. Conventionally survey on the SPS in NPPs, it needs two preliminary process. One is dividing into two of SPS along longitudinal direction and other is pressing to be flat. However, this kind of work not only have low productivity but also workers are exposed to radiation for a long time. To solve it, we developed equipment of inspector which can measure on the outer and inner sides of SPS. It would be minimizing the exposure time of workers to radiation and greatly reducing inspection cost.

2. Body

2.1 Component and function of apparatus

- Bench and instrument holder consisting Al material.
- Ball transfers consisting of a ball mounted in a housing with ball transfer bearings that allow the ball to rotate in all directions which is suitable for turning or diverging parts of conveying system. It is supported by 3 Boll-transfers at the left and right of the SPS and also minimized the friction generated during advance and rotation. Boll-transfer has a low contact area with the SPS, so the contamination transfer rate is low, and it is easy to replace in case of contamination.
- Front (rear) motor switch installed on the control box side by side with the front (rear) motor speed controller, has the role of stopping, moving forward, and rotating the motor.
- Holder for Instrument can hold detector properly and worker can adjust the height of holder for check the result value. (w×d×h=65×100×30mm).
- Holder for detector can put the probe to keep the gap between SPS and surface of probe within 1.5cm using adjusting nut. (w×d×h=170×95×10mm).
- Power terminal box installed at the lower left of the bench and consists of an earth leakage breaker and an adapter.



Fig. 1. Ball-transfer



Fig. 2. Motor-Shaft Assembly.

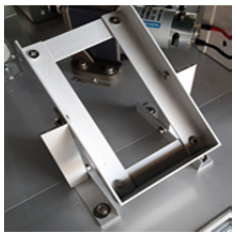


Fig. 3. Holder for Instrument

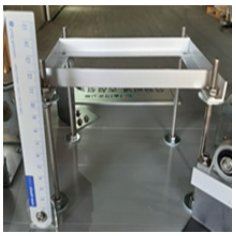


Fig. 4. Holder for detector.

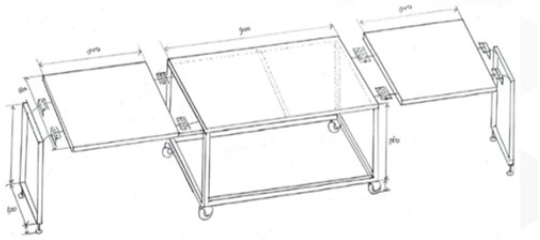


Fig. 5. Drawing of SPS inspector.



Fig. 6. Final completion of SPS inspector.

2.2 Step of operation inspection

Step 1: Fixing the support by deploying the auxiliary worktables on both sides. Step 2: Adjusting to 1.5cm gap between detector holder

and SPS. Step 3: After setting the speed of the front motor, set the speed of the rear motor as to front one. Step 4: After confirming that the front drive shaft and the rear drive shaft operate normally, insert the steel pipe scaffold in the forward direction**.**

2.3 Result of velocity test

In order to check 5cm/sec as required by the procedure, the speed was measured by marking it at an arbitrary point on the surface of the SPS and installing a tape measure in the axial direction. Circumferential direction speed was measured by checking 360 degree rotation speed of SPS.

Table 1. Result of velocity test

	Length for test	Elapsed Time(sec)	Remark
Axial	5cm	1	
Circum ferential	15cm	3	r=2.4cm

2.4 Comparison of traditional and new approach

In the traditional contamination inspection, the inspection quantity varies depending on the fatigue level of the worker but when the SPS inspector was used, 30 pieces per hour could be completely inspected on a 6m basis. In radiation management area, inspection on the board could significantly reduce the radiation effect from the contaminated floor than the conventional method.

Table 2. Result of comparison of two cases

Division	Worker	SPS inspector
Elapse time / 1EA	4~6min	2min
Required Persons	2~3	1
Gap between SPS and detector	Person by person	1.5 cm (uniform)

As above Table 2, SPS inspector is more effective in terms of accuracy and save time of the contamination inspection than human do. Also, the inspector rotate the SPS automatically that is more efficient for continuous work than worker rotate the SPS as in the conventional method.

3. Conclusion

This SPS contamination inspection equipment was manufactured for testing to prove its feasibility, and it is believed that it would be possible to further reduce time of contamination inspection and manpower. When manufacturing prototype equipment, we are going to expand 2 more equipment by compensating the defect.

By using the above product, it is possible to accurately comply with the procedures and prevent the case of that the contaminated SPS is taken out due to human error. In the future, if work-related of SPS is completed and the decayed SPS is subjected to contamination inspection for export, this equipment is expected to be used continuously.

REFERENCES

[1] Jae Sung Shin, Seong Yong Oh, and Hyunmin Park, “Decontamination With a Single-mode Continuous Wave Fiber Laser for Nuclear Decommissioning”, Journal of Korea Radioactive Waste Society (2020).

[2] Myung Suk Lee, Yong Yuk Jin, Kyung Min Lee, and Jin Uu Lim “Pipe cutting device for radioactive contamination inspection”, Korea Intellectual Property Office.

RESRAD Code Sensitivity Analysis and Safety Assessment for Clearance of Radioactive Waste

Yeo Chong Cho* and Jong Soon Song
Chosun University, 309, Pilmun-daero, Dong-gu, Gwangju, Republic of Korea
*chowon2662@khnp.co.kr

1. Introduction

In 2017, the dismantling of Kori unit 1, the first nuclear power plant in Korea, was confirmed, and by 2033, permanent suspension of 14 nuclear power plants was realized. Therefore, the generation of landfill wastes subject to clearance of wastes such as concrete and soil is expected to increase in the process of dismantling nuclear facilities and restoring the site. internally, the RESRAD-ONSITE Code is the most widely used for the safety evaluation of the clearance of landfill waste, and the evaluation is performed by adopting the representative value based on the RESRAD default value and the KINS/RR-144 report as the characteristic parameter of the landfill site. However, due to the selection of conservative input parameters focusing on the ease of verification of regulatory requirements, the estimated exposure dose is overestimated, and the impact on clearance is very large. Therefore, in this study, in order to secure clearance suitability and safety, the characteristics and sensitivity of major parameters in dose evaluation were analyzed, input parameters for efficient clearance were considered, and safety evaluation was performed.

2. Input Parameter Analysis and Application

2.1 Characteristics of Clearance Wastes

The waste to be evaluated is spent activated charcoal that has been charged into the HVAC system of nuclear power plant, and its main characteristics are as follows.

Table 1. Characteristics of clearance wastes

Type	Quantity(kg)	Dose rate (μSv/h)	Contamination
charcoal	3,400	0.14 ~ 0.17	BKG

2.2 Radionuclide Concentration

In the existing clearance case, conservatively, the maximum radionuclide concentration of the representative sample was applied as the representative concentration of the total waste. However, since the total amount of waste is landfilled on the same site during actual landfilling, this study conducted a practical evaluation by applying the average concentration of all wastes according to the regulatory guidelines.

Table 2. Evaluation result by maximum and average activity (mSv/y)

TDose(t)	Max. concentration	Av. concentration
Max. dose	7.966E-04	5.750E-04
5 year	1.381E-05	8.796E-06

2.3 Dose Conversion Factor

The exposure age group was evaluated by applying six age groups. In addition, in order to evaluate as a single age group, the evaluation was performed by applying twice that of ICRP 72 adult DCF, and the conservatism of the single age group evaluation was confirmed.

Table 3. Results of exposure dose by DCF (Max. dose) (mSv/y)

ICRP72 DCF×2	RESRAD 7.2 DCF			
	Age 1	Age 5	Age 15	Adult
1.305E-03	5.812E-04	3.705E-04	3.310E-04	5.750E-04

2.4 Safety Evaluation Times

Previously, a conservative assumption was made that the general population resides immediately after the landfill, but according to the Waste Control Act, the follow-up management period is required within 30 years after the landfill closure, so the evaluation was made on the assumption that 5 years had elapsed after the landfill was closed.

Table 4. Results of exposure dose by evaluation times (mSv/y)

TDose(t)	Age 1	Age 5	Age 15	Adult
0 year	5.81E-4	3.71E-4	3.31E-4	5.75E-4
5 year	9.03E-6	7.57E-6	7.32E-6	8.80E-6

2.5 Cover Depth

Cover depth was applied to 0.6 m based on the covering standard of the Waste Control Act. In fact, even after the clearance waste is landfilled, the thickness of the cover depth is expected to be thicker than that of households because general waste is additionally landfilled.

Table 5. Exposure dose result by thickness of the cover depth (mSv/y)

Thickness (m)	0 years	1 years	5 years	10 years
0.3	5.748E-04	5.749E-04	1.113E-04	6.433E-05
0.6	2.822E-04	4.073E-04	8.796E-06	3.077E-06
1.2	2.442E-04	3.905E-04	3.599E-06	1.397E-08

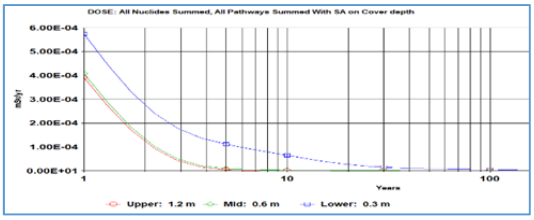


Fig. 1. Sensitivity analysis result by cover depth.

2.6 Density of Contaminated Zone

As for the density of the contaminated zone, 0.53 g/cm3, which is the density of spent activated charcoal, is applied, and it is a conservative application because the apparent density increases due to compaction work in the landfill and cover process. As a result of the sensitivity analysis, the exposure dose increased as the density increased.

Table 6. Exposure dose result by density of contaminated zone (mSv/y)

Density (g/㎤)	0 years	1 years	5 years	10 years
0.53	2.822E-04	4.073E-04	8.796E-06	3.077E-06
0.75	3.932E-04	5.722E-04	1.032E-05	3.088E-06
1.5	7.715E-04	1.135E-03	1.548E-05	3.110E-06
3	1.528E-03	2.260E-03	2.580E-05	3.143E-06

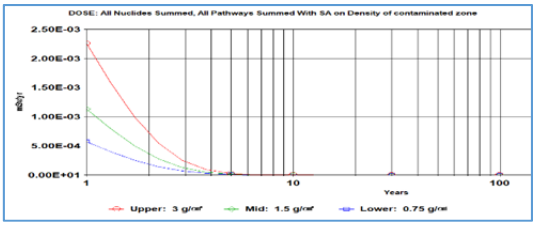


Fig. 2. Sensitivity analysis result by density of contaminated zone.

2.7 Precipitation

Using the data from the Meteorological Administration, the average rainfall of 1.44 m/y in the last five years of Yeosu, the expected landfill site, was applied. As a result of the sensitivity analysis, as the precipitation increased, the exposure dose decreased due to the hydrological effect.

2.8 Other Input Parameters

Other input parameters were entered as shown in Table 7.

Table 7. Other input parameters

Input Parameter	Value
Area of contaminated zone(㎡)	3.21
Thickness of Contaminated Zone(m)	2
Length Parallel to Aquifer Flow	2.02
Density of cover material(g/㎤)	1.53
Wind speed(m/s)	3.88
Inhalation rate, Dietary data	KINS/RG-N02.02,
Non-dietary data	KINS/RR-144
Storage times before use data	KINS/RG-N02.02,

3. Safety Evaluation Results

As a result of clearance safety evaluation, individual and collective doses of landfill workers and residents satisfied the allowable dose for clearance level under the Nuclear Safety Act.

Table 8. Estimated exposure dose to individual and collective

	TDose(t)	Individual dose (μSv/y)	Collective dose (man-Sv/y)
Worker	0 year	3.548E-01	7.096E-06
Resident	5 year	9.031E-03	3.329E-07

4. Conclusion

In this study, a clearance safety evaluation was performed using RESRAD-ONSITE Ver 7.2 for spent activated charcoal generated from nuclear power plants. Effectiveness was examined through the characteristics and sensitivity analysis of input parameters, and practical input parameters were applied by reviewing the latest literature and reports to avoid conservative assumptions. The evaluation result satisfies the allowable dose for clearance, but it was evaluated somewhat more conservatively than the intention of this study due to the domestic environment of the input parameters and some different conditions. In the future, if an input parameters reflecting the domestic conditions is developed, a systematic system is established, and an evaluation is performed in accordance with the characteristics of the waste, the estimated radiation dose can be more accurately predicted.

REFERENCES

[1] KINS, "Development of Regulatory Requirements for Clearance of Radioactive Waste, RR-144" (2002).
[2] KINS, "Safety Analysis on Clearance of Radioactive Waste, RG-N12.08" (2015).
[3] ANL, "User's Guide for RESRAD-ONSITE Code, ANL/EVS/TM 18/1" (2018).

Preliminary Studies on Neutron Activation of Concrete from Cyclotron Facilities and Applicability of Decay-in-Storage for Decommissioning Waste Management

Se Geun Lee and Jae Hak Cheong*
Kyung Hee University, 1732, Deogyeong-daero, Giheung-gu, Yongin-si, Gyeonggi-do, Republic of Korea
*jhcheong@khu.ac.kr

1. Introduction

During decommissioning of nuclear facilities, neutron activation of structural materials is the largest fraction of the source term inventory especially for reactor and accelerator facilities [1]. At this point, for the proper planning and safe implementation of decommissioning, neutron activation evaluation is essential [1]. In Korea, there are many accelerator facilities which are used to produce PET radiotracer, especially ^{18}F-FDG. ^{18}F-FDG is produced via ^{18}O(p,n)^{18}F reaction and secondary neutron is generated from (p,n) reaction. Generated secondary neutrons interact with structural materials of cyclotron facility and occur neutron induced activation during its operation period. After operation period, neutron activation derives generation of decommissioning waste which is contaminated volumetrically. In this study, several prior studies were analyzed to confirm neutron activation level of cyclotron facilities. And a hypothetical cyclotron and concrete vault room modelling is conducted for preliminary calculation of neutron activation of the cyclotron facility. And incident neutron flux of concrete wall is obtained from MCNP6 calculation. Also, neutron activation assessment was conducted with FISPACT-II for each assessment point. From calculated radioactivity concentration of concrete walls of vault room and cyclotron components, sum of fractions (SoF) with clearance level of each activation product (AP) are derived in this study. Finally, applicability of decay-in-storage strategy was confirmed for management of decommissioning waste from cyclotron facilities

2. Materials and Methods

In this study, the prior studies which addressed the specific radioactivity of each AP were analyzed to calculate SoF. Figure 1 shows SoF along with elapsed decay time for seven cases collected in this study. Most cases, both Co-60 and Eu-152 with same 0.1 Bq/g of clearance level and 5.27 and 13.5 years of half-life, respectively, were the most critical radionuclides to determine SoF of concrete.

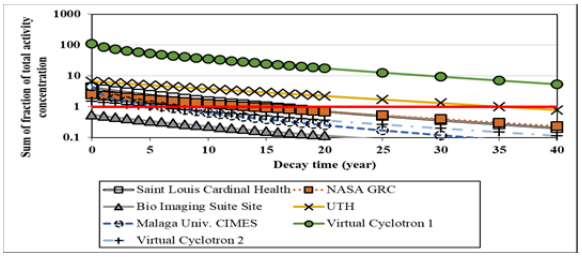


Fig. 1. Overall framework to assess neutron activation of the cyclotron facility established in this study.

Considering the maximum 15-year decay period, the SoF of 5 out of 7 cases decreased to less than union. It implies the decay-in-storage strategy could be possibly applied to concrete waste from decommissioning of cyclotron facilities.

In this study, procedure of neutron activation assessment consists of two steps: neutron flux calculation and production, depletion and decay of radionuclide calculation. There are several commercialized computational codes for neutron activation assessment [1]. Incident neutron flux is calculated by MCNP6 computational code and radionuclide production, depletion and decay are calculated by FISPACT-II computational code in this study. Following Figure 2 shows the overall framework to assess neutron activation in this study.

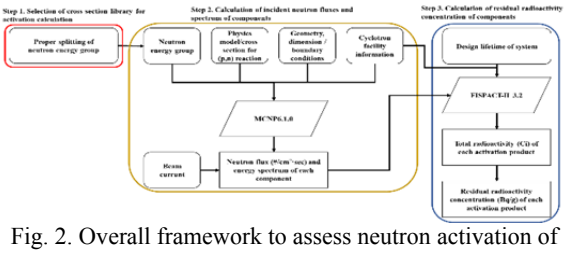


Fig. 2. Overall framework to assess neutron activation of the cyclotron facility established in this study.

It is very important that selecting proper cross-section of neutron activation reaction and splitting neutron energy group. Furthermore, different with nuclear reactor facilities, in cyclotron facilities, neutrons are produced by (p,n) reaction which is calculated by physics model or cross-section library such as Bertini, ISABEL or TENDL, etc. Regarding previous study and preliminary evaluation, TENDL-2019 library is selected to obtain neutron yield from (p,n) reaction in the cyclotron facility [2]. Also, EAF

VITAMIN-J library is selected to calculate activation, especially APs of concrete components. Other assumptions of target system are shown in Table 1.

Table 1. Assumptions of target system for neutron activation assessment in this study

Category	Assumption
Operation history	2 hours/day, 5 days/week, 50 weeks/year, 10 years
Concrete type	NBS 04
Impurity contents	Co-59 10 ppm, Cs-133 1 ppm Eu-151 0.5 ppm Eu-153 0.5 ppm

3. Results and Discussions

Figure 3 shows total incident neutron flux of each point of concrete wall calculated by MCNP6.1.0. Despite it is not shown explicitly in Figure 3, both thermal and fast neutron flux was decreased with the distance from the cyclotron target and the depth of concrete. Furthermore, neutron flux was increased ahead the beam direction.

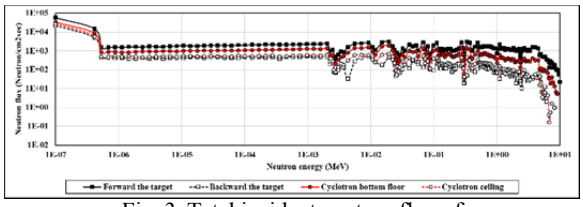


Fig. 3. Total incident neutron flux of each point of concrete wall.

Based on the results of MCNP6 calculations, radioactive concentrations of major APs were calculated by FISPACT-II code. For analyzing impacts of neutron activation to radioactive waste generation, radioactivity concentration for each major AP was calculated as Figure 4. All of 4 APs are generated by activation of impurity nuclide. The most activated, concrete forward the target has decreasing radionuclide concentration by depth of concrete wall, except forward the target. The radionuclide concentration is increased slightly around 5~10 cm depth shown in Figure 4.

The SoF of the most activated concrete is calculated along with elapsing decay time to confirm the applicability of decay-in-storage to manage radioactive waste from decommissioning of the cyclotron facility, shown in Figure 5 which exists within the variance of prior studies.

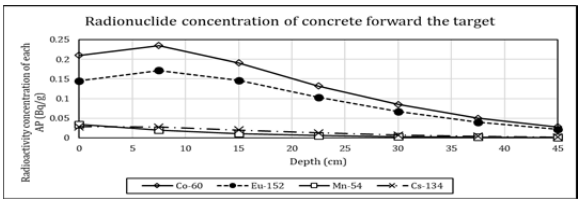


Fig. 4. Radioactivity concentration of concrete forward the cyclotron target.

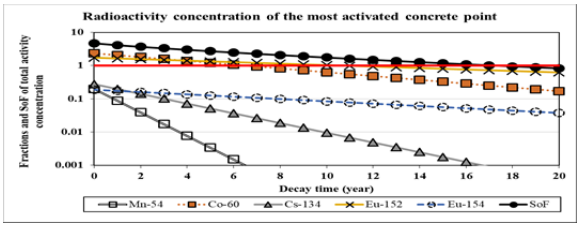


Fig. 5. Radioactivity concentration of concrete forward the cyclotron target.

As shown in Figure 5, the most critical AP for SoF is Co-60 with 2.35 of fraction with clearance level, immediately after the end of the cyclotron operation. However, along with elapsed decay time, the dominant AP become Eu-152 which has longer half-life than Co-60. After around 17-year of decay time, the period that can be used as a controlled area such as radioactive isotopes storage room after demolition cyclotron body, the most activated part of concrete based on the assumption of this study could be treated as clearance waste.

4. Conclusion

Based on several prior studies on activation of concrete from cyclotron facilities, it might be applicable that decay-in-storage to manage decommissioning waste. Also, following the preliminary calculation in this study, the impurity control can be essential and decay-in-storage can be one of options for decommissioning cyclotron facilities.

REFERENCES

[1] IAEA, Methodologies for Assessing the Induced Activation Source Term for Use in Decommissioning Applications, Safety Report Series No.95 (2019).

[2] M. Bakhtiari, L. M. Oranj, Nam-Suk Jung, Arim Lee, Hee-Seock, Lee, Estimation of neutron production yields from $H_2{}^{18}O$ as the ^{18}F-production target bombarded by 18-MeV protons.

A Study of the Nuclear Inventory Evaluation for Decommissioning Radioactive Waste Scaling Factor Analysis

Hwayoon Kang and Yongsoo Kim*
Department of Following Nuclear cycle Engineering, Hanyang University,222 Wangsimni-ro, Seongdong-gu, Seoul 133-791, Korea
*yongskim@hanyang.ac.kr

1. Introduction

With the end of the operational permit for Kori-1 nuclear power plant, Korea's first nuclear power plant, it will begin decommissioning the plant after shutting down its operation in 2017.

In addition, a total of 7.08 million drums will be generated based on the 200L standard by 2095 when the decommissioning of the nuclear power plant is completed as a result of predicting the amount of 30 nuclear power plants planned under the energy conversion policy in the future.

By level, the number of mid-levels is estimated at 3.5 million (5%), low-levels at 3.47 million (49%), and extremely low-level at 3.26 million (46%) [1].

In the case of operating wastes generated in Korea, Radioactive nuclides of drums are applied as a scaling factor, which is an indirect measurement method. To date, but no specific method of assessing radionuclides for decommissioning waste has been established.

Therefore, we will examine the scaling factor of waste generated during the operation of nuclear power plants and the scaling factor developed at overseas nuclear power plants and would like to examine how to assess the nuclear end-to-end high volume centered on the scaling factor for decommissioning waste.

2. Methods and Examples

In the case of Kori unit 1, the final decommissioning waste to be delivered to the waste disposal site through decontamination and regulation clearance is estimated to be about 14,500drum [1].

As a result of comparing the amount of waste generated from overseas nuclear power plants,
If the IAEA disassembles one PWR of 900-1300 MWe, calculated at 13,613drums, this is estimated to be similar to the expected generation of decommissioning waste at Kori Unit 1 at present.

The characteristics of decommissioned wastes are generated in large quantities in a short period of time compared to those of operational wastes, and they vary in form and have low levels.

However, there is a difference that large scale wastes and extremely low-level wastes are generated in large quantities compared to operating wastes. Except for this, the disposal process of medium and low-level waste is assumed to be carried out in a similar manner to the operation waste.

The method of assessing the nuclear inventory of the decommissioned waste was reviewed through the method of assessing the nuclear inventory of the operational waste.

2.1 Methods for evaluating nuclides inventory

In order to assess the radioactive nuclides in the medium and low-level waste generated from nuclear power plants, a separate detailed method of assessing the high nuclear inventory is required. In general, direct measurement methods are used, centering on the scaling factor method.

First, take a representative sample of the waste subject to analysis and conduct a radiochemical analysis to examine the correlation between the radioactive nuclides subject to evaluation.

Based on this, Key nuclide, which is easy to measure, analyzes the correlation with the difficult DTM nuclide and ensures satisfactory correlation.

Using both the scaling factor method and the non-destructive direct measurement, after measuring the concentration in Key nuclides through direct measurement, the scaling factor is applied to predict the radioactivity of DTM nuclides [3].

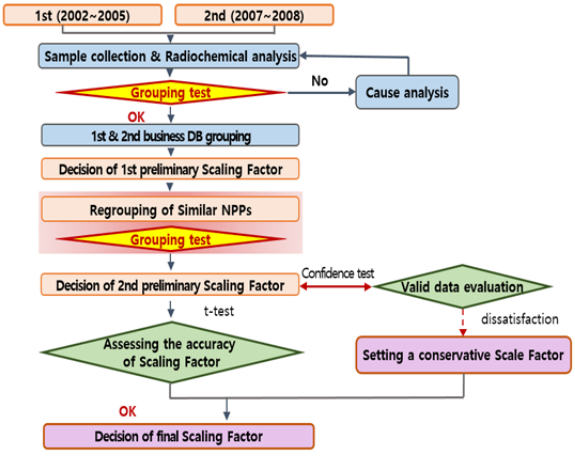


Fig. 1. determining scaling factor [3].

2.2 Examples of domestic and international scaling factors

Various wastes generated from nuclear power plants are classified into DAW (Dry Active Waste), concentrate radioactive waste, waste resin, and

waste filters. DAW that is most frequently generated by catch (26%) is based on the assessment of the nuclear load of catch. [1] DAW is a solid waste with various characteristics that occur during the operation of a nuclear power plant, and the currently developed scaling factor is as shown in Table1.

Table 1. Scaling Factor (DAW)

DTM Nuclides	Kori1	Kori2	Hunul2	Hanbit2
C-14	0.0519	0.0112	0.0568	0.0568
Fe-55	2.29	3.08	6.3	6.3
Ni-59	0.0838	0.0213	0.151	0.151
Ni-63	5.62	1.16	0.651	0.651
Sr-90	0.0963	0.0385	0.703	0.703

Table2 shows an example of LTP (License Termination Plan) for US MY nuclear power plants, comparing the current domestic operational nuclear power plants with the waste balance factor of overseas decommissioned plants. The MY nuclear power plant was permanently shut down in 1996 at 860MWe, which is comparable to the Kori-1 reactor, referring to the analysis of samples collected in 1998. Examples of application of scaling factors for internal structures such as waste resins, waste filters, and reactor coolant pumps can be checked[6].

For the same comparison of the currently applied scaling factors, the difference was compared by comparing the factors [5] for the waste paper equivalent to domestic nuclear power plant operating waste and the decommissioning waste of the U.S. Main Yankee.

Table2. Comparison of Scaling factors between Domestic and Overseas (Resin) [5], [6]

DTM Nuclides	ETM Nuclide	Korea		USA
		Kori1	Hunul2+ Hanbit2	Maine Yankee
C-14	Co-60	0.288	0.0673	0.005274
Fe-55	Co-60	1.03	4.57	0.462300
Ni-59	Co-60	0.817	1.21	-
Ni-63	Co-60	12.5	1.02	1.632000
Sr-90	Cs-137	0.452	0.565	0.006116

The comparison of the scaling factor shows a difference of at least twice as much as C-14 compared to the Kori-1 plant, about 70 times the difference between Sr-90 nuclides. It is confirmed that it has a conservative value compared to MY.

Thus, it is necessary to improve accuracy by updating additional data through periodic verification as the first applied metric for operational nuclear power plants. This is because it prevents overestimation and maintains reasonable values when assessing nuclides inventory.

3. Conclusion

Decommissioning radioactive wastes generate a variety of intermediate and low level wastes, and in this paper, domestic and foreign data were investigated to confirm the predicted amount of various decommissioning radioactive wastes.

In the event of decommissioning Kori unit 1, the key to developing a method of assessing the nuclides inventory is how far the scaling factor, which is direct and indirect measurement, will be applied in accordance with the methodology previously presented by the IAEA.

The application of the scaling factor to decommissioning radioactive waste at Kori-1 is an important task that will serve as a prior criterion for nuclear power plants that will be decommissioned in the future. The more accurate the actual measured value is within the margin of error, the more reliable it can be. However, for all nuclides emitting alpha/beta-rays, there are practical difficulties in direct measurement, so the radioactive nuclides analysis of decommissioning radioactive wastes is required by applying an indirect method of scaling factor.

REFERENCES

[1] 2018 Intermediate and low level radioactive waste management implementation plan, Korea Radioactive Waste Agency (2018).

[2] Jeong Hae Yong, Prospects for regulation of decommissioning radioactive waste, Korea Institute of Nuclear Safety (2019).

[3] KINS/GR-297, Development of Regulatory Technology for Radioactive Waste, Korea Institute of Nuclear Safety (2005).

[4] Kang Il Jung and 3 others, Comparison of Radionuclide Inventory Between Predicted and Measured Activity of Dry Active Waste From Korea Nuclear Power Plant, Korea Radioactive Waste Agency (2017).

[5] An Hui Jin and 2 others, Comparison of the Development of Radioactive Waste Scaling Factor between Korea and the US, Korea Hydro & Nuclear Power (2015).

[6] Tranceuranic and Other hard to detectRadionuclides in Main Yankee Sample Media (2001).

Pressurized Heavy Water Reactor Spent Resin Mixture Transfer System Processor Development

Kyu-Ho Lee*, Ha-Young Oh, Bong-Ki Ko, Hyeon-Oh Park, and Seung-Geon An
Sunkwang T&S Co.,Ltd., Sunkyung Officetel 20F, #3, Gongwon-ro, Guro-gu, Seoul 08298, Republic of Korea
*khlee@sktns.co.kr

1. Introduction

In December 2019, the permanent shutdown of Wolsong Unit 1, PHWR (Pressurized Heavy Water Reactor) was decided, accordingly there is a need for treatment of the spent resin mixture stored in the spent resin storage tank of PHWR. In the case of PWR (Pressurized Water Reactor), generated spent resin treated through the SRDS (Spent Resin Drying System) at constant cycle. On the other hand, in the case of PHWR, the spent resin storage tank stored in form of mixture of zeolite, activated carbon and spent resin, it is impossible to dispose as it stands.

Spent resin and mixture (zeolite, activated carbon) must separate for the treatment of generated spent resin of PHWR, prior to transfer of spent resin mixture shall be preceded. When designing the spent resin storage tank, upper part of the spent resin storage tank designed manhole, test hole and resin inlet to ensure stability in operation of the NPP, lower part of the resin storage tank designed resin outlet to prepare for the decommissioning plan, so transfer of spent resin made it possible. However, up to the present, the operator of the NPP, KHNP (Korea Hydro & Nuclear Power Co., Ltd.) has been confirmed no specific plan for transfer of spent resin mixture through resin outlet.

This study developed a system for transfer processing the generated spent resin mixture in PHWR which is a step that should be preceded for treating spent resin stored in the spent resin storage tank of PHWR.

2. Body

2.1 Characteristic analysis of the spent resin storage tank of PHWR

The spent resin storage tank of PHWR is rectangular concrete structure, upper part of the spent resin storage tank has manhole and test hole to check the spent resin mixture storage volume, sampling and storage state to ensure resin inlet to transfer generated spent resin in each system and the stability of the operation of NPP. Also, to prepare to the next permanent shutdown, lower part of the spent resin storage tank designed resin outlet for transfer spent resin mixture.

The spent resin storage tank of PHWR stored in form of mixture of zeolite, activated carbon and spent resin. The spent resin mixture show differences in the fluid's liquidity due to density differences, the spent resin storage tank is consist of gradient phenomenon that zeolite, activated carbon are mainly stored in the lower part of manhole side, spent resin is mainly stored test hole side. In addition, long term storage caused to harden spent resin mixture and prior study confirmed that the input of the machinery was restricted below a certain depth when sampling spent resin mixture by opening manhole.

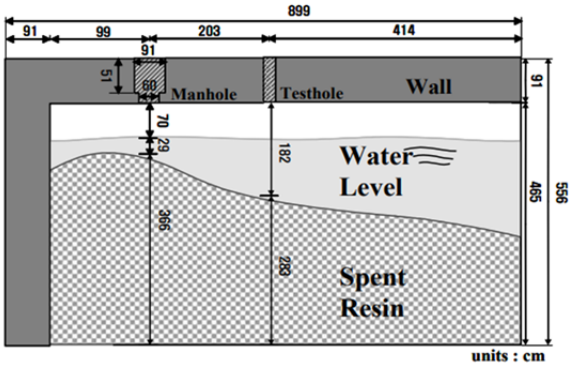


Fig. 1. Structure and internal estimation appearance of spent resin storage tank of PHWR.

Located space in resin outlet is very narrow, so It has been confirmed that the space was unsuitable for treating spent resin mixture.

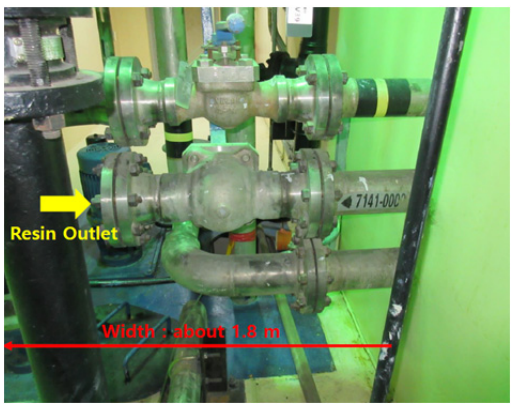


Fig. 2. Wolsong Unit 1 spent resin outlet space and pipe.

2.2 Process design for Spent resin mixture transfer system

Through characteristic analysis of the spent resin storage tank of PHWR, transfer spent resin mixture using the resin outlet was restrict, we looked for other plan. First, impeller installation or the injection of high pressure water was considered to give liquidity to the hardened mixture in the spent resin storage tank. However, the installation of impeller on upper part of the spent resin storage tank is limited, there is a possibility that a large amount of tritium, the representative nuclear species of the PHWR, may leak during the injection of high-pressure water, so countermeasure such as additional installation of equipment need to be prepared. Second, the method of transfer the spent resin mixture was considered through manhole located at upper of the spent resin storage tank. Currently, manhole and test hole in upper the spent resin storage tank are non-radiation protection area, the area are being used as a maintenance unit of KEPCO KPS, when transferring spent resin mixture, it is necessary to establish temporary radiation protection area. It was in consideration of stability of work and installation of additional equipment during transfer of spent resin mixture, It was concluded that it is reasonable to transfer spent resin mixture through upper of the spent resin storage tank.

A typical pump for transporting substances with liquids are used a diaphragm pump. However, when the prior study, the membrane of the pump was damaged by the particle surfaces of zeolite and activated carbon during long transfer of spent resin mixture. Therefore, rolled vacuum pump, corresponding to the special pump was selected.

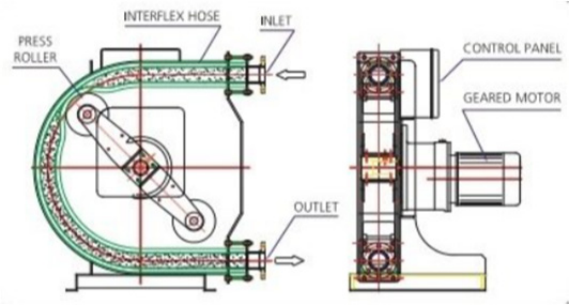


Fig. 3. Rolled vacuum pump diagram.

Rolled vacuum pump can transfer materials such as gravel along with liquid and It is excellent that the compression and hose resilience by rotating the compression roller. Normal and reverse rotation are also possible, which can solve other foreign substances(straps, gloves, work clothes, bags, etc.) jamming phenomenon that can occur when transfer spent resin mixture.

Also, liquid shall be accompanied when transferring substances due to the characteristics of rolled vacuum pump. It is designed for smooth transfer by creating fluid liquid around the pipe inlet of rolled vacuum pump by using liquid waste in the spent resin storage tank. This method has an additional positive effect of mitigating the hardening phenomenon of spent resin mixture.

3. Result

The characteristics analysis of the spent resin storage tank at PHWR confirmed the hardening and gradient phenomenon of the spent resin mixture, considering requirement of the NPP site, method of transfer of the spent resin mixture through upper part of the spent resin storage tank was selected. Accordingly, rolled vacuum pump, the special pump suitable for transfer of spent resin mixture, was selected, and ultimately ‘Process for transfer system of spent resin mixture in the spent resin storage tank of PHWR’ was designed.

4. Conclusion

The permanent suspension of Wolsong Unit 1 raised the need for spent resin mixture treatment, accordingly in this study, development of process for transfer system was carried out to transfer spent resin mixture in the spent resin storage tank, which should be preceded for spent resin treatment. However, it is judged that it should be accompanied by on-site applicability assessment of the actual NPP.

Acknowledgement

This Study was supported by a Korea Institute of Energy Technology Evaluation and Planning (KETEP) grant funded by the Korean government (No. 20191510301110).

REFERENCES

[1] Kyu-Tae Park, Jung-Min Yoo, Hyeon-Oh Park, Young-Ku Choi, Development of the PHWR Spent Resin Treatment Technology to Secure Disposal Safety, (2018).

5분과

제염해체 (Oral)

Synthesis of Prussian Blue Functionalized CoCr Layered Double Hydroxides to Treat Cesium and Iodate together

Jueun Kim[a], Jaehyuk Kang[a], and Wooyong Um[a,b,c,*]
[a]Division of Advanced Nuclear Engineering, POSTECH, 77, Cheongam-ro, Nam-gu, Pohang, Korea
[b]Division of Environmental Science & Engineering, POSTECH, 77, Cheongam-ro, Nam-gu, Pohang, Korea
[c]Nuclear Environmental Technology Institute, POSTECH, 77, Cheongam-ro, Nam-gu, Pohang, Korea
*wooyongum@postech.ac.kr

1. Introduction

Radioactive cesium (Cs-137) and iodine (I-125/ 129) have become an emerging issue because these elements have high radiotoxicity and solubility and can be easily volatilized at high temperature [1].

Layered double hydroxides (LDHs) are anionic clay known as hydrotalcite-like materials. These LDHs are composed of the positive charged layer with the exchangeable anions to maintain the structural charge balance. Our previous study [2] reported that CoCr LDHs have a high IO_3^- sorption capacity by anion exchange and redox effect. Also, Prussian blue (PB) has a high selectivity of Cs^+ by cation exchange with K^+ and ion trapping effect [3]. Based on this research, CoCr LDHs and PB could become the promising precursors to synthesize the combined sorbent for simultaneous Cs^+ and IO_3^- removal.

Therefore, our main objective of this study is to synthesize the novel PB functionalized LDHs to enhance the removal efficiencies of both Cs^+ and IO_3^- at the same time and identify the removal mechanism.

2. Material and Method

2.1. Synthesis PB-LDH

CoCr LDHs were prepared according to our previous study [2] and used for preparing PB-LDH. The 2.7 g of CoCr LDHs were dispersed into 20 mL of deionized water, and 10 mL of 4 mol/L $FeCl_2$ was then slowly added into solution under magnetic stirring. Subsequently, 10 mL of 3 mol/L $K_4Fe(CN)_6{\cdot}3H_2O$ was dropped into the mixed solution at 20 mL/hr, reacted for 1 hr, centrifuged and dried at 96 ℃ for 12 hrs. The obtained PB-LDH was washed with DIW five times and dried at 96 ℃ for 12 hrs.

2.2 Characterization

The zeta potential for surface charge analysis, powder X-ray diffraction (XRD) for crystallinity identification were used to characterize the physicochemical properties of the PB-LDH.

2.3 Sorption experiments

The equilibrium experiments were investigated to compare removal efficiencies of CoCr LDHs, PB, and PB-LDH. The pH variation sorption experiments were performed to describe the effect of initial pH on removal of Cs^+ and IO_3^- and stability of the PB-LDH. The concentration of Cs and I were analyzed by inductively coupled plasma mass spectrometer (ICP-MS) with NexION 300D (Perkin Elmer).

3. Results and Discussion

3.1 Characterization of PB-LDH

Table 1. Zeta potential values of CoCr LDHs, PB, and PB-LDH

CoCr LDHs	PB	PB-LDH
+44.3 mV	-2.86 mV	-30.0 mV

CoCr LDHs showed high positive zeta potential value due to their positive charged layers (Table 1). However, PB-LDH showed highly negative zeta potential value, which is similar to zeta potential value of original PB. These results can be interpreted that PB was formed on the surface of CoCr LDHs during the synthesis of PB-LDH.

The characteristic peaks of PB and LDHs were observed in XRD patterns of PB-LDH (Figure 1). The peak around 11.57° indicate (003) plane of CoCr LDHs. In addition, the peaks at 17.96°, 25.39°, and 36.33° showed the presence of potassium cobalt hexacyanoferrate hydrate. The rest crystalline phases are CoO(OH) and Co_3O_4, which could be caused by CoCr LDHs. After Cs^+ and IO_3^- removal, the intensity of CoO(OH) and Co_3O_4 slightly decreased due to dissolution of PB-LDH.

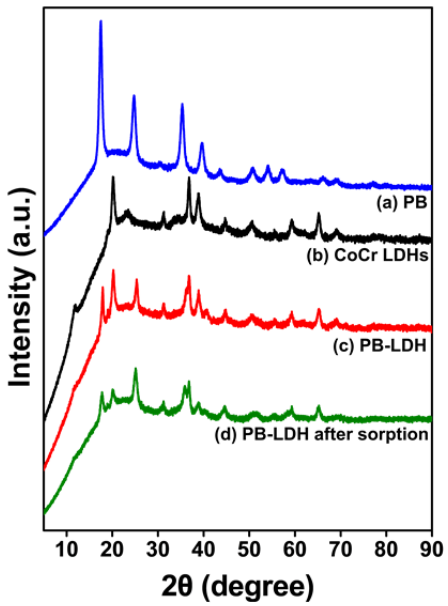


Fig. 1. XRD patterns of PB, CoCr LDHs, PB-LDH,and PB-LDH after Cs^+ and IO_3^- sorption.

3.2 Co-sorption properties of PB-LDH

Table 2. Removal efficiencies of PB, CoCr LDHs, and PB-LDH (Target solution concentration = 5 mg/L, Reaction time = 3 d)

Removal efficiency [%]	$CsIO_3$		$CsCl$	$NaIO_3$
	Cs^+	IO_3^-	Cs^+	IO_3^-
PB	99.8	0.00	99.3	6.86
CoCr LDHs	0.266	92.6	2.36	92.8
PB-LDH	99.7	89.8	99.7	88.6

The PB-LDH simultaneously removed Cs^+ (99.7%) and IO_3^- (89.8%), while CoCr LDHs and PB showed reasonable removal efficiencies (>90%) only for IO_3^- and Cs^+, respectively (Table 2).

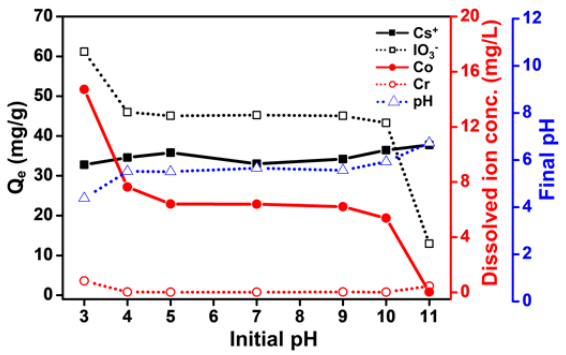


Fig. 2. Effect of initial pH on removal.

In the initial pH range of 4-10, the final pH seems to be constant due to the pH buffer effect of the PB-LDH (Figure 2). Cs^+ removal was not affected by the initial pH, however, IO_3^- removal significantly decreased above pH 11 due to the deprotonated surface. The plenty of Co ions were detected in the final solution, especially under pH 3, due to the dissolution of CoO(OH) and Co_3O_4. The released Cr concentration did not exceed the acceptable limit of drinking water by World Health Organization (0.05 mg/L), except pH 3 condition. As a result, the optimum pH conditions to utilize the PB-LDH are between 4-10.

4. Conclusion

From this study, PB-LDH could become a promising sorbent for simultaneous Cs^+ and IO_3^- removal, which can reduce the operation cost of treating waste solutions in radioactive waste management.

ACKNOWLEDGEMENT

This work was supported by the National Research Foundation of Korea (NRF) grant funded by the Korean government (MSIP: Ministry of Science, ICT and Future Planning) (No. NRF-2016R1D1 A1B02013310).

REFERENCES

[1] ORNL/NUREG/TM-25, "BEHAVIOR OF IODINE, METHYL IODIDE, CESIUM OXIDE, AND CESIUM IODIDE IN STEAM AND ARGON", (1976).

[2] Jaehyuk Kang et al., "Nanostructured MgFe and CoCr Layered Double Hydroxides for Removal and Sequestration of Iodine Anions", Chemical Engineering Journal, 380, 122408 (2020).

[3] Husnul Aulia Alamudy et al., "Selective adsorption of cesium from an aqueous solution by a montmorillonite-prussian blue hybrid", Chemical Engineering Journal, 349, 595-602, (2018).

A Chemical Decontamination Process for Corrosion Oxide Layers on Carbon Steel Heat Transport System in PHWR

Naon Chang [1,2], Heechul Eun[2,*], Huijun Won[2], Wangkyu Choi[2], Seonbyeong Kim[2], and Yongsoo Kim[1]
[1]Department of Nuclear Engineering, Hanyang University, Seoul 04763, Korea
[2]Department of Decommissioning Technology Research, Korea Atomic Energy Research Institute, Daejeon 34057, Korea
*ehc2004@kaeri.re.kr

1. Introduction

Before decommissioning, the decontamination process is required to be applied to a primary coolant circuit to reduce the radiation expose to the workers [1]. The main sources of radioactive material are corrosion oxide layers in the primary coolant circuit generated during reactor operation. The Hydrazine Base Reductive metal Ion Decontamination (HyBRID) process is developed by KAERI to dissolve the Fe-rich oxide layer such as Fe_3O_4 in the pressurized water reactor (PWR) [3]. The HyBRID process can be used to decontaminate the corrosion oxide layer on a heat transport system in a pressurized heavy water reactor (PHWR). Because the corrosion oxide layer in the PHWR is mainly consisted of Fe_3O_4 [4]. The corrosion oxide layer in the PHWR is much thicker than that in the PWR as shown in Table 1[4]. However, the thick Fe_3O_4 oxide layer can degrade the performance of the HyBRID process. Because the high concentration of Fe ions in the process solution can prevent the occurrence of Fe_3O_4 dissolution reaction. Therefore, the spent process solution, which is the process solution remained after finishing the decontamination cycle, is necessary to be replaced by fresh process solution. The composition of fresh process solution is the same as initial condition of HyBRID process solution. However, a secondary wastes generation can be increased when the process solution is frequently replaced. To resolve this problem, the decontamination process using recycled HyBRID spent process solution without replacement was suggested for applying it to the decontamination of the thick corrosion oxide layer on the heat transport system in the PHWR [5]. The recycling method is consisted of a precipitation, a filtration, and a make-up steps. In the precipitation step, the dissolved metal ions and SO_4^{2-} ions in the spent process solution are precipitated by injecting $Ba(OH)_2$. In the filtration step, the precipitates are removed and a purified process solution is obtained. In the make-up step, the purified solution reduces to the fresh process solution. The flow diagram of the PHWR decontamination process was shown in Fig. 1.

In this study, the effective control method of above decontamination process of thick corrosion oxide layer in the PHWR. The control method includes the monitoring method, which can be used in decontamination site in the nuclear power reactor.

Table 1. Characteristics of corrosion oxide layers in the reactor [4]

Reactor Type		Deposit Thickness (μm)	Deposit Density (g/cm^3)	Specific Weight (mg/cm^2)
PWR	Pipe	3	4	1.2
	SG	2	4	0.8
CANDU	Pipe	75	4	30
	SG	25	4	10

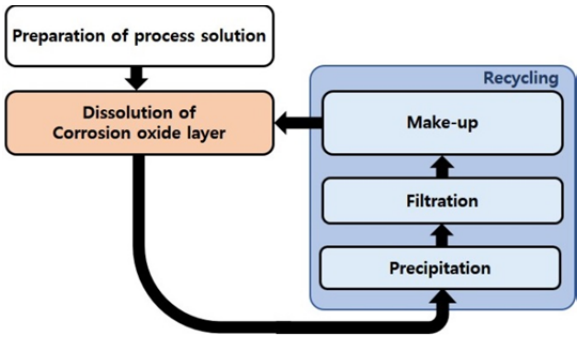


Fig. 1. Flow diagram of corrosion oxide layer decontamination process on the heat transport system in the PHWR using recycled HyBRID spent process solution.

2. Methods

2.1 Dissolution test of Fe_3O_4

The dissolution tests of Fe_3O_4 (Junsei, 94.0 %) were conducted by using the HyBRID process solution surrogate. The HyBRID process solution surrogate was consisted of 1,600 ppm of $N_2H_4 \cdot H_2O$ (Junsei, 98.0), 2,600 ppm of H_2SO_4 (Showa, 97.0 %), and 31 ppm of $CuSO_4$ (Junsei, 97.5 %). The pH value of the surrogate is 2.75. When the dissolution test was performed, 0.37 g, 0.66 g, 1.25 g and 1.84 g of Fe_3O_4 were injected in 1 L of each surrogate. The dissolution test was conducted by using water bath at 95 °C with 200 rpm mixing.

2.2 Analysis

During and after the Fe_3O_4 dissolution test, the concentrations of Fe ions in the surrogates were investigated by using AA analysis method (AAnalyst 400, Perkin Elmer co.). The pH was also analyzed during and after the dissolution test by using pH meter (Orion Star™ A211 Benchtop pH Meter, Thermo Fisher Scientific).

3. Results and Discussion

When the 0.37 g and 0.66 g of the Fe_3O_4 w343 dissolved in the surrogates (Initial [Fe] = 250 ppm and 450 ppm), the Fe_3O_4 were dissolved completely less than 2 h and 4 h each. When the 1.25 g and 1.84 g of the Fe_3O_4 were dissolved in the surrogates (Initial [Fe] = 850 ppm and 1250 ppm),, the concentrations of Fe ions were saturated from 4-5 h. Therefore, it is confirmed that the decontamination cycle was finished. This meaning is that it is necessary to be recycled by performing the recycling method.

The pHs were increased and decreased during the dissolution test. The increase in pH was caused by the acid-induced dissolution reaction, which is the dissolution reaction between Fe_3O_4 and H^+ ion [6]. The decrease in pH was occurred by the reductive dissolution reaction, which is the dissolution reaction between Fe_3O_4 and H^+ and e^- ions [6]. When the dissolution reactions were finished, it was confirmed that the pH values were decreased to 2.75. This pH value was the same with the initial pH value of the HyBRID process solution. Therefore, the decontamination process can be easily controlled by monitoring the pH value during the decontamination cycle.

Acknowledgement

This work was carried out under the Nuclear R&D program (NRF-2017M2A8A5015144) funded by the Ministry of Science, ICT and Future Planning (MSIP).

REFERENCES

[1] E. G. Lim, “South Korea’s Nuclear Dilemmas”, Journal for Peace and Nuclear Disarmament, 2(1), 297-318 (2019).
[2] W. K. hoi et al, KAERI/RR-4230/2016, KAERI (2017).
[3] Decontamination Handbook, TR-112353, July (1999).
[4] H. C. Eun et al., “Method for decontamination oxide layer”, 10-2020-0036610 (2020).
[5] S. J. Keny et al., “Radiation effects on the dissolution kinetics of magnetite and hematite in EDTA- and NTA-based dilute chemical decontamination formulation”, Radiation Physics and Chemistry, 72, 475-482, (2005).

Evaluation of the Nuclide Inventory for the SG Crossover Leg in Kori Unit 1

Jonghoa Kim*, Homin Jeon, Jihyun Yu, Seunggi Jeong, Sunghoon Kim, Kyeongho Han, and Jangsoo Seo
Sae-An Enertech Corporation, 184 Gasan Digital 2-ro, Geumcheon-gu, Seoul, Korea
*jhkim4198@sae-an.co.kr

1. Introduction

The methods for evaluating the nuclide inventory present on the inner surface of component subject to decommissioning NPP are an indirect measurement method that collects and measures a sample that can prove the representativeness of component subject to decommissioning, and a direct measurement method that measures using ISOCS (In Situ Object Counting System) on the external surface of a component subject to decommissioning, and MicroShield computer program that estimates the nuclide inventory on the inner surface of component using the dose rate of a component subject to decommissioning and the radioactivity of the sample[1].

In this study, the nuclide inventory was evaluated by ISOCS for the SG crossover legs in Kori unit 1, which was permanently shutdown on June 18, 2017. And the contact dose rate calculated by inputting the nuclide inventory evaluated by ISOCS into the MicroShield computer program was compared with the contact dose rate measured directly by survey meter.

2. Materials and Methods

2.1 ISOCS

ISOCS consists of a portable HPGe detector, a geometry composer computer program for calculating detection efficiency, portable lead shields, etc., and the detection efficiency of the detector is calculated by modeling the measurement object as a radiation source. In addition, ISOCS allows quantitative evaluation of nuclides and radioactivity is possible regardless of the size of the measurement object. Portable HPGe detector of ISOCS used in this study is as follows[2,3].

- Company: CABERRA
- Detector Model: GC2018
- Relative Efficiency: ≥ 20%
- Resolution: ≤ 1.8 keV (^{60}Co 1332 keV)

2.2 MicroShield Computer Program

The MicroShield computer program uses 16 fixed geometry models for radiation shielding evaluation of point sources, line sources, and volume sources using the point kernel method. The basic concept of the point kernel method is to divide the volume source into a large number of small point sources and regard each as a point source, and add up the respective contributions. MicroShield computer program has a built-in dose-radiation conversion program, so that the radioactivity can be inferred for the energy fraction of each nuclides[4,5].

2.3 Measurements Methods

The reasons for selecting the SG crossover legs in Kori unit 1 as the nuclide inventory measurement point are that the contact dose rate is the highest in reactor coolant system loop, and the field conditions for ISOCS measurement are relatively better than other measurement points. In addition, a lead shielding was installed so that the dead time of the detector was less than 5%. The ISOCS geometry model of the SG crossover legs is shown in Figure 1.

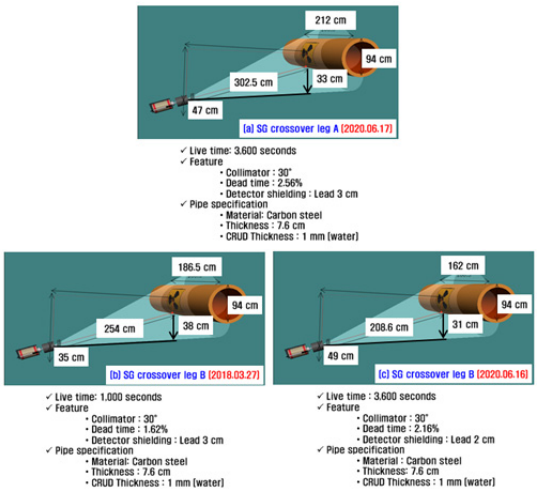


Fig. 1. ISOCS geometry model of the SG crossover leg A and B.

The verification of the nuclide inventory of the SG crossover legs measured and analyzed by ISOCS was verified by the relative deviation between the contact dose rate calculated by inputting the nuclide inventory evaluated by ISOCS into the MicroShield computer program and the contact dose rate measured directly by survey meter. The calculation formula is as follows.

$$RD = \frac{|\text{MicroShield Calculation} - \text{Measured}|}{\text{MicroShield Calculation}} \times 100\% \quad (1)$$

3. Results and Discussions

3.1 Nuclide Inventory

Table 1 and Fig. 2 shows the nuclide inventory and gamma spectrum of the SG crossover legs in Kori unit 1. In the case of the SG crossover leg B, ^{58}Co, ^{60}Co and ^{65}Zn were detected in March 2018, but only ^{60}Co was detected in June 2020. And the ^{60}Co radioactivity was 1.12×10^{70} Bq/cm^3 in March 2018, and 5.50×10^{6} Bq/cm^3 in June 2020, which decreased by about 49.1%.

Table 1. Nuclide inventory of the SG crossover leg A and B

Nuclide	Half-life	Radioactivity		
		SG crossover leg A	SG crossover leg B	
		June 2020	March 2018	June 2020
^{58}Co	70.86 d	N/D	1.40×10^{6} Bq/cm^3	N/D
^{60}Co	5.271 y	2.79×10^{7} Bq/cm^3	1.12×10^{7} Bq/cm^3	5.50×10^{6} Bq/cm^3
^{65}Zn	244.3 d	N/D	1.07×10^{6} Bq/cm^3	N/D
Total		2.79×10^{7} Bq/cm^3		5.50×10^{6} Bq/cm^3

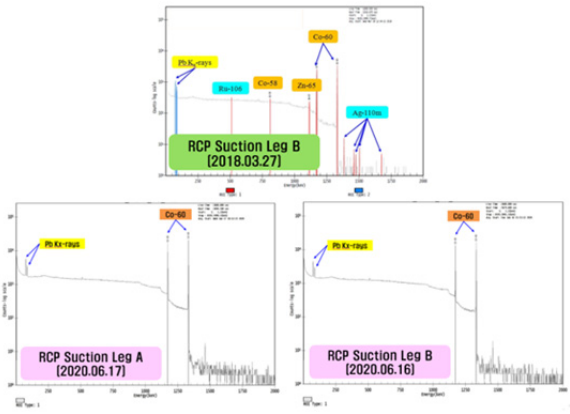


Fig. 2. Gamma spectrum of the SG crossover leg A and B.

3.2 Relative Deviation

The contact dose rates calculated by the MicroShield computer program for the nuclide inventory of the SG crossover legs measured in June 2020 were evaluated as 4.91 mSv/h and 0.95 mSv/h, respectively. And the contact dose rates measured directly by survey meter are 4.1 mSv/h and 1.0 mSv/h, respectively. Therefore, the relative deviations of SG crossover legs A and B were evaluated as 16.5% and 5.3%, respectively.

4. Conclusion

In this study, the nuclide inventory was evaluated by ISOCS and MicroShield computer programs for the SG crossover leg A and B in Kori unit 1. ^{58}Co, ^{60}Co and ^{65}Zn were detected in March 2018, but only ^{60}Co was detected in June 2020. This is thought to be because the radioactivity of some nuclides was attenuated below the background level of the measurement space due to the inherent half-life of the nuclides. ISOCS has not been able to perform measurements at many points, due to the limited equipment mobility and space utilization. In the future, it will be performed to measure the radioactivity inventory at more measurement points using CZT (CdZnTe) detector, which is advantageous for mobility and space utilization.

Acknowledgments

This work was supported by the Korea Institute of Energy Technology Evaluation and Planning (KETEP) and the Ministry of Trade, Industry & Energy (MOTIE) of the Republic of Korea (No. 20191510301310).

REFERENCES

[1] H. TOUBON. B. NOHL, S, LEFEVRE, M. CHIRON, K. BOUDERGUI, P. PIN, New Methodology for Source Location and Activity Determination in Preparation of Repairing or Decommissioning Activities, IRPA 2006 15-19 May 2006, Paris, France.
[2] CANBERRA, Model S573 ISOCS Calibration Software Technical Reference Manual, (2012).
[3] CANBERRA, Genie 2000 Spectroscopy Software Operation Manual, (2013).
[4] Grove Software, "MicroShield® Computer Program (ver. 10.03)", (2015).
[5] Grove Software, "MicroShield® User's Manual", (2015).

Integration of Soil Washing and Water Treatment Techniques for Separation of Radioactive Elements From Soils Impacted by Nuclear Power Plants

Yongju Choi*, Jihyeon Jung, Hojae Song, Seonyoung An, Seoyoung Choi, Jong Kwon Choe, and Kyoungphile Nam
Seoul National University, 1 Gwanak-ro, Gwanak-gu, Seoul, Republic of Korea
*ychoi81@snu.ac.kr

1. Introduction

Soils near nuclear power plants (NPPs) under operation or those at decommissioned NPP sites are often found to contain radioactive elements, such as ^{137}Cs, ^{90}Sr, ^{60}Co, at unacceptable levels. However, an efficient and cost-effective technology for soil decontamination is not currently available in practice. This framework should include not only a mainstream process for soil treatment but also a sidestream process to deal with wastes (e.g., washwater produced from soil washing). This study is aimed to design a framework that integrates soil washing and washwater treatment processes with a potential to exhibit feasibility in practical applications. Challenges involved in the integration of the two processes are identified and discussed.

2. Materials and methods

2.1 Materials

The current experimental work was conducted using non-radioactive isotopes of Cs, Cr, and Co with an assumption that different isotopes of the same element behave almost the same under the experimental conditions employed in the work. A soil sample was collected at a location adjacent to a former NPP site in Korea. The sample was found to show Cs, Sr, and Co concentrations of 1.16, 90.11, and 10.18 mg/kg, respectively, which are all significantly higher than the background concentrations of the elements previously reported for Korean soils.

2.2 Overview of Laboratory Experiments

Soil washing was conducted by agitating the soil sample with deionized water or an aqueous solution of EDTA, citric acid, oxalic acid, phosphoric acid, or calcium chloride. Various reagent concentrations, liquid-to-solid ratios, and washing durations were tested.

For washwater treatment, chemical coagulation, chemical coagulation with adsorbent supplement, and adsorption were studied. Alum was used as a coagulant and zeolite and ion exchange resin as adsorbents. Water laden with Cs, Cr, and Co was prepared with a variety of compositions to study possible composition of washwater produced from soil washing processes. Coagulant and adsorbent dose and contact time were also varied as they should considerably impact the treatment efficiency.

3. Results and Discussion

3.1 Soil Washing

The study soil showed relatively uniform concentration distribution across its particle size range. In addition, washing with deionized water did not result in significant reduction in solid-phase concentration of Cs, Cr, and Co. Accordingly, it was concluded that the study soil cannot be decontaminated at a reasonable efficiency if a soil washing process relies only on physical mechanisms (e.g., particle separation, abrasion). Soil washing experiments with various aqueous reagents showed less than 50% removal efficiencies for all cases except for a case that used 1 M $CaCl_2$ solution for Sr removal. A high removal efficiency of 68.2% observed for this exceptional case can be attributed to the high propensity of Ca^{2+} to replace Sr^{2+} bound to soil particles because of the chemical similarity of Ca^{2+} and Sr^{2+}.

3.2 Wastewater Treatment

Alum coagulation was effective at removing suspended particles from washwater. Particle removal efficiencies of greater than 99.5% was achieved when water containing 2000 mg/L of <38 μm-sized soil particles was dosed with 30 and 60 mg/L alum. However, the alum treatment itself was not effective at removing dissolved-phase Cs, Sr, and Co.

When zeolite was supplemented in the alum coagulation process, significant reduction in the dissolved-phase Cs, Sr, and Co was observed. For example, at a zeolite dose of 0.5 g/L and alum dose of 10 mg/L, removal efficiencies of 91.15%, 99.93%, and 99.96% were observed for dissolved concentrations of Cs, Sr, and Co, respectively. Interestingly, the removal efficiency of the dissolved-phase elements using this hybrid water treatment process decreased with an increased dose of alum, which can be attributed

to the acidity of alum. At low pH, the zeolite surface becomes less negatively charged or turns to be positive, which reduces the electrostatic attraction between the adsorbent surface and the cationic contaminants.

Zeolite and a commercial ion exchange resin (CMP 28) showed excellent adsorption capacity of the study elements, with maximum adsorption capacities of 2×10^5 mg/kg or greater. However, the adsorbents showed only moderate selectivity toward Sr^{2+} in the presence of Ca^{2+}. This result implies that it would be highly challenging to treat washwater from a soil washing process employing $CaCl_2$ reagent via adsorption, either as a process following coagulation or coagulation supplemented with adsorbents.

4. Conclusion

This study identifies important design principles for a decontamination process of soils impacted by nuclear power plants. First, it should be examined how radioactive elements are bound to soil particles: based on the concentration distribution among different soil particle size range and the resistance of radioactive elements against reagent-free washing, it should be determined whether reagents are to be used or not. Once the use of reagents is determined to be necessary, selection of reagents should be made under consideration of the efficiency of the sidestream process of washwater treatment. Coagulation process, which is employed to remove particulates from washwater, should also be designed under consideration of its impact on adsorptive removal of dissolved residual contaminants, which may be combined with or follow the coagulation process.

Radioactivity Concentration Derivation for Conditional Recycling of Decommissioning Wastes

Kiwon Kang, Hyeongjin Byeon, Eunyeong Choi, and Jaeyeong Park*
Department of Nuclear Engineering, Ulsan National Institute of Science and Technology, 50 UNIST-gill, Eonyang-eup, Ulju-gun, Ulsan, 44919, Republic of Korea
*jypark@unist.ac.kr

1. Introduction

In Korea, A clearance level of radioactive waste in the International Atomic Energy Agency (IAEA) safety guide No. RS-G-1.7[1] has been applied without a consideration of specific domestic situation. However, the clearance level in IAEA report were the most conservative value among the values calculated in all scenarios such as landfill, melting, and housing no matter what the characteristic of radioactive waste is.

In this study, conditional clearance level was analyzed for some scenarios that assumed regulated uses of recycled radioactive waste in limited area. By considering domestic exposure situation during the recycling process, conditional clearance level was derived through dose assessment for each situation.

2. Dose assessment methodology

The recycling scenarios of radioactive waste which can limit access of public are listed up in Table . All products in scenarios are assumed to be used only in the nuclear industry under regulation.

Table 1. Conditional recycling scenarios

No	Material	Description	Exposure pathway
M1	SUS304	200L drum	External (Worker)
M2		320L drum	
M3		Iso-1496 1AA	
M4	Ductile cast iron	KBS-3 SNF cask	
M5	Iron	Rebar for disposal facility	
C1	Concrete	Underground silo drum disposal container	External Inhalation Ingestion (Worker)
C2		Silo backfill	
C3		Near surface disposal facility	
C4		Radiation control area building aggregate	

Scenario in cement recycling consists of recycled cement components manufacture, transportation, and utilization. Internal exposure such as inhalation and ingestion was considered only at the manufacturing scenarios whereas it was not considered at transporting or using the finished product stages because radioactive dust is less likely to occur at that process. So, dose assessment was conservatively conducted using the exposure scenario of worker in the manufacturing stage.

Scenario in metal waste recycling include exposure of workers who carry metal deregulated waste, are on duty at melting facilities, and handle final recycled products. Through dose assessment in three scenarios, the final conditional clearance level was derived using the dose in the scenario showing the highest dose.

For dose assessment, internal exposure coefficients for workers are taken from the International Commission on Radiological Protection (ICRP) publication 68[2]. The dose assessment model and conservative values of essential parameters are derived from IAEA safety reports series No. 44 [3].

2.1 External exposure (Microshield pro)

The dose conversion factor of external dose is determined by various factors such as the geometry of the source, the shielding-absorption effect of the source itself, and distance from the source. So, the external dose conversion factor was calculated using Microshield pro Version 12[4] which is the commercial code developed mainly for dose assessment of photon and gamma rays. After modeling the geometry and composition of recycled products in Table using a program by referring to the LILW management implementation plan of Korea Radioactive Waste Agency (KORAD)[5], the dose conversion factor of external exposure per unit activity concentration was derived.

2.2 Target radionuclide

Each scenario was analyzed with the 13 radionuclides (^{3}H, ^{14}C, ^{59}Fe, ^{58}Co, ^{60}Co, ^{59}Ni, ^{63}Ni, ^{90}Sr, ^{94}Nb, ^{99}Tc, ^{129}I, ^{137}Cs, ^{144}Ce) considered domestic Nuclear Safety Commission Notification

Table 2. Comparison of IAEA clearance level with conditional clearance level from conditional scenarios

Nuclide	Decay mode	IAEA Clearance level [Bq/g]	Ratio (Clearance level of conditional scenario / Clearance level of IAEA)								
			M1	M2	M3	M4	M5	C1	C2	C3	C4
^{3}H	β	100	110.25	110.25	110.25	110.25	110.25	70.63	70.63	70.63	70.63
^{14}C	β	1	724.64	724.64	724.64	724.64	724.64	391.88	391.88	391.88	391.88
^{55}Fe	ε	1	1.75	1.75	1.75	1.75	1.57	1.57	1.57	1.57	1.57
^{58}Co	ε,γ	1	13.70	13.70	5.45	1.39	0.94	1.15	1.30	0.58	0.36
^{60}Co	β,γ	0.1	10.59	10.59	4.92	1.13	0.81	0.98	0.74	0.44	0.30
^{59}Ni	ε	100	79.37	79.37	79.37	79.37	79.37	67.31	67.31	67.31	67.31
^{63}Ni	β	100	33.44	33.44	33.44	33.44	33.44	26.82	26.82	26.82	26.82
^{90}Sr	β	1	16.39	16.39	16.39	16.39	16.39	12.63	12.63	12.63	12.63
^{94}Nb	β,γ	0.1	12.59	16.56	6.62	1.66	1.13	1.23	1.31	0.69	0.44
^{99}Tc	β	1	632.91	632.91	632.91	632.91	632.91	429.24	429.54	429.26	428.84
^{129}I	β	0.01	450.45	450.45	450.45	450.45	450.45	325.56	430.59	404.14	392.21
^{137}Cs	β,γ	0.1	37.69	45.87	20.10	5.28	2.48	4.31	5.41	2.14	1.18
^{144}Ce	β,γ	10	5.79	9.52	4.28	1.14	0.91	0.84	0.97	0.43	0.27

3. Result and discussion

As presented in 3. Result and discussion, significant ratio differences in conditional clearance level are shown depending on the radioactive decay mode of the nuclide. Since there is little effect of external exposure from beta-emitting radionuclides (e.g. ^{3}H, ^{14}C, ^{63}Ni,^{90}Sr, ^{99}Tc, and ^{129}I), the conditional clearance levels show a mitigated value of 10 to 700 times larger than clearance levels suggested by IAEA.

On the other hand, external radiation-dominant radionuclide which emits gamma-rays in the process of radioactive decay showed that the conditional clearance level was more conservative than the current regulations in some scenarios. Conditional clearance level of gamma-emitting radionuclide tends to represent more conservative values as the size of recycled product grow. However, given that the clearance level of IAEA is the logarithm rounded value of the original concentration in the maximum exposure scenario, it is considered as an understandable level.

4. Conclusion

In this study, the safety of each scenario was verified for recycled items containing beta or gamma nuclides. Upon recycling products under the regulation at limited area, the clearance level of beta-emitting radionuclides may be up to 700 times higher than the current standard. Even, in the case of gamma-emitting radionuclides, the mitigated concentration standards may be applied for specific scenarios like using a relatively small radioactive waste disposal container.

Recycled products considered in this study are finally disposed of at the radioactive waste disposal sites and those are systematically managed for several hundred years even after they are closed. So, it is cleared that recycled products are not exposed to the public and radioactive waste repositories could be used more efficiently.

As a further study, it is worthwhile to analyze the clearance level by sensitivity of parameter used at dose assessment and investigate efficient parameter for conditional scenario considering domestic working environment.

REFERENCES

[1] IAEA, “Application of the Concepts of Exclusion, Exemption and Clearance”, IAEA, Safety Guide No. RS-G-1.7, (2003).

[2] ICRP, “Dose Coefficients for Intakes of Radionuclides by Workers”, ICRP Publication 68, Ann. ICRP 24 (4), (1994).

[3] IAEA, “Derivation of Activity Concentration Values for Exclusion, Exemption and Clearance”, IAEA Safety report series No. 44, Vienna, (2005).

[4] Grove Software, Microshield Pro Version 12, User’s Manual Version 12, (2020).

[5] KORAD, “LILW management implementation plan, (2018).

Numerical Calculations for Performance Prediction of Ventilation Unit of Thermal Cutting System Developed for Kori Unit 1 Reactor Vessel Dismantling

Kyuho Chang*, Haewoong Kim, Kwangsoo Park, and Heedong Sohn
Doosan Heavy Industries & Construction, 22 DoosanVolvo-ro, Seongsan-gu, Changwon-si, Gyeongsangnam-do, 51711, Republic of Korea
*gyuho.jang@doosan.com

1. Introduction

To dismantle a radiologically activated reactor vessel, the reactor vessel must be cut to a size that can be stored in a disposal drum. In the past, radiologically activated reactor vessels were cut by applying underwater mechanical cutting methods, but recently, there have been cases in which reactor vessels are cut by flames in the air, mainly in countries advanced in decommissioning such as Germany. Although the method of thermal cutting in the air has advantages in terms of schedule and cost over the method of mechanical underwater cutting, there is a risk that pollution may spread to other wastes and workers in the decommissioning workspace if the fumes generated during thermal cutting of radioactive waste are not removed appropriately.

In this background, the performance of ventilation unit in thermal cutting systems is very important. In this paper, a case of performance prediction of ventilation unit using numerical calculations will be introduced.

2. Thermal Cutting System developed for Kori unit 1 Reactor Vessel Dismantling

2.1 Configurations of thermal cutting system

The thermal cutting system developed for Kori unit 1 reactor vessel dismantling consists of reactor vessel lifting tool, gentry crane, thermal cutting robot arm, shielding tent and ventilation unit. As shown in Figure 1 & 2, the fume generated during thermal cutting is introduced into the ventilation unit along the duct connected to the shielding tent due to the pressure gradient and flow rate developed by the centrifugal fan installed at the rear of the HEPA filter allows the fume from the shielding tent to enter the ventilation unit.

3. Numerical modeling & Procedure for Performance Prediction of Ventilation Unit

In this paper, numerical calculations were applied to predict the resistance curve of ventilation system. By comparing the calculated resistance curve with the rated flow and pressure of the centrifugal fan, the capacity of the centrifugal fan was assessed whether it is sufficient or not. The prediction of the resistance curve of ventilation unit was calculated using the commercial code ANSYS CFX version 16.2.

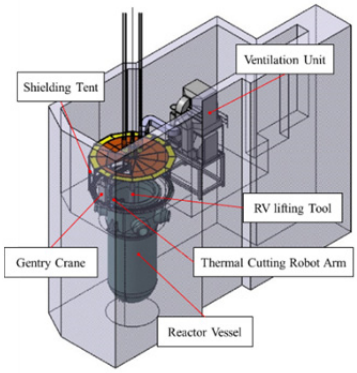


Fig. 1. Configurations of thermal cutting system developed for Kori unit 1 reactor vessel.

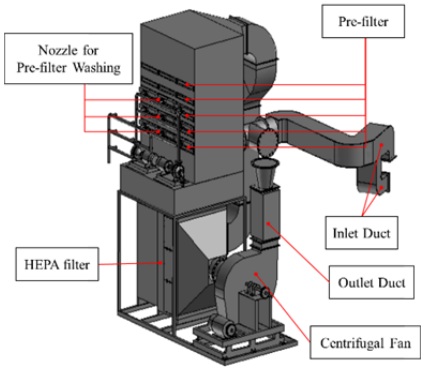


Fig. 2. Configurations of ventilation unit.

3.1 Modeling of ventilation unit for numerical calculations

To ensure the efficiency and accuracy of calculations, a hybrid type grid system was prepared that uses prism elements and tetrahedron elements. After creating triangular grids on the wall of the ventilation unit, 10 stage of prism-type boundary layer grids was created vertically on the surface. The first stage of the boundary layer grids was sufficiently clustered to the wall so that it was located in the viscous sublayer ($y^+<10$) so that the turbulence boundary layer

profile was not predicted too stiff when applying the standard k-ω turbulence model[1]. The inertia zone, excluding the boundary layer, generated tetrahedron grids. For efficient calculation, pre-filter and HEPA filter were modeled as porous media, and the resistance coefficients of porous media were obtained through trial and error so that the pressure drop through the porous medium calculated by numerical tests was equal to the pressure drop provided by the filter supplier.

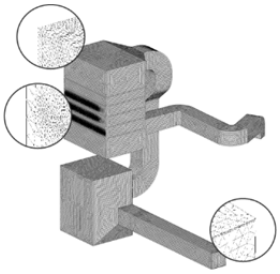


Fig. 3. Grid generations.

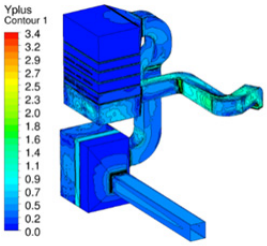


Fig. 4. y^+ distributions.

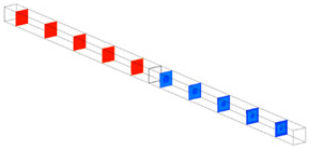


Fig. 5. Numerical tests for obtaining resistance coefficient of the pre-filter.

4. Numerical Calculation Results

4.1 Flow structures in ventilation unit

Because inertial resistance is dominant, the pressure-drop by the filter increased as the flow rate increased, and the resistance of the flow rate and the resistance of the filter resulted in a strong recirculation flow before the pre-filter and HEPA filter. It is observed that flow is uniformly distributed in cross section due to resistance of pre-filter and HEPA filter, and the pressure drop at each stage of pre-filter was same.

4.2 Performance prediction of ventilation unit

In Figure 8, the resistance curve of the ventilation unit predicted by numerical calculations and the rated operating point of the centrifugal fan were compared. Since the total pressure transferred by the centrifugal fan at the rated flow rate of the centrifugal fan is higher than that of the ventilation unit, it is expected that the capacity of the centrifugal fan is sufficient to maintain the negative pressure in the shielding tent.

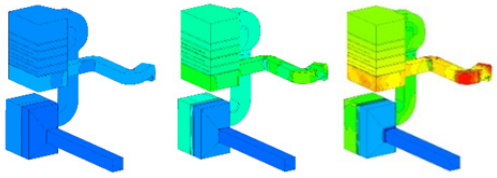


Fig. 6. Total pressure distributions on the ventilation unit wall (from left; Q/Q_{rated} = 0.3, 1.0, 1.5).

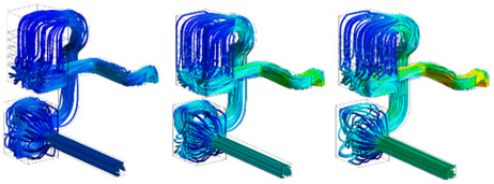


Fig. 7. Streamlines in the ventilation unit (from left; Q/Q_{rated} = 0.3, 1.0, 1.5).

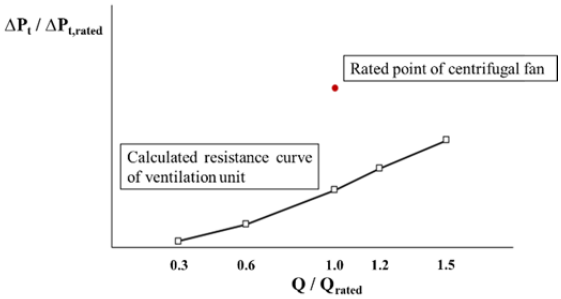


Fig. 8. Comparison of the calculated resistance curve of ventilation unit with rated point of the centrifugal fan.

5. Conclusion

In this paper, the resistance curve of the ventilation system was calculated using numerical calculation, the performance of the ventilation system was evaluated by comparing the calculated resistance curve with the capacity of the turbomachinery. As a result of calculation, it was shown that the performance design of the ventilation unit was done appropriately.

ACKNOWLEDGEMENT

This research was supported by a grant from Energy Technology Development Program Funded by Ministry of Trade, Industry and Energy of Korean Government (No. 20161510300430).

REFERENCES

[1] Wilcox, D.C., "Multiscale model for turbulent flows", In AIAA 24th Aerospace Sciences Meeting. American Institute of Aeronautics and Astronautics, (1986).

Analysis of Plasma Cutting Process Using High Speed Camera and Cutting Signals

Dae-Won Cho*, Dong-Hyun Kim, and Jeong Suh
Busan Machinery Research Center, Korea Institute of Machinery and Materials, Busan, 46744
*dwcho@kimm.re.kr

1. Introduction

There is various cutting method to cut the metal materials such as plasma cutting, bandsaw cutting and laser cutting [1-3]. Among the various cutting method, the plasma cutting is the widely used because the cutting speed relatively high and the sensitivity is relatively small. This study conducted a study on plasma arc cutting process monitoring through high-speed camera and waveform analysis. The independent variables were the cutting speed and current, and the analysis was performed on the cutting waveform such as arc plasma characteristics and the resulting voltage according to the change of the corresponding value.

2. Main Title

2.1 Experimental setup

Fig.1 shows schematics of the plasma cutting process which recorded the images from the high speed camera and the synchronized waveforms such as current and voltage. The material is SUS304 steel with 20mm thickness.

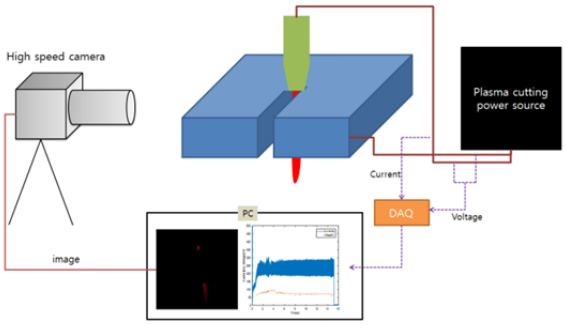


Fig. 1. Schematics of the plasma cutting process.

2.2 Experiment conditions

This study designed the input variables cutting speed (3 levels: 100mm/min, 150mm/min, 200 mm/min) and plasma current (3 levels: 150A, 190A, 225A) .

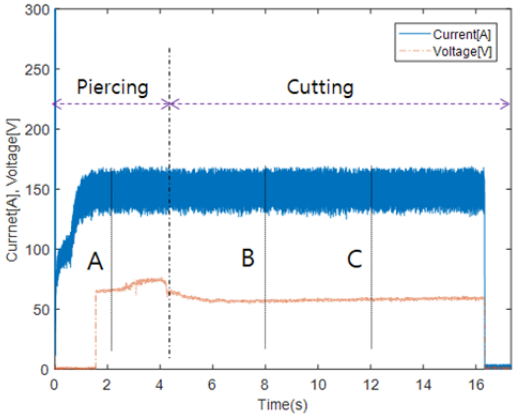


Fig. 2. Waveforms of current and voltage.

3. Results and discussion

This study could compare the high speed images with the synchronized waveform; therefore, it is possible to compare the detail images and the signals. In the beginning stage, the cutting torch maintained the position and do not move in 2 to 4 seconds because, stationary cutting torch can sufficiently blow the molten pool downward by arc forces and gas pressure. The measured cutting signals such as current and voltage varied in the stationary section (piercing) as shown in Fig. 2. The current value increased and fluctuated in the stationary section and then it became stable and the only vibrated signals are measured.

On the other hand, the voltage values increased in the beginning section and the intensity of arc plasma is relatively stronger and bright at A section in Fig.3. However, the voltage value and the arc plasma light can be stable after the welding torch moving as shown in Fig. 3

Fig. 4 shows the arc plasma for different cutting speed. As the cutting speed increases, the difference of cutting length for top and bottom surface also increases because the high cutting speed induced the weak downward molten pool flow.

The measured voltage value is highly related with the arc plasma length and it is also related with the unstable arc shape such as double arcing. This study investigated the detail cutting signals along with the high speed images, kerf of top and bottom surface.

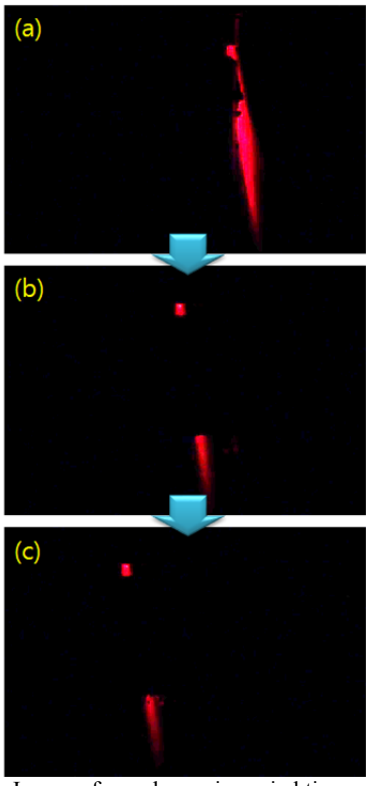
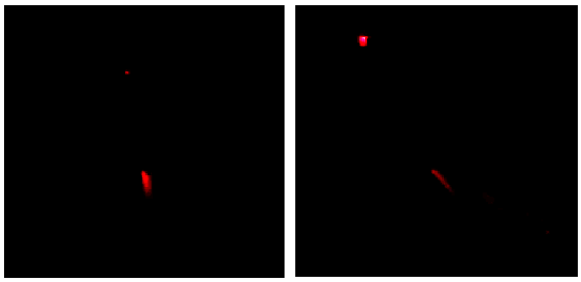


Fig. 3. Image of arc plasma in varied time period.


(a) 150A, 100mm/min (b) 150A, 200mm/min
Fig. 4. Image of arc plasma for different cutting speed.

4. Conclusion

In this study, changes in kerf width, cutting length difference according to current, cutting speed plasma cutting were confirmed.

Acknowledgements

This work was supported by the National Research Foundation of Korea (NRF) grant funded by the Korean government (MSIP: Ministry of Science, ICT) (No.2017M2B 2B1072888).

REFERENCES

[1] P. Hilton, D. Lloyd, "Advances in Decommissioning Using Laser Cutting", WMS Journal, 1(4), (2016).
[2] F. W. Bach, H. Steiner, G. Schreck, G. Pilot, "Analysis of results obtained with different cutting techniques and associated filtration systems for the dismantling of radioactive metallic components", Commission of the European Communities, (1993).
[3] P.E. Lainetti, Cutting techniques for facilities dismantling in decommissioning projects, International Nuclear Atlantic Conference, (2011).

Planning and Design of Decommissioning Site Remediation Focusing on Radionuclide and Site Media Characteristic

In-Ho Yoon*, Sung-Man Kim, Ilgook Kim, Chan-Woo Park, Hee-Man Yang, Youngho Sihn, Changyun Roh, and Sang-Bum Hong
Decontamination and Decommissioning Research Division, Korea Atomic Energy Research Institute (KAERI)
1045 Daedeokdaero, Yuseong-gu, Daejeon 305-353, Republic of Korea
*ihyoon@kaeri.re.kr

1. Introduction

Serious environmental contamination with radionuclides resulted from the Fukushima Daiichi nuclear accident in Japan, and a very large amount of soil in a wide area became contaminated [1]. In addition to this critical accident, unintended leakages of radioactive substances from various nuclear facilities have also contaminated the environment, and most of the radio-contaminated soils are subject to low-level wastes [2]. Remediation of radio-contaminated soil has been attempted with various techniques, such as soil washing, phytoremediation, thermal treatment and electroremediation. Although considerable progress has been made in the development of soil remediation techniques for some radionuclides such as U and Co, the removal of radioactive cesium(Cs) from soil has been relatively inefficient or has required high energy consumption owing to the strong and irreversible interaction of Cs with 2:1 clay minerals in the soil [3]. The efficient and economical environmental remediation requires detailed information on site media characteristics. It is necessary to derive the concept of soil restoration considering the mobility of radioactive contamination according to site media characteristics.

2. Safety evaluation for site reuse

Release criteria was established for investigating and evaluating residual contamination for site release in environmental remediation of nuclear facilities. In addition, the Derived Concentration Guideline Level (DCGL) of each radionuclide shall be evaluated using site characteristics. A computer code (RESRAD) is used to assess site safety. In order to ensure reliability of assessment, the sensitivity analysis should be preceded to select input factors that reflect the site characteristics. The Final Status Survey (FSS) procedure for site release is standardized for each facility. In addition, it is needed for the integrated management of measurement and evaluation data. The assessment should be carried out with accurately measurement system for surveying the residual contamination in site.

3. Planning and design of decommissioning site remediation focusing on radionuclide and site media characteristic

The geochemical properties of the site medium are analyzed, such as the size distribution, formation, organic/inorganic matter, moisture content, and etc. in the soil in nuclear facility sites. In addition, it is necessary to assess the mobility in accordance with the distribution coefficient (K_d) of radionuclides. The efficient strategy for site-specific remediation can be established through the mobility of radionuclides according to site media characteristics. We can select the optimization of site remediation and evaluate the amount of generated waste and the disposal cost through radionuclide and site media characteristic.

4. Conclusions

Through the mobility of radionuclides according to site media characteristics, the efficient strategy for site-specific remediation can be established. In the future, it is necessary to develop the site remediation model including cost models and radionuclide release. Through this, it is expected that it will be used to select more optimized remediation technologies in the decommissioning planning of nuclear power plant.

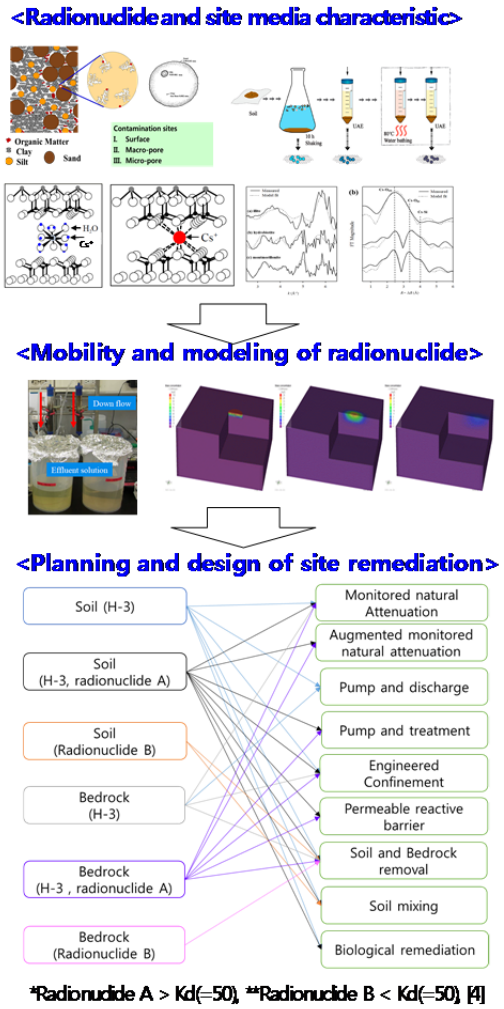


Fig. 1. The procedure of the selection of remediation method.

REFERENCES

[1] Yamamoto, T. J. Nucl. Sci. Technol., 49, 1116-1133, (2012).

[2] Zhu, Y., Shaw, G. Chemosphere, 41, 121-128, (2000).

[3] Park, C.W. Kim, B.H. Yang, H.M. Seo, B.K, Lee, K.W. J. Hazar. Mater. 327, pp 127-134. (2017).

[4] EPRI, Groundwater and Soil Remediation Guidelines for Nuclear Power Plants, Technical Report, (2011).

5분과

제염해체 (Poster)

Pre-Decommissioning Activities for the Decommissioning of CANDU-6 (Canadian Case)

Kwangsoon Choi*, Mugap Shin, and Jaihoon Jung
KEPCO E&C, 269 Hyeoksin-ro, Gimcheon-si, Gyeongsangbuk-do, Republic of Korea
*kschoi@kepco-enc.com

1. Introduction

This paper summarizes the preliminary decommissioning activities in the CANDU (CANada Deuterium Uranium)-PHWR(Pressurized Heavy Water Reactor) decommissioning waste management review report developed through technical cooperation with CNL(Canadian Nuclear Laboratories).

2. Reference Case

2.1 Design

This report focuses on a generic single unit 600 MW(e) CANDU-PHWR. There are three CANDU 6 reactors that were built and started up around the same time as Wolsong-1 : Point Lepreau, Embalse, Gentilly-2. Therefore, above Canadian units are a suitable match to Wolsong-1 in terms of reactor design and time of construction and connection to the grid.

2.2 Operating History

The typical design life of a CANDU reactor, before refurbishment, is about 30 years. It is assumed that the reference unit has been operated for 25 years under a constant neutron flux (100% capacity) and there has been a decay period of 5 years.

2.3 Refurbishment

For the reference case, no refurbishment activities have been considered nor has the waste generated been included.

3. Pre-Decommissioning Activities

3.1 Decontamination

Decontamination will be required if the gamma fields associated with the out-of-core portions of the PHTS (Primary Heat Transport System) are high or if the system is contaminated with fission products and actinides as a result of fuel defects during the life of the reactor.

The expected wastes generated from decontamination include: oxide waste from mechanical decontamination, spent ion-exchange resin, compactable waste, non-compactable waste, and spent liquid filters [1][2].

3.2 Defueling and Storage of Spent Fuel

Management of spent fuel is an important part of decommissioning. When the reactor is shutdown, it is assumed that there is spent fuel in the storage pool generated from the last 10 years.

Table 1. Waste Generation froe Decontamination

Waste Description	Volume	Remarks
Oxide waste	3 m3	From mechanical decontamination
Spent ion exchange resin	60-75 m3	
Compactable waste	26 m3	Volume is before compaction.
Non-compactable waste	1.2 m3	
Spent liquid filters	0.08 m3	

3.3 Draining of Tritiated Heavy Water Systems

The tritium concentrations referenced in this paper are calculated using next assumption : the moderator system is continuously detritiated using the Wolsong Tritium Removal Facility, which keeps the tritium concentrations much lower than 10 Ci/kg. At end of life, the total inventory of tritiated heavy water will need to be stored outside the reactor and auxiliary buildings, in stainless steel drums in a purpose-built facility. The concentration of tritium in the heavy water is much higher than the international drinking water standard of 10,000 Bq/L and it will need several centuries to meet the limit considering the half-life of tritium of 12.3 years.

4. Remaining Total Inventory

After the spent fuel and tritiated heavy water (D2O) have been removed, the systems have been decontaminated and all radwaste has been removed off site, the remaining activity will be mainly in the reactor and building structures that have been activated such as pressure tubes, the reactor vessel and biological shielding. The total inventory of spent fuel, tritiated heavy water and the expected radiological inventory left in the

structures are summarized in Table 1. As shown in the table, the removal of all irradiated fuel, and tritiated heavy water (and after decontamination) results in a reduction of >99.9% in the radioactivity inventory present after reactor shutdown.

Table 2. Radiological Inventory following Pre Decommissioning compared to Total Radiological Activity

	Ci	Bq	%
Spent fuel	8.10E+08	3.00E+19	98.6%
Tritiated D2O	1.11E+07	4.10E+17	1.3%
Structures	9.14E+05	3.38E+16	0.1%
Total	8.22E+08	3.04E+19	100%

5. Conclusion

In Korea, radioactive waste generated during pre- decommissioning activities are not classified as decommissioning waste. However, considering domestic conditions, those are likely to be processed during the decommissioning phase. Therefore, the Canadian case can be referenced for Wolsong unit 1 Decommissioning Project.

REFERENCES

[1] G. Xu, et al. “A Methodology for Estimation of Resin-Waste Volume Generated from Decontamination of Primary Heat Transport System Prior to Retube”, 153-79140-401-000/ACB-06-031, (2006).

[2] C. F. Wong et al., “Identification and Characterization of Operational Wastes Generated from CANDU Retube”, 153-79000-TN-001, Rev0, (2006).

A Study for Maximizing Detection Efficiency and Image Resolution in Nuclear Power Plant

Changyeon Yoon[1] and Taewoong Lee[2,*]
[1]KHNP Central Research Institute, 70, Yuseong-daero 1312beon-gil, Yuseong-gu, Daejeon, Korea
[2]Global Institute of Technology, KEPCO KPS, 211, Munhwa-ro, Naju-si, Jeollanam-do, Korea
*superdapo@kps.co.kr

1. Introduction

The conventional scintillator detectors which consist of lutetium series such as LSO, LYSO or LGSO are widely used in various fields. These scintillators have high atomic number and density, and hence, their detection efficiencies are very high. However, the pixel sizes of scintillators limit their positional resolution which is directly related with image resolution. In order to compensate this problem, pixelized CZT semiconductor detector which has high energy and position resolution was used. Since the atomic number and density of CZT were relatively lower than those of scintillators, detection efficiency of CZT was low, as well. However, since pixelized CZT can track the interaction position inside detectors, both of photoelectric events and Compton scattering can be used for effective interaction. Therefore, the detection efficiency improves significantly[1]. In this research, the performance of CZT semiconductor with Compton scattering was compared with that of scintillators.

2. Method

The Monte Carlo simulation was run by GATE 5.0. The atomic ratios of LYSO and LGSO were $Lu_{1.9}Gd_{0.1}SiO_5$ and $Lu_{0.4}Y_{1.6}SiO_5$[2]. The voxel sizes of LYSO and LGSO were 7 mm × 1.5 mm × 1.5 mm. A water cylinder whose radius and height were 10.39 mm and 1.5 mm was surrounded by forty scintillators.

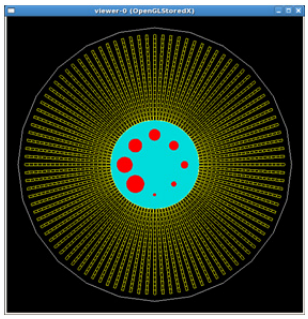


Fig. 1. Position and size of sources.

CZT consisted of one hundred 20 mm × 0.5 mm × 1 mm detector module made of 1 mm × 0.5 mm × 1 mm voxel. Size of water cylinder was same for scintillators. Eight disk sources with various radii from 0.3 mm to 2.05 mm with 0.25 mm step. (cf. Fig. 1).

For Compton technology, the sequence of Compton scattering events followed by the photoelectric event was analyzed by using Compton scattering formula.

The image reconstruction method was filtered backprojection and three kinds of evaluation methods were used. The first method was the comparison of reconstructed images using photoelectric events only and those using both photoelectric events and Compton scattering events. The second method was visual evaluation using various source sizes explained above. The third method was the comparison of relative standard deviation (RSD) for the largest sources for each detector system.

3. Results

Table 1. Detected counts for each detector system.

	LYSO PET	LGSO PET	CZT PET
Photoelectric events only	311078	1499760	311325
Photoelectric & Compton scattering	354345	1665079	369375

Table 1 showed the detected counts for LYSO, LGSO, and CZT system. For all system, the detection efficiency increased when both of photoelectric events and Compton scattering events were used as effective events. The detection efficiency of LGSO system was almost five times higher than other systems since the ratio of the lutetium whose atomic number and density were the largest among the elements in the detectors. The detection efficiency of CZT was almost same with that of LYSO since the ratio of the lutetium was only 0.4 for LYSO system.

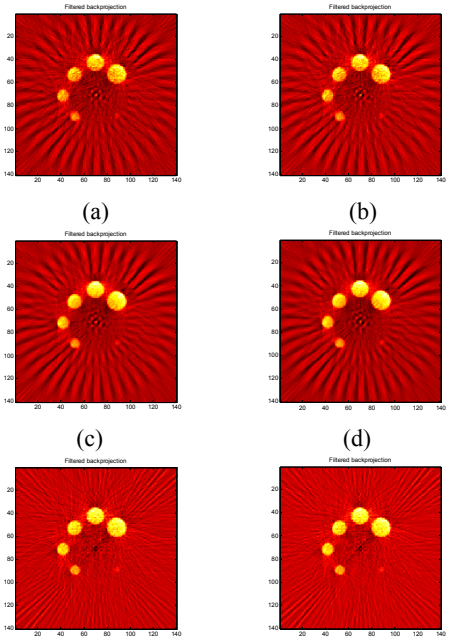


Fig. 2. Filtered backprcjection images.
(a) LYSO system with photoelectric events only
(b) LYSO system with photoelectric and Compton
(c) LGSO system with photoelectric events only
(d) LGSO system with photoelectric and Compton
(e) CZT system with photoelectric events only
(f) CZT system with photoelectric and Compton.

As shown in the Fig. 2, the images reconstructed by using both photoelectric events and Compton scattering events showed less noise than those by using photoelectric events only. The images of LGSO showed less noise than those of LYSO since the detection efficiency of LGSO was much higher than that of LYSO. In the viewpoint of image resolution, the image of CZT system showed all sources while other systems could not showed the smallest source.

Table 2. RSD of each detector system.

	LYSO PET	LGSO PET	CZT PET
Photoelectric events only	0.0687	0.0683	0.0706
Photoelectric & Compton scattering	0.0678	0.0677	0.0701

The RSD of 10×10 pixels in the largest source of each detector was shown in Table 2. For all system, the RSDs with Compton technology were lower than those of conventional system. In other words, the quality of reconstructed images for every detector systems were improved by using Compton technology. The RSD of LGSO was the highest among detectors due to its high detection efficiency.

4. Conclusion

For all material, the efficiency with Compton scattering was always high, and hence the image quality was improved by using Compton technology. CZT detector showed best image resolution by visual inspection and LGSO detector showed the highest detection efficiency. In addition, noise of reconstructed image for every detector systems were almost similar.

In conclusion, the Compton technology was effective to all detector systems, and hence, the image resolution of CZT detector was the highest. Therefore, CZT semiconductor detector with Compton technology is the most effective system for nuclear power plant.

REFERENCES

[1] Changyeon Yoon, Wonho Lee, Taewoong Lee, “Simulation for CZT Compton PET - Maximization of the Efficiency for PET by Using Compton Event”, Nucl. Instr. And Meth. A (2011).

A Study on the Dose Assessment of Workers in the Transition Period

Jong Soon Song and Hak Yun Lee*
Chosun University
*leehakyun1@naver.com

1. Introduction

A permanently shut down nuclear plant must be decommissioned through immediate dismantling or deferred dismantling. Immediate dismantling is performed after an average of five years from the permanent shutdown. During the transition period between the time of the permanent shutdown and the start of dismantling, decontamination work is performed to remove elements that interfere with dismantling and efficiently manage the exposure of dismantling workers. Since most works are carried out near highly contaminated devices because of the characteristics of tasks during the transition period, it is necessary to study the impact of exposure of workers in advance. Therefore, this study analyzed the tools and calculations to assess the impact of exposure in the working environment during the transition period. The analysis result can be used as the optimal indicator to ensure worker safety in the continuous nuclear plant decommissioning market expected in the future.

2. Transition Period

2.1 Work Scenario

Tasks performed during the transition period of nuclear plant decommissioning include decontaminating and removing elements that can interfere with dismantling and lowering radiation levels. TRS No. 420 (Transition from Installations, Technical Report Series No. 420) published by IAEA classified nine workloads during the transition period. Table 1 shows the activities during the transition period, as specified by IAEA.

Table 1. Transitional work activities

Workload during Transition period
Removal of Spent Fuel
System Cleanout Operation
Treatment, Conditioning, Storage and/or Disposal of Waste
Decontamination or Fixing of Contamination
Characterization & Inventory of Radioactive Materials
Consideration of Systems
Preparation of a Facility's rooms and Buildings
Protection from External or Internal Events
Removal of Minor Components

If the tasks using remote control and robots are conservatively excluded, radiation exposure is likely in all activities of the above nine workloads. In particular, a significant exposure is expected in the case of decontaminating large structures, such as the nuclear reactor and steam generator.

3. Exposure Evaluation Method

Dose assessment is divided into external and internal exposures. This study covers the external exposure only, excluding the internal exposure that occurs through breathing. External exposures are divided into direct exposure directly from equipment or pipes that contain or are contaminated with radioactivity and submersion that is the exposure by entering an airborne radioactive area contaminated with inert gases or other nuclides. The point kernel method is the leading method for assessing external exposure. This section describes the point kernel method and the software applying it.

3.1. Point-Kernel Method

The Point-Kernel method is an approximate but efficient approach for evaluating photon responses in shielding analyses. However, the method lacks rigor, and it has limitations in high precision cases. Nevertheless, the method is still successfully applied in design and safety analysis works. When the method is correctly applied, it can provide fairly good results for gamma radiation.

The main idea of Point-Kernel method is that a radiation source can be seen as consisting of a series of discrete elementary cells (point kernels), and the dose rate at the detecting point is composed of the contributions of all point kernels to the detecting point. The total dose rate from a point kernel isotropic with energy, E, to the detecting point is given by:

$$D(r,E) = C(E)S(E)B(E,t(E))\frac{e^{-t(E)}}{4\pi r^2} \qquad (1)$$

3.2. VISIPLAN software

VISIPLAN transmits the results of radiation dose computation and 3D data by using internet

technology and it enables users to personally compute the radiation doses for work scenarios within a 3D environment as a tool developed by SCK-CEN. The method used in the evaluation of the radiation dose considers the location of workers, duration of their work, and the ensuing geometrical and source distribution changes in the 3D computer simulation of the workplace based on Point-kernel computation.

In the establishment stage of VISIPLAN modeling, modeling is executed on the bases of the technological structure design, measurement technology, assessment of the facility structure through laser scanning, technical data on the region through the collection of information on the substance, , and by comprehensive data collection on the radiologic information.

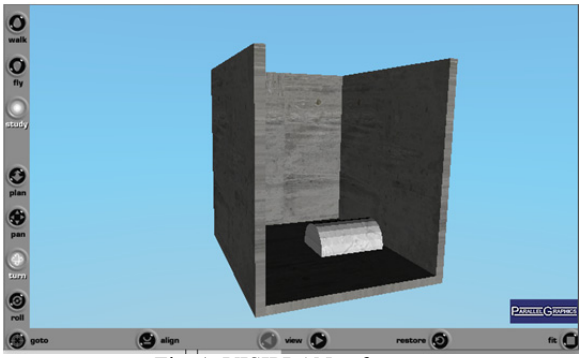


Fig. 1. VISIPLAN software.

4. Conclusion

This study discusses the methodology to assess radiation exposure in preparation for exposure to workers that can occur during the transition period before the start of dismantling after permanent the shutdown of nuclear facilities.

Because of the characteristics of the working environment that occur near major radiated structures during the transition period, the impact of external exposure is likely to be larger than that from internal exposure. Therefore, this paper analyzed the point kernel method to assess external exposures and the VISIPLAN code applying it.

Since the VISIPLAN code can assess the exposure impact according to workers' movements through the spatial dose rate, we determined that it was optimal for the transition period characterized by many movements.

Therefore, we plan to apply the radiological distribution of major structures to VISIPLAN to assess the exposure impact according to the scenarios of tasks during the transition period. We expect the assessed exposure impact to be an essential factor in establishing work guidelines and safety standards for workers during the transition period.

ACKNOWLEDGEMENT

This work was supported by Korea Institute of Energy Technology Evaluation and Planning (KETEP Project no.20191510301120) and Ministry of Trade, Industry and Energy, Republic of Korea.

REFERENCES

[1] IAEA, "Radiological Characterization of Shut Down Nuclear Reactors for Decommissioning Purposes", Technical Reports Series No. 389 (1998).

[2] F. Vermeersch and C. Vanbosstraeten, "Software VISIPLAN: a powerful tool for optimization.", 2nd EC/ISOE Workshop on occupational exposure management ant NPPs (2000).

Evaluation of the Preliminary Dose Rate of the New-Type Disposal Container According to the Predicted Value of the Radionuclides Inventory of the Decommissioning Concrete Waste

Ho-seog Dho*, Tae-man Kim, Rin-ah Kim, and Chun-hyung Cho
Korea Radioactive Waste Agency, 174, Gajeong-ro, Yuseong-Gu, Daejeon, 34129, Korea
*ehghtjr@korad.or.kr

1. Introduction

In countries that have decommissioning most commercial NPPs, large-capacity disposal containers are used to efficiently dispose of decommissioning wastes that occur in large quantities in a short period of time. In Korea, such a large-capacity disposal container is also being developed, and shielding design is carried out in accordance with the technical standards of NSSS [1].

However, the surface dose rate limit of 10mSv/h or less suggested in the current Acceptance Criteria in Korea may cause excessively high exposure, so it is not suitable for large-capacity containers (here 'large-capacity' refers to the storage weight of waste). In this study, we intend to produce basic data for setting the surface dose limit of a large-capacity disposal container developed for decommissioned NPP's radioactive waste.

2. Limits on the surface dose rate of overseas disposal containers

Limits on the surface dose rate of overseas disposal containers. In most countries, the surface dose of large-capacity disposal containers is set to be less than 2mSv/hr.

2.1 France

The ANDRA specification sets 2 mSv/h as the contact dose rate limit for packages that are to be stored at the CSA. The radioactivity of finished metal containers shall comply with the requirements from ANDRA technical specification ACO.SP. ASRE.99-002.

2.2 Sweden

The containers are arranged side-by-side in two rows and stacked three full-height or six half-height containers on top of each other. For waste packages to be deposited in BLA, the maximum permissible surface dose rate is 2 mSv/h, and 0.1 mSv/h at a distance of 2 meters.

2.3 US

Radiological acceptance criteria for Waste Isolation Pilot Plant (WIPP) repository, US, surface dose rate is contact handled drums surface dosage rate is 2 mSv/h, and 0.1 mSv/h at a distance of 2 meters. otherwise requires packaging in remote-handle cask.

2.4 UK

The external dose rate from the waste package shall enable safe handling of the waste package during transport and the geological disposal facility operational period and shall comply with regulatory limits for transport. The external dose rate of the waste package should be compatible with the dose rate at 1 meter from any external surface of a transport package, not exceeding 0.1mSv/h and the dose rate on its external surface not exceeding 2mSv/h.

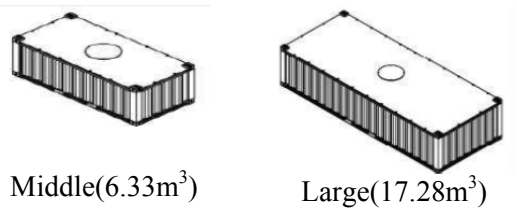
2.5 Russia

The container shall provide protection against ionizing radiation so that the equivalent dose rate at any point on its surface does not exceed 2.0 mSv/h and at a distance of 1 m from the surface does not exceed 0.1 mSv/h (GOST R 51824-2001).

3. Evaluation of dose rate of new-type disposal container

3.1 Specifications of new-type disposal container

In the 'Development of Waste Package, Transportation, and Disposal Containers for Decommissioning Wastes of NPP', dedicated by KETEP and supervised by KORAD, a new-type disposal container was developed as shown in Fig. 1.



Middle(6.33m^3) Large(17.28m^3)

Fig. 1. The new-type disposal container.

3.2 Decommissioned NPP's Bio-shield Concrete Radionuclide Inventory Assumption

Recently, research on the evaluation of Radionuclide Inventory in relation to Decommissioned NPP is underway. Among them, a reference that evaluated Decommissioned NPP's Bio-shield Concrete Radionuclide Inventory was used as a source term for wastewater [2].

Table 1. Impurity nuclides Reaction Concentration of impurity and Activity

Impurity nuclides Reaction Concentration of impurity[ppm]	Case1	Case2	Case3	Case4
Li-6 (n, α)H-3	-	-	20	20
Co-59 (n, γ)Co-60	3.92	10	10	9.8
Ni-58 (n, p)Co-58	-	-	30	25.84
Ni-62 (n, γ)Ni-63	-	2.2	-	-
Cs-133 (n, γ)Cs-134	1.2	1.2	1.2	1.3
Eu-151 (n, γ)Eu-152	0.17	0.8	1	0.55
Total Activity(Bq/g)	2.44E+03	8.62E+03	1.27E+04	8.14E+03

3.3 Disposal container surface dose rate evaluation result

The surface dose of medium and large (2 types) disposal containers was evaluated using the Bio-shield Concrete Radionuclide Inventory.

Table 2. The Surface dose rate evaluation result

(mSv/h)

Disposal container Type	Case1	Case2	Case3	Case4
Middle	4.76.E-01	1.85.E+00	2.29.E+00	1.40.E+00
Large (with Soft-bag)	3.23.E-01	1.26.E+00	1.55.E+00	9.50.E-01
Large	3.57.E-01	1.39.E+00	1.71.E+00	1.05.E+00

4. Conclusion

The reason the new-type disposal container was developed by applying the NSSS standard is that it is used for both packaging and transportation.

In this study, in order to set the surface dose rate limit of large-capacity disposal containers used for decommissioned NPP's radioactive waste, we evaluated the dose rate of a disposal container containing 'Radioactive concrete waste' analyzed by conservative assumptions.

In countries that have experienced the decommission of most NPPs, the surface dose rate limit of disposal containers is set to 2mSv/h or less. Accordingly, in Korea, if a new-type developed disposal container is used, it will be possible to satisfy 2mSv/h or less even if the radioactive concrete waste, which is assumed to be conservative, is stored.

However, the actual radiographic evaluation data for decommissioning waste is not presented in the published FDP of Kori Unit 1 yet.

Therefore, it is necessary to determine whether or not to revise the Acceptance Criteria by evaluating the surface dose rate of the disposal container based on the measured inventory of radionuclides in the waste.

Acknowledgement

This work was supported by the Korea Institute of Energy Technology Evaluation and Planning (KETEP Project No. 20193210100120) and the Ministry of Trade, Industry & Energy (MOTIE) of the Republic of Korea.

REFERENCES

[1] NSSS No.2071-56, Regulations for the Packing and Transport of Radioactive Materials, etc.

[2] G.Y Cha, The effects of impurity composition and concentration in reactor structure material on neutron activation inventory in pressurized water reactor, KNFCWT vol.14 no.2, (2016).

Review on Site Remediation and Release of Nuclear Power Plant During Decommissioning

Cheon-Woo Kim*, Kwang-ho Jo, and Hyejin Jung
KHNP-CRI, 70, 1312-gil, Yuseong-daero, Yuseong-gu, Daejeon 34101, Korea
*cheonwoo@khnp.co.kr

1. Introduction

Site remediation should be undertaken to restore the radioactive contaminated soil and groundwater to un-restricted release or restricted release in the final stage of nuclear power plant decommissioning. Its purpose is to protect the people and the environment from potential harmful effects due to exposure to ionizing radiation. It is the final goal of decommissioned nuclear facilities and the site and building are reused to suit the purpose. When establishing plans and strategies, which are the initial stages of decommissioning, consider the plan to release the nuclear power plant site. There are two types of site release, one is un-restricted release and the other is restricted release, the first is called greenfield and the latter is called brownfield. Some examples of greenfield and brownfield are as follows. Of the fifteen nuclear facilities that have been decommissioned in the United States, eight facilities (Big Rock Point, CVTR, Conn. Yankee, Maine Yankee, Saxton, Shippingport, Trojan, Yankee Rowe) have been released to greenfield, five (Elk River, Fort St. Vrain, Pathfinder, Rancho Seco, Shoreham) are being used as thermal power plants (brownfield), and two (BONUS and PIQUA) are entombed (brownfield). In addition, all three nuclear facilities (Gross Welzheim, Niederaichbach, VAK Kahl) in Germany were released to the greenfield, and JPDR in Japan was reused as a nuclear facility (brownfield) [1].

Fig. 1 shows a picture of the Maine Yankee nuclear power plant in operation and a picture that was released to greenfield after decommissioned in 2007.



Fig. 1. Maine Yankee nuclear power plant in operation (left) and greenfield (right) after decommissioning.

Fig. 2 shows a picture of Rancho Seco nuclear power plant that was partially dismantled and converted into a thermal power plant. In this case, the site release is called restricted release and is generally referred to as brownfield.



Fig. 2. Rancho Seco nuclear power plant which was converted into thermal power plant after decommissioning.

2. Procedure for Site Release

2.1 Un-restricted/Restricted Release

In general, the main procedure for site release is the MARSSIM (NUREG-1575) developed by the multi-agency of the United States, and the RESRAD code is used to evaluate the specific radioactivity of residual nuclides. The MARSSIM is a regulatory guidance document outlining the process and steps to be taken in order to survey a site for radiological contamination and to verify that it has been sufficiently cleaned for release for other uses. Major processes recommended by the MARSSIM include HSA, Scoping Survey, Characterization Survey, Remedial Action Support Survey, and Final Status Survey [2]. In un-restricted release, all exposure pathways should be considered. In the case of farmer scenario representing greenfield, the farmer lives on the site for 24 hours and consumes water, plant foods, meat, milk, fish, soil, etc. However, there is a difference in evaluating some cases of brownfield, such as industrial worker, suburban resident, recreationist, etc. excluding exposure pathways.

2.2 Guideline for Site Release

A facility is considered decommissioned when an approved end state has been reached. In order words, a site can be released when the radiation level of residual radioactivity at a site

meets a site release criteria. Site release criteria can be:

- Allowable dose to a future user of the site (i.e., 0.1mSv/y)
- Concentrations for various radionuclides in soil, concrete or groundwater (these values have been determined by a dose based calculation)

If the site release criteria is dose-based**,** site release limits which is measurable concentrations called the DCGL (Derived Concentration Guideline Level) needs to be determined by dosed modeling codes such as the RESRAD which was developed by Argonne National Lab. under funding by the US DOE and the US NRC or the DandD which was developed by Oak Ridge National Lab. under funding by the US NRC. The DCGL is the concentration of residual radionuclides in the soil, distinct from the background and concentration that causes a dose corresponding to the site release standard when uniformly distributed throughout the site.

3. Discussion

After completion of the decommissioning of the Korean nuclear power plant, the site needs to be restored based on the NSSC Notice titled "Criteria for reuse of the site and remaining buildings. In the case of Korea, restricted release is planned, and the annual effective dose rate is 0.1mSv, and it must be verified that the effective dose rate not exceed 1mSv per year even if safety measures or restrictive conditions fail [3]. The evaluation period affecting the DCGL is considering 1,000 years, and the specific radioactivity of about 20 nuclides such as H-3, C-14, Mn-54, Fe-55, Co-60, Ni-63, Sr-90, Nb-94, Tc-99, Cs-137, Eu-152, Eu-154, Eu-155, Pu-238, Pu-240, Pu-241, Am-241, Cm-244, etc. The DCGL value for the industrial worker scenario (i.e., brownfield) of C-14, a representative nuclide of interest, is 1.23E+05 Bq/g based on 0.25mSv/y criteria for the Rancho Seco nuclear power plant and 1.25E+02 Bq/g based on 0.1mSv/y criteria for the ZORITA nuclear power plant. In the case of both nuclear power plants, these are the result of evaluation with the RESRAD code. The criteria for classification of soil contamination and non-contamination are the DCGL, and are classified as soil separation technology as shown in Fig. 3. Soils less than the DCGL can be reused for landfilling, and soils above the DCGL are separated into Low-Level Waste (LLW) and Very Low-Level Waste (VLLW) and sent to the final disposal facility after removing contamination.

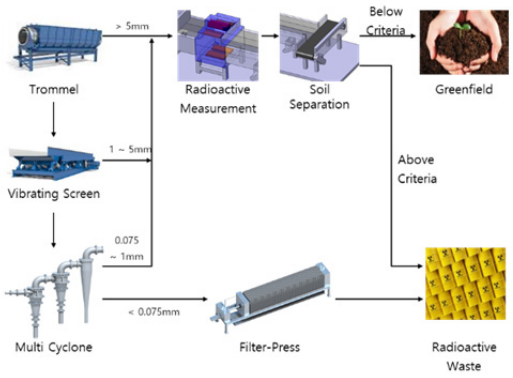


Fig. 3. General equipment configuration used to restore contaminated soil in nuclear power plant.

4. Conclusion

After the decommissioning of nuclear power plant in Korea is completed, the site is expected to be promoted for restricted release rather than un-restricted release. For the remediation and release of the nuclear power plant site, the site will be restored to satisfy the DCGL value derived based on the annual effective dose rate proposed by the NSSC notice. The number of nuclides and specific radioactivity of DCGL were obtained using the RESRAD code and described in the Final Decommissioning Plan which will be submitted to the Korean nuclear regulatory body.

REFERENCES

[1] US EPRI, "KHNP/EPRI Decommissioning Technology Workshop", Daejeon, Sept. 5-6 (2017).

[2] US DOE/US EPA/US DOD/US NRC, "Multi-Agency Radiation Survey and Site Investigation Manual (MARSSIM)", NUREG-1575, Rev. 1, August (2000).

[3] Korean Nuclear Safety & Security Commission Notice, "Criteria for reuse of the site and remaining buildings", 2016-33 (2016).

Constructability Review Considering Installation and Dismantling of NSSS Equipment in the Early Phase of the Project

Jun Hee Lee* and Sung Hyun Jeon
KEPCO E&C, 269 Hyeoksin-ro, Gimcheon-si, Gyeongsangbuk-do, Korea
*lee516@kepco-enc.com, hjsj@kepco-enc.com

1. Introduction

The life cycle of a Nuclear Power Plant(NPP) is composed of about 10 years of construction period, about 40-60 years of commercial operation, and about 15 years of decommissioning period.

This study intends to present major considerations for improving the constructability related to the installation and dismantling of NSSS (Nuclear Steam Supply System) equipment, which are the main processes of construction and decommissioning work during this period.

2. Scope and review of constructability

2.1 Constructability range

Constructability means integrating the knowledge and experience of construction in all phases of a project (design, purchase, construction, commissioning and operation, etc.).

And according to the U.S. CII (Construction Industry Institute, US), Constructability can increase the possibility of cost reduction only when it is considered in the early basic design phase of project.

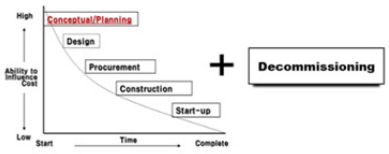


Fig. 1. Effect of Constructability Review by Project Phases and Addition of Decommissioning Phase.

Currently, constructability review focused on work during the construction period, but in the future, work in the decommissioning period should be also be considered. Additional work for the decommissioning phase is required to be considered in the early phase of the project.

2.2 Constructability review

❍ In this study, matters related to equipment, which are the critical path during the construction and decommissioning period of new NPP project, are subject to constructability review, and the main constructability review contents are as follows.

- Analysis of transportation methods, installation methods, and related processes for timely installation
- Review of applicability of large-capacity crane
- Determining the appropriate plan for the installation and dismantling of NSSS equipment in the early phase of the project

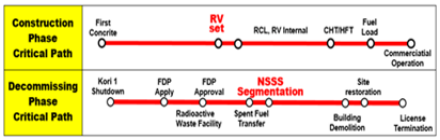


Fig. 2. Major Milestones of Construction and Decommissioning Phases.

❍ Major targets for reflection of constructability review results

- Reflection when developing a general arrangement at the early phase of the project through a parallel constructability review
- Reflection in equipment hatch, structure calculation and drawings of related buildings

3. Constructability review for NSSS equipment of new NPP project

3.1 Purpose and Key feature

❍ The purpose of constructability review is to derive the optimal design plan and develop the construction schedule by reviewing the installation and dismantling plan of NSSS equipment in the early phases of the new NPP project.

❍ Key features of new NPP for constructability review

- As the outer diameter of the RVA (Reactor Vessel Assembly) increases due to the application of an integrated RVA (that is composed of RVA, Steam Generator, Internal, Reactor Coolant Pump and Pressurizer), equipment hatch cannot be used when it brings into the Reactor Containment & Auxiliary Building(RCAB).
- The RCAB is square and the ceiling crane is applied to the overhead crane.

3.2 NSSS equipment installation plan review of the New nuclear power plant (Installation in using Open Top Method)

❍ Problems when applying integrated RVA
- No measures to prevent deformation of joints between internals when applying integrated RVA

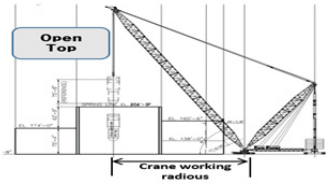


Fig. 3. RVA Installation Applying Open Top Method.

❍ Application of separation of RVA and internal equipment
- Separate installation of RVA and internal (Steam Generator, Internal, Reactor Coolant Pump and Pressurizer) to complement problems when applying integrated RVA
  - RVA installation: Open Top Method
  - RVA internal equipment: Side Method (bring into the RCAB through equipment hatch)
- Large-capacity cranes used in commercial NPP project can be applied

3.3 NSSS equipment dismantling plan review of the New nuclear power plant (Taking out in using the Side Method)

❍ Side Method
- In the decommissioning phase, the Open Top method cannot be applied as the prevention of radioactive contamination must be considered together. Therefore, it is necessary to review the Side Method
- NSSS equipment: After taking out the RVA internal equipment through the equipment hatch, and then taking out RVA through the temporary opening

❍ Operation of temporary opening and platform
- Temporary opening
  - Since the outer diameter of the RVA is larger than the equipment hatch, it is required to install a temporary opening on the outer wall of the RCAB to take out the RVA. After taking out the RVA, the temporary opening is closed to prevent radioactive contamination.
- Platform: Operation of the platform on the outside wall of RCAB

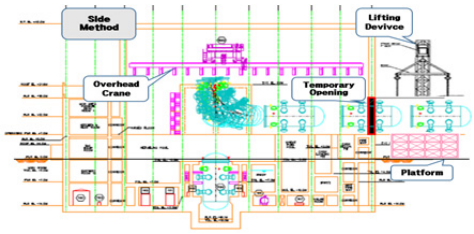


Fig. 4. RVA Dismantling Applying Side Method.

4. Conclusion

This study is expected to derive the following optimal plans and review the effects through constructability analysis for the installation and dismantling of NSSS equipment during construction and decommissioning period of the project.

❍ Construction: Open Top Method
- Convenience of work
- Prevention of deformation between RVA Internals

❍ Decommissioning: Side Method
- Prevention of radioactive contamination compared to Open Top Method

❍ Expected effect through constructability analysis at the early phase of the project
- Derivation of the optimal outputs through construction method and schedule review
- Satisfying the requirements for structure and equipment arrangement considering the decommissioning work of regulatory agencies and project owner
- Project Life Cycle cost reduction effect can be expected through constructability for engineering, construction and decommissioning period.
- Reducing risks through preliminary review of various project risks

REFERENCES

[1] KEPCO E&C, Evaluation of Decommissioning Source Terms and Wastes for the Pressurized Water Nuclear Power Plant and Heavy Nuclear Power Plant, Final Report, (2016).

[2] KEPCO E&C, Smart Project, Reactor Containment & Auxiliary Building(RCAB) General Arrangement Drawing, (2016).

[3] TLG Services, Inc., Guidelines for Producing Commercial Nuclear (AIFF/NESP-036), (1986).

[4] C.B. Tatum, J.A. Venegas and J.M. Williams, Constructability Improvement during Conceptual Planning, Stanford University, (1986).

A Study on Assessment of Lead-Free Dual-Layered Shielding for Radiation Shielding Rates During Decommissioning of Steam Generator in Kori Unit 1

Taewoong Lee*, Heechul Youn, and Nakjeom Kim
Global Institute of Technology, Kepco KPS, 211, Munhwa-ro, Naju-si, Jeollanam-do, R.O.Korea
*superdapo@kps.co.kr

1. Introduction

Based on the detailed milestone of the decommissioning process, the Kori-1 nuclear power plant (NPP) will undergo a decommissioning of structures, systems, and components from 2022 to 2030. During the decommissioning process, the external exposure dose and dose reduction method should be estimated to protect the dismantling workers. Moreover, it is essential to evaluate the radiation protection of dismantling workers in the final decommissioning plan. In recent years, owing to advances in nanotechnology, radiation shielding using nanoparticles has been applied for radiation protection. Radiation shielding using nanoparticles improves the radiation shielding rate owing to the reduction in pore space between the nanoparticles [1].

In this study, to reduce the external exposure dose during the dismantling of the steam generator (S/G) in the decommissioning of the NPP, the performance of the Pb-free shielding was estimated based on optimized conditions. This study may offer guidelines for decreasing the external exposure dose to dismantling workers for radiation safety.

2. Material and Methods

Figure 1 shows a schematic diagram of the Pb-free shielding and the simulation setup in the MCNP6 code.

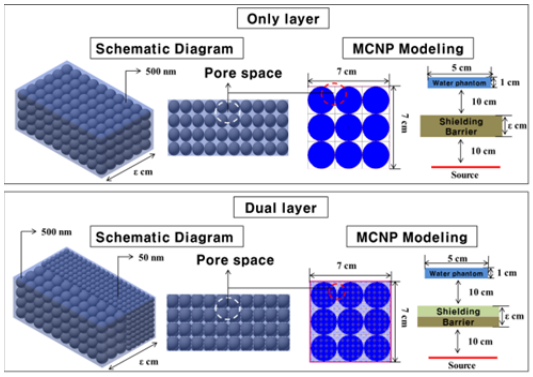


Fig. 1. Schematic diagram of radiation shielding barrier and simulation setup.

The radiation source inside the S/G was utilized to estimate the external dose for the dismantling workers in the S/G (i.e., water chamber and U-tube). The radiation source of the S/G was obtained from the results of crud analysis in the S/G of the Kori-1 NPP [2]. However, because the large components will be dismantled in year 2026, i.e., nine years after the permanent shutdown of the Kori-1 NPP, the radionuclide inventories utilized for the MCNP simulation were calculated based on their physical half-lives. Hence, radionuclides with relatively short half-lives were excluded, whereas ^{54}Mn, ^{60}Co, ^{65}Zn, ^{106}Ru, and ^{144}Ce, which had relatively long lives, were utilized as the radiation source.

Table 1. Radiation source of steam generator (S/G)

Isotopes	Estimated activity in 2026 (Bq)	
	Chamber	U-Tube
^{54}Mn	2.29×10^{-2}	5.1×10^{0}
^{60}Co	7.18×10^{7}	1.6×10^{10}
^{65}Zn	2.28×10^{-5}	5.1×10^{-3}
^{106}Ru	3.67×10^{0}	8.2×10^{2}
^{144}Ce	2.6×10^{-3}	5.8×10^{-1}
Total activity after decontamination (DF = 7)	1.03×10^{7}	2.29×10^{9}

3. Results

Figure 2 and table 3 show the representative dismantling process of the S/G with human participation.

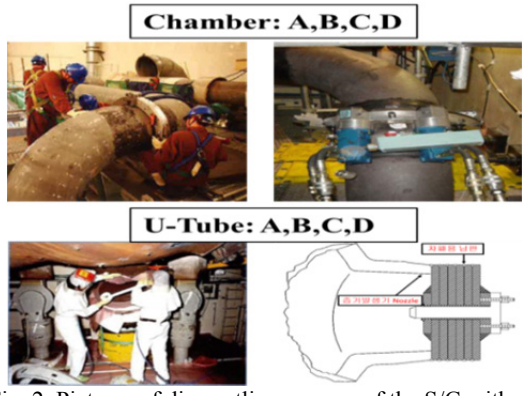


Fig. 2. Pictures of dismantling process of the S/G with human participation.

Table. 2. dismantling process of the S/G with human participation.

Maintenance activity description			
Chamber		U-Tube	
A 128h	Cut steam line piping at steam nozzle on upper shell and downstream	E 149h	Cut steam generator shell at the transition cone
B 100h	Cut feed water piping at its junction with upper shell and upstream from the junction		
C 121h	Decontaminate channel head and tube sheet, and cut steam generator at channel head	F 400h	Plug all pipe ends to prevent spread of contamination and to reduce the radiation field
D 448h	Cut and remove reactor coolant inlet and outlet piping		

*Fig. 2 and table 2. Pictures of dismantling process of the S/G with human participation.

As shown in Fig. 3, the equivalent doses with the dual-layered Pb-free shielding for the dismantling process of the S/G decreased. During the dismantling of the water chamber and U-tube region, the average equivalent doses with the Pb-free shielding of the HVL and TVL reduced by approximately 50% and 90%, respectively. Table 4 summarizes the comparison of the equivalent dose reduction achieved using Pb-free shielding for the dismantling of the S/G.

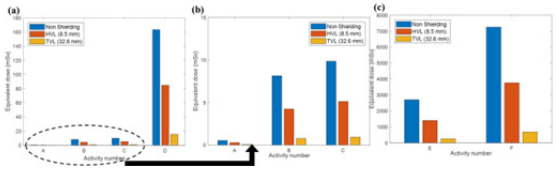


Fig. 3. Comparison of equivalent dose reduction achieved using Pb-free shielding for dismantling process of S/G: (a) water chamber; (b) partial enlarged image of (a); and (c) U-tube region.

Table 3. Summary of equivalent doses for dismantling process of steam generator.

Equivalent doses (mSV)							
HVL (8.5 mm), TVL (32.6 mm), Material (WC-Co:15.9 g/cm^3)							
Chamber					U-Tube		
	Non	HVL	TVL		Non	HVL	TVL
A	5.3×10^{1}	2.7×10^{-1}	5.1×10^{-2}	E	2.6×10^{3}	1.4×10^{3}	2.5×10^{2}
B	8.1	4.2	0.7				
C	9.8	5.1	0.9	F	7.2×10^{3}	3.7×10^{3}	6.8×10^{2}
D	163.2	84.7	15.5				

4. Conclusion

The equivalent doses for the dismantling process of the S/G can be reduced significantly by the WC-Co Pb-free shielding. Hence, it can prevent dismantling workers from the external exposure dose. Our simulation results demonstrated the feasibility of using dual-layered Pb-free shielding to reduce the external exposure dose in the dismantling of S/G.

REFERENCES

[1] Electric Power Research Institute, “Technology Development to Improve Radiation Shielding for Material Inspections”, EPRI Report, 1016770 (2008).

[2] Son *et al.*, “The assessment and reduction plan of radiation exposure during decommissioning of the steam generator in Kori Unit 1”, JNFCWT, 16, 377-287 (2018).

Optimization of Lead-Free Dual-Layered Shielding for Radiation Exposure During Decommissioning of Steam Generator in Kori Unit 1

Taewoong Lee*, Seongmin Jo, and Nakjeom Kim
Global Institute of Technology, Kepco KPS, 211, Munhwa-ro, Naju-si, Jeollanam-do, R.O.Korea
*superdapo@kps.co.kr

1. Introduction

The Kori-1 nuclear power plant has been permanently shut down since 2017, and the dismantling of its major structures, systems, and components are currently in progress. The conventional methods cause Pb poisoning to the human body as well as secondary waste generation during Pb disposal. In addition, if small pinholes are present in the Pb plate, the radiation shielding rate is degraded. In recent years, owing to advances in nanotechnology, radiation shielding using nanoparticles has been applied for radiation protection. Radiation shielding using nanoparticles improves the radiation shielding rate owing to the reduction in pore space between the nanoparticles. Several studies have demonstrated the superiority of Pb-free shielding using nanoparticles [1]. New materials for Pb-free shielding have been developed from the composition ratio of various polymers and high-density metals. These studies demonstrated that the performance of Pb-free shielding using nanoparticles was better than that of shielding using microparticles. The linear attenuation coefficients of Pb-free materials improved because of their high atomic number and high density. In this study, we propose a dose reduction method involving dual-layered lead-free shielding. To determine the best performing shielding material, several types of Pb-free materials were tested and their shielding performances compared using Monte-Carlo simulation.

2. Material and Methods

2.1 Geometrical design of Pb-free radiation shielding barrier

Figure 1 shows a schematic diagram of the Pb-free shielding and the simulation setup in the MCNP6 code. As shown in Fig. 1, the Pb-free shielding was constructed in a dual layer comprising nanoparticles. An advantage of this structure is the reduction in pore space between the radiation shielding materials, resulting in an improved radiation shielding rate. The overall size of the Pb-free shielding was 7 cm × 7 cm × ε cm, where the thickness (ε) of the Pb-free shielding barrier is the variable to be optimized to achieve a high performance. The distance between the center of the water phantom and the radiation source and that between the Pb-free shielding and the water phantom was set to 10 cm. The water phantom comprised a cylinder of height 5 cm and diameter 1 cm. The diameters of the Pb-free material of each layer were 500 and 50 nm. The materials used for the Pb-free shielding were WC-Co, Mo, Bi_2O_3, and $BaSO_4$, whose densities were 15.09, 10.22, 8.9, and 4.5 g/cm^3, respectively.

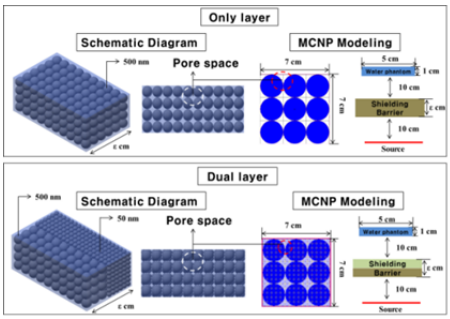


Fig. 1. Schematic diagram of radiation shielding barrier and simulation setup.

3. Results

The equivalent dose rates and radiation shielding rates of each structure for various source energies were compared, as shown in Fig. 2. To estimate the equivalent dose rates, the activity of the source was set to 1 mCi, and WC-Co was used as the material for the Pb-free shielding. The equivalent dose rates decreased with the increasing thickness of the Pb-free shielding. However, the equivalent dose rates increased with the incident γ-ray energy, primarily owing to the decrease in performance of the radiation shielding because of the increase in radiation penetration with the incident γ-ray energy.

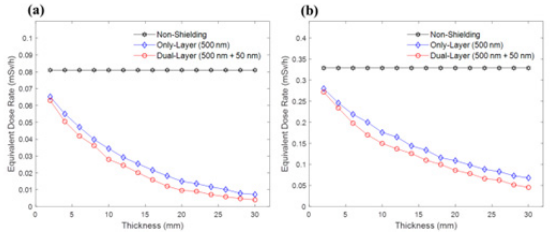


Fig. 2. Comparison of equivalent dose rates for various energies: (a) ^{137}Cs (662 keV) and (b) ^{60}Co (1173 and 1332 keV).

In summary, because of the reduction in the pore space between the radiation shielding materials, the Pb-free shielding with the dual-layered material was performed better than conventional shielding with only layered materials.

The radiation shielding performance was proportional to the density and atomic number of the material. No significant difference was observed between Pb and WC-Co, which outperformed other materials. However, as shown in Fig. 3, WC-Co exhibited the best performance when its thickness exceeded 5 mm, whereas no significant improvements were observed when its thickness was less than 2 mm. Under the same simulation conditions, Bi_2O_3, Mo, and $BaSO_4$ yielded worse performances than WC-Co.

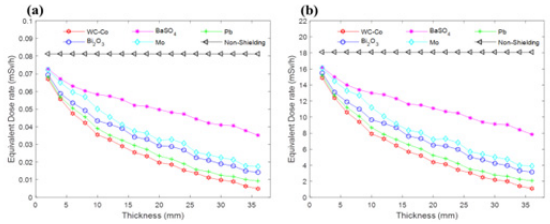


Fig. 3. Comparison of equivalent dose rates for various materials using sources of S/G: (a) water chamber and (b) U-tube region.

4. Conclusion

In this study, the optimized design parameters for dual-layered Pb-free shielding were estimated. The dual-layered Pb-free shielding performed better than the conventional shielding with only layered materials. Moreover, the study indicated the results of the better shielding effect of nanoparticles. WC-Co performed better than the other materials tested as its density was the highest.

REFERENCES

[1] Electric Power Research Institute, “Technology Development to Improve Radiation Shielding for Material Inspections”, EPRI Report, 1016770 (2008).

DOI Coded Aperture Imager Monitoring the Distribution of Gamma Nuclides in Decommissioning of Nuclear Power Plant

Taewoong Lee[1], Hyounggun Lee[2], Nakjeom Kim[1], and Wonho Lee[3,*]
[1]Global Institute of Technology, Kepco KPS, 211, Munhwa-ro, Naju-si, Jeollanam-do, R.O.Korea
[2]Department of Bio-Convergence Engineering, Korea Univ, 145, Anam-ro, Seoul, R.O.Korea
[3]School of Health and Environmental Science, Korea Univ, 145, Anam-ro, Seoul, R.O.Korea
*wonhol@korea.ac.kr

1. Introduction

The Kori-1 nuclear power plant has been permanently shut down since 2017, and the dismantling of its major structures, systems, and components are currently in progress. For the accurate verification of the location for the radiation γ-sources it is important to monitor the dose distribution of γ-sources in the decommissioning of the nuclear power plant [1].

In recent years, 3D position-sensitive scintillators that can measure depth-of-interactions (DOIs) have been developed. Hence, several DOI scintillator detectors coupled to silicon photo-multipliers (SiPMs) are used for nuclear medicine and industrial applications. In this paper, a DOI coded-aperture imager using a 3D position-sensitive scintillator detector is proposed to monitor the γ-sources in decommissioning of NPP. Given that the 3D position-sensitive scintillator consisting of four scintillator arrays could obtain the information of the DOI, the quality of the reconstructed image should be improved, because the position uncertainty of depth information decreased. Using a Monte Carlo simulation, the performance of the DOI coded-aperture imager was evaluated and compared with that of conventional coded-aperture imagers. To combine data from four different layers, a hybrid maximum likelihood expectation maximization (h-MELM) method was applied. Moreover, several types of scintillators were tested and compared with respect to their resolution-variance (RV) curves, detection efficiencies, and signal -to-noise ratios (SNRs).

2. Material and Methods

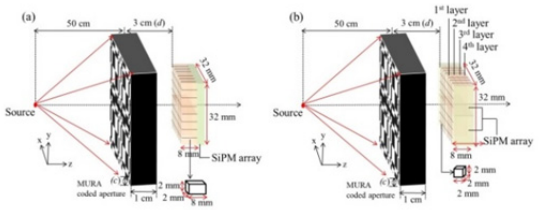


Fig. 1. Geometry of (a) conventional coded aperture imager and (b) DOI coded aperture imager.

As shown in Fig. 1(b). Each layer in the DOI coded-aperture imager was a 16 × 16 array of 2 mm × 2 mm × 2 mm cubic scintillation crystals. The design of the DOI coded-aperture imager is based on a pixelated scintillator array coupled with a commercially available array of silicon photo-multipliers. Therefore, the size of each scintillator element should be matched with that of the element of SiPM array. To match the sizes of the mask pixels and detector pixels, the elemental area of mask is chosen as 2 mm × 2 mm.

Maximum likelihood expectation maximization (MLEM) is an iterative procedure used to determine the maximum probability estimates of the parameters of a Poisson distribution model. The DOI coded aperture imaging system determined the interaction position from four different layers. To combine the data from four different layers, a hybrid MELM (h-MLEM) method was applied, as follows:

$$\lambda_j^{n+1} = \lambda_j^n \cdot \frac{\Sigma_i \frac{c_{ij}^{L_1} y_i^{L_1}}{\Sigma_k c_{ik}^{L_1} \lambda_k^n} + \Sigma_i \frac{c_{ij}^{L_2} y_i^{L_2}}{\Sigma_k c_{ik}^{L_2} \lambda_k^n} + \Sigma_i \frac{c_{ij}^{L_3} y_i^{L_3}}{\Sigma_k c_{ik}^{L_3} \lambda_k^n} + \Sigma_i \frac{c_{ij}^{L_4} y_i^{L_4}}{\Sigma_k c_{ik}^{L_4} \lambda_k^n}}{\Sigma_i c_{ij}^{L_1} + \Sigma_i c_{ij}^{L_2} + \Sigma_i c_{ij}^{L_3} + \Sigma_i c_{ij}^{L_4}} \quad (1)$$

3. Results

Figure 2 shows the SNRs of each modality for various source energies. As the iterations increased, the resolution of the reconstructed image improved, but the background noise also increased; hence, the reconstructed image of the 20th iteration was chosen, which showed a high resolution without a significant background noise peak. The SNRs of the DOI coded-aperture imager were considerably higher than those of the conventional coded-aperture imagers. In summary, the performance of the DOI coded-aperture imager was superior over the widest range of energies (122 - 1275 keV).

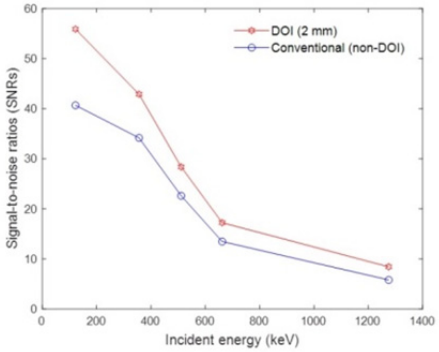


Fig. 2. Signal to noise ratios (SNRs) vs. incident radiation energy for the conventional coded aperture imager and DOI coded aperture imager (20th iteration).

Figure 3 presents the RV curves of each modality for various source energies. The RV curve shows that a system curve closer to the origin represents better performance. The reconstructed image from the DOI coded-aperture imager showed a lower background noise level than the conventional coded-aperture imager, because effective events with less position uncertainties yield better information for image reconstruction.

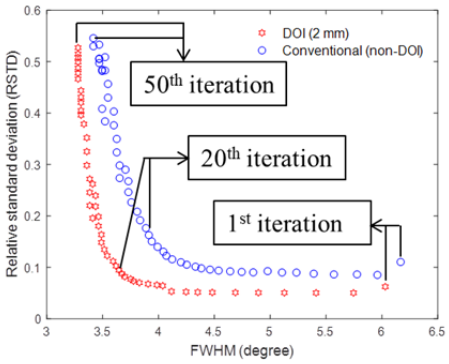


Fig. 3. Resolution-variance curves for reconstructed image using the h-MLEM algorithm: ^{137}Cs radiation source (662 keV).

4. Conclusion

The DOI coded-aperture imager demonstrated higher signal-to-noise ratios (SNRs) in the reconstructed images, when compared with conventional coded-aperture imagers with 2D pixelated scintillators.

ACKNOWLEDGEMENTS

This work was supported by the Nuclear Safety Research Program through the Korea Foundation Of Nuclear Safety (KoFONS) using the financial resource granted by the Nuclear Safety and Security Commission (NSSC) (No. 1903006) and the National Research Foundation of Korea (NRF) grant funded by the Korea government (MSIT) (No. 2020R1A2C1005924) of the Republic of Korea.

REFERENCES

[1] Electric Power Research Institute, “Use of Portable Gamma Detector Systems During Decommissioning”, EPRI Report, TR-3002015953 (2019).

Dual-Anti Mask Methods for Monitoring the Distribution of Gamma Nuclides in Decommissioning of Nuclear Power Plant

Taewoong Lee[1], Nakjeom Kim[1], and Wonho Lee[2,*]
[1]Global Institute of Technology, Kepco KPS, 211, Munhwa-ro, Naju-si, Jeollanam-do, R.O.Korea
[2]School of Health and Environmental Science, Korea Univ, 145, Anam-ro, Seoul, R.O.Korea
*wonhol@korea.ac.kr

1. Introduction

The Kori-1 nuclear power plant has been permanently shut down since 2017, and the dismantling of its major structures, systems, and components are currently in progress. To protect dismantling workers from external exposure dose during decommissioning, it is necessary to monitor the distribution of the γ-rays in the decommissioning. A coded aperture imaging, which provides a high efficiency high resolution in the reconstructed image of the γ-ray, is used to monitor the nuclear materials emitting γ-rays. Among the various types of coded apertures, the squared-shaped modified uniformly redundant array (MURA), which is suitable with common photo devices, has been utilized for industrial applications, decontamination and decommissioning (D&D) [1].

In this study, a compact MURA coded mask imaging system using dual-anti mask method was developed, and its performance was compared and evaluated for high energy gamma radiation sources. In the dual anti-mask method, the information of not only the first shadow image but also the second shadow image was simultaneously used to reconstruct the radiation images of all γ-ray energies. Subsequently, to integrate data from the two different shadow images, the hybrid update maximum likelihood expectation maximization (h-MLEM) method was applied.

2. Material and Methods

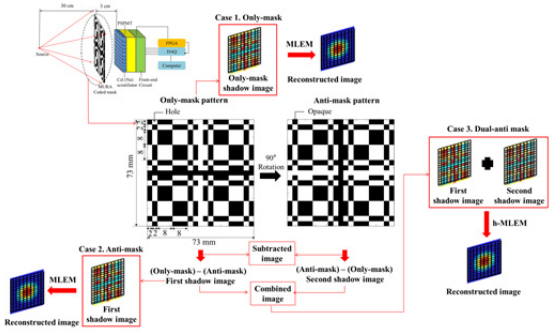


Fig. 1. Schematic diagram of the dual-anti mask imaging system with MURA coded aperture.

As shown in Fig. 1, three separate collimation methods can be defined:

1. Only-mask method (case 1): the incident radiation passes through a MURA coded mask and forms shadow of mask on the detector. Consequently, all effective events form only-mask shadow image which is utilized for the image reconstruction.

2. Anti-mask method (case 2): if the only-mask is rotated by 90°, all holes of the original MURA coded mask pattern are replaced by opaque elements. The mask that becomes anti-symmetric by 90° rotation is known as the "anti-mask." The anti-mask method utilizes only the first shadow image using the background subtraction method for the image reconstruction.

3. Dual-anti mask method (case 3): the incident radiation passes through a mask and anti-mask. Subsequently, the types of two different shadow images with the subtraction of background events can be acquired in the detector plane. The first shadow image can be obtained by subtracting shadow image of anti-mask from shadow image of only-mask, and the second shadow image can be obtained in reverse order. Dual-anti mask method utilizes the information from both first shadow image and second shadow image simultaneously for the image reconstruction. We combined the datasets from the first shadow image and second shadow image using Eq. (1).

The h-MLEM method was used to combine the information from the first and second shadow images as shown in Eq. (1).

$$\lambda_j^{n+1} = \lambda_j^n \cdot \frac{\sum_i \frac{c_{ij}^F Y_i^F}{\sum_k c_{ik}^F \lambda_k^n} + \sum_i \frac{c_{ij}^S Y_i^S}{\sum_k c_{ik}^S \lambda_k^n}}{\sum_i c_{ij}^F + \sum_i c_{ij}^S} \quad (1)$$

3. Results

Figure 2 show the reconstructed images of each modality for various incident radiation energies. Using the shadow image that includes the subtraction of background events leads to a higher-performance reconstructed image. Especially, as the dual anti-mask method utilized two

shadow images with reduced background noise, the performance of the dual-anti mask imaging was higher than that of the conventional imaging as shown in Fig. 2.

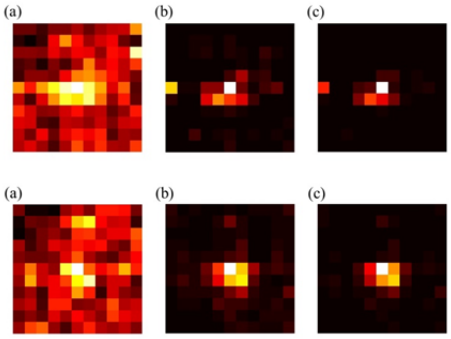


Fig. 2. Reconstructed image obtained using the MLEM and the h-MLEM method for ^{60}Co (1173 keV and 1332 keV (30th iteration)): (a) Only-mask, (b) anti-mask, and (c) dual-anti mask.

Hence, the reconstructed image obtained by the dual-anti mask method showed the high performance such as the least noise and the fewest artifacts among the three collimation methods.

4. Conclusion

In this study, the reconstruction method of the h-MLEM was used to reconstruct each modality image. As two different shadow images can contribute effective information to the reconstructed images simultaneously, the results of the dual-anti mask method offer lower background noise in the reconstructed images. The results of this study demonstrated the availability of using dual-anti mask imaging as a means of monitoring the position and distribution of high energy gamma radiation source in decommissioning of NPP.

ACKNOWLEDGEMENTS

This work was supported by the Nuclear Safety Research Program through the Korea Foundation Of Nuclear Safety (KoFONS) using the financial resource granted by the Nuclear Safety and Security Commission (NSSC) (No. 1903006) and the National Research Foundation of Korea (NRF) grant funded by the Korea government (MSIT) (No. 2020R1A2C1005924) of the Republic of Korea.

REFERENCES

[1] Electric Power Research Institute, “Use of Portable Gamma Detector Systems During Decommissioning”, EPRI Report, TR-3002015953 (2019).

Construction of the Advanced Remote Dismantling System Testbed

Jonghwan Lee*, Dongjun Hyun, Jae Sung Shin, Ikjune Kim, Sungmoon Joo, and Jaehyun Ha
Korea Atomic Energy Research Institute, 111, Daedeok-daero 989beon-gil, Yuseong-gu, Daejeon, Republic of Korea
*jhl@kaeri.re.kr

1. Introduction

The dismantling process of high-radioactive core facilities in nuclear power plants is a complex process that requires various technologies and equipment while also considering economic feasibility and safety [1]. The basic concept of advanced remote dismantling system under development is to perform robot-based remote dismantling work safely and efficiently by optimizing the dismantling process in real time based on design data and environmental information of the dismantling site. This study briefly describes the construction of a testbed for the experiment and verification of advanced remote dismantling system technology based on the robot and the environmental information feedback.

2. Configuration of the system framework

Advanced remote systems must meet a number of functional requirements, such as command generation for robot and device control, acquisition and processing of three-dimensional environmental information, simulation-based dynamic process re-planning, and interactive remote control for site information-based optimal processes. Figure 1 shows the overall system framework for interoperating modules based on these functional requirements [2].

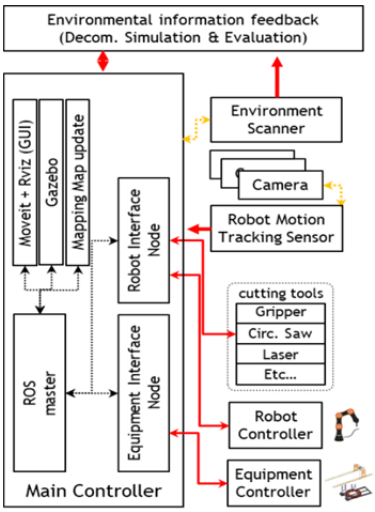


Fig. 1. System framework of the advanced remote dismantling system.

3. Construction of the system testbed

The system testbed is for the experiment and verification of the designed system framework. This testbed consists of two robots and a underwater cutting experimental pool, a three-dimensional underwater laser scanner system with radiation proof, a robot-linked laser cutting head and generator, auxiliary gas supply and collection facilities, and so on. The components of the testbed are integrated and driven in conjunction with three-dimensional environmental data processor, environmental information-based real-time decommissioning process simulation workstation, robot and device control unit. Figure 2 shows briefly the configuration of the testbed.

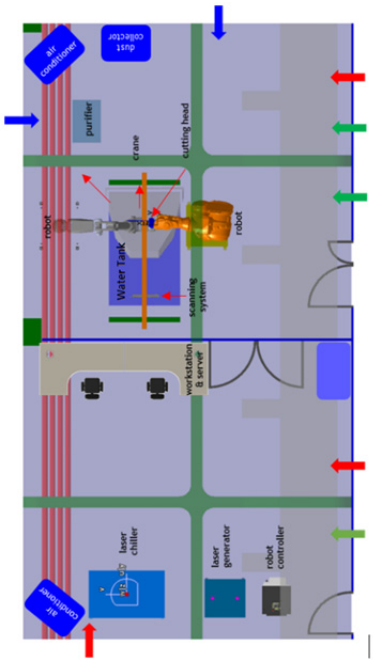


Fig. 2. Layout of the advanced remote dismantling system testbed.

Two robots and laser cutting devices for remote cutting are operated by a mobile workstation for integrated control and a server for robot system control. The mobile workstation for integrated control acquires and processes three-dimensional environmental information through the radiation resistant underwater laser scanner system, and performs real-time process

simulation based on the processed three-dimensional environmental information. The server for robot system control works in conjunction with the mobile workstation to simultaneously control remote cutting equipment such as robot and laser cutting hardware. The workstation and server for integrated control and simulation were applied with various component technologies developed for the advanced remote dismantling system such as technologies for acquiring and processing three-dimensional environmental information under water, remote interconnection technology, real-time dismantling process simulation and integrated evaluation technology based on environmental information feedback, high efficiency underwater laser cutting technology, etc.

4. Conclusion

The built testbed will provide a platform for testing and verification of the advanced remote dismantling system that can economically and safely dismantle highly radioactive nuclear facilities in the next year. Through this process, we will check the integrated performance of the advanced remote dismantling technology, and secure the progressive technology for remote dismantling of the core facilities of high-radioactive nuclear power plants.

ACKNOWLEDGEMENT

This work was supported by the nuclear research and development program (2017M2A8A5015146) through the National Research Foundation of Korea, funded by the Ministry of Science and ICT, Republic of Korea.

REFERENCES

[1] I. Kim, B. Choi, D. Hyun, J. Moon, J. Lee, K. Jeong, et al., “A framework for a flexible cutting-process simulation of a nuclear facility decommission”, Annals of Nuclear Energy, 97, 204-207 (2016).
[2] J. Lee, S. Joo, D. Hyun and I. Kim, “Design of the Advance Remote Dismantling System Framework”, Proceedings of the Korean Radioactive Waste Society SPRING 2018, 16, 279-280, (2018).

Preliminary Review of Applicability of Site Configuration Management to Nuclear Power Plants Under Decommissioning

Ga Hyun Chun and Jae Hak Cheong*
Dept. of Nuclear Engineering, Kyung Hee Univ., 1732 Deogyoung-daero, Giheung-gu, Yongin-si, Gyeongi-do
*jhcheong@khu.ac.kr

1. Introduction

During decommissioning of nuclear power plants (NPPs), configuration of the site has been changed due to dismantling or remediation actions. Configuration management of operating NPPs have currently been conducted, however, only conducted for Structures, Systems, and Components (SSCs). Not only for SSCs but for the plant sites during decommissioning, licensee cannot arbitrarily release the sites after removing the residual contamination until the relevant radioactivity criteria have been met. Thus, it is necessary to manage configuration properties of the sites including radiological properties. There is no experience in decommissioning of NPPs in Korea. However, overseas countries such as United States, there are plenty of experiences of decommissioning nuclear facilities including NPPs. Particularly, some regulations and guides on how to release and reuse the sites have been proposed from the past to the present. Therefore, some guides on decommissioned sites have been analyzed and some options for the configuration management have been propsed by applying the analyzed guides.

2. Methodology

In this chapter, some guides on sites have been reviewed for configuration management.

2.1 Regulatory Guide 1.86

Regulatory Guide 1.86 is a guide describing methods and procedures considered acceptable by the regulatory staff for the termination of operating licenses for nuclear reactors [1]. The licensee should perform comprehensive radiation survey to ensure that the surface contamination is below the acceptable surface contamination level before unrestricted reuse. When measuring residual surface contamination, measurements of average contamination should not be averaged over more than $1m^2$.

2.2 NUREG/CR-2082

NUREG/CR-2082 is a guide to give guidance and direction on how the licensee shall carry out a final survey, such that its design, procedures and results can be compared with existing standard with validity [2]. The radiation survey procedure is classified into preliminary survey and final survey. It is important to conduct a simple preliminary survey to establish an efficient plan before performing final survey. In the final survey, the site is divided into “survey unit” which is subdivided into a rectangular grid system which referred as “survey block”. NUREG/CR-2082 have proposed proper size of survey block or numbers of measurement points.

2.3 NUREG/CR-5849

NUREG/CR-5849 is a revised version of the previously published guidance NUREG/CR-2082 as a guidance for radiation survey for termination of operating licenses [3]. The radiation survey procedure of NUREG/CR-5849 consists of background survey, scoping survey, characterization survey, remediation control survey, final status survey and confirmatory survey. The sites are divided into “Affected area” and “Unaffected area” for designing final status survey, and these areas are subdivided into survey unit. NUREG/CR-5849 have suggested measurement averaging size or numbers per survey unit of affected area and unaffected area.

2.4 MARSSIM

Multi-Agency Radiation Survey and Site Investigation (MARSSIM) is a detailed guidance for giving guide whether or not the site reuse criteria is satisfied by performing radiation survey. The procedure of evaluating radiological characteristics in MARSSIM consists of site identification, Historical Site Assessment (HSA), scoping survey, characterization survey, remedial action support survey and Final Status Survey (FSS). Areas are initially classified as "Impacted area” and a "Non-impacted area” and for designing FSS, the impacted areas are subdivided into survey units according to the expected radioactive contamination level. Class 1 areas before remediation are areas with residual activity concentrations that exceed the DCGL (Derived Concentration Guideline Level). Class 2 areas are areas where residual activity concentrations

that exceed the DCGL are not expected. Class 3 areas are areas that have a low probability of containing areas with residual activity. Table 1shows the suggested survey unit areas for each site classification in MARSSIM.

Table 1. Suggested survey unit areas in MARSSIM

No	Class 1	Class 2	Class 3
Structures	Up to 100m^2	100 to 1,000m^2	No limit
Land areas	Up to 2,000m^2	2,000 to 10,000m^2	No limit

3. Site Configuration Management during Decommissioning Process

In this chapter, some options of configuration management for decommissioned sites applying guides analyzed in previous chapter.

3.1 Applying Regulatory Guide 1.86

Regulatory Guide 1.86 can be applied for configuration management of decommissioned sites. As can be seen in Chapter 2.1, the measurement of contamination should not be averaged over 1m^2, therefore the site can be divided into multiple survey unit with 1m^2 square grid as shown in Figure 1.

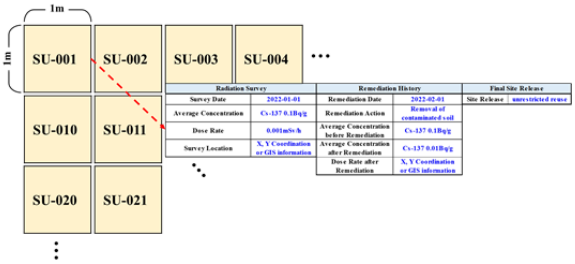


Fig. 1. Site configuration management based on Regulatory Guide 1.86.

3.2 Applying MARSSIM

Based on MARSSIM methodology, it is possible to propose a configuration management option for each survey unit in which the site is divided using graded approach. Configuration management can be performed for each radiation survey stage. The properties to be managed for each radiation survey step maybe different as shown in Figure 2.

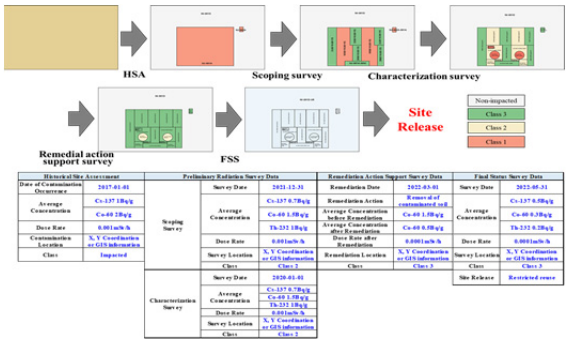


Fig. 2. Site configuration management based on MARSSIM.

4. Conclusion

In this study, guidance documents of United States have been analyzed and the radiation survey procedures and the systems of classifying the site have been investigated. Also, options of site configuration management by applying Regulatory Guide 1.86 and MARSSIM have been suggested. However, for applying in the real field, it is necessary to derive an effective option by analyzing pros and cons between these methods and properly utilizing the advantages of two methods. This study may contribute to ensuring reliability of site release during decommissioning of NPPs.

Acknowledgement

This work was supported by the Korea Institute of Energy Technology Evaluation and Planning (KETEP) and the Ministry of the Trade, Industry & Energy (MOTIE) of the Republic of Korea (No.20191510301290).

REFERENCES

[1] U.S. Atomic Energy Commission, Termination of Operating Licenses for Nuclear Reactors, Regulatory Guide 1.86 (1974).

[2] Oak Ridge National Laboratory, Monitoring for Compliance with Decommissioning Termination Survey Criteria, NUREG/CR-2082 (1984).

[3] Oak Ridge National Laboratory, Manual for Conducting Radiological Surveys in Support of License Termination, NUREG/CR-5849 (1992).

[4] U.S NRC, Multi-Agency Radiation Survey and Site Investigation Manual (MARSSIM), NUREG-1575, Rev.1 (2000).

Applying AOPs to Illite for Efficient Cesium Removal in Liquid Waste

Jaeeun Kang[1,*], Juhyeok Lee[1], Jimo Lee[1], Ingyu Song[2], and Won-Seok Kim[1]
[1] Division of Advanced Nuclear Engineering (DANE), Pohang University of Science and Technology (POSTECH), 77, Cheongam-ro, Pohang, South Korea
[2] Division of Environmental Science and Engineering (DENE), Pohang University of Science and Technology (POSTECH), 77, Cheongam-ro, Pohang, South Korea
*jenny94@posteh.ac.kr

1. Introduction

Radioactive cesium (^{137}Cs) is a major nuclide that occurs during nuclear power plants (NPPs) accidents or NPPs decontamincation. In particular, ^{137}Cs has posed critical environmental risks due to its high solubility to migrate via aqueous media in the subsurface. According to the prior studies, the illite is one of the mica clay minerals that has known to be an effective adsorbent for the removal of Cs because of its selective and specific adsorption sites, called 'frayed edge sites (FES)' [1]. However, cesium mainly tends to be adsorbed to FES of illite.

In order to solve these problems, we conducted artificial weathering to illite through Advanced Oxidation Processes (AOPs) that generate hydroxyl radicals. In other words, radicals, unstable and highly reactive intermediates, are expected to affect the mineral surface.

The objective of our research is to compare the Cs removal efficiencies of three AOPs-treated illites which are Fenton reaction (FR), Fenton-like reaction (FLR) and Plasma reaction (PR).

2. Materials and Methods

2.1 Materials

To proceed with the adsorption experiment, we used illite collected in Yeongdong and classified into particles of 75 μm or less by sieving. The simulated liquid waste was prepared with a solution of 1ppm concentration using the ^{133}Cs having the same chemical properties as radioactive cesium. The ratio of the soil to solution ratio is 100 and the adsorption experiments were performed with 0.1g of soil.

2.2 Methods

2.2.1 Fenton and Fenton-like reaction

To improve the adsorption capacity of illite, AOPs was applied as FR, FLR, and PR.

As catalysts for the FR and FLR, $FeSO_4$ and $CuSO_4$ were used, respectively, and a 0.1 M of hydrogen peroxide (H_2O_2) was prepared to generate hydroxyl radicals ($OH\cdot$) by reacting with the catalysts.

Table 1. Experimental conditions for Fenton reaction (FR) and Fenton-like reaction (FLR)

	Catalyst		H_2O_2	Final pH
FR	$FeSO_4$	0.6 M	0.1 M	2.36
FLR	$CuSO_4$	0.6 M		2.13

After adding catalysts and 2 g of illite to 50 mL beakers, 12.5 mL of H_2O_2 was added each (Table 1). Since the FR and FLR are most active around pH 2, a small amount of 1 M HCl solution was added immediately to maintain pH between 2~2.5. After stirring for 24 hours, 10 mL of 0.1 M NaCl was dropped to stop the reaction [2]. The reactant was centrifuged at 3000 rpm for 10 minutes and then dried in an oven at 70°C overnight.

2.2.2 Plasma reaction

To weather the illite through plasma, 3 g of illite was placed on the sample holder and exposes plasma under the following conditions (Table 2). In order for the plasma to react evenly with the illite, it was stirred with a stick occasionally.

Table 2. Experimental conditions for plasma reaction (PR).

	Power	Gas	Reaction time
PR	100 W (2.45 GHz)	Argon 2 SLM*	Few seonds per spot

*SLM : Selective Layer Melting

The findings suggest that the surface of illite permanently becomes pinkish once it is exposed to oxidative plasma. In addition, optical emission spectra (OES) was used for qualitative analysis of radicals generated by plasma.

2.2.3 Adsorption experiments

Adsorption experiments proceeded to triplicate to ensure reproducibility. The time taken for Cs to reach adsorption equilibrium is ~3 days, thereby the adsorption time is based on 5 days

for sufficient saturation. After 5 days, the mixtures were centrifuged at 3000 rpm for 10 minutes. The supernatant was analyzed using an Inductively Coupled Plasma Mass Spectrometer (ICP-MS). The concentration of cesium before and after adsorption was caluclated to evalaute adsorption efficiency by the following equation:

$$\text{Adsorption efficiency (\%)} = \frac{(C_0 - C_{eq})}{C_0} \times 100 \quad (1)$$

where C_0 is the initial concentration of cesium, and C_{eq} is the equilibrium concentration of cesium after adsorption.

3. Results

3.1 Adsorption experiments

We investigated that the adsorption of cesium with illite which was modified through various reaction. However, in the AOPs except plasma reaction, precipitates are generated and 3.7% is mixed as precipitates in 0.1 g of each solids. Additionally, the adsorption experiments for cesium were performed using 0.1 g of those precipitates. The precipitates produced by the FR and FLR showed the adsorption efficiencies of ~ 1.7% and 0% for cesium. Although these effects were insignificant, the adsorption efficiencies of the FR and FLR illite were corrected.

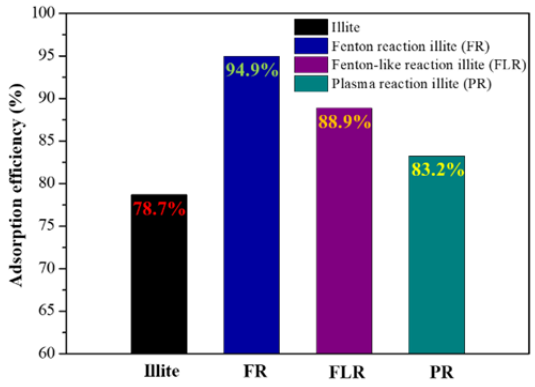


Fig. 1. Adsorption efficiencies depending on illites treated with AOPs.

Among the illites treated with the AOPs, FR illite indicated the highest adsorption efficiency of ~ 95% (Fig 1). The Fenton reaction uses ferrous ions to react with hydrogen peroxide, producing hydroxyl radicals as shown in equation:

$$H_2O_2 + Fe^{2+} \rightarrow OH\cdot + OH^- + Fe^{3+} \quad (2)$$

The hydroxyl radicals with strong oxidizing ability act on illite to reduce the stability of minerals. Other AOPs including the Fenton reaction also generated the hydroxyl radicals which affect on the surface of illite. It is especially notable that the FES present in the interlayer not only adsorbs cesium, but also adsorbs on the surface of minerals.

4. Conclusion

For adsorption experiments, we treated the illite with AOPs. Based on our results, it was found that all illites treated with AOPs showed relatively higher adsorption efficiency than natual illite. Because of the hydroxyl radicals generated by the AOPs, the surface of illite is modified. Although natural illite selectively absorbs cesium with FES, our results provide new evidence in increased adsorption for cesium on the surface through AOPs.

ACKNOWLEDGEMENT

This work was supported by the Korea Institute of Energy Technology Evaluation and Planning (KETEP) and the Ministry of Trade, Industry & Energy (MOTIE) of the Republic of Korea (No. 20181510300800).

REFERENCES

[1] Lee, J., Kang, J., & Kim, W.S. (2020). Removal of radioactive cesium in secondary wastewater after soil-washing process. Journal of Korean Society of Environmental Engineers, 42(8), 405-413.

[2] Abou-Shady, A., Bahnasawy, N., & Eissa, D. (2020). Effects of Fenton oxidation on soil mineral stability determined by the Taguchi approach. Journal of the Saudi Society of Agricultural Sciences, 19(4), 270-275.

Studies on Characteristics of $HMnO_4$, a Strong Oxidizing Reagent for NPP Chromium Oxide Decontamination, Prepared by Cation Ion Exchange of KMnO4

Junho Shin[1,*], Seungyeop Han[1], Hyojung Kim[1], Jongho Jeon[1], Wonzin Oh[1], Sang-June Choi[1], Jae Kwan Park[2,*], Byung-Chul Lee[2,*], and Ki-Chul Kim[3]
[1]Kyungpook National University, 80 Daehak-ro, Buk-gu, Daegu 41566, Republic of Korea
[2]Hannam University, 1646 Yuseong-daero, Yuseong-gu, Daejeon 34054, Korea
[3]KEPCO KPS, 69-46 Munsan 2 Sandan1-Ro, Qedong-Eup, Gyeongju-si, Republic of Korea
*sa011107@knu.ac.kr

1. Introduction

A study on the preparation characteristics of HMnO4, a strong oxidizing reagent for the NPP chemical decontamination, was conducted by the ion exchange method using IRN77 and $KMnO_4$.

It was found in the studies that the resin can be decomposed during the stay in the ion exchange contactor and its decomposition products can cause the loss of $HMnO_4$ during the chromium oxide chemical decontamination.

But the cation resins based on ST_DVB matrix were known to be resistant to the oxidizing agents including $KMnO_4$[(2)], even though $KMnO_4$ is used as a TOC measurement agent, oxidizing organics in the water. Jiangbo Li et al(2020)[(1)] recently showed 99% destruction of the spent resin by a microwave enhanced Fenton producing ·OH radicals which surround the surface of resin and break them into small molecule organics and also O_2, CO_2 as in the figure 1 below.

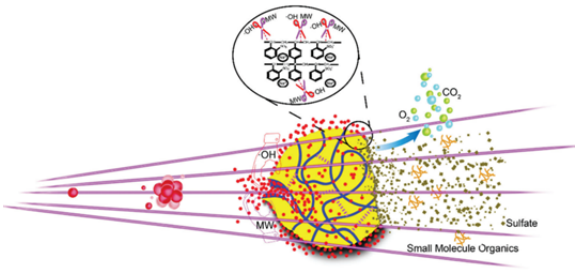


Fig. 1. a scheme in which resins are decomposed by microwave reinforced pentons that produce OH active oxygen.

2. Methods

2.1 Experiments

The batch and column reactors were used as the ion exchange contactors. The Cr_2O_3 pellet decontamination in the HMnO4 prepared by cation exchange was carried out to investigate its loss caused by the resin degradation products. The breakthrough experiments were carried out by changing the flow rate, Q= n BV/hr and the concentration of $KMnO_4$, where n of IRN77 provided by the Amberlite is 8~50.

2.2 Theory

The oxidation reactions of Cr_2O_3 and H_2O by $HMnO_4$ can be expressed as the followings.

$$Cr_2O_3+2MnO_4^-+H_2O \rightarrow 2HCrO_4^-+2MnO_2 \quad (1)$$

$$MnO_4^{-+}+ \rightarrow MnO_2+4/3H_2O \quad (2)$$

The oxidation reaction of the resin degradation organic products like carboxyl acid can be expressed as follows:

$$H_2C_2O_4+2/3MnO_4^- \rightarrow 2/3MnO_2+2CO_2+4/3H_2O \quad (3)$$

3. Results and discussion

3.1 Effect of resin degradation on loss of HMnO4

The figure 2 showed the Cr2O3 pellet decontamination behaviors using the HMnO4 prepared by IRN77 batch ion exchange contactor, where HMnO4 solution was heated at 95℃ for 50 min in advance of Cr pellet decontamination.

The loss of HMnO4 are expected by two roots, one of them is self-decomposition by H2O(3) and the other is oxidation of the resin degradation products as in the equation (2) and (3), respectively.

The experimental results showed that the first root loss is small and negligible comparing the loss due to the resin degradation products.

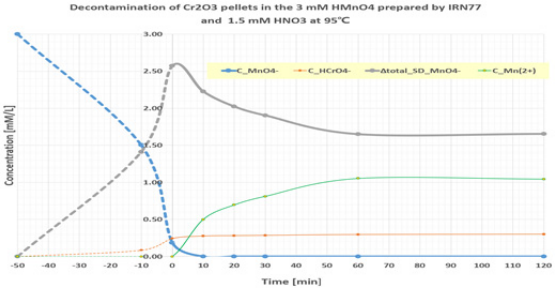


Fig. 2. Cr_2O_3 oxidative decontamination using the HMnO4 prepared by batch contactor.

3.2 Break through behaviors depending on the C_KMnO4 and flow rate, Q=n x BV/hr

The resin degradation products might be small but were difficult to identify their phases, size and species. The figure 3 showed the results of breakthrough experiments depending on the concentration of KMnO4 and flow rate, Q = n BV/hr.

Figure 3_(a) showed good cation exchange behavior, while figure 3_(b) showed poor due to resin degradation.

And more the figure (b) showed that the resin degradation products caused the degradation of cation exchange capacity, especially at n ≤ 15, where comparing with those in figure (a), KMnO4 concentration was higher and the contact time, T_residence = BV/Q ∝ 1/n, was relatively longer in the continuous ion exchange column contactor.

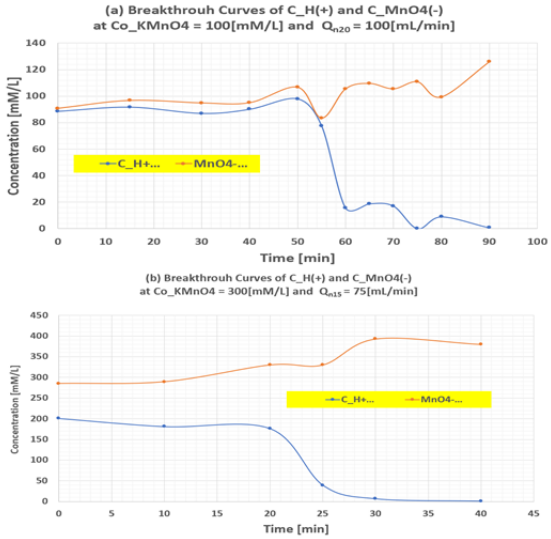


Fig. 3. Breakthrough of C_H^+and_MnO_4^- in IX column at different concentration and flow rate.

4. Conclusion

The iRN77 resin degradation characteristics during the cation exchange of KMnO4 were studied experimentally and the following conclusions were obtained in the experimental range.

1. The ion exchange resin based on the ST DVB matrix such as IRN 77 can be degraded during ion exchanging the strong oxidant like KMnO4 in case of long contacting and high concentration.

2. The resin degradation products can cause a loss of HMnO4 during the NPP oxidative chemical decontamination.

Acknowledgement

This work was supported by the Korea Institute of Energy Technology Evaluation and Planning (KETEP) and the Ministry of Trade, Industry and Energy (MOTIE) of the Republic of Korea (No. 20191510301310).

References

[1] Jiangbo Li et al, Energy Engineering, vol 117 no 3 (2020).

[2] Boweman et al, BNL-NUREG-51987(1988).

[3] Hyun Kyu Lee, wonzin oh, JRNC Vol 317, no 3 (2018).

Identification Algorithm Based on Neural Network for Gamma Spectra in Low Level Activity Measurement

Inhye Hahm*, Eunjoong Lee, Byungchae Lee, Young-Su Kim, Junha Kim, and Sang Bum Hong
Korea Atomic Energy Research Institute, 111 Daedeok-daero 989beon-gil, Yuseong-gu, Daejeon, Republic of Korea
*hih@kaeri.re.kr

1. Introduction

In Korea, it is expected that more than 40% of the cost of decommissioning nuclear power plants will be spent on waste management [1]. There is a growing need for safe and cost-effective management of radioactive waste. The method of handling radioactive waste typically begins with the characterization of waste, along with the conditions for the acceptance of waste, will determine on the possible measures that the waste must take before it reaches its final disposal or clearance. Accurate characterization can help to reduce costs and increase safety if we know whether the waste is radioactive or not, and which nuclides are present.

Although it is not difficult to identify radioisotope in a spectrum using established methods, there could also be situations in which the level is close to the signal from the isotope. This can happen when the radioactivity of the isotope is very low or the measurement time is short. In such cases, machine-learning algorithms may be more suitable to correctly interpret the data and detect the presence of certain isotopes with more confidence [2].

Since decommissioning waste is generated in large quantities in a short period, it is possible to reduce the effort in the analysis process if the identification and quantification is possible with a short time measurement. In this study, we suggested a neural network based algorithm that automatically identifies gammy-ray spectra for sources with very low activity.

A high purity germanium (HPGe) detector was used for measurement, and the measurement time was performed in less than 60 seconds, targeting a spectrum that is difficult to identify with the existing peak search algorithm (GENIE-2000).

2. Methods

2.1 Overview

In order to enhance stability, reliability, and availability of assets, nuclear technology has increased its interest in using data-driven methods. Machine-learning algorithms have been implemented for a variety of applications in spectroscopy, such as calibration drifts, data uncertainties, peak overlapping, and isotope classification among many others [3].

Artificial neural networks (ANNs) are computer structures inspired by the biological neural networks that form brains, typically called neural networks. An ANN is based on a set of unit or nodes called artificial neurons that are linked. Like the synapses in a biological brain, each connection can send a signal to other neurons.

By inputting the energy observed in each channel of the detector, information on each nuclide was learned and the identification of the nuclide was output. (Figure 1) The activation function for the output layer is the softmax which is traditionally used for classification.

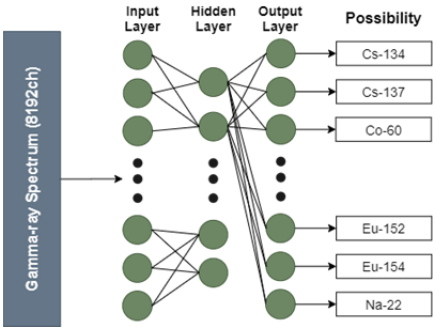


Fig. 1. Overview of neural network composition.

2.2 Training, validation and test sets creation

In general, learning is conducted with a training set, and this learning process is evaluated through a validation set for proper stop. The performance of the ANNs is evaluated through test sets.

The efficiency of the algorithm based on ANN depends primarily on what data is used for training. As the training accuracy is higher, over fitting may occur, so it is also important to secure enough data.

A source with weak radioactivity was used to take into account the situation where there was no significance difference from the background. ^{60}Co, ^{137}Cs and ^{152}Eu gamma reference sources were used, and the radioactivity is as follows respectively: 2.32E+04(Bq), 2.93E+03(Bq), 1.39E+05 (Bq).

Each source was measured at 0.5m, 1m, and 2m distances from the HPGe detector for 60 seconds, respectively, and it was confirmed that the measurement result was not identified by GENIE-2000 software due to the small difference from the background (Figure 2). One data set consisted of the number of 120 spectra from 8192 channel, and 12 data sets were obtained for each nuclide. In the same way, 4 sets of background data were also measured.

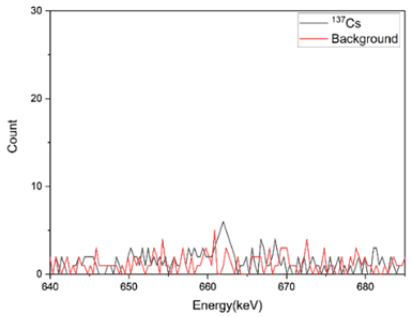


Fig. 2. Comparison of Cs-137 and background measurement results.

These data were randomly shifted for the peak regions of each nuclide, and 10% of the 5000 spectra was allocated to the validation set. The test set used spectra measured by a similar method, and soil measurement data including reference source.

2.3 Hyper-parameter tuning

In order to find the optimal parametric configuration that maximizes the network efficiency, several parameters implemented in the neural network algorithm have been varied: the number of layers, the number of neurons, and the activation function in each layer, the learning rate of the optimizer [4] In this study, it was observed that increasing the number of layers increase the risk of overfitting.

3. Result and discussion

In this study, the loss was calculated using mean squared error (MSE)

$$\mathrm{MSE} = \frac{1}{\mathrm{N}}\sum_{i=1}^{N}(y_i - \hat{y}_i)^2 \qquad (1)$$

where y_i is the true value of output, and $\hat{y}_i$ is the calculated output.

Even in the relatively low epoch, the learning process terminated, which seems to be because the types or radioisotope were not diverse. The performance of the learned neural network is more than 95% accurate.

Through this study, the possibility of gamma spectrum analysis in low level activity measurement was confirmed. By experimenting with various measurement environments and nuclides, the algorithm will be improved so that it can be used to measure decommissioning waste and sites.

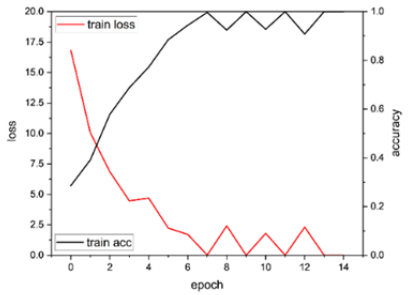


Fig. 3. Train accuracy and loss according to number of epochs.

Acknowledgements

This work was supported by a grant from the National Research Foundation of Korea (NRF), funded by the Korean government, Ministry of Science, ICT and Future Planning (No. 2017M2 A8A5015143).

REFERENCES

[1] KEPCO International Atomic Energy Graduate University, “Final report on technology development of regulatory elements for nuclear power plant decommissioning waste management and radiation environment impact verification”, NSSC (2018).

[2] E. Masala and L. Blomeley, “Machine-Learning Algorithm for Shielded Special Nuclear Materials Detection”, CNL Nuclear Review (2019).

[3] M. G. Fernandez, K. Higley, A. Tokuhiro, K. Welter, W. K. Wong, and H. Yang, “Status of research and development of learning-based approach in nuclear science and engineering: A review, Nuclear Engineering and Design, Volume 359 (2020).

[4] M. Kamuda, J. stinnett, and C.J. Sullivan, “Automated Isotope Identification Algorithm Using Artificial Neural Networks”, IEEE transaction on Nuclear Science (2017).

Tritium Removal Behaviors of Protonated Lithium Metal Compounds in Water

Chan Woo Park*, Sung-Wook Kim, Youngho Sihn, and In-Ho Yoon
[1]Decommissioning Technology Research Division, Korea Atomic Energy Research Institute, Yuseong-gu, Daejeon, Republic of Korea
*chanwoo@kaeri.re.kr

Abstract

A large amount of radioactive tritium can be produced in nuclear power plant. The boron activation contributes the most to tritium source in the effluent stream of pressurized-water reactors. On the other hand, neutron bombardment of deuterium mainly contributes to the production of tritium in heavy water reactor. Accidental release of such tritiated water can cause contamination of the aquatic environment such as groundwater and can produce tremendous amount of liquid waste. In addition, the liquid waste containing considerable amount tritium has been produced as a result of the Fukushima nuclear accident in Japan. However, separations of hydrogen isotopes are still technically challenging because chemical properties of hydrogen isotopes are very similar.

In this presentation, we report the exchange behaviors of hydrogen isotopes between various protonated lithium metal compounds and tritiated water. Protonated lithium metal compounds were prepared by acid-treatment of various lithium metal compounds including spinel-structured lithium manganese oxide (LMO), spinel structured (LMNCO), layered lithium cobalt oxide (LCO), and olivine-structured lithium iron phosphate (LIP). The prepared materials are denoted as PMO (protonated lithium manganese oxide), PMNCO (protonated lithium manganese nickel cobalt oxide), PCO (protonated lithium cobalt oxide), and PIP (protonated lithium iron phosphate), respectively.

Elemental contents of Li and transition metal (Mn, Co, Ni) in the compounds were analyzed to verify the formation of protonated lithium metal compounds by replacement of Li^+ with H^+ via acid-treatment. The weight fraction of Li in the compounds was significantly reduced after the acid treatment of the lithium metal compounds because Li^+ was replaced by H^+ via the treatment. The X-ray diffraction (XRD) analysis was also performed to analyze changes in crystal structures of the compounds after the acid treatment. The XRD patterns showed a slight peak shift to higher angles after the acid treatment, and it implies the lattice structure was shrieked by Li^+/H^+ exchange.

To analyze tritium removal behavior of the protonated lithium metal compound, the tritiated water was mixed with protonated lithium metal compounds for the desired time. The supernatant was separated and filtered with ultrafiltration membrane. The radioactivity of tritium remaining in the supernatant was determined by a liquid scintillation counter (Hidex 300SL). Among the various protonated lithium metal compounds, the PMNCO could remove largest amount of tritium in light water. The highly electronegative metal components present in the protonated lithium metal compounds seems to enhance exchange of proton with tritium in water.

Logistical Simulation for Concrete Treatment Process in Decommissioning

Bong-su Yoon*, David Kessel, and Chang-Lak Kim
KEPCO International Nuclear Graduate School
658-91 Haemaji-ro, Seosaeng-myeon, Ulju-gun, Ulsan, Republic of Korea
*ss156@hanmail.net

1. Introduction

In October 2015, the Atomic Energy Commission reviewed and decided on the policy direction to prepare for the safe and economic dismantling of Kori-1 without a hitch and strategically prepare for the future nuclear dismantling market. This means that the NPP Business Project is expanding into the entire life cycle considered from development-oriented to decommissioning.

According to the draft decommissioning plan, the steps for site remediation are as shown in Table 1. [1]

Table 1. The Decommissioning Plan

Contents	Period
1. Prepared in advance	~ 2017.06
2. Approval of decommissioning	~ 2022.06
3. Dismantling	~ 2029.12
4. Site remediation	~ 2031.12

The dismantling of concrete buildings is carried out for two years, and an efficient disposal process is needed to dispose of large quantities of concrete waste as planned. Therefore, this report is intended to be modeled using the Flexsim software to implement specific processes that minimize factors that could affect the dismantling schedule and maximize clearance.

2. Literature Review

2.1 Concrete Properties

The concrete is composed of 35% porous cement paste and the remaining 65% of the aggregate. The cement paste exhibits the properties of adhesion in response to water, and the aggregate consisting of quartz or limestone is entangled, enabling the formation of structures.

The contamination of concrete is closely related to the movement of moisture and its adsorption quantity. According to Bladley's Formula, the thickness of the adsorption layer is about 4.5Ă at 50% relative humidity. [2] This can be inferred that concrete contamination occurs only on the concrete surface or on the leak.

Most contaminations are concentrated in porous cement paste. The cement paste has a smaller adhesion strength from about 300℃ according to the change in the properties of hydration products, and thermal destruction of aggregates can occur at temperatures above 573℃.

2.2 Decontamination of Radionuclide

Concrete waste can be largely classified by means of contamination and radiation by radioactive materials.

Since concrete is theoretically a waterproof material, contamination can only occur on the surface. Thus, if the contamination of concrete is removed by radioactive materials in an appropriate method, the level of radioactivity is reduced to a level that can be clearance.

Radiated concrete is closely related to the properties of materials and the location of structures. In other words, substances close to the reactor and with large neutron reactivity cross-section are highly likely to be contaminated by radiation. Radiated concrete studies show that concrete radiation is close to MDA at a thickness of more than 20cm.

3. Application of Technology

3.1 Pretreatment of concrete building

To dismantle a concrete building, separation is necessary according to the degree of contamination of the concrete. For this purpose, appropriate pretreatment shall be performed. Mechanical grinding is performed for surface contamination of concrete. The type of shaving machine determines the grinding thickness and capacity. Contamination by radiation can be separated by non-contaminated concrete and radial concrete using cutting. Diamond Wire Saw method is suitable for small, closed working environments.

3.2 Classification by concrete component

Concrete of low contamination level are classified as aggregate and concrete paste by the process below. Aggregates can be clearance, and concrete pastes are treated as radioactive waste.

Crush → Heat → Mill → Sieve

Each process shall be established on the basis of the technical standards currently used. [3]

3.3 Procedure for clearance of concrete waste

Clearance of concrete is carried out by the following process:

a. Selection of wastes for clearance using surface radiation dose rate
b. γ-emit nuclide, Gross α/β analysis
c. Obtaining Permit
d. Disposal in landfill

4. Simulation

4.1 Assumptions in Simulation Modeling

Modeling finds motifs in the classification of radioactive wastes and the use of aggregate regeneration of concrete wastes. Because the Flexsim software is capable of continuous fluid based types and discrete continuous simulations, the necessary methods were used for each process. Also, the Flexsim software should set the quantified data. Therefore, the modelling process is simplified and the numbers are quantified as representative values.

4.2 Input Data

The total amount of concrete was assumed to be 11,370 tons, and the set value in each process was determined using machine certification, which is currently widely used in the industry. Table 2 shows as the input data used in the model.

Table 2. Input Data in Model

ITEM (or process)	Capacity
Wire Saw	2.7m^2/hour
Shaving	12 m^2/hour
Surface measuring	15 m^2/hour
Crushing	20 m^2/hour
Heating	3.5 m^2/hour
Milling	30 m^2/hour
Sieving	3.5 m^2/hour
HPGe Detector	1.6 tons/1000sec
Gross α/β count	1.6 tons/hour *5times
γ Detector	2 tons/hour

4.3. Simulation Model

The concrete's treatment process model is simulated as shown in Figure 1. This model is based on the treatment of concrete waste at the actual nuclear power plant. The classification and pre-treatment of concrete waste is performed using a fluid-type process, and an event-type process is used for clearance of concrete.

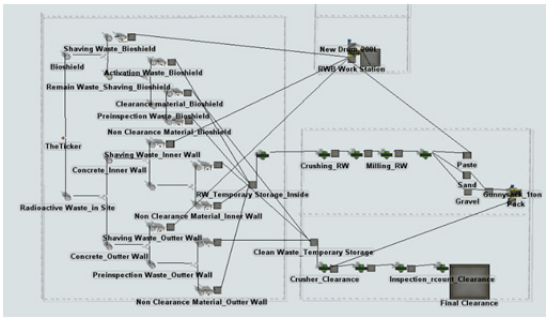


Fig. 1. Aerial View of Concrete's Treatment Process.

5. Conclusion

In this study, the concrete treatment process simulation was presented based on the technology currently used in the industrial site.

In the case of the scenario assuming 11,370 tons of concrete, 5,181 drums of radioactive wastes (200L size of drum) and 10,929 drums of clearance wastes (1,000L size of drum) are generated. And the results show that it takes about 6,066 hours to complete treatment of concrete waste. This indicated that concrete waste could be disposed of during the building dismantling period (two years) as proposed in the draft decommissioning plan.

The critical paths of each process are 'Wall Shaving', 'Heating of Radioactive Waste' and 'Cross α/β Count'. If the exact total amount of concrete is calculated, this simulation will help to calculate the number of people and equipment of the Critical Path.

ACKNOWLEDGEMENT

This work was supported by the Korea Institute of Energy Technology Evaluation and Planning (KETEP Project No. 20204010600130) and the Ministry of Trade, Industry & Energy (MOTIE) of the Republic of Korea.

REFERENCES

[1] KHNP, Final Decommissioning Plan for Kori Unit 1 Abridgement, (2020).
[2] Dong-woo Ryu, Prediction Model of Moisture Distribution Considering Simultaneous Transfer of Heat and Moisture in Concrete, (2009).
[3] I.P Binkhorst, Technology for Resue of Contaminated Concrete Constituents, (1998).

Choosing a Knowledge Management Strategy for Decommissioning of NPP

So-Yoon Kim*, David Kessel, and Chang-Lak Kim
KEPCO International Nuclear Graduate School
658-91 Haemaji-ro, Seosaeng-myeon, Ulju-gun, Ulsan, Republic of Korea
*soyooon@gmail.com

1. Introduction

The decommissioning of NPP is a long-term project, so it is important to preserve and utilize knowledge. The application fields of use of NPP decommissioning knowledge management (KM) include recording, managing, and improving the efficiency and utilization of all data produced in the NPP decommissioning project, making objective decisions based on data, collecting opinions from stakeholders, and public acceptance.[1] This paper intends to present a model that can be applied to decommissioning project. To propose a framework for KM, Analytic Network Process (ANP) was used as a decision-making tool.

2. Background of KM

2.1 Knowledge type

The knowledge of an organization is created through the continuous interaction between the explicit knowledge and tacit knowledge of the members of the organization. Explicit knowledge is the knowledge that can be easily expressed and understood and easily transferred to others. Tacit knowledge is difficult to express and transfer to others.[2] Tacit knowledge includes intuitive knowledge that is difficult to teach, such as innovative thinking or body language.

2.2 Definition of KM

KM is the processes of capturing, handling and using knowledge that exists within an organization.[2] KM relies on an understanding of knowledge, which consists of discrete or intangible skills that a person or institution possesses.

3. KM Strategy Decision Analysis

For successful KM implementation, an organization must be able to evaluate and select a KM strategy that is more favorable to the project. It is a Multi-Criteria Decision Making (MCDM) problem that must consider several complex factors [3].

3.1 Analytic Network Process (ANP)

The ANP presents an optimal solution through a more accurate approach to the real world in the case of interdependence between each level in the decision-making process or within the same level and a complex decision-making environment. Unlike AHP expressing dependencies between layers in one-way hierarchical arcs, ANP allows the expression of dependencies in each layer or within the same layer as two-way arcs.[3] In general, ANP proceeds through the following 5 steps:

a. Create a decision-making network that expresses the relationship.
b. Perform a pair-wise comparison between each element.
c. Calculate the relative importance of each factor.
d. Create a Super-matrix in which all elements on the network are arranged in rows and columns of a matrix, and the importance of each element is a column vector.
e. Super-matrix is multiplied to an infinite square to calculate the stabilized importance.

3.2 Decision-making framework

To make a decision, it is required to calculate and select an evaluation group, such as the clustering of purpose, competency, and strategy of KM. Fig. 1 is a decision-making framework that utilizes ANP to evaluate and select knowledge management strategies that are more advantageous for NPP decommissioning project.

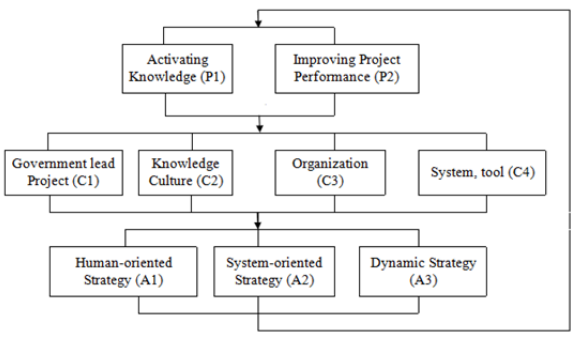


Fig. 1 Decision-making framework.

3.3 Application of ANP

A survey was conducted with five people with knowledge related to the decommissioning of NPP. To quantify the importance of each item, a two-way comparison was performed using Saaty's nine-point scale ranging from 1 to 9. After conducting the survey, the geometric mean value was used for analysis. Also, Super Decisions 2.10.0, a program dedicated to ANP, was used.

3.4 Analysis of results

First, as shown in Table 1 below, through the unweighted super-matrix, it can be seen that each knowledge management strategy represents its knowledge management purpose. From a human-oriented strategy, "Activating Knowledge" (0.857), from a system-oriented strategy, "Improving Project Performance" (0.857) showed relatively important. In terms of dynamic strategy, "Activating Knowledge" (0.667) showed relatively high importance.

Table 1. The unweighted super-matrix

Clusters	Alternative			Competency				Purpose	
	A1	A2	A3	C1	C2	C3	C4	P1	P2
A1	0	0	0	0.099	0.571	0.232	0.168	0	0
A2	0	0	0	0.537	0.143	0.184	0.484	0	0
A3	0	0	0	0.364	0.286	0.584	0.349	0	0
C1	0	0	0	0.000	0.143	0.289	0.101	0.086	0.182
C2	0	0	0	0.143	0.000	0.379	0.433	0.424	0.091
C3	0	0	0	0.429	0.429	0.000	0.466	0.331	0.364
C4	0	0	0	0.429	0.429	0.331	0.000	0.159	0.364
P1	0.857	0.143	0.667	0	0	0	0	0	0
P2	0.143	0.857	0.333	0	0	0	0	0	0

Also, as a result of finding out which factors play a relatively important role according to the purpose of knowledge management, from the perspective of Activating Knowledge, "Knowledge Culture", and from the perspective of Improving Project Performance, "Organization" and "System or tool".

And the overall priorities were obtained from the limit super-matrix shown in Table 2. The most considered purpose was "Activating Knowledge" (P1) due to the highest priority of 0.141; the most important competency was "Organization" (C3) due to the highest priority of 0.161, and the desired alternative was Strategy "Dynamic Strategy" (A3) due to the highest priority of 0.103.

Table 2. The limit super-matrix

Clusters	Alternative			Competency				Purpose	
	A1	A2	A3	C1	C2	C3	C4	P1	P2
A1	0.072	0.072	0.072	0.072	0.072	0.072	0.072	0.072	0.072
A2	0.076	0.076	0.076	0.076	0.076	0.076	0.076	0.076	0.076
A3	0.103	0.103	0.103	0.103	0.103	0.103	0.103	0.103	0.103
C1	0.072	0.072	0.072	0.072	0.072	0.072	0.072	0.072	0.072
C2	0.134	0.134	0.134	0.134	0.134	0.134	0.134	0.134	0.134
C3	0.161	0.161	0.161	0.161	0.161	0.161	0.161	0.161	0.161
C4	0.133	0.133	0.133	0.133	0.133	0.133	0.133	0.133	0.133
P1	0.141	0.141	0.141	0.141	0.141	0.141	0.141	0.141	0.141
P2	0.109	0.109	0.109	0.109	0.109	0.109	0.109	0.109	0.109

4. Conclusion

This ANP analysis on nuclear decommissioning projects shows that an appropriate evaluation KM strategy is essential to the purpose and strategic choice. Before the introduction of KM, priority should be preceded by clarifying the objectives of the NPP decommissioning projects. This is because the necessary strategies and competencies in the project vary according to the main purpose.

ACKNOWLEDGEMENT

This work was supported by the Korea Institute of Energy Technology Evaluation and Planning (KETEP Project No. 20204010600130) and the Ministry of Trade, Industry & Energy (MOTIE) of the Republic of Korea.

REFERENCES

[1] KAERI, "The State-of-the-Art Report for the Knowledge Management System for the Radioactive Waste Repository", KAERI/ AR-900/2011, (2011).

[2] Martie Maria Squier, "The principles and practice of knowledge management", Built Environment and Information Technology University of Pretoria, (2003).

[3] Young-Chan Lee, "Decision Making Framework for Achieving Successful Knowledge Management", Article in The Journal of Information Systems, (2009).

Establishment of Restricted Recycling Scenarios of Very Low Level Waste From Decommissioning and Preliminary Radiological Assessment of Potential Risk

In Gyu Chang and Jae Hak Cheong*
Dept. of Nuclear Engineering, Kyung Hee Univ., 1732 Deokyoung-daero, Giheung-gu, Yongin-si, Gyeonggi-do
*jhcheong@khu.ac.kr

1. Introduction

A large amount of waste is generated when the nuclear power plant is decommissioned, and it is necessary to consider a plan for the treatment of decommissioning waste. Restricted recycling of decommissioning waste in public has difficulty due to the problem of acceptability of residents. Therefore, a scenario of restricted recycling within the nuclear industry can be considered. There are some cases of the recycling of decommissioning waste abroad, and in Europe there is a report that presents a list of restricted recycling scenarios and evaluates the economics not radiological assessment [1].

In Japan, there is a case of recycling waste from nuclear power plants as welding tables or chairs on the site of the nuclear power plant. In Spain, concrete waste from decommissioning the nuclear power plant is used as a backfill material for radioactive waste storage facilities, and waste from the storage of medium and low level radioactive waste recycled as grout/concrete for filling the container. In the case of the UK, it was recycled as an ISO container barrier for transporting low-level radioactive waste. In Germany, it was recycled as a container for radioactive waste. In the United States, decommissioning waste was recycled by making shielding blocks or type B waste containers [2].

However, regulatory standards for restricted recycling have not yet been established, and research on them is necessary.

2. Methodology

2.1 Establish Restricted Recycling Scenarios

The majority of decommissioning waste are steel and concrete. The scenario of restricted recycling of steel and concrete, which is an extremely low level radioactive waste, within the nuclear industry was established. In EUR-18041 report, restricted recycling scenarios are listed. Table 1 shows scenarios of restricted recycling.

Table 1. List of EUR-18041 restricted recycling scenarios

Material	Scenario
Stainless Steel	Vitrified Waste Product Canisters
Stainless Steel	Waste Drums
Carbon Steel	Waste Disposal Box
Carbon Steel	ISO Transport Container
Carbon Steel	Reinforcing Bars
Carbon Steel	Granulate and Fibres
Aluminum	Storage Canister
Copper	Spent Fuel Disposal Container
Concrete	Shield Walls
Concrete	Prefabricated Concrete Pieces
Concrete	Immobilisation Medium for Drums

In addition, restricted recycling scenarios have been established for domestic situation. In the case of carbon steel, a scenario for recycling with DOT-17H drums was selected. In the case of concrete, a scenario of recycling as a concrete disposal container with recycled aggregate and silo backfill with crushed concrete waste was selected.

Table 2. List of restricted recycling scenario considered by domestically

Material	Scenario
Carbon Steel	DOT-17H Drum
Concrete	Silo backfill
Concrete	Disposal container

In the case of restricted recycling, it is assumed that all of the recycling facilities exist in the nuclear industry because it is recycling within the nuclear industry, and it is assumed that steel recycling facilities exist within the site of a nuclear power plant and concrete recycling facilities exist within the site of a repository.

In the case of steel waste, the throughput was assumed to be 100 ton, and in the case of concrete, it was assumed to be 100 ton. Each of amount is assumed by data of report and research.

2.2 Evaluation of Exposure Dose

The methodology for evaluating the restricted recycling scenario is shown in Fig.1. First, a restricted recycling scenario is established, and

radiological assessment is conducted using the default values within RESRAD, IAEA report. At this time, an additional consideration should be given offsite dose as dust escape from the factory during the waste processing. Therefore, it was evaluated using Reg.Guide 1.109 model. The allowable concentration for each type of nuclide was derived from the results of the radiation exposure dose by workers and offsite dose assessment. Based on the derived results, the concentration of very low level radioactive waste and the concentration of low level radioactive waste were compared. We consider range of very low level radioactive waste therefore we need to decide the result is int this range and reasonable or needed to be more considered.

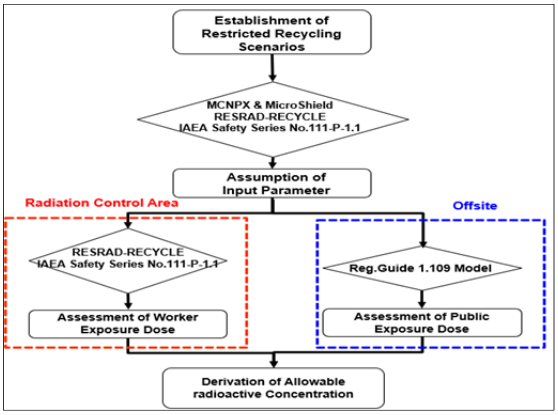


Fig. 1. Methodology of radiological assessment of restricted recycling.

2.3 Derivation of Allowable Nuclide Concentration of Restricted Recycling

In the case of restricted recycling, since recycling is carried out in a controlled situation within the nuclear industry, it is expected that a dose limit higher than 10 μSv/y, the allowable dose for clearance waste, is expected. However, even if decommissioning waste is recycled within the nuclear industry, it is not reasonable to allow up to 20 mSv/y, the annual dose limit of radiation workers, because it includes workers not radiation worker in the recycling process, and restricted recycling at dose of 1 mSv/y, the dose limit of the general public. Based on this, the restricted recycling allowable concentration (draft) was presented.

3. Results

In the process of recycling decommissioning waste, the exposure dose per unit radioactivity concentration received by workers was evaluated, and dose assessment for offsite dose was conducted. Based on this, the restricted recycling allowable concentration (draft) was derived. The resulting restricted recycling allowable concentration (draft), very low level radioactive waste concentration, and low level radioactive waste concentration limit were compared. In this study, a preliminary radiological assessment of the restricted recycling of DOT-17H drums was conducted.

As a result, it was evaluated that the radioactivity concentration was high for each nuclide due to controlled situation and relatively short working time because of little amount of decommissioning waste.

4. Conclusion

Most of the large amounts of waste generated when decommissioning nuclear power plants are wastes subject to clearance waste or very low level radioactive waste. In this study, a preliminary assessment of restricted recycling was conducted and a restricted recycling allowable concentration (draft) was derived. Based on the data on the amount of very low level radioactive waste generated at the time of decommissioning a nuclear power plant, it is expected to be able to derive a clearer evaluation of the radiation exposure of workers per unit radioactivity concentration, offsite dose, and a restricted recycling allowable concentration.

Therefore, this study is expected to be used as basic data for research on restricted recycling.

ACKNOWLEDGEMENT

This work was supported by the Nuclear Safety Research Program through the Korea Foundation Of Nuclear Safety (KoFONS) using the financial resource granted by the Nuclear Safety and Security Commission (NSSC) of the Republic of Korea (No. 1605008).

REFERENCES

[1] U.S. Nuclear Regulatory Research, “RADIOLOGICAL ASSESSMENTS FOR CLEARANCE OF MATERIALS FROM NUCLEAR FACILITIES”, NUREG-1640, (2003).

[2] International Atomic Energy Agency, “Application of Exemption Principles to the Recycle and Reuse of Materials from Nuclear Facilities”, Safety Series No. 111-P-1.1, (1992), Vienna.

The Effect of ICRP's New Internal Dosimetry Models on Occupational Internal Exposure During Dismantling of Radioactive Concrete

Siwan Noh* and Seungnam Yu
Korea Atomic Energy Research Institute, 989 Daedeok-daero, Yuseong, Daejeon 34057, Korea
*snoh@kaeri.re.kr

1. Introduction

In the current occupational internal dosimetry, internal dose coefficients and bioassay functions provided in ICRP (International Commission on Radiological Protection) Publication 68[1] and 78[2] based on Publication 60[3] are used. Recently, ICRP developed new recommendations on occupational internal dosimetry based on Publication 103[4] to provide revised internal dose coefficients and bioassay functions that reflect the latest data and dosimetry systems throughout Publication 130[5], 134[6], 137[7], and 141[8] that are called the series of OIR (Occupational Intakes of Radionuclides).

In decommissioning of nuclear power plants, the amount of concrete waste accounts for a large portion of the total waste and some concrete such as bio-shield concrete are radioactive by neutron activation. In the process of dismantling radioactive concrete, internal exposure to workers can occur mainly by inhalation of aerosol during cutting operation.

Although internal dosimetry based on ICRP Publication 60 is currently used, OIR models are expected to be used in the near future. Therefore, in this study, we evaluate the effect of OIR internal dosimetry models on concrete dismantling worker by comparing internal doses calculated from existing models with doses calculate from OIR models.

2. Materials and Methods

First of all, we selected major nuclides that mainly contribute to the internal exposure of workers during radioactive concrete dismantling from previous study [9,10]. In this study, ^{3}H, ^{55}Fe, ^{60}Co, ^{152}Eu, and ^{154}Eu are selected as major nuclides.

Internal dosimetry is largely divided into prospective and retrospective dosimetry. In the prospective dosimetry, only internal dose coefficients are used to calculate internal exposure of workers since intake activities are already estimated. In retrospective dosimetry, however, bioassay functions such as intake retention and excretion functions in addition to internal dose coefficients are needed to estimate intake activities of workers.

Along with dose coefficients, the OIR provides the dose per content functions, *z(t)* needed for the bioassay and these functions are calculated by dividing internal dose coefficients by intake retention or excretion function. Therefore, committed effective doses are calculated by multiplying the measured activities from bioassay and dose per content function for corresponding elapsed time. In this study, we compare internal dose coefficients and dose per content function of whole-body retention for ^{3}H, ^{55}Fe, ^{60}Co, ^{152}Eu, and ^{154}Eu based on Publication 60 and 103. Publication 60 based internal dose coefficients and intake retention functions are converted into the type of *z(t)* and compared to *z(t)* provided in OIR.

In case of prospective dosimetry, OIR is applied to internal dose calculation of worker for dismantling scenarios and intake activities from previous study [9,10] and calculated doses based on ICRP 60 and OIR are compared. Table 1 shows the activity concentrations of major nuclide in radioactive concrete based on the previous study.

In this study, we considered only inhalation as intake route and AMAD of 1 and 5 μm as particle size of inhaled aerosol. In case of absorption type, default absorption type for each nuclide by Publication 68 and OIR, and the chemical form of ^{3}H is assumed as HTO, respectively.

Table 1. Activity concentrations of major nuclide in radioactive concrete

Study 1 [9]	Activity Conc. [Bq/g]	Study 2 [10]	Activity Conc. [Bq/g]
^{3}H	1.15E+05	^{55}Fe	1.38E+04
^{60}Co	5.22E+03	^{152}Eu	8.65E+03
^{55}Fe	2.83E+03	^{60}Co	3.58E+03
^{152}Eu	1.63E+01	^{154}Eu	7.93E+02
^{154}Eu	5.60E-01		

3. Results and Discussion

Table 2 shows the internal dose coefficients for major nuclides provided in ICRP 68 and OIR. In case of ^{3}H, it can be seen that the internal dose coefficient increases by 10% with OIR

application. For ^{55}Fe, the coefficients decrease by 60% and 80% for 1μm and 5 μm AMAD, respectively. For ^{60}Co, the coefficients increase by 15% for 1μm AMAD and decrease by 9% for 5μm AMAD. For ^{152}Eu, the coefficients decrease by 10% and 33% for 1μm and 5μm AMAD, respectively. For ^{154}Eu, the coefficients decrease by 10% and 33% for 1μm and 5 μm AMAD, respectively.

Table 2. Internal dose coefficients for major nuclides provided in ICRP 68 and OIR (Sv/Bq)

Nuclide	Publication 68			OIR		
	Type	1μm	5μm	Type	1μm	5μm
^{3}H	HTO	1.8E-11		HTO	2.0E-11	
^{55}Fe	F	7.7E-10	9.2E-10	M	3.1E-10	1.9E-10
^{60}Co	M	9.6E-09	7.1E-09	M	1.1E-08	6.5E-09
^{152}Eu	M	3.9E-08	2.7E-08	M	3.5E-08	1.8E-08
^{154}Eu		5.0E-08	3.5E-08		3.6E-08	1.9E-08

Table 3 and 4 show the relative committed effective dose of concrete dismantling worker for the scenario by previous study based on ICRP 68 and OIR, respectively. In case of the Study 1, committed effective doses for 1μm AMAD increase by 11% and dose for 5μm AMAD decrease by 12% because the internal dose coefficient of ^{60}Co, which mainly contribute to dose for the Study 1, increase for 1μm AMAD and decrease for 5μm. In case of the Study 2, committed effective doses for 1μm decrease by 11% and dose for 5μm decrease by 34% because the internal dose coefficient of ^{152}Eu, which mainly contribute to dose for the Study 2, decrease for 1μm AMAD and significantly for 5μm AMAD.

Table 3. Committed effective dose for the scenario from Study 1 based on ICRP 68 and OIR (relative value)

Nuclide	ICRP 68		OIR	
	1μm	5μm	1μm	**5**μm
^{3}H	2.1		2.3	
^{60}Co	50.1	37.1	57.4	33.9
^{55}Fe	2.2	2.6	0.9	0.5
^{152}Eu	0.6	0.4	0.6	0.3
^{154}Eu	0.03	0.02	0.02	0.01
Total	55.0	42.2	61.2	37.1

Table 4. Committed effective dose for the scenario from Study 2 based on ICRP 68 and OIR (relative value)

Nuclide	ICRP 68		OIR	
	1μm	5μm	1μm	**5**μm
^{152}Eu	337.2	233.5	302.6	155.6
^{154}Eu	39.6	27.7	28.5	15.1
^{60}Co	34.3	25.4	39.3	23.2
^{55}Fe	10.6	12.7	4.3	2.6
Total	421.8	299.3	374.8	196.6

Fig. 1 shows the dose per content function, *z(t)* for 5μm AMAD using ICRP 68 and OIR. We can see around 10% and 20% increase for ^{3}H and ^{60}Co while a 15%, 5.6%, and 6.8% decrease for ^{55}Fe, ^{152}Eu, and ^{154}Eu at 7 days of elapsed time.

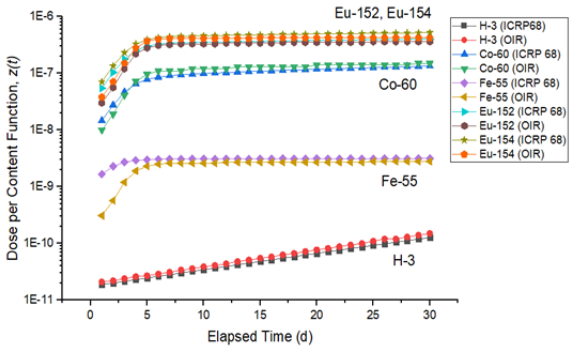


Fig. 1. Dose per content function of whole-body retention, z(t) for 5μm AMAD using ICRP 68 and OIR.

4. Conclusion

In this study, we evaluate the effect of OIR internal dosimetry models on concrete dismantling worker by comparing internal doses calculated from existing models with doses calculate from OIR models. It is confirmed that internal dose of concrete dismantling workers may increase or decrease at a significant level when applying the OIR models.

REFERENCES

[1] ICRP, ICRP Publication 68 (1994).
[2] ICRP, ICRP Publication 78 (1997).
[3] ICRP, ICRP Publication 60 (1991).
[4] ICRP, ICRP Publication 103 (2007.)
[5] ICRP, ICRP Publication 130 (2015).
[6] ICRP, ICRP Publication 134 (2017).
[7] ICRP, ICRP Publication 137 (2017).
[8] ICRP, ICRP Publication 141 (2019).
[9] C.W.Lee et. al., Prog.Nucl.Energ., 126, 103401 (2020).
[10] J.Park et. al., JNFCWT 18(2), 157-167(2020).

A Study on Radiological Inventory Evaluation for RV/RVI and Bio-Shield Concrete of a 1,000MW PWR NPP With Three-Loop

Jae-Hun Ko[a,*], Dong-Gyu Lee[a], Nak-Hoon Sung[a], Jae-Yong Oh[b], and Cheon-Woo Kim[b]
[a]Korea Nuclear Engineering & Service, #5, Hyundai Plaza, 798-1 Yuseong-daero, Daejeon, Korea
[b]KHNP Central Research Institute, 1312-70 Yuseong-daero, Yuseong-gu, Daejeon, Korea
*kojh4@kones21.com

1. Introduction

Radioactive inventory evaluation of nuclear power plant (NPP) is essential in establishing decommissioning plan by providing information about radiation environment, waste amount and cost evaluation. In this study, a three-loop PWR NPP with a design life of 40 years was analyzed and the radioactive inventory of the reactor vessel (RV), the reactor vessel internals (RVI) and bio-shield concrete irradiated to neutrons was calculated.

2. Methods and Results

The activation evaluation of RV/RVI was carried out using a combination of MCNP/ ORIGEN-2 computational codes, and the evaluation procedure is as shown in Fig. 1[1].

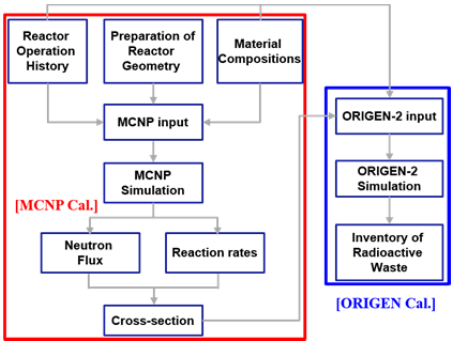


Fig. 1. Procedure of activation evaluation.

The neutrons from fuels located outside of the reactor core have greater effect on activation of the structural components than on the fuels inside. Based on analysis of the power distribution of the fuels located outside of the core, it can be concluded that there are four representative cycle groups among which a representative cycle was selected for each cycle group, as shown in Fig. 2. The distribution of neutron sources for activation evaluation applied radial and axial power distributions of the selected representative cycles. Then, depletion calculations were performed by selecting one fuel of representative cycle using the ORIGEN-ARP module of the SCALE6.1 computer code. The modified material compositions of the fuel were applied as a results of depletion calculation.

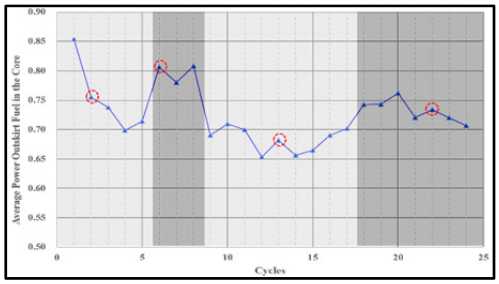


Fig. 2. Selected four representative cycles

As shown in Fig. 3, a detailed MCNP6 modeling was carried out based on the design drawings of the 1,000MW 3-loop PWR NPP[2]. The model contains RVI such as baffle plate, former, barrel, neutron shield panel, and guide tube, and RV such as reactor vessel, insulation, and top/bottom heads. In addition, there is a 2m thick bio-shielded concrete outside the reactor, and the concrete was modeled by dividing 50cm in the radial direction. 157 fuels are located within the reactor core and boron-containing coolant is circulating between RV and RVI. The materials of the RV/RVI and bio-shield concrete are carbon steel, stainless steel and concrete, respectively, and the content of material compositions and impurities follows NUREG/ CR-3474[3].

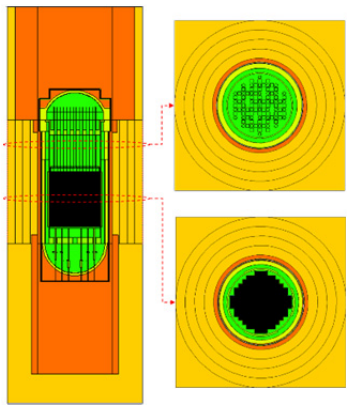


Fig. 3. Analysis model for activation Evaluation.

The names and detailed locations of each part of RVI and RV are shown in Figure 4.

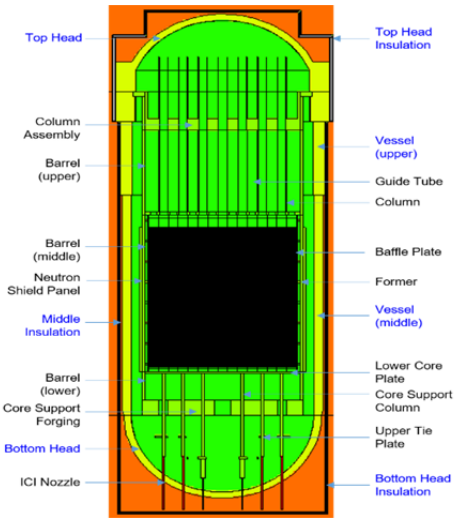


Fig. 4. RV/RVI analysis model.

Boron concentration in the coolant is one of the important factors to calculate the neutron flux in each component in the RV/RVI. Therefore, average boron concentration of representative cycle was applied as input factors on the calculation of neutron flux using MCNP6. Table 1 shows a variation of the neutron flux in each component at the end of cycle (EOC) of the representative cycle.

Table 1. Neutron Flux of major components

Item	Major components	Neutron Flux [#/sec·cm^2]
RVI	Baffle plate	6.52E+13
	Baffle Former	1.93E+13
	Barrel (middle)	7.21E+12
	Neutron Shield Panel	6.19E+12
RV	Vessel (middle)	4.44E+10
	Middle Insulation	1.58E+10
Concrete	Concrete 1	8.91E+09
	Concrete 2	8.38E+07
	Concrete 3	3.62E+05

The (n, γ) reaction libraries of some nuclides in the PWRU50.LIB of ORIGEN2 code were modified with the activation cross-section library generated by the MCNP simulation[4]. To calculate the radioactive inventory for the reactor to be evaluated after design life using the ORIGEN2 code, input factors such as EFPD (effective full power day), the neutron flux for each component and 7.5 years cooling time were used. Fig. 5 shows classification of the radioactive waste and the total activity in each component of the RV/RVI and bio-shield concrete.

[Reactor Vessel Internals]

Components	Location	Activity (Bq)	Waste Level
Baffle plate	Side	9.21E+16	ILW
Baffle former	Side	1.18E+16	ILW
Barrel (fuel region)	Side	1.45E+16	ILW
Neutron shield panel (4ea)	Side	4.49E+15	ILW
Upper core plate	Upper	3.65E+15	ILW
Lower core plate	Lower	4.67E+15	ILW
Core support column	Lower	3.31E+14	ILW
Barrel (above fuel region)	Upper	6.11E+12	LLW
Guide tube	Upper	5.04E+13	LLW
Upper Column	Upper	2.18E+13	LLW
Barrel (under fuel region)	Lower	7.18E+13	LLW
Core support forging	Lower	2.12E+12	LLW
Total Activity (Bq)		1.28E+17	

[Reactor Vessel]

Components	Location	Activity (Bq)	Waste Level
Reactor vessel (middle)	Side	1.66E+14	LLW
Insulation (middle)	Side	3.39E+13	LLW
Reactor vessel (upper)	Upper	1.41E+11	LLW
Top head	Upper	1.33E+09	VLLW
Top head insulation	Upper	5.80E+10	LLW
Bottom head	Lower	7.00E+10	LLW
Bottom head insulation	Lower	4.54E+11	LLW
Total Activity (Bq)		2.00E+14	

[Bio-Shield Concrete]

Components	Location	Activity (Bq)	Waste Level
Concrete Segment 1	0~50cm	1.43E+13	LLW
Concrete Segment 2	50~100cm	3.25E+11	LLW
Concrete Segment 3	100~150cm	2.20E+09	VLLW
Concrete Segment 4	150~200cm	-	C.W
Total Activity (Bq)		3.62E+14	

Fig. 5. Results of activation evaluation.

3. Conclusion

The radiological inventory assessments were carried out to classify radioactive waste for the 1,000MW PWR NPP with three-loop. The major nuclides determining waste classification of the activated RV/RVI and bio-shield concrete are as follows: (listed in order of high specific activity)

- RVI : ^{60}Co, ^{63}Ni, ^{59}Ni, etc.
- RV : ^{60}Co, ^{55}Fe, ^{152}Eu, etc.
- Concrete : ^{60}Co, ^{152}Eu, ^{154}Eu, etc.

The RVI components adjacent to the active fuel region were classified as ILW, while the other RVIs and all the RVs except the top head were classified as LLW. In the case of bio-shield concrete, waste classification cannot be determined because the results of neutron flux calculations for concrete thicknesses from 1.5 m to 2.0 m are not available. However, it could be assumed to be classified as clearance waste (C.W), when inferred from the results of the specific activity of each nuclide for "Concrete 3" classified as VLLW.

REFERENCES

[1] Dong-Keun Cho, et al., “Radiological characteristic of decommissioning waste from a CANDU reactor”, NET Vol.43, No.6 December 2011.

[2] Los Alamos National Laboratory, “Version 1.0, MCNP-A General Monte Carlo N Particle Transport Code, MCNP6™ User’s Manual”, LA-CP-13-00634, Ver. 6, 2013.

[3] NUGEG/CR-3474, “Long-lived activation products in reactor materials”, U.S. NRC, 1984.

[4] ORNL, " ORIGEN2 : Isotope Generation and Depletion Code Matrix Exponential Method", June, 2002.

Technical Review on Release of Radioactive Building in European Commission

Jihwan Yu* and Hangrae Cho
KHNP-CRI, 70, 1312-gil, Yuseong-daero, Yuseong-gu, Daejeon, 34101, Republic of Korea
*liu20893283@khnp.co.kr

1. Introduction

The purpose of this study is to review the European Commission's clearance regulation for the recycling or reuse of buildings and building debris contaminated by radioactive materials generated from nuclear power plant decommissioning, and devise measures for clearance of buildings that occur when nuclear facilities are decommissioning in Korea.

The study on the Release of Radioactive Materials and Buildings from Regulatory Control by the European Commission provides basic considerations for clearance, including the radiological concept and factors influencing the decision to clearance[1].

2. The radiological concept for clearance

Clearance is based on the concept of triviality of expose, this is generally related to the stipulation that the effective dose expected to be incurred by any member of the public due to cleared materials is of the order of 10 μSv or less in a year[Fig 1].

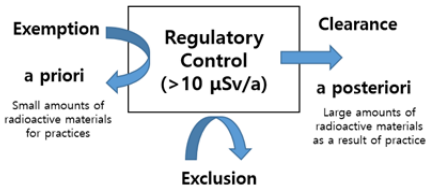


Fig. 1. Relationship of Exemption, clearance and Exclusion.

Consequently, cleared waste may be treated as normal waste and materials cleared for reuse or recycling may be sold or transferred to any other party and used for any purpose without being considered to be radioactive.

2.1 Differences between clearance of materials and clearance of buildings

While the basic concepts are the same for clearance of materials and clearance of buildings, there are important differences in the implementation of clearance of materials and clearance of buildings.

- Unconditional clearance of materials requires mass specific clearance levels and for those materials with a measurable surface also surface specific clearance levels in order to limit the surface activity (release of dust etc.).
- Clearance of buildings, on the other hand, needs to take account of a much more limited set of exposure scenarios. Clearance levels for buildings are usually expressed as surface specific activity levels (relating to the activity on and beneath the surface).

2.2 Radiological modeling for Clearance option

The surface contaminated metals require surface specific and mass specific clearance levels, bulk materials such as building rubble requires mass specific clearance levels only, and building surfaces (floors, walls, ceilings) require surface specific clearance levels or mass specific clearance levels in combination with the definition of penetration depth.

Figure 2 provides a schematic representation of the pathways and scenarios included in the radiological model for clearance of metals, as used in the EC RP 89 [2].

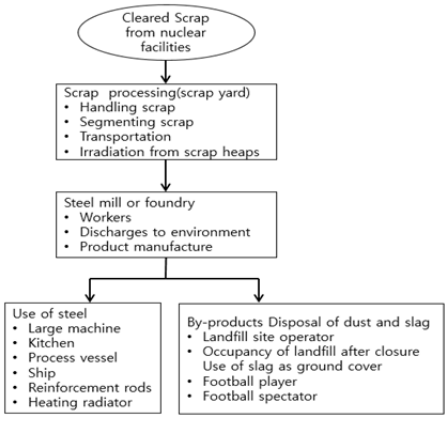


Fig. 2. The radiological model for clearance of metals.

Figure 3 provides a schematic representation of the pathways and scenarios in the radiological model for clearance of buildings and of building rubble, as used in EC RP 113 [3].

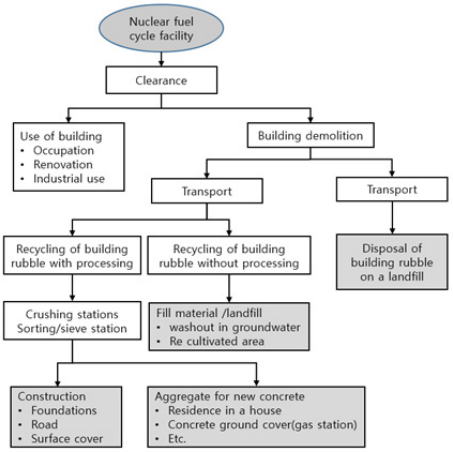


Fig. 3. The radiological model for clearance of buildings and building rubble.

2.3 Clearance levels

Clearance levels that have been calculated with the radiological models presented in Section 2.2 are summarized in Table 1.

Table 1. Overview of clearance levels calculated with the radiological models.

Purpose	^{3}H	^{14}C	^{63}Ni	^{60}Co	^{137}Cs	^{90}Sr	Unit
Unconditional clearance, RP 112/1	100	10	100	0.1	1	1	Bq/g
Unconditional clearance, RS-G-1.7	100	1	100	0.1	0.1	1	Bq/g
Metal scrap for recycling or reuse, RP 89	1,000	100	10,000	1	1	10	Bq/g
Building rubble, RP 113	100	10	1,000	0.1	1	1	Bq/g
Building for reuse, RP 113	10,000	1,000	10,000	1	1	100	Bq/cm^2
Buildings for demolition only, RP 113	10,000	10,000	100,000	1	10	100	Bq/cm^2

3. Conclusion

In this study, European's release regulation were reviewed. With reference to these examples, we intend to establish clearance measures for release criteria of buildings applicable to nuclear facilities in Korea.

REFERENCES

[1] Release of Radioactive Materials and Buildings from Regulatory Control, OECD/NEA (2008).
[2] Recommended radiological protection criteria for the recycling of metals from the dismantling of nuclear installations, European Commission (1998).
[3] Recommended radiological protection criteria for the clearance of buildings and building rubble from the dismantling of nuclear installations, European Commission (2000).

Efficient Decomplexation of Co-EDTA Mixed Radioactive Waste by Advanced Oxidation Process

Juhyeok Lee[1] and Wooyong Um[1,2,3,*]
[1]Division of Advanced Nuclear Engineering, POSTECH, 77, Cheongam-ro, Nam-gu, Pohang, Korea
[2]Division of Environmental Science & Engineering, POSTECH, 77, Cheongam-ro, Nam-gu, Pohang, Korea
[3]Nuclear Environmental Technology Institute (NETI), POSTECH, 77, Cheongam-ro, Nam-gu, Pohang, Korea
*wooyongum@postech.ac.kr

1. Introduction

Ethylenediaminetetraacetic acid (EDTA, $C_{10}H_{16}N_2O_8$) is chelating agent that is used in decontamination of radioactive wastes. EDTA presents a high level of complexing capacity with respect to heavy metals such as Fe, Co, Cu, and Ni as well as radioactive ^{60}Co. The distribution of Co-EDTA in natural waters poses a threat to the ecological environment, which seriously threatens human health and environments. In addition, it is not recommended to dispose of the mixed radioactive waste with complexing chelates in repository [1].

Advanced Oxidation Processes (AOPs) have been described as effective methods for oxidizing the Co-EDTA waste due to the efficient capacity for mineralizing most of organic contaminant. Among the AOPs, Fenton reaction and peroxymonosulfate (PMS) reaction that yield highly oxidant radicals, such as hydroxyl radical ($OH\cdot$) and sulfate radical ($SO_4^{\cdot-}$), respectively are used to decompose the Co-EDTA.

In this study, decomplexation efficiency of Co-EDTA was studied using Fenton and PMS reaction as a function of pHs, [catalyst]/[Co-EDTA], [oxidant]/[Co-EDTA], reaction time, and temperature. Through these experiments, an optimized condition with the highest decomplexation efficiency was determined for Co-EDTA.

2. Experimental

2.1 Materials

Ethylenediaminetetraacetic acid disodium cobalt salt hydrate (powder, min. 98% $C_{10}H_{12}CoN_2Na_2O_8 \cdot xH_2O$, TCI Co., Ltd.) was used for target material in this research. Deionized water (DIW) was used for the preparation and dilution of the solution. As oxidant for AOP, hydrogen peroxide solution (H_2O_2 30wt% in H_2O, Sigma-Aldrich Co. LLC) and potassium peroxymonosulfate (powder, $2KHSO_5 \cdot KHSO_4 \cdot K_2SO_4$, Sigma-Aldrich Co. LLC) were used. As a catalyst for Fenton reaction, Iron(Ⅱ) sulfate heptahydrate (powder, ≥99.0% $FeSO_4 \cdot 7H_2O$, Sigma-Aldrich Co. LLC) was used. Nitric acid (≥65% HNO_3, Sigma-Aldrich Co. LLC) and sodium hydroxide solution (1 M NaOH, Samchun pure chemical Co., Ltd.) were used to adjust the pH. All materials used in the experiment were used without any pre-treatment.

2.2 Analytical instruments

Electron spin resonance spectrometer (ESR, EMXplus-9.5/2.7, Bruker, USA) was used to identify the formation of active radicals. Ultraviolet-visible spectrophotometer (UV-VIS, UV-2600, Shimadzu, Japan) and Inductively coupled plasma mass spectrometer (ICP-MS, NexION 300D, PerkinElmer, USA) were used to measure the change of Co-EDTA and the cobalt concentration before and after decomplexation through AOP, respectively. X-ray diffraction (XRD) and Fourier-transform infrared spectroscopy (FT-IR) were used to identify the mineral phase and vibrational structure of precipitation, respectively.

2.3 Methods

To make 1.78 mM Co-EDTA solution, add 20 mL of DIW and 14 mg of Co-EDTA reagent to a 50 mL beaker and stir on a hot plate for 1 h. Depending on the type of experiments, catalyst and oxidant were added to react with Co-EDTA solution. Then, 65% HNO_3 or 1 M NaOH was added to the solution to adjust the pH from 1 to 13. The solution was stirred at 300 rpm for 0 to 150min on a hot plate. After the reaction, 1 M NaOH was added to the solution to increase the pH of the solution to above 8, and cobalt ions in solution decomposed from Co-EDTA were precipitated in the form of cobalt hydroxide. Then, centrifugation was performed at 3,000 rpm for 15 minutes using a centrifuge and then filtered with a 45 μm syringe filter to separate the impurities that may remain in the supernatant.

3. Results and Discussion

3.1 ESR analysis

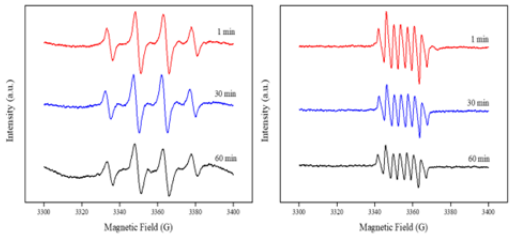


Fig. 1. DMPO spin-trapping ESR spectra recorded in Fenton reaction (left) and PMS reaction (right).

As shown in Fig. 1, the characteristic signals of DMPO-OH and DMPO-SO_4 were detected using DMPO as the spin trapping reagent. It indicates the generation of OH· radicals and $SO_4^{\cdot-}$ radicals in Fenton and PMS reaction, respectively.

3.2. Optimization

In effect of pH, optimum pH that resulted in the highest decomplexation efficiency of Co-EDTA was determined by conducting the reaction at various pH values, while holding the other operating parameters constant: [Co-EDTA] = 1.78 mmol/L, temperature = 25°C, reaction time = 120 min, [$FeSO_4 \cdot 7H_2O$] = 17.8 mmol/L, and [PMS] = 0.142 mol/L. In addition, in Fenton reaction with low oxidant concentration, H_2O_2 was used in the same concentration as PMS (0.142 M), and in Fenton reaction with high oxidant concentration, 1.78 M of H_2O_2 was used.

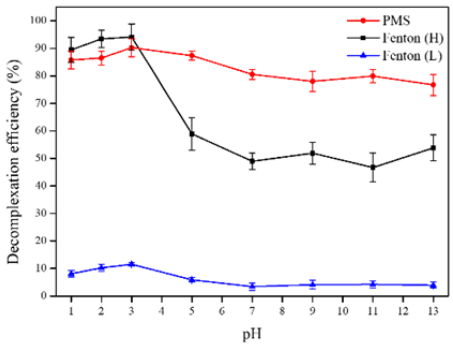


Fig. 2. Effect of pH on the decomplexation of Co-EDTA by Fenton and PMS reaction; Fenton (H)=Fenton reaction with high oxidant concentration; Fenton (L)=Fenton reaction with low oxidant concentration.

As shown in Fig. 2, decomplexation efficiency of Co-EDTA by Fenton reaction depended strongly on initial pH. The highest decomplexation efficiency was shown when the pH was around 3.0. But, the decomplexation efficiency by Fenton reaction dramatically decreased at pHs higher than 3.0. Meanwhile, at the same oxidant concentration as PMS reaction, the decomplexation efficiency of Co-EDTA by Fenton reaction was significantly lower than that of PMS reaction. In PMS reaction, the highest decomplexation efficiency was also found at pH =~3.0, but it showed to decrease gently with increasing pHs. Therefore, if the PMS reaction is used, high decomplexation efficiency can be obtained without additional pH adjustment compared to Fenton reaction. In addition, PMS reaction showed much higher decomplexation efficiency at the same oxidant concentration. Therefore, the amount of oxidant used can be also significantly reduced in PMS reaction.

4. Conclusion

Decomplexation of Co-EDTA was studied using radicals generated from Fenton and PMS reaction, respectively. In effect of pH, the decomplexation efficiency of Co-EDTA is strongly influenced by variable pH conditions in Fenton reaction. The optimum pH was found to be around 3 in Fenton reaction. In PMS reaction, it showed evenly high decomplexation efficiency at the overall pH condition. Therefore, high decomplexation efficiency can be obtained without additional pH adjustment in PMS reaction, suggesting better treatment technology for decomplexing the mixed radioactive waste.

REFERENCES

[1] R. Thomas, K. Lawlor, M. Bailey, and L. Macaskie, "Biodegradation of Metal-EDTA Complexes by an Enriched Microbial Population" Applied and Environmental Microbiology, 64(4), 1319-1322 (1998).

Tritium Extraction From Cement Mortar According to Heating Temperature

Ki Joon Kang*, Jun Woo Bae, and Hee Reyoung Kim
Ulsan National Institute of Science and Technology
*roffl1234@unist.ac.kr

1. Introduction

There were the various forms of tritium like gaseous tritium (HT), tritiated water (HTO), organically bound tritium (OBT) in environment [1-2]. Recent research showed about risks of internal exposure due to tritium absorption by respiration or intake. Therefore, tritium should be removed from materials contaminated to tritium and disposed. Tritium was extracted from cement mortar sample by heating method and analyzed by LSC (Liquid Scintillation Counter) in this study.

2. Material and Method

2.1 Sample Preparation

Cement mortar powder and tritiated water with tritium concentration of 6778.67±14.93 kBq/L were mixed to make cement mortar sample. Mixing mass ratio between cement mortar powder and tritiated water was 5 vs 1. Remaining mixing ratio between cement mortar powder and tritiated water, the mass used in making cement mortar dough was increased to make cement mortar sample of 5 groups with same mixing ratio and different mass. The size of each cement mortar sample was fit to the sample boat of high temperature furnace with entrance area of 1.25 mm x 14.5 mm. cement mortar samples were dried for 24 hours in room temperature. Cement mortar samples were shipped to sample boat of high temperature furnace.

2.2 Tritium Extraction

Sample boats including cement mortar samples were inserted to high temperature furnace work tube. Oxygen and air gas tanks were connected to work tube inlet, and then were flowed to work tube outlet. Tritium capture bottles including 0.1 M nitric acid were connected to work tube outlet. Heating temperature for tritium extraction was 200 ℃ in high temperature furnace. Heating duration was set to 9 hours. Three nitric acid solutions with the concentration of 0.1 M were used to know extraction rate of tritium as heating duration. Nitric acid volume was 20 mL and replace term was 3 hours. After heating for 9 hours, 0.1 M nitric acid solutions were replaced with new one and cement mortar sample was heated to extract remaining tritium at the temperature of 600 ℃ for 5 hours. Finally, the process of heating at 600 ℃ for 5 h was repeated for the comparation with MDA (Minimum Detectable Activity) value. Samples were heated at each temperature condition of 200 °C, 250 °C, 300 °C, 350 °C, and 400 ℃ for 9 h. And then, tritium extraction rate for 9 hours was compared to each other.

2.3 Tritium Analysis

All nitric acid solutions used in capturing extracted tritium from cement mortar samples were used in making LSC cocktail solution. LSC cocktail solution was consist of 8 ml of nitric acid and 12 ml of the liquid scintillator (GOLDSTAR, MERDIAN Biotechnologies Ltd) in a plastic vial. LSC cocktails were measured and analyzed in LSC.

3. Results

Considering 9 hours heating for 9 hours, tritium radioactivity concentration from sample group 1 to 5 during the first 3 hours interval were 4.07 ± 0.04, 4.15 ± 0.05, 4.65 ± 0.05, 4.30±0.06, and 4.48±0.05 Bq/g, respectively, at a heating temperature of 200 ℃ on table 1. The values for the second 3 hours were 0.72±0.02, 0.98 ± 0.03, 1.07 ± 0.02, 1.24 ± 0.03, and 0.85±0.02 Bq/g. The values for the third 3 hours were 0.46±0.02, 0.60±0.02, 0.54±0.02, 0.76±0.02, and 0.57±0.02 Bq/g. In all sample group, tritium concentrations became low as heating duration is gone. It can be guessed that most of tritium were extracted in first 3 hours. And then, according to position of tritium in cement mortar sample, tritium extraction can be different. Most of the tritium on the surface of cement mortar sample is extracted during the initial 3 hours, and it may take a long time to extract because the tritium is more difficult to escape from the sample as it was in the center of the cement mortar sample. However, if tritium is present in cement mortar sample with a chemical bond state other than its physical distribution, there may be tritium that cannot be extracted even if heating duration is increased.

After heating for 9 hours, tritium radioactivity concentrations at the temperature of 600 ℃ for 5 hours (9~14 hours) were similar to those of third 3 hours (6~9 hours). In sample groups of 1 and 5, tritium radioactivity concentrations for 5 hours were even higher than those of third 3 hours. It means that there may be tritium cannot be extracted at the temperature of 200 ℃ even if heating duration was increased. And total tritium radioactivity concentrations in cement mortar sample from each sample groups (1~5) were different as 5.89 ± 0.05, 6.31 ± 0.07, 6.72±0.06, 6.80±0.07, 6.63±0.06 Bq/g. From group 1 to 5, although mixing ratio between cement mortar power and tritiated water was same, tritium contamination was different.

Table 1. Radioactivity concentration of extracted tritium for each 3 hours interval at 200 ℃

Sample group	Radioactivity concentration (Bq/g)		
	0~3 hours	3~6 hours	6~9 hours
1	4.07±0.04	0.72±0.02	0.46±0.02
2	4.15±0.05	0.98±0.03	0.60±0.02
3	4.65±0.05	1.07±0.02	0.54±0.02
4	4.30±0.06	1.24±0.03	0.76±0.02
5	4.48±0.05	0.85±0.02	0.57±0.02
Sample group	Radioactivity concentration (Bq/g)		
	9~14 hours	Residual after 14 hours (<MDA)	
1	0.65±0.02	0.007 (<0.027)	
2	0.59±0.02	0.011 (<0.036)	
3	0.46±0.02	0.011 (<0.033)	
4	0.51±0.02	0.013 (<0.042)	
5	0.73±0.02	0.008 (<0.029)	

Tritium extraction rates for 9 hours at the temperatures of 200 °C, 250 °C, 300 °C, 350 °C, and 400 ℃ were shown in Table 2. The rates corresponding to 9 h of heating are 79.26 % ± 4.24, 84.94 % ± 3.74, 89.46 % ± 1.77, 95.76 % ± 1.51, and 98.43 % ± 0.41. With an increase in the heating temperature, the average extraction rate increases, but the standard deviation decreases. Although heating duration was increased to 9 hours, at the temperatures of 200, 250, and 300 °C, the existence of tritium chemically compounded can have a dominant effect to tritium extraction rate. However, those effect was decreased as heating temperature was increased.

Table 2. Maximum and average tritium extraction rate (%) for 9 hours interval at each temperature

Tritium extraction rate	Heating temperature (℃)		
	200	250	300
Average (%)	79.26 ± 4.24	84.94 ± 3.74	89.46 ± 1.77
Maximum (%)	84.62	88.43	91.86

Tritium extraction rate	Heating temperature (℃)	
	350	400
Average (%)	95.76 ± 1.51	98.43 ± 0.41
Maximum (%)	97.09	98.92

5. Conclusion

The study confirmed that tritium in cement mortar sample can be extracted by heating method under melting temperature. When heating temperature higher than 350 °C and a heating duration longer than 9 h are required to achieve an extraction rate of 95 %. At the temperature under 350 ℃, although heating duration increase, tritium extraction rate can be different according to tritium distribution and bonding types in cement mortar sample. If temperature is higher than 350 ℃, the fluctuation of tritium extraction rate can be minimized regardless of tritium distribution and bonding types in cement mortar sample.

Acknowledgments

This research was supported by by the Industrial Technology Innovation Program (20191510301210, Development of Dismantling Technology for the Volume Reduction of Radioactively Contaminated Tanks) funded by the Korea Institute of Energy Technology Evaluation and Planning (KETEP, Korea).

REFERENCES

[1] S.B. Kim, N. Baglan, P.A. Davis, Current understanding of organically bound tritium (OBT) in the environment, J Environ Radioact, 126 (2013) 83-91.

[2] S. Hisamatsu, Y. Takizawa, Tritium transfer from diet to human, Journal of Radioanalytical and Nuclear Chemistry-Articles, 197 (1995) 271-280.

Development of WBS for CANDU Nuclear Power Plant

Minhee Kim*, Chang-Lak Kim, and Sanghwa Shin
KEPCO International Nuclear Graduate School
*min850zzang@naver.com

1. Introduction

The CANDU type Wolsong unit 1 nuclear power plant is expected to be decommissioned due to permanently shutdown in 2019. According to the power reactor information system of the IAEA, as of October 6, 2020, there are 9 CANDU-type nuclear power plants that have been permanently shutdown [1].

The work breakdown structure (WBS) is a hierarchical structure for decommissioning project. The international structure for decommissioning costing (ISDC) of the OECD/NEA presented the principle of cost estimation through WBS [2].

In case of foreign countries, WBS provided by ISDC or self-developed WBS has been used. In Korea, the Korea Atomic Energy Research Institute developed the WBS for research reactors. The Korea Hydro & Nuclear Power Co. developed the WBS under the scenario of immediate decommissioning of the pressurized water nuclear power plant [3].

There is no case for WBS development of CANDU-type nuclear power plant in Korea. In addition, WBS considering the structure of nuclear power plant is not identified. Therefore, in this study WBS has been developed for CANDU-type nuclear power plant.

2. WBS Development Method

2.1 WBS structure analysis

For the development of WBS, decommissioning handbook [4] published by DOE and ISDC report were analyzed. Furthermore, WBS used in decommissioning of the Oyster Creek, Pilgrim, and Indian point nuclear power plants in the United States were reviewed.

The analysis results are as follows. First, WBS has a hierarchical structure. The topmost level (Level 1) of the structure encompasses the overall project. The next level consists of the sub-items of the high level.

Second, WBS has a basic structure of cost estimation. The ISDC presented the relationship among the accounting structure, ISDC and WBS. The WBS relationship with accounting structures can derive the cost data [2][4][5].

2.2 WBS Development

In this study, WBS with CANDU-type nuclear power plant structure was developed by referring to the analysis result. Each hierarchical structure of WBS is established as follows.

Level 1 considered the main decommissioning tasks, the basic data and other costs for costs estimation. Table 1 is Level 1 of the developed WBS.

Table 1. Level 1 of WBS with CANDU-type nuclear power plant structure

WBS ID	WBS description
1	Pre-decommissioning Action
2	Dismantling, Segmenting and Demolition
3	Waste processing, Storage and Disposal
4	Site infrastructure and operation
5	Miscellaneous expenditures

Level 2 in WBS ID-2 is classified as a reactor building, service building and turbine building. Level 3 is classified as a room and area of each building. Level 4 describes the components and equipments inside the room/area. The unit cost factor(UCF) as presented in AIF/NESP-036 reports may be applied to components, equipment and structure. Through this WBS, the decommissioning cost of Wolsong unit 1 can be estimated. Figure 1 is a part of the developed WBS.

Sub-items of WBS ID-1 consist of the basic information for each building components and equipments of a nuclear power plant and the labor cost for cost estimation. Sub-items in WBS ID-3 are items related to decontamination, volume reduction, disposal, transport and storage of waste. WBS ID − 4 and 5 applied to ISDC, an international recommendation.

3. Conclusion

The purpose of this study is to present WBS for the cost and schedule estimation of decommissioning CANDU-type nuclear power plants. The calculation method is as follows: 1) to confirm the basic information and labor cost items entered into WBS; and 2) to select the component or equipment of the nuclear power plant structure. The cost and schedule can be

estimated by multiplying the basic information of the structure and UCF.

In conclusion, the WBS developed by applying the CANDU type structure is expected to be able to estimate the cost and schedule more easily by selecting the decommissioning work configuration.

ACKNOWLEDGEMENT

This study was supported by the Korea Institute of Energy Technology Evaluation and Planning of the Republic of Korea (No. 20201510300130).

REFERENCES

[1] https://pris.iaea.org/PRIS/WorldStatistics/ShutdownReactorsByType.aspx

[2] OECD/NEA, "International Structure for Decommissioning Costing", Radioactive Waste Management 2012.

[3] KAERI, "Analysis on Technology for Methodologies of Decommissioning Cost Assessment of Nuclear Facility", September 2019.

[4] DOE, "Decommissioning Handbook", 1994.

[5] P. Krishna, "Notification of Revised Post-Shutdown Decommissioning Activities Report and Revised Site-Specific Decomm-issioning Cost Estimate for Pilgrim Nuclear Power Station", November 2018.

[6] T. S. LaGuardia, "Guidelines for Producing Commercial Nuclear Power Plant Decommissioning Cost Estimates", AIF/NESP- 036, May 1986.

WBS ID	WBS description
1	**Pre-decommissioning Action**
1.1	Collection of information of internal/external facilities.
1.1.1	quality of the material
1.1.2	contamination status
1.1.3	size
1.1.4	radioactive level
1.1.5	nuclide characteristic
1.4	Matters relating to labour force
1.4.1	work force
1.4.2	monthly salary
1.4.3	number of working days
2	**Dismantling, Segmenting and Demolition**
2.1	Reactor Building
2.1.2	Steam Generator Room
2.1.3	Reactor Area
2.1.3.1	Steel liner
2.1.3.2	Calandria Vault Wall
2.1.3.3	Ordinary Concrete
2.1.3.4	Embedment Ring
2.1.3.41	Calandria Tube
2.1.3.42	Calandria Side Tube Sheet
2.1.4	New Fuel Loading and Service Room
2.1.5	Spent Fuel Transfer Room
2.2	Service Building
2.3	Turbine Building

WBS ID	WBS description
3	**Waste processing, Storage and Disposal**
3.1	Decontamination / Volume reduction
3.1.1	decontamination
3.1.3	waste package
3.2	Transport
3.2.1	Vehicles
3.3	Storage
3.3.2	storage containers
3.4	Disposal
3.4.1	disposal method
4	**Site infrastructure and operation**
4.1	Site security and surveillance
4.1.1	Procurement of general security equipment
4.2	Site operation and maintenance
4.3	Operation of support systems
4.3.1	Electricity supply systems
4.4	Radiation and environmental safety monitoring
4.5	Final cleanup, landscaping and refurbishment
4.6	Final radioactivity survey of site
4.7	Perpetuity funding/surveillance for limited or restricted release of property
5	**Miscellaneous expenditures**
5.1	Owner costs
5.2	Taxes
5.3	Insurances
5.4	Asset recovery

Fig. 1. Part of WBS developed to reflect CANDU-type nuclear power plant structure

Sulfate Radical Advance Oxidation Process for Degradation of Spent Resin

Muhammad Aamir Hafeez, Junsung Jeon, Junkyu Park, and Wooyong Um*
Division of Advanced nu-clear Engineering (DANE), Pohang University of Science and Technology (POSTECH) -77, Cheongam-ro, Nam-Gu, Pohang, Gyeongbuk, 790-784, Republic of Korea.
*wooyongum@postech.ac.kr

1. Introduction

Ion exchange resins are extensively used in nuclear power plants to remove the radioactive contaminates i.e., ^{60}Co, ^{65}Zn, ^{51}Cr, ^{125}Sb, ^{58}Ni, ^{14}C, ^{59}Ni, ^{54}Mn, ^{133}Ba, and ^{137}Cs produced by the nuclear reactions in reactor core. Once completing their useful life, these are removed from nuclear facility as "spent resins". Therefore, treatment and disposal of spent resins produced from nuclear industry is essential to reduce their potential hazard to human and environment. Many researchers have already investigated the conventional Fenton/Fenton-like advance oxidation processes (AOPs) for volume/weight reduction of spent resins, which is mainly dependent on the production of hydroxyl radicals by the reaction of H_2O_2 with transition metals. The recent research on sulfate radicals based on advanced oxidation process (SR-AOPs) received increasing attention due to enhanced performance over hydroxyl radical based advanced oxidation process (HR-AOPs). SR-AOPs are superior in terms of higher selectivity of ($SO_4^{\cdot-}$) to react with organic compounds via electron transfer reactions, longer half-life of ($SO_4^{\cdot-}$), and its tendency to interact with organic compounds over a wide pH range [1]. In this study, we optimized the reaction conditions for effective degradation of the spent cationic resin using SR-AOPs.

2. Experimental

2.1 Material and Methods

The cation exchange resin used was nuclear grade (strongly acidic H^+ form) Amberlite IRN-77. All the experiments in this study were performed under non-radioactive conditions. All reagents were analytical grade, 30% H_2O_2 (m/m) purchased from Junsei Chemicals Japan, and Amberlite IRN-77, copper sulfate $CuSO_4 \cdot 5H_2O$ cobalt sulfate $CoSO_4 \cdot 7H_2O$, Peroxymonosulfate (PMS) ($KHSO_5 \cdot 0.5KHSO_4 \cdot 0.5K_2SO_4$) in the form of oxone salt purchased from Sigma-Aldrich in Korea.

2.2 Dissolution of Resin

Dissolution of resin was performed using 500 mL, three-necked round-bottom flask (with a stirrer bar) immersed in an oil bath placed on a hotplate as shown in Fig. 1. The reactor was thermo-regulated at 90°C ± 3°C and magnetic stirrer was used for 3h reaction. Fresh Amberlite IRN-77 resin (5g) were mixed with 0.02M $CuSO_4 \cdot H_2O$ catalyst solution in a 150 mL glass beaker for 10 min followed by pH adjustment of 2 using 4M NaOH solution. Then, the mixture was introduced into the reactor. About 1.59 mL H_2O_2/g loaded resin was inserted using dual channel peristaltic pump with flow rate of 0.053mL/min for 2.5h, and reaction was stopped after 0.5h mixing under the same conditions. Physicochemical properties of dissolved resin are listed in Table 1.

Table 1. Characterization of dissolved resin

pH	1.16
COD	80,000 mg/L
TOC	22,000 mg/L
Conductivity	28ms/cm

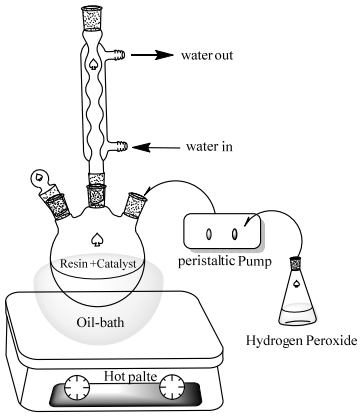


Fig. 1. Schematic diagram for dissolution of resin.

2.3 *Resin degradation by SR-AOPs*

Transition metals such as Co, Fe, Cu and Mn have been widely applied for PMS activation to generate the $SO_4^{\cdot-}$ by following equation (1).

$$Mn^+ + HSO_5^- \rightarrow M^{(n+1)} + SO_4^{\cdot-} + OH^- \qquad (1)$$

All the experiments was conducted in homogeneous batch conditions for 120 minutes. The desired amount of diluted resin was added in 150 mL glass beaker and placed on a hotplate with an IKATRON ETS-D5 temperature probe, maintaining predetermined temperature. Then, appropriate volume of 80mM Co^{2+} as catalyst and 320mM PMS as oxidant from their perspective stock solutions were introduced, respectively. The reaction time was monitored after adjusting the required pH using 4MNaOH and 4M H_2SO_4. The initial volume of reaction solution was 100 mL. The efficiency of SR-AOPS were evaluated by the COD reduction rate. COD of the all experiments was measured by the COD digital reactor block (DRB200) equipped with a spectrophotometer (DR3900) by HACH, USA.

3. Results and Discussion

3.1 Effect of initial pH

The efficiency of SR-AOPS depends on the generation of ($SO_4^{\cdot-}$) radicals. The initial pH plays a vital role in the generation and stability of $SO_4^{\cdot-}$radicals. The pH was varied from 2-11 at constant temperature in order to investigate the optimal pH for the maximum COD removal. The highest COD removal efficiency was achieved at pH of 9 as shown Fig. 2.

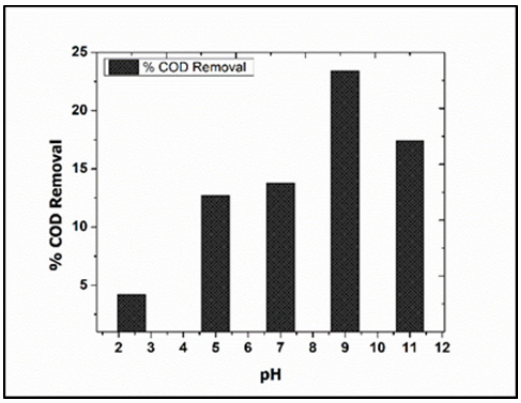


Fig. 2. Effect of pH on (%) COD removal, initial COD=1000 mg/L, Co^{2+} (0.4mM), PMS (4mM) volume=100 mL reaction time 120 min, at room temperature.

3.2 Effect of temperature & reagent dosages

The catalyst (Co^{2+}) and oxidant (PMS) dosage significantly affected the COD removal (%) of spent resin. As we increased the dosage of oxidant from 4mM to 60mM at fixed catalyst concentration of (4mM), it generated more sulphate radicals. After optimizing the effective reagent dosage, the effect of reaction temperature on % COD removal was also evaluated. Increasing temperature also resulted in highest % COD removal. A maximum of 96% COD removal for spent resin was achieved at 80°C for 120 minutes as shown in Fig.3.

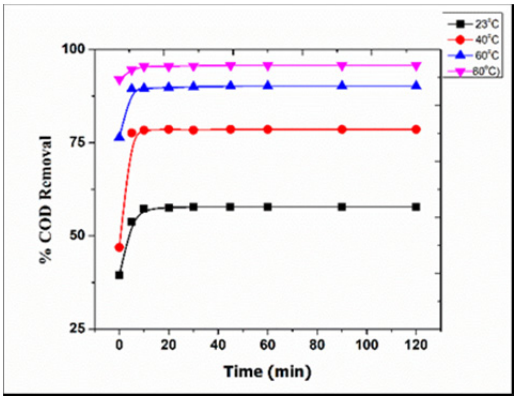


Fig. 3. Effects of temperature & dosage on (%) COD removal, initial COD=1000 mg/L, Co^{2+} (4mM), and PMS (60mM) pH=9 in 100 mL volume for 120 min

.

4. Conclusion

In this study, we performed SR-AOPs for effective degradation of spent resin by optimizing the initial pH, dosage of catalyst & oxidant, and reaction temperature as key factors. We successfully achieved 96 % COD removal of spent resin using following optimized dosage of Co^{2+} (4Mm) as catalyst, PMS (60Mm) as oxidant, and 80°C reaction temperature for 120 minute.

Acknowledgment

This work was supported by the National Research Foundation of Korea (NRF) grant funded by the Korean government (No. NRF-2019M2A7A 1001811).

References

[1] J. Wang, S. Wang, “Activation of persulfate (PS) and Peroxymonosulfate (PMS) and application for the degradation of emerging contaminants”, Chemical Engineering Journal, 334, 1502-1517 (2018).

Analysis on Radioactive Waste Level of the Reactor Internals According to the Content of Impurities

Gilyong Cha[1], Soonyoung Kim[1,*], Minhye Lee[1], Minchul Kim[2], and Hyunmin.Kim[2]
[1] RADCORE Co., Ltd., #A516, 17 Techno 4-ro, Yuseong-gu, Daejeon, Republic of Korea
[2] KHNP CRI, 70, 1312-gil, Yuseong-daero, Yuseong-gu, Daejeon, Republic of Korea
*sykim@radcore.co.kr

1. Introduction

Radioactive materials generated during the operation of a nuclear power plant remain in the nuclear power plant even after permanent shutdown. Also, the neutron induced activation in the core, core internals and bio-concrete are a major source of radiological pollution, accounting for more than 99% of the total radioactivity in a commercial reactor operated for 30 years. SSCs(system, structure and components) of a commercial reactor with a high-temperature and high-pressure environment are mainly made of steel materials such as SS-304. Elements other than Fe contained in iron ore may be contained as impurities in the steel during the smelting process, and additional impurities may be added in the steel manufacturing process as well. It is well known that this fact can lead to changes in the inventory of radionuclide[1][2]. In this study, the effect of impurities in neutron induced activated steel materials on the determination of radioactive waste levels was evaluated using computational analysis.

2. Computational Method

2.1 Computational Codes

Each computational codes for calculating the neutron flux and the radioactivity inventory are required to evaluate the inventory. The neutron flux calculation code simulates the behavior of neutrons generated from the core's nuclear fuel and calculates the neutron flux and energy spectrum at user-specified locations. In addition, the radioactive inventory calculation code calculates the amount of each radionuclides inventory using neutron information generated from the neutron flux calculation code. In this study, the MCNP code[3] was used to calculate the neutron flux, and the FISPACT code[4] was used to calculate the radioactivity for activation. The detailed evaluation system is shown in Figure 1.

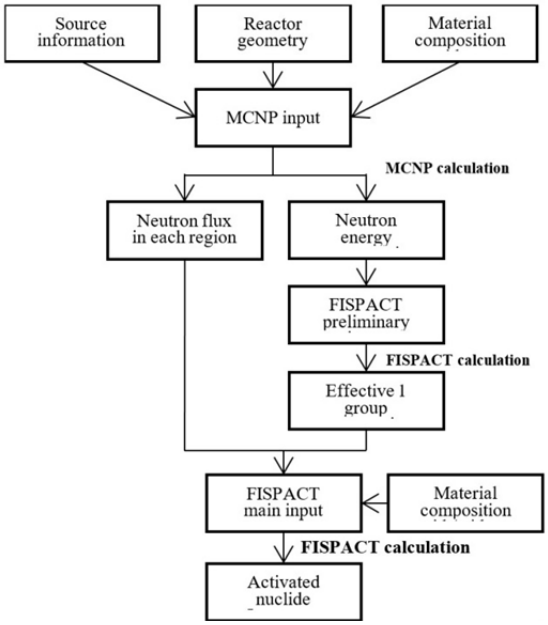


Fig. 1. MCNP/FISPAT computational code system.

2.2 Material of Reactor Internals

NUREG/CR-3474[5], published by the US NRC, evaluated the content of constituent elements and impurity nuclides in SS-304, materials of nuclear power plant SSCs, through radioactivity analysis of several nuclear power plants in the country. On the other hand, in Korea, there is no large-scale chemical assay experience on the effect of impurities contained in structures around the core on the generation of radionuclides, so this study was based on the material information of NUREG/CR-3474.

3. Results

SSCs composed of SS-304 material, used to support fuel and core in the reactor, have a maximum neutron flux of 1E+14 #/cm^2-sec order when operating a nuclear power plant. Radioactive waste levels were calculated based on SS-304, which was irradiated at 1E+13#/cm^2-sec in the core for 30 years and cooled for 10 years. And then, conditions for change the level of radioactive waste were analyzed according to the impurity content.

For SS-304 radioactive waste to be classified as ILW(Immediate Level Waste), the specific

activity of at least one of Co-60, Ni-59 and Ni-63 must exceed the low-level disposal limit(V/L must exceed 1 in Table 1). Ni-59 and Ni-63 are produced by the activation of Ni element contained in SS-304 by about 10%, and Co-60 is mainly produced by activation of Co impurities. Therefore, the radioactivity change by nuclide according to the content of Co impurities was investigated, and the results are shown in Table 1.

Table 1. Activities of Co-60, Ni-59 and Ni-63 for condition of Co Impurities

Nuclide	LLW limit (Bq/g)	Co 229 ppm		Co 2570 ppm		Co 1850ppm	
		V, value(Bq/g)	V/L	V, value(Bq/g)	V/L	V, value(Bq/g)	V/L
Co-60	3.70E+07	5.03E+07	0.89	5.56E+08	9.89	2.60E+08	7.12
Ni-59	7.40E+04	5.25E+05	7.10	5.25E+05	7.10	5.25E+05	7.10
Ni-63	1.11E+07	5.84E+07	5.26	5.84E+07	5.26	5.84E+07	5.26

As a result of evaluating the range of the Co impurity content (229 ppm ~ 2570 ppm) measured in NUREG/CR-3474, it was evaluated that the effects of Co-60 and Ni-59 were similar when the Co-60 impurity was 1850 ppm. In other words, SS-304 with Co impurities less than 1850 ppm will determine the waste level regardless of whether impurities are applied, and SS-304 with more than 1850 ppm of Co impurities is evaluated to increase the level of radioactive waste.

On the other hand, the activity of Co-60 in SS-304 irradiated with a relatively low neutron flux(about 1E+05~1E+10 #/cm^2-sec) is dominant in determining radioactive waste levels. Therefore, For SSCs composed of SS-304, which are relatively far from the core, the level of radioactive waste can be determined from self-disposal to LLW depending on the content of Co impurities.

4. Conclusion

In this study, the effect of the impurity content in the SS-304 material constituting the reactor internals on the level of radioactive waste was evaluated. In terms of long-term disposal, the waste level of SS-304 material is determined by long-lived nuclides such as Ni-59 and Ni-63, and only some SS-304 with particularly high Co impurities can change the waste level from LLW to ILW. On the other hand, in the range below the LLW, the influence of the content of Co impurities on the level of radioactive waste was evaluated to be dominant. The results of this study can be used to establish the effective nuclear decommissioning waste management strategies in the future.

REFERENCES

[1] IAEA, “Radiological Characterization of Shut Down Nuclear Reactors for Decommissioning Purposes”, IAEA Technical Report Series No. 389, (1997).

[2] Gil Yong Cha, et, al., “The Effects of Impurity Composition and Concentration in Reactor Structure Material on Neutron Activation Inventory in Pressurized Water Reactor”, JNFCWT vol.14, no.2, pp. 91-100 (2016).

[3] Denise B. Pelowitz, et, al., “MCNP6 User’s Manual”, LA-CP-13-00634, rev.0, (2013).

[4] R. A. Forrest, “FISPACT-2007 Manual”, UKAEA FUS 534, (2007).

[5] J. C. Evans, et, al., “Long-Lived Activation Product in Reactor Materials”, NUREG/CR-3474, (1984).

Performance Evaluation of Non-Radioactive Contaminated Soil Separation, Coagulation and Dewatering Using Pilot Scale Soil Decontamination System

Seongjoo Kang, Minhyuk Yoon, Kukjin Seo, Woohyeon Rhee, Seungil Kim, and Dukwon Kang*
Elim-Global Co. Ltd., 767, Sinsu-ro, Suji-gu, Yongin-si, Gyeonggi-do, Republic of Korea
*dukwon.kang@elim-global.com

1. Introduction

With the decision to decommissioning the Kori-1 reactor in June 2017, 10 nuclear reactors will be decommissioned sequentially until 2030. In the case of Korea, it has a narrow national territory unlike other countries that operate nuclear power plants, so it is necessary to seek ways to restore and recycle nuclear sites through decommissioning them as soon as possible. Under the long-term operation of the nuclear reactor, the site and its surrounding areas are contaminated with trace amounts of radioactive materials, and large amounts of contaminated waste will be generated upon decommissioning the nuclear power plant. Due to the atmospheric release of radioactive materials from the Fukushima Daiichi nuclear accident, the surrounding soil was contaminated and radioactive nuclides such as Cs, Co., and Sr are in contact with the surrounding residents through various channels, causing social problems, causing pathological or toxicities in the human body. Thus, in the end, there is a desperate need for decontamination techniques that can effectively deal with them. Generally, there are various methods of purifying contaminated soil such as solidification, stabilization, reclamation, soil ingot, plant purification, and soil washing, but among them, soil washing method is known as the most economical and technically stable method.

In this study, the soil cleaning process was carried out by mixing the soil artificially contaminated with the original soil using non-radioactive nuclides, and it was intended to evaluate the effective concentration and fixation of pollutants by adding powder-type natural polymeric condensate to the effluent containing fine soil. In addition, the residual supernatant water in the coagulation is being recycling for soil washing process and may contain residual non-radioactive nuclides. For this part, the separation process using for removing the radioactive species will be announced at the next conference and in this study, we would like to introduce the results of dehydration of the condensed lower sludge and drying.

2. Method

2.1 Artificial contaminated soil preparation

The soil used in the experiment was collected from forest soil and field soil around 5cm above the surface layer of the nuclear power plant area, and then separated the each fraction using a sieve (more than 5mm, 5mm to 2mm, 2mm to 0.75mm, 0.75 to 0.19mm, 0.19 to 0.075mm) in each step. The soil was artificially spiked using CsCl and $CoCl_2$, and the pollution concentration of the spike solution was 100 mg/kg. For about three weeks, it was naturally dried by mixing it equally with the spike solution and 1:1 ratio. Because soil that has been completed of natural drying cannot simulate natural contaminated soil when it is discharged with simple water washing, it was verified whether it was discharged through simple stirring and ultrasonic washing.

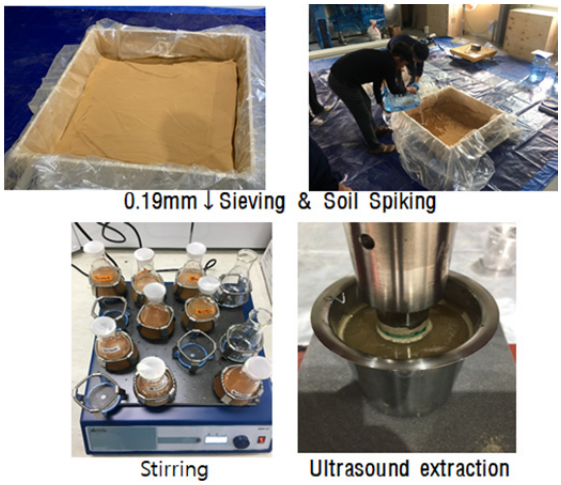


Fig. 1. Artificial contaminated soil & leaching test.

2.2 Pilot scale soil washing system

The sample for pilot scale testing we used was sandy soil in Gyeonggi-do, which had similar characteristics to soil around nuclear power plants, was mixed with artificial soil for soil washing process. The soil decontamination process was divided into four stages of washing & separation, solid-liquid separation, dehydration, and drying, separating and retrieving soil, and collecting fine particles contained in the cleaned water treated with contaminated soil, and the supernatant water was composed to be recycled

according to the degree of contaminant.

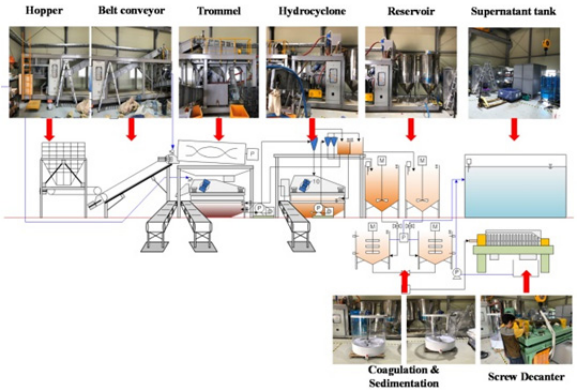


Fig. 2. Pilotscale soil separation, coagulation and dewatering system.

2.3 Coagulation, Dehydration and Drying process

Various kinds of commercial coagulation agents were applied to wash effluent containing fine particle containing solution in the upper and lower parts of hydro-cyclone to induce coagulation. The deposited sludge was discharged using a screw decanter centrifuge and then dried at 60°C using dry oven.

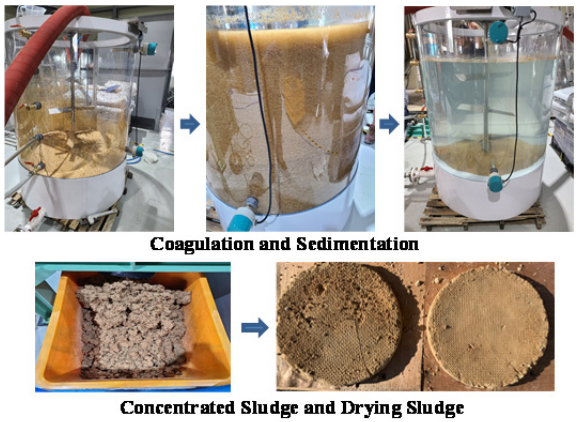


Fig. 3. Coagulation and dewatering Process.

3. Results

In the case of target soil, consisted mainly the sandy soil including the amount of fine soil content. Although there is a difference in degree in the elution characteristics of cesium in each soil specimen, the liquid samples of ICP-MS showed that in the case of soil contaminated by artificial contamination, cesium released by stirring was somewhat lower in the range of 0.02 to 0.209 mg/L. In addition, at 19.38 KHz, a current of 0.4 A was applied to induce elution, but there was no significant difference in elution (washing) efficiency.

When natural powder coagulant were applied after the soil washing process, the turbidity and SS concentration of the superior water were found to be below 10 mg/L in comparison to the initial concentration, and the concentration of Cs and Co dissolved in the supernatant water was also rarely detected. In the case of fine soil particles, it was confirmed that fine soil particles mixed with contaminant, which are present in the water in the form of suspended solids, were concentrated and discharged through the dehydration process.

4. Conclusion

It has been confirmed that soil contaminated with non-radioactive nuclides has minimal elution effect by water washing and is suitable for application to soil washing process. In addition, it was found that Cs were mostly found in micro-contaminated soil of less than 0.2mm. It was confirmed that the supernatant water separated through the coagulation and sedimentation process can be reused or discharged through the post-processing facility. In the future, purification efficiency by scenario will be assessed through continuous process of 1m^3/hr or more, and dehydrated cakes that have been dried will also be evaluated for integrity of the solidification.

ACKNOWLEDGEMENT

This work was supported by the Korea Institute of Energy Technology Evaluation and Planning (KETEP) and the Ministry of Trade, Industry & Energy(MOTIE) of the Republic of Korea (No. 20181510300800).

REFERENCES

[1] Grasso, D., Butkus, M.A., O'sullivan, D., and Nikolaidis, N.P., "Soil-washing design methodology for a lead contaminated sandy soil," Wat. Res., 31, 3045-3056 (1997).

[2] Choi, J.Y., Kim, S.K., Yang, D.B, & Kim, K.R (2014). A novel in situ clean-up system for metal contaminated seabed sediment, Korean Environmental Dredging Society, 4(1), 49-59.

Fabrication of Nanocomposite-Based Plastic Scintillator

Hara Kang[1,2], Sang Bum Hong[2,*], Changhyun Roh[2,3,*], and Jae Hak Cheong[1,*]
[1] Department of Nuclear Engineering, Kyung-Hee University, Suwon, Gyeonggi-do, 17104 Republic of Korea
[2] Decommissioning Technology Research Division, Korea Atomic Energy Research Institute, Yuseong-Gu, Daejeon, 34057 Republic of Korea
[3] Quantum Energy Chemical Engineering, University of Science and Technology (UST), 217 Gajeong-ro, Daejeon 34113, Republic of Korea
*sbhong@kaeri.re.kr; *chroh@kaeri.re.kr; *jhcheong@khu.ac.kr

1. Introduction

Beta-ray emitters such as 3H, 14C, and 36Cl, which have high mobility in the environment occurring at the decommissioning site, are considered significant isotopes due to their majority occurrence via neutron activation. However, the existing methods for beta-ray evaluation, LSC have shortcomings that consume much time and human resources for pretreatment and sampling, and "scaling factor", using as an auxiliary method, have less accurate because it is estimated indirectly using formulas for the number of the "key gamma-emitter". Therefore, many studies have been conducted on measuring beta rays using plastic scintillators as an alternative and supplemental method [1, 2].

Plastic scintillators have been used to measure beta-ray detector due to its composition with the low atomic number materials, despite low detection efficiency and bad energy linearity. Moreover, small penetration and short range of the beta-emitter challenges beta-ray in-situ measurement. To solve these challenges, some nanomaterials which have some optical advantages to elevating photoluminescence quantum yield have emerged for the fabrication of the plastic scintillators with advanced light yield [3]. Therefore, various attempts to overcome these shortcuts of conventional plastic scintillators have been made.

In this study, we present characteristics of nanocomposite based plastic scintillator with advanced light yield via fabrication with nanomaterials and evaluated the beta-ray detection efficiency.

2. Scintillation Process

Some nanocomposites have noticed in recent decades due to their unique optical properties that cannot be found in conventional bulk particles for plastic scintillator fabrication. One of the major optical characters of the colloidal nanoparticle mentioned above is called quantum confinement effects, that can control emission wavelength with the difference between energy states, blue shift with a diameter of the nanomaterial decreased. Another optical property of the nanomaterial is Localized Surface Plasmon Resonance (LSPR), a phenomenon that can be observed when metal particles in nanometer size that smaller than the wavelength of the light absorb a certain wavelength of light. Free electrons of the material surface oscillate strongly in groups, it makes an enhanced local electromagnetic field around the particles.

When the beta-ray incident in the scintillator, the radiation grants its energy to the surrounding material, excites the electron from the ground state, and returns to a stable state by emitting scintillation with the difference of the wavelength between the excited state and the ground state. In this experiment, scintillation processes are taken apart with three routes (Fig. 1). The light absorbed by the epoxy matrix transferred its energy to the fluorescence material (PPO, POPOP), otherwise transferred to nanoparticles directly (Route 2). Also, the light absorbed in the matrix transferred the energy to nanoparticles and fluorescents in turn (Route 3).

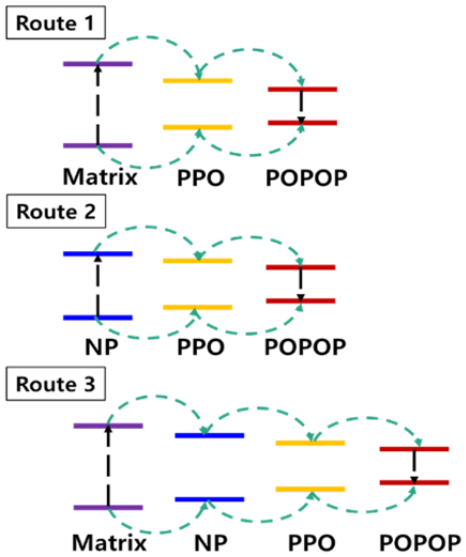


Fig. 1. Scheme of the scintillation process of the nanomaterial loaded scintillator.

3. Fabrication Process for Nanocomposite Scintillator

Two kinds of fluorescents, one is PPO as the primary solute and the other is POPOP as a wavelength shifter was added in epoxy monomer, and CdTe, Gd_2O_3, perovskite nanomaterial was loaded in the monomer solvent, respectively. Then, the solvent was stirred for 2 hours at room temperature for even dispersion of the materials. To remove air bubbles in the monomer solution, the solvent in stainless steel was put alone for 1 hour. Then, the solution was heated in the electric oven at high temperature for two days for polymerization. For easy removal of stainless-steel mold from polymerized scintillator, the scintillator ejected from the oven at 80 ℃ and injected into cold water for quenching. By demolding from stainless-steel mold, the nanomaterial loaded scintillators were prepared.

4. Result and Discussion

4.1 Chemicals and Characteristics

All reagents used were purchased from Sigma -Aldrich on a high purity. To evaluate the optical properties of manufactured scintillators and commercial scintillators, transmittance, and photoluminescence emission spectrum were measured.

4.2 Beta-ray measurement

Two kinds of fabricated scintillators of 2 mm thickness and 5 cm diameter and commercial scintillator, BC-400, with identical geometry were used for performance comparison to measure beta-ray. The PMT used in the experiment was 2-inch diameter 9266B (ET enterprises), and Multi-Channel Analyzer used NIMBIN (Canberra). beta-ray sources measured inside an optical enclosure designed to minimize the interference from the light, and area sources, ^{14}C and ^{90}Sr were measured. For the reliability of the experiment, each measurement was repeated three times for 10 minutes, and the distance between the source and the detector was 5 cm. The beta-ray spectra of scintillators, perovskite loaded scintillators and commercial scintillators with only PPO and POPOP were measured.

5. Conclusion

To overcome the low light efficiency and low energy linearity caused by the composition of a low atomic number of existing plastic scintillators, a plastic scintillator applied advanced technology was manufactured by adding nanomaterials.

To demonstrate the improvement of optical properties, the transmittance and fluorescence emission photometric values were measured. The fluorescence emission strength of the manufacturing scintillator was analyzed. Also, two types of fabricated scintillators to evaluate detection efficiency, scintillators with only fluorescents (PPO and POPOP), scintillator with nanomaterials, and one commercial scintillator were used to measure beta ray emitter of ^{90}Sr. Radiation measurements were conducted inside the optical enclosure to minimize light interference, and the thickness of the scintillator was optimized through MCNP6 computational simulation.

ACKNOWLEDGEMENT

This work was supported by a grant from the National Research Foundation of Korea (NRF), funded by the Korean government, Ministry of Science and ICT [No. 2017M2A8A5015143].

REFERENCES

[1] S. Toshikazu, Y. Yuji, “Development of Beta-ray Spectrometer for Radiation Emergency Accidents”, J. of Nucl. Science and Technol., supplement 5, 546-548 (2008).
[2] L. Anumaija, F. Pascal, S.K. Marja, G, Florence, “Digital Autoradiography (DA) in Quantification of Trace Level Beta Emitters On Concrete”, J. Radioananl Nucl. Chem., 298, 133-161 (2013).
[3] C, Quishui, W. Jing, Q. Xiangyu, et al., “All-inorganic perovskite nanocrystal scintillators”, Nature, 561, 88-93 (2018).

Cutting Simulation Method Based on the 3D Scanned Environmental Information for Nuclear Facility Dismantlement

Ikjune Kim*, Dongjun Hyun, Jonghwan Lee, Sungmoon Joo, and Jaehyun Ha
KAERI, Daedeok-daero 989-111, Yuseong-gu, Daejeon, 34057, Republic of Korea
*ikjunekim@kaeri.re.kr

1. Introduction

We are developing a system that performs cutting operations with the scenarios created based on the digital mockup of the nuclear facility. However, the digital mockup and actual sites may differ, so that cutting activity in the scenario which is created based on the digital mockup might be inapplicable for actual physical cutting operations [1].

So, we used the 3D scanning method to acquire the actual site data to which the digital mockup is aligned. And by the result of the alignment we update the digital mockup and the dismantling scenarios. Before deploying the updated scenario to the physical cutting system, it is simulated in the digital environment to check the cutting path of the equipment and the cutting result.

Existing cutting process simulation method [2] creates the cutting result model in the process modeling procedure, which is done before the digital mockup update process of the actual physical cutting operations. And at the simulation stage, it hides the cut target model and shows the cut result model to animate the cutting action. Hence, it produces the inaccurate geometry of the cutting result model with respect to the updated cutting motion and geometry of target model, despite it is very important to evaluate the cost of the cutting operations.

In this study, we propose the method to simulate the cutting result model with the updated digital mockup in the physical cutting operations.

2. Methodology

The concept of the dismantling control system is shown in Fig. 1. The concept system has two main parts, simulation system and physical system. In the simulation system, the user defines the cutting scenario and deploy the scenario to physical system which is composed of actual cutting device such as robot manipulator and laser cutter.

In the operational loop, at the end of each activity of physical system, simulation system updates the digital mockup and the next cutting scenario based on the environmental information. Using the updated scenario and the model, the user simulates and checks the activities and send it to physical system to proceed the cutting operation.

The focus of this study is how the simulation system creates the cutting result more exactly base on the environmental information. Hence, we do not create the cutting result model in the cutting scenario definition phase because the cutting result model cannot be updated with the transformation matrix that is calculated from digital mockup to environmental information alignment. Rather, we create the cutting result model on the fly inside the simulation stage.

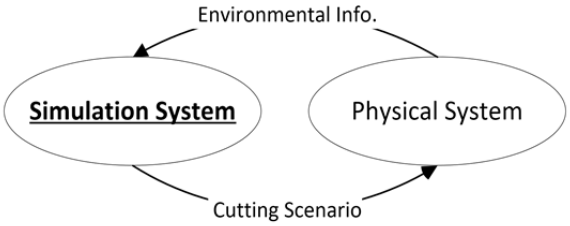


Fig. 1. Concept of the dismantling control system.

To do so, we have implemented the device model observer in the simulation system. When the cut activity is simulated, the observer is also activated. The observer observes all the resources regarding the cut activity simulation, and creates the cutting volume based on the shape and motion of the cut device at every time step with which cut the target model.

At the end of each time step, observer performs the Boolean remove operation, subtracting the cutting volume from the target model. Therefore the cut result model is created in the simulation stage based on the updated scenario and the digital mockup.

By the proposed methodology, even if the digital mockup model is updated in the cutting operation, simulation system still creates the exact cut result model. Hence the user can exactly evaluate the cost of the cut activity and the mechanical properties of the cut result model.

3. Conclusion

In this study, we have developed a simulation system which creates the exact cut result model based on the updated digital mock-up by the 3D scanned environmental information. This is a core component of our concept of dismantling control system. We expect that the proposed dismantling concept enables the cutting operation more accurate and fast. So far we couldn't deploy entire methodology to our testbed, in the future we have to test the methodology with real cutting operation.

Acknowledgement

This work was supported by the nuclear research and development program (2017M2A8A5015146) through the national research foundation of Korea funded by the Ministry of Science and ICT.

REFERENCES

[1] I. Kim, B. Choi, D. Hyun, J. Lee, K. Jeong, S. Kang, S. Moon, et al., "Environmental Information Feedback Framework for Nuclear Facility Decommission", Korean Nuclear Society Autumn Meeting, (2017).

[2] I. Kim, B. Choi, D. Hyun, J. Moon, J. Lee, K. Jeong, et al., A framework for a flexible cutting-process simulation of a nuclear facility decommission, Annals of Nuclear Energy, vol. 97, pp. 204-207, (2016).

Integrated Control Framework of Remote Dismantling System in Radiation and Underwater Environment

Dongjun Hyun*, Ikjune Kim, Sungmoon Joo, Jaehyun Ha, and Jonghwan Lee
Korea Atomic Energy Research Institute, 989-111 Daedeok-daero, Yuseong-gu, Daejeon, Korea
*dongjunn@kaeri.re.kr

1. Introduction

The integrated control framework proposed in this paper is a control system associated with a digital manufacturing platform, which allows the cutting process to be verified prior to execution by process simulation. The goal of the integrated control framework is to ensure that the remote dismantling system is operated directly by a simulated dismantling scenario, despite differences between digital mockup and the actual dismantling site. The task of this study is data conversion between the digital manufacturing platform and hardware control system, as well as 3d registration to correct the difference from the actual site and 3d data acquisition in radiation and underwater environment.

2. Remote Dismantling System

2.1 Overview of remote dismantling system

The remote dismantling system in this study features spatial perception based teleoperation technology and high payload dual robotic arms and underwater laser cutting technology.

2.2 Hardware configuration

Hardware of the remote dismantling system consists of dual robotic arms with elevation system and orthogonal and cylindrical cross crane system and linear/rotary stage system and bandsaw system (see Fig.1).

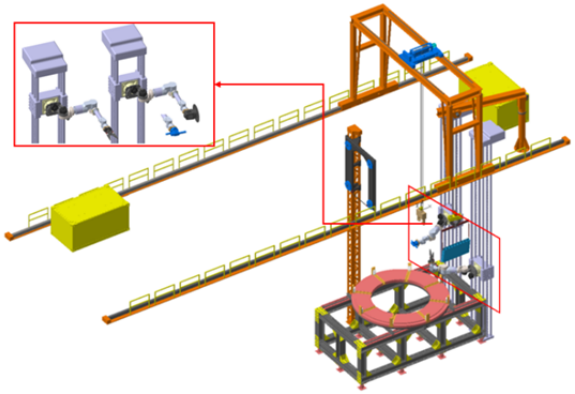


Fig. 1. Hardware configuration.

3. Integrated Control Framework

The integrated control framework consists of a digital manufacturing system, a control system and a remote dismantling system, and each system operates by organically interworking with various functional modules included (see Fig. 2).

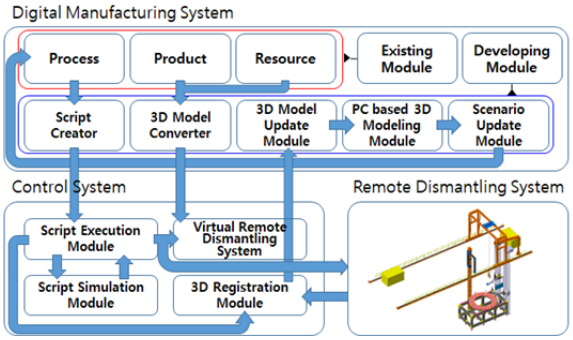


Fig. 2. Integrated Control Framework.

3.1 System operation using converted data

A script creator and a 3d model converter are developed to convert data of the existing module to input of the control system. Converted input of the control system are verified through the script simulation module and the virtual remote dismantling system and then used to operate the actual remote dismantling system (see Fig.3).

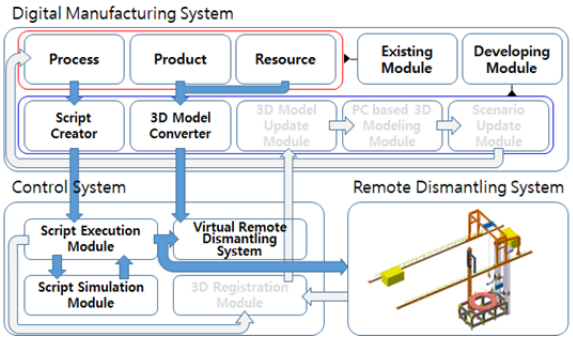


Fig. 3. System Operation Framework.

3.2 Input correction using 3d registration

Input error caused by difference between 3d mockup and the actual site is corrected by the 3d registration module and then data of the digital manufacturing system is updated (see Fig.4).

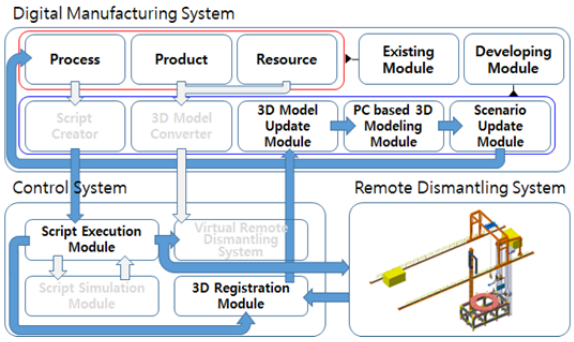


Fig. 4. Correction of 3D Model.

3.3 3d data acquisition and processing

3d data acquired in radiation and underwater environment contain error caused by refraction in a protection glass and water surface and is corrected by the refraction compensation module. After that, the corrected raw data is transmitted to the 3d data registration module through a process of segmenting raw data into appropriate regions because the raw data has a larger capacity and contains a larger area than necessary (see Fig.5).

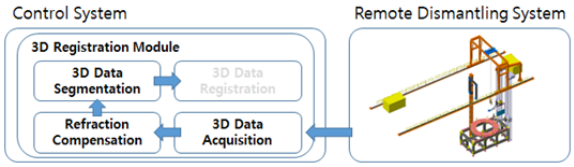


Fig. 5. 3D Data Acquisition and processing.

4. Experimental Results

4.1 System operation using converted data

A CRDM pipe bundle cutting test on a scaled reactor head is performed in a testbed [1] (see Fig. 6).

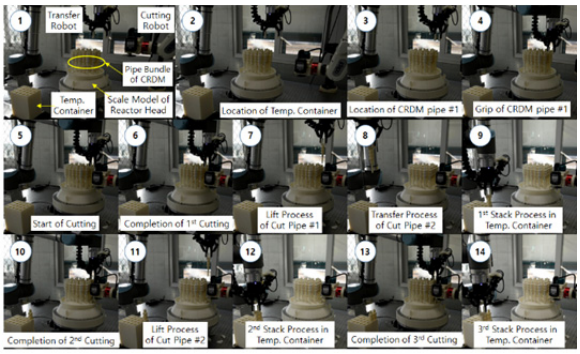


Fig. 6. CRDM Pipe Bundle Cutting Test.

4.2 Input correction using 3d registration

The robot input coordinates for cutting the CRDM pipe have been corrected by 3d registration (see Fig.7).

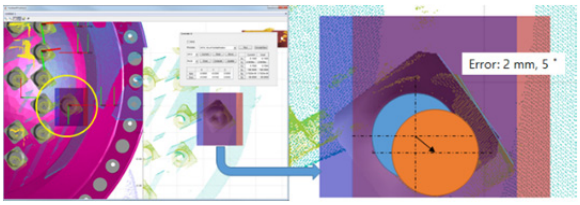


Fig. 7. Error correction using 3d registration.

4.3 3d data acquisition and processing

3d data acquisition and processing test is performed using a scaled reactor head in a simple pool (see Fig.8).

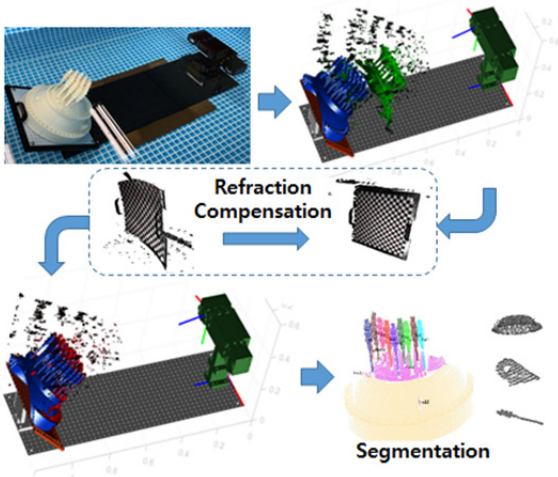


Fig. 8. 3d data acquisition and processing test.

5. Conclusion

The achievements of the proposed integrated control framework is demonstrated by experimental results.

Acknowledgements

This work was supported by the nuclear research and development program (2017M2A8A5015146) through the National Research Foundation of Korea, funded by the Ministry of Science and ICT, Republic of Korea.

REFERENCES

[1] Hyun D., Kim I., Joo S., Lee J., Kang S., “Development of Testbed for Advanced Remote Dismantling System”, Korea Radioactive Waste Society Fall Conference, (2018).

Disposal and Treatment for Decommissioning Solid Waste of Advanced Fuel Science Building at KAERI

Byungyoun Min*, Hyojin Aan, Undong Choi, Jinho Park, and Seungkook Park
NUDECOM, 401. E-6 BLDG, Korea Atomic Energy Research Institute, 989-111 daedeok-daero, Yuseong-gu, Daejeon, Republic of Korea
*bymin085@naver.com

1. Introduction

In korea, the management plan and strategy such as treatment, decontamination, packing, disposal (included self-disposal) about decommissioning wastes is insufficient because there is no decommissioning experience of nuclear facilities except for decommissioning of research reactor and uranium conversion plant.

To make a decommissioning activity plan of Advance Fuel Science Building, it is very important to establish and approach characteristics of facility, treatment for decommissioning waste, decontamination, packing and disposal.

Therefore, the management plan of efficient and rational decommissioning wastes considering the characteristics of decommissioning wastes such as the demolition, cutting, decontamination, volume reduction, packing, transportation and disposal etc. needs to establish.

For this purpose, the decontamination, treatment, packing and disposal of generated decommission solid waste during a decommissioning activity of Advanced Fuel Science Building(AFSB) has been suggested and approached.

2. Physical inventory assessment

To make a decommissioning plan of nuclear facilities, it is very important to investigate and identify characteristics of facilities for decommissioning. That is why the characteristics survey result of nuclear facilities for decommissioning are widely used to predict the amount of decommissioning waste and to provide estimates of exposures about the decommissioning work stage of each facility. For this purpose, the physical inventory of Advanced Fuel Science Building has been evaluated. The physical inventory assessment was performed by using results of MCNP 3D modeling based on the drawings and actual data of facilities [1]. The assumptions for calculating radioactive waste are as follows.

- Depth of concrete surface scabbling : 0.2cm(wall)×0.5cm(floor)×0.1cm(ceiling)
- Metal radioactive waste: 13% of the total amount of metal waste (as a result of dismantling with KRR)

Concrete waste is generated by 6,061 tons, with radioactive waste accounting for about 0.8 percent of the total. Compared to the total amount of concrete, the amount of concrete generated by salt-making work such as a scabbling is very small.

Table 1. Sessions for KRS conference

	Building (tons)			Equipment (tons)		
	Conc.	Metal	Others	Conc.	Metal	Others
Inventory	7,699	6.58	0.27	-	1,781	2.53
Industrial waste	6009	5.97	0.27	-	1,576	2.53
Radioactive Waste	52	0.46	0	-	206	0
Total	6,061	6.58	0.27	-	1,782	2.53

3. Results

The classification, decontamination, and packaging of waste for final disposal (including self-disposal) use the KAERI's radioactive waste treatment facility currently under construction. Dismantled radioactive wastes are classified in detail according to the material and level of radioactivity, and transported to and stored in the storage area of the comprehensive radioactive waste disposal facility using a 200L or 4m^3 storage container. In case of wastes generated during the dismantling process, decontamination work is carried out at the site.

3.1 Concrete waste

Radioactive concrete waste (powder type waste) generated during dismantling is 52 tons in the form of powder. Radioactive concrete wastes of dispersion material shall be transported to the final disposal site after cement solidification.

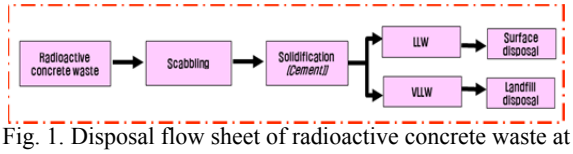


Fig. 1. Disposal flow sheet of radioactive concrete waste at AFSB.

3.2 Metal waste

When a dismantle AFSB, small size metal waste of 0.4 tons from building and 206 tons from equipment are generated, respectively [2].

Although it is classified as low-level waste during dismantling activities, all of it can be disposed of self-disposal by performing steam injection, ultrasonic and melt decontamination. Melt decontamination is effective for self-disposal after remove contaminated parts using steam, brushes and abrasive stones decontamination. In the case of highly corrosive carbon steel, the decontamination is carried out after removing part of the contaminated part using brush, abrasive stone, ultrasonic chemical decontamination, etc.

Based on experience in the decontamination, treatment, and disposal of metal wastes generated during dismantling of uranium conversion facilities and KRR-2, Because of the simple form of contamination and type of radionuclides in AFSB, relatively physical decontamination techniques such as swabbing, washing, scrubbing, brushing, steam injection, abrasive stone and ultrasonic decontamination by workers will be able to be treated as very low-level or self-disposal wastes.

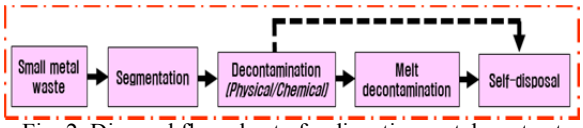


Fig. 2. Disposal flow sheet of radioactive metal waste at AFSB.

4. Summary

The approach of disposal and treatment for decommissioning solid waste generated during decommissioning activity of advanced fuel science building are as follows.

- Physical inventory assessment for decommissioning solid waste at Advanced Fuel Science Building.
- Approach of decontamination and disposal for treatment and final disposal of decommissioning solid waste such as concrete powder waste and small size metal waste.
- Approach of packing and disposal of decommissioning solid waste.

The result will be applied as decontamination, packing, and disposal for generated decommissioning solid waste during decommissioning activity of Advanced Fuel Science Building.

REFERENCES

[1] The physical and radiological inventory assessment for an initial decommissioning plan of nuclear fuel cycle facilities, KAERI/TR-7281/2018.

[2] The Approach of disposal and treatment for decommissioning solid waste at Advanced Fuel Science Building, NDC/TR-006/2020.

6분과

방사선환경 및 안전 (Oral)

Exercises of Aerial Radiation Measurements Using a Manned Helicopter

Young-Yong Ji[1,*], Hyon-Sock Chang[2], and Hee-Jin Kim[3]
[1] Korea Atomic Energy Research Institute, 989-111 Daedeok-daero, Yuseong, Daejeon 34057, Korea
[2] SI Detection Co. Ltd., Daejeon 34051, Republic of Korea
[3] Nuclear Safety Division, Busan Metropolitan City, Busan 47545, Republic of Korea
*yyji@kaeri.re.kr

1. Introduction

According to lessons learned from the accident of Fukushima Daiichi nuclear power plant (FDNPP), the importance of environmental radiation survey has increased to quickly assess the radioactive deposits in the ground. In general, the aerial radiation measurements is widely applied to diverse fields, such as the mineral exploration and emergency response [1-2]. With respect to the nuclear accidents, the purpose of aerial radiological survey is to support the decision making at the emergency through rapidly detecting properties of radioactive plume and making a radiation map due to the deposited radionuclides. Especially, a radiation map over wide area around the accident place at the early stage would be fundamental data to designate evacuation zones and build recovery strategies.

A variety of aerial measuring system (AMS) has been equipped in a manned helicopter for the efficient response depending on the dose rate level. A large volume NaI(Tl) detectors with a size of 2"x4"x16" (2L) and 4"x4"x16" (4L) are generally used for the purpose having a high counting efficiency in the airborne gamma-ray spectrometry. An array system with three or four large volume NaI(Tl) detectors has been widely used in global aerial radiological measurements. In addition to hardware system, it is very important to prepare methods and procedure to assess the radioactive deposition from measured ambient radiations at diverse flight heights.

There are much time and cost constrains to fully possess the AMS including analysis methods and procedures, because an experimental verification process should be repeatedly conducted using a manned helicopter at diverse geometries. As a preliminary study using manned helicopters, exercises of aerial radiation measurement was conducted using a 4"x4"x16" NaI(Tl) detector (1EA). Especially, ambient dose rates at 1 m above the ground was estimated from the AMS at above 300 m height ad compared with results of carborne survey around the same sites.

2. Method and Results

2.1 Rotary-wing aircraft

In this study, two kinds of helicopter, which means rotary-wing aircraft, were supported for exercises using the AMS around Busan Metropolitan City. The first helicopter is Mi-172 (Russia) of civil passenger version manufactured and the second is AW-139 (Italy) equipped with autonomous navigation system (ANS) for the purpose of a wide range of missions, such as firefighting, search and rescue, and emergency medical service. In the case of Mi-172, there was no ANS in helicopter so that the airborne survey was conducted by manually operating the flight following the flight lines. As shown in Fig. 1, the attenuation of incident photons to a detector was first evaluated by measuring the ambient dose rate inside and outside of a helicopter.



Fig. 1. The evaluation of photon attenuation due to a rotary-wing aircraft (AW-139).

2.2 Corrections in the AMS

The attenuation correction factor due to the flight height should be first determined to convert measured dose rate during aerial survey into one at 1 m above the ground. A hovering is performed at diverse altitudes in the relatively flat land. However, in this study, the MCNP simulation was conducted by modeling the infinite half space with uniform photons distribution of natural radionuclides. The photon intensity was calculated by considering the radioactivity distributions in the ground of natural nuclides of ^{214}Pb, ^{214}Bi, ^{228}Ac, ^{212}Pb, ^{212}Bi, ^{208}Tl, and ^{40}K.

To apply the attenuation correction factor, flight heights were accurately determined during airborne survey. A radar altimeter should be

equipped outside a helicopter and its data have to be then linked with gamma-ray spectrometry. However, this was not supported to helicopters in this study. The flight height was finally calculated by using GPS altitude in the AMS and DEM (Digital Elevation Model) altitude around the survey site, as shown in Fig. 2.



Fig. 2. Flight altitude on the ground.

2.3 Airborne gamma-ray spectrometry

The first aerial radiological survey was performed around the Gwangan-Suyeong, Busan for the purpose of making radioactive map of ambient dose rate at 1 m above the ground. The flight height was about 300 m above the ground. The measured dose rate at flight heights can be divided into those from deposited in the ground and background radiation by used helicopter and AMS itself. The background radiation was then evaluated from dose rates measured above the diverse sea levels, as shown in Fig. 3. The contrast of radiation map was definitely identified between the land and sea around the survey site. The calculated dose rate from the AMS was then compared with one of carborne survey around the same survey site.

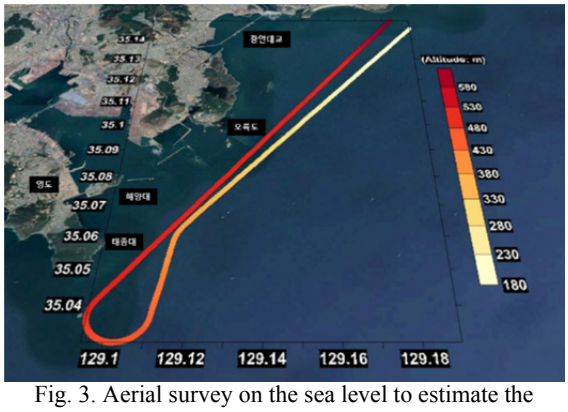


Fig. 3. Aerial survey on the sea level to estimate the background dose rate.

The 2nd aerial radiological survey was also conducted on the assumption that the radioactive plume is dispersed to the direction of Haeundae, Busan, due to the accident of Kori NPPs. The aerial survey was then conducted by following the designated flight lines of about 180 km from Gori NPPs to Haeundae, with the help of the ANS. Figure 4 shows the measured dose rate during the aerial measurement. The flight height was about 800 m due to high mountains in the flight route.



Fig. 4. The aerial measurement using a manned helicopter from Gori NPPs to Haeundae.

3. Conclusion

The aerial radiological survey can be applied to supporting the decision making at the emergency response through rapidly detecting the property of radioactive plume and making radiation map due to deposited radionuclides in the ground. For a preliminary study, exercise using the AMS was successfully performed to assess the ambient dose rate at 1 m above the ground through the wide area. Finally, it could be concluded that periodical experiments should be conducted to enhance the ability of airborne gamma-ray spectrometry.

ACKNOWLEDGEMENTS

This work was performed under the auspices of the Ministry of Science and ICT of Korea, NRF contract No. NRF-2020M2A8A4025462.

REFERENCES

[1] IAEA Airborne Gamma Ray Spectrometer Surveying, Technical Reports Series No. 323 (1991).
[2] Y. Sanada et al., Temporal variation of dose rate distribution around the Fukushima Daiichi nuclear power station using unmanned helicopter, Appl. Radiat. Isot. 118: 308-316 (2016).

Calculation of Minimum Detectable Concentrations for Mobile In-Situ Gamma Detector Using Outdoor-Field Data

Se-Won Park*, Chanki Lee, and Hee Reyoung Kim
Ulsan National Institute of Science and Technology, 50 UNIST-gil, Ulju-gun, Ulsan, Korea
*ycg03105@unist.ac.kr

1. Introduction

The radiation survey and site investigation process at decommissioning site is performed through scanning, sampling and direct measurements [1]. For the effective and fast RSSI process, mobile gamma detection system was developed [2] and it can be used as a scanning or direct measurement. In this study, Minimum Detectable Concentrations (MDCs) were calculated to identify applicability of mobile gamma detection system for decommissioning sites.

2. Methods

2.1 Detection sensitivity of detector

The sensitivity of the detector used as direct measurement can be expressed as a static MDC and sensitivity of scanning is represented by scan MDC and these are calculated using Equations (1) and (2), respectively [1][3].

$$\text{Static MDC} = \frac{3+4.65\sqrt{C_B}}{T\,\varepsilon\frac{A}{100}} \quad [\text{dpm}/100\ \text{cm}^2] \qquad (1)$$

where, C_B is the background counts during T, T counting time (min), ε the detector efficiency, and A the probe area (cm^2) [3].

$$\text{Scan MDC} = \frac{60\,d'\sqrt{C_{Bi}}}{i\sqrt{p}\,\varepsilon\frac{A}{100}} \quad [\text{dpm}/100\ \text{cm}^2] \qquad (2)$$

where, d' is selected based on the required true-positive (1-β) and false-positive rates (α), C_{Bi} the background counts during the time interval i, i the observation time interval (sec) that probe is over the hot spot, $\sqrt{p}$ the surveyor efficiency [3].

The relevant observation interval i is based on the scan speed and areal extent of the hot spot and can be calculated by Equation (3) [3][4].

$$i = \frac{\text{Length of the hotspot}}{v} \quad [s] \qquad (3)$$

Where, the length of the assumed hotspot (m) is the length passed in the direction of the detector, v (m/s) is scan speed for detector [3][4].

3. Results and Discussion

3.1 Detection sensitivity results

The $DCGL_W$ for surface soil of Maine Yankee is 0.86 pCi/g. It converted to 7636.80 Bq/m^2 by assuming soil density is 1.6 g/cm^3 and thickness of the contaminated is 0.15 m [1][4] to compare with MDCs. The static MDC in field was 594.78 Bq/m^2, and Fig.2 shows the scan MDC based on the scan speed and hotspot size [4].

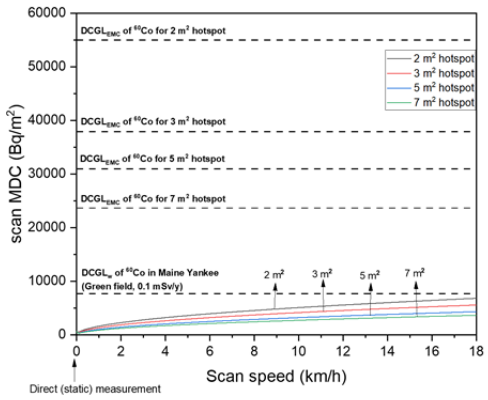


Fig. 1. Scan MDC according to hotspot size and scan speed [4].

4. Conclusion

The static MDC had a value of 7.79% of the $DCGL_W$ for surface soil of the Maine Yankee and the scan MDC at a speed of 18 km/h or less had a value lower than the $DCGL_{EMC}$ of the assumed hotspot. Therefore, it was confirmed that the mobile gamma detection system had sufficient performance to evaluate the $DCGL_W$ for surface soil of Manie Yankee using direct measurements and scanning at the decommissioning site.

ACKNOWLEDGEMENT

This work This work was supported by the 'Development of integrated mobile radioactive contamination detection system' of the Korea Institute of Energy Technology Evaluation and Planning (KETEP) granted financial resource from the Ministry of Trade, Industry & Energy, Republic of Korea (NO. 20171510300590).

REFERENCES

[1] Multi-Agency Radiation Survey and Site Investigation Manual (MARSSIM), NUREG-1575, Rev. 1, Nuclear Regulatory Commission, Washington, DC, (2000).

[2] C. Lee, S-W Park, H.R. Kim, Development of mobile scanning system for effective in-situ spatial prediction of radioactive contamination at decommissioning sites, Nuclear Instruments and Methods in Physics Research, A 966 (2020) 163833.

[3] Minimum Detectable Concentrations with Typical Radiation Survey Instruments for Various Contaminants and Field Conditions, NUREG-1507, Nuclear Regulatory Commission, Washington, DC, (1998).

[4] C. Lee, S-W Park, H.R. Kim, Applicability of a mobile in-situ gamma detector with different scan speed for finding hotspots in decommissioning sites, Nuclear Engineering and Technology, Submitted. (2020).

Development of Radiation Localization Algorithm Using Recursive Bayesian Inference

Hwa Jeong Han[1], Sang Hun Shin[2], Beom Kyu Kim[1], and Byung Gi Park[1,*]
[1]Soonchunhyang University, [2]FNC Technology Co. Ltd.
*byunggi@sch.ac.kr

1. Introduction

Predicting the location and distribution of radioactive materials released into the atmosphere in the event of a nuclear power plant accident is fundamental in establishing response strategies to protect residents and the environment. Radioactive material diffuses in the form of atmospheric particulates, sinks to the ground, and deposits on the ground. The process of determining and quantifying the surrounding area affected by the emitted radioactive material can be performed by measuring the intensity of the radioactive material at an arbitrary point in space.

The intensity of the radioactive source and the distance between the radioactive source and the detector follows an inverse square approximation. There are several statistical methods suitable for obtaining estimates of the location and distribution of the radioactive source based on radiation data collected by the detector. Various statistical methods are discussed in the previous paper [1]. In the paper, the radiation localization system is designed, and system structures are described.

2. Localization estimation based on RBE PF using radiation intensity signal

The system to be implemented in this paper is a system that estimates the position of the radioactive plume in space using the particle filter of the RBE algorithm with the radiation signal collected by the detector. The process is briefly expressed as a flow chart as shown in figure 1. The flowchart is performed as follows.

The collected measurement data is loaded, and the measurement data is sorted and classified. The data may be estimated by applying a particle filter to estimate the position of the radioactive plume in space. Radiation distribution is represented by 2D or 3D contour mapping. It saves position estimation and contour mapping results.

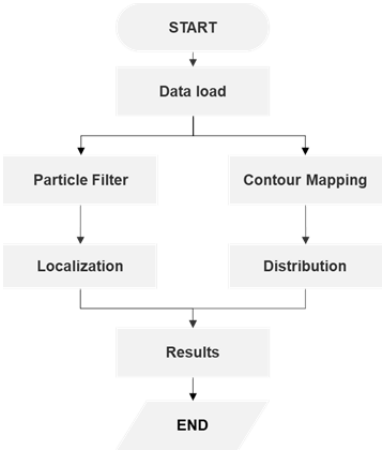


Fig. 1. Localization estimation flow chart.

2.1 Data load

Data stored from the detector different the number and size of data according to the number of detectors and measurement time. Therefore, it should be modeled to be able to load the big size of data. Also, it can be loaded according to the save format of the data.

Data classification can be selected by channel or by coordinates (altitude or coordinates of the ground), etc., and parallel processing is performed using clusters so that all large amounts of data can be read and processed.

2.2 Particle filter

The particle filter of RBE is applied to estimate the position of radioactive plume using the data processed through the above process. Particle filters work in the following process.

Particles with zero weight are randomly spread in the measuring area. The weights of particles are updated using the location of particles and the radiation intensity data measured by the detector. In order to allow the particles to quickly locate the plume, the particles that are detected most like the plume are given weights according to the predicted value. Particles with small weights are deleted, and particles with large weights are copied to form multiple particles. It is determined by calculating the similarity between the estimated actual plume position value of each particle through the predicted value [2-3].

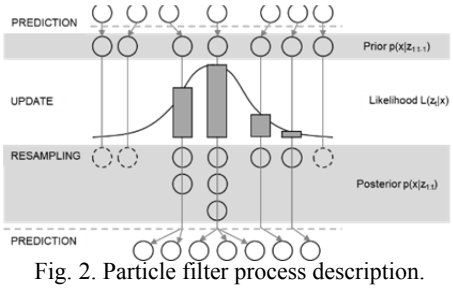


Fig. 2. Particle filter process description.

Assuming that a UAV with detectors is flying in space, and particles are generated to track the current plume location, each particle has its own coordinates. The distance between the coordinates of each UAV is calculated, and the distance between the radiation intensity observed by the detector is calculated, and the weight of the particle is derived through the similarity between the two distances. A method for calculating the particle weight based on the radiation intensity can be described as follows. In the particle filter, the observation step is performed to update the weight of each particle. The probability or similarity for each particle is calculated based on the measured radiation intensity observed by the detector.

The particle filter algorithm quickly finds the plume location so that particles distributed throughout the world can be performed by repeating the resampling process several times. However, if the plume moves too fast or the user's location changes rapidly, the changed location Finding the point very slowly.

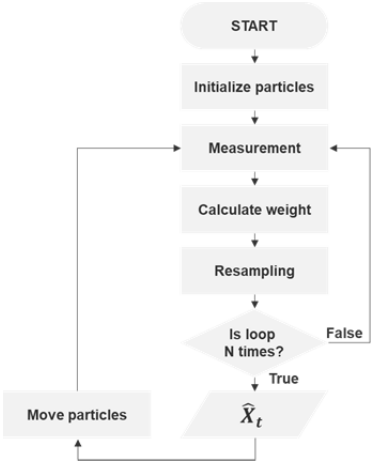


Fig. 3. Particle filter flow chart.

The process of performing the position estimation algorithm using the particle filter proceeds in steps of generating, observing, predicting, and moving particles. In the step of moving particles, a process of probabilistically predicting the result value using a random number called the Monte Carlo method is performed. do. At this time, a random number is generated to move the particles, which uses a random walk technique, which refers to randomly moving the coordinates of each particle within a predetermined range. If the distribution of particles is too narrow, the possibility of convergence to local minimization is high. Conversely, if the distribution of particles is too wide, there is a problem that a position estimation error increase [2-3].

2.3 Contour mapping

Contour mapping representing the radiation distribution can be drawn using classified data. Using the accumulated 2D data, 3D contour mapping according to altitude can be described.

2.4 Save results

The position estimated by the particle filter and the result expressed through contour mapping can be saved in an external directory, and the storage format can be designated as text, spreadsheet, graph, etc.

3. Discussion

In this study, we have suggested the methodology of the radiation localization using RBE PF. The methodology was evaluated in the computer simulation. The simulation result shows that this methodology can be applied to the localization estimation.

ACKNOWLEDGEMENTS

This work was supported by the National Research Foundation of Korea (NRF) grant funded by the Korean government (MSIT) (No. 2020M2D2A 206253811).

REFERENCES

[1] H. J. Han et al., “Review of Airborne Radiation Mapping and Radiation Detection Algorithms for Radiometric Surveys”, Proc. Of the KRS 2020 Spring Conference, 18(1), 347-348, online.
[2] Dawn An, Nam Ho Kim, Joo Ho Choi, “A Comparison Study of Model Parameter Estimation Methods for Prognostics” J. Comput. Struct. Eng. Inst. Korea, 4(4) (2012).
[3] Brewer, E. “Autonomous Localization of 1/R^2 Sources Using an Aerial Platform.” (2009).

Comparison of Gross and Photopeak Counts for Underwater Measurements Based on $YAlO_3$:Ce Spectrometer

Chanki Lee* and Hee Reyoung Kim
Department of Nuclear Engineering, Ulsan National Institute of Science and Technology, Ulsan, South Korea
*lck1992@unist.ac.kr

1. Introduction

Various kinds of radioisotopes have been generated by operations of nuclear power plants or accelerators in nuclear industry. In order not these radioisotopes to be released into water, development of in-situ measurement techniques is required. In water medium, however, having around 10^3 times larger density than air, so different approaches should be applied for the underwater radiation to be measured effectively, including materials, communication, and data analysis methods. In this study, therefore, we explains our developed spectrometer design based on $YAlO_3$:Ce scintillator. Then, we discuss the usefulness and timeliness of representative two data types, gross and photopeak counts, in a quantitative way.

2. Spectrometer design

2.1 Sensing module

We selected the $YAlO_3$:Ce single crystal as a scintillator material, thanks to its features of high density, chemical stability, and mechanical and radiation hardness, as well as appropriate levels of optical performance such as light yield (~ 40% of NaI:Tl) and photopeak absorption coefficient. To have small size and light weight but enough efficiency for exempt quantity, the crystal was produced in Φ2 ×2-inches size. The crystal was connected to a photomultiplier tube (PMT) with the same diameter and relatively short 64 mm length, and incorporated together with voltage divider by Al body as well as magnetic shield.

2.2 Communication module

A multichannel analyzer (MCA) was manufactured to be customized to be small size with laminated 2 layers of printed circuit boards. The MCA processes the sensing module signals, and stores data from processed signals. The data types include gross counts for every 1 s and accumulated spectrum of 1024 energy channels for 300 s. The data are transmitted onto surface by RS-422 communication through 8 pins underwater cable, where the cable also charges built-in Li ion battery pack for the PMT, and controls the MCA on/off remotely. Once underwater data are transmitted to the surface, the communication module on surface can transmit overall data to end user PC via LTE router.

2.3 Watertight housing

Φ80 × 420-millimeters cylindrical watertight housing was made to seal the abovementioned sensing module, MCA, and the battery pack. Body and back-end-cap was made of Al-6061 alloy, and the body thickness (t_{min}) was set as 3 mm based on Equation (1), where P is the pressure, R is the inside radius, and S is the maximum allowable stress.

$$t_{min} = \frac{PR}{3S-0.6P} \quad (1)$$

We used 3 mm of polyetheretherketone (PEEK) resin and carbon nanotube (CNT) compounds as a window material for front-end-cap. It is because of its similar yield stress (~ 100 MPa) and much lower density (~ 1.3 g/cm^3) and effective atomic number (~ 6.3 [1]), compared with Al-6061. The overall design of the spectrometer in the watertight housing is shown in Fig. 1.

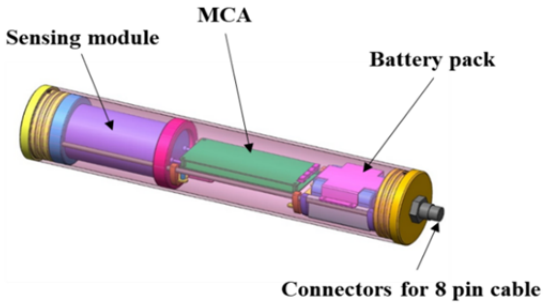


Fig. 1. Overall design of the spectrometer in the watertight housing.

3. Experimental methods

The gross counts and energy spectrum counts were obtained by the spectrometer for maximum 1,800 s from ^{137}Cs and ^{60}Co radioisotopes, which were located in 0.8 × 0.8 × 0.8-m^3 tank both with and without water supply. Source-detector distance was controlled from 50 mm up

to 400 mm. Then, their efficiencies and 3-sigma standard deviations for different acquisition time were calculated and compared.

4. Results and discussion

Fig. 2 shows a set of gross and photopeak efficiency values of ^{137}Cs without water supply from obtained energy spectrum.

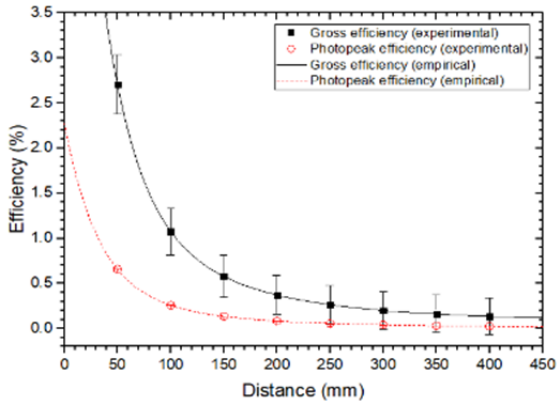


Fig. 2. Gross and photopeak efficiency values as a function of distance.

Because gross efficiency values are higher than photopeak efficiencies for all cases, they can provide relatively timely information for high radioactivity region with shorter acquisition time. Also, they can reliably find signals beyond background level at longer range of maximum ~ 300 mm than photopeak counts, where attenuation of gamma-ray occurred severely. Such tendency was more prominent in water than in air and for higher energy ^{60}Co than for ^{137}Cs, because contribution of attenuated counts was larger. Their relative standard deviations became higher as the source-detector distance increases, and gross counts were not distinguishable from background after ~ 300 mm for all cases.

5. Conclusion

The $YAlO_3$:Ce scintillation spectrometer was designed, developed, and preliminarily tested for use in underwater radiation measurement. Comparison between gross and photopeak counts at different distances shows that gross counts can be a more efficient data than the other for finding high radioactivity region, despite of their huge standard deviation results. Stability test for different temperature and flow velocity as well as dose rate calibration of the spectrometer will be conducted to provide useful raw data for mapping algorithms.

ACKNOWLEDGEMENT

This work was supported by the Ulsan City Support Project Research Fund of the Ulsan National Institute of Science and Technology (UNIST) under Grant 1.200051.01.

REFERENCES

[1] L. Birnbacher et al., “Accurate effective atomic number determination with polychromatic grating-based phase-contrast computed tomography”, Optics Express, 26(12), 15153 (2018).

Introduction of Modular Design Based Mobile Air Cleaning System

Jong Seong Kim[1], Kaphyun Yoo[1,*], Jungsu Oh[1], Hyun Chul Lee[2], Doo Yong Lee[2], Dukhee Lee[3], Junghyuk Shin[4], and Byunggi Park[5]
[1] Century Corporation, 5th floor, Magok jungangro 86, Gangseo-gu, Seoul, Rep. of Korea
[2] FNC Technology Co., Ltd., 32F, 13 Heougdeok 1-ro, Giheung-gu, Yongin-si, Gyeounggi-do, Rep. of Korea
[3] SOLTI Co., Ltd., 106, Gongdan 1-daero 322beon-gil, Siheung-si, Gyeounggi-do, Rep. of Korea
[4] NAC Co., Ltd., 54, Cheomdanyeonsin-ro, 288beon-gil, Buk-gu, Gwangju, Rep. of Korea
[5] Soon Chun Hyang University, 22 Soonchunhyang-ro, Shinchang-myeon, Asan-si, Chungnam, Rep. of Korea
*kaphyoo@century.co.kr

1. Introduction

The radioactive contaminants like an aerosol can be produced by the metal and concrete cutting as well as scarifying concrete during decommissioning of NPPs. The relatively small size of radioactive materials is floated in the air. These can contaminate working area and can be released to the outside. Once this happens, the field workers and residents nearby site would be exposed from the radiation. During the decommissioning, existing Air Clearing Unit (hereafter ACU) might be primarily operated to clean the air condition. In addition, the mobile ACU can be used to protect the workers from the local radioactive materials with existing ACU to meet ALARA principle. This paper introduces the project to develop the mobile ACU specially used for the decommissioning of NPPs.

2. Project Overview

The project to develop the mobile ACU used for the decommissioning of NPPs has started from May, 2020, which is funded from KETEP (Korea Institute of Energy Technology Evaluation and Planning). Fig. 1 shows the development task with organization.

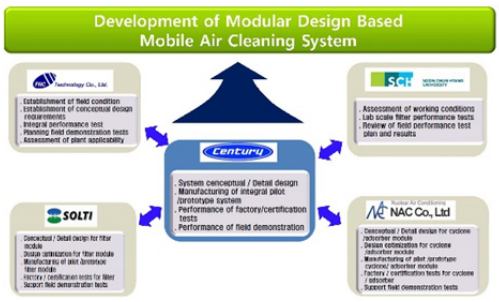


Fig. 1. Development task with organization.

5 organizations (Lead: Century corporation, Participation: FNC Technology, SOLTI, NAC and Soonchunhyang University) have been performing the technology development by April, 2023. The main tasks to develop the mobile ACU are as;

(1) Assessment of working conditions:
- Characteristics of aerosol and gas produced from decommissioning process, method, working condition, and so on.
- Characteristics of working environment such as working location, area, procedure, and so on.

(2) Design of mobile ACU:
- Design requirements based on the assessment results of working conditions.
- Review of applicable code and standards, licensing requirements.
- Performance of component and system design

(3) Manufacturing of mobile ACU
- Pilot / Prototype mobile ACU

(4) Performance tests
- Lab scale component performance tests
- Integral system performance tests
- Factory performance tests
- Certification tests based on KEPIC-MH or industry requirements
- Field demonstration tests

3. Design Concepts

The mobile ACU used for decommissioning NPPs has to have following capabilities;

(1) Minimization of secondary radio
(2) active waste
(3) Installation in limited space
(4) Easy handling and maintenance
(5) Operation with existing ACU

Fig. 2 shows the key elements and system configuration for the proposed mobile ACU. The proposed mobile ACU is based on modular design, which consists of filter module, adsorber module and control & monitoring module.

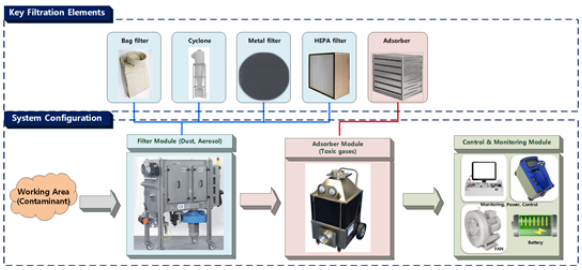


Fig. 2. Key filtration elements and system configuration for proposed mobile ACU.

The filter module consecutively consists of bag filter or cyclone as a pre-filter, metal filter as a medium filter and HEPA. Most of the radioactive dust and aerosol sized over 0.3μm are filtered through the pre- and medium filters. Since these filters would be permanently or semi-permanently used with cleaning, the amount of radioactive particulate would be significantly reduced for the HEPA filtration load. This can minimize the secondary waste from the replacement of HEPA. The adsorber module filled with a specialized adsorption material such as metal impregnated charcoal can be equipped with the filter module to remove the toxic gases such as NOx, SO_2 as well as CO. The mobile ACU can be operated by the control & monitoring module where the signal from instruments such as a differential pressure and/or radioactivity is monitored, the fan speed is controlled with instrumentation by an inverter.

Fig. 3 presents operation scheme for the proposed mobile ACU.

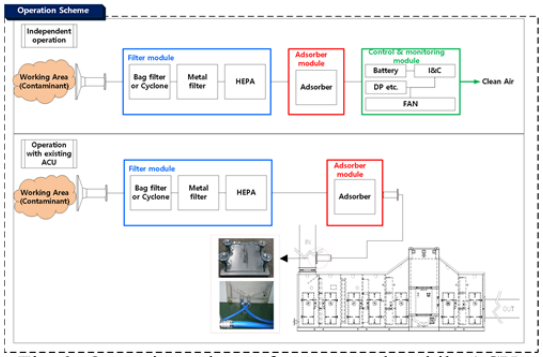


Fig. 3. Operation scheme for proposed mobile ACU.

According to the working area conditions, the unit filter module is serially connected to the unit adsorber module by flexible pipe or a number of filter modules are parallelly connected each other by a manifold. The mobile ACU can be operated either independently with control & monitoring module or by combining with the existing ACU without control & monitoring module.

4. Performance Test Plan

Fig. 4 shows the performance test plan for the proposed mobile ACU. The performance tests for the mobile ACU consist of the lab-scale filter performance test, integral performance test, factory performance test and certification test. The factory & certification tests would be conducted with KEPIC-MH as well as industry standards. On the other hand, the system performance on normal and various abnormal conditions would be confirmed by integral performance tests.

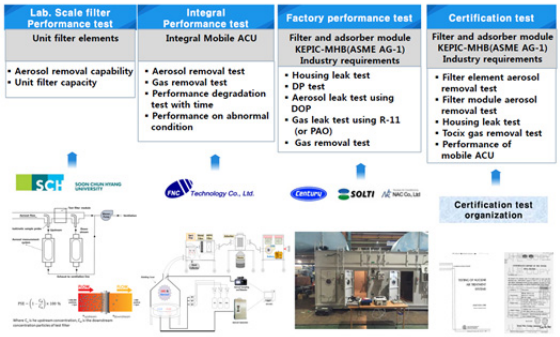


Fig. 4. Performance test plan for proposed mobile ACU.

The field demonstration test is planned for the prototype of proposed mobile ACU. This will be performed with a cutting test mockup or test bed in the planned decommissioning research institute, but this needs to be discussed in the future.

5. Conclusion

The mobile ACU used for the decommissioning of NPPs is one of the important devices to protect the field workers and residents nearby decommissioning site from radioactive materials. The modular design based mobile ACU is proposed and is in the designing phase. It will be realized with project plan in near future.

ACKNOWLEDGEMENTS

This work was supported by the Korea Institute of Energy Technology Evaluation and Planning (KETEP) grant funded by the Korea government (Ministry of Trade, Industry and Energy) (No. KETEP- 20201510300190).

Comparison of Annual Atmospheric Dispersion Factors of Continuous and Purge Releases of Gaseous Radioactive Effluents

Na-Hyun Kim[1,*], Won-Tae Hwang[2], and Chang-Lak Kim[1]
[1]KEPCO International Nuclear Graduate School, 658-91, Haemaji-ro, Seosaeng-myeon, Ulju-gun, Ulsan, Republic of Korea
[2]Korea Atomic Energy Research Institute, 111, Daedeok-daero 989 beon-gil, Yuseong-gu, Daejon, Republic of Korea
*hiskgus@gmail.com

1. Introduction

Although releasing radioactive material issue has been treated importantly from the start of operation Kori unit 1 to its shut down in June 2017, it is a recent to get attention to dispersion of radioactive material to atmospheric since people became interested in environmental issues with their life enhancing.

To evaluate the extent of dispersion gaseous radioactive material of normal operating nuclear power plants, XOQDOQ computer code is used to calculate atmospheric dispersion factor assuming that gaseous radioactive material is released only continuously [1]. However, in reality, both continuous and purge releases are simultaneously done in normal operation in a nuclear power plants.

The variation of the atmospheric dispersion factor values was evaluated based on annual purge time and compared to ones of continuous release. The three years meteorological data from 2008 to 2010 at the Kori and Wolsong sites were used to compare with atmospheric dispersion factors.

2. Material and Method

2.1 Meteorological Evaluation of Atmospheric Dispersion

To evaluate atmospheric dispersion, the XOQDOQ computer code was applied, which has been developed in U.S. NRC for the purpose of regulation of radioactive effluents. The code provides independent atmospheric dispersion evaluation of continuous or purge releases of radiological material at commercial nuclear power reactors and relevant nuclear facilities. It is based on the theory that material released to the atmosphere will be normally distributed by following a straight-line Gaussian plume model [2].

2.2 Meteorological Data Analysis

Meteorological data was measured according to the technical standards of NSSC Notice 2017-26 [3]. These standards are applicable to the safety evaluation of sites acceptability for construction and operating permits of nuclear power plants and relevant facilities sites.

The data observed in the meteorological towers was organized by statistics analysis, called Joint Frequency Distribution (JFD). To create the JFD, seven atmospheric stability classes (A~G) and eleven wind speed classes (<0.5, 0.5~1.0, 1.1~1.5, 1.6~2.0, 2.1~3.0, 3.1~4.0, 4.1~5.0, 5.1~6.0, 6.1~8.0, 8.1~10.0, 10.0< m/sec) for sixteen directions were designated.

In case of the calm, it was proportionally distributed with non-calm wind probability. The effect of recirculation and stagnations were reflected but the building wake was not considered.

3. Result and Discussion

The JFD of meteorological data was divided to 7 classes as shown in Table 1.

Table 1. Distribution on Atmospheric Stability Grades

	Unstable Grade			Neutral	Stable Grade		
	A	B	C	D	E	F	G
Kori	20.6	3.2	3.4	22.6	34.3	13	2.9
	27.2				50.2		
Wolsong	9	3.8	4.2	30.7	35.2	12.7	4.5
	17				52.4		

*Unit: percentage (%)

The percentages of stable conditions were greater than the unstable ones for both sites.

The Exclusion Area Boundary (EAB) is basically determined meeting the requirements of 10 CFR 100.11, 700m radius from the each Kori Units, 560m from Shin Kori Units and 914m from Wolsong Units. Considering the EAB of two sites, the receptor location was selected to 1 kilometer. Within 16 directions, the highest atmospheric dispersion factor was compared for both releases.

3.1 Results of the Atmospheric Dispersion Factors

As the annual purge release time went up from 100 hours to 8760 hours, the X/Q values in ordinate were rapidly decrease down and finally convergence to the value of continuous release in every 4 types of release as shown in Figure 1.

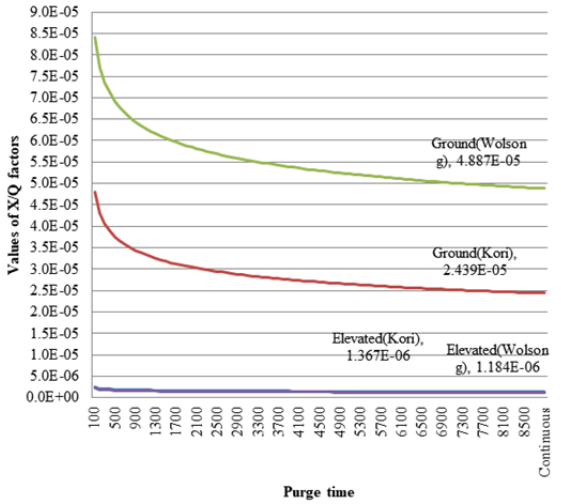


Fig. 1. Result of atmospheric dispersion factors using meteorological data of Kori and Wolsong.

As shown in Table 2, it can be expected to 50 percent of quantitative effect of full time continuous release with less than 2 hr/day (600 hours/365 days) purge release in everyday for a year. The value range of X/Q factor will not be significantly changed depend on the purge time with exceeding 2 hours in a day.

Table 2. X/Q Values and purge release time by percentages

%		Ground (Kori)	Elevated (Kori)	Ground (Wolsong)	Elevated (Wolsong)
90	X/Q	2.674E-05	1.471E-06	5.238E-05	1.284E-06
	hr	4800	4700	4900	4600
80	X/Q	2.909E-05	1.574E-06	5.590E-05	1.383E-06
	hr	2700	2700	2900	2500
50	X/Q	3.615E-05	1.885E-06	6.644E-05	1.683E-06
	hr	600	600	700	600

3.2 Comparison

To compare the X/Q factors in aspect of the purge and continuous release, the maximum and minimum value of X/Q factors were identified at 8760 hours and 100 hours respectively. Therefore, it was verified that the purge release values were less than two times of the continuous release values (1).

$$\frac{Maximum\ value\ (\frac{X}{Q} factor\ of\ 100\ hour\ purge\ release)}{Minimum\ value\ (\frac{X}{Q} factor\ of\ Continuous\ release)} < 2 \quad (1)$$

4. Conclusions

In general, it has been assumed that releases from nuclear power plants were continuous when calculating the atmospheric dispersion factor in Korea.

In this study, the annual atmospheric dispersion factors of purge release were calculated according the purge time and compared with the factors of continuous release.

It was found that the value of only purge release were not greater than 2 times of continuous release one even though in the worst meteorological case.

Moreover, by the fact that the mean value of them was applicable around 600 hours purge release time, it can be satisfactory to release more than that time, typically the normal operation nuclear power plants. Since Gaussian plume model has high reliability in flat geography it could be expected conservative approach when applying it to South Korea geography which has lots of mountainous area.

This conclusion is expected to provide important information nuclear industry and the operation of the expected nuclear facilities.

ACKNOWLEDGEMENT

This work was supported by the Korea Institute of Energy Technology Evaluation and Planning (KETEP Project No. 20204010600130) and the 2020 Research Fund the KEPCO International Nuclear Graduate School (KINGS), the Republic of Korea.

REFERENCES

[1] U.S. NRC Regulatory Guide 1.111, U. S. NRC, Washington, D.C. (1977).

[2] NUREG/CR-2919, XOQDOQ, U. S. NRC, Washington, D.C. (1982).

[3] NSSC Notice 2017-26, Nuclear Safety and Security Commission (2017).

Comprehensive Wireless Radiation Monitoring System for Decommissioning Nuclear Power Plants

Yun-Sam Kim, Younggil Kim, Donggu Kim, Jungsik Kim, Misuk Jang*, and Seoung Rae Kim
Nuclear Engineering Services & Solutions Co., Ltd., 2F, 756-27 Daedeok-daero, Yuseong-gu, Daejeon, 34055, Korea
*nessrnd@ness.re.kr

1. Introduction

Currently, about 55 percent of nuclear power plants over 30 years old have been operating around world [1]. Decommission of theses aged plants has become a new topic of research in the field of nuclear power plant. Korea is also waiting for the Kori#1 reactor to be decommissioned after a permanent shutdown, and the number of nuclear power plants to be decommissioned will continue to increase, such as Wolseong#1.

The decommissioning nuclear power plants, despite having lower radiation leakage than those in operation, have a possibility of radiation leakage. To detect radiation leakage early during plant decommissioning, a wireless monitoring system, which is easier to install than wired, is required.

In this paper, we introduce a summary of the wireless radiation monitoring system for decommissioning nuclear power plants.

2. Wireless Radiation Monitoring System

2.1 Wireless Radiation Monitoring System Design

Wireless radiation monitoring system consist largely of location-based ADRs to detect personal radiation exposure, earplugs to inform workers of their surroundings, radiation monitoring server to manage dose information, and wireless communication networks.

The location-based ADR not only allows workers to know the current radiation exposure by themselves, but also sends the location and radiation dose of workers to the radiation monitoring server to inform workers of their condition or hazardous situations. It also informs operation status of the location-based ADR or information on the surrounding risks to the worker through the earplugs.

The decommission of nuclear power plants produces a lot of noise, such as cutting and removing equipment, and the use of earplugs is required to protect workers from noise. These earplugs keep workers from noise but prevent workers from receiving information from the radiation management server or ADR alarms. Our earplugs are connected to a location-based ADR using Bluetooth, and the information delivered by the location-based ADR is converted to voice. This allows workers to be protected from outside noise and to perform safer tasks by allowing them to check the required information by voice.

The radiation monitoring server is responsible for monitoring location and dose information delivered by the location-based ADR, determining risks, and informing the surroundings. The radiation monitoring server and location-based ADR are wirelessly connected and use the ISM band's internal wireless network for personal information protection. The radiation monitoring server analyzes the information received from the location-based ADR to determine if a hazardous situation has occurred in the plant, and notifies the surrounding workers of the hazard when hazard if a hazardous situation occurs.

2.2 Operation of Wireless Radiation Monitoring System

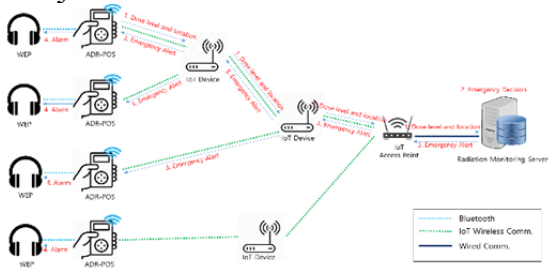


Fig. 1. Wireless Radiation Monitoring System Communication.

Figure 1 shows the operation of the wireless radiation monitoring system. Location-based ADR measures radiation and periodically transmit values to the radiation monitoring server at predefined time if it determines that it is within a safe range. The position-based ADR also sends its position calculated using UWB and triangulation along with radiation measurements. The transmission of these data uses 2.4 GHz ISM band communication protocol, such as ZigBee [2], etc., or lower frequency communication.

Frequency higher than 2.4 GHz is not used due to low transmittance, making it difficult to transmit long-distance within the plant. The radiation monitoring server stores information received from location-based ADR and shows it to the system administrator.

When radiation beyond the safe range is detected in the worker's space, the location-based ADR first sends warning information to the worker's earplugs using Bluetooth. The earplugs then convert the warning message into voice and inform the worker to evacuate immediately. At the same time, the ADR sends its location and radiation value to the server using a non-scheduled wireless communication section. Upon receiving the warning information, the server receives radiation information from various devices around the location-based ADR to verify the accuracy of the warning. If the warning is deemed accurate, the server sends warning to the location-based ADRs around the hazard, and the ADRs receiving that information inform the worker of the risk location information and the need for evacuation.

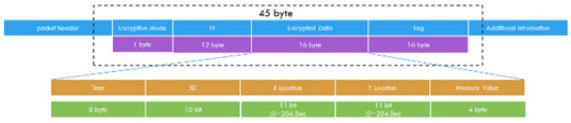


Fig. 2. Network Packet Definition.

Figure 2 defines network packet for transmitting location information and radiation values. Network packets include ID, location information and radiation value of each ADRs. Of these, location information excludes height information even though ADRs get 3D location information. All packets are encrypted and transmitted because ADR and the actual user's information can be mapped using the ID of the network packet and there is a possibility of personal information leakage.

3. Conclusion

In this paper, we proposed the wireless radiation management system which can identify radiation leakage that may occur during nuclear power plant decommissioning early, and is easier to install and operate than wired. When using our system, workers can evaluate immediately if they have been exposed to radiation in an unintended situation, and the surrounding workers can also recognize the danger, making safe work possible. In addition, since the field supervisor can monitor the location of the workers in real time, it is possible to take the rescue work of the accident worker faster from an unexpected accident.

ACKNOWLEDGEMENT

This work was supported by the Korea Institute of Energy Technology Evaluation and Planning (KETEP), granted financial resources from the Ministry of Trade, Industry & Energy of the Republic of Korea (No. 20191510301060).

REFERENCES

[1] PRIS, "Power Reactor Information System: Past, Present and Future", (2019).
[2] ZigBee Alliance, https://zigbeealliance.org.

6분과

방사선환경 및 안전 (Poster)

Introduction of Auto G-Factor Calculation Program

Sungyeop Joung* and Young-Yong Ji
Korea Atomic Energy Research Institute, Daejeon 34057, Republic of Korea
*jsy1003@kaeri.re.kr

1. Introduction

Dose conversion from a measured energy spectrum for counts obtained using a gamma-ray spectrometer can be achieved from a G-factor. This means the theoretical detector response function to make a spectrometric determination of the dose rate. Monte Carlo simulation can be calculated, such as the Monte Carlo N-particle (MCNP) code. This G-factor calculation process is not a hard but quite time-consuming and complicated process. Therefore, we make the automated G-factor calculation program with simple input variables to reduce calculation time and mistakes.

2. Definition and calculation process of G-factor

The G-factor is a function of a detector's response to incident photons. The Monte Carlo calculation could achieve this factor. That means this G-factor also depends on the response function of the gamma radiation detector [1]. The following equation can calculate the G-factor.

$$\dot{X} = \int n(E)G(E)dE, \qquad (1)$$

Where $\dot{X}$ is dose rate, E is incident radiation energy, $n(E)$ is count rate of energy E, and $G(E)$; a G-factor is the dose conversion factor of the measured count rate. The G-factor unit can be μR/h/cps, nGy/h/, or μSv/h/, etc.

The radiation spectrum can be derived by the response function archived from the Monte Carlo calculation. Equation 2 shows this response function.

$$n_i = R_{ij}\emptyset_j, \qquad (2)$$

Where n_i is the count rate of the ith channel of the measured spectrum, R_{ij} is response function that means measured count rate per incident gamma radiation fluence of energy E_i, and $\emptyset_j$ is incident radiation fluence with energy E_j. Figure 1 shows an example of the response matrix. Equation 3 shows the relation between gamma radiation fluence and exposure dose rate.

$$\dot{X} = C\left(\frac{\mu_{en}}{\rho}\right)_{air} E_j\emptyset_j \equiv \left(\frac{\dot{X}}{\emptyset}\right)_j \emptyset_j, \qquad (3)$$

Where C is unit conversion constant, $(\mu_en/\rho)_air$ is mass-energy absorption coefficient in the air, E_j is incident radiation energy, $(\dot{X}/\emptyset)_j$ is a conversion factor of incident radiation fluence to dose rate. Equation 4 shows the relation between G-factor and inverse response matrix and $\dot{X}$ which is derived from equation 1 to 3.

$$G_i = \left(\frac{\dot{X}}{\emptyset}\right)_j R_{ij}^{-1}, \qquad (4)$$

Where i and j means measured radiation in the gamma energy spectrum and incident radiation energy, and G_{ij} means radiation detector G-factor.

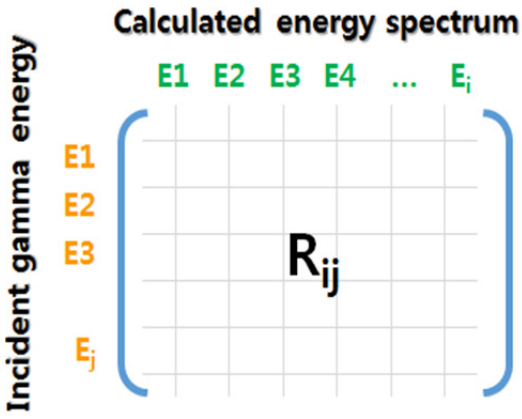


Fig. 1. an example of the response matrix.

3. Auto G-factor calculation program

We use the python language to program the auto G-factor calculation program because it is easy to read, improved productivity, interpreted language, and supports vast libraries with open-source. Figure 2 shows the screenshot of the auto G-factor calculation code. This code contains 3 parts.

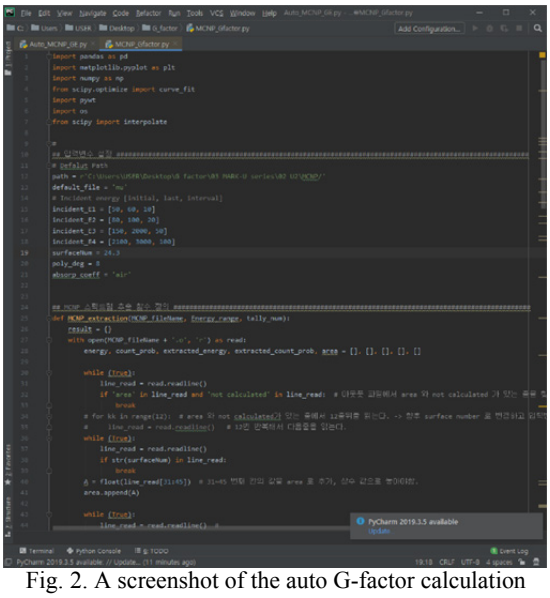


Fig. 2. A screenshot of the auto G-factor calculation program.

3.1 Input variables

The first part of the auto G-factor calculation program consists of input variables. These variables are the input path of Monte Carlo simulation output, output file name, incident energy of simulated output, and incident surface number.

3.2 Output extraction and inverse matrix calculation

The second part of this program consists of output spectrum extraction and incident surface area of the detector. After this process, the program calculates the inverse matrix of the response function. This part used the NumPy library to calculate the inverse matrix and matrix multiplication.

3.3 Polynomial fitting and G(E) factor calculation

The last part of the program is composed of polynomial fitting of calculated response function and G(E) factor coefficients. This part used the Pandas library for polynomial fitting.

4. Result

We compared the result of the auto G-factor calculation program and the result from a conventional method. Figure 3 shows the G-factor of the CZT detector calculated from the program and the conventional method. This shows these results are consistent well.

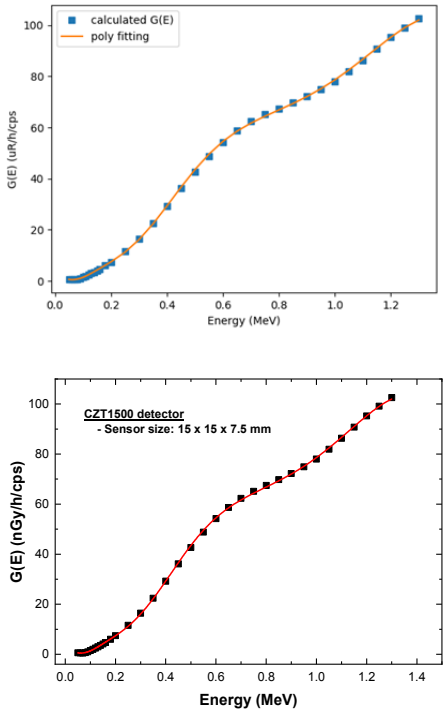


Fig. 3. G-facor of the CZT detector calculated from Auto G-factor calculation program and conventional method.

5. Conclusion

We introduced the auto G-factor calculation program and verified. We believe this code will help users understand and calculate of G-factor.

REFERENCES

[1] Ji YY, Hong DS, Kim TK, Kwak KK, Ryu WS, “Application of the dose conversion factor for a NaI(Tl) detector to the radwaste drum assay”, Radiat Meas 46:503–509 (2011).

Analysis on Activation Source Term for Soil Sample at KIJANG Research Reactor

Ji Sung Park*, Gyuhong Roh, and Byungchul Lee
Korea Atomic Energy Research Institute, 111, Daedeok-daero 989beon-gil, Yuseong-gu, Daejeon, Republic of Korea
*jspark13@kaeri.re.kr

1. Introduction

In KIJANG research reactor (KJRR), neutron activation analysis (NAA) facility is to be installed for radioactive analysis of various samples through the pneumatic transport system(PTS) during normal operation. A representative application of NAA is the analysis of soil samples. In natural soil contains various elements. Each element in soil becomes radioactive after neutron irradiation, and releases a gamma ray. In this paper, the radioactive source term of the soil sample is evaluated to determine the appropriate decay time for handling the radioactive soil sample.

2. Methods and Results

2.1 Contents of Soil

Since natural soil contains different compositions depending on the region, season, and weather and no reference soil sample is designated in Korea, Montana soil [1] among NIST soil samples is employed as the reference sample in this paper. Among various elements in Montana soil sample, the certificated nuclides for exact content of each element are shown in Table 1. Whereas, although the exact content has not been certificated, the nuclides which are considered to have a significant effect on the assessment of radioactivity are shown in Table 2.

Table 1. Certified Content List in Montana Soil Sample

Element	Mass Fraction (%)	Element	Mass Fraction (μg/g-soil)
Al	6.53 ± 0.09	Sb	19.4 ± 0.8
Ca	2.88 ± 0.08	As	105 ± 8
Fe	2.89 ± 0.06	Ba	726 ± 38
Mg	1.05 ± 0.03	Cd	41.7 ± 0.25
P	0.086 ± 0.007	Cu	114 ± 2
K	2.45 ± 0.08	Mn	638 ± 28
Na	1.14 ± 0.03	Hg	6.25 ± 0.19
S	0.042 ± 0.001	V	81.6 ± 2.9

Table 2. Non-certified Content List in Montana Soil Sample

Element	Mass Fraction (μg/g-soil)	Element	Mass Fraction (μg/g-soil)
Br	5	La	40
Ce	69	Mo	1.6
Cs	6.1	Nd	31
Cr	47	Rb	110
Co	10	Sm	5.9
Dy	5.6	Sc	9
Eu	1.1	Th	14
Ga	15	W	3
Au	0.03	U	2.6
Hg	7.3	Yb	2.7
Ho	1	Y	25
In	1.1	Zr	230
I	3		

2.2 Calculation of Activation Source Term

In KJRR, NAA facility is to be installed at two irradiation holes outside the reactor core (Figure 1). The sample employed for the radioactivity analysis is 1 gm of soil. The soil sample is put in a polyethylene (PE) capsule and the PE with soil sample is irradiated in the irradiation hole of NAA. Since it is expected that the radioactivity of the irradiated PE capsule be low compared to that of the irradiated soil sample, only the radioactive source term of the soil sample is considered in this evaluation. The irradiation time is taken as10 minutes and 60 minutes, and the decay times after irradiation are considered to be 0 min, 1 min, 10 min, 30 min, and 60 min.

The radioactive source term is evaluated using the ORIGEN code [2] in the SCALE Code Package. The radioactivity of soil sample is estimated under the irradiation at the thermal neutron flux of 4.98E+12 n/cm2-sec in the ORIGEN calculation. Then, the gamma-ray source term is obtained by multiplying the radioactivity of the nuclides by the gamma-ray branching ratio [3].

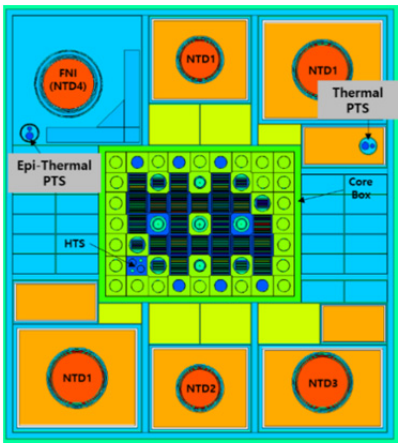


Fig. 1. Irradiation holes for NAA in KIJANG Research Reactor.

2.3 Results and Discussion

As a result of the irradiation of the soil sample at KJRR, the radioactivity of 45 nuclides from the irradiation for 10 and 60 minutes are calculated. Among 45 nuclides, 15 nuclides having high activity are shown in Table 3.

Table 3. Activity of Soil Sample at KJRR

Nuclide	Activity of Soil Sample (Bq)	
	10 min irradiation	60 min irradiation
Al-28	1.524E+09	1.596E+09
Mg-27	5.127E+07	1.176E+08
Mn-56	2.185E+07	9.750E+07
V-52	1.628E+07	1.932E+07
Na-24	5.434E+06	3.197E+07
Cu-66	3.062E+06	4.118E+06
Dy-165	6.180E+05	3.639E+06
As-76	4.390E+05	2.605E+06
Eu-152m	3.595E+05	2.090E+06
Ba-139	2.961E+05	2.064E+06
Cu-64	1.817E+05	1.066E+06
K-42	1.168E+05	6.848E+05
Sb-122	2.945E+04	1.764E+05
La-140	2.397E+04	1.429E+05
Sm-153	2.064E+04	1.247E+05

Using the radioactivity of 45 nuclides, gamma spectra depending on irradiation time and decay time are obtained by multiplying the radioactivity of 45 irradiated nuclides by gamma-ray branching ratio of each nuclide. The result is shown in Figure 2. Then total gamma-ray intensity for each case is calculated finally as shown in Table 4. The total gamma intensity for the case of 60 min irradiation and 60 min decay is higher than that for the case of 10 min irradiation and 10 min decay. Since the shape of spectra, therefore, is similar in all evaluation case as shown in Figure 2, it can be expected that the irradiation time gives more influence on total gamma intensity than the decay time.

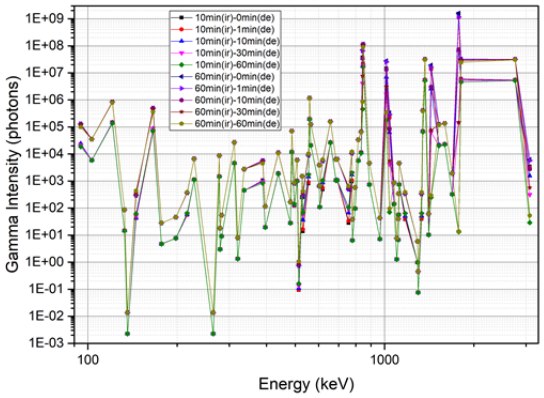


Fig. 2. Gamma Spectra of Activated Soil at KJRR.

Table 4. Total Gamma Intensity of Activated Soil at KJRR

Decay Time (min)	Total Gamma Intensity (photons)	
	10 min Irradiation	60 min Irradiation
0	1.630E+09	1.930E+09
1	1.219E+09	1.494E+09
10	1.341E+08	3.314E+08
30	4.127E+07	2.069E+08
60	3.269E+07	1.791E+08

4. Conclusion

The source term of the irradiated soil sample at NAA hole in KJRR is evaluated using the ORIGEN code. The total gamma intensities immediately after irradiation for 10 min irradiation and 60 min irradiation are evaluated as 1.630E+09 photons and 1.930E+09 photons, respectively. And the total gamma intensities at 60 min decay after 10 min irradiation and 60 min irradiation are evaluated as 3.269E+07 photons and 1.791E+08 photons, respectively. These evaluated results can be utilized to determine the decay time requirements to reduce the radiation exposure of workers as possible during the NAA experiment.

REFERENCES

[1] NIST Standard Reference Material 2711 (Montana Soil), 18 July 2013.
[2] Scale: A Comprehensive Modeling and Simulation Suite for Nuclear Safety Analysis and Design, ORNL/TM-2005/39, Version 6.1, Vols. I-III, June 2011.
[3] Table of gamma ray (Decay diagram), http://atom.kaeri.re.kr.

Development of Regulatory Guidance on Conditional Clearance for the Disposal, Recycling and Reuse of Activated Medical LINAC Components

Byeonghyeon Park*, Minchul Song, Jonghoon Park, and Jaeho Lee
Korea Institute of Nuclear Safety
*hpark@kins.re.kr

1. Introduction

In Korea, since the early 2000s, as interest in radiation therapy has increased, the development and introduction of radiation therapy devices have been expanded, and their use has been steadily increasing. On the other hand, the lifespan of the linear accelerator for treatment is known to be at the level of 10 to 20 years, and the introduction of treatment devices reflecting new technologies is increasing, and the demand for disposal is increasing accordingly.

Unlike general X-ray devices, linear accelerators with more than a certain energy generate neutrons by photonuclear reactions between X-rays and surrounding materials, and these neutrons create unintended radioisotopes. Therefore, when the linear accelerator is to be discarded, it is necessary to confirm whether the clearance criteria are met through quantitative analysis of radioactive nuclides, but the method and contents are difficult to achieve. The components of the linear accelerator for treatment vary in shape and material, and if the analysis is performed without selection for all parts, the burden of enormous cost is incurred, so when considering economic and social costs, the justification of the regulation against the radiation risk is poor. Therefore, it is necessary to develop guidelines that enable licensees to easily measure and make judgments while simultaneously satisfying the criteria for clearance.

2. Method

2.1 Proxy nuclide

Table 1 shows the nuclides that can be generated by radiation in consideration of the material of the linear accelerator component. Co-60 was selected as a proxy nuclide to be used to determine whether or not to satisfy the clearance criteria from a measurement point of view by comprehensively considering the half-life of the nuclide, radiation emission, production yield, and radiological hazard. In lead and aluminum, Co-60 is not produced as a major produced nuclide, but considering that the clearance concentration. of Co-60 is the lowest and easy to measure, all measured values are assumed to be due to gamma ray from Co-60 and the result is adequately conservative.

Table 1. Exposure pathways for conditional clearance of activated accelerator [1]

Material	Nuclides generated	Reference nuclides
Lead	Tl-204, Sb-124	Sb-124
Copper	Fe-55, Co-57, Co-60	Co-60
Aluminum	Na-22	Na-22
Iron	Mn-54, Fe-55, Co-57, Co-60	Co-60, Mn-54

2.2 Selection of measurement instrument and Dose assessment

Although it is possible to measure the radioactivity concentration using HPGe detectors, in this case, there are too many factors to be considered, and the result value is distorted due to the uncertainty of the factor itself. In addition, the clearance concentration of Co-60 is 0.1Bq/g, which requires too much effort and time to measure up to this value. Therefore, rather than focusing on accurately measuring an object that is difficult to measure, the approach was based on the dose rate using GM counter, and the radioactivity and radioactivity concentration corresponding to the dose rate was evaluated by using computer simulation with MCNPX and Microshield. In addition, a sufficiently conservative assumption was made so that the result does not underestimate the risk, and a standard source is used for verification of the computer simulation. Based on the estimated activity or activity concentration, it is possible to evaluate whether the clearance criteria are met. If such a measurement method is recommended, it is expected that any licensees can easily perform the measurement and judge the result.

2.3 Scenarios for clearance of induced components

The clearance concentration for radioisotopes is a fairly conservative value, and considering the reality that radioactive waste is disposed of in a specific scenario and is very difficult to measure, a conditional clearance level can be provided to promote the convenience of the licensees. In medical linear accelerators, the components radio-activated are all metals, and they are limited to being reused or recycled by

metal related facilities. In addition, due to the characteristics of metals, internal exposure occurs only when reprocessed in a foundry, and only external exposure is considered for residents or workers in facilities other than foundry. Therefore, it is possible to determine whether or not it is possible to dispose of radioactive parts by limiting them to WF, WO, RF, RH, and RP among the above IAEA scenarios [2].

Since Co-60 was selected as the proxy nuclide, the radioactivity concentration that satisfies the clearance criteria for each scenario (Actual: 10μSv/y, Low probability: 1mSv/y) based on Co-60 is as follows. In the case of Co-60, the RH scenario determines the clearance concentration, and considering the entire scenario, it can be seen that the effect of external exposure is 1,000 times higher than that of internal exposure for the same nuclide.

Table 2. Exposure pathways for conditional clearance of activated accelerator [1]

Receptors	Pathways
1. Disposition route: Transfer of accelerator components for refurbishment	
1.1 Workers handling activated component	External exposure
1.2 Workers refurbishing components	External exposure Inhalation of re-suspended dust
2. Disposition route: Disposal of the activated component via normal waste streams and metal recycling	
2.1 Workers handling activated component	External exposure
2.2 Workers at landfill	External exposure
2.3 Workers at foundry / recycling facility	External exposure Inhalation of re-suspended dust

Table 3. Conditional clearance level for metal recycling scenarios for Co-60

Scenario	Exposure pathways	Concentration(Bq/g)	
		Actual	Low Prob.
WF	External exposure	2.1	4.9
	Inhalation	2.8E5	6.5E5
	Ingestion	1.6E3	2.9E3
WO	External exposure	1.1	4.9
RH	External exposure	0.03	0.3
RP	External exposure	0.5	4.0
	Inhalation	8.2E4	4.1E4
	Ingestion	82	4.1E2

3. Result

It can be seen that the main exposure pathway for determining the clearance concentration of Co-60 is the RH (Resident house) scenario. The geometry of this scenario assumes a room with a size of 3m×4m×2.5m and 20cm thick walls inside the building. IAEA SRS-44 provides the dose rate of external exposure per radiation concentration of Co-60 that a resident can receive from a height of 1m in the middle of the room as 0.794μSv/h/(Bq/g). To verify this, a building uniformly contaminated with Co-60 1Bq/g was computerized with MCNP6, and as a result of the simulation, it was confirmed that the radiation dose rate at the occupant's location was similar to the above value.

Therefore, in order for the effect of internal exposure to be at a level similar to that of external exposure, it should be higher than 800μSv/h. If it is less than 0.1μSv/h at the distance from the surfaces of radio-activated component, it is expected that it can be regarded as non-activated from a regulatory point of view.

4. Conclusion

As described above, it was confirmed that there is a limitation in accurately measuring radioactivity for each nuclide for components having various geometries and materials. Therefore, we propose a method of selecting proxy nuclides and estimating the radioactive concentration of proxy nuclides based on the radiation dose rate, and the standard is 0.1μSv/h at a distance of 1 cm from the surface. This proposal is an example of conditional clearance discussed in the IAEA, and will be limitedly applied only to linear accelerators for treatment that are not many in use and have completed understanding what kind of components are.

Additional research will be supported to prove the validity of the guidelines for determining radiation using a general portable survey meter.

Based on the results of this study, it is expected that it will be a way to ensure sufficient safety while making the regulatory decision on the disposal of radioactive parts more efficiently.

REFERENCES

[1] Commission on Radiological Protection, “Clearance of Accelerators and the removal of accelerator parts from radiation protection areas” (2009).

[2] IAEA, “Derivation of activity concentration values for exclusion, exemption and clearance” (2005).

Review on Effectiveness of Current Discharge Limit Based on Radiation Dose for Gaseous Radioactive Effluent From Korean Nuclear Power Plants

Soyun Kim, Ji Su Kang, and Jae Hak Cheong*
Dept. of Nuclear Engineering, Kyung Hee Univ., 1732 Deokyoung-daero, Giheung-gu, Yongin-si, Gyeonggi-do
*jhcheong@khu.ac.kr

1. Introduction

Radioactive effluent discharged during the normal operation of Korean Nuclear Power Plants (NPPs) is controlled by the discharge limit based on radioactivity concentration (Bq/m^3) and exposure dose of the public (i.e. dose constraints). In Korea, the dose constraints for the radioactive effluent are listed in the Nuclear Safety and Security Commission (NSSC) Notice No.2019-10 as shown Table 1 [1]. This safety standard is based on the 10 CFR 50 Appendix I of the United States Nuclear Regulation Commission (USNRC) [2]. However, the specific technical reason has not been suggested in the process of reference the dose constraint of US.

Table 1. Annual Dose Constraints of Korea [1]

		Exposure Type	Korea
Facility	Gaseous	Gamma air dose	0.1 mGy
		Beta air dose	0.2 mGy
		Effective dose of External exposure	0.05 mSv
		Skin equivalent dose of External exposure	0.15 mSv
		Equivalent dose of radioactive iodine, H-3, C-14, particulates	0.15 mSv
	Liquid	Effective Dose	0.03 mSv
		Maximum equivalent dose	0.1 mSv
Site		Effective dose	0.25 mSv
		Thyroid equivalent dose	0.75 mSv

Furthermore, the current dose constraints of Korea are relatively complex than international average. For instance, 4 of 5 standards of gaseous effluent (other than equivalent dose of radioactive iodine, tritium, and carbon 14) is based on external exposure by noble gases. Effective dose for gaseous effluent of intake scenario is not considered. Otherwise, most of other nations are using relatively simple dose constraint by integrating effective dose of the gaseous and liquid effluents as shown Table 2. Therefore, this study aims to the validation of the technical base of the current dose constraint of Korea and the US. Also, this study suggests the re-calculated dose constraint based on the gaseous effluent data of Korea NPPs from 2009 to 2019.

Table 2. Dose Constraints of other nations (mSv/y)

	IAEA	UK	GER	JPN	FIN
Facility	0.3	0.3	0.3	0.05	0.1
Site	-	0.5	-	-	-

2. Methodology

2.1 Bases of 10 CFR 50 Appendix I.

This study reviewed the technical bases of 10 CFR 50 Appendix I in the document USNRC Docket RM-50-2 (1974) [3] written about the initial concluding statement of 10 CFR 50 Appendix I. According to the report, the initial design objectives were that annual total body dose to the individual living near the boundary of a site from radioactive material released in either liquid or gaseous effluent from all reactors at the site will generally be less than 5 percent of average doses from natural radiation background which was in the range of 100 ~125 mrem/y in US at that time. Thus, the initial dose constraint for either gaseous or liquid effluent was about 5 ~6.5 mrem/y. Then, external dose from gaseous effluent was separated into total-body dose from gamma radiation and skin dose from beta radiation. The annual total body dose constraint remained in 5mrem and annual dose to the skin increased to 15mrem which was the 1/2 of 1% of the radiation dose limits for a member of the public recommended by ICRP-9, 3rem. The annual gamma and beta air dose were limited to 10 mrad/y and 20 mrad/y to keep the annual dose not to exceed 5 mrem to the total body or 15 mrems to the skin. In the case of radioactive iodine, H-3, C-14 and other particulates, the initial design objective was to limit the annual radioactivity of I-131 not more than 1 Ci (37 Bq) and annual dose to any organs under 15 mrem.

Likewise, the current dose constraint of 10 CFR 50 Appendix I adjusted the average annual total dose of individual in US of 1960s and the does limit of ICRP-9 (1966) in decision making process. Also the dosimetry concept of 10 CFR 50 Appendix I has remained ICRP-2 since initial

concluding statement.

Now, dose constraints of radioactive effluent in Korea has been calculated based on ICRP-60 dosimetry concept but regulated by dose constraints based on ICRP-2 concept and 1960~1970s technical base of US.

2.2 Methodology

The methodology to re-calculate the dose constraint is shown in Figure 1 as a flowchart.

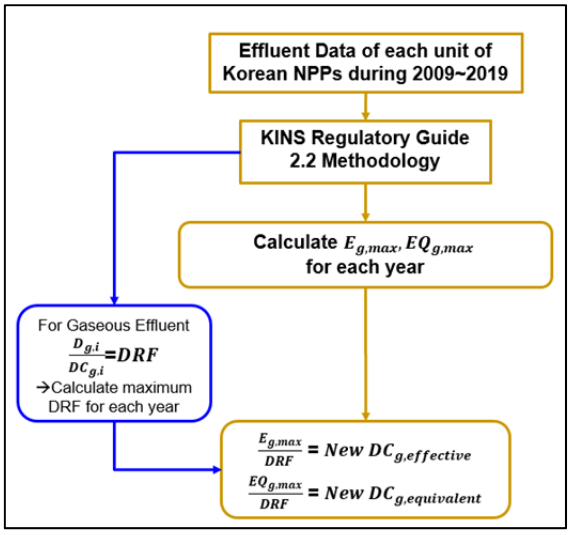


Fig. 1. Flow chart of the process to re-calculate the dose constraints based on the gaseous effluent data from 2009 to 2019.

The input data is the gaseous effluent data of each unit of Korean NPPs from 2009 to 2019 [4]. By using KINS Regulatory Guide 2.2 methodology based on USNRC Regulatory Guide 1.109 Rev.1 and IAEA Safety Standards No. 115 [5]. $D_{g,i}$ is the calculated dose based on current regulatory standard by using the methodology. Subscript i means each exposure dose type shown in the column 3 in Table 1. $DC_{g,i}$ is the current dose constraint of each type of exposure by gaseous effluent and DRF is 'dose ratio factor' which is $D_{g,i}$ divided by $DC_{g,i}$. The verification of the calculation was conducted by comparing the results of "The Annual Report on the Environmental Radiological Surveillance and Assessment around the Nuclear Facilities" written by KINS [6]. At the same time, the KINS 2.2 Methodology also calculates $E_{g,max}$, the maximum effective dose among the six groups of each year for gaseous effluent, and $EQ_{g,max}$, the maximum equivalent dose among the age groups of each year for gaseous effluent. For each year, divide $E_{g,max}$ by maximum DRF of each year to obtain the range of proper level of effective dose as the dose constraint for gaseous effluent ($New\ DC_{g,effective}$). And the same calculation for $EQ_{g,max}$ to obtain the proper level of equivalent dose as the dose constraint for gaseous effluent ($New\ DC_{g,equivalent}$).

3. Conclusion

The dose constraints of radioactive gaseous effluent in Korea has been using the numerical values of 10 CFR 50 Appendix I which was based on 1970s data and decision-making process. Also, current system is more complex than international trend due to calculate 5 types of exposure by gaseous effluent. 4 of 5 types are based on external exposure by noble gases. To evaluate the validation of current dose constraint, this study suggested the methodology to calculate proper level of effective dose and maximum equivalent dose as the dose constraint for gaseous effluent.

Acknowledgement

This work was supported by the Nuclear Safety Research Program through the Korea Foundation of Nuclear Safety (KOFONS), granted financial from the Nuclear Safety and Security Commission (NSSC), Republic of Korea (No.2003017).

REFERENCES

[1] The Nuclear Safety Security Commission, Standards for Radiation Protection, etc, NSSC Notice No.2019-10, (2019).

[2] USGPO, Domestic Licensing Production and Utilization Facilities, 10 CFR 50.

[3] USNRC, Docket RM-50-2 "Guides on Design Objectives for Light-Water Cooled Nuclear Power Reactors" (1974).

[4] KHNP, Environmental radiation survey and evaluation report around nuclear power plants, (2009~2019).

[5] KINS, Offsite Dose Calculation Manual, KINS/RG-N02.02, (2016).

[6] KINS, The Annual Report on the Environmental Radiological Surveillance and Assessment around the Nuclear Facilities, (2012~2019).

Preliminary Safety Assessment of Incineration of Decommissioning Waste for Clearance

Ji Hoon Han and Jae Hak Cheong*
Dept. of Nuclear Engineering, Kyung Hee Univ., 1732 Deokyoung-daero, Giheung-gu, Yongin-si, Gyeonggi-do
*jhcheong@khu.ac.kr

1. Introduction

Corresponding to the decommissioning of NPP, it is estimated to be generated the bulk amount of decommissioning waste. Since most of the decommissioning wastes would be classified as for clearance, they can be disposed of by means of landfill, incineration, and recycling by the Article 107 of Enforcement Decree of the Nuclear Safety Act. In the case of KINS/RR-144 report, it derived the radioactivity concentration for clearance by combining a generic approach and a specific approach. However, there are limitations that the assessment was only for the wastes generated from NPP on the operation and limited the subject of off-site incineration as the oil of which contaminated by H-3 and C-14.

Therefore, this study proceeded with the preliminary safety assessment for the incin-eration of decommissioning waste for clearance with the reflection of the characteristics of decommissioning waste.

2. Methodology

2.1 Selection of Radionuclides

From the decommissioning of research reactors, Co-60 and Cs-137 were detected as major nuclides in the combustible decom-missioning waste for clearance. Thus, including H-3, C-14 which considered in the KINS/RR-144 report, H-3, C-14, Co-60, and Cs-137 are selected as the major nuclides for the safety assessment.

2.2 Selection of Scenarios

The following three scenarios were chosen as the major scenarios that could be exposed most to the contaminated materials by incineration.

- A Worker on an incineration facility handling incineration ash
- A Resident near an incineration facility
- A Worker on a landfill facility

Each scenario has adopted applicable path-ways among external, inhalation, and ingestion.

Table 1. Considered Scenarios and Pathways

Scenarios	Pathway	Description
Incineration Facility Worker (WI)	EXT	External exposure on ash
	INH	Inhalation of resuspended dust
	ING	Inadvertent ingestion of dust
Resident Near Incineration Facility (RI)	INH	Inhalation of contaminated -airborne materials
	ING	Ingestion of contaminated -foodstuffs
Landfill Worker (WL)	EXT	External exposure on landfill
	INH	Inhalation on landfill
	ING	Inadvertent ingestion of dust

2.3 Assessment Models

- Mathematical Model

Since there is no particular calculation model for incineration workers, the mathematical model is applied on the basis of IAEA Safety Reports Series No. 44 (SRS-44) which used to derive the clearance levels.

$$D_{EXT,i} = C_i e_{EXT,i} f_d f_c t_e e^{-\lambda t_1} DF \quad (1)$$

$$D_{INH,i} = C_i e_{INH,i} f_d f_c t_e C_{dust} V e^{-\lambda t_1} DF \quad (2)$$

$$D_{ING,i} = C_i e_{ING,i} f_d f_c q e^{-\lambda t_1} DF \quad (3)$$

C_i : Activity concentration of nuclide i [Bq/g]
$e_{EXT,i}$: Dose coefficients of nuclide i for external exposure [(μSv/y)/(Bq/g)]
$e_{INH,i}$: Dose coefficients of nuclide i for inhal-ation [μSv/Bq]
$e_{ING,i}$: Dose coefficients of nuclide i for ingestion [μSv/Bq]
f_d : Dilution factor [-]
f_c : Concentration factor [-]
t_e : Exposure time [h/y]
C_{dust} : Dust concentration [g/cm^3]
q : The quantity ingested per year [g/a]
V : Breathing rate [m^3/h]
λ : Decay constant [1/y]
t_1 : Decay time before the start of the scenario [y]
DF : Decay factor during the scenario [-]

- Regulatory Guide 1.109 Model

Regulatory guide 1.109 model is a calculation model of annual doses to a person from effluents of NPP for the purpose of evaluating compliance with 10 CFR Part 50 Appendix I.

- RESRAD Model

RESRAD-Onsite 7.2 is a computer code designed at Argonne National Laboratory for estimating radiation doses to an individual located on top of contaminated soil.

2.4 Input Parameters

Referring to the decommissioning report of Maine Yankee NPP, the amount of decommissioning waste for incineration is set to 1,000 tons and they assumed to be incinerated in one facility. The radioactivity concentration is set to 1 Bq/g. Applied parameters were chosen conservative values and major input parameters are shown in table 2.

Table 2. Major Input Parameters Applied in the Scenarios

	WI	RI	WL
Receptor	Adult (Worker)	Adult (Public)	Adult (Worker)
Dose Coefficients	SRS-44 ICRP-72	ICRP-72	ICRP-72
f_d	1	1	0.1
f_c	H, C : 0.1 Co, Cs : 10	H, C : 1 Co, Cs : 0.1	H, C : 0.1 Co, Cs : 10
t_e	SRS-44	-	SRS-44
V	KINS/RG-N02.02	KINS/RG-N02.02	KINS/RG-N02.02
C_{dust}	SRS-44	-	RESRAD
q	EPA*	KINS/RG-N02.02	EPA*
λ	ICRP-107	ICRP-107	ICRP-107
t_1	SRS-44	KINS/RG-N02.02	-
X/Q	-	KINS/RR-144	-
etc.	-	KINS/RG-N02.02	RESRAD

*EPA, “Exposure Factors Handbook” (2017)

3. Calculation Results

The clearance levels derived by the dose calculation results of each scenario are shown in table 3. A near logarithmic rounding approach was also applied to derive the clearance levels.

Table 3. Clearance Levels of Each Scenario

	WI	RI	WL	CL*
H-3	10000	100	100000	100
C-14	1000	1	10000	1
C-60	0.1	0.1	0.1	0.1
Cs-137	0.1	1	1	0.1

* Clearance levels in NSSC Notice No. 2020-6 attached table 1

4. Conclusion

It is found that the current clearance levels are valid to the incineration scenarios. The nuclides that have the most impact are H-3 and Co-60 and they have a risk to over 10 μSv/y. Although the derived clearance level is the same as the current regulatory status, the risk can be handled in the perspective of ALARA like limiting the quantities for incineration or increase the number of workers, etc.

Because there was not much data about the quantities and about the work data for incineration of decommissioning wastes for clearance, the assumptions that applied in this study are conservative to handle uncertainty caused by insufficient data. Therefore, there needs to carry out in-depth studies about the radioactivity partitioning in incineration ash, working parameters, and decommissioning waste data management to reduce its uncertainties of safety assessment.

ACKNOWLEDGEMENT

This work has supported by the Nuclear Safety Research Program through the Korea Foundation Of Nuclear Safety (KoFONS) using the financial resource granted by the Nuclear Safety and Security Commission (NSSC) of the Republic of Korea (No. 1605008).

REFERENCES

[1] Korea Institute of Nuclear Safety, “Development of Regulatory Requirements for Clearance of Radioactive Waste”, KINS/RR-144 (2002).

[2] International Atomic Energy Agency, “Derivation of Activity Concentration Values for Exclusion, Exemption and Clearance”, Safety Reports Series No. 44 (2005).

Comparative Analysis of HH-XRF Spectra for UO_2 Using Monte Carlo Simulation

Jaeyeong Jang and Woojin Kim*
Korea Institute of Nuclear Nonproliferation and Control, 1418, Yuseong-daero, Yuseong-gu, Daejeon, 34101, Republic of Korea
*kimwj@kinac.re.kr

1. Introduction

Handheld X-ray Fluorescence (HH-XRF) analysis is a technology that is able to be applied to the forensics of unidentified nuclear materials [1]. For this, measurement data on several nuclear materials is required in advance. However, since nuclear material is strictly managed, it is often difficult to obtain measurement data. Therefore, a methodology that obtains a measurement data for nuclear material using Monte Carlo simulation was suggested.

In this study, experiment and simulation on UO_2 pellets were performed as a preliminary study for this methodology. Comparative analysis was conducted on the energy spectra obtained from the experiment and MCNP6 simulation.

2. Material and Method

2.1 HH-XRF measurement for UO_2 pellet

The experiment was performed using Bruker S1 titan 600 HH-XRF, and a UO_2 pellet having a density of 10.53 g/cm^3 was measured. The specifications HH-XRF and experimental setup was shown in Table 1 [2].

Table 1. Specification of HH-XRF and experimental setup [2].

	Category	Value
X-ray tube	Target	Rh (ρ = 12.41 g/cm^3, thickness = 0.65 μm)
	Window	Be (ρ = 1.85 g/cm^3, thickness = 125 μm)
	Collimator	Al alloy + Cu alloy
Detector	Detector type	Silicon Drift Detector
	Detector depletion depth	500 μm
	Detector active area	20 mm^2
	Detector shield	Fe alloy
Experimental setup	Sample type	UO_2 (ρ = 10.53 g/cm^3)
	Accelerating voltage	50 kV
	Current	9.85 μA
	Measurement time	60 sec



Fig. 1. Instruments for experimental measurements: Bruker S1-Titan 600 HH-XRF, desktop kit, and UO_2 pellet.

2.2 MCNP6 simulation

The principle of HH-XRF analysis is to measure the secondary X-ray generated by irradiating the primary X-ray to the sample with a detector. Therefore, first, the primary X-ray was simulated using the MCNP6 code. As shown in Figure 2, a primary X-ray was generated by transporting electrons of 50 keV by an accelerating voltage to a 0.65 μm of Rh target. The calculated energy distribution of primary X-ray was applied as a source term to the reconstructed HH-XRF as shown in Fig. 3. The energy spectrum of the secondary X-ray incident on the silicon drift detector (SDD) was calculated using the F8 tally and GEB (Gaussian Energy Broadening) option, correcting the energy broadening in physical radiation detector.

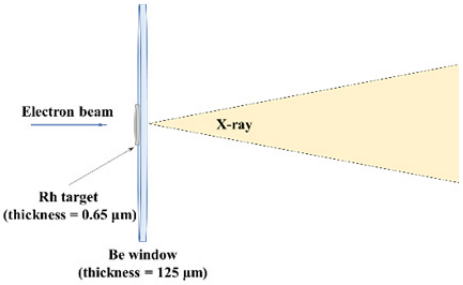


Fig. 2. Geometry for the production and emission of the X-ray in MCNP6 simulation.

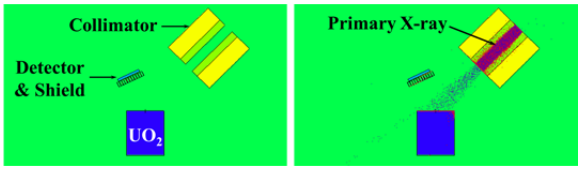


Fig. 3. Cross-sectional view of the MCNP6 geometry model of the HH-XRF and UO_2 pellet.

3. Results and Discussion

Figure 4 shows the energy spectra of the UO_2 pellet sample using HH-XRF. Here, U-Lα_1 and U-Lα_2 lines (13.6, 13.4 keV) and U-Lβ_1 and U-Lβ_2 lines (17.2, 16.4 keV) by fluorescent X-rays were mainly produced. In addition, the peaks at 3.1 and 3.3 keV were determined as M lines of U. In the energy range of 0 to 10 keV, noise peaks occurred due to materials constituting HH-XRF components. Since the intensity of noise peaks was even lower than that of U fluorescent X-rays, it is determined that there is little effect on the detection of U.

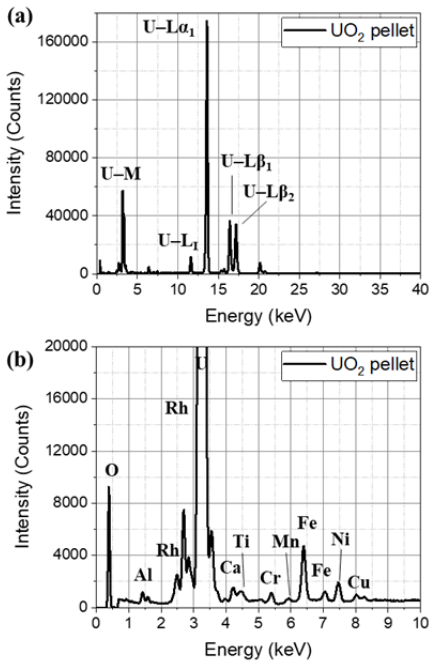


Fig. 4. Measured energy spectra from the UO_2 sample in the (a) whole energy region, (b) low energy region.

Figure 5 shows the energy spectrum of the primary X-ray calculated by MCNP6. Based on the direction of incidence of electrons, it was averaged over a range of 180°. The main peaks of the spectrum were the characteristic peaks of Rh target, Kα_1 (20.2 keV), Kβ_1 (22.7 keV) and Lα_1 (2.7 keV), Lβ_1 (2.8 keV), etc.

Figure 6 shows the energy spectra obtained through experiments and MCNP6 simulation. The spectrum of MCNP6 was normalized based on the total counts of experiment. It is shown that most of the characteristic peaks were consistent. In order to quantitatively analyze the similarity of the spectrum calculated by the simulation, the coefficient of determination (R^2) between the spectra was calculated and was 0.91.

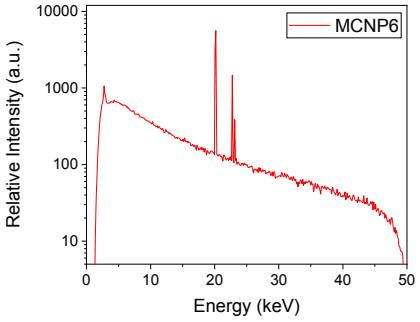


Fig. 5. Energy spectrum of primary X-ray through MCNP6 simulation.

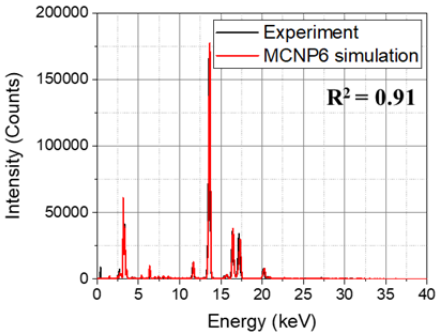


Fig. 6. Measured and MCNP6 simulation energy spectra for the UO_2 pellet sample.

4. Conclusion

The experiment for the nuclear material, UO_2 pellet, using HH-XRF was simulated using the MCNP6, and energy spectrum similar to the actual experimental results was obtained. Based on the result, measurement data on nuclear materials that cannot be used for experiments can be obtained. In the future, a data library of necessary nuclear materials will be constructed and applied to nuclear forensic studies using HH-XRF.

Acknowledgement

This work was supported by the Nuclear Safety Research Program through the Korea Foundation of Nuclear Safety (KOFONS) and the Nuclear Safety and Security Commission (NSSC) of the Republic of Korea (Grant No. 1804026).

REFERENCES

[1] Moody, K., Grant, P., Hutcheon, I., Nuclear Forensic Analysis, Boca Raton: CRC Press, 2015.

[2] Bruker Corporation, S1 TITAN User Guide, November 2015.

Evaluation of Radiological Hazard Parameter of Domestic Building Raw Materials

Myeogn-Hoon Joo*, Dae-Hyeon Kim, Eun-Ji Park, Seok-Hwan Han, and Sung-Gyu Leem
Hanil Nuclear. Co., Ltd., 3F, 45, Deokcheon-ro, Manan-gu, Anyang-si, Gyeonggi-do, Republic of Korea
*jooz81@hanilnuclear.co.kr

1. Introduction

Naturally Occurring Radioactive Materials (NORM) exist in all construction materials collected from nature, and as these are used as raw materials for apartments, humanity is being constantly exposed to natural radiation. In the World, the amount of exposure from nature is generally known as 2.4 mSv for one year, but the annual exposure by nature is known to be more than that due to the use of granite in the uranium belt area, industrialization, and technological development etc. It is continuously exposed to low doses from nature, but the radioactive risk is always latent, and it is not known from which point the damage caused by the exposure will occur.

Currently, apartments are over 80% of the total number of houses in Korea, and most construction materials are obtained from these natural materials. Building materials are managed by applying the radioactivity level index (EU RP112) in Korea. To measure natural radionuclides, uranium decay series ^{226}Ra, thorium decay series ^{232}Th, and ^{40}K were analyzed using a high-purity germanium gamma spectroscopy analyzer (HPGe). The radioactivity level index, radium equivalent radiation, external exposure index, internal exposure index, absorbed dose, and annual effective dose can be calculated from the analyzed radioactivity concentration of the radionuclides (Radiological Hazard Parameter). Studies on the radioactive hazards of such building raw materials are continuing abroad. In Korea, many studies are being conducted at the Korea Atomic Energy Research Institute and other research organizations and school institutions. Gamma spectroscopy analysis was performed on the sand, aggregate, cement, concrete, brick, tile, and paint materials used as building raw materials, and radioactive hazard parameter values were calculated based on the measured radioactivity values.

This study used building raw materials used in the construction of apartments from 2018 to 2019 as samples. Also, about 10,000 sample samples (Bulk) from 23 countries in Europe were compared with the standards suggested by the UNSCEAR.

2. Material & Method

As the measurement sample, the original sample was grinded/dried, and a sample obtained using a 200 um standard sieve was used as the final measurement sample. After sealing the measuring container, maintaining the equilibrium for about 4 weeks, and then measured using 30% HPGe (BSI, Canberra).

2.1 Radioactivity concentration determination

$$C = \frac{N}{P\varepsilon tf} \ (^{226}\text{Ra}(^{214}\text{Pb}), \ ^{232}\text{Th}(^{228}\text{Ac}), \ ^{40}\text{K}) \quad (1)$$

The radioactivity value was determined according to ISO 18589-3:2012.

2.2 Radium equivalent radioactivity

$$R_{eq} = C(^{226}Ra) + 1.43 * C(^{232}Th) + 0.077(^{40}K) \quad (2)$$

For the evaluation of radium equivalent radioactivity (^{226}Ra, ^{232}Th, ^{40}K), the radioactivity of 1 Bq/kg, 0.7 Bq/kg, and 13 Bq/kg, respectively, were used as the same gamma-dose. The equilibrium radium radiation from dry materials should be less than 370 Bq/kg and the external dose should be 1.5 mSv/y (UNSCEAR 2000).

2.3 Radioactivity index (RP112)

$$I_r = \frac{C_{Ra}}{300} + \frac{C_{Th}}{200} + \frac{C_K}{3{,}000} \leq 1 \quad \text{(bulk)} \quad (3)$$

$$I_r = \frac{C_{Ra}}{700} + \frac{C_{Th}}{500} + \frac{C_K}{8{,}000} \leq 1 \quad \text{(intermediate)} \quad (4)$$

$$I_r = \frac{C_{Ra}}{1{,}700} + \frac{C_{Th}}{1{,}200} + \frac{C_K}{20{,}000} \leq 1 \quad \text{(superficial)} \quad (5)$$

(Bulk / Intermediate / superficial raw material)

2.4 External exposure index

$$H_{ex} = \frac{C_{Ra}}{370} + \frac{C_{Th}}{259} + \frac{C_K}{4810} \leq 1 \quad (6)$$

2.5 Internal exposure index

$$H_{in} = \frac{C_{Ra}}{185} + \frac{C_{Th}}{259} + \frac{C_K}{4{,}810} \leq 1 \quad (7)$$

2.6 Determination of absorbed dose

$$D\left(\frac{nGy}{h}\right) = 0.462 * C_{Ra} + 0.604 * C_{Th} + 0.0417 * C_K \quad (8)$$

The absorbed dose rate in the air is due to the emission of gamma rays from each representative natural radionuclide emitted from the building's raw materials and was calculated as nGy/h. Also, the absorbed dose is 55 nGy/h in a room simulation, 4 m × 5 m × 2.8 m concrete building. (UNSCEAR 2000).

2.7 Determination of annual effective dose

$$D_{eff}\left(\frac{mSv}{y}\right) = D\left(\frac{nGy}{y}\right) \times \left(\frac{0.7Sv}{Gy} \times \frac{8{,}760h}{y} \times 0.8\right) \times 10^{-6} \quad (9)$$

The dose conversion factor was applied as 0.7 Sv/Gy and the indoor occupancy factor was 0.8 (UNSCEAR 2000) and was based on the indoor annual effective dose of 0.39 mSv/y (ICRP 1990).

Table 2. Building raw materials value

LIST	n	R_{aq}	I_r	H_{ex}	H_{in}	D	D_{eff}
[1)]Sand	24	230.59	0.87	0.65	0.73	108.79	0.53
[2)]Aggregate	124	201.23	0.75	0.57	0.65	94.79	0.47
Cement	39	150.38	0.54	0.44	0.57	69.44	0.34
Concrete	26	162.66	0.61	0.46	0.54	76.96	0.38
Tile	2	197.68	0.12	0.58	0.71	92.48	0.45
Brick	7	154.65	0.23	0.44	0.53	72.82	0.36
Paint raw material	7	116.38	0.07	0.35	0.45	54.68	0.27
[3)]Europe member states, 23	10k	121.81	0.45	0.35	0.43	57.31	0.28
UNSCEAR 2008	-	370	≦1	≦1	≦1	84	0.48

*series,
1) not mineral sand (without Zirconium sand, Bauxite, Ilmenite, Rutile).
2) Crushed Aggregate (< 5 mm), Coarse Aggregate (10-25 mm).
3) ^{226}Ra, ^{232}Th and ^{40}K activity concentrations in European brick, concrete, cement, natural gypsum: comparison with the European soil. Average values and ranges, UNSCEAR 2000.

3. Results

Table 1. shows the comparison with the average (10,000 samples) of building materials in 23 European countries. In this study, sand, aggregate, and tile in the effective dose category in Table 1. exceeded the recommendations of the UNSCEAR, and only sand exceeded the effective dose standard in the annual effective dose. In terms of annual effective dose, 7,000 hours were used in domestic studies, but (in this study) 8,760 hours were applied by the UNSCEAR. (8,766 hour/year, ICRP 1990).

4. Conclusion

Among building raw materials, radioactivity of uranium, thorium, and potassium of sand, aggregate, cement, concrete, tile, brick, and paint stocks worn from 2018-2019 was measured. When comparing the average factor values of each of the 23 European countries, except for absorbed dose and annual effective dose, all other factors were mostly lower than the recommendations of the UNSCEAR. When compared for each individual sample, there were some construction materials with high values, but in terms of average values, it was found that most of them were below the recommended value. Since some items have a small number of samples, we intend to monitor the radiation of building raw materials used in domestic apartments by collecting more data in the future.

Hanil Nuclear Co., Ltd. maintains the KS Q ISO/IEC 17025 QC system, and is recognized for its analysis method using international test methods such as ISO, IEC, EPA, ASTM, and national notices, and publishes the international certification report in the field of radioactivity measurement. We are conducting radioactivity measurement of construction materials and general industrial raw materials requested by domestic industries.

REFERENCES

[1] Characterization of the natural radionuclides in various industrial products and a study on safety management, KAERI/RR-4043/2015.
[2] J.H. Al-Zahrani, Estimation of natural radioactivity in local and imported polished granite used as building materials in Saudi Arabia, Journal of Radiation Research and Applied Sciences 10 (2017) 241-245.
[3] UNSCEAR, United Nations, & Scientific committee on the effects of atomic radiation (2000), Sources and effects of ionizing radiation: Sources(Vol.1). United Nations Publications.
[4] UNSCEAR, United Nations, & Scientific committee on the effects of atomic radiation (2008), Report of the united nations scientific committee on the effects of atomic radiation: Fifty-sixth session. United Nations Publications (10-18 July 2008) (No.46).
[5] EC, 1999b. Radiological Protection Principles Concerning the Natural Radioactivity of Building Materials. Radiation Protection 112. European Commission, Brussels.

Analysis of DCGL Derivation Cases at License Termination

Gang Woo Ryu, Se Jong Lee, Min Seong Kim, Hyeok Jae Kim, and Kwang Pyo Kim*
Kyung Hee University, 1732 Deokyoungdaero, Giheung-gu, Yongin-si, Gyeonggi-do, 17104, Korea
*kpkim@khu.ac.kr

1. Introduction

Kori Unit 1 was permanently shut down in 2017, and about 10 units including Wolsung Unit 1 are expected to be permanently shut down by 2030. In Korea, Final Decommissioning Plan (FDP) must be submitted to NSSC (Nuclear Safety and Security Commission) for decommissioning. Table 2 of the NSSC Notice No.2020-8 states that Derived Concentration Guideline Level (DCGL) should be evaluated and reported in FDP.

There is insufficient experience in decommissioning of nuclear facilities in Korea. Therefore, it is necessary to review foreign cases for the decommission. Relatively many decommissions of nuclear facilities have been performed in the US. The DCGL derivation cases were reported in License Termination Plan (LTP) in the US. The objective of this study was to analyze DCGL derivation cases at license termination in the US.

2. Materials and Methods

In this study, we focused on the case of decommissioning in the US, which has a lot of experience in decommissioning. The cases at Yankee Rowe, Connecticut Yankee, SONGS 1, and Rancho Seco nuclear power plants were analyzed. Analyses were performed focusing on the dose criteria, scenarios, calculation codes, and radionuclides for the DCGL derivation.

3. Results

3.1 Yankee Rowe

Yankee Rowe nuclear power plant applied 0.1 mSv/y as a dose criterion when deriving DCGL. DCGL was derived by applying 0.25 mSv/y to the initial LTP, but in the final step, DCGL was derived by applying 0.1 mSv/y, which is the criterion of the Massachusetts Department of Public Health (MDPH).

DCGLs was derived for soil and building. When deriving the soil DCGL, resident farmer scenario was used, and RESRAD-ONSITE was used. When deriving the building DCGL, it was derived for the building expected to remain after decommissioning. Building occupancy scenario was used. The RESRAD-BUILD was used for the DCGL derivation.

A total of 22 radionuclides were concerned including H-3, C-14, Co-60, Sb-125, Cs-137, and Pu-238.

3.2 Connecticut Yankee

Connecticut Yankee nuclear power plant applied 0.19 mSv/y as a dose criterion when deriving DCGL. The dose limit in the State of Connecticut is 0.19 mSv/y.

The DCGL was derived for soil and building. When deriving the soil DCGL, resident farmer scenario was used, and RESRAD-ONSITE was used. When deriving the building DCGL, building occupancy scenario was used.

A total of 20 radionuclides were concerned including H-3, C-14, Mn-54, Co-60, Cs-137, and Pu-238.

3.3 SONGS 1

SONGS nuclear power plant site has three units including SONGS 1, 2, 3. The licenses for all three units refer to a common plant site. License of SONGS 1 will not be terminated until Units 2 and 3 are decommissioned. Therefore, Final status survey will be conducted after decommissioning of all of the plants. At the present time, all of the units in SONGS site are expected to release in 2042, and accordingly, the final regulatory limits are not clearly known.

Therefore, SONGS 1 used Screening DCGL given in NUREG-1757. Conservatively established a nominal limit is 10% of DCGL.

A total of 15 radionuclides were concerned including H-3, C-14, Mn-54, Co-60, I-129, Cs-137, and Pu-238.

3.4 Rancho Seco

Rancho Seco nuclear power plant decided to reuse the building without completely dismantling them. The purpose was not to release the site unrestricted, but to restricted. Rancho seco nuclear power plant applied 0.25 mSv/y as a dose criterion when deriving DCGL.

DCGL was derived for soil and building. When deriving the soil DCGL, industrial worker scenario was used, and RESRAD-ONSITE was used. Resident farmer scenario was concerned but

total dose exceeds 0.25 mSv/y for approximately 30 years following license termination. When deriving the building DCGL, building occupancy, renovation/demolition, and industrial worker scenario were used.

C-14, Co-60, Ni-63, Sr-90, Cs-134, and Cs-137 were concerned for the soil, and 26 radionuclides including the above 6 were concerned for the building.

4. Conclusion

In this study, DCGL derivation cases in the US were analyzed. Dose criteria applied for the nuclear power plants were different one another. The dose criteria were set by the state and related agencies to which the power plant belongs were applied, in addition to the criteria given in 10 CFR 20 subpart E. In general, resident farmer scenario and RESRAD-ONSITE were used to derive soil DCGL, building occupancy scenario and RESRAD-BUILD were used to derive building DCGL. Radionuclides concerned were similar for each case except for some radionuclides. This study results are expected to be used as basic data when deriving domestic DCGL.

ACKNOWLEDGEMENTS

This work was supported through the KoFONS using the financial resource granted by NSSC (No.1805016).

REFERENCES

[1] NSSC Notice 2020-8, "Standard Format and Content of Decommissioning Plan for Nuclear Facilities", (2020).

[2] EPRI, "Final Status Survey and Site Release Experience Report", (2008).

Table 1. Comparison of dose criterion, calculation computer code, scenario, radionuclides for each nuclear power plant

	Yankee Rowe	Connecticut Yankee	SONGS 1	Rancho Seco
Dose criterion	0.1 mSv/y	0.19 mSv/y	0.25 mSv/y	0.25 mSv/y
Scenario	Resident farmer, Building occupancy	Resident farmer, Building occupancy	Resident farmer[a]	Industrial worker[b], Building occupancy, Building renovation
Computer code	RESRAD-ONSITE, BUILD	RESRAD-ONSITE, BUILD	DanD[a]	RESRAD-ONSITE, BUILD
Radionuclide	H-3, C-14, Fe-55, Co-60, Ni-63, Sr-90, Nb-94, Tc-99, Ag-108m, Sb-125, Cs-134, Cs-137, Eu-152, Eu-154, Eu-155, Pu-238, Pu-239/240, Pu-241, Am-241, Cm-243/244	H-3, C-14, Mn-54, Fe-55, Co-60, Ni-63, Sr-90, Nb-94, Tc-99, Ag-108m, Cs-134, Cs-137, Eu-152, Eu-154, Eu-155, Pu-238, Pu-239, Pu-241, Am-241, Cm-243	H-3, C-14, Mn-54, Fe-55, Co-60, Ni-63, Sr-90, Tc-99, I-129, Cs-137, Eu-152, Pu-238, Pu-239, Pu-241, Am-241,	H-3, C-14[c], Na-22, Fe-55, Ni-59, Co-60[c], Ni-63[c], Sr-90[c], Nb-94, Tc-99, Ag-108m, Sb-125, Cs-134[c], Cs-137[c], Pm-147, Eu-152, Eu-154, Eu-155, Np-237, Pu-238, Pu-239, Pu-240, Pu-241, Pu-232, Am-241, Cm-244

a DanD Code and resident farmer scenario were used to derive Screening DCGL
b Industrial worker scenario was used for both soil and building DCGL
c Radionuclides concerned soil DCGL derivation

Review of Radiation Dose Assessment for the Processed Products

Byung Min Lee[1], Jae Kwon[1], Jong Hyeok Park[1], Jung Hwan Jang[2], and Kwang Pyo Kim[1,*]
[1]Kyung Hee University, 1732 Deokyoungdaero, Giheung-gu, Yongin-si, Gyeonggi-do, 17104, Korea
[2]Korea Institute of Nuclear Safety, 62 Gwahak-ro, Yuseong-gu, Daejeon, 34142, Korea
*kpkim@khu.ac.kr

1. Introduction

Radioactive materials can be used for various purposes in many fields. With the development of technology, the number and types of processed product artificially containing radioactive nuclides are increasing. Recently, concerns about processed product containing radioactive nuclides have increased. Since processed products are closely related to the lives of the public, it is possible that consumers are exposed to processed products. Therefore, it is necessary to identify the radiation dose due to the processed products.

The objective of this study was to review the domestic and foreign radiation dose due to processed products. Dose assessment for processed products in domestic and foreign country were also reviewed.

2. Dose assessment for processed products

2.1 Korea

The Nuclear Safety and Security Commission (NSSC) conducted exposure dose assessment due to processed products in Korea. The NSSC conducted the dose assessment for about 100 products annually [1]. The NSSC categorized the processed products into body fit products, health supplement products, building materials and industrial processed products. Dose assessments were conducted in the order of surface radiation dose rate measurement, radionuclide analysis, and dose assessment using radiation transport codes. Table 1 shows dose assessment results according to processed product. The highest annual effective dose was about 928 μSv/yr for building materials. It was followed by body fit products (671 μSv/yr), industrial processed products (617 μSv/yr), and health supplement products (61 μSv/yr).

Table 1. Annual effective dose according to processed product group in Korea

Classification	Annual effective dose (μSv/yr)			
	2014	2015	2016	2017
Body fit products	15	< 1	30	671
Health supplement products	8	< 1	61	-
Building materials	152	85	928	83
Industrial processed products	1	617	272	-

2.2 US

The National Council on Radiation Protection and Measurements (NCRP) analyzed the radiation dose of American from various radiation sources in US. The NCRP No.160 presented the results of dose assessment for various radiation sources, including processed products in 2009 [2]. The NCRP categorized the processed products into cigarette, building materials, mining and agriculture, glass and ceramics, fossil fuel, and others sources. Dose assessment for processed products was analyzed based on data evaluated by various organizations related health physics. Table 2 shows dose assessment results according to processed product group analyzed by the NCRP. The highest annual effective dose was about 300 μSv/yr for cigarette. It was followed by Building materials (70 μSv/yr), and highway and road construction materials (40 μSv/yr).

Table 2. Annual effective dose according to processed product group in the US

Classification	Annual effective dose (μSv/yr)
Cigarette	300
Building materials	70
Mining and agriculture	10
Glass and ceramics	< 1
Fossil fuel	5
highway and road construction materials	40
Other sources	-

2.3 UK

In the 20th century, the National Radiological Protection Board (NRPB) had assessed exposure dose periodically in the UK. Since then, Health Protection Agency (HPA) and Public Health

England (PHE) have been conducting the research of radiation exposure dose. HPA presented the results of British exposure dose due to processed products containing radioactive materials in 2005 [3]. The HPA categorized processed products into Radioluminous item, smoke monitors, glass, glaze, geological specimens, and camera lenses. Dose assessment for processed products was analyzed based on data evaluated by various organizations including the NRPB. Table 3 shows dose assessment results according to processed product group analyzed by the HPA. The highest annual effective dose was about 200 - 300 μSv/yr for photographic lenses. It was followed by geological specimens (100 μSv/yr), and glass (50 μSv/yr).

Table 3. Annual effective dose due to processed products in the UK

Classification	Annual effective dose (μSv/yr)
Radioluminous item	11
Smoke alarm	< 1
Glass	50
glaze	< 1
Geological specimens	100
Photographic lenses	200 - 300

3. Conclusion

In this study, we reviewed the dose assessment for processed products in Korea, the US, and the UK. This study result can be used as basic data for radiation safety management.

ACKNOWLEDGMENTS

This work was supported through the KoFONS using the financial resource granted by NSSC (No. 1803013).

REFERENCES

[1] KINS, “Investigation and Analysis of Actual State of Safety Management for Radiation in the Natural Environment”, KINS/GR (2014-2017).
[2] NCRP, “Ionizing Radiation Exposure of the Population of the United States”, NCRP No.160 (2009).
[3] HPA, “Ionizing Radiation Exposure of the UK Population”, HPA-RPD-001 (2005).

Review of Studies Assessing Radiation Dose to Residents Due to the Radioactive Effluent From Nuclear Facilities

Hyun Jun Na[1], Min Young Lee[1], Hyeung Woo Nam[1], Jae Bin Heo[1], Jin Ho Park[2], and Kwang Pyo Kim[1,*]
[1]Kyung Hee University, 1732 Deokyoungdaero, Giheung-gu, Yongin-si, Gyeonggi-do, 17104, Korea
[2]Korea Institute of Nuclear Safety, 62 Gwahak-ro, Yuseong-gu, Daejeon, 34142, Korea
*kpkim@khu.ac.kr

1. Introduction

Artificial exposure results from radiation sources created unnaturally. In 2002, artificial exposure was about 19% of total exposure of the Korean population [1]. Artificial exposure is divided into medical exposure, occupational exposure, and exposure by other artificial sources such as radioactive effluent from nuclear facilities.

Nuclear facilities include nuclear power plants, radioactive waste disposal facility, and other nuclear facilities. Radiation dose to residents may occur by radioactive effluent from these nuclear facilities. Therefore, it is necessary to investigate radiation dose to residents due to the radioactive effluent from nuclear facilities in order to identify artificial exposure.

The objective of this study is to review studies assessing radiation dose to residents due to the radioactive effluent from nuclear facilities. Therefore, we investigated studies assessing radiation dose to residents due to the radioactive effluent from nuclear power plants, radioactive waste disposal facility, and other nuclear facilities.

2. Exposure dose assessment studies

2.1 Nuclear power plant

Domestic nuclear power plants include Kori, Hanbit, Hanul, and Wolsung. Korea Institute of Nuclear Safety (KINS) assessed the radiation dose to residents due to the radioactive effluent from these nuclear power plants in 2017 [2].

Dose assessment was conducted using the Integrated Dose Assessment Code Package for KINS (INDAC). INDAC is a program that has been modified to conform the GASDOS, LIQDOS program to ICRP 60 recommendations based on US Reg. Guide 1.10. Information such as radiation sources, atmospheric dispersion factor, and dilution water flow rate for the dose assessment was utilized. Information such as ingestion rate, respiration rate, and processing period was utilized by the default values of INDAC.

Table 1 shows the radiation dose to residents by nuclear power plants. The criteria for effective dose and radiation dose to the thyroid are 0.25 mSv/yr and 0.75 mSv/yr [3]. Effective doses ranged 3.74×10^{-2} to 6.80×10^{-2} mSv/yr. Radiation doses to the thyroid ranged 3.52×10^{-2} to 6.45×10^{-2} mSv/yr. Effective dose and radiation dose to the thyroid by nuclear power plants were less than the dose criteria.

Table 1. Radiation dose to residents by nuclear power plants

Site	Radiation dose (mSv/yr)	
	Effective dose	Radiation dose to the thyroid
Kori	5.95×10^{-2}	5.95×10^{-2}
Hanbit	3.74×10^{-2}	3.52×10^{-2}
Hanul	4.83×10^{-2}	4.54×10^{-2}
Wolsung	6.80×10^{-2}	6.45×10^{-2}

2.2 Radioactive waste disposal facility

Korea Radioactive Waste Agency (KORAD) assessed the radiation dose to residents due to the radioactive effluent from radioactive waste disposal facility in 2017 [4].

Dose assessment was conducted using Radiological Dose Calculation Program Package (RADCAP). RADCAP was developed by KORAD based on ICRP 60 in consideration of the environmental characteristics of medium and low-level radioactive waste disposal facility site. In order to assess atmospheric dispersion factor, KORAD measured meteorological data through onsite weather station. Atmospheric dispersion factor was assessed by XOQDOQ using the meteorological data.

Table 2 shows the radiation dose to residents due to the radioactive waste disposal facility. Effective dose and radiation dose to the thyroid were both 2.08×10^{-6} mSv/yr. Effective dose and radiation dose to the thyroid were less than the dose criteria.

Table 2. Radiation dose to residents by radioactive waste disposal facility

Category	Radiation dose to residents (mSv/yr)
Effective dose	2.08×10^{-6}
Radiation dose to the thyroid	2.08×10^{-6}

2.3 Other nuclear facility

Other nuclear facilities include research reactor, nuclear fuel processing plants, isotope waste incineration facilities, radioactive isotope waste management facility, and so on. Domestic other nuclear facilities are located in Daeduck site.

Korea Atomic Energy Research Institute (KAERI) assessed the exposure dose to residents due to the radioactive effluent from other nuclear facilities in 2017 [5]. KAERI calculated the total radiation dose to residents by other nuclear facilities in Daeduck site. Dose assessment was conducted using ENDOS program. ENDOS was developed by KAERI based on ICRP 60. In order to assess atmospheric dispersion factor, KAERI measured meteorological data through onsite weather station. Atmospheric dispersion factor was assessed by XOQDOQ using the meteorological data.

Table 3 shows the total radiation dose to residents by other nuclear facilities in Daeduck site. Effective dose and radiation dose to the thyroid were 8.78×10^{-4} mSv/yr and 1.20×10^{-2} mSv/yr. Effective dose and radiation dose to the thyroid were less than the dose criteria.

Table 3. Total radiation dose to residents by other nuclear facilities

Category	Radiation dose to residents (mSv/yr)
Effective dose	8.78×10^{-4}
Radiation dose to the thyroid	1.20×10^{-2}

3. Conclusion

In this study, we reviewed studies assessing radiation dose to residents due to the radioactive effluent from nuclear facilities. Radiation doses to residents were calculated using computer programs such as INDAC, RADCAP, and ENDOS. The radiation doses to residents due to the radioactive effluent from nuclear power plants, radioactive waste disposal facility, and other nuclear facilities were less than the dose criteria. The results of this study are expected to be used as basic data for researching artificial exposure of the population.

ACKNOWLEDGMENTS

This work was supported through the KoFONS using the financial resource granted by NSSC. (No. 1803013).

REFERENCES

[1] [1]KINS, “Radiation Environment in Korea”, KINS/GR-356 (2009).
[2] [1]KINS, “The Annual Report on the Environmental Radiological Surveillance and Assessment around the Nuclear Facilities”, KINS/AR-140 (2017).
[3] [1]NSSC Notice 2017-36, “Notice of Standards for Radiation Protection”, (2017).
[4] KORAD, “Around the Site of Medium and Low Level Radioactive Waste Disposal Facilities Radiation Environment Survey Report”, (2018).
[5] KAERI, “Environment Radiation Monitoring Around the Nuclear Facilities”, KAERI/RR-4329/2017 (2018).

Outdoor Air Control Unit With Heat Pipes System for Reducing Radioactive Liquid Waste

Youngwoo Kwon*, Seonho Noh, Heeseok Kang, Youngkuk Jang, and Ilje Cho
Korea Atomic Energy Research Institute, 989-111 Daedeok-daero, Yuseong-gu, Daejeon, 34057
*kyw@kaeri.re.kr

1. Introduction

The Korea Atomic Energy Research Institute operates the Nuclear Cycle Experimental Research Facility which has radiation controlled area in the laboratory with the aim of realizing pyroprocessing technology. During summer, the facility should maintain proper temperature and humidity to manage analysis and experiment equipment. However, about few tons of condensate are generated every year due to the air conditioner.

This paper is mentioned about reducing the amount of liquid radioactive waste by using OAC with Heat Pipe System.

2. OAC with Heat Pipe System

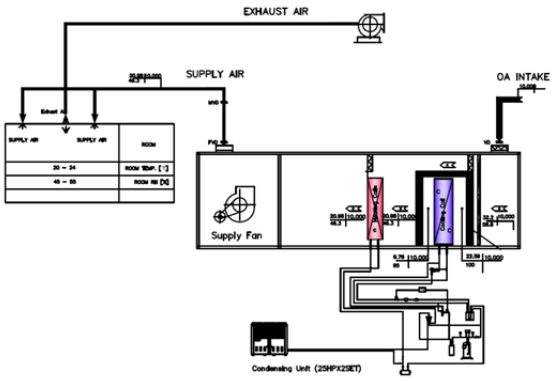


Fig. 1. OAC with Heat Pipes System.

OAC with Heat Pipe reduces load of cooling coil through pre-cooling. It makes the reheating load free to maintain proper relative humidity and temperature.

Briefly, the outdoor air is pre-cooled through heat exchanging in heat pipes. Then, the pre-cooling air passes through the cooling coil and becomes very humid and low temperature air. Lastly, the air passes through the heat pipes again before air supply. The air is reheated and gets the proper temperature and humidity. This system saves more energy due to higher energy absorption during the rainy season.

3. Simulation Results

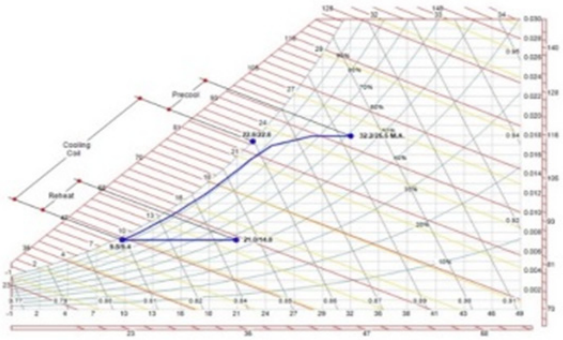


Fig. 2. Psychometric chart.

3.1 Equations

$$q_T = G\Delta h = q_S + q_L = GC_p\Delta t + G\Delta h = \gamma QC_p\Delta t + \gamma Q\Delta h \quad (1)$$

$$h = ha + xhv = cpt + x(r + cvt) \quad (2)$$

$$L = G(x_2 - x_1) = \gamma Q(x_2 - x_1) \quad (3)$$

The psychometric chart shows the results of a simulation based on the Nuclear Cycle Experimental Research Facility. The condition of outdoor air was based on the average temperature and humidity during the summer in Daejeon, and the air volume was assumed to be 10,000m^3/h. Total energy saving and condensate generation were calculated by using Psychometric Analysis.

As a result, a condensate of 122.5 kg/h will be collected. Fig.3 shows how much moisture can be removed from the laboratory per hour. Air temperature of supply will be 21 degrees Celsius and the relative humidity will be 46.3 percent. A total of 76,048W of energy can be saved by pre-cooling and re-heat processes.

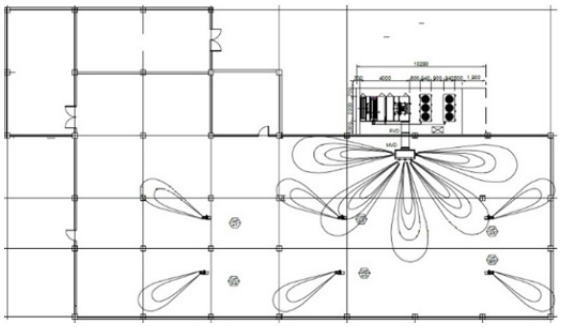


Fig. 3. Air Circulation Diagram.

The above picture is designed to achieve optimal effects by considering the conditions of the Nuclear Cycle Experimental Research Facility. The concept is designed by considering various factors such as air circulation, equipment placement plan, external air volume, optimal number of ventilation, damper system, and power supply.

Among the various above, the air circulation section is described in this paper. The direction of the OAC is transverse. When the external air is supplied in the diffuser fan, the air circulation goes from left to right. To make the air circulation smoothly in the facility, an air circulation fan should be installed so that air circulation can change the flow front to back or back to front using the longitude air circulation method.

4. Conclusion

According to the data, if OAC with Heat Pipe dehumidification system is applied to radiation controlled area, radioactive liquid waste can be dramatically reduced. Also, improves indoor air quality, increases dehumidifying capacity of air conditioning equipment. It is effective for sensitive equipment and space to be managed with proper humidity and temperature.

REFERENCES

[1] John Dieckmann, 2003, Dedicated Outdoor Air Systems, ASHRAE Journal, May 2003.

[2] ANL-7959 Hot Fuel Examination Facility /North Facility Safety Report, February 1975, Argonne National Laboratory pp. 42-53.

Comparison of Indoor Thermal Environment by Exhaustion in Spring and Summer

Heeseok Kang*, Youngwoo Kwon, Seonho Noh, Youngkuk Jang, and Ilje Cho
KAERI, 989-111 Daedeokdaero, Yuseong, Daejeon, 34057, Korea
*hskang1@kaeri.re.kr

1. Introduction

Although the operation of the test facility is organically connected in various fields, the thermal environment of the laboratory is a major factor affecting the health and efficiency of the workers in the laboratory, and it is recognized as an important item for both the operator and the operator of the facility. The operation of the test facility is organically connected to various fields such as air temperature and humidity, noise, and cleanliness. It is recognized as an important item for both operators and workers.

The thermal environment of the laboratory has the effect of raising the room temperature by combining the radiant heat of the facility due to sunlight and the heat generated from the indoor laboratory equipment. In the laboratory, ventilation through supply and exhaust air and room temperature control by various methods of cooling and heating are performed.

2. Exhaust System in Facility

2.1 Reinforced ventilation by additional exhaust fan

The nuclear cycle test center of the Korea Atomic Energy Research Institute(KAERI) is operating a total of six exhaust gases and laboratory ventilation, and one exhaust system for pure laboratory ventilation. The ventilation method corresponds to the third type of ventilation, and the interior is maintained at negative pressure by the exhaust fan, and air does not leak to the outside through gaps such as doors and windows, so there is no fear of external contamination by laboratory air. Fig. 1 shows a conceptual diagram of the exhaust and ventilation system of the nuclear cycle test laboratory. As shown in the figure, the exhaust gas generated from the various experimental devices on the first floor passes through the exhaust system on the third floor connected by an exhaust duct, and then passes through the filter bank to be discharged to the outside. Laboratory ventilation is designed to ventilate the laboratory by opening the end of the exhaust duct and passing through the exhaust system and then passing through the filter bank to the outside. Therefore, the six exhaust systems are operated to discharge exhaust gas from the experimental device and to ventilate the room. In addition, an additional exhaust system is being operated considering only laboratory ventilation. In the previous experiment of this paper, in order to examine the effect on the indoor thermal environment caused by the operation of an additional exhaust fan during the spring, the outside of the laboratory (T1) and the inside of the exhaust chamber (T2), and the third floor of the exhaust passage from the first floor to the third floor. Changes in temperature (T4, T5) in the space (T3) and the laboratory space on the first floor were observed.

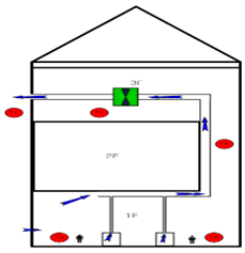
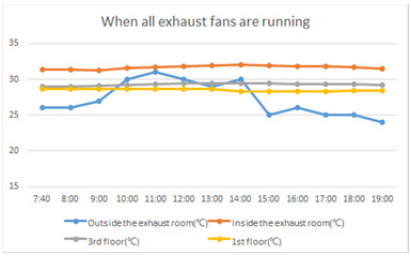


Fig. 1 Conceptual exhaust diagram in the laboratory.

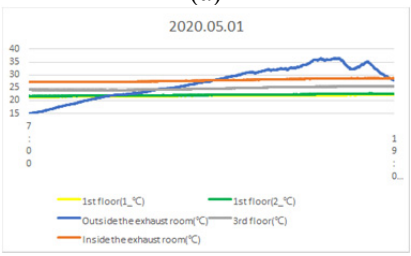
2.2 Comparison of indoor temperature by running exhaust fan in spring and summer

Previous Fig. 2(a) shows the temperature change inside and outside the laboratory when all 7 exhaust fans were operated during the spring season. Since the temperature sensor is adjacent to the building wall, it has been confirmed that it is affected by the radiant heat of the wall. The sudden drop in temperature after 2 pm was thought to be related to the radiant heat of the wall by sunlight. To compare the temperature of the spring season, the temperature change for a specific day from May to August is shown in Fig. It is shown in 2(b), (c), (d), (e). The external temperature in May and June was above 35°C in the evening, and the result was that the wall facing west was influenced by radiant heat from sunlight in summer. The outside temperature in July and August differs from that in May and June, which was seen as the influence of rainy weather. Even when the air conditioner is not operated in the

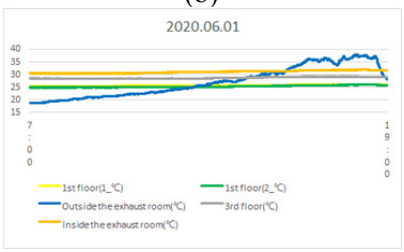
summer, the indoor temperature is steadily maintained without being significantly affected by the gradual increase in the external temperature (T1). This result could be said to be a single result indicating that the ventilation of the exhaust fan is well maintained.



(a)



(b)



(c)



(d)



(e)

Fig. 2 Comparison of indoor temperature by running exhaust fan in spring and summer; (a)Spring season, (b)in May, (c)Summer season (in June), (d)Summer season(in July), (e)Summer season(in August).

3. Conclusions

The conditions of the spring and summer seasons were compared with respect to the temperature of the laboratory with both exhaust and ventilation fans running. It was unreasonable to confirm the consistent trend due to the irregularities of the weather, but the following results were confirmed. It was confirmed that the indoor temperature was steadily maintained without being significantly affected by the gradual increase in the external temperature in both the spring and summer seasons with all exhaust fans running. In the future, it was necessary to obtain temperature observation data in more various weather conditions.

A New Approach to Determine Critical Distance Radius of Self Powered Neutron Detector by Using Least Square Fitted Charge Density

Hyuk Han* and ChangJe Park
Nuclear Engineering Dept., Sejong Univ., 209 Neungdong-ro, Gwangjin-gu, Seoul Korea 143-747
*hyuk2229@sju.ac.kr

1. Introduction

Self-powered neutron detector (SPND) is one of devices for in-core neutron fluxes detecting without external electricity source. SPND consists emitter, insulator and collector. When neutrons reacted with emitter material, it generates electrons and these electrons cross insulator area to make signal in collector area. For calculating sensitivity of SPND, space charge effect is one of important component. Because, MCNP code which for calculate sensitivity, cannot describe exact space charge effect. So, for calculation, appropriate assumptions are required. H. D. Warren suggest one of this calculation models with electric field for SPND [1][2]. In this paper, different calculation model from H. D. Warren's for electric field with charge density profile expressed in liner, quadratic and cubic form, is suggested and compared with H. D. Warren's result [3].

2. Theory

Space charge effect is that the potential limits the current by the charge present in the space. Usually, electrons are emitted in emitter material and negatively charged. However, as electrons continue to be released, the cathode becomes relatively polarized and pulls the electrons back together, blocking the movement of electrons to release them, forming a space charge around them to form a cloud-like electron cloud. When calculated electric field is zero, space charge cloud is there and that distance from emitter origin point is called critical distance. It is important in SPND, because electrons need to cross this space charge area to generate signals. In the H. D. Warren's paper, E(r) is suggested as next form.

$$E(r) = \frac{2A}{r_i}\left\{\frac{r}{r_i} - \left[\frac{1-k^2}{2\ln(1/k)}\right]\frac{r_i}{r}\right\} \quad (1)$$

When A is constant related with radiation intensity, r_i is outer radius of the insulator and k is r_e/r_i which r_e is emitter radius. With this equation, critical distance r_0 can derive as next form.

$$r_0 = r_i\left[\frac{1-k^2}{2\ln(1/k)}\right]^{1/2} \quad (2)$$

3. Equations

In the cylindrical symmetry, electric field E obeys Poisson equation [4].

$$\frac{\partial E}{\partial r} + \frac{E}{r} = \frac{\rho(r)}{\varepsilon} \quad (3)$$

Where r is arbitrary distance which unit is cm, $\rho(r)$ is the charge density profile and ε is material dielectric constant and unit is V/m.

$$\frac{\partial E}{\partial r} + \frac{E}{r} = \frac{\rho(r)}{\varepsilon} \rightarrow E' + \frac{E}{r} = \frac{\rho(r)}{\varepsilon} \quad (4)$$

For solving this equation, 1st linear non-homogeneous ordinary differential equation' solution is needed. Finally, electric field E(r) can be derived in boundary condition of insulator inner and outer radius.

$$E(r) = \frac{1}{r\varepsilon}\left(\int_{r_i}^{r}\rho(r)rdr - \frac{1}{\ln\left(\frac{r_o}{r_i}\right)}\int_{r_i}^{r_o}dr\frac{1}{r}\int_{r_i}^{r}\rho(r)rdr\right) \quad (5)$$

If $\rho(r)$ assumed as constant form, electric field E(r) can be expressed as next equation.

$$\rho(r) = a,$$
$$\int_{r_i}^{r}\rho(r)rdr = \left[\frac{1}{2}ar^2\right]_{r_i}^{r} = \left(\frac{1}{2}ar^2\right) - \left(\frac{1}{2}ar_i{}^2\right)$$
$$\int_{r_i}^{r_o}dr\frac{1}{r}\int_{r_i}^{r}\rho(r)rdr = \int_{r_i}^{r_o}\frac{1}{r}\left[\frac{1}{2}ar^2\right]_{r_i}^{r}dr$$
$$= \int_{r_i}^{r_o}\left(\frac{1}{2}ar\right)dr - \left(\frac{1}{2}ar_i{}^2\right)\times\int_{r_i}^{r_o}\frac{1}{r}dr$$
$$= \left[\frac{1}{4}ar^2\right]_{r_i}^{r_o} - \left(\frac{1}{2}ar_i{}^2\right)\times ln\left(\frac{r_o}{r_i}\right)$$
$$= \left(\frac{1}{4}ar_o{}^2\right) - \left(\frac{1}{4}ar_i{}^2\right) - \left(\frac{1}{2}ar_i{}^2\right)\times ln\left(\frac{r_o}{r_i}\right) \quad (6)$$

As result, next equation can be derived when charge density profile assumed as constant form.

$$E(r) = \frac{1}{r\varepsilon}\left(\left(\frac{1}{2}ar^2\right) - \frac{1}{\ln(r_o/r_i)}\left(\left(\frac{1}{4}ar_o{}^2\right) - \left(\frac{1}{4}ar_i{}^2\right)\right)\right) \quad (7)$$

And critical distance result can be expressed as next equation.

$$r_0 = \left[\frac{2\left(\left(\frac{1}{4}ar_o{}^2\right) - \left(\frac{1}{4}ar_i{}^2\right)\right)}{a \times ln(r_o/r_i)}\right]^{1/2} \quad (8)$$

When a=1, critical distance equation derived same as Warren's general critical distance equation.

$$r_0 = r_i\left[\frac{1-k^2}{2\ln(1/k)}\right]^{1/2}$$
$$* k = \frac{r_{emitter}}{r_{insulrator}} = \frac{r_{inner}}{r_{outer}} \quad (9)$$

4. Conclusion

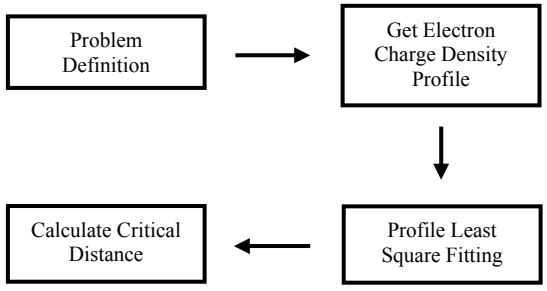


Fig. 1. Critical Distance Calculation Algorithm.

In this study, equations to calculate critical distance for SPND with charge density profile trend line and its results are suggested. Fig. 1 show whole algorithm of calculation. Result effectiveness were verified by compared with H. D. Warren's derivation results. In the future, charge density profile will be assumed as liner, cubic, quadratic form and critical distance calculation conducted.

Reference

[1] H. D. Warren, "Calculational Model for Self-Powered Neutron Detector" (1972).

[2] H. D. Warren and N. H. Shah, "Neutron and Gamma-Ray Effects on Self-Powered In-Core Radiation Detectors" (1974).

[3] Dekking, Michel, "A modern introduction to probability and statistics: understanding why and how" (2005).

[4] N. P. Goldstein, "A MONTE-CARLO Calculation of the Neutron Sensitivity of Self-Powered Detectors" (1973).

[5] Hyunsuk Lee and Deokjung Lee "New calculational model for self-powered neutron detector based on Monte Carlo simulation" (2014).

Preliminary Study on Neutron Shielding of Moderating Materials Using an SiPM-Based ^{4}He Detector System

Kyung Taek Lim, Sungmin Kim, Wonjong Song, and Heejun Chung*
Korea Institute of Nuclear Nonproliferation and Control (KINAC)
1418, Yuseong-daero, Yuseong-gu, Daejeon, 34101, Republic of Korea
*hjchung2@kinac.re.kr

1. Introduction

To verify the integrity of spent nuclear fuel assemblies in a dry cask via passive neutron tomography, a prototype safeguards apparatus equipped with ^{4}He gas scintillation detectors has been developed. In particular, the designed system acquires a cross-sectional image of the cask system by measuring fast and thermal neutrons emitted from the cask simultaneously.

In this work, we investigate the degree to which the ^{4}He scintillation detector can be utilized to evaluate the neutron attenuation of two moderating materials using a ^{252}Cf source.

2. Methodology

Fig. 1 depicts the experiment setup for neutron shielding evaluation of two moderating materials as summarized in Table 1.

Table 1. Summary of the material properties

Item		Moderating material	
		Resin-1	Resin-2
Chemical Composition (Wt%)	Al	14.93	21.6
	H	5.05	5.70
	B	1.05	1.40
	C	35.13	26.70
	O	-	23.50
	N	-	0.90
	O + Zn (balance)	43.84	-

The detector was positioned so that the middle segment would be in parallel to the resin blocks. As for the moderating materials, a total of 20 blocks, each having a 1-cm thickness, were used for both Resin-1 and Resin-2 to measure the neutron shielding with increasing material thickness. The ^{252}Cf source was also placed 27 cm apart from the detector center to account for the resin block thickness and the minimum gap projected between the detector and cask in future experiments.

It should be emphasized that despite the utilized detector's ability to detect neutrons using three-independent segments, it was reported that each segment has slightly varying optical properties, particularly in the outer segments [1]. Thus, the characterization of detector properties and the neutron shielding experiment are restricted to using only the middle segment.

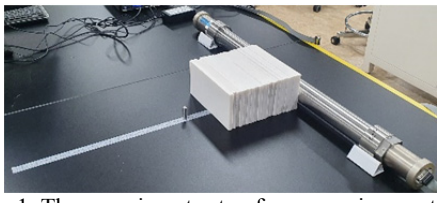


Fig. 1. The experiment setup for measuring neutron shielding of two different materials using a ^{4}He (Arktis S670e) detector and a ^{252}Cf source.

3. Result and Discussion

The characterization of the S670e detector was first carried out before performing the neutron shielding experiment for the following reasons: 1) inconsistency in the recorded neutron counts due to the detector's angular orientations, and 2) statistical fluctuation in the measurement due to the long-term operation.

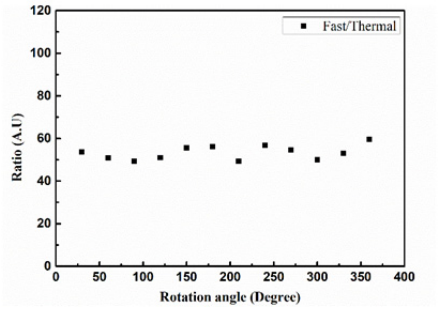


Fig. 2. The fast/thermal ratio measured as a function of orientation angles.

According to the provided operation manual [2], each segment is equipped with four SiPM-pairs placed in the middle along its longitudinal direction. In this regard, the detection efficiency could vary depending on the angular orientation. Thus, we measured the fast-to-thermal neutron ratio of ^{252}Cf source at various angles by rotating the detector from 0 to 360 degrees as shown in Fig. 2. We notice the measured ratios fluctuate with the changing rotation angle and hence the detector orientation should be fixed to eliminate possible discrepancies in the measured quantities.

On the other hand, it is widely known that SiPMs are temperature-dependent devices. Fig. 3 reports the variation in the measured neutron counts and the detector temperature with increasing operation time. Also, each measurement corresponds to a data acquisition time of 5 minutes.

From the result, we can see that the change in the ratio and the temperature have a similar trend with increasing operation time. Also, the ratio change is nearly 5% for a temperature change of approximately 1.0 °C for 480 min of operation. However, the observed ratio fluctuation due to temperature variations is not as significant as one would expect from the typical temperature-coefficient of an SiPM.

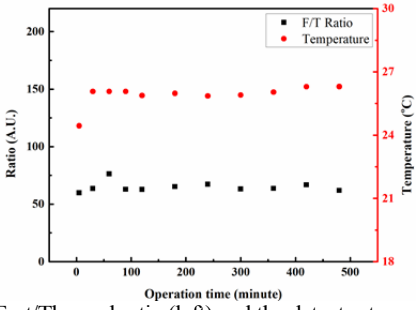


Fig. 3. Fast/Thermal ratio (left) and the detector temperature (right) measured as a function of operation time.

Fig. 4 and Fig. 5 show the fast and thermal neutrons measured with increasing thickness from 0 to 20 cm for Resin-1 and Resin-2. The degree to which the fast neutron decays with increasing material thickness is nearly the same for both Resin-1 and Resin-2. On the contrary, a clear difference is shown in the thermal neutron measurements where the Resin-2 is more effective in absorbing the moderated thermal neutrons. It is interesting to see that the number of thermal neutrons increases from 0 to 5 cm and starts decreasing with increasing thickness. The reason is that a minimum attenuation length is required for the moderated thermal neutrons to be absorbed by the shielding material without penetration.

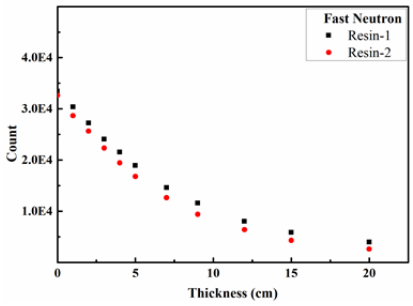


Fig. 4. Fast neutrons measured as a function of shielding thickness for two moderating materials.

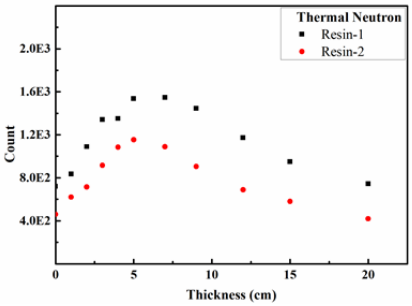


Fig. 5. Thermal neutrons measured as a function of shielding thickness for two moderating materials.

4. Conclusions

This work demonstrated the neutron shielding effectiveness of two different moderating materials using the commercially available ^{4}He detector system. Future work will focus on analyzing the shielding properties of the investigated materials and comparing them with MCNP simulation.

Acknowledgment

This work was supported by the Nuclear Safety Research Program through the Korea Foundation of Nuclear Safety (KoFONS) using financial resources granted by the Nuclear Safety and Security Commission (NSSC) of the Republic of Korea (No. 1804025).

REFERENCES

[1] C. Barker et al., "Pulse shape analysis and discrimination for silicon-photomultipliers in helium-4 gas scintillation neutron detector," EPJ Web Conf., 170, 07002 (2018).

[2] Arktis Radiation Detectors Ltd., "Arktis S-670(e) Detector Series Operating Manual," Oct. 14, (2020).

7분과

방사화학 (Oral)

Evaluation of ^{55}Fe in Radioactive Waste With Liquid Scintillation Counting

Kyunghun Jung*, Garam Park, Jungbo Yoo, Tae-Hong Park, and Jaiil Park
Korea Atomic Energy Research Institute, 989-111 Daedukdaero, Yuseong, Daejeon, 34057, Korea
*kyunghunjung@kaeri.re.kr

1. Introduction

In accordance with the Nuclear Safety and Security Commission Notice No. 2020-11, the delivery regulation of low and medium level radioactive waste, the concentration of some radionuclides in low and intermediate radioactive waste must be determined before its disposal. Radioactive waste is produced not only in nuclear power plants, but also in research institutes, schools, hospitals, industrial sites, and other places dealing with radioactive materials. The waste form is also very diverse, including paper, resin, filter, vinyl, plastic, sludge, and solidified materials. Radioactive Waste Chemical Analysis Center in KAERI has developed radioactive waste analysis methods, including radiochemical separation of the radionuclides specified in the disposal regulations [1].

Among the radionuclides to be analyzed, ^{55}Fe is produced by activating a stable isotope of iron and has a half-life of 2.74 years. It captures an electron whose energy of 231 keV and emits 5.9 and 6.5 keV X-rays, and 5.0-6.5 keV Auger electrons during its decay. Therefore its radioactivity can be detected by two types of devices, an X-ray detector and a Liquid Scintillation Counter (LSC).

Taddei et al. [2] analyzed the radioactivity of ^{55}Fe using the two methods and reported that LSC was capable of lowering the detection limit. Notably, there is a risk of overestimation because the LSC method is susceptible to even a small amount of interfering nuclides. In the case of X-ray analysis, however, the self-shielding effect of the target sample may occur. The paper also reported that the X-ray possibly underestimated the radioactivity due to the influence of ^{137}Cs and ^{60}Co, when they were not completely removed from sample.

We have been using an X-ray detector to analyze ^{55}Fe. However, in our environment, the detection efficiency of x-ray analysis is only a few percents. In addition, our sampling protocol barely produces a uniformly spread sample for counting.

The LSC method, which has a detection efficiency of 40% or more with respect to the x-ray analysis method, has advantages that the sample amount for counting can be reduced and the sample can be prepared uniformly. Therefore, we report the results of examining whether LSC can be used to analyze ^{55}Fe in our circumstance, where the radioactive waste can possess a variety amount of Fe.

2. Experiment

2.1 Sample Preparation

A solution containing 3, 5, 8, 10, 20, 30, 50 and 80 mg of Fe was prepared using Fe carrier solution in HNO_3 to find a quenching index dependency on Fe weight. 1 mL of diluted ^{55}Fe certified reference material (7055, Eckert & Ziegler) was added to the carrier solution and then distilled water was added up to the whole volume of 10 mL. 10% NH_4OH was added to adjust the pH of samples to 9-10 to precipitate $Fe(OH)_3$, which was centrifuged and then dried using IR ramp. The precipitate was dissolved in 5 mL of 2M H_3PO_4 to obtain transparent color. Finally a LSC cocktail (Ultima Gold LLT, Perkin-Elmer) was added to make a total of 20 mL of measurement solution.

2.2 Measurement

The radioactivity of the prepared sample was measured using a LSC apparatus (Quantulus GCT 6220, Perkin-Elmer). All samples were measured for 10 min so that its 2-sigma percent was 1 % or less. The sample vial was cleanly wiped with ethanol to prevent detector from a noise due to electrostatic effects. The maximum value of the energy range measured by the LSC was set to 6.6 keV, which is slightly larger than the maximum energy of the Auger electron of ^{55}Fe. The transformed Spectral Index of the External standard (tSIE) was adopted as a quench parameter in this experiment.

A measurement efficiency of the LSC equipment was calculated from a count value of the sample and the CRM concentration put in the sample. Fig.1. shows the relationship between measurement efficiency and quench parameter. It was confirmed that the quenching effect varies with respect to the contained Fe weight in the sample.

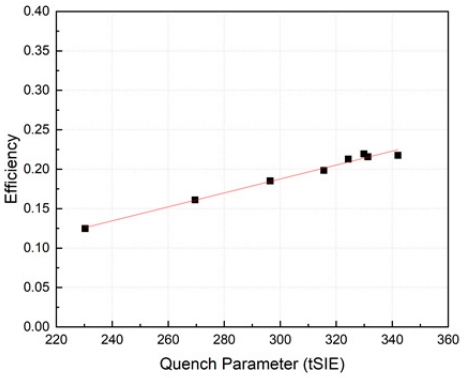


Fig. 1. Quench correction curve of ^{55}Fe.

3. Conclusion

A measurement efficiency of the LSC device using the sample prepared according to our protocol was estimated to be about 20 % at the maximum. This is about six times higher than the X-ray measurement method, which currently has a measurement efficiency of around 3 % in our environment.

REFERENCES

[1] Chang Heon Lee, Myung Ho Lee, Sun Ho Han, Yeoung-Keong Ha and Kyuseok-Song, "Systematic radiochemical separation for the determination of ^{99}Tc, ^{90}Sr, ^{94}Nb, ^{55}Fe and ^{59,63}Ni in low and intermediate radioactive waste samples", J Radioanal Nucl Chem, 288, 319-325 (2011).

[2] M. H. T. Taddei, J. F. Macacini, R. Vicente, J. T. Marumo, S. K. Sakata and L. A. A. Terremoto, "A comparative study using liquid scintillation counting and X-ray spectrometry to determine ^{55}Fe in radioactive wastes", J Radioanal Nucl Chem, 295, 2267-2272 (2013).

Manufacture of Leaching Resistance Cement Waste Form Including KJRR Simulated Liquid Waste

Gi Yong Kim[a,b], Junhyuck Im[b], Dae Seok Hong[b] , and Jong Sik Shon[b,*] , and Tae-Hong Park[a]
[a] Radwaste Radiochemical Analysis Team, Korea Atomic Energy Research Institute, 111 Daedeok-daero, Yuseong-gu, Daejeon, Korea
[b] Operational Radwaste Control Team, Korea Atomic Energy Research Institute, 111 Daedeok-daero, Yuseong-gu, Daejeon, Korea
*njsshon@kaeri.re.kr

1. Introduction

Ki-Jang Research Reactor (KJRR) is planning to build the Ki-Jang, Busan at 2022. It is important to safely dispose of low-and intermediate level radioactive waste from operation of the research reactor. One of the efficient way to treat radioactive waste is cement solidification. The cement solidification method is simple and efficient than other solidification method, but has a lower leaching resistance. Hence, this study was focused on the development of cement solidification for an enhancement of cesium leaching resistance. We used loess to improve the cesium leaching resistance of KJRR cement waste form containing KJRR simulated liquid waste. A leaching test was carried out using KJRR simulated liquid waste containing 3 g L^{-1} of cesium for 90 days. Loess showed that KJRR cement waste form made cesium leaching resistance 21.1% higher than the control (KJRR cement, without loess). All KJRR cement waste form should meet the waste acceptance criteria for final disposal such as leaching test, and compressive strength tests.

2. Methods and Results

2.1 Materials

Portland cement (Type I) and loess were purchased from SSangyong, Greenbio. NaCl, Na_2SO_4 and CsCl were purchased from Sigma-Aldrich (Mo, USA). All other chemicals used are of analytical or research grade.

2.2 Component of KJRR simulated liquid waste

The KJRR (Ki-Jang Research Reactor) simulated liquid waste constituents are as follows: Na_2SO_4 106.53 g L^{-1}, NaCl 64.28 g L^{-1}, and Cs^+ 3 g L^{-1} [1].

2.3 Manufacture of KJRR cement

The KJRR cement waste form(including KJRR simulated liquid waste) were manufactured in accordance with the Korean Industrial Standard (KS-L-5109) [2]. The mechanical mixer was purchased from Jl-206 (Jeil Precision, Korea). The KJRR cement waste forms were made at W/C 0.7 considering the result of a free-standing water test (Fig 1a).

And we added loess to improve the cesium leaching resistance of KJRR cement (S/C S; loess, C; cement) from 1 and 10 wt.% (Fig. 1b). And KJRR cement waste form solidified while under curing at room temperature with relative humidity of 40 to 60 % for 28 days. After 28 days, the uniformity of the KJRR cement waste form was visually confirmed.

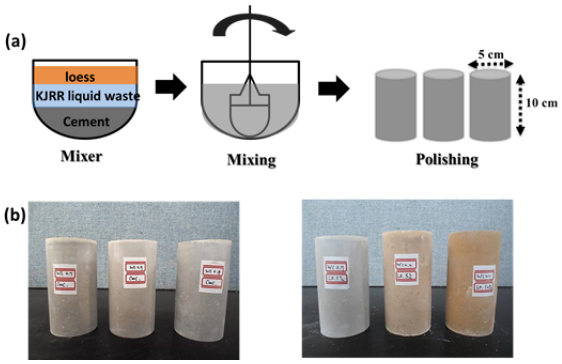


Fig. 1. (a) Schematic diagram showing a KJRR cement waste form including KJRR simulated liquid waste, (b) Real images of KJRR cement waste form, and (c) Loess KJRR cement waste form.

2.4 Leaching test of KJRR cement waste form

As shown in figure 2. We analyzed pH and electronic conductivity(Eh) of KJRR cement waste form with a leaching time. It was confirmed that the pH increased with loess content of KJRR cement waste form.

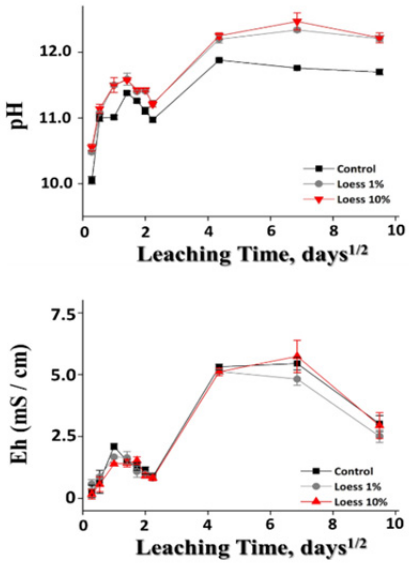


Fig. 2. Measures of pH and electronic conductivity with a leaching time of KJRR cement waste form: (a) pH, (b) Eh.

The cumulative fraction leacheded (CFL) of cesium according to the change of loess content was calculated using the ANS 16.1 test method from USA. The leaching resistance was determined by considering the degree of cesium ions leached during the leaching test, and the cumulative fraction leach was defined as the equation below [3].

$$CFL = \frac{\sum A_i}{A_0} \quad (1)$$

A_i= Cumulative leaching amount of material A during the leaching interval

A_0= Initial content (g) of the material A.

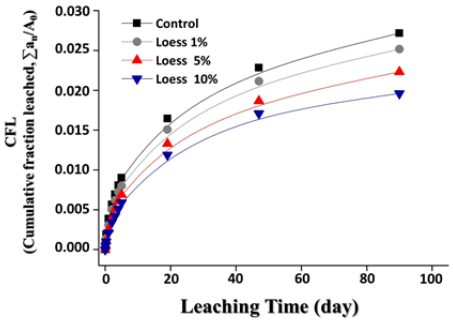


Fig. 3. Cumulative fraction of Cs^+ leached in loess KJRR cement waste form.

It was confirmed that KJRR cement waste form containing loess was less Cs^+ leaching than control sample (KJRR cement waste form, without loess) (Fig. 3).

2.5 Compressive strength test of KJRR cement waste form

Table 1 shows the compressive strength results of the KJRR cement and loess KJRR cement. All experiment groups were satisfied with the final disposal facility.

Table 1. Compressive strength test of KJRR cement(control) and loess KJRR cement

Compressive strength (Mpa)*		
Component	Number	Results
Control	**1**	27.6
	2	26.8
	3	25.3
Loess 1%	**1**	15.2
	2	16.2
	3	14.8
Loess 5%	**1**	15.4
	2	12.3
	3	14.9
Loess 10%	**1**	17.2
	2	15.5
	3	14.8

* Compressive strength acceptance criteria ≥ 3.45 MPa [3]

3. Conclusions

In this study, we made a KJRR cement waste form with KJRR simulated liquid waste. In addition, we used loess to improve the cesium leaching resistance of KJRR cement waste form. We demonstrated that loess successfully isolated the KJRR cement waste form based on an SEM-EDS spectrum analysis. A leaching test was carried out using simulated KJRR liquid waste containing 3 g L^{-1} of cesium. Loess KJRR cement waste form achieved a cesium leaching resistance 21.1% higher than the control value. In addition, all experimental groups were satisfied with the final disposal facility, such as the compressive strength and leaching test.

REFERENCES

[1] J.S. Shon, et al., “Treatment and Disposability of Intermediate Level Liquid Radwastes generated by Fisson Moly Production”, Proc. of the Korean Radioactive Waste Society, 15 (2017).

[2] W.H. Jang, et al., "A Study on Operating Range of Cement Solidification for Final Disposal of Radioactive Soil”, Journal of Korea Society of Waste Management, 34 (2017).

[3] G.Y. Kim, et al., “Characterization of cement solidification for enhancement of cesium leaching resistance”, Journal of Nuclear Fuel Cycle and Waste Technology, 16(2), 189-193 (2018).

Strontium Isotope Detection by Combination of Laser-Induced Breakdown Spectroscopy (LIBS) and Molecular Laser-Induced Fluorescence (MLIF)

Sung-Uk Choi and Jong-Il Yun*
Department of Nuclear and Quantum Engineering, KAIST, Daehak-ro 291, Yuseong-gu, Daejeon 34141, Republic of Korea
*jiyun@kaist.ac.kr

1. Introduction

The natural abundance of strontium isotopes varies depending on their origin due to the decay of long-lived ^{87}Rb ($t_{1/2} = 4.9\times10^{10}$y). Therefore, strontium could be utilized as a geological indicator for determining the origin of ore [1]. In particular, strontium could be the signature material for nuclear forensics, tracking the origin of uranium ore concentrate (UOC). However, the typical isotope detection method such as mass spectrometry cannot be used to the onsite identification for nuclear forensics due to its complex measurement procedure. The combination of laser-induced breakdown spectroscopy (LIBS) and molecular laser-induced fluorescence (MLIF) could be a promising solution to this issue. LIBS-MLIF consists of the two processes for signal enhancement: 1) generation of a plasma plume by a high energy pulse laser, and 2) excitation of molecules in plasma by a resonant wavelength laser. These step-by-step processes enable not only the amplification of the fluorescence signal, but also the selectivity of isotopes.

In the present study, strontium isotopes were detected with regard to the emission and excitation spectra of strontium monoxide by LIBS-MLIF. The stable isotopes of strontium could be clearly resolved at individual rotational band heads. The results demonstrated the feasibility of LIBS-MLIF for the detection of strontium isotopes.

2. Experimental

Fig. 1 shows the schematic diagram of the experimental set-up. The Q-switched Nd:YAG lasers (Quantel, Brilliant, 10 Hz, λ=266nm) generated the plasma on the surface of the sample. Thereafter, an optical parametric oscillator (OPO) laser (OPOTEK Inc., Vibrant HE) excited the species in the plasma by resonant wavelength for the electronic transitions of interest. The fluorescence signal was detected by a Czerny-Turner spectrometer (Andor Technology, shamrock sr-3030i) with an intensified charge-coupled device (Andor Technology, iStar).

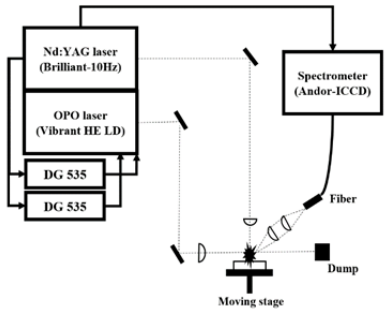


Fig. 1. Schematic diagram of LIBS-MLIF configuration.

The measurement conditions were optimized for the detection of strontium monoxide emission. The energies of Nd:YAG and OPO laser were set at 40 mJ and 3 mJ, respectively. The inter-pulse delay and gate delay were optimized to 5 μs and 15 μs, respectively.

For sample preparation, the strontium monoxide powder (Aldrich, 99.9% purity) was pelletized with KBr binder in pellets on a one-centimeter scale.

3. Result and discussion

3.1 Strontium oxide emission spectrum

The SrO molecular radical in laser-induced plasma could be generated in the following two ways: 1) direct extraction as an intact molecule from the sample, or 2) recombination of the atomized strontium and oxygen. These SrO radicals release intense emission in the wide spectral range [2]. As shown in Fig. 2, the SrO molecular emission from $A^1\Sigma^+\rightarrow X^1\Sigma^+$ transition system was observed in the range from 780 to 900 nm by using the LIBS system. The three vibrational bands (1-0, 2-0, and 3-0) could be identified.

However, it is not easy to distinguish the isotope in this complex molecular emission. Therefore, MLIF system is needed to be supplemented to resolve individual isotopes. The (2-0) vibrational band was selected to be applied for excitation, since it has an intense rotational branch head and a relatively large isotopic shift (0.15 nm).

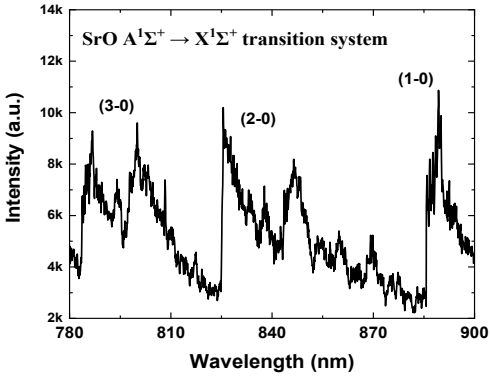


Fig. 2. SrO emission spectrum using single LIBS system.

3.2 LIBS-MLIF emission spectra

The natural strontium consists of three major stable isotopes (^{88}Sr = 82.58%, ^{87}Sr = 7.00%, and ^{86}Sr = 9.86%). Thus, molecular radicals of ^{88}SrO, ^{87}SrO, and ^{86}SrO exist in laser-induced plasma from the strontium sample. They have an isotopic shift of about 70 pm per one mass number [2], which could be selectively excited by fine-tuning of laser wavelength.

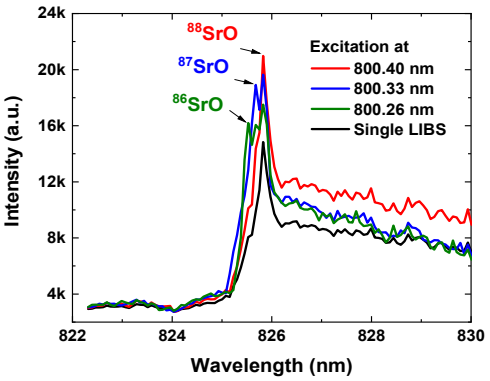


Fig. 3. SrO emission spectrum of LIBS-MLIF with excitation wavelengths.

Fig. 3 shows the SrO emission spectra of LIBS-MLIF configuration. The rotational branch head of each isotope was significantly amplified depending on the excitation wavelength. Although the individual LIBS-MLIF spectra of strontium isotopes were not perfectly resolved, the characteristic emission feature of each isotope could be clearly identified. Contrary to LIBS-MLIF, the emission spectrum generated only by LIBS (black line) cannot be resolved due to an overlap of the emission between strontium isotopes. The combined LIBS-MLIF method therefore offers a possibility of isotope detection, that is not possible with LIBS.

3.3 Isotope-resolved excitation spectra

Although the strontium isotopes could be distinguished in emission spectra, it was limited by the resolution of the spectrometer (40 pm). To clearly identify the isotopes, the excitation spectrum was measured, which can be obtained with respect to the intensity dependence of the specific emission peak as a function of excitation wavelength, , as shown in Fig. 4. The strontium isotopes could be more clearly distinguished with the fine laser resolution (10 pm).

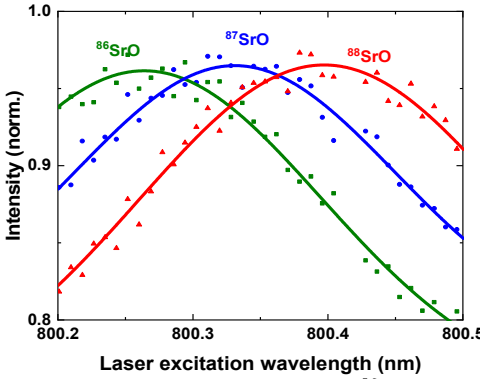


Fig. 4. SrO excitation spectra (intensity of ^{86}SrO at 825.78 nm ^{87}SrO at 825.85 nm, ^{88}SrO at 825.93 nm) with measured data (point) and Gaussian fitting (lines).

4. Conclusion

In the present study, strontium isotope detection was conducted by LIBS-MLIF configuration. Strontium monoxide molecular radicals were utilized as the fluorescence signal sources. The isotope-resolved emission and excitation spectra were measured by fine-tuning of incident laser wavelengths. This study demonstrated the feasibility of LIBS-MLIF for nuclear forensic analysis using strontium isotopes.

REFERENCES

[1] Z. Varga et al., Application of lead and strontium ratio measurements for the origin assessment of uranium ore concentrates, Anal. Chem. 81 (2009) 8327–8334.

[2] X. Mao et al., Laser Ablation Molecular Isotopic Spectrometry: Strontium and its isotopes, Spectrochim. Acta B 66 (2011) 767–775.

Coordination Mode-Dependent Stability and Optical Property Changes of Am(III)-Aliphatic Dicarboxylate Complexes

H.–K. Kim[1,*], K. Jeong[2], H.–R. Cho[1], E. C. Jung[1], K. Kwak[3], and W. Cha[1]
[1] Nuclear Chemistry Research Division, KAERI, Daejeon 34057, Republic of Korea
[2] Department of Chemistry, Korea Military Academy, Seoul 01805, Republic of Korea
[3] Department of Chemistry, Korea University, Seoul 02841, Republic of Korea
*hkim11@kaeri.re.kr

1. Introduction

Physicochemical interactions of long-lived radionuclides determine their migration behaviors in the natural aquatic systems. Understanding the chemical complexations of the radionuclides are required for the long-term safety assessment of the deep geological disposal of high-level radioactive wastes. A carboxylic group in small and macro organic matters is one of the key function groups that strongly interact with actinides ions and thus increase their mobility [1]. In this study, we investigated the Am(III) interactions with a series of aliphatic dicarboxylate ligands with an increasing carbon chain length. UV-Vis spectrophotometry coupled with a liquid waveguide capillary cell (LWCC), time-resolved laser fluorescence spectroscopy (TRLFS), ATR-FTIR were used in a combinatorial approach for speciation of the complexes, determining formation constants, and examining coordination mode of each ligand. Molecular structures and bonding properties of the complexes are predicted by DFT calculations.

2. Experimental

Sample preparations ^{241}Am was purified as described in our previous study [2]. Quantitative and qualitative analysis of the purified ^{241}Am were carried out by using liquid scintillation counting, gamma and alpha radiation spectrometry. Sodium dicarboxylate **s**olutions were prepared in 1 M $NaClO_4$ and pHs were adjusted to be in pH~6 by adding $HClO_4$. Am(III) solutions were also prepared in 1 M $NaClO_4$ and pH~6. Am(III)-dicarboxylate samples were prepared by adding dicarboxylate solutions into fixed volume of Am(III) solutions.

UV-Vis-LWCC, TRLFS, ATR-FTIR UV-Vis absorption spectra were measured by using Cary3 (Varian) coupled with a LWCC (WPI) with a path length of 100 cm. Luminescence spectra were collected by TRLFS equipped with a nanosecond pulsed laser (OPO, Vibrant B, OPOTEK Inc.) as an excitation source (503 – 507 nm, ~3.5 mJ), a spectrograph (SR-303i, Andor Technol.), and an intensified CCD (ICCD, iStar, Andor Technol.). All the measurements were carried out at 25℃. Data analysis was carried out by using OriginPro 2015 and HypSpec programs.

Samples for IR spectral measurements were prepared with Eu(III) instead of Am(III), because of the limited amount of the ^{241}Am in stock as well as the difficulty in handling the highly radioactive materials. A FTIR spectrometer (Nicolet 5, Fisher Sci.) was used with a diamond ATR cell of 9 reflections (Concentrate 2^{TM}, Harrick).

DFT calculations Gaussian 16 package was used for the calculations with 6-31G(d) basis set. The small-core scalar-relativistic effective core potential was used with an ECP60MWB_SEG basis set. The B3LYP functional was used for geometric optimization and frequency calculation. Solvation effect of water was modeled by including the first coordination shell around Am, and the rest of the solvent was approximated by applying the dielectric continuum model.

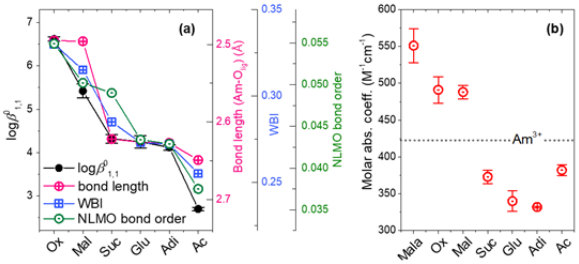


Fig. 1. (a) Correlation of the stability of the Am(III) complexes with bond length, Wiberg bond index (WBI), and natural localized molecular orbital (NLMO) bond order, (b) Molar absorption coefficient change depending on the ligands.

3. Results and discussion

Absorption spectra of Am(III) were shifted towards the longer wavelength direction, as increasing the ligand concentrations. Speciation of the Am(III) complexes for each ligand were conducted based on the absorption spectral changes and stability constants were calculated.

Ligand-dependent molar absorption coefficient changes appeared as shown in Fig. 1.

Luminescence spectra of Am(III) in the presence of each ligand exhibited significantly enhanced intensities along with red-shifts. Luminescence lifetimes are also considerably prolonged as complexation progresses, and deduced hydration number changes suggest bidentate bindings of the examined dicarboxylates. An additional hydroxyl group aids formation of 6- and 5-membered ring structures via tridentate bindings of a malate ligand. FTIR spectral changes provide insights into the coordination-mode, either side-on or end-on binding of each ligand. DFT calculations provide bonding properties between Am and oxygen atoms of ligands such as bond lengths and bond orders. The calculation results support the experimentally suggested coordination mode for each ligand [3,4]. Correlations of the coordination modes with stability, bond distance, bond order, and molar absorptivity will be discussed in the presentation.

REFERENCES

[1] McCarthy JF, Sanford WE, Stafford PL: "Lanthanide Field Tracers Demonstrate Enhanced Transport of Transuranic Radionuclides by Natural Organic Matter". Environ. Sci. & Technol., 32:3901-3906 (1998).

[2] Kim H-K, Cho H-R, Jung EC, Cha W: "Radioanalytical and spectroscopic characterizations of hydroxo- and oxalato-Am(III) complexes". J. Nucl. Fuel Cycle and Waste Technol., 16:397-410 (2018).

[3] Kim H-K, Jeong K, Cho HR, Jung EC, Kwak K, Cha W: "Spectroscopic speciation of aqueous Am(III)–oxalate complexes". Dalton Trans., 48:10023-10032 (2019).

[4] Kim H-K, Jeong K, Cho H-R, Kwak K, Jung EC, Cha W: "Study of Aqueous Am(III)-Aliphatic Dicarboxylate Complexes: Coordination Mode-Dependent Optical Property and Stability Changes". Inorg. Chem., 59:13912-13922 (2020).

Anodic Dissolution Behaviors of Inconel-600 Depending on Ni and Fe Additives in LiCl-KCl

Younghwan Jeon, Jungho Hur, Seungmin Ohk, and Jaeyeong Park*
Department of Nuclear Engineering, Ulsan National Institute of Science and Technology,
50 UNIST-gil, Ulju-gun, Ulsan 44919, Republic of Korea
*jypark@unist.ac.kr

1. Introduction

A steam generator (SG) is a component which converts secondary water into steam by using primary hot coolant. A lot of dismantled SGs were produced in Korea by replacement and permanent shutdown of nuclear power plant. Additionally, 10 nuclear power plants will be expired within 10 years with a number of used SGs production. During the operation, stress corrosion cracking (SCC) are induced in SG tubes and radioactive elements in primary coolant due to CRUD, uranium and fission products from damaged fuel, deposit on the primary side of SG tubes and inside the cracks of SG tubes. Hidden radioactive elements in cracks disturb conventional chemical and physical decontamination processes and this is why SG tubes would be classified into a low-level radioactive waste (LLW) [1].

In Korea with a limited capacity and area of radioactive waste repositories, the SG tubes would be troublesome wastes. A molten salt based electrorefining can be a solution to decontaminate the contaminants on the surface and inside the cracks of the tubes and to recycle the decontaminated tubes. To make the process feasible and enhance the radionuclide removal efficiency, it is necessary to understand anodic dissolution behavior depending on various operating conditions such as molten salt compositions and applied currents and potentials.

In this study, anodic dissolution behaviors of Inconel-600 in two different initial molten salt compositions (LiCl-KCl with 5 wt.% $NiCl_2$ or $FeCl_2$) at 500℃ were investigated in galvanostatic and potentiostatic conditions. Applied potential and current density ranges were set to dissolve only Cr and Fe, not Ni which is the largest content of Inconel-600 to enhance the electrical efficiency of the decontamination process. The microstructures and compositions of the Inconel-600 on the anode and cathode deposits, after some amount of charges were passed, were analyzed by SEM-EDS and ICP-OES.

2. Experimental

LiCl-KCl (Alfa Aesar, 99.99 %), $NiCl_2$ (Alfa Aesar, 99.99 %), $FeCl_2$ (Alfa Aesar, 99.99 %) were used for electrolyte of LiCl-KCl-5 wt% $NiCl_2$/$FeCl_2$. Ag wire with 1 mm diameter (Alfa Aesar, 99.99 %) in LiCl-KCl-1 wt% AgCl was used as reference electrode and Inconel-600 plate for anode, and two tungsten rods with 3.175 mm diameter (Alfa Aesar, 99.99 %) for cathode.

All electrochemical experiments were performed in a glove box which restrict oxygen and moisture concentrations to be less than 0.1 ppm under Ar gas (99.99 %) environment. The cell temperature was maintained to the desired temperature within 1℃ by proportional-integral-derivative (PID) controller of the furnace and temperature was measured by K-type thermocouple in dummy cell with same position of electrochemical cell.

As shown in

Table 1 experimental sets were conducted. Whole experiments were performed at 500℃. Multi-potentiostat of PARSTAT MC200 and PARSTAT 1000 including VersaStudio software were used to apply potential or current density at the anode. Potential and current density change of anode and cathode were collected during the experiments.

Table 1. A summary of the Experimental matrix for different electrolytic additives

Test ID	Electrolyte (Balanced LiCl-KCl)	Applied current density (mA/cm^2) Applied Potential (V vs. 1 wt% Ag/AgCl)
NG* 1-4	5 wt% $NiCl_2$	+5, 10, 20, 30
NP* 1-4		+0.15, 0.20, 0.25, 0.30
FG* 1-4	5 wt% $FeCl_2$	+5, 10, 20, 30
FP* 1-4		+0.00, 0.05, 0.10, 0.15

*N; $NiCl_2$, F; $FeCl_2$ based, G; galvanostatic, and P: potentiostatic condition.

3. Results and Discussion

In the potentiostatic dissolution (NP, FP), a Cr-Fe depletion zone was observed (Fig. , Fig.) and its thickness was decreased at positive

potential in both molten salt systems. A lot of microcracks larger than 10 μm on the anode surface were observed in LiCl-KCl-5 wt.% $FeCl_2$ molten salt (Fig. (e)), but not in LiCl-KCl-5 wt.% $NiCl_2$. Due to the microcracks of the anode in $FeCl_2$ added salts, microparticles less than 20 μm, containing more than 10 wt.% Cr, fell out of the Inconel specimen. In the case of $NiCl_2$ added salt, the size of the Cr-Fe depletion zone was larger than 40 μm, and the content of Cr and Fe in the zone was less than 2 wt.%.

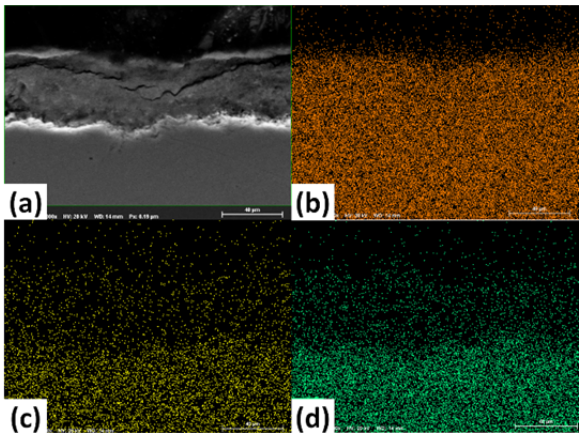


Fig. 1. SEM-BSE (a) and EDS mapping (b, c, d) images of anode cross section of NP with applied potential of +0.20 V. Target element in (b): Ni; (c): Fe, (d): Cr.

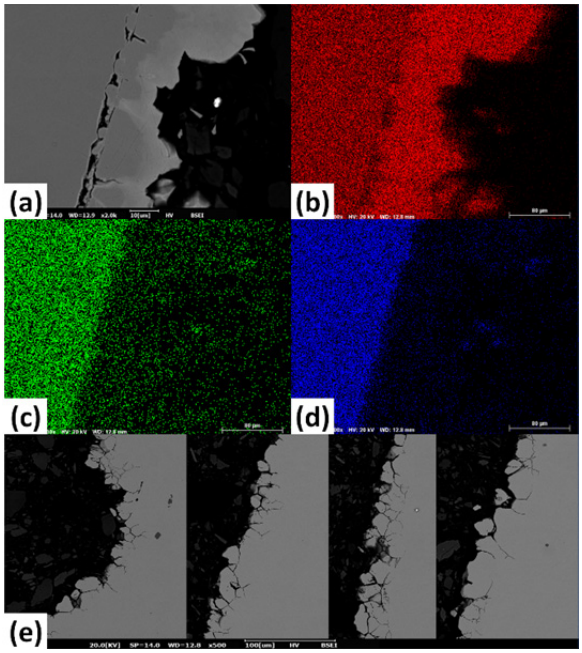


Fig. 2. SEM-BSE (a, e) and EDS mapping (b, c, d) images of anode cross section of FP with applied potential of +0.20 V. Target element in (b): Ni; (c): Fe, (d): Cr.

In the galvanostatic dissolution (NG, FG), the thickness of the Cr-Fe depletion zone was less than 5 μm in both salts, and the contents of Cr-Fe in the depletion zone was larger than 15 wt%, which is less than the potentiostatic method. Similar to the potentiostatic experiments, microcracks on the Inconel 600 surface were observed in LiCl-KCl-$FeCl_2$ but not in LiCl-KCl-$NiCl_2$. The cathode deposits were identified as high purity Ni and Ni-Fe intermetallic in $NiCl_2$ added salts and $FeCl_2$ salts respectively.

4. Conclusion

In this study, anodic dissolution behaviors microstructural changes of Inconel-600 in LiCl-KCl with $NiCl_2$ or $FeCl_2$ additives were investigated. Uncontaminated section of SG tubes and Ni in Cr-Fe depletion zone can be recycled by extracting whole elements except for Ni in Cr-Fe depletion zone. By optimizing applied anode potential and current density which affect ionization behaviors and micro-structural change of anode, decontamination efficiency can be maximized.

ACKNOWLEDGEMENT

This work was supported by the National Research Foundation of Korea grant funded by the Ministry of Science and ICT, Republic of Korea. (2019M2A7A1001758).

REFERENCES

[1] Krause, G., Amcoff, B., Robinson, J. "Options for Steam Generator Decommissioning", NEA-PREDEC, (2016).

Two-Step Zr Metal Preparation Combining Electrorefining and Thermal Decomposition

Jungho Hur, Younghwan Jeon, Seungmin Ohk, and Jaeyeong Park*
Department of Nuclear Engineering, Ulsan National Institute of Science and Technology, 50 UNIST-gil, Ulju-gun, Ulsan 44919, Republic of Korea
* jypark@unist.ac.kr

1. Introduction

Zirconium has been considered as a critical material in the nuclear industry due to its good mechanical performance and low neutron absorption cross-section in the reactor environment. However, after the reactor period, Zr-based alloys such as nuclear fuel cladding, pressure tube, and calandria tube are activated by neutron activation. They are classified as intermediated level radioactive waste which is required to be decontaminated in the context of effective waste management and recycling of valuable materials.

The decontamination method for spent Zr-based alloys especially spent nuclear fuel (SNF) cladding, has been studied by many researchers using the molten salt electrorefining method [1,2]. The fluoride-based process has the advantage of simpler electrochemical behavior (single redox behavior: Zr^{4+}/Zr), but the disadvantages of high process temperature and corrosion issue. Process temperature and corrosion issues are critical in the view of scaling up the process. The chloride-based process can be operated in lower temperatures than the fluoride-based process but has complicate valence stated of Zr with disproportion reaction which may cause co-deposition of ZrCl. The change of the focus in the decontamination process from direct Zr recovery to ZrCl may offer a better option that suppresses detachment of electrochemical deposition, reacts at a more positive potential, and increases the process efficiency.

In this study, a new decontamination method considering thermal decomposition reaction ($4ZrCl(s) \rightarrow ZrCl_4(g)+3Zr(s)$) is proposed based on the proven and analyzed major process. Also, the process conditions are suggested.

2. Experimental

2.1 Electrodeposition of ZrCl

Electrochemical experiments for ZrCl recovery was conducted at 450℃ in a glove box system using LiCl-KCl-2 wt% $ZrCl_4$ electrolyte. Applying potential was -1.1 V (vs. 1 wt % Ag/AgCl) for ZrCl production.

2.2 Thermal decomposition reaction of ZrCl

The vacuum distillation furnace was used for thermal decomposition reaction experiments with various conditions to explore the effect of temperature, pressure, and reaction time. Tantalum crucible was chosen due to its non-reactivity with the sample. The temperature increased at a rate of 200℃/h and cooled with a rate of 0.04~0.06℃/s.

Table 1. Test matrix of thermal decomposition

No.	Temperature (℃)	Pressure (torr)	Reaction time (h)
1	600	760	12
2		1.7~1.8	12
3		1.7~1.8	24
4	800	760	12
5		1.7~1.8	12
6		1.7~1.8	24
7	1100	760	12
8		1.7~1.8	12
9		1.7~1.8	24

3. Results

3.1 Electrodeposition of ZrCl

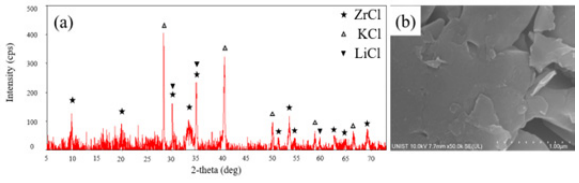


Fig. 1. (a) XRD result and (b) SEM image of ZrCl.

Electrodeposited ZrCl was analyzed by X-ray diffraction (XRD) and scanning electron microscopy (SEM) as shown in Fig.1. Only ZrCl and electrolyte was observed by XRD. ZrCl has a densely layered morphology which results from an octahedral crystal structure.

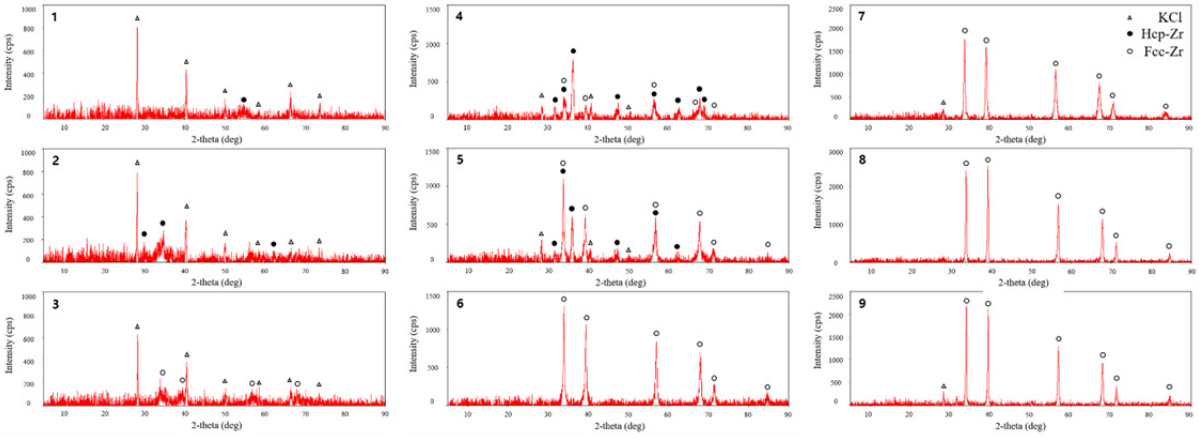


Fig. 2. XRD analysis of produced Zr in case 1-9.

3.2 Thermal decomposition of ZrCl

XRD results of case 1-9 are shown in Fig. 2. It seems that thermal decomposition reaction occurred but insufficient crystallization of Zr, in case 1-3, based on the disappearance of ZrCl peaks and observation of small Zr peaks. In case 4-6, two crystal phases of Zr (Hcp-Zr, Fcc-Zr) appeared and the phase of Zr is stable to be Fcc-Zr with longer reaction time. When 1100 ℃, only Fcc-Zr was shown in case 7-9. The results imply that the crystallographic phase transition also occurs as well as the thermal decomposition reaction of ZrCl. It can be summarized as

$$4ZrCl(s) \rightarrow ZrCl_4 + 3HCP\text{-}Zr(s) \qquad (1)$$

$$HCP\text{-}Zr(s) \rightarrow FCC\text{-}Zr(s) \qquad (2)$$

It was also ensured that residual electrolyte in ZrCl sample was eliminated during the thermal decomposition reaction. The process of higher temperature and low pressure make effective diminish of electrolyte so that it can ensure the purity of Zr.

4. Discussion

Major processes of the newly proposed decontamination method are electrodeposition as ZrCl and thermal decomposition of ZrCl into Zr which were experimentally proven by this study. Additionally, processes of spent molten salt purification and arc melting are required to minimize secondary waste and solidify Zr powder as shown in Fig. 3. Spent molten salt purification process introduces a liquid cadmium electrode to recover residual ions and make intermetallic compounds. Cd in the intermetallic compound will be distilled and recycled into salt purification. Recovered residual ions will be sent to a long-term disposal facility and arc melted Zr can be recycled after a short-term cooling period.

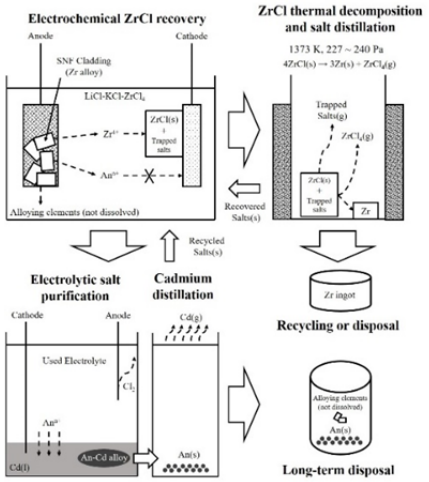


Fig. 3. Proposal of new decontamination process considering thermal decomposition of ZrCl.

5. Conclusion

A new decontamination process of spent Zr-alloy considering the thermal decomposition reaction of ZrCl is proposed based on the experimental results of major processes.

REFERENCES

[1] S. Sohn, J. Park, I.S. Hwang, “Electrolytic recovery of high purity Zr from radioactively contaminated Zr alloys in chloride salts”, Int. J. Electrochem. Sci., 3897–3909 (2018).

[2] C.H. Lee, K.H. Kang, M.K. Jeon, C.M. Heo, Y.L. Lee, “Electrorefining of zirconium from zircaloy-4 cladding hulls in LiCl-KCl molten salts”, J. Electrochem. Soc., 159(8) D463–D468 (2012).

Thermal Behaviors of Nuclear Fuel Samples and Cladding Materials by Using In-Situ High-Temperature XRD

Sang Ho Lim [a,c], Jeongmook Lee [a], Dong Woo Lee [a], Young-Sang Youn [b], Jong-Yun Kim [a,c], Tae-Hyung Kim[a], and Junghwan Park[a]
[a]Nuclear Chemistry Research Team, Korea Atomic Energy Research Institute, Daejeon, Republic of Korea
[b]Department of Chemistry, Yeungnam University, Gyeongbuk, Republic of Korea
[c]Department of Radiochemistry & Nuclear Nonproliferation, University of Science and Technology, Daejeon, Republic of Korea
*slim@kaeri.re.kr

1. Introduction

Understanding the thermal behaviors of nuclear fuel and cladding materials is one of the critical issues in securing the safety of operating nuclear power plants. Metallic fuels have been considered candidate nuclear fuels for sodium-cooled fast reactors (SFRs).

2. Experimental section

The six types of metallic fuels were manufactured by the injection casting method at a casting temperature of approximately 1893 K under dynamic vacuum condition, to perform HT-XRD measurements, metallic fuels with a diameter of 5.5 mm were sliced with a thickness of approximately 1.0mm. All samples were polished with 2000 grit SiC paper and then rinsed with absolute ethanol. To minimize the oxidation, the samples were quickly mounted on a tungsten heating strip in BRUKER-AXS D8 ADVANCE system (Bruker) equipped with an HTK-2000N high-temperature chamber (Anton Paar).

Pure Zr (Sigma-Aldrich Korea Ltd.) and ZIRLO™ (Westinghouse Electric Co.) were prepared with a diameter of 6.35mm and with the area of approximately 10 x 10mm^2, respectively. Both samples were polished with 2000 grit SiC paper and then rinsed with ethanol. To minimize oxidation under air caused by the high oxygen affinity of zirconium (ΔG = -1037 kJ/mol at standard conditions), the sample was quickly loaded on the tungsten (W) heating strip within minutes after polishing and placed under vacuum.

3. Results & discussions

From a study of the six types of uranium-based alloys with 10wt% Zirconium to monitor change in the lattice constants as a fuction of temperature and the phase transformation using in situ HT-XRD. We observed that only orthorhombic α-U diffraction patterns appeared below 843 K in the case of all the metallic fuels. Pawley refinement of the HT-XRD data indicated anisotropic lattice thermal expansion in the metallic fuels with an increase in the annealing temperature. The a and c lattice parameters of α-U increased as temperature was elevated, whereas the b lattice parameter remained almost constant as compared to those obtained at room temperature. To the best of our knowledge, this is the first report on the HT-XRD analysis of the lattice thermal expansion of metallic fuels upon annealing.

For in situ HT-XRD experiments using pure Zr and ZIRLO™ samples to compare their properties. We observed that only hexagonal Zr diffraction patterns emerged at 30 °C in both Zr and ZIRLO™. In addition, as the temperature increased, Zr was oxidized above 1110 °C and ZIRLO™ was oxidized above 1230 °C. Through the analysis results of in situ HT-XRD spectra using Pawley refinement, we found that the c-axis lattice parameter of ZIRLO™ constantly increased as a function of temperature while that of Zr sample was irregular, indicating that the change in the c/a ratio of ZIRLO™ was much more stable than that of Zr sample.

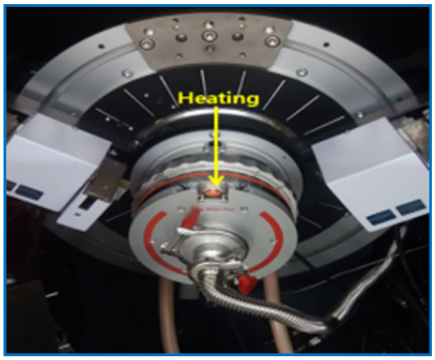


Fig. 1. In-situ high-temperature equipment installed in AXS D8 ADVANCE XRD system.

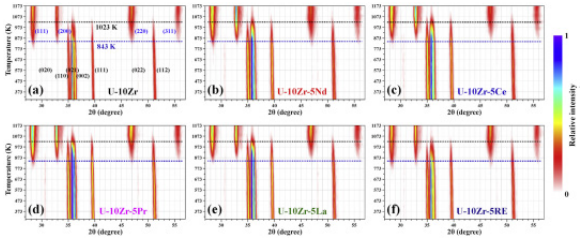


Fig. 2. 2D views of in situ HT-XRD data (a) U10Zr, (b) U10Zr-5Nd, (c) U10Zr5Ce, (d) U10Zr-5Pr, (e) U10Zr-5La, and (f) U10Zr-5RE metallic fuels are annealed from 303 to 1173 K with an interval of 30 K.

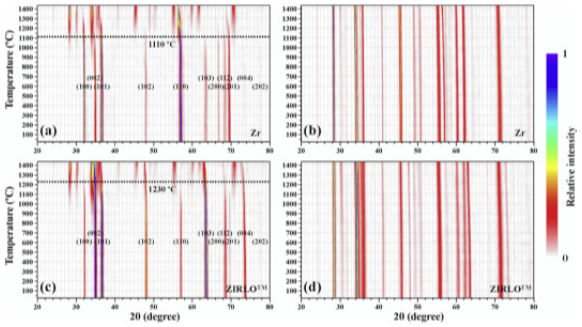


Fig. 3. 2D views of in situ HT-XRD spectra obtained during (a, c) heating from 30 to 1430 _C and (b, d) cooling from 1430 _C to 30_C at intervals of 40 _C for (a, b) Zr and (c, d) ZIRLO™ specimens.

Acknowledgement

This work was supported by the National Research Foundation of Korea (NRF) grant funded by the Korean government (MSIP; No.2012M2A8A5 025925).

REFERENCES

[1] G.L. Hofman, L.C. Walters, T.H. Bauer, Metallic fast reactor fuels, Prog. Nucl. Energy 31 83-110 (1997).

[2] A. Karahan, N.C. Andrews, “Extended fuel swelling models and ultra high burnupfuel behavior of UePueZr metallic fuel using FEAST-METAL”, Nucl. Eng. Des. 258 26-34 (2013).

[3] Y.C. Kang, M.M. Milovancev, D.A. Clauss, M.A. Lange, R.D. Ramsier, “Ultra-high vacuum investigation of the surface chemistry of zirconium”, J. Nucl. Mater. 281 57-64 (2000).

[4] N. Stojilovic, E.T. Bender, R.D. Ramsier, Surface chemistry of zirconium, Prog. Surf. Sci. 78 101-184 (2005).

7분과

방사화학 (Poster)

Determination of ^{90}Sr and ^{63}Ni in Low- and Intermediate-Level Radioactive Waste

Kyeonghui Bae*, Sora Choi, Kyunghun Jung, Jung Bo Yoo, and Tae-Hong Park
Nuclear Chemistry Research Division, Korea Atomic Energy Research Institute(KAERI), 111 Daedeok-daero-989, Yuseong-gu, Daejeon, 34057, Korea
*kyeonghui1@kaeri.re.kr

1. Introduction

Drums of low- and intermediate-level radioactive waste in the Korea Atomic Energy Research Institute (KAERI) is in urgent need of disposal. To resolve the issue by transporting to the repository, the concentration of regulatory radionuclides such as ^{3}H, ^{14}C, ^{55}Fe, ^{58,60}Co, ^{59,63}Ni, ^{90}Sr, ^{94}Nb, ^{99}Tc, ^{129}I, ^{137}Cs, ^{144}Ce, and gross α should be identified according to the Notice of Nuclear Safety and Security Commission (NSSC) No. 2020-11 [1].

Among them, we have focused on the determination of ^{90}Sr and ^{63}Ni nuclides that are pure beta emitter [2,3]. Since they emit low beta energy, 546 and 67 keV, respectively, the whole quantification process that leads to reliable results is important [2,4]. This work describes extraction chromatography methods, which were used for the separation, purification and measurement of ^{90}Sr and ^{63}Ni. Due to its high counting efficiency, a liquid scintillation counter (LSC) was used for the detection of radioactivity. The validity verification of separation procedure and calibration of LSC are also covered.

2. Experimental

2.1 Reagents and equipment

The standard solutions of Sr, Ni, and Ca (10 mg/mL) were purchased from Accustandard, USA. The certified reference standard solutions of ^{90}Sr (19SR090GV5) and ^{63}Ni(2114-16-1) were produced by Korea Research Institute of Standards and Science, and Eckert&Ziegler, respectively. UltimaGold LLT (PerkinElmer, USA) was used as scintillation cocktail. All chemicals were analytical grade reagents and used without further purification.

Inductively coupled plasma-optical emission spectrometer (ICP-OES, Thermo Jarrell Ach, USA) was employed for the quantitative analysis of Sr. Separated ^{90}Sr and ^{63}Ni were counted in LSC with double photomultiplier tubes (PerkinElmer, USA).

2.2 Separation of Sr

Certified reference material and inactive standard solution (3 mg) were used for calibration and validity confirmation, respectively.

A Ca standard solution was added to 50 mL centrifuge tube including a Sr carrier solution, and then 1,520 mg of oxalic acid was dissolved in the solution. After adjusting pH to 4.5~5 with 10% NH_4OH, the supernatant was separated through centrifugation (3500 rpm, 5 min.). The Sr(Ca)-oxalate precipitation was washed twice with 10 mL of 0.3 M ammonium oxalate, and dissolved in 5 mL of 8 M HNO_3, which was poured into the prepared Sr-resin column, followed by 15 ml of 8 M HNO_3. The ^{90}Sr nuclide was collected with the elution of 10 mL of 0.05 M HNO_3. 0.1 mL of the Sr solution was diluted with 10 mL of 0.05 M HNO_3 for the quantitative analysis using ICP-OES. 10 mL of UltimaGold LLT was added to the remaining solution for the LSC measurement.

2.3 Separation of Ni

The inactive standard solution (2.0 mg) was used for calibration and validity confirmation. 10% NH_4OH was added to the Ni carrier solution to adjust pH to 9~10 and DI water was added up to a total volume of 100 mL.

The solution was passed through the prepared Ni-resin column using a peristaltic pump. 20 mL of 0.1 M ammonium oxalate and 10 mL DI water were added to the column, sequentially. The Ni was eluted with 10 mL of 9 M HCl and the eluent was further purified with the anion exchange chromatography.

The chemical yield was estimated with the precipitation of $Ni(DMG)_2$,[5] the radioactivity of ^{63}Ni was determined with LSC.

2.4 LSC calibration

For ^{90}Sr and ^{63}Ni calibration curves, at least 10 standard samples were prepared including a blank, non-radioactive standard.

In case of ^{90}Sr, 3.0 mg of inactive Sr was used for the recovery determination. The same amount of CRM and 5 mL of 8 M HNO_3 were added. After the separation, different amounts of

nitromethane as a quenching material were added to the samples except the blank. The radioactivity of the ^{90}Sr sample was measured for 10 minutes using LSC.

For ^{63}Ni, the same amount of CRM, 2 mL of 0.7 M HCl, and 18 mL of UltimaGold LLT were added to all samples. Different amounts of nitromethane was also added to the samples except the blank. The radioactivity of the ^{63}Ni sample was measured for 30 minutes.

3. Results and discussion

Results of validity confirmation are as follows: The recovery rates of Sr and Ni are 88.27±0.01% and 90.17±0.07%, respectively. Since the values are higher than our criterion, 85%, our separation process is validated.

Calibration has to be carried out regularly for reliability of measurement.

Due to ^{90}Y formation, it is better to measure ^{90}Sr by LSC as soon as possible after separation. The radioactivity of ^{90}Sr was corrected in this work.

4. Conclusion

We carried out the validity verification of the determination methods of ^{90}Sr and ^{63}Ni nuclides developed in KAERI. The results are expected to improve reliability of our radiochemical analysis for radioactive wastes disposal.

REFERENCES

[1] Notice No. 2020-11 of the Nuclear Safety and Security Commission (NSSC) (2020) Acceptance criteria for the delivery of low and intermediate level radioactive waste.

[2] Basavaraju A., Venkataramaiah P., Gopala K., and Sanjeeviah H., Inner bremsstrahlung accompanying beta decay in ^{90}Sr-^{90}Y, Phys. Rev. C, 28, 333-336 (1983).

[3] X. Hou, L. F. Østergaard, S. P. Nielsen, Determination of ^{63}Ni and ^{55Fe} in nuclear waste samples using radiochemical separation and liquid scintillation counting, Analytical Chimica Acta, 535, 297-307 (2005).

[4] C. H. Lee, M. Y. Suh, K. Y. Jee, and W. H. Kim, Rapid separation of nickel for ^{59}Ni and ^{63}Ni activity measurement in radioactive waste samples, J. Radioanal. Nucl. Chem., 298, 1221-1226 (2013).

[5] C. H. Lee, M. H. Lee, S. H. Han, Y. K. Ha, K. Song, Systematic radiochemical separation for the determination of ^{99}Tc, ^{90}Sr, ^{94}Nb, ^{55}Fe and ^{59,63}Ni in low and intermediate radioactive waste samples, J. Radioanal. Nucl. Chem., 288, 319-325 (2011).

Effect of H_2O Adsorption on Cladding Material

Dong Woo Lee [a], Sangjune Park [b], Ki-jeong Kim [c], Jeongmook Lee [a], Young-SangYoun [b], Jong-Yun Kim [a,d], and Sang Ho Lim [a,d,*]

[a]Nuclear Chemistry Research Team, Korea Atomic Energy Research Institute, Daejeon, Republic of Korea

[b]Department of Chemistry, Yeungnam University, Gyeongbuk, Republic of Korea

[c]Pohang Accelerator Laboratory, Pohang University of Science and Technology, Gyeongbuk, Republic of Korea

[d]Department of Radiochemistry & Nuclear Nonproliferation, University of Science and Technology, Daejeon, Republic of Korea

*slim@kaeri.re.kr

1. Introduction

Among the waste materials in nuclear plant process, zirconium and its alloys have been extensively used for cladding and structural materials. The cladding materials are mainly composed zirconium with interesting properties over other materials such as a low thermal neutron absorption cross-section, high corrosion resistance. Cladding materials serves to completely seal the nuclear fuels in the fuel rod to prevent the external release of fission products generated from nuclear fuels by irradiation. [1, 2]

In order to generate electrical energy, they are always contacted with water to transfer the heat energy produced from the nuclear fuels to water. Consequently, oxidation of the cladding surface by water is inevitable. Because this oxidation degrades the cladding performance, the reaction between the cladding and water should be studied to understand the oxidation phenomenon on the cladding surface.

The cladding material is fabricated with small quantities of niobium, tin, and iron, which are minor alloying elements, to improve the corrosion resistance and mechanical strength.

In this work, we performed experiments on the coverage and temperature dependence of cladding with H_2O adsorption using synchrotron-based high-resolution photoemission spectroscopy (HRPES). Because synchrotron based HRPES renders it possible to change the photon energy, we can obtain a highly surface-sensitive signal from materials based on the universal curve. We determined that even before the deposition of H_2O, the Zr 3d HRPES profile obtained from cladding material exhibited several peaks related to zirconium oxidation states, indicating that the surface of material comprises zirconium metal and zirconium oxides. After the exposure of experiment, the relative quantity of zirconium metal decreased, whereas the total zirconium oxide quantity including oxidation state of zirconium increased. Sequentially, we annealed a sample with H_2O adsorbed on cladding material to check the temperature dependence. To the best of our knowledge, the coverage and temperature dependence of cladding material with H_2O adsorption have not been systematically studied using synchrotron based HRPES.

2. Experimental

The sample preparation for the HRPES, cladding material was polished with 3000 grit SiC paper, and rinsed with deionized water. The amount of H_2O exposure is expressed in Langmuir (L) which is calculated as the product of the H_2O molecule pressure and the exposure time ($1L=10^{-6}$ Torr·s). HRPES data were obtained using the 8A2 beamline at the Pohang accelerator laboratory (PAL). All the core-level spectra of the sample with H_2O adsorbed on cladding materials were recorded at room temperature using a high-performance electron analyzer (SCIENTA2002, Sienta-Omicron) at photon energies of 400, 630, and 710 eV for Zr 3d, where the total spectral resolution at each photon energy was 0.15 eV, determined by measuring Au Fermi-edge. HRPES data were obtained with a pass energy of 20 eV for Zr 3d of 0.05 eV. All the spectra were measured in the normal-emission mode, and analyzed using a standard nonlinear least squares fitting procedure with Voigt functions.

3. Results and discussion

Fig. 1 shows the Zr 3d HRPES spectrum obtained from cladding material before the deposition of H_2O. As the primary analysis in this study involves the Zr 3d spectra, we reduced the photon energy up to 400 eV to obtain the most sensitive Zr 3d HRPES profiles.

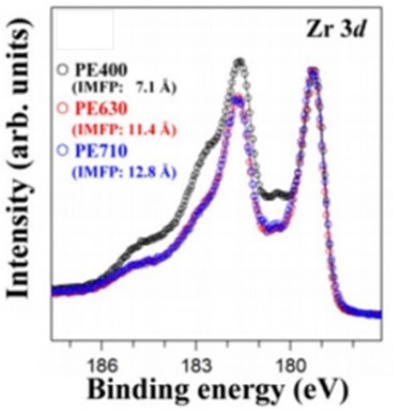


Fig. 1. (a) Zr 3*d* HRPES spectrum obtained from cladding material before the deposition of H_2O. Black, red, blue open circles in (a) indicate Zr 3*d* spectra acquired at the photon energies of 400, 630, and 710 eV, respectively, which were normalized using Zr $3d_{5/2}$ peak of zirconium metal at 179.3 eV.

Fig. 1 displays the Zr 3d spectra acquired at photon energies of 400, 630, and 710 eV, respectively. The Zr 3d profiles obtained at photon energies of 630 and 710 eV were similar; however, that obtained at 400 eV was different. The electron inelastic-mean-free-paths (IMFPs) at photon energies of 400, 630, and 710 eV for Zr 3d, using the NIST electron inelastic-mean-free-path database (Version 1.2) with an algorithm developed by Tanuma, Powell, and Penn. In particular, the IMFPs for Zr 3d indicates that the spectrum at a photon energy of 400 eV contains more surface information compared to the others. Therefore, only the Zr 3d spectrum measured at a photon energy of 400 eV will be considered henceforth.

4. Conclusions

In this research, we investigated the effect of the cladding with H_2O adsorption using synchrotron-based HRPES. Using the analysis of the Zr 3d, HRPES profiles obtained from cladding material before H_2O exposure, we measured the existence of various species in cladding. After the deposition of H_2O on cladding, the relative proportion of zirconium metal decreased, whereas that of the total zirconium oxides increased, indicating that H_2O reacted with zirconium metal in matrix.

ACKNOWLEDGEMENT

This work was supported by the National Research Foundation of Korea (NRF) grant funded by the Korean government (MSIP; No.2012M2A8A5 025925).

REFERENCES

[1] N. Yoshitaka, A. R. Krauss, L. Yuping, D. M. Gruen, Initial oxidation of zirconium and Zircaloy-2 with oxygen and water vapor at room temperature. J. Nucl. Mater. 228, 346–353, (1996).
[2] N. Stojilovic, E. T. Bender, R. D. Ramsier, High-temperature Auger electron spectroscopy of Zircaloy-4. Appl. Surf. Sci. 252, 1806–1811, (2005).

Measurement of Recovery for the Validation of Pretreatment Method in Decontamination Paper Samples

Kwang-Soon Choi*, Simon Oh, Jae-seok Lee, Hye-Ryun Cho, and Tae-Hong Park
Nuclear Chemistry Research Division, Korea Atomic Energy Research Institute, 111 Daedeok-daero-989, Yuseong-gu, Daejeon 34057, KOREA
*nkschoi@kaeri.re.kr

1. Introduction

Drums containing low and intermediate levels of radioactive waste samples have been managed temporarily at the Korea Atomic Energy Research Institute (KAERI). To dispose these wastes in a repository permanently, the Nuclear Safety and Security Commission (NSSC) has been specified the radioactive waste acceptance criteria. Therefore, the activity of nonvolatile nuclide such as ^{144}Ce, ^{58,60}Co, ^{137}Cs, ^{55}Fe, ^{94}Nb, ^{59,63}Ni, ^{90}Sr, ^{99}Tc, and total alpha in radioactive waste samples should be determined.

First of all, sample pretreatment is needed to measure the activity of alpha, beta and gamma emitting nuclides. Dry ashing method has been used for sample pretreatment because of allowing the decomposition of a large sample size [1]. And microwave digestion has been used to dissolve coal ash owing to advantage of high heating efficiency [2]. A quality assurance of sample pretreatment is very important to increase the reliability of the activity of nonvolatile nuclides measured.

2. Experiment

2.1 Dry ashing of sample

To validate the sample pretreatment method of dry radioactive waste samples such as paper, ICP-AES standard solutions of nine elements as shown in Table 1 were added to a sheet of decontamination paper in a glass beaker. Put the beaker in an electric furnace, and the temperature of the electric furnace was increased step wise from 200 to 450 ℃ in 50 ℃ increments, and maintained for 5 h at every step.

Table 1. The amount of 9 elements added

Element	Amount (μg)
Cs	100
U	200
Ce, Co, Ni	1000
Fe, Nb, Re, Sr	2000

2.2 Dissolution of ash produced

To enhance the solubility of Ce_2O_3, a produced ash was dissolved with H_2O_2. Two mL of H_2O_2 by dividing it by 0.5 mL was added to a microwave digestion vessel containing ash plus 10 mL of HNO_3. After each addition of 0.5 mL of H_2O_2, the microwave digestion vessel containing HNO_3 plus ash was heated on a hot plate at 200 ℃ for 3 min. Two mL of HCl and 0.25 mL of HF were added to the vessel, and the vessel was heated on a hot plate at 200 ℃ for 15 min. After cooling, a high-performance microwave digestion system was used to dissolve undissolved residue following heating on a hot plate.

2.3 Measurement of nine elements

For measurement of recovery in a solution of ash produced, eight elements such as Ce, Co, Fe, Nb, Ni, Re (surrogate of ^{99}Tc), Sr, U, and Cs were measured by ICP-AES and by ICP-MS, respectively.

3. Results & discussion

3.1 Dissolution of ash produced

The ash produced was completely dissolved by the above sample pretreatment method. If 2 mL of hydrogen peroxide (H_2O_2) is added at once, the solution overflows out of the vessel. Thus H_2O_2 was added with 0.5 mL increment.

3.2 Measurement of nine elements

Eight elements except Fe were quantitatively recovered. And the recovery of Fe was 118.1 % (2362 μg). Since the amount of Fe founded was greater than 2000 μg added, additional tests were conducted to see if Fe existed in the decontamination paper itself. The amount of Fe in a blank decontamination paper was 367 μg. Thus the amount of Fe in the sample was corrected to 1995 μg. The validation of the pretreatment method was verified since the recovery was within the range of 95~105%, as shown in Table 2, and the relative standard deviation was less than 10%.

Table 2. Recovery of 9 elements in decontamination paper

Element	Recovery (%)	SD
Ce	96.8	5.0
Co	98.4	3.8
Cs	98.0	1.3
Fe	99.8	5.4
Nb	101.5	3.4
Ni	99.9	5.0
Re	99.6	4.5
Sr	99.9	2.9
U	96.5	4.2

4. Conclusions

A sample treatment method for the dissolution of ash produced by heating decontamination paper was validated through measurement of recovery. Nine elements were quantitatively recovered using mixed acid including H_2O_2. This procedure will be applied to dry radioactive waste samples generated from nuclear power plant and nuclear research facility.

REFERENCES

[1] Ming Y, Bing L (1998) Determination of rare earth elements in human hair and wheat flour reference materials by inductively coupled plasma mass spectrometry with dry ashing and microwave digestion. Spectrochim Acta 53B:1447

[2] Low F, Zhang (2012) Microwave digestion for the quantification of inorganic elements in coal and coal ash using ICP-OES. Talanta 101:346

Determination of Reduction Yield of Metallic-Metal Oxide Products from Pyroprocessing of Spent Nuclear Fuels: Development of In-Hotcell Procedure

Young Hwan CHO*, Tae Hong Park, and Sang Eun Bae
Korea Atomic Energy Research Institute
*yhcho@kaeri.re.kr

1. Introduction

The current method of determining reduction yields of metal-oxide mixtures is the bromine method. Numerous studies have been conducted using this method [1]. However, there are many restrictions to apply this method under a highly radioactive environment. A modified bromine method has been developed to enable it to be carried out in a hot cell environment.

2. Modification of Bromine Method

2.1 Bromine method

Figure 1 shows the concept of chemical procedures of the bromine method. It is a multi-step process requiring various types of manipulations. It is extremely difficult to carry ut in a limited space and high radioactive hot cell. Modification of the procedures is required.

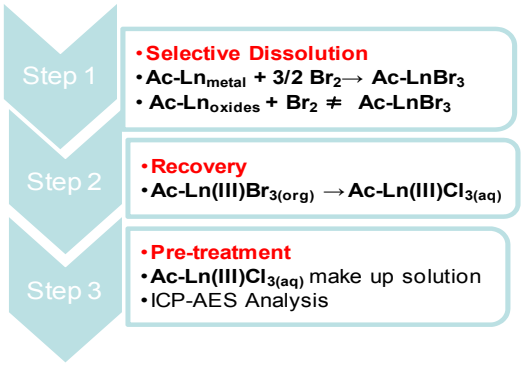


Fig. 1. Chemical scheme of bromine method.

2.2 Modification of the method

Some part of the procedures can be simplified through the pre-checking experiments. Figure 2 shows the comparison of the existing and modified method. For example, the centrifugation procedure for solid-liquid phase separation has been confirmed to be replaceable by filtering method.

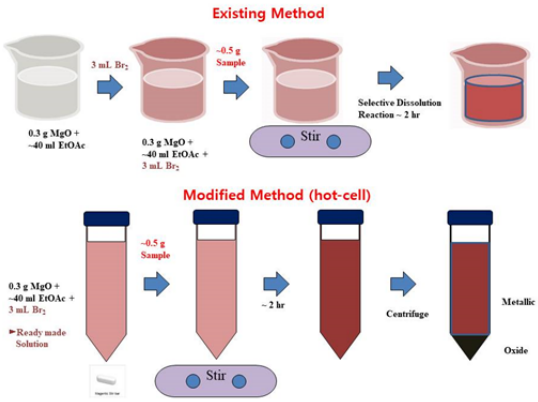


Fig.2. Comparison of (1) existing bromine method and (2) modified in-hotcell bromine method.

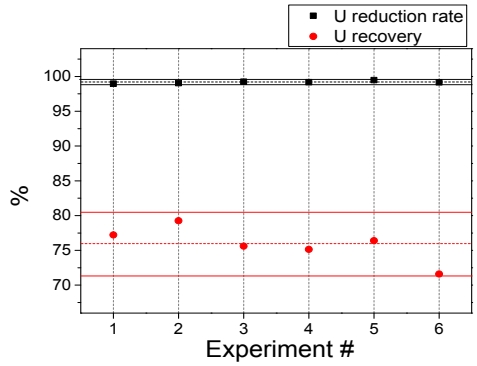


Fig. 3. Reduction yield of reference samples for in-hotcell bromine method validation.

Figure 3 verifies that the existing bromine method can be replaced with a new method.

Based on the modified procedure and pre-checked experimental data, the new bromine method applicable to the hot cell environment was developed [2]. This allows complicated bromine method procedures to be carried out efficiently even in narrow and highly radioactive hot cell.

Besides, a shielded ICP-AES system has been established. A home-made glove box system was interfaced with ICP-AES spectrometer, and performance test has been done. And a radiation resistant, hot cell space saving, modular type centrifuge has been designed and built for use inside of the chemical hot cell.

3. Summary

A modified bromine method has been developed to enable it to be carried out in a hot cell environment. The effectiveness of the new method has been verified through thorough experimental examination. This allows complicated bromine method procedures to be carried out efficiently even in narrow and highly radioactive hot cell.

REFERENCES

[1] Tae-Hong Park, Young-Hwan Cho, Byungman Kang, Jong-Goo Kim, Kyungwon Suh, Jihye Kim, Sang-Eun Bae, Jong-Yun Kim, Jeffery J. Giglio, Matthew M. Jones "Constituent analysis of metal and metal oxide in reduced SIMFUEL using bromine-ethyl acetate", J. Radioanaly Nucl Chem., 316, 1253-1259 (2018) and references therein.

In-Situ Qualitative Monitoring of Metal Ions in LiCl-KCl Melt

Chan-Yong Jung, Hwa-Kyeung Jeong, and Sang-Eun Bae*
Nuclear Chemistry Research Division, Korea Atomic Energy Research Institute
989-111 Daedeok-daero, Yuseong-gu, Daejeon, 34057, Korea
*sebae@kaeri.re.kr

1. Introduction

Pyrochemical process and molten salt process has attracted much attention in that the electrochemical process recovers the unreacted uranium and reduces the volume of high-level wastes in spent nuclear fuel. Since the uranium and transuranium (TRU) elements are recovered during the pyrochemical process [1,2], it is critical to monitor the nuclear material flow in the molten salt during the process operation. It is well known that electrochemical and spectroscopic techniques can be used to monitor the concentration of nuclear materials in the molten salts [1]. We investigated the electrochemical behavior and characterization of uranium and lanthanide elements in molten salts. Sometimes, it can be useful to easily monitor the formation and existence of the nuclear materials in the molten salts. In this work, we studied feasibility of the electrochemical technique for in-situ qualitative monitoring during the pyrochemical process.

2. Experimental

All the experiments were carried out in a glove box under Ar where O_2 and H_2O level were maintained to be less than 1 ppm. Lithium chloride (LiCl)/potassium chloride (KCl) eutectic salts (anhydrous beads), and silver chloride (AgCl) were obtained from Sigma Aldrich. Europium chloride ($EuCl_3$), samarium chloride ($SmCl_3$), and uranium chloride (UCl_3) were purchased from Alfa Aesar (purity ≥ 99.99%). Electrochemical measurements were performed in a quartz tube (20 mm in outer diameter and 2 mm in wall thickness). W wire (Alfa Aesar, dia. 0.2 mm) and glassy carbon (Alfa Aesar, dia. 2 mm) electrodes were used as the working and counter electrodes, respectively. The W wire electrode was mechanically polished with sand paper prior to use. The reference electrode was Ag wire immersed in 1 mol% AgCl-LiCl-KCl melt. The Electrochemical measurements were performed using a Gamry Reference 3000.

3. Results and Discussion

Fig.1 shows cyclic voltammograms (CV) obtained from W electrode immersed in LiCl-KCl containing uranium chloride and some lanthanides chloride. Around 0.4 V, -0.3 V and -0.9 V, the redox currents of $Eu^{2+/3+}$, $U^{3+/4+}$ and $Sm^{2+/3+}$ are observed. The currents for the lanthanide redox reactions increased as the lanthanide ions were added. These results mean that the redox reactions of U and lanthanide ions are not interrupted each other.

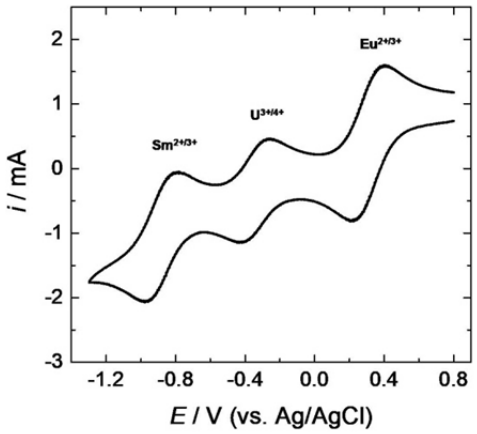


Fig. 1. CV results obtained from W wire in LiCl-KCl melt containing uranium chloride, europium chloride, and samarium chloride.

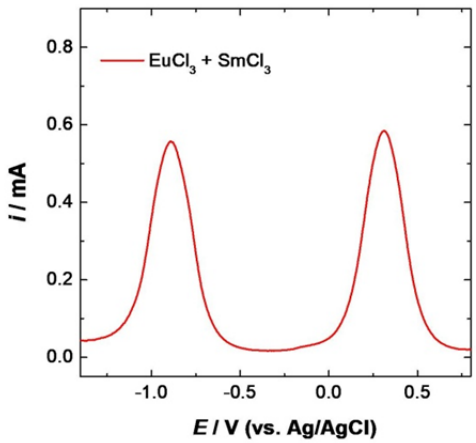


Fig. 2. SWV results obtained from W wire in LiCl-KCl melt containing europium chloride and samarium chloride.

Fig. 2 shows square wave voltammetry (SWV) results obtained from W electrode immersed in

LiCl-KCl containing europium and samarium chloride. In the square wave voltammetric curve, the currents at +0.3 V and -0.95 V are observed, attributed to reduction of Eu(III) and Sm(III), respectively. As the concentrations of europium and samarium chlorides and the number of the electrons during the reactions are the same each other, the current response and FWHM are almost similar. The results indicate that it can be useful for extracting information about the existence of the metal ions in the melt.

4. Conclusion

To develop an in-situ qualitative monitoring for use in the pyrochemical, electrochemical techniques, CV and SWV, were tested. The currents in the CV and SWV results appeared at the same potential region. The electrochemical reactions of uranium and lanthanide ions were not perturbed by one another. This means that the CV and SWV can be used for in-situ qualitative analysis of uranium and lanthanide ions in the molten salt.

REFERENCES

[1] D.-H. Kim, S.-E. Bae, T.-H. Park, J.-Y. Kim, C.-W. Lee, and K. Song, Microchemical Journal, 114, 261-265 (2014).

[2] T. Inoue, L. Koch, Development of Pyroprocessing and its future direction, Nucl. Eng. & Technol., 40, 183-190 (2008).

[3] Y.J. Park, S.-E. Bae, Y.H. Cho, J.Y. Kim, K. Song, UV–vis absorption spectroscopic study for on-line monitoring of uranium concentration in LiCl–KCl eutectic salt, Microchem. Journal, 99, 170-173 (2011).

Determination of EDTA in Radioactive Wastes in the Presence of Iron Using UV-Vis Spectrophotometer

Hyejin Cho* and Jail Park
Korea Atomic Energy Research Institute, 111 Daedeok-daero-989, Yuseong-gu, Daejeon 34057
*hcho921@kaeri.re.kr

1. Introduction

A variety of chemical decontamination processes are used to remove the build-up of radioactive-activated metals and corrosion products from the cooling systems of nuclear power plants. All of these decontamination processes use chelating agents, such as ethylene diamine tetra acetic acid (EDTA), nitrile tri acetic acid (NTA), oxalic acid, and citric acid, to complex the released radionuclides. However, these chelating agents, enhancing the mobility of radionuclides and actinides from the depository, are potentially harmful to the environment [1, 2]. Due to the vital importance of EDTA analysis in radioactive wastes from the point of view of environmental analytical chemistry, several analytical methods have been reported for its quantitative assay. Among these, the xylenol orange (XO) indicating method has been selected as a suitable method for radwastes with good performance. However, the precision and accuracy of the analysis were considerably decreased in the presence of iron in the samples when using the XO indicating method. In this study, the effects of Fe(II) and Fe(III) to determine the concentration of EDTA were investigated.

2. Results and Discussions

The intensity of the red-colored zirconium-XO complex formed in a strong acid medium is reduced in the presence of free EDTA or its metallic complexes through formation of a more stable zirconium-EDTA complex. The reduction in color intensity is a measure of total EDTA in the sample reported as mg/L of EDTA. This method involves an extraction process and sequential measurements of transmittance at a specific wavelength, at 535 nm, is spectrophotometer to determine the wt % of EDTA in a solution.

Chemical decontamination using EDTA involves the dissolution of metal oxides from the system's surfaces. Thus, it is very possible for radwastes to have EDTA and other metal oxides or metal-EDTA complexes. Among them, iron oxides are one of the most common metal oxides and are widespread in the nuclear industry. Also, EDTA has a high affinity for ferric ions, so the effects of ferric ions should be considered for precise analysis of EDTA.

The solution including 10 ppm of EDTA shows the value of 25 % transmittance (% T) by UV-vis spectrophotometric analysis. The spectrum, presented in Fig 2, shows that the addition of Fe(II) (red line) and Fe(III) (blue line) to the 10 ppm EDTA solution, the value of % T is decreased to 22 and 11 % T, respectively. This result explains that the presence of Fe(III) in the solution significantly affects to the EDTA analysis while Fe(II) has less effects on the analytic results.

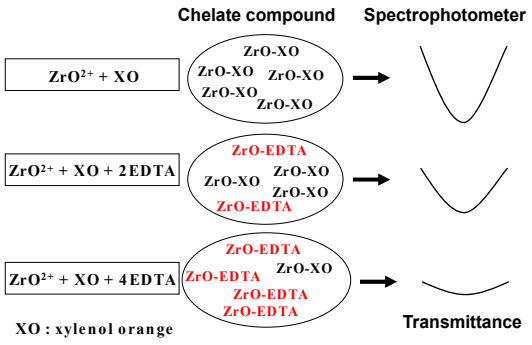


Fig. 1. Principle of EDTA determination.

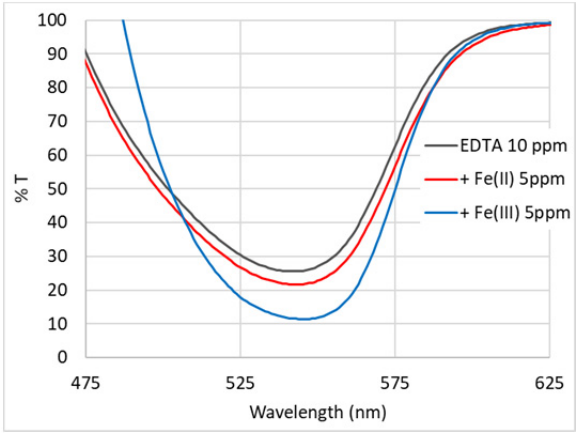


Fig. 2. The effects of Fe(II) and Fe(III) in the determination of EDTA concentration.

More detailed experimental results will be discussed.

3. Conclusion

The contents of EDTA in radioactive wastes are required to be thoroughly analyzed for the secured disposal. Thus, the XO method was successfully applied for the determination of EDTA. However, it is found that the precise analysis of EDTA cannot be conducted in Fe(III) containing solutions. In order to explain this behavior, further experiments will be carried out in the near future.

REFERENCES

[1] J. L. Means, D. A. Crear, and J. O. Duguid, “Migration of radioactive wastes: radionuclide mobilization by complexing agents”, Science, 200(4349), 1477-1481 (1978).
[2] M. Sillanpaa, and M. L. Sihvonen, “Analysis of EDTA and DTPA”, Talanta, 44(8), 1487-1497 (1997).

Synthesis of Actinide Chloride Complexes from Actinide Oxide in High Temperature Molten Salt

Hwakyeung Jeong and Sang-Eun Bae*
Nuclear Chemistry Research Division, Korea Atomic Energy Research Institute, 111 Daedeok-daero 989 beon-gil, Yuseong-gu, Daejeon, 34057, Republic of Korea
*sebae@kaeri.re.kr

1. Introduction

As lanthanide and actinide oxides are not fully reduced to their metal form during an electro-reduction process, it is needed to find a way to covert the lanthanide / actinide oxides to chloride complexes in a pyrochemical process [1]. Recently, molten salt reactor (MSR) has attracted much attention. In the MSR, the molten salt containing the actinide halogen complexes are used as a coolant [2]. Therefore, it is also important to synthesize a lanthanide / actinide chloride complex for studying the chemical and physicochemical behaviors of the MSR coolant. In this work, we studied that the actinide chloride can be achieved from its oxide forms in LiCl/KCl molten salt by using aluminum chloride.

2. Experimental

Lithium chloride/potassium chloride (LiCl /KCl) eutectic salts, Aluminum chloride ($AlCl_3$), and Lithium oxide (Li_2O) were obtained from Sigma Aldrich. Thorium dioxide was supplied from KAERI stock material. All the experiments were carried out in a glove box under Ar where O_2 and H_2O level were maintained to be less than 1 ppm. Electrochemical measurements were performed in a quartz tube (20 mm in outer diameter). W wire (Alfa Aesar, dia. 0.2 mm, S= 0.21 cm^2) and glassy carbon (Alfa Aesar, dia. 2 mm) electrodes were used as the working and counter electrodes, respectively. The W wire electrode was mechanically polished with sand paper prior to use. The reference electrode was Ag wire immersed in 2.5 mol% AgCl-LiCl-KCl melt. The Electrochemical measurements were performed using a Gamry Reference 3000.

3. Results and Discussion

In order to conversion of the actinide dioxide to the actinide chloride complex in LiCl-KCl melt, we chose ThO_2 as a representative of actinide dioxides.

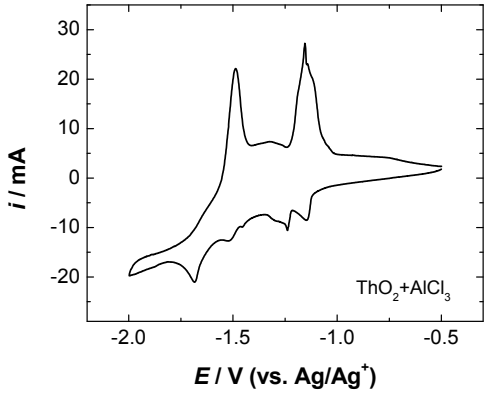


Fig. 1. Cyclic voltammogram obtained from a W wire (S= 0.21 cm^2) immersed in LiCl-KCl melt containing 1 wt% ThO_2 and 1 wt% $AlCl_3$. Scan rate= 200 mVs^{-1}. Temperature= 773 K.

In this work we introduced $AlCl_3$ into the melt to dissolve ThO_2 and to get rid of the oxygen from the oxide. Fig. 1 shows a cyclic voltammogram obtained from a W wire immersed in LiCl-KCl melt containing ThO_2 after the addition of $AlCl_3$. $AlCl_3$ is gasified to Al_2Cl_6, which is highly reactive with oxygen and provides chloride ions. The mechanism of the reaction can be described as shown below [2].

$$3ThO_2(s) + 2Al_2Cl_6(l) \rightarrow 3ThCl_4(l) + 2Al_2O_3(s) \quad (1)$$

Pair of peaks at -1.67 and -1.5 V is attributed to the electrodeposition and dissolution reactions of Th, and the other peaks may be related to the formations of Al and Th-Al alloy. The peaks at -1.67 and -1.5 V denote that the $ThCl_4$ was produced in the melt. Since the amount of $AlCl_3$ was added in excess compared to ThO_2, it can be expected that Al^{3+} still remains in the molten salt so that it is needed to remove the Al^{3+} from the melt. In order to get rid of the Al^{3+}, we investigated the change in electrochemical behavior while adding Li_2O.

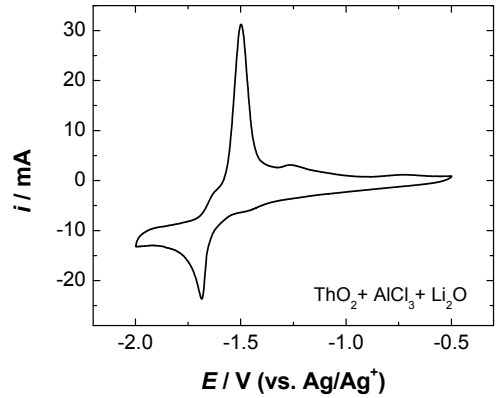


Fig. 2. Cyclic voltammograms obtained from a W wire (S= 0.21 cm^2) immersed in LiCl-KCl melt containing 1 wt% ThO_2, 1 wt% $AlCl_3$ and Li_2O. Scan rate= 200 mVs^{-1}. Temperature= 773 K.

Fig. 2 shows a cyclic voltammogram obtained after Li_2O was stoichiometrically added. As the time went by, all of the peaks related to Al disappeared and only the peaks of Th remained. This result indicates that the Al^{3+} was removed from the melt by adding the oxygen ion. Thus, $ThCl_4$ was successfully produced in the LiCl-KCl.

Acknowledgement

This work was supported under the mid- and long-term nuclear research and development program through the National Research Foundation of Korea (NRF-2017M2A8A5014716) funded by the Korean Ministry of Science and ICT.

References

[1] Sang-Eun Bae,* Dong-Chul Choi, and Tae-Hong Park*, Proceedings of the Korean Radioactive Waste Society Conference, 604-605 (2018).
[2] Ya-Lan Liu, Yong-De Yan, Wei Han, Mi-Lin Zhang*, Li-Yong Yuan, Kui Liu, Guo-An Ye, Hui He, Zhi-Fang Chai and Wei-Qun Shi*, RSC Advances, 3, 23539-23547 (2013).

Studies on the Chemical Synthesis and Characterization of Lead (II) Oxide Nanoparticles Prepared With Cationic, Anionic and Non-ionic Surfactants

Viktoriya Kim[1,2], Dong Woo Lee[2], Jung Hwan Park[1,3], Jeongmook Lee[2], Tae-Hyeong Kim[2], Jong-Yun Kim[1,2], and Sang Ho Lim[1,2,*]
[1]Radiochemistry and Nuclear Nonproliferation, University of Science and Technology, Republic of Korea
[2]Korea Atomic Energy Research Institute, Republic of Korea
[3]Department of Nuclear & Quantum Engineering, Korea Advanced Institute of Science and Technology, Republic of Korea
*slim@kaeri.re.kr

1. Introduction

Lead oxide exists in many forms such as PbO, PbO_2, Pb_2O_3, and Pb_3O_4. Recently, PbO has attracted more attention, due to its use as an important industrial material, which has been widely utilized in batteries, gas sensors, pigments and paints, ceramics, and glass industry and as a catalyst in synthetic organic chemistry [1]. Lead oxide has two different crystalline crystal structures α-PbO (tetragonal form) and β-PbO (orthorhombic form). PbO nanoparticles' morphologies can play important roles in their properties. Lead oxide may appear in a various forms including nanoplates, nanostars and nanodendrites [2], nanorods, nanopowders, nanosheets and nanotubes [3].

This present work describes the chemical synthesis of lead oxide nanoparticles using lead (II) acetate as precursor in the presence of various cationic, anionic and non-ionic surfactants. Surfactants were used to control the size and morphology of producing PbO nanoparticles. The effects of surfactants, temperature and catalyst addition rate on lead oxide formation was studied. The size, morphology and crystal of PbO particles were analysed using scanning electron microscope (SEM), transmission electron microscopy (TEM) and X-ray powder diffraction (XRD).

2. Experimental details

2.1 Materials

All chemicals and reagents in this work were used as received without further purification: lead (II) acetate trihydrate (Thermo Fisher, 99%), sodium hydroxide (Merck, 99%), cetyltrimethylammonium chloride (CTAC, Fluka, ≥98%), cetyltrimethylammonium bromide (CTAB, Sigma-Aldrich, 95%), sodium dodecyl sulfate (NaSDS, Sigma-Aldrich, ≥99%), polyoxyethylene sorbitol (Tween 20, Sigma-Aldrich), sorbitan tristearate (Span 65, Sigma-Aldrich), *polyvinyl alcohol* (PVA, Sigma-Aldrich, 99%).

2.2 Lead oxide synthesis

As illustrated in Figure 1, 10 mL of the aqueous surfactant solution whose concentration was 3xCMC (Critical Micelle Concentration depends on the type of surfactant) was mixed with 50 mL of 0.8 M $Pb(C_2H_3O_2)_2 \cdot 3H_2O$ in de-ionized water (step 1) and stirred on a magnetic stirrer at room temperature for 1 hour (step 2), then the resultant solution was heated to 60-90 ºC, after that 50 mL of 14.5 M NaOH in de-ionized water was added slowly (average rate ranged from 6 to 48 drops per minute) (step 3) and stirred on a magnetic stirrer at 60 - 90 ºC for 1 hour after adding the entire volume of NaOH. At this stage, the colour of the suspension solution turned to red-orange, indicating the formation of lead (II) oxide. The resultant precipitate was filtered on a Buchner funnel, washed with de-ionized water and ethanol repeatedly, then dried in a drying oven at 100 ºC for two hours and at 240 ºC for another two hours, after filtration the dried precipitate was ground in a mortar.

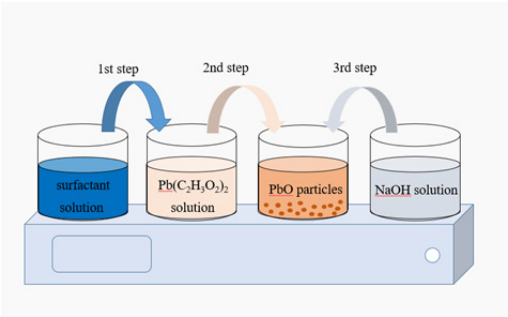


Fig. 1. Schematic illustration of PbO synthesis.

3. Results and discussion

The obtained SEM results indicated that the average size of the lead oxide particles synthesized without the use of surfactants was 5 μm, in the presence of the surfactants CTAC and PVA the size decreased fifty times 0.1 μm. In addition, in the presence of the same surfactants, lead oxide

without impurities was successfully synthesized and confirmed by the results of XRD.

Table 1. General table of experimental conditions and obtained results

I.D.	Surfactant	C[1] [mM]	T[2] [ºC]	PbO	D[3] [μm]
1	Without surfactant	-	90	V_i[4]	5-10
2	CTAC	3.3	60	V[5]	0.1-0.5
3	NaSDS	24.6	60	X[6]	~10
4	Tween 20 /Span 65	0.18 /0.06	60	X[6]	5-7
5	Tween 20	0.18	60	X[6]	1-3
6	PVA	0.3	60	V[5]	0.1-0.5
7	CTAB/ Span 65	2.7 /0.06	80	V_i[4]	1-2

[1]C: concentration of surfactants
[2]T: temperature of solution when adding catalyst
[3]D: size of synthesized PbO particles
[4]V_i: formation of lead oxide with impurities of unknown origin
[5]V: formation of pure lead oxide
[6]X: no formation of pure lead oxide

As can be seen in Table 1, in the case of using NaSDS, Tween 20/Span 65, Tween 20 surfactants, the formation of lead oxide did not occur, with the use of CTAB/Span 65 surfactants, the formation of lead oxide occurred, but with unknown impurities, the size of the PbO particles varied on average from 1 to 7 μm.

4. Conclusion

Chemical synthesis of PbO nanoparticles has been carried out with cationic, anionic and non-ionic surfactants. Studies have shown that in the presence of surfactants PVA and CTAC the size of synthesized particles decreases from 5 μm to 0.1 μm, due to the properties of surfactants to prevent particle aggregation and stabilize them.

REFERENCES

[1] A. Bratovcic, “Synthesis, Characterization, Applications, and Toxicity of Lead Oxide Nanoparticles”, Intech Open (2020).
[2] K.C. Chen, C.W. Wang, Y.I. Lee, H.G. Liu. “Nanoflakes and nanostars of β-PbO formed at the air/water interface”. J. Colloids and Surfaces A: Physicochemical and Engineering Aspects, 373(1-3), 124-129 (2011).
[3] L. Shi, Y. Xu, Q. Li, “Controlled growth of lead oxide nanosheets, scrolled nanotubes, and nanorods. Crystal Growth Design, 8(10), 3521-3525 (2008).

Characterization of Material for Immobilization of Radioactive Waste : Structure, Leaching Test, and γ-Irradiation

Hye Ran Noh[1,2], Dong-Woo Lee[2], Tae-Hyeong Kim[2], Jeongmook Lee[2], Jong-Yun Kim[1,2], and Sang Ho Lim[1,2,*]
[1] Radiochemistry and Nuclear Nonproliferation, University of Science and Technology, Daegeon 34113, Republic of Korea
[2] Nuclear Chemistry Research Division, Korea Atomic Energy Research Institute, Daejeon 34057, Republic of Korea
*slim@kaeri.re.kr

1. Introduction

Immobilization of high-level waste (HLW) radionuclides is still an international challenge that has occupied much attention. One way to effectively dispose of HLW would be to immobilize them into inert and stable host materials such as glass or crystalline phases. Up to now, a number of host phases including britholites, monazite, synroc and zircon are being considered to act as waste forms materials. Unlike previous studies, we propose to apply new candidate material for the immobilization, Titanium Tellurium Oxide, $TiTe_3O_8$. The primary motivation that let us to experiment is it can be possible to contain various multivalent cations (Er^{3+}, Ce^{4+} and Te^{6+}) at the Ti^{4+} site [1, 2] and has excellent acid resistance. In this study, we would evaluate its susceptibilities to leaching and *γ*-irradiation under conditions which may exist in geologic storage sites.

2. Experimental

2.1 Materials and preparation

We used the solid-state reaction method to prepare $TiTe_3O_8$ pellets by combining TiO2 (SHOWN, 99.0%) and TeO2 (Alfa Aesar, 99+%) in a molar ratio of 1:3 respectively. The mixture calcination was carried out during 12 h at 650 °C and then cooled to room temperature.

2.2 Leaching experiments

The leaching experiment was performed using the MCC-1(Materials Characterization Center-1) method (90 °C, 7 days), and were additionally performed with 0.01M HCl and 0.01M NaOH solutions to see chemical durabilities at acidic and alkaline conditions.

2.3 γ-irradiation experiment

Prior to irradiation, the pellet was put into a bottle and irradiated by ^{60}Co γ-rays (Korea Atomic Energy Research Institute, Jeongeup) in air with dose of 10 kGy during an hour.

2.4 X-ray diffraction (XRD)

XRD patterns were performed with a Bruker AXS D8 Advance X-ray Diffractometer using Cu Kα radiation. XRD data was collected in the range from 10° to 80° using a 0.02° step size.

3. Results and Discussion

3.1 Structure of $TiTe_3O_8$

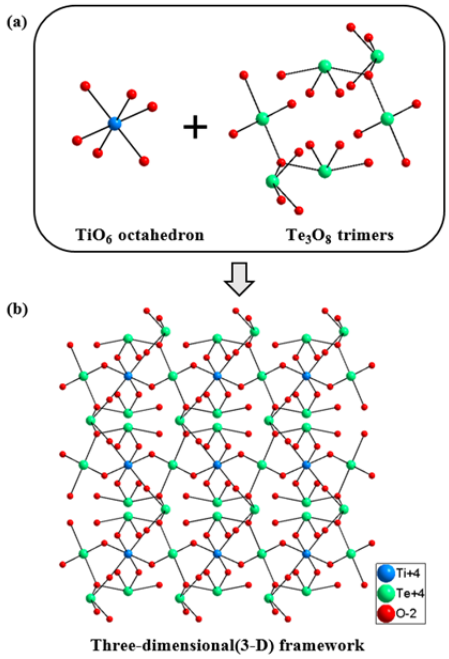


Fig. 1. Ball-and-stick representations of (a) TiO_6 octahedron and Te_3O_8 trimers by corner sharing of TeO_4 seesaw groups (b) a framework of $TiTe_3O_8$.

The titanium tellurite, $TiTe_3O_8$ crystallizes in the cubic space group *Ia-3* (206) with 3-D framework structure. The framework backbone is composed of TiO_6 octahedra and TeO_4 polyhedra containing Ti–O–Te and Te–O–Te bonds. The Ti^{4+} cation is connected to six oxygen atoms in an octahedral coordination environment. The Te^{4+} cation is bonded to four oxygen atoms in seesaw environments. And the three TeO_4 polyhedra share their corners through one O atom and form Te_3O_8 trimers. The Ti^{4+} cation is shared by

two Te_3O_8 trimers in an asymmetric coordination environment. Each trimer is further connected by a TiO_6 octahedron along the [100] direction, which results in infinite bands running through the [010] direction, thereby resulting in the formation of a 3-D framework.

3.2 Leaching experiment

In Fig. 2, XRD patterns of leached samples at HCl (pH 2.0), deionized water (pH 6.6) and NaOH (pH 12.0) are shown. All patterns are the same as those of sample before leaching, regardless of acidic and alkaline conditions. It means it has excellent aqueous/chemical durability as there are no huge variations in the crystal structure.

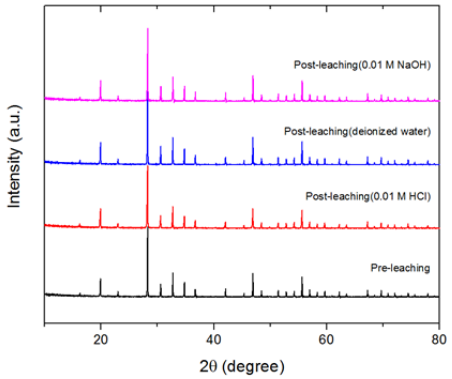


Fig. 2. XRD patterns of pre- and post-leach $TiTe_3O_8$ at various pH-values from pH 2 to pH 12 range.

3.3 γ-irradiation experiment

Fig. 3 shows the XRD patterns of the sample both before and after γ-irradation. The pattern was similar to that of the pristine sample and no special peak and shift were observed. In other words, it indicates that new material or phase wasn't formed and total volume expansion wasn't observed. Furthermore, there is no significant decrease in intensity in a specific peak, so it is not considered its crystalline was rendered amorphous.

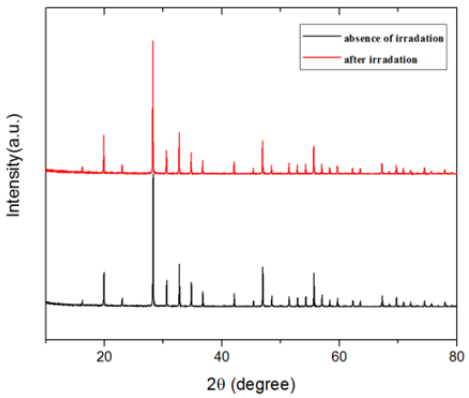


Fig. 3. XRD patterns of $TiTe_3O_8$ under γ -ray irradiation.

4. Conclusion

From $TiTe_3O_8$, we observed its stability of structure under leaching and γ-ray irradiation. In leaching experiment, there are no huge variations in the crystal structure regardless of pH and thus we can explain it has excellent aqueous/chemical durability. In γ-irradiation testing, it shows worthwhile radiation resistance toward its chemical structure and crystal structure. In addition to these experiments, we will conduct further experiments to verify whether the leach rate is within acceptable limits for immobilization.

REFERENCES

[1] N. Ghrini, R. Karray, J.P. Laval, A. Kabadou, A. Ben Salah, "X-ray powder diffraction and Raman vibrational study of new doped compound $TiTe_3O_8:Ce^{4+}$", J. Mater. Environ. Sci. 6, 989-996 (2015).

[2] I.B. Ayed, S. Elleuch, A.B. Ahmed, A. Kabadou, "Effect of erbium doping on vibrational and optical properties of $TiTe_3O_8$" J. Alloy. Compd. 791, 1088-1097 (2019).

Determination of Lanthanides in a High Salt Matrix Using Liquid-Liquid Extraction

Jihye Kim* and Sang-Eun Bae
Nuclear Chemistry Research Team, Korea Atomic Energy Research Institute, Daejeon 34057, Korea
*jihyekim21@kaeri.re.kr

1. Introduction

Lanthanides (Ln) have been widely applied to many fields of geology, biology, and agriculture. The determination of lanthanides has been reported using various analytical techniques such as inductively coupled plasma optical emission spectrometry (ICP-OES), inductively coupled plasma mass spectrometry (ICP-MS), ion chromatography (IC), and capillary electrophoresis (CE). However, most analytical methods for measuring trace lanthanides have not been validated for highly saline samples. Here we have developed a liquid-liquid extraction (LLE) technique for sample pretreatment from high salt matrix such as seawater (~ 0.6 M NaCl).

LLE as the most common sample treatment technique has been used for sample cleanup and pre-concentration of lanthanides. LLE is simple, robust, and compatible with many analytical techniques such as ICP-OES, ICP-MS, and CE. In this study, the parameters influencing the LLE of lanthanides were investigated. For extraction of lanthanides, bis(2-ethylhexyl) phosphate (HDEHP) was used as a carrier in heptane solvent. To return the lanthanides from a heptane solvent to an aqueous phase (termed back extraction process), high concentration of acidic aqueous solution (6 M HCl) and octanol was used to dissociate the Ln-HDEHP complexes. Under the optimized conditions, the extraction recoveries were ~100% for 12 lanthanides in 0.6 M NaCl.

2. Materials and methods

2.1 Liquid-Liquid extraction

Lanthanides sample solution (donor phase, pH 2.5) was prepared in 0.6 M NaCl (such as seawater). A 10 mL of donor solution containing lanthanides was transferred into the vial. A 1 mL of organic phase (0.25 M bis(2-ethylhexyl) phosphate as a carrier in heptane) was added on the top of the donor solution. Extraction was done by vortexing vigorously for 10 min. After extraction, the phases were separated by centrifugation at 3000 g for 10 min and the donor phase was discarded by a pipet. The principle of the extraction of Lns was demonstrated as Fig. 1.

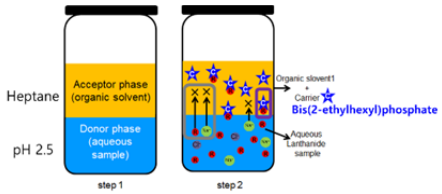


Fig. 1. LLE principle for the extraction of Lns from highly saline sample.

To remove the carrier in a final step of extracts and to decrease the Ln-HDEHP complexes, back extraction method was added to this LLE process. 1 mL of octanol was added into the organic phase (extract). Back extraction was achieved with four times, sequential steps using 1 mL of 6 M HCl. In the back extraction process, the final sample extracts were mixed for 10 min and then separated by centrifugation at 3000 g for 10 min. After centrifugation, two organic phases (heptane and octanol) were discarded and the aqueous phase was transferred to a new vial. After extraction, the aqueous phase (final volume of 4 mL) was injected into ICP-MS to measure the extraction recovery. The modified LLE principle and procedure are shown in Fig. 2 and Fig. 3, respectively.

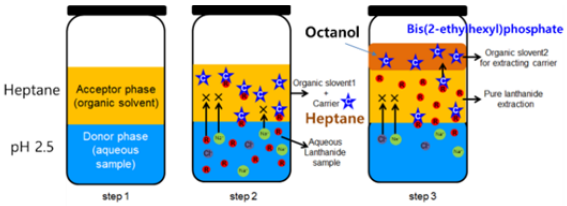


Fig. 2. Modified LLE principle for the extraction of Lns from highly saline sample (included back extraction).

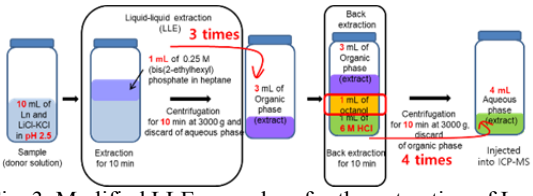


Fig. 3. Modified LLE procedure for the extraction of Lns from highly saline sample.

3. Results and discussion

The extraction of lanthanides from the aqueous to organic phase can be calculated using K values (partition coefficient). The fraction of

total Lns transferred to organic phase is (1-q, q: the fraction Lns), and the molarity in organic phase is (1-q)m/V_2. (Here, V_1 is the volume of aqueous phase and V_2 is the volume of organic phase) The fraction remaining in aqueous phase after 1st extraction is calculated by eq 1.

$$q = \frac{v_1}{v_1 + Kv_2} \quad (1)$$

After n extractions, each with volume V_2, the fraction remaining in the aqueous phase is shown in eq 2.

$$q^n = \left(\frac{v_1}{v_1 + Kv_2}\right)^n \quad (2)$$

Thus, many small extractions are more effective than a few large extractions. We optimized the extraction step by comparing sequential extractions from Fig. 4. In this study, 3 times extraction steps were performed from aqueous phase to organic phase to achieve the high extraction efficiency.

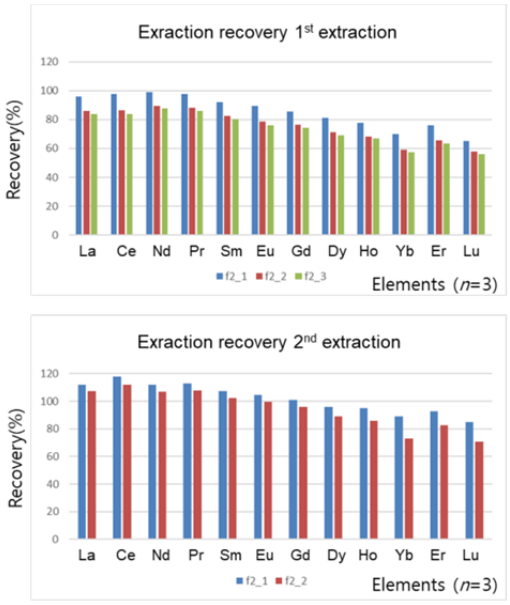
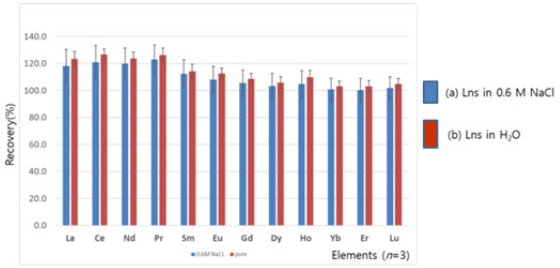


Fig. 4. Extraction recoveries (a) 1st extraction and (b) lanthanides from aqueous phase to organic phase.

Fig. 5 described the extraction efficiencies using optimum conditions. Most cases, 100% extraction recoveries for Lns were achieved by liquid-liquid extraction from highly saline sample. Further, the extraction recoveries were very similar to the extraction recoveries of Lns in pure water.



Donor phase: La, Ce, Nd, Pr, Sm, Eu, Gd, Dy, Ho, Yb, Er, Lu (0.6 M NaCl or not)
Organic phase: heptane + 0.25 M carrier [bis(2-ethlyhexyl)phosphate]
Back extraction: 6 M HCl with octanol

Fig. 5. Comparison of extraction recoveries between (a) lanthanides in a high salt matrix and (b) lanthanides in pure water.

4. Conclusions

LLE has developed for the extraction of 12 Lns in a high salt matrix (0.6 M NaCl such as seawater). The modified LLE was included the back extraction step to remove the carrier and to decrease the Ln-HDEHP complexes. The advantages of this proposed method are good extraction efficiencies (~100%) and good sample cleanup. Furthermore, this proposed method is applicable to determination of trace amounts of Lns in spent fuel cell containing molten LiCl-KCl salt.

Reference

[1] C.W. Noack, D. A. Dzombak, and A.K. Karamalidis "Determination of rare earth elements in hypersaline solutions using low-volume, liquid-liquid extraction" Environmental Science & Technology 49, 9423-9430 (2015).

Sample Preparation and Characterization of ε- Particles in CeO_2

Hyun Myung Choe[1,2], Hye Ran Noh[2,3], Dong Woo Lee[2], Jeongmook Lee[2], Junghwan Park[2], Tae-Hyeong Kim[2], Jong-Yun Kim[2,3], and Sang Ho Lim[2,3,*]
[1]Department of Chemistry, Sogang University, Seoul, Republic of Korea
[2] Korea Atomic Energy Research Institute, 111, Daejeon, Republic of Korea
[3] University of Science & Technology, Daejeon, Republic of Korea
*slim@kaeri.re.kr

1. Introduction

The deep geological disposal method has been internationally considered as the final disposal of spent nuclear fuels (SNFs) [1]. This method has risks such as the exposure of SNFs to groundwater due to container failure or unpredictable natural disasters. SNF is a complex, heterogeneous system in terms of its chemical composition and microstructure. The irradiated oxide fuel forms a complex multiphasic system containing >30 fission products. The noble metals group, which is represented in SNF mainly by Mo, Ru, Rh, Pd, and Tc, is not incorporated in the crystal lattice of UO_2 but found as metallic inclusions trapped in the inter and intragranular pores and in the grain boundaries. [2] ε-particle is the metallic phase that forms as inclusions at the grain boundaries in the UO_2 fuel during reactor operation. This metal is composed of Pd, Mo, Rh, Ru, and Tc [3]. This difference in behaviours observed with and without ε-particle present indicates a clear role for these particles in suppressing the oxidation of UO_2. The most likely explanation is that the H_2 dissociation reaction is catalyzed on these particles, which act as galvanically coupled anodes within the fuel matrix, leading to a decrease in inhibition of UO_2 oxidation/corrosion [4].

This study uses CeO_2 as a surrogate for UO_2. It has the same cubic crystal structure (space group no.225) with almost the same lattice parameters (CeO_2 = 0.5411nm and UO_2 = 0.5471), and not much has been studied with CeO_2. So, there is little information about the effect ε-particles on the physicochemical properties of the manufacturing method of CeO_2 containing ε-particle and its structural characterization. Thus, we studied the sample preparation and characterization of ε-particles in CeO_2.

2. Experimental

The CeO_2 (99.995%, Sigma Aldrich), MoO_2 (99%, Sigma Aldrich), and MoO_3 (99.98%, Sigma Aldrich) (MoO_2 and MoO_3 weighed as 0, 1, 3, 5 wt%) powders were mixed and pelletized. The sample pellets were sintered in the tube furnace at 1100℃ for 18h with an H_2 atmosphere. The surface morphologies of prepared pellets were observed by scanning electron microscope (SEM), energy dispersive X-ray spectroscopy (EDS) (JEOL, JSM-6610LV), X-ray diffraction (XRD) data were obtained by Bruker D8 Advance system in the 2θ range of 5°to 120° with a scanning step of 0.02°/0.1s and using Cu Kα line source (beam current 40Ma at 40Kv) at room temperature. The lattice parameters of the samples were calculated from XRD spectra with refinement.

3. Results

CeO_2 and MoO_2 or MoO_3 were sintered using a tube furnace. The SEM image can confirm the structure before and after the sample, and it can be confirmed that ε- particles exist at the CeO_2 grain boundary. Figure 1 shows the XRD powder pattern before sintering. In the $Ce_{0.95}Mo_{0.05}O_{2+X}$ pattern, MoO_3 picks could be identified. After XRD measurement before and after sintering, a comparative analysis was performed.

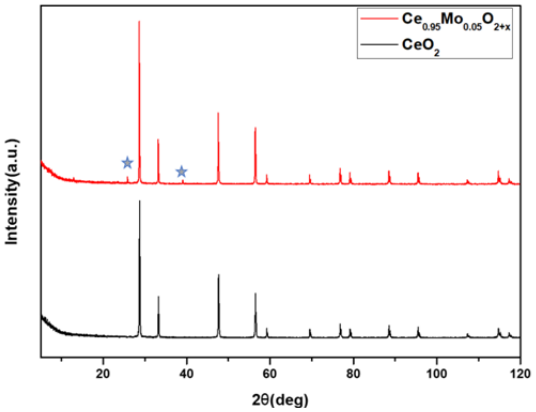


Fig. 1. X-ray diffraction patterns data for CeO_2 and $Ce_{0.95}Mo_{0.05}O_{2+x}$ (★:MoO_3).

4. Conclusion

The formation of ε -particles at the grain boundaries of CeO_2 was analyzed through SEM. And the overall distribution of the sample was

analyzed through EDS mapping. And the structure formation analysis was performed through XRD measurement before and after sintering.

REFERENCES

[1] Kleykamp, H. The chemical state of the fission products in oxide fuels. J. Nucl. Mater. 131, 221–246 (1985).

[2] Cordara, T. Microstructural evolution of UO2 pellets containing metallic particles of Ru, Rh and Pd during dissolution in nitric acid solution: 3D-ESEM monitoring. Hydrometallurgy, 188(July), 182–193 (2019).

[3] Zhu, Z., Noël, J. J. & Shoesmith, D. W. Hydrogen peroxide decomposition on simulated nuclear fuel bicarbonate/carbonate solutions. Electrochim. Acta 340, (2020).ater. 484, 332–338 (2017).

[4] Shoesmith, D. W. The inhibiting effects of hydrogen on the corrosion of uranium dioxide under nuclear waste disposal conditions. 346, 16–23 (2005).

Investigation on Crystallographic Properties of Zr and Its Alloy Through the Use of In-situ High Temperature X-ray Diffraction

Tae-Hyeong Kim[1,*], Dong Woo Lee[1], Jeongmook Lee[1], Junghwan Park[1], Jong-Yun Kim[1], Young-Sang Youn[2], and Sang Ho Lim[1,3,*]
[1]Korea Atomic Energy Research Institute, 111 Daedeok-daero 989beon-gil, Yuseong-gu, Daejeon, Republic of Korea
[2]Yeoungnam University, 280 Daehak-ro, Gyeongsan, Gyeogbuk, Republic of Korea
[3]University of Science and Technology, 217 Gajeong-ro, Yuseong-gu, Daejeon, Republic of Korea
*slim@kaeri.re.kr

1. Introduction

Zirconium alloys are widely used in various applications since Zr has high hardness, ductility, and corrosion resistance. Small amount of metals such as tin, niobium, iron, chromium, and nickel were added to improve its mechanical strength and corrosion resistance. One of the main applications of zirconium alloys is the cladding of fuel rods in pressurized and boiling water nuclear reactors due to low thermal neutron absorption cross-section of Zr [1]. The high temperature behavior of fuel cladding has been interesting since the fuel cladding is the primary barrier separating the fuel and environment.

In the present work, we investigated the crystallographic property of Zr and its alloy by using *in-situ* high temperature X-ray diffraction to understand its behaviors at high temperatures.

2. Experimental

Disc type of Zr (Sigma-aldrich) and its alloy with a diameter of 6.35 mm were prepared. Both were polished with 2000 grit SiC paper and then rinsed with ethanol before the measurement.

The X-ray diffraction was measured using a Bruker D8 Advance (Bruker AXS) diffractometer equipped with a HTK 2000N (Anton Paar) heating chamber. Cu Kα radiation at a voltage of 40 kV and a current of 40 mA filtered through a Ni foil was used as X-ray source. XRD patterns were measured with scan range of 20-80°, scanning step of 0.02°, and step time of 0.1 s. The samples on W heating strip heated up from 30 °C to 1400 °C with heating rate of 30 °C/min. The pressure was kept below 1.8×10^{-6} torr during the measurement.

3. Results and Discussion

Fig. 1. shows the *in-situ* high temperature X-ray diffraction patterns of Zr and its alloy at 30 °C and 1430 °C. The hexagonal close-packed structure of Zr was only observed for both samples at 30 °C. No patterns related to additional metal ions was observed in zirconium alloy. At 1430 °C, the hexagonal Zr crystal structure disappeared whereas new diffraction patterns related to monoclinic and tetragonal Zr oxide (ZrO_2) appeared. Additional rhombohedral Zr oxide (Zr_3O) for Zr alloy was assigned.

Contrary to the expectation, the oxidation was observed instead of temperature-induced phase transformation [2] from the hexagonal closed-packed crystal structure to the body-centered cubic crystal structure at 863 °C. The equilibrium partial pressure of oxygen of the oxidation of Zr was calculated based on the NIST Chemistry WebBook TDB [3]. At the transition temperature, the equilibrium partial pressure was around 10^{-41} atm. The pressure during the measurement was not enough to prevent oxidation. Even under reducing H_2 environment, the oxidation of Zr was observed by ex-situ XRD measurement

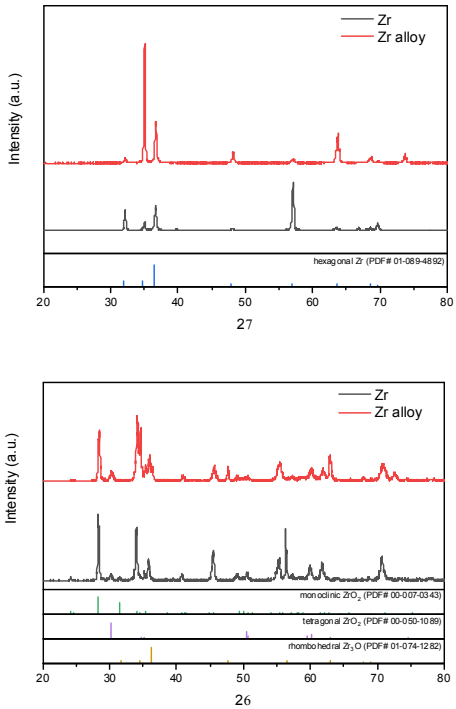


Fig. 1. *In-situ* high temperature X-ray diffraction pattern of Zr and its alloy at (top) 30 °C and (bottom) 1430 °C.

The lattice parameter of Zr and zirconium alloy for the hexagonal Zr crystal structure was determined within the temperature range of 30 ^{o}C to 830 ^{o}C using Pawely refinement. The data measured above 830 ^{o}C were excluded for the reliability. The a- and c-axes lattice parameter of both samples increased with increasing temperature, but the changes in the c-axis lattice parameter were quite different. The c-axis lattice parameter of zirconium alloy was more stable than that of Zr, causing a distinct difference in the c/a ratio. Therefore, the lattice thermal expansion of zirconium alloy was more stable than that of Zr.

4. Conclusion

The crystallographic characterization of Zr and its alloy were investigated by using *in-situ* high temperature in the temperature range of from 30 ^{o}C to 1430 ^{o}C. Both Zr and its alloy were oxidized instead of temperature-induced phase transformation due to its extremely low equilibrium partial pressure of oxygen for the oxidation. Based on the Pawely refinement, more stable lattice thermal expansion of zirconium alloy was observed, which is expected to suppress the rapid degradation of its mechanical properties.

Acknowledgement

This work was supported by the grant from the Nuclear Research and Development Program of the National Research Foundation of Korea funded by the Korean Ministry of Science and ICT (Grant code: 2017M2A8A5014719).

REFERENCES

[1] G. S. Brady, H. R. Clauser and J. A. Vaccari, *Material handbook (15th edition)*, McGraw-hill Professional (2018).
[2] I. Schnell, and R. C. Albers, “Zirconium under pressure: phase transitions and thermodynamics”, *Journal of Physics: Condensed Matte*r, 18, 1483-1494 (2006).
[3] M. W. Chase Jr., “NIST-JANAF thermochemical tables”, Journal of Physical and Chemical Reference Data Monograph 9 (1998).

Study on Improving the Sensitivity of Nuclear Material Analysis With LA-ICP-MS Using Desolvator

Jeongmook Lee [a], Dong Woo Lee [a], Tae-Hyeong Kim [a], Junghwan Park [a], Jong-Yun Kim [a,b], and Sang Ho Lim [a,b,*]

[a]Nuclear Chemistry Research Team, Korea Atomic Energy Research Institute, 111, Daedeok-daero 989 Beon-gil, Yuseong-gu, Daejeon, 34057, Republic of Korea

[b]Department of Radiochemistry & Nuclear Nonproliferation, University of Science and Technology, Gajeong-ro 217, Yuseong-gu, Daejeon, 34113, Republic of Korea

*slim@kaeri.re.kr

1. Introduction

Laser ablation inductively coupled plasma mass spectrometry (LA-ICP-MS) has been successfully applied to determine trace elements and isotope ratios in U-10 Mo fuel [1] and irradiated nuclear fuel [2-4]. LA-ICP-MS offers accurate, quick, and quantitative measurement with simple sample preparation and high sensitive chemical analysis. It is expected that LA-ICPMS would be very useful to analyze nuclear materials.

Desolvator provides the highest performing ICP-MS sample introduction system. Membrane desolvator maximizes ICP-MS sensitivity by that sweep gas removes solvent vapor while the analyte transport efficiency remains high. For the solution sample, the sensitivity of ICP-MS with desolvator generally increases by 5~10 times compared to that without the use of desolvator. In this study, we tried to confirm the possibility of improving the sensitivity for solid samples by connecting a desolaver to LA-ICP-MS. If this is possible, it will be possible to analyze the component using a smaller solide sample.

2. Experimental

LA-ICP-MS system consisted of ICP-MS (Element XR, Therrmo Scientific) and a laser ablation system (LSX213, Teledyne CETAC Technologies). Fig.1 shows LA system, desolvator and ICP torch. A NIST-SRM (Standard Reference Materials) 612 glass was also used to evaluate the capability of our LA-ICP-MS with desolvator setup. The sample line form LA system is cut and divided into a T shape to allow the ablated materials by 213 nm laser source to meet the hot air form desolvator. This mixture was introduced into the ICP torch with argon sampling and carrier gas. The ablated materials were ionized through the plasma and entered the mass detector. Spot analysis was used for LA-ICP-MS measurement.

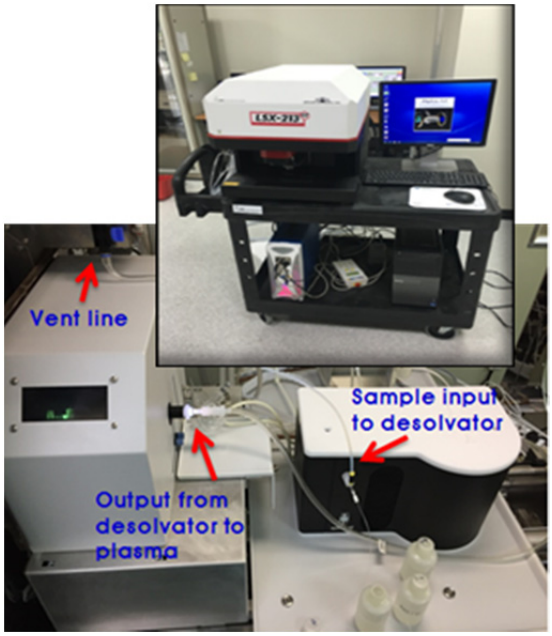


Fig. 1. Overview of system. LA equipment (up), ICP torch (left) and desolvator (right).

3. Results and discussion

^{238}U, one of the main isotopes in NIST-SRM, 612 was measured to confirm the sensitivity. ^{238}U sensitivity was ~10^4 cps when desolvator was not used under optimized conditions. On the other hand, when the desolvator was used, the sensitivity was ~10^6 cps, which showed a sensitivity improvement of about 100 times. It seems that the hot and dry air from the desolvator removes moisture from the ablated sample and increases the sample concentration relatively. Alternatively, it is assumed that hot and dry air improves the ionization efficiency of the sample in the ICP torch.

4. Conclusions

It was confirmed that the sensitivity was improved by about 100 times by applying the desolvator to LA-ICP-MS in the analysis of solid samples just as the sensitivity of liquid

samples is improved by using a desolvator. This shows that when analyzing solid radioactive samples, it is possible with a smaller amount, and suggests an analysis attempt that is safer and generates a smaller amount of analytical waste.

REFERENCES

[1] G. J. Havrilla and J. Gonzalez, Demonstration of femtosecond laser ablation inductively coupled plasma mass spectrometry for uranium isotopic measurements in U-10Mo nuclear fuel foils, Los Alamos National Laboratory, LA-UR15-24319 (2015).

[2] Y.-K. Ha, S. H. Han, H. G. Kim, W. H. Kim, and K. W. Jee, Shielded laser ablation ICP-MS system for the characterization of high burnup fuel, Nuclear Engineering and Technology, Vol.40, p.311 (2008).

[3] Y.-K. Ha, J. Kim, Y. S. Jeon, S. H. Han, H. S. Seo, and K. Song, Local burnup characteristics of PWR spent nuclear fuels discharged from YEONGGWANG-2 nuclear power plant, Nuclear Engineering and Technology, Vol.42, p.79 (2010).

[4] Y.-K. Ha, J.-G. Kim, Y. S. Park, S. D. Park, and K. Song, Behaviors of molybdenum in UO_2 fuel matrix, Nuclear Engineering and Technology, Vol.43, p.309 (2011).

2020 추계학술논문요약집

발행인 김경수

발행처 한국방사성폐기물학회

주 소 대전광역시 유성구 대덕대로 989번길 111
한국원자력연구원 원자력성과확산관(E7) 202호

연락처 **Tel** +82-42-861-5851, +82-42-866-4205
Fax +82-42-861-5852 **E-mail** krs@krs.or.kr

인쇄처 신진기획인쇄사 **Tel** +82-42-638-7887

Abstracts of Proceedings of the
Korean Radioactive Waste Society AUTUMN 2020

www.krs.or.kr

KOREAN RADIOACTIVE WASTE SOCIETY

사단 한국방사성폐기물학회
법인 Korean Radioactive Waste Society